EVALUATION OF SEISMIC RESISTANCE OF TRADITIONAL OTTOMAN TIMBER FRAME HOUSES

A THESIS SUBMITTED TO THE GRADUATE SCHOOL OF NATURAL AND APPLIED SCIENCES
OF
MIDDLE EAST TECHNICAL UNIVERSITY

BY

YASEMİN DİDEM AKTAŞ

IN PARTIAL FULFILLMENT OF THE REQUIREMENTS
FOR
THE DEGREE OF DOCTOR OF PHILOSOPHY
IN
ARCHITECTURE

AUGUST 2011

Approval of the thesis:

EVALUATION OF SEISMIC RESISTANCE OF TRADITIONAL OTTOMAN TIMBER FRAME HOUSES

submitted by **YASEMİN DİDEM AKTAŞ** in partial fulfillment of the requirements for the degree of **Doctor of Philosophy in Restoration, Middle East Technical University** by,

Prof. Dr. Canan Özgen
Dean, Graduate School of **Natural and Applied Sciences** ____________________

Assoc. Prof. Dr. Güven Arif Sargın
Head of Department, **Architecture** ____________________

Assoc. Prof. Dr. Neriman Şahin Güçhan
Supervisor, **Architecture Dept., METU** ____________________

Assoc. Prof. Dr. Ahmet Türer
Co-supervisor, **Civil Engineering Dept., METU** ____________________

Examining Committee Members:

Assist. Prof. Dr. Güliz Bilgin Altınöz
Architecture Dept., METU ____________________

Assoc. Prof. Dr. Neriman Şahin Güçhan
Architecture Dept., METU ____________________

Prof. Dr. Zeynep Ahunbay
Architecture Dept., İTÜ ____________________

Prof. Dr. Ömür Bakırer
Architecture Dept., METU ____________________

Prof. Dr. Uğurhan Akyüz
Civil Engineering Dept., METU ____________________

Date: **22.08.2011**

I hereby declare that all information in this document has been obtained and presented in accordance with academic rules and ethical conduct. I also declare that, as required by these rules and conduct, I have fully cited and referenced all material and results that are not original to this work.

Name, Last Name : Yasemin Didem Aktaş

Signature :

ABSTRACT

EVALUATION OF SEISMIC RESISTANCE OF TRADITIONAL OTTOMAN TIMBER FRAME HOUSES

Aktaş, Yasemin Didem
Ph.D., in Restoration, Department of Architecture
Supervisor : Assoc. Prof. Dr. Neriman Şahin Güçhan
Co-Supervisor : Assoc. Prof. Dr. Ahmet Türer

August 2011, 359 pages

The aim of this study is to evaluate the seismic resistance of traditional Ottoman timber frame "*hımış*" structures, which form the major part of Turkey's cultural heritage, from an engineering point of view. On the other hand, the seismic resistance of traditional Ottoman timber frame structures was not evaluated from an engineering perspective.

For the aim of seismic resistance evaluation of traditional Ottoman timber frame houses, the TUBITAK (the Scientific and Technological Research Council of Turkey) project numbered 106M499 was carried out. Within this framework, 16 tests were carried out in the Structural Mechanics Laboratory of Middle East Technical University, by means of 8 1-1 scale timber frames of different geometrical configurations and material, carefully selected from traditional houses in Safranbolu, representing Ottoman timber frame "*hımış*" technique. The frames were tested without and with different infill/covering types, and parameters that directly or indirectly indicate the behavior of a structure under earthquake loading were derived from the results obtained at the end of experimental work. In addition, capacity calculations were carried out for each test, using ATC-40 procedure.

The results demonstrated that Ottoman timber frame "*hımış*" houses are seismically resistant, and yet there are a number of important points that should be obeyed in their construction regarding size of diagonal elements, size and placement of openings, intervals between vertical studs, as well as connection details. It is also seen that certain infill/covering materials/methods are more advantageous than the others; for example, covering techniques results in a higher amount of maximum lateral load that the frame can bear under the same displacement. Infill with masonry blocks results in a larger increase in weight than in load bearing capacity. The conclusions drawn are intended to be used not only in the conservation of such structures but they are also expected to direct modern seismically resistant constructions.

Keywords: timber frame, Ottoman house, seismic resistance, earthquake, adobe infill, brick infill, *bağdadi*, *şamdolma*

ÖZ

GELENEKSEL OSMANLI AHŞAP ÇERÇEVELİ KONUTLARININ DEPREM DAYANIMLARININ DEĞERLENDİRİLMESİ

Aktaş, Yasemin Didem
Doktora, Restorasyon, Mimarlık Bölümü
Tez Yöneticisi : Doç. Dr. Neriman Şahin Güçhan
Ortak Tez Yöneticisi : Doç. Dr. Ahmet Türer

August 2011, 359 pages

Bu çalışmanın amacı, Türkiye'de yer alan konut mimarisinin büyük çoğunluğunu oluşturan geleneksel Osmanlı "*hımış*" konut yapılarının sismik dayanımlarının bir mühendislik bakış açısıyla incelenmesidir. Bu amaçla gerçekleştirilen 106M499 kodlu TÜBİTAK projesi çerçevesinde, Orta Doğu Teknik Üniversitesi Yapı Mekaniği Laboratuvarı'nda, geleneksel Osmanlı "*hımış*" tekniğini örnekleyen Safranbolu evlerinden seçilen, farklı malzemelerde ve farklı geometrik konfigürasyonlara sahip olacak şekilde inşa edilmiş birebir ölçekli 8 adet çerçeve, dolgusuz ve dolgulu/kaplamalı şekilde test edilmiş ve yapının deprem yükü altındaki davranışına ilişkin doğrudan ya da dolaylı fikir verecek parametreler elde edilmiştir.

Sonuçlar geleneksel Osmanlı "*hımış*" konut yapılarını sismik direncinin yüksek olduğunu, buna karşılık bu yapıların inşasında, çapraz elemanların (payanda) boyutları, pencerelerin boyutlandırılması ve çerçeve içindeki konumları, ahşap dikmeler arasındaki boşluklar ve bağlantılara ilişkin uyulması gereken bir dizi kural olduğunu göstermiştir. Buna ek olarak, belli dolgu/kaplama türlerinin diğerlerine göre daha avantajlı olduğu da gözlemlenmiştir. Örneğin, kaplama teknikleri ile

çerçevenin aynı deplasman değeri altında daha fazla yüke dayanabildiği görülmüştür. Yığma dolgulu çerçevelerde, dolgusuz örneklere kıyasla gerçekleşen ağırlık artışı yük taşıma kapasitesindeki artıştan fazladır. Bu çalışma sonunda ulaşılan sonuçların, yalnızca halihazırda var olan geleneksel Osmanlı "*hımış*" konut yapılarınında gerçekleştirilen koruma çalışmalarında kullanılması değil, aynı zamanda depreme dayanıklı modern yapı tasarımını da yönlendirmesi beklenmektedir.

Anahtar kelimeler: ahşap çerçeve, Osmanlı konutu, deprem dayanımı, deprem, kerpiç dolgu, tuğla dolgu, *bağdadi, şamdolma*

ACKNOWLEDGEMENTS

I would like to thank Assoc. Prof. Dr. Neriman Şahin Güçhan, for her insight, and invaluable and careful guidance throughout this study. She was always willing to allocate time to discuss the progress and the results of our study; therefore she played an indispensible role on the final state of this thesis.

I want to express my deepest gratitude to Assoc. Prof. Dr. Ahmet Türer for his guidance and encouragements not only for this dissertation but also for the contributions he has made to other fields in my life. He has always been an unending source of inspiration. I feel truly privileged that I have had the opportunity to work with him, for more than seven years already, and I hope from the bottom of my heart that this association will always be.

I also want to acknowledge that Uğurhan Akyüz was the project supervisor of this project and surely one of the persons that made it possible.

I am deeply grateful to Ömür Bakırer, Güliz Bilgin Altınöz and Zeynep Ahunbay for making this study a better one with their invaluable feedbacks.

The experimental part of this study could not be completed without the invaluable contributions of Barış Erdil, also known as “Eküri”. Working with you made all that tiresome work easy and enjoyable. The staff of Structural Mechanics Laboratory and Ahmet and Himmet Çelen from Beypazarı also made a great contribution to this study. Thank you!

Balkardeşim, Selüm, Ezgi, Burcik, Nagiş, Beyhan, Gökhan, Emre, Murat, and Semoş deserve also a big and sincere acknowledgement for encouraging me all that time and keeping me at work.

Bilge, who I neglected so much… Your daughter is already a big girl and she doesn’t even know her aunt, Yasemin :(Thank you for your limitless understanding.

Maryam and Pourang, with golden, or rather crystal hearts… Thank you for sharing your dreams and including us in them…

I am also deeply grateful to Belüş and Efe for their unconditional love and support.

I want to thank to all the special friends of mine, Filüş, Cem, and Emine, for being in my life and making it always more beautiful, even from far away. Thank you Pufu, for being so soft and velvety all the time…

And, thank you Ceyhan, my best friend, my love, my family… Thank you for what you are and what you have always brought to my life.

TABLE OF CONTENTS

LIST OF FIGURES

FIGURES

LIST OF TABLES

TABLES

CHAPTER 1

INTRODUCTION

Turkey is a seismically active country and prone to earthquake induced damages. Taking into consideration that a major part of the registered built heritage in Turkey is composed of traditional Ottoman timber frame "*hımış*" houses, the need for an evaluation of these structures from an engineering point of view is apparent. In spite of the presence of a number of studies in the relevant literature, claiming the timber frame *hımış* houses have an inherent seismic resistant property, nearly none has been said on the experimental basis of an engineering approach. The traditional Ottoman timber frame *hımış* structures are hybrid constructions, where the foundation and the ground floor are made of masonry and the upper floors and the roof are made of timber frames. Since the seismic performance of masonry structures is a highly focused subject so far by many scholars, this thesis aims to make up such a deficiency in this field by concentrating on the behavior of timber frame section of traditional Ottoman timber frame *hımış* houses under seismic demand.

1.1. A BRIEF HISTORY OF USE OF TIMBER AS A CONSTRUCTION MATERIAL

Timber is one of the oldest construction materials. In the attempt of ancient men to understand the qualities that the naturally occurring substances held, timber must have attracted attention immediately as a material of construction, since it is a readily available material in wooded areas. It is also a light material, which rendered permanent and transportable shelters possible (Wright, 2000: v2, 5).

Since timber is an organic, and hence easily degradable material, our knowledge on ancient use of timber is more limited than those on other ancient materials. Wright (2000: v2, 13-14) lists the sources of our information on ancient use of timber as follows:

> (1) Actual remains of wooden building elements, (2) Negative impressions left in more permanent material by completely decayed wood (…), (3) Ancient pictorial representations (…), (4) Literary and epigraphic references, (5) Analogical evidence from building forms in other more permanent materials, e.g. stone and mud brick – on the prevalent assumption that the forms of much of the building derives from wood originals.

In Paleolithic Period, unsettled hunters and gatherers are believed to have constructed the first temporary shelters with circular plan by using easily available materials such as branches, wattle and mud (Acar, 1996: 380). Even though it is claimed that no permanent housing was made until the "Neolithic Revolution" (Özdoğan, 1996: 19), Acar (1996: 381) suggests that continuous settlements were found before the beginning of agricultural activities in Mesolithic Age, which are composed of structures not much different than those constructed in Paleolithic Period.

In Neolithic buildings in Middle East, on the other hand, wood was started to be considerably processed by trimming them into timber (Wright, 2000: v1, 21) and plans turned to be rectangular in shape rather than circular, mostly in Aceramic Neolithic Age (Acar, 1996: 382-383). Again in the Neolithic period, in the continental Europe, there were so-called round and long houses, where timber was used together with stone in the former and alone in the latter (Wright, 2000: v1, 26-27).

In ancient Asia Minor, the houses were mostly constructed using adobe blocks reinforced by timber elements from the Late Chalcolithic Age onwards. This type of construction can be seen in nearly all Anatolia, including the well-known sites such as Beycesultan and Kültepe (Kaneš). It is known that the stone foundation of Beycesultan Palace was constructed upon transversally laid timber blocks (Lloyd and Müller, 1998: 35). Lloyd and Müller underlines that use of timber frames has a long tradition in Anatolia and other places in Middle East (such as northern Syria), most probably against earthquakes, since such a construction technique is nearly not at all observed in Mesopotamia, where there is limited seismic activity (Lloyd and Müller, 1998: 35). In Hittite settlements, the roofing of the houses were built using timber, however, there are no traces left from these upperstructures (Neve, 1996: 103). Mellink (1975: 204) informs us that walls, made of adobe and timber, were also found in the upper Hittite layers of Zile-Maşat Höyük.

When Anatolia is concerned, the tomb chambers with timber construction in the Phrygian tumuli should also be noticed (Wright, 2000: v1, 101-102). Perrot and Chipiez (1892: 118, 205) argue that the stone pillars inside the Phyrigian tombs recalls wooden posts in a loft and the only reason for this is that a wooden post would not bear the heavy roof. It was underlined that the false plasters in front of these stone carved tombs must also be inspired from their wooden originals. They also claim that the Phrygian houses must have been constructed using timber, also because the rocks in the area have a soft loose texture and trees are abundant (Perrot and Chipiez, 1892: 118).

Fellows (1840: 129-131) claims that the Lycian rock carved tombs might be an imitation of Lycian timber houses since these tombs reflect, to a large extent, timber construction technique (Figure 1). Perrot and Chipiez (1892: 353) underline that the Lycian land is full of forests and timber “must at all times have been the sole industrial means of the country”. They also suggest that the Lycian monumental architecture was influenced by and reproduced from timber frame house constructions, where the spaces between main beams were infilled with timber elements of square pieces, so that the surface is divided into panels and “they (Lycians) for centuries went on repeating in their necropolis forms suggested by the only style of architecture they had known at the outset-that which, in building the house, used none but squared and unsquared pieces of timber” (Perrot and Chipiez, 1892: 353, 357). After Fellows (1840: 129), also Işık and Yılmaz (1996: 171) suggest that this ancient tradition of timber construction still lives in modern granaries, as corroborated by Perrot and Chipiez (1892: 364).

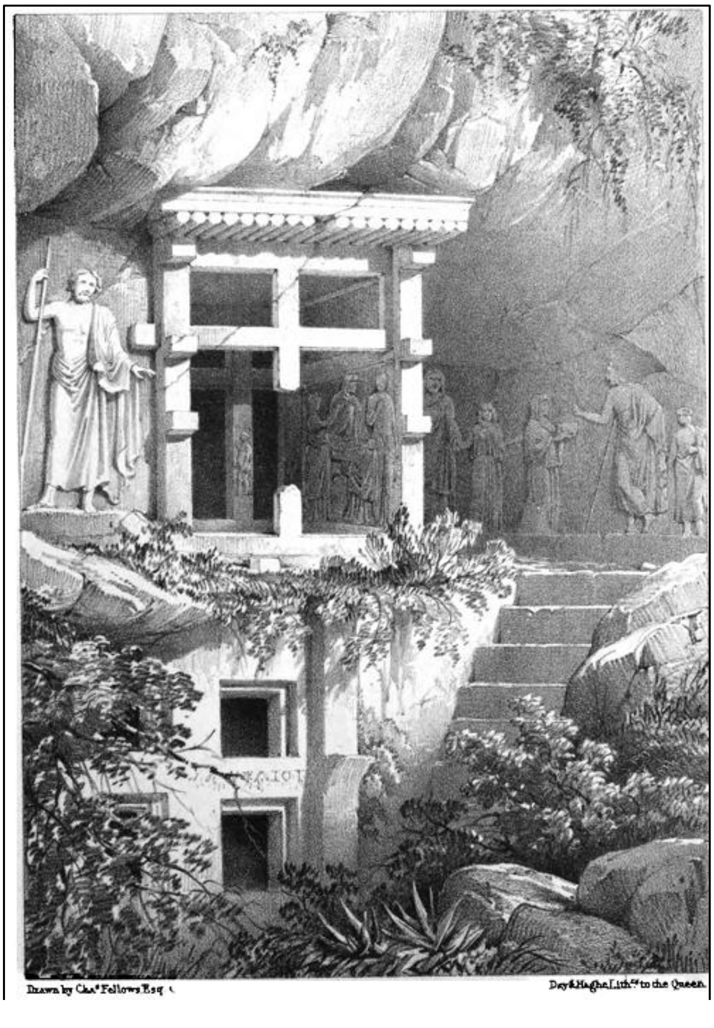

Figure 1: Drawing of a Lycian rock tomb at Myra by John Murray (after Felllows, 1840)

Another ancient use of timber was timber roofing by the Greek (Hamlin, 1904: 55). However, as underlined by Wright (2000: v1, 101-102) it is not correct to generalize this kind of a use since there is little material survived to our time. Although flat terrace or slightly pitched terrace roofing was more common, certain plan types show us that gable roofing, for instance, was not unknown but only a rare case. Hamlin (1904: 49), on the other hand, suggests that the Doric frieze and cornices might be originated from wooden construction.

The roofing of the houses in pre-dynastic Egypt is considered to be of timber (Lloyd and Müller, 1998: 73). Some monumental details, on the other hand, for example, at Karnak, Kalabshe, Amada and Abydos, show resemblance to timber construction (Hamlin, 1904: 12). Hamlin (1904, 26) claims also that the domestic architecture in ancient Egypt must have been of timber and adobe, because this is the only way to explain why they are now totally disappeared. He also explains that there are relief pictures at monumental structures, depicting the construction of timber frame structures and their infilling with adobe (Hamlin, 1904: 27). The flat stone roofing of monumental structures is assumed to come down from these houses (Lloyd and Müller, 1998: 117). Also columns in the stone monuments have vegetative decorations such as papyrus or palm, therefore are most probably imitations of timber precedents (Lloyd and Müller, 1998: 118; Wright, 2000: v2, 5).

Romans were familiar with the timber truss and the structural advantages it offers (Guiliani, 1990: 56-59). In addition to gable roof, they used timber also for the purpose of "centering and shuttering of arcuated construction" as well as for bridge construction (Wright, 2000: v1, 114). Romans are also distinguished for a variety of specialized tools for any kind of construction work, including carpentry. Trees appropriate for certain climatic conditions were well known (Adam, 2006: 92-93). Romans achieved timber joints by nails and spikes (Ulrich, 2007: 59) as well as through a variety of interlaced connection methods (Adam, 2006: 104-105; Ulrich, 2007: 59-70). Within the territories of the Roman Empire, only in the North, in Britain or in Germany, timber floors were common (Adam, 2006: 213). They also used gluing as a joining means to assemble two or more planks side by side to obtain a flat panel (Ulrich, 2007: 70). Vitruvius gives also important information regarding the use, preferred types, and production of timber. According to Vitruvius (tr.by. Morgan, 1914: 41, 58), fir, for example, is preferable for its light-weight and strength, and yet it catches fire very rapidly, while oak is particularly suitable for underground uses because of its durability, and alder should be used in foundations of buildings to be constructed in swampy regions. In addition, since the wall thickness was limited by public law (Vitruvius, tr.by. Morgan, 1914: 58-63), thinner timber frame walls (*opus craticium* or *muri craticii*) were preferred over brick or adobe walls in house constructions (Lugli, 1957: v1, 44).

In the eastern Roman Empire, the use of wooden tie beams was frequent. "As masons constructed the walls, they built tie beams into the thickness of walls and nailed or toggled them together at the corners to aid in stabilizing the construction until the mortar set to its ultimate hardness."

(Ousterhout, 1999: 192). The same reinforcement technique was valid also for the construction of arches and vaults. “Nailed or toggled to another, the wooden beams created a series of tension rings that secured the building against deformation, thus allowing construction to proceed at a rapid rate.” (Ousterhout, 1999: 210-211). Ousterhout (1999: 207-208) underlines also the fact that “surviving timber elements in a structure may contribute to its dating”. The use of timber in foundations was rare in Byzantine period (Ousterhout, 1999: 161-162). Eyice (1996: 207-208) underlines that Byzantines must have built timber structures in highly wooded areas, however no traces were left from those. A small number of remains that are thought to belong to Byzantine dwellings are all masonry structures. On the other hand, the author suggests that the wooden *böcekhane* buildings by İznik Lake are probably examples representing Byzantine construction tradition (Eyice, 1996: 207-219). There are findings supporting that Byzantines constructed their houses in Anatolia mostly by using adobe (Rheidt, 1996: 230).

In the Seljuk cities, as in Principalities period, nearly nothing is available regarding dwellings (Tanyeli, 1996: 416-423). In the former case, it may be assumed that for the upper class of the society, tent was still an essential part of the sheltering tradition (Tanyeli, 1996: 423). Also for the latter case, even though there are traces belonging to several urban pavilions and mansions, Tanyeli (1996: 423) suggests that rural housing outside the cities, possibly in tents, were still preferred, based on the Ibn Battuta’s travel notes.

Ottomans, on the other hand, especially after 16th century, established a well-established timber frame housing tradition, which still comprises the majority of the Turkey’s heritage. Based on a comprehensive literature review, the general characteristics of the Ottoman timber frame housing are defined in detail in the next sections.

1.2. TIMBER FRAME HOUSES DURING THE OTTOMAN ERA

The traditional timber frame houses in Turkey have been denominated in different ways by different scholars. They are called as Turkish House (e.g. Eldem, 1984), Turkish Hayat House (e.g. Kuban, 1995), Anatolian House (e.g. Asatekin, 1994) and Ottoman House (e.g. Cerasi, 1998; Arel, 1982) by different scholars. In this study, the Ottoman house term is preferred since the general form and design principles of this construction tradition was first developed in Western Aegean Region (Kuban, 1996: 4) and successfully applied to a vast area, from the Southern Middle Anatolia to Black Sea Coasts of Romania, Crimea, Bulgaria, Macedonia, Bosnia Herzegovina, Mora, until Croatia and Hungary in the north that was under German influence, where the Ottoman Empire spread, regardless of drastic differences in climate[1] (Kuban, 1996: 4; Eldem I, 1984: 19-20, 93), and based on such characteristics such as available materials of construction, topography and site properties and economic constraints (Günay, 1998: 66) (Figure 2-Figure 8).

Figure 2: Traditional Ayaş houses (Neriman Şahin Güçhan archive)

[1] Sözen (2001:126) claims that in the Balkan countries (except southern Greece and Dalmatian coasts) the evolution of Ottoman house with timber construction has been easier in comparison to in Syria, Egypt and Iraq, because there was not an established housing tradition. This is also because the Ottomans embraced this region as their favorite expansion zone (Akın, 1996: 269). The Ottoman effect in Balkan countries can still be easily observed by means of a high number of still standing examples. Akın (1996: 267-271) draws attention to the fact that also the building terminology reveals this fact (i.e. *hayat* vs. *hayati*, *şahnişin* vs. *sahnissi* etc.).

Any valid plan type of traditional Ottoman house with timber frame construction, including varieties formed by projections can be observed also in the Balkans. Not only rooms keep their multi-functional characteristics but also *başoda* exists also in these examples. In the meantime, however, like in the eastern parts of the Empire, also in the case of Balkan countries the end-product dwelling was affected by the regional traditions as well. Therefore, housing with partial (such as Albania and Bosnia) or sometimes with no influence (such as northern Bulgaria, southern Greece, Croatia, Aegean islands, etc.) from Ottoman architecture can also be observed in some areas. For example, in Bulgarian houses with open sofa plan type no *eywan* exists at all. Similarly, in Northern Greece, houses where rooms are not directly opened to sofa, but instead to an inner corridor, can be observed. The same situation is valid also for certain parts of Bosnia Herzegovina and Bulgaria; there is generally a kitchen-like space between rooms and sofa (Akın, 1996: 271-273).

Kuban (1995: 232-237) underlines also that some local changes were started to occur towards the 19th century, when the modernization (westernization) process was in rise, especially in the houses of non-Muslim community, according to their needs, in Balkan countries and in the Thrace (especially in Edirne). For example, in Bulgarian houses, *hayat* was not much accentuated anymore, therefore from the plan layout point of view the house was strongly different than a conventional Ottoman house, while façade still preserved its features. One should also bear in mind that many Balkan scholars argue that the origins of such houses should be sought in Byzantine dwelling architecture, and not in Ottomans' once presence in the area. Yet, the divergences of Balkan houses from traditional Ottoman houses as we observe in Anatolia and Istanbul are much fewer than their similarities (Akın, 1996: 273-276).

Figure 3: Traditional Beypazarı houses (Neriman Şahin Güçhan archive)

Figure 4: Traditional Güdül houses (Neriman Şahin Güçhan archive)

Figure 5: Traditional Cumalıkızık houses (Neriman Şahin Güçhan archive)

Figure 6: Traditional Sürmene houses (Neriman Şahin Güçhan archive)

Figure 7: Traditional Şirince houses (Neriman Şahin Güçhan archive)

Figure 8: Traditional Rize houses (Neriman Şahin Güçhan archive)

Şahin Güçhan (2007b: 2-3), groups the Ottoman house researchers/scholars according to three areas of interest. The first group of scholars makes an evaluation on plan typology and space organization of Ottoman houses, while the second group of scholars uses geographical factors as the primary parameters. The third group adds social and economic factors into consideration. Since the content of this study does not include the sociological/economic factors that shaped traditional Ottoman timber frame structures, only the former two factors will be discussed below.

TYPOLOGICAL STUDIES ON SPATIAL CHARACTERISTICS OF TRADITIONAL OTTOMAN TIMBER FRAME HOUSES

This group of scholars accepts the room and *sofa* as the primary elements forming the plan layout of the Ottoman houses. The relationship of rooms with *sofa* and their order defines the plan layout. In this typological order, rooms are separated by means of an outer, inner or a central *sofa* (Figure 9). *Sofa* is used as a circulation space, as well as like a room in appropriate weather conditions (Kuban, 1995: 144), which is similar to Arabic *tarma* or Persian *liwan* (Ünlü, 1996: 248). Sofa is also a gathering area of the house. Any kind of social activities, such as wedding ceremonies took place here. Sometimes, *eywan*s can be seen adjacent to these sofas, generally located in a cove left between two rooms. In addition to this, *sekilik*s were formed by elevating the floor level by several steps. They are open at their two or three sides and may turn out to be *köşk*, which are distinguished with many windows (Eldem I, 1984: 97, 123; Sözen, 2001: 81).

Based on visual documents, as well as limited information given by *wakfiyya*s, it is known that in the 15th and 16th centuries, the majority of the houses were single story - *bayt-i sufli* - (Eldem I, 1884: 83;

Kuban, 1995: 48; Faroqhi, 1998: 169) and had an outer *sofa*[2] (called *hayat* by Kuban). In these single story houses, the floor level was generally elevated by some 1.5 – 2 m to take more advantage of sunlight, especially in narrow streets of big cities, as well as to avoid rising damp (Sözen, 2001: 81). After 16th century, when the houses had more than 1 storey, plan layouts started to diversified.

The lower space was used either as an empty space where supporting upright elements were located, or as a deposit area, animals' shelter or the like (Eldem I, 1984: 96). Eldem underlines also that even in the later periods, where number of floors increased to two or three, the main living space is always only one and the highest of these floors. The floor found in between was normally lower in height and while it was originally used as a winter floor and for service spaces, after the 19th century its differences from the main upper floor were nearly diminished (Eldem I, 1984: 96, 123). Mezzanine floor concept also appears in the 17th century (Günay, 1998: 42). When 18th century arrives, a new plan type develops, which is characterized with a central sofa. Also later, the plan type has always been characterized by the position of sofa (Eldem I, 1984: 96, 215; Sözen, 2001: 82) (Figure 9).

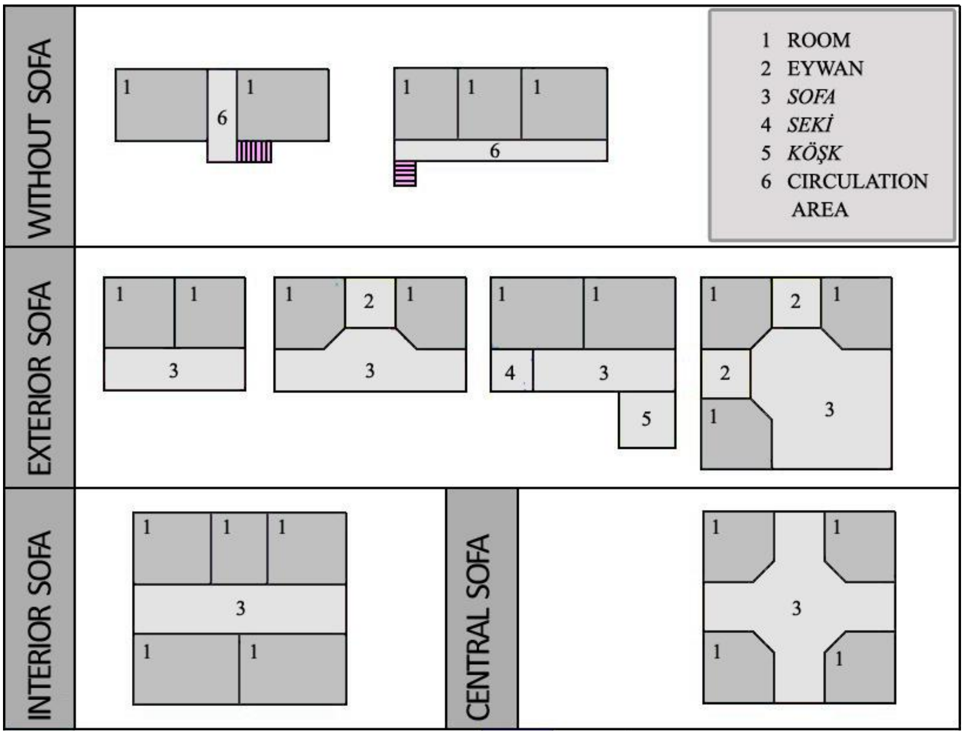

Figure 9: Plan types of Ottoman house (based on Eldem, 1968)

[2] There are scholars suggesting that the *sofa* was originated from very early Anatolian examples since similar spaces were found in Neolithic Hacılar. Also the Hittite *hilani* houses have such semi open spaces that can be evaluated as a *sofa* (Ünlü; 1996: 249).

The number, location and direction of the rooms in each floor were deeply affected by the plan type. The rooms are multifunctional in these houses. The same space is used for sitting, dining and sleeping purposes. The necessary objects for eating or sleeping are kept in the cabinets, inserted into walls, when they are not necessary (Eldem III, 1984: 80; Sözen, 2001: 72-81). There was built-in furniture in these rooms, such as *sedir*s, closets, *seki*s etc. Some scholars argue that this kind of a room concept has been derived from tent, where different activities took place as well[3].

It is also because of the fact that the size and shape of a room can easily be altered by not changing much its relation with the rest of the house, i.e. the room is more or less an independent entity within the house opening directly to sofa, that the scholars used that allegory between a tent and a room in an Ottoman house.

In addition to these, there is also a *başoda*, which is utilized to accept the guests. It is the largest, most ornamented and generally located at the corner of the plan layout. In some cases, especially in the men's room (*selamlık*), the room is divided into two parts by means of a change in floor elevation. The lower part, located at the entrance is called *sekialtı*, whose width is somewhat determined by the diameter of the door frame (Eldem I, 1984: 96; Eldem III, 1984: 15; Kuban, 1995: 113; 134; Sözen, 2001: 80-81).

TYPOLOGICAL STUDIES ON GEOGRAPHICAL CHARACTERISTICS OF TRADITIONAL OTTOMAN TIMBER FRAME HOUSES

In this approach, the houses are grouped based on the geographical locations they are placed in. Kazmaoğlu and Tanyeli (1979) define the socio-cultural background as the most important factor forming traditional architecture of a region. Based on such a criterion, they divide Anatolia into two as (1) where "original Anatolian synthesis" in housing is observed and (2) transition regions. The former, which is defined as "*hımış*", includes Western-Northwestern Anatolia, Eastern Black Sea Region, the city of Konya and the city of Istanbul, while the latter includes the rest, namely Bodrum, Kayseri, Eastern Anatolia and Southeastern Anatolia (Kazmaoğlu and Tanyeli, 1979: 34). Among

[3] Anton Bammer (1996: 234-247), for example, suggests that the Ottoman architecture has deeply been affected by Turkish-Mongolian tents called *yurt* and bases his argumentation on semi nomadic traces of moving to highland camps, *yayla*s, in summers, multi functionality or rooms, summer, and separate winter and summer rooms. Kuban (1996: 4-5) claims that also the use of rooms in a traditional Ottoman house resembles that of a tent since in both cases, the central area is empty and sitting group surrounds the space. Some other scholars, such as Cerasi (1998) oppose this assumption, claiming that Turkish house is a product of contributions of different cultures, belonging to different ethnic groups, unified through Ottoman culture (Cerasi, 1998: 132, 139). However, Rheidt (1996: 230) suggests that also in Byzantine dwellings, rooms were multifunctional, therefore the use of rooms for multiple purposes must be an already established tradition in Anatolia. Tanyeli (1996: 426) underlines that even though the etymological link between the words *oda* (room) and *otağ* (tent) is conspicuous; relating the foundations of Ottoman house and nomadic habits to use tents as shelters is too direct.

these, in Konya, Bodrum, Eastern and Southeastern Anatolian Regions the common construction material is not timber. Based on Kazmaoğlu and Tanyeli (1979), the classification of timber construction types is tabulated in Table 1 and showed in Figure 10.

Table 1: A classification of timber construction types based on Kazmaoğlu and Tanyeli (1979)

Original Anatolian Synthesis		
Region	**Dominant Construction Techniques**	**Notes**
Western-Northwestern Anatolia	*Hımış* structures with adobe or brick infill	
Eastern Black Sea Region	*Hımış* structures with stone infill.	Small size infill materials, even boulders. Symmetrical plan schemes, closed *sofa* type. Uncovered construction
Istanbul	Timber construction.	Plan schemes with closed *sofa*. Western influence.
Transition Regions		
Region	**Dominant Construction Techniques**	**Notes**
Kayseri	A combination of timber and stone construction	Inner and closed *sofa* types.

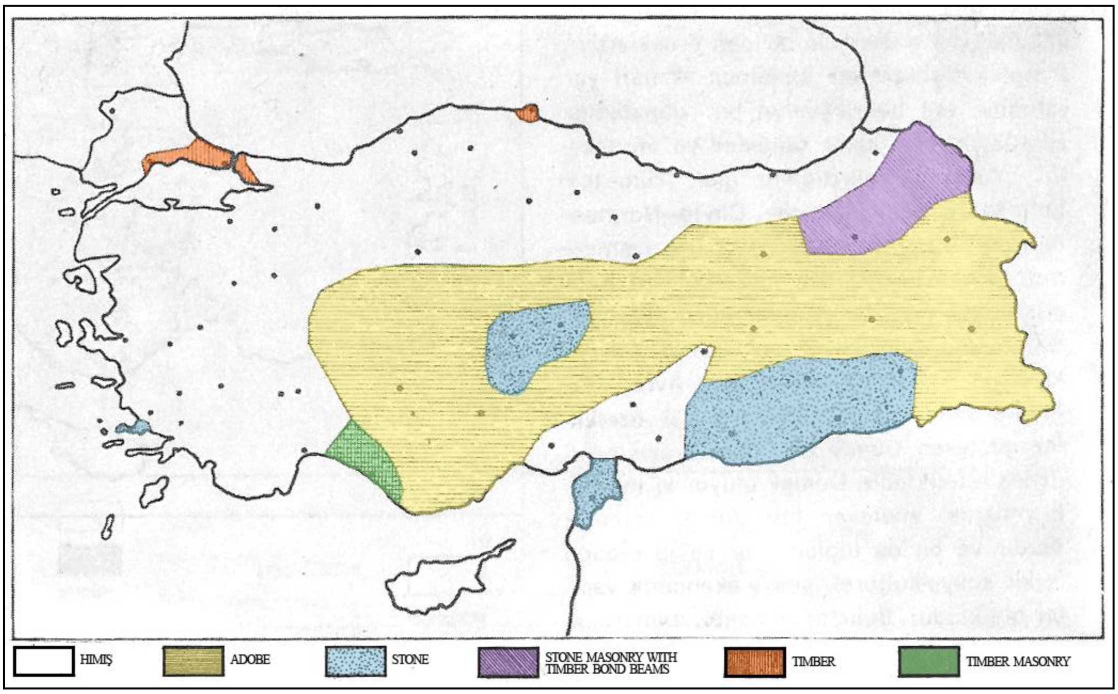

Figure 10: Geographical distribution of *hımış* structures and other construction types (recolored after Kazmaoğlu and Tanyeli, 1979)

Cerasi (1998, 120-129) investigates in detail the way of adapting one or more elements of neighboring cultures' housing tradition to eventually form Ottoman houses. According to him, the final product of traditional Ottoman timber frame "*hımış*" structures the effects of different ethnic groups have cumulatively formed the traditional "*hımış*" houses (Cerasi, 1998: 116), therefore one may claim that these type of constructions are hybrid not only from structural point of view, but also on the basis of the cultural background they were born into.

1.3. TRADITIONAL TIMBER FRAME OTTOMAN "HIMIŞ" HOUSES

Traditional timber frame Ottoman "*hımış*" house is a hybrid construction system, where the ground floor is built in masonry and the upper floors and the roof are composed of timber frames. This counter-distinction between the construction techniques of ground and upper floors, which was probably a conscious choice, is illustrated in Figure 11 by Şahin Güçhan (1995: 173).

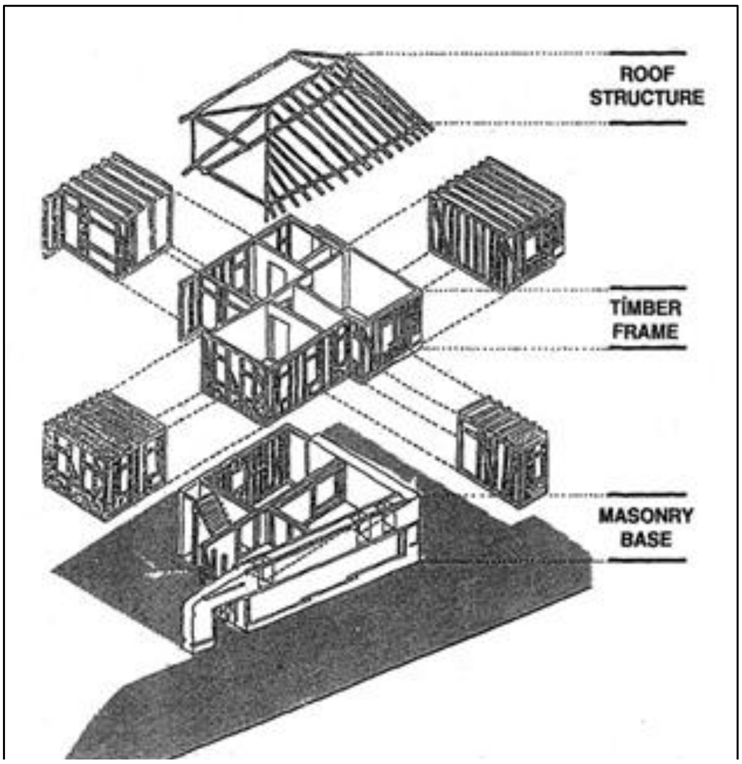

Figure 11: Sections of a timber frame house in Ankara (after Şahin, 1995)

The earliest standing examples to "*hımış*" structures belong to the 17th century, while the latest examples of this type of construction belong to 19th century. Faroqhi (1998: 169) confirms that there were two story timber houses in the 16th century. In fact, from the drawings of the traveler Peter Coeck of Aelst[4], we know that multiple story timber houses existed in the first half 16th century (Coeck, 1533, tr. by. Sir William, 1873). A detail from one of his woodcuts is seen in Figure 12.

Figure 12: A detail from a woodcut of Peter Coeck of Aelst (after Coeck, 1533, tr. by. Sir William, 1873)

Building methods utilized for the construction of a timber Ottoman house has evolved as to have very simple details (Günay, 1998: 66). This brings also along the speed and ease in reconstruction of houses after a devastating fire sweeps them off, as frequently occurred throughout the history (Kuban, 1995: 238) and in line with lack of sense of permeability that can be observed in the "institutional and psychological context of Ottoman society" (Cerasi, 1998: 120). Moreover, the construction techniques do not exhibit much regional varieties (Kuban, 1995: 239).

[4] "(...) to Sophia, 15 miles. This town derives its name from the church, outside the bazaar, called St. Sophia (...) Most of the people are Turks. There are very few stone houses, most being of timber or earth." (Coeck, 1533, tr. by. Sir William, 1873: 27).
"(...) a new village, passing by Philippopoli, and then the river Staunch [Stanimacki] (which) was in old times built by King Philip (...) and are Turkish villages of straw, wood, and clay." (Coeck, 1533, tr. by. Sir William, 1873: 28). "Except for the old churches (...) the buildings are all in the Turkish fashion, of wood and clay." (Coeck, 1533, tr. by. Sir William, 1873: 29).

The ground floor, in *hımış* houses, built on top of stone foundations, is generally made of rubble stone masonry or adobe with timber lintels (hatıls) at regular intervals as well as of cut stone or alternating courses of stone and brick[5] (Kafesçioğlu, 1955: 60; Eldem III, 1984: 162). In the case that the ground floor was not constructed of cut stones, big cut stones were placed anyways where the main uprights, supporting the actual timber frame, would bear (Eldem III, 1984: 162).The ground floor might also be constituted by singular vertical timber elements, with the gap in between filled with non-load bearing masonry or not[6] (Kafesçioğlu, 1955: 58).

The ground floor fits with the generally irregular planimetric geometry of the house. The upper floors, on the other hand, are more regular in shape and larger by means of *çıkma*s (Şahin Güçhan, 2007b: 35, 61).

In the early period houses (17th century), it was common that also upper floors were constructed of masonry except for the façade where the projection was located (Eldem I, 1984: 123). The upper floors are constructed as timber frames, which are the smallest module of a timber frame storey. A timber frame is a façade of a room of *sofa*. They are constituted of vertical, horizontal and diagonal elements. The timber elements used for the construction of the timber skeleton are always single-piece elements (Aksoy and Ahunbay, 2005; 53). The cross-sections are approximately 12x12 – 15x15 cm and the interval between the studs varies between 1.30 m and 1.50 m for Northwestern Anatolian houses (Kafesçioğlu, 1955: 64-66). These values are about 12x12 cm and approximately 50 cm for Ankara houses (Kömürcüoğlu, 1950: 63).

Diagonal braces were used in a variety of configuration and inclination angle. In Northwestern Anatolia, this angle changes between 30 and 45°. Generally the corner posts are supported by diagonals, however it is also possible that the studs located in the middle are supported by diagonal bracing at two sides (Kafesçioğlu, 1955: 64-66).

Floor joists are placed approximately 40-50 cm apart from each other (Kuban; 1995: 243) and directly upon these joists, and single-piece-from-end-to-end floorboards are nailed (Eldem III, 1984: 163).

It is important to point that before placing the infill material, all frame system, including the roof, is generally completed[7].

---

[5] In some settlements (for example in Kastamonu, Çankırı and Göynük) it is common to use the masonry walls in only one or two facades (Kafesçioğlu, 1955: 60).

[6] One should bear in mind that even though infill is not designed to carry vertical loads, it will increase the overall stiffness under lateral loading.

[7] However, Kuban reports that De Kay, during his visit in Istanbul in the beginning of the 19th century, notes as follows: "(…) The operation of painting goes simultaneously with the labor of the carpenter and the mason" (Kuban, 1995: 238)

1.3.1. SECTIONS OF TIMBER FRAME OTTOMAN *HIMIŞ* HOUSES

Traditional timber frame Ottoman "*hımış*" house is a hybrid construction system, where the ground floor is built in masonry and the upper floors and the roof are composed of timber frames. Brief information regarding these masonry and timber frame sections is given below.

1.3.1.1. MASONRY SECTION

The masonry sections of an Ottoman house are composed of foundations and ground floor walls.

Şahin Güçhan (1995: 175-180) classifies the foundations of timber frame "*hımış*" houses as discontinuous, continuous or composite (Figure 13). The discontinuous foundations, especially common in Northwestern Anatolia as well as Beypazarı and Nallıhan, are composed of timber posts that are not jointed to each other at foundation level, but sit on roughly finished stone bases, i.e. the single footing foundations, which stick out of the ground approximately 25-30 cm (Figure 14, Figure 15).

In case of continuous foundations, there is a, mostly rubble stone, masonry wall of some depth under the ground and through the external edges of a structure, as in Ankara. In composite foundations, on the other hand, the edges of a building are supported by continuous foundations, whereas the inner axis or partition walls with discontinuous ones (For more information see Şahin, 1995: 175-180). In Central Anatolian village houses investigated by Kafesçioğlu (1949: 12), the foundation is approximately 1 m, while for Birgi houses within the content of the study by Diri (2010: 87), the foundation depth varies between 60 and 150 cm.

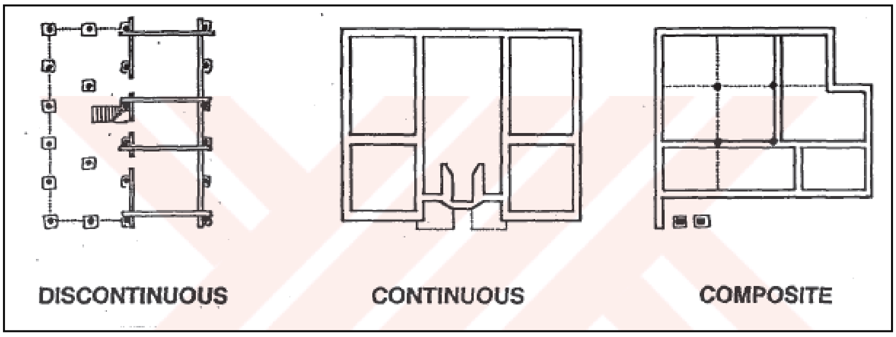

Figure 13: Schematic representation of different foundation types in timber frame structures (after Şahin, 1995)

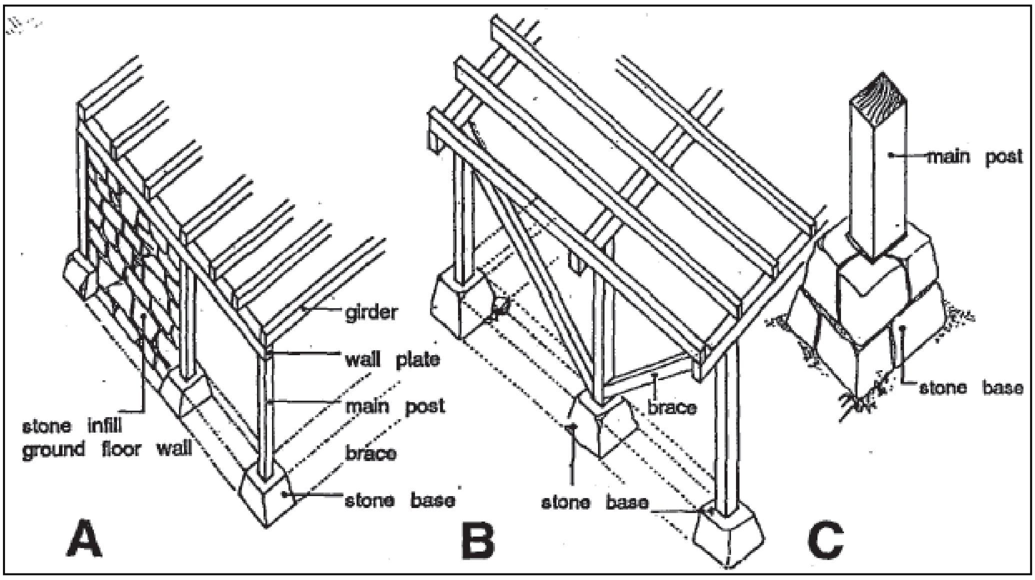

Figure 14: Discontinuous foundations (after Şahin; 1995)

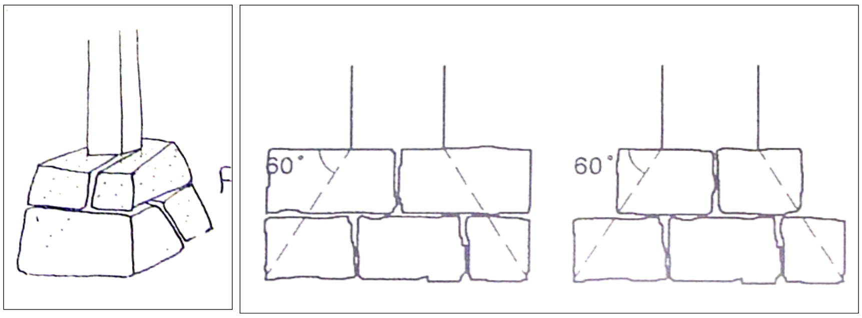

Figure 15: Examples to single footings (after Kafesçioğlu (1955) and Soygeniş (2008), respectively)

Ground floors were generally constructed in stone masonry, not only for load bearing purposes but also to protect timber from rising damp (Kuban, 1995: 241). The houses where upper floors are supported by masonry base and those where upper floors are carried by high timber posts (sometimes with non-load bearing masonry infill between these posts) should be distinguished. For instance, Ankara houses are generally from the former group, while Beypazarı houses belong to the latter one (Şahin, 1995: 173-174).

In the masonry ground floors, cut stones were rarely used. Rubble stone masonry with or without additions of brick is the most frequently seen material in ground floor walls (Eldem III, 1984: 172). In the houses where ground floor walls are made of stone masonry, it is possible also that the foundation is constructed as subbasement (Aksoy and Ahunbay, 2005: 51). The use of cut stone walls in the ground floors is an exception and depends on economic conditions of the house owner. The wall thicknesses vary between 60 and 75 cm for early period Ottoman houses (17th century), as confirmed by Eldem (1984), while Kömürcüoğlu (1950) says that the wall thicknesses are 60-90 cm, and sometimes even thicker in Ankara houses. (Kafesçioğlu, 1955: 46-50; Eldem, 1984: 123; Kömürcüoğlu, 1950: 57). Diri (2010: 94), on the other hand, informs us that the thickness of ground floor wall is in between 65-70 cm for exterior walls, while interior partition walls in the ground floor are 50 cm thick in Birgi houses. The height of ground floor is 2.5 – 5.0 m in the case of Northwestern Anatolian houses (Kafesçioğlu, 1955: 62).

In masonry ground floors, timber lintels are used at certain vertical intervals. The interval between timber lintels is 150-180 cm in traditional Birgi houses (Diri, 2010: 97). Diri (2010) informs us that these timber lintels may be rounded or rectangular, with a cross-section of 10-15 x 10-15 cm, again for Birgi houses. The lintels are connected to each other every 50-70 cm by means of tie beams, 6x10 cm in sectional size (Diri, 2010: 97).

Another important point is that the connection of masonry ground floor to the timber frame system above for the overall seismic behavior of the structure Figure 16-Figure 17. Kuban informs us that the upper story timber skeleton is fastened to the ground floor masonry walls via the wooden beams embedded within the upper part of masonry (Kuban, 1995: 241). The base beams can be constituted of more than one piece of timber, connected to each other by means of nails (Aksoy and Ahunbay, 2005: 53). It should be born in mind that the seismic resistance of timber frame section can govern the seismic resistance of the whole structure, provided that the timber frame upper floors and masonry ground floor are properly connected to each other, and masonry ground is seismically resistant.

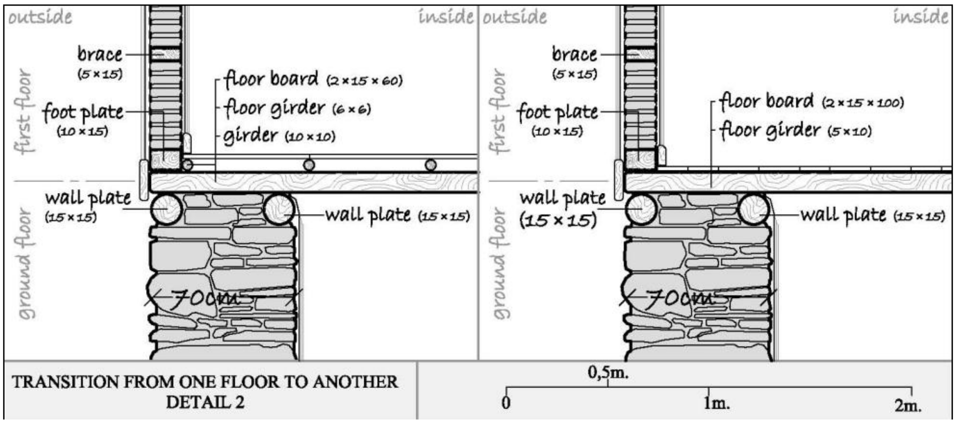

Figure 16: Detail of use of masonry wall in the lower floor and timber frame wall in the upper floor; use of girder and floor girders together at floor change (left), use of only floor girders at floor change (right) (after Diri, 2010)

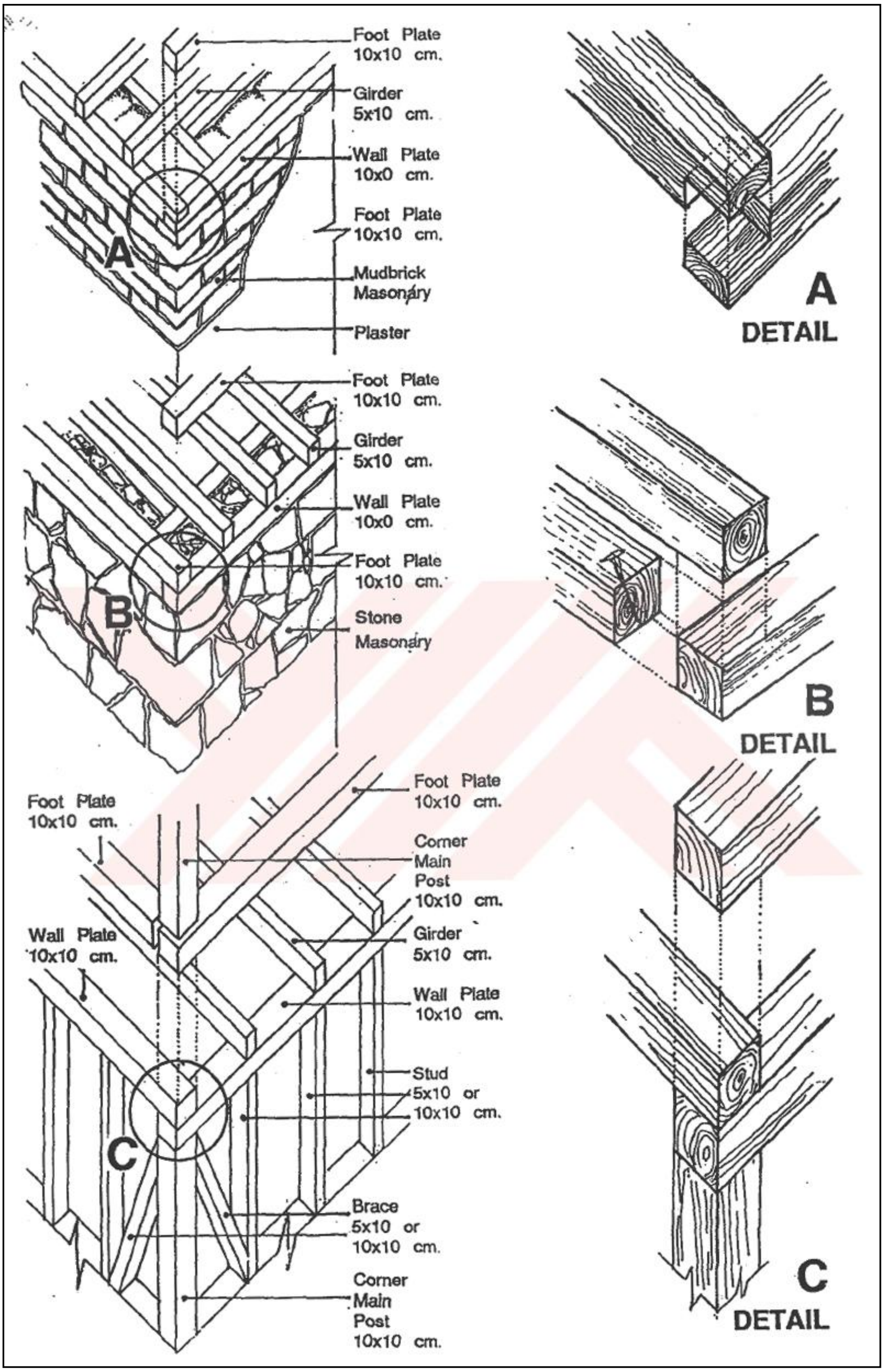

Figure 17: Connection details between the masonry and timber frame sections (after Şahin, 1995)

1.3.1.2. TIMBER FRAME SECTION

As mentioned above, the floors on top of the masonry base are made of timber frames in Ottoman houses. A single frame, forming façade of a room or a *sofa*, is the smallest module forming the timber frame section in an Ottoman house. The timber frames in traditional Ottoman timber frame *hımış* houses are composed of horizontal and vertical elements, and diagonal braces, configured inside the area delimited by a wall plate, a foot plate and two main posts. As can be seen in Figure 18, two horizontal elements i.e. beams, which are wall and foot plates, and two vertical elements, which are main posts delimits the frame's outer borders. These elements are larger in size than the other horizontal and vertical elements inside the frame, i.e. studs and posts. The diagonal elements, namely braces, are also generally thicker than the other elements. Each timber frame is a module that corresponds to one side of a room.

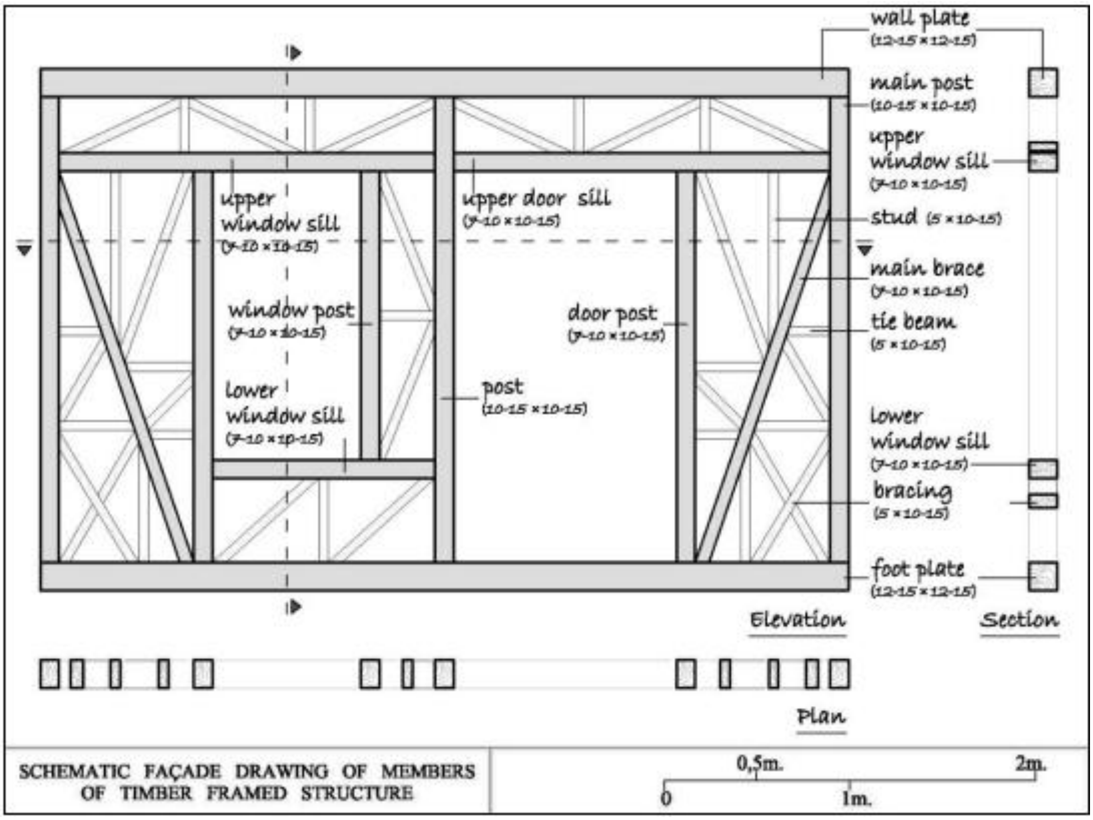

Figure 18: Timber frame elements in a room facade in Birgi (after Diri, 2010)

1.3.1.3. INFILL/COVERING

The intervals between the vertical, horizontal and diagonal timber elements were filled using an appropriate infill material, such as brick, timber, adobe or stone (Eldem III, 1984: 172) (Figure 21). The choice of infill material depends on the material availability of the region. For example, in the northwestern Anatolian houses (as far as we are informed by the travelers' notes, including Istanbul), use of adobe prevails (Kafesçioğlu, 1955: 46; Kuban, 1995: 238), which is produced in a variety of dimensions, while in the Black Sea region it is stone. In Figure 19, the schematic drawings for different infill examples in Birgi are seen.

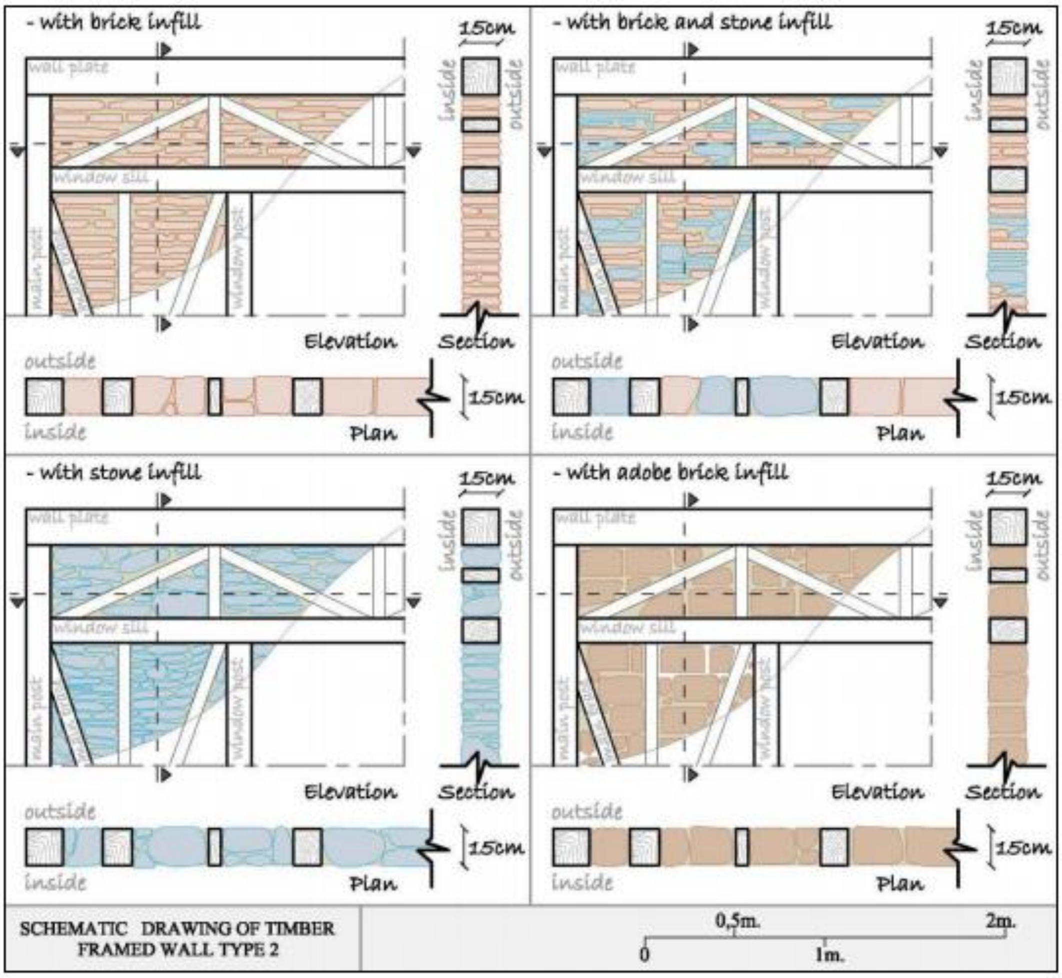

Figure 19: Schematic representations of different infill types (after Diri, 2010)

A widely used covering technique, which was first appeared in the 18th century as an application to the walls, is called *bağdadi*, where wooden laths were nailed onto the timber frame and then, plaster was applied (Kuban, 1995: 245) (Figure 20). In Ankara use of *bağdadi* is common and brick is also seen in few examples (Şahin, 1995: 206-207).

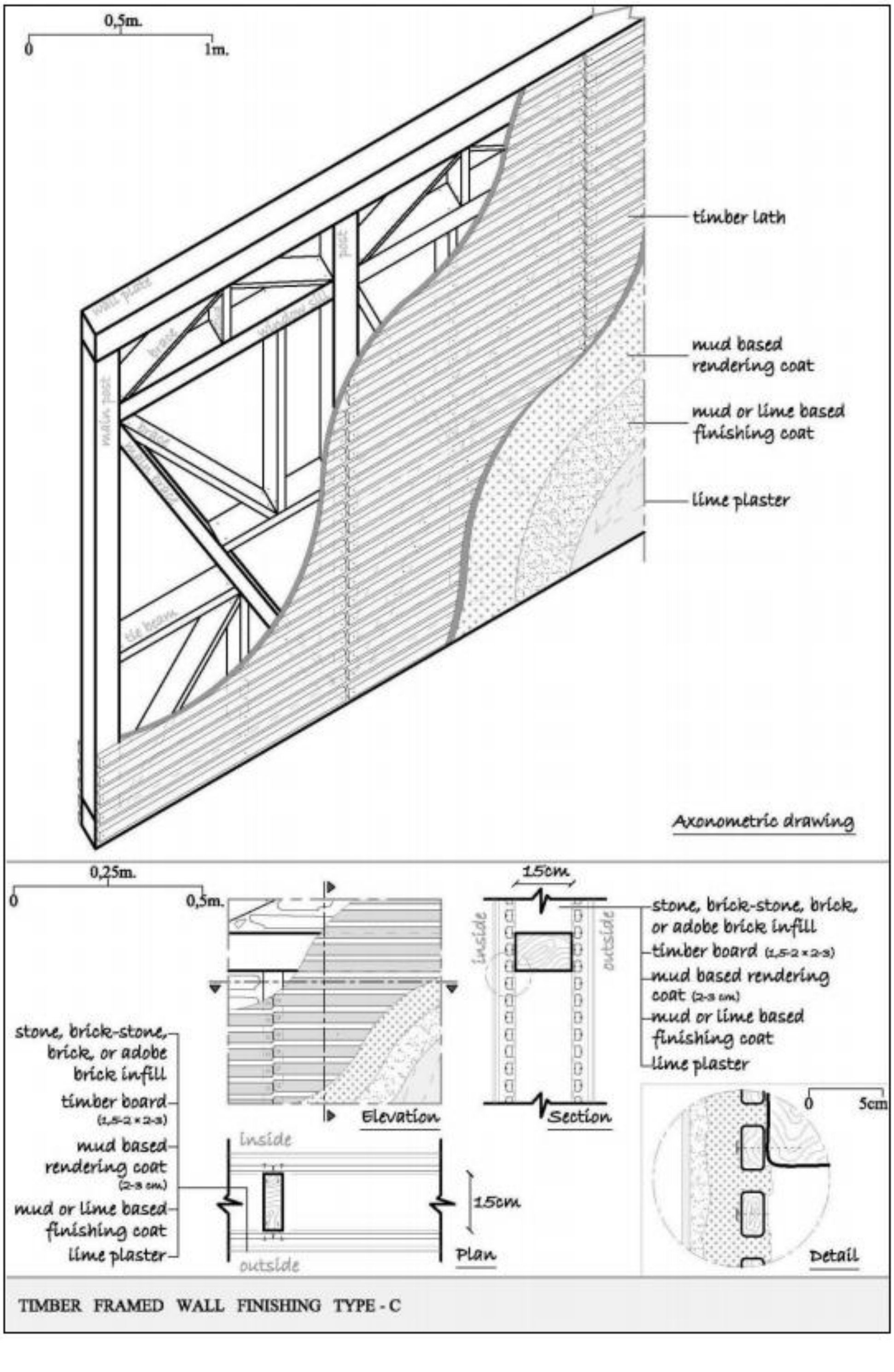

Figure 20: Schematic representation of *bağdadi* covering (after Diri, 2010)

Weather boarding was another technique that was frequently used between the end of the 18th century and the beginning of the 19th century mostly in Istanbul and Thrace. It was applied at the facades facing the prevailing wind and rain direction (Eldem I, 1984: 311).

The wall thickness of timber frame walls with infill/covering is nearly a quarter of that of the ground floor; approximately 20 cm, except for the walls into which built-in cabinets were inserted (Eldem, 1984: 123-124).

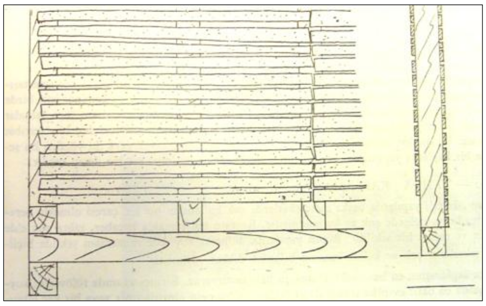

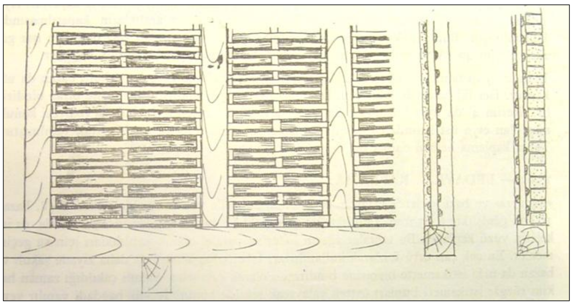

Figure 21: Two different types of *bağdadi* (after Kafesçioğlu; 1955)

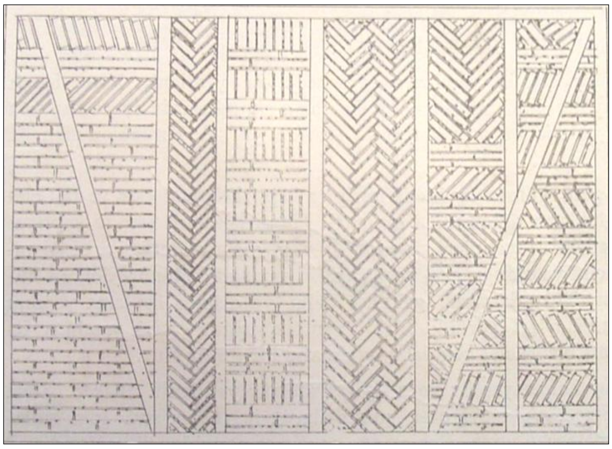

Figure 22: Brick infill (after Kafesçioğlu, 1955) and an example to brick infill, laid in *herring-bond* style, in Ankara. (no 17 located on Oksuzler Street, Erzurum neighborhood)[8]

[8] The photographs belong to the author unless specified otherwise.

1.3.1.4. PROJECTIONS

Projections (jetties) are one of the very common and distinguishing features of timber frame Ottoman houses. The projections actually did not exist till the second half of the 16th century[9] (Kuban, 1995: 171; Günay, 1998: 15) since, based on visual documents and limited information given by *wakfiyya*s, it is known that in the 15th and 16th centuries, the majority of the houses were single story - *bayt-i sufli* - (Faroqhi, 1998: 169).

There are a variety of examples of projections, from short ones to those continuing along a whole façade, as well as in terms of construction systems. Projections are used as an element completing the living spaces at the upper floors, into right rectangular shapes, in the case that the sitting lots of the houses are not complete quadrilaterals, which was indeed widespread, especially in the cities (Kafesçioğlu, 1955: 76). Other reasons for projections are to increase usage area and to have a more complete view of the street (Evren, 1959: 7).

Based on their construction systems, the projections can be grouped as (1) simple cantilever projections (*konsol çıkmalar*), (2) corbelled projections (bindirmeli çıkmalar), and (3) braced projections (göğüslemeli çıkmalar). The simple cantilever projections are constructed simply by extending floor beams towards outside (Kafeçioğlu, 1955: 76). They are especially used when the projection length is relatively small (less than 70 cm) and are the only way to obtain a projection until 1650-1700 (Eldem III, 1984: 162, 170) (Figure 23). Corbelled projections, on the other hand, are made as layers of overlapping of timber beams perpendicular to each other and are commonly seen in Ankara and Kastamonu (Kafeçioğlu, 1955: 80) (Figure 24). In braced projections, which are preferred in case of longer salience is desired, the bulging section is braced from outside by diagonal timber braces (Kafeçioğlu, 1955: 82; Şahin, 1995: 200; Eldem III;, 1984: 162) (Figure 25). These diagonals may be inserted onto the wall at one end, or may be based on a horizontal element (*hatıl*) embedded in the wall (Kuban, 1995: 243; Eldem III, 1984: 170).

---

[9] Eldem (1984), on the other hand, limits the date when projections start to appear as the second half of the 17th century (Eldem, 1984: 123).

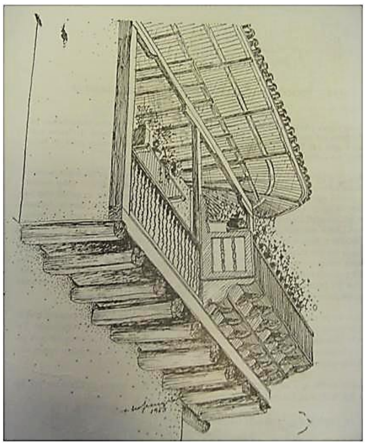

Figure 23: An example to simple cantilever projections (after Kafesçioğlu, 1955)

Figure 24: An example to corbel projections in Safranbolu (Neriman Şahin Güçhan archive) (1993)

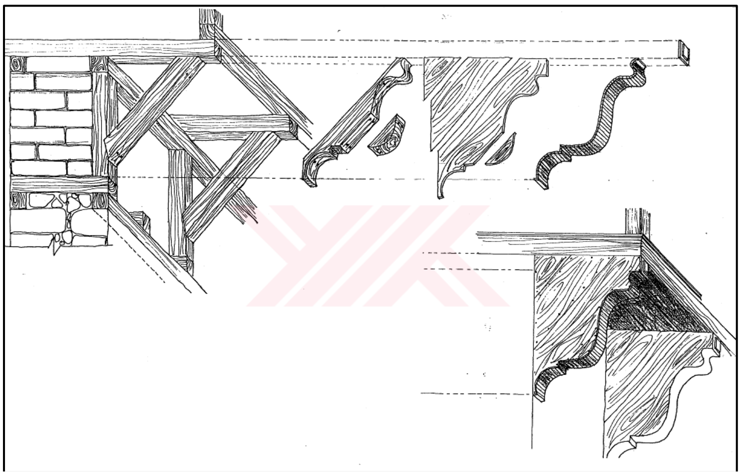

Figure 25: An example to supported projections (after Şahin, 1995)

1.3.2. ROOFS

Kuban (1995) informs us that most 16th century Istanbul houses had a flat roof (Kuban, 1995: 238). Within the existing stock of traditional Ottoman timber frame houses, the oldest of which is from 17th century, roof is generally a four-hip roof or – for small buildings or for those adjacent to other buildings at their two sides – a gable one, with wide eaves covered mostly with clay tiles, but sometimes also with slates or shingles so as to be appropriate to climate and available material in the region.

The early period houses (17th century) had only one single roof, while as the plan got more complicated by means of the addition of projections, roofs were also elaborated accordingly. Eaves were sheathed with timber laths or were covered with *bağdadi* and then plaster.

In some of the earlier incomplete houses, there is no boarding under roof covering. It can occasionally be seen that roughly cut elements, having larger sections than those required structurally, were used for roof construction. The most commonly used timber type for roofing is poplar, especially in central and east central Anatolia. The main horizontal elements were placed in the direction of the shorter side of the plan. Other longer beams were placed on those in perpendicular direction. Uprights sit onto the crossing points of them and were held together by tie beams. Kuban says that there was no ridge beam and rafters met at the top line. Rafters were 6-7 cm in diameter and placed at 30-45 cm intervals. Jointing was weak or lacking. The underneath of roof was nearly always sheathed with timber laths or covered by *bağdadi* and plaster, except for some secondary spaces like depot or stable (Kuban, 1995: 229, 245-247; Eldem III, 1984: 162-163, 170) (Figure 26).

Rafters may be extended to obtain inclined eaves. Alternatively, ceiling beams may be extended; in this case horizontal eaves were obtained (Kuban, 1995: 247).

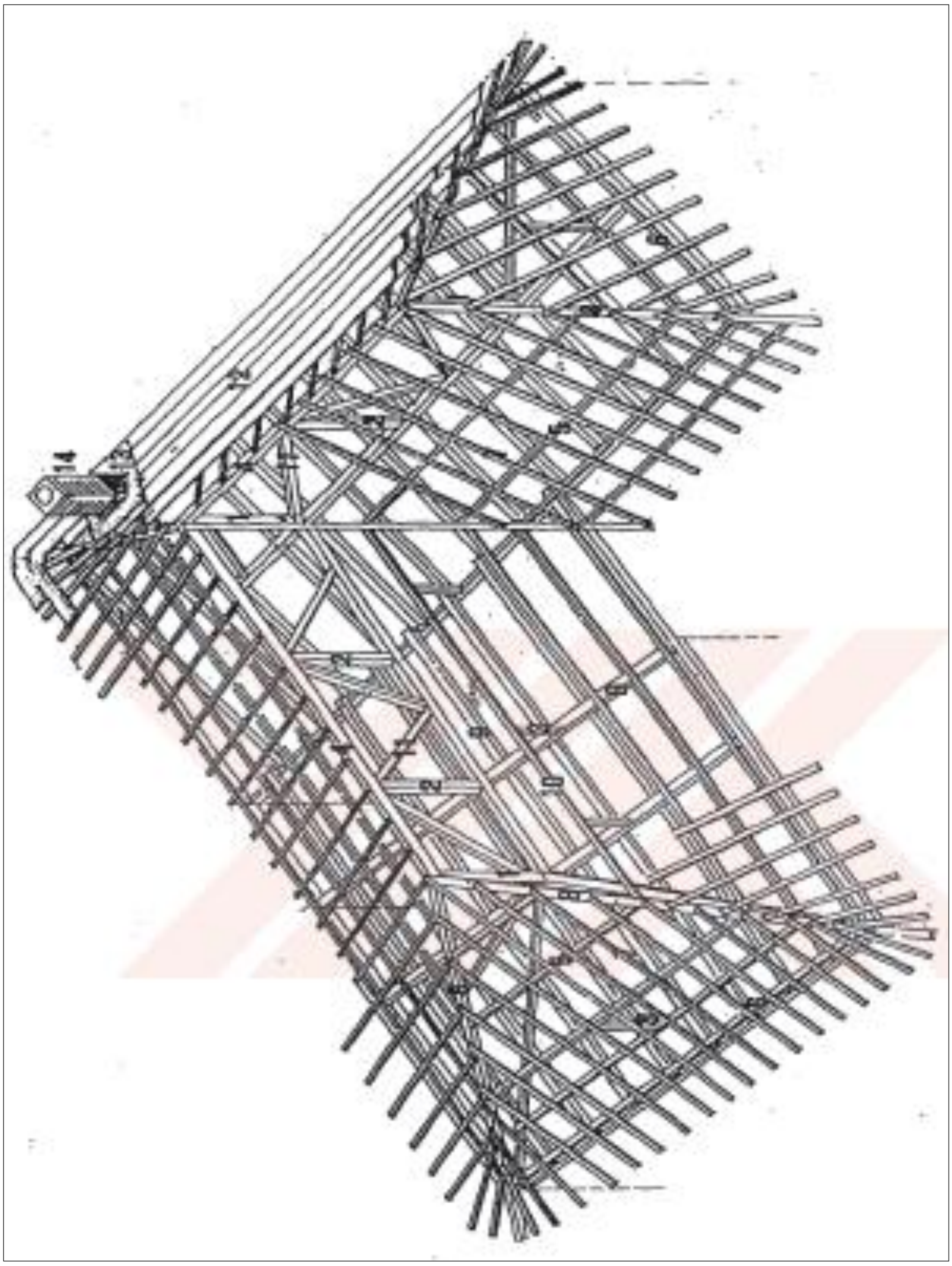

Figure 26: Roof structure observed in Cingoz St., 20, Ulucanlar Quarter, where 1 stand for corner post, 2 king post, 3 post, 4 ridge purlin, 5 purlin, 6 end purlin, 7 rafter, 8 angle rafter, 9 beam, 10 tie beam, 11 brace, 12 roof board, 13 zinc sheet and 14 brick chimney (after Şahin, 1995)

1.3.3. WOOD TYPES AND CONNECTIONS / JOINTS USED IN TRADITIONAL OTTOMAN HOUSES

A variety of wood types had been used for building Ottoman houses. Depending on the local availability of material, several of the widely used wood types are pine, oak, chestnut, horn beam, juniper, cedar, fir and poplar. Pine is the most commonly used one, while oak, chestnut and cedar were for the relatively rich houses. Poplar was generally used for roofing (Kuban, 1995: 239; Eldem III, 1984: 163). On the other hand, Kafesçioğlu (1949) mentions that poplar was used for construction material for the whole house in the Middle Anatolian village houses (Kafesçioğlu, 1949: 11).

Building methods utilized for the construction of a timber Ottoman house has evolved as to have very simple details (Günay, 1998: 66). In Ottoman houses with timber frame construction, nearly the sole connection tool is nails in structural timber sections (Kuban, 1995: 243; Kafesçioğlu, 1955: 66). The length of these wrought nails (*dövme* çivi) varies between 9 and 20 cm for Northwestern Anatolian houses (Aksoy and Ahunbay, 2005: 53).

In addition to the nailed connections, single housing or mortise and tenon joints can also be observed (Kuban, 1995: 243), especially in the connections between base beams with each other, posts at the edges with base beams, upright elements with their caps, floor beams and projection supports, and those in the roof (Aksoy and Ahunbay, 2005: 53). For examples of such connections, please see (Figure 27-Figure 32).

Figure 27: Chamfered joint in the base beam of a house in Yalova (Aksoy and Ahunbay; 2005)

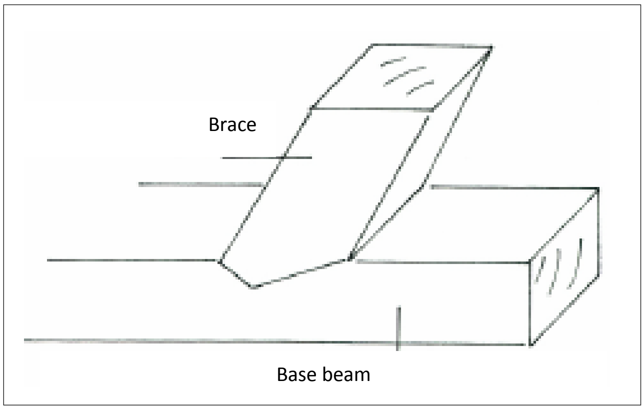

Figure 28: Base beam – upright connection of a house in Akçakoca (Aksoy and Ahunbay; 2005)

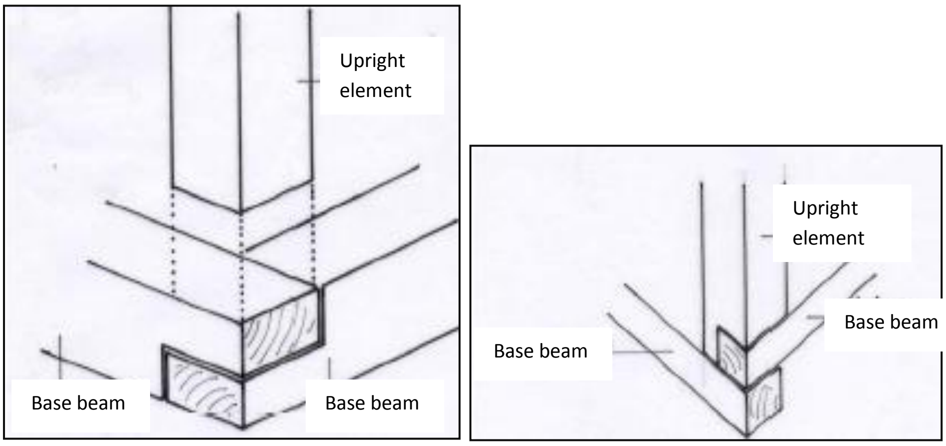

Figure 29: Base beam and upright – base beam connections, respectively, of a house in Gölcük (Aksoy and Ahunbay; 2005)

Figure 30: Upright element – horizontal element connection of a house in Yukarı Değirmendere (Aksoy and Ahunbay; 2005)

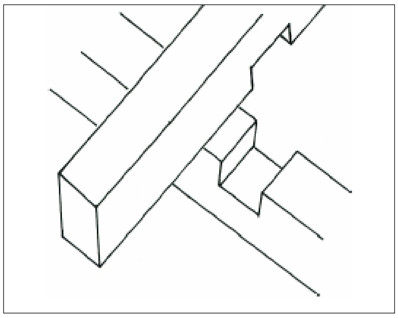

Figure 31: Diagonals connection of a house in Akçakoca (Aksoy and Ahunbay; 2005)

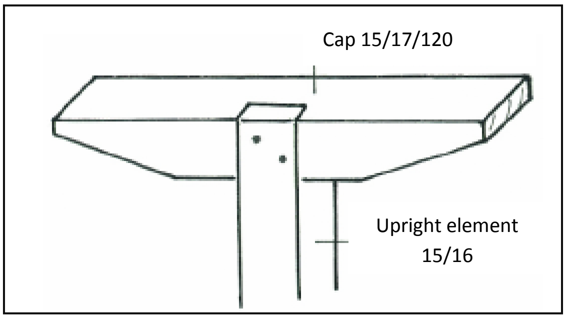

Figure 32: Upright element – cap connection of a house in Adapazarı (Aksoy and Ahunbay; 2005)

1.4. SEISMIC RESISTANCE OF STRUCTURES WITH TIMBER FRAME CONSTRUCTION

In many parts of the world, the seismic resistance of timber frame structures, whether they are modern or historic, has been observed and appreciated. The technical qualities of traditional timber frame structures, which are very much associated with vernacular architecture taken into consideration mainly for its cultural/artistic/architectural features, have rarely been investigated (Şahin-Güçhan, 2007a: 841). The seismic resistance of timber structures is partially caused by the high ductility, high energy dissipation capacity and lower weight in comparison to, for example, reinforced concrete and steel structures.

Yet, for a timber frame to be seismically resistant, several other criteria are needed to be fulfilled. First of all, timber used must be strong and ductile enough to dissipate energy originated by earthquake. Another important aspect is connections. The connections between individual members should be sufficiently strong to hold them together. In addition, bracing is needed to make the structure resistant to lateral loading (Tobriner, 2000: 3-4).

Tobriner (2000: 5-6) claims that timber frame structures having bracings have an intrinsic seismic resistance. However, other factors belonging to individual structures under investigation should also be taken into account while making an assessment. Normally, a structure having a more regular plan, and composed of load bearing elements with similar characteristics seismically more resistant. Equal floor heights, having low height to base ratio are other factors contributing a more appropriate configuration (Tobriner, 2000: 5-6).

There can be seen a variety of damages occurring at timber structures. Cracking and falling of plaster, mortar failure, connection problems, large lateral displacements, dislodgement of masonry infill and failure problems are among those (Doğangün *et.al*., 2006: 981).

Tobriner (2000: 9) reports that M. Hasan Boduroğlu observed the damage occurred after sixty earthquakes in rural areas of Turkey between the years of 1925 and 1984 and concluded that *bağdadi* constructions performed better than *hımış* ones (Tobriner, 2000: 9). Şahin Güçhan (2007a: 848) states also that "in *bağdadi* technique, the timber laths increase the resistance of the building against lateral forces, and thus against earthquakes as they are light and function as additional ties and provide a certain elasticity."

In the case of Turkey, there is an extensive tradition of timber construction. We know that Istanbul was fully constructed of timber (residential structures) starting from the 17th till the beginning of 20th century. According to the reports given after 1688 Izmir Earthquake, this city was also full of timber structures by then and masonry was used only for foundations and lower parts of the walls (Tobriner, 2000: 2). Tobriner also states that there was a consciousness about the seismic resistance of timber structures at least in the 17th century in Istanbul. Written documents have testimonial proofs regarding how the people of the city were impressed to see the performance of timber structures after the 1894 Istanbul earthquake (Tobriner, 2000: 2).

Therefore, considering the discussions given above, it can be seen that the studies on timber structures included detailed reports on damaged buildings (timber ones and others), laboratory experiments and analytical modeling. Therefore, also the relevant literature can be classified and reviewed under three main titles, which are (1) historical observations, (2) experimental studies, and (3) analytical studies.

1.4.1. REPORTS BASED ON IN-SITU HISTORICAL OBSERVATIONS

In the relevant literature, there are many observations, made after a number of historic and contemporary earthquakes, which report that the timber frame structures behave better under earthquake loading than masonry and reinforced concrete structures. For example, it is known that after 1509 great Istanbul Earthquake, known also as *Kıyamet-i Suğra*, which was reported from Greece, Transylvania and even Cairo (Ambraseys and Finkel, 1995: 37), the Ottoman authorities prohibited the construction of masonry structures and allowed timber frame “*hımış*” structures, claiming that the masonry structures resulted in larger casualties (Şahin Güçhan, 2007: 842).

After 1755 Lisbon Earthquake, a new type of braced half-timber construction called *gaiola pombalina* was developed against seismic risk. In this system, wooden skeleton having a series of x bracing are inserted into masonry structures (Figure 33). This is a mutual relation; masonry protects timber from fire whereas timber renders the structure more resistant against earthquake (Tobriner, 2000). The *gaiola* system was primitively tested by soldiers randomly stamping on the floors and stipulated by law.

Figure 33: Pombalina construction (after Lopes, 2010)

Also after the 5 successive earthquakes in Calabria, Italy, in 1783, for the first time in history, a governmental commission was founded and a timber construction system was developed to reconstruct collapsed settlements under the influence of *gaiola*. This system was called *Casa Baraccata*, where the timber bracings were placed not within the sectional thickness of the wall but on the surface (Figure 34) and the basics of this type of construction was stipulated law in 1785 until 1854. *Gaiola pombalina* and *casa baraccata* are of the first serious attempts for technical innovation (Tobriner, 2000: 2; Tobriner, 1999: 64-65; Tobriner, 1997: 110, 113-114).

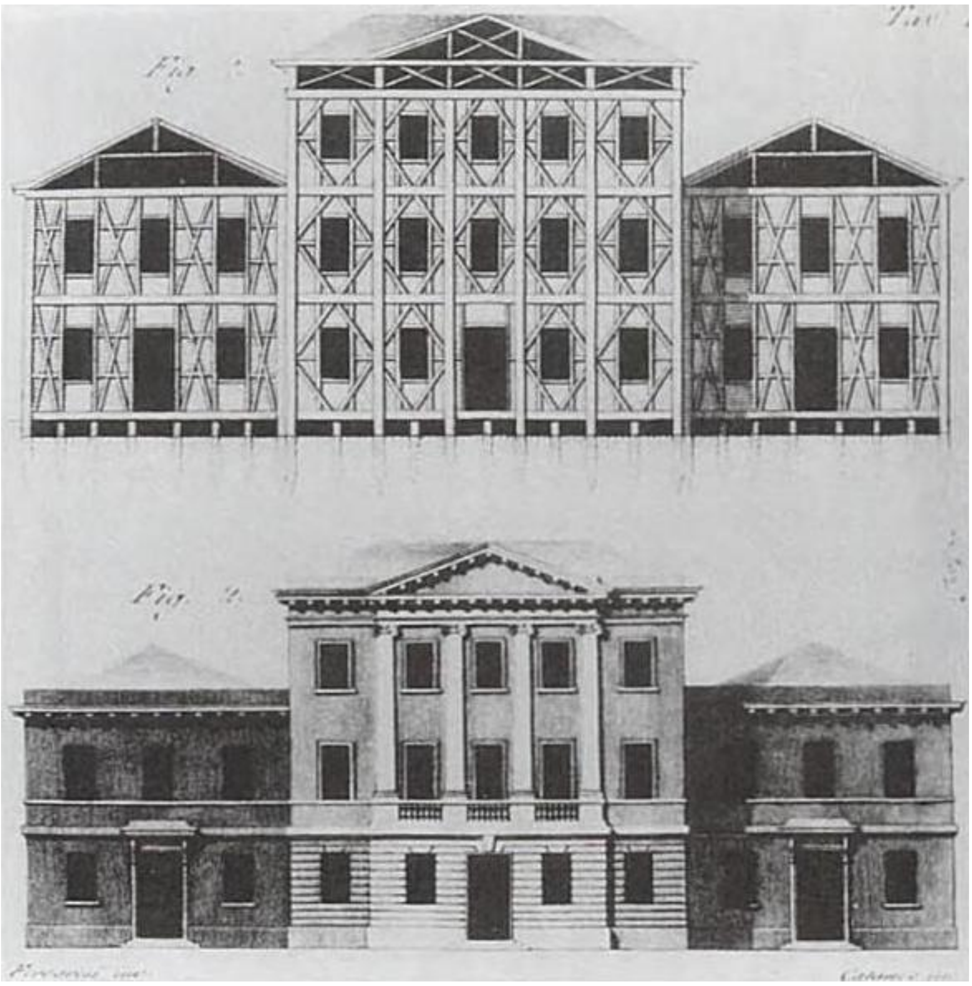

Figure 34: Drawing of Casa Baraccata (Drawing by Giovanni Vivenzio in *Istoria de' Tremuoti avvenuti nella provincia di Calabria Ulteriore e nella città di Messina nell'anno 1783, e di quanto nelle Calabrie fu fatto per lo suo risorgimento fino al 1787. Preceduta da una teoria, ed istoria generale de' tremuoti*, Naples: Stamperia Regale, 1788) (after Tobriner, 1999)

In Lima, Peru there is also used a similar system called *quincha*, which consists of multiple layers of vertical and horizontal elements of timber or cane, to then fill with earth and mud (Minke, 2001: 28; Cuadra and Chariarse, 1992: 87). Another traditional timber frame is *bahareque* of San Salvador, which is constructed by a frame, formed using crudely trimmed timber elements (sometimes with the use of cane and bamboo) with mud infill (Figure 35) (Bommer *et al.*, 2002: 408; López *et al.*, 2004).

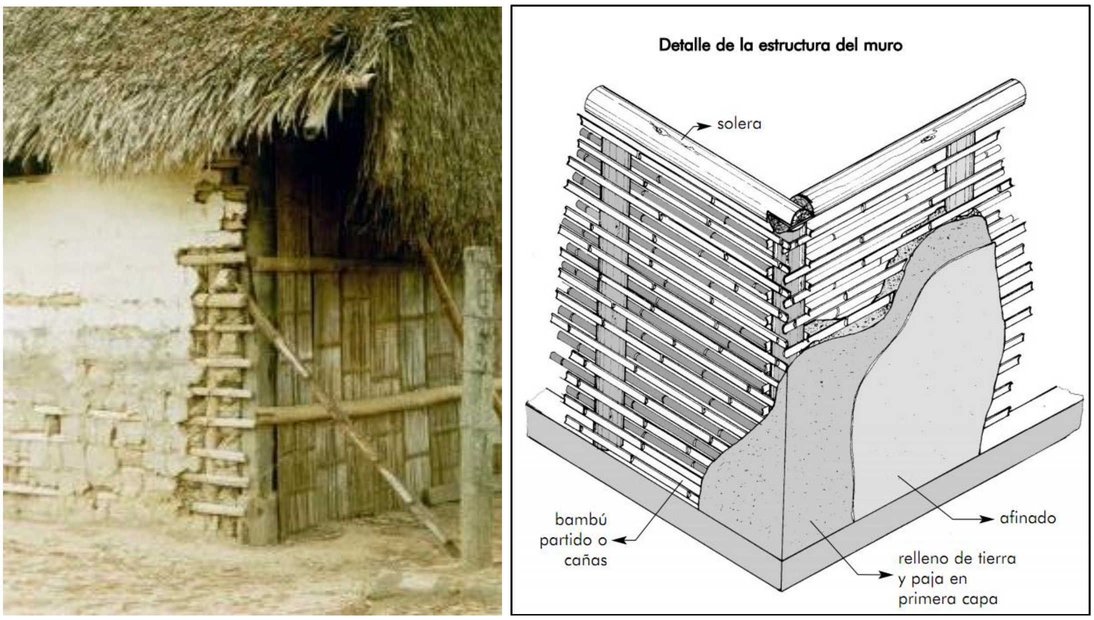

Figure 35: *Quincha* (www.inbar.int) and *bahareque* constructions (Aedo and Olmos; 2002), respectively

It is noteworthy that D. Eginitis, the director of the Observatory of Athens, who was personally invited to Istanbul after the 1894 earthquake by Abdulhamid II himself for a post-disaster report, "greeted with pleasure that the buildings in Istanbul are not entirely built of masonry as in other regions". Because "if it was the case, the loss could have been more serious". Eginitis clearly states that "the timber-framed buildings have resisted the earthquake amazingly. While some old timber structures of a mediocre quality were still standing, some well-built, nice and new masonry buildings, even the ones joined with steel, were destroyed" (Şahin-Güçhan, 2001: 22; Şahin-Güçhan, 2007a: 842-843; Genç and Mazak, 2001: 29-31).

According to the observations reported by Rainer and Karacabeyli (2000: 3-4) after the 1994 Northridge Earthquake in California in USA, in many multi-story wood frame apartment blocks, the weakest first stories were damaged, which then caused the collapse of the whole structure. Also Lam *et al.* (2002: 277) underlines the loss of life and property occurred due mainly to wooden structures. This situation was attributed to poor quality control, improper nailing, etc.

It was reported by Rainer and Karacabeyli (2000: 4) after the 1995 Kobe Earthquake in Japan that in this devastating earthquake, the majority of the timber structures constructed before or during the World War II were collapsed, however younger timber constructions were standing perfectly. Therefore, one should consider the effect of deterioration and aging as well as bad or insufficient maintenance. Lam *et al.* (2002: 277-278) stresses the lack of sufficient lateral resistance systems like shear walls and horizontal diaphragm systems in those post and lintel structures that were collapsed.

> Braces were often lacking or improperly installed. The connection details at the corners of the wall frame did not have sufficient capacity to resist tension load, resulting in separation of the corner connections (…) and decay in the wood members from termite attacks also contributed to the collapse of some of the buildings (Lam *et al.*, 2002: 277-278).

After the 1999 Kocaeli and Düzce Earthquakes in Turkey, it was seen that the *hımış* structures had no or little damage. The more recent reinforced concrete apartment blocks, on the other hand, were damaged extensively. The statistical study conducted by Gülhan and Özyörük Güney in 2000 is remarkable so as to reveal the difference between heavily damaged reinforced concrete structures and timber frame ones. Even though the detailed inventory made by Tobriner (2000) according to the villages around Düzce gives more scattered information, it still indicates the seismic resistance of timber frame structures (Şahin-Güçhan, 2007a: 844-845; Doğangün *et.al*., 2006: 982; Tobriner, 2000: 7-9; Gülhan and Özyörük Güney, 2000: 2-3).

2000 Orta Earthquake in Çankırı, Turkey resulted in heavy damage in rural areas, where most of the damaged structures were made of rubble stone or adobe masonry. In Çerkeş district, on the other hand, where the majority of the houses are two story timber frame structures, no structural damage was observed (Demirtaş *et al.*, 2000: 13).

After the 2005 Kashmir Earthquake: The traditional Kashmir timber frame masonry structures, "*Dhajji-dewari*" were remained intact, whereas especially some forms massive masonry structures, such as rubble stone masonry ones, were extremely vulnerable against seismic loading. It was observed that the walls of a lower masonry story were collapsed to a large extent whereas the timber frame upper story was not inflicted by any damage (Rai and Murty, 2005: 2-3).

Similarly, according to the observations made by Şahin-Güçhan (2007a), in the 1970 Gediz Earthquake, the most affected parts of the damaged timber structures were masonry sections like the exterior walls of ground floor, service walls and chimneys. Even in the case that loosening of infill materials occurred, the timber frame remained intact (Figure 36). *Bağdadi* constructions performed better than the ones with masonry infill. The modification of ground floor for new openings (or to enlarge the existing ones) had a negative effect on seismic behavior (Figure 37) (Şahin-Güçhan, 2007a: 843-844). It is also known that a large part of Gediz was also destroyed by fires after earthquake (Gürpınar *et al.*,1981: 144)

Figure 36: An example showing the destroyed masonry ground floor in Iğdiş Village after 1970 Gediz Earthquake (after Şahin-Güçhan, 2007a)

Figure 37: A timber-framed building damaged due to the weakening of the ground floor by enlargement of the openings (after Şahin-Güçhan, 2007a)

In spite of many examples where *hımış* houses are claimed to have behaved well, in Sultandağı Earthquake (or Çay Earthquake) (February 3, 2002), they were heavily damaged.

> "Most of the injuries and casualties in the region are associated with the total collapse of *hımış* buildings. *Hımış* buildings had been widely preferred in rural areas three or four decades ago and were traditionally built by their residents without engineering considerations. Thick perimeter

> walls and heavy roofs are common features of *hımış* buildings providing heat insulation of the structure. The observed performance level of *hımış* buildings indicated heavy damage and total collapse due to the poor strength and brittle behavior of the walls and considerable mass of the buildings. Observations suggest that due the lack of rigid diaphragm action, most of the walls responded individually during the seismic attack. Moreover observation on collapsed buildings indicated that as a consequence of weak connections between the perimeter and orthogonal partitioning walls, separation occurred and most of the thick perimeter walls collapsed in the out of plane direction." (Erdik et al., 2002a: 5-6).

In another publication, the authors repeat that most of the damage in the region was due to the *hımış* structures, "built by their residents without engineering considerations" (Erdik et al., 2002b: 3). It is also known that liquefaction phenomena played an important role in the damage after Çay Earthquake (Koçyiğit *et al.*, 2002: 12).

Bayülke (2001) also underlines that seismic resistance depends rather on the construction quality than construction material (Bayülke, 2001: 14-15). He exemplifies the 1967 Mudurnu Valley and 1970 Gediz Earthquakes, where, he claims, most of the damage was occurred because of *hımış* structures or in *hımış* structures themselves. However, for the former earthquake, Kalafatçıoğlu (1968) states that "as a result of the earthquake, (timber) structures slightly inclined towards west, and plaster on the interior walls took off" (Kalafatçıoğlu, 1968: 132). Grabert (1971: 28), on the other hand, describes the latter earthquake as follows:

> (…) timber buildings were constructed either without a basement floor or simply as *bağdadi*. These buildings show that upper floors got deformed a little less than the ground floor. The ground floor loosely sits directly on soil without a foundation or a basement (...).

Bayülke (2001) mentions also 1923 Kanto Earthquake. Even though, damage to timber structures was partially due to the spreading fires all along the disaster area, photographs show also many timber structures failing under earthquake loading (Figure 38-Figure 39).

Figure 38: The Akasaka district, one of Tokyo's residential areas, lies in ruins after the 7.9 magnitude earthquake on Sept. 1, 1923. (AP Photo)
(taken from http://www.theatlantic.com/infocus/2011/03/1923-kanto-earthquake-echoes-from-japans-past/100025/)

Figure 39: Many People sit on street car railway in front of their crushed houses in Japan 1923 after an earthquake. Fortunately, this area did not suffer from fire. (AP Photo)
(taken from http://www.theatlantic.com/infocus/2011/03/1923-kanto-earthquake-echoes-from-japans-past/100025/)

Also after Kobe earthquake thousands of traditional timber structures were collapsed. This huge damage may be attributed to the slender framing system in contrast with heavy and bulky roof structures of traditional timber Japanese houses as well as lack of a proper foundation. In addition, it is known that timber houses collapsed after Kobe Earthquake lacked sufficient diagonal bracing, increasing the structures' ability to bear lateral loads (Tobriner, 1998).

Bahareque houses in San Salvador are known not to have behaved well either, under seismic loading (Yoshimura and Kuroki, 2001: 58-60). Bommer *et al.* (2002: 410) clearly state that most of the damaged houses after two earthquakes in 2001 were *bahareque* and adobe ones, while those with a more solid timber framing behaved significantly better. It was observed that the *bahareque*s that survived the 1965 earthquake were all constructed two-three years prior to the disaster. López *et al.* (2004: 302) partially attributes the high death toll to the collapse of *bahareque*s. López *et al*. (2004: 8-9), on the other hand, gives more detailed information regarding 1936 El Salvador Earthquake, claiming that poorly constructed *bahareque*s collapsed, while well-constructed ones survived the earthquake. Among the potential problems that may be related to the *bahareque* houses that were collapsed during the earthquake, these were listed: (1) faulty tying, and (2) heavy tile roof as well as (3) decayed timber and (4) loose subsoil (López *et al*., 2004: 9).

1.4.2. EXPERIMENTAL STUDIES

In addition to the above mentioned observations reported by different scholars, there is a variety of experimental studies carried out to test the structural behavior and resistance of timber structures. Among the experimental studies, one can list the short term monitoring tests such as static lateral loading test conducted either on a model constructed in the laboratory environment or in-situ on the real structure. By means of such application, the lateral load bearing capacity of timber structure as well as the failure mode in this type of loading can be determined. In addition, dynamic tests carried out by means of accelerometers, microtremors etc. to determine the basic vibration characteristics of a structure are common.

Fujita *et al.*, (2004) in their study conducted a forced static lateral loading test in elastic range as well as a cyclic loading test until the failure in the main beam is observed. They carried out also dynamic tests, not only as an independent testing set, but also between successive loadings to see whether or not the vibration tests have an effect on vibration characteristics of the structure. Fujita *et al.*, (2004) concluded that the infill helps to improve the lateral load bearing capacity of a timber structure (Fujita *et al.*, 2004: 46). Yasumura and Yasui (2006) carried out a series of pseudodynamic tests on plywood timber frames with openings and obtained hysteretic parameters that are not much different from each other for different opening configurations (Yasumura and Yasui, 2006: 67).

There is also a variety of non-destructive and semi-destructive evaluation techniques applicable in case of the diagnosis, condition assessment and mechanical/material characterization of timber structures. The techniques mentioned by Kasal and Anthony (2004: 102), are several non-destructive methods necessary for a thorough visual inspection, those for species identification, stress wave and ultrasonic methods, pin driving and screw withdrawal methods, resistance drilling and digital radioscopy, and several semi-destructive techniques like core drilling and tension micro specimen technique. It was further concluded that the non-destructive or semi-destructive techniques developed for timber structures are reliable tools for diagnosis of eventual problem areas and yet they can hardly be defined as reliable when material properties are to be determined. Therefore, it is a better idea to use the results obtained from such methods for material characterization for only in a comparative basis.

Kandemir-Yucel *et al.*'s study (2007) is a detailed example for the application of infrared thermography, together with the use of ultrasonic pulse velocity measurements for the purpose of evaluating the state of degradation of timber elements existing at a historical structure. The application of infrared thermography with ultrasonic methods is concluded to be effective for the condition assessment of timber structural elements (Kandemir-Yucel *et al.,* 2007: 247).

Cointe *et al.* (2007) used monitoring tools (potentiometers to measure displacements at critical locations) and non-destructive techniques (measurement of wood's density by drilling) to validate the analytical model of a nearly four hundred year old timber frame bell tower in France chosen for this purpose (Cointe *et.al.*, 2007: 347). Yamasaki *et al.* (2010) developed a method to determine the modulus of elasticity of timber using stress wave propagation velocity and concluded that their method is effective not only for elasticity estimation, but also for the identification of species (Yasamaki *et al.*;, 2010:386). Shaji *et al.* (2000) developed and experimentally validated a method based on ultrasonic velocity readings in order to inspect and assess the condition of existing timber structures. Gilfillan and Gilbert (2001) developed a slightly destructive technique based on the pull-out strength of a probe, made for the purpose, which is inserted to the timber surface at right angles, and they obtained a reasonable correlation between the results obtained by different methods (Gilfillan and Gilbert, 2001: 387-388).

Agency for Cultural Affairs of Japan suggests that (Uchida *et al.*, 2000) three different elements defining earthquake resistance of traditional Japanese timber structures of post and beam system. These are (a) column rocking, (b) clay walls and (c) single columns with suspended clay walls. The experimental studies conducted by the authors showed the reliability of this approach (Uchida *et al.*, 2000: 8).

The connections are required to transfer seismic load through the timber frame to the foundation (Lam *et al.*, 2002: 276). Timber joints are components affecting the mechanical performances of timber structures at first hand, being the weakest points in the structure; normally the connections fail when the wooden elements are still in the elastic range (Parisi, *et al.*, 2002: 1183; Chen *et al.*, 2003: 2731).

Within the framework of a four-year research project entitled ‘Reliability and design of innovative wood structures under earthquake and extreme wind conditions’ conducted at the University of British Columbia (UBC) between August 1997 and July 2001, Lam *et al.* (2002) concluded that load-displacement relation of timber structures under seismic loading is highly dependent on load path (Lam *et al.*, 2002: 284).

Parisi *et al.* (2002) tested the connections under cyclic and monolithic loadings or traditional connections, where metal, if any, was used only to prevent dissembling of wooden parts. The reinforcement and retrofitting of these connections are always made with the introduction of additional metal pieces. To determine the efficiency of these interventions, a testing program was carried out within the framework of the research activity conducted at the Structural Testing Laboratory of the University of Trento and at the Institute for Wood Technology of the National Research Council at S. Michele all’Adige, Italy. The testing of connections under monotonic and cyclic loads as well as that of assembled roof trusses showed different levels of efficiency of different retrofitting methods. As a conclusion, one can say that the most effective retrofitting is the one made using simple bolts (Parisi, *et al.,* 2002: 1191).

Leijten (2009) attempted to determine the withdrawal capacity of washers in bolted timber connections. Popovski *et al.* (2003) attempted to determine the behavior under seismic load and failure modes of braced timber frames, with different connections. The study showed that the seismic behavior of the timber frame drastically change with different connections and that, in bolted connections, the behavior depends, to a large extent, on bolt slenderness (Popovski *et al.*, 2002: 399). Sawaka *et al.* (2008), on the other hand, investigate the effect of decay on shear performance of dowel-type timber joints. The authors controlled the amount of decay by wetting the samples and concluded that, in decayed samples, stiffness, yield capacity and maximum load bearing capacity all get lower (Sawaka *et al.*, 2008: 361).

Assessment of the current condition, as well as the remaining service life of a structure is also an important issue arising especially in case of historical structures. For this reason, Van de Kuilen (2007) tried to develop a model for the assessment of service life of timber foundations, based on a large amount of experimental data, previously obtained by ultrasonic testing, Pilodyn hammer testing, drilling and full scale pile testing to determine density and strength values of timber elements underground. The study took also the influence of decay into consideration. The model formed in this manner was found to be satisfactory (Van de Kuilen, 2007: 161).

There is a number of shaking table tests, carried out on timber frame structures. Popovski *et al.* (2003; 1089) used shaking table technique to test five different connection types. Four of these are bolted connections, while the last one is a timber riveted connection. The authors conclude that very different failure modes were observed with different connections and underline that the behavior of a timber frame is totally defined by the connection details (Popovski *et al.,* 2003: 1099). Heiduschke *et al.* (2009: 323) also carried out a number of seismic tests by means of shaking table tests on small and full scale frames. They concluded that frames with moment connections have an excellent ability to bear seismic loading (Heiduschke *et al.*, 2009: 338).

One of the very few experimental studies on traditional timber frame architecture was carried out by Fang *et al.* (2001) on a model representing the ancient Chinese architecture. The authors carried out dynamic tests on a full scale model with traditional connection details in order to obtain typical vibrational characteristics of an ancient Chinese timber frame house (Fang *et al.*, 2001: 1351-1352).

As a result, there is little work done for the aim of determining structural characteristics of traditional timber frame structures. Moreover, conventional connectors, such as nails, were nearly not at all studied and standardized modern connectors were focused.

1.4.3. MODELING STUDIES

Studies on modeling of timber structures, although an important tool to understand their static, cyclic and dynamic behavior, did not find an extensive application so far, unlike that of masonry. The above mentioned research project entitled 'Reliability and design of innovative wood structures under earthquake and extreme wind conditions' conducted by the University of British Columbia (UBC) aimed also to develop the analytical models for the structural analysis of timber structures as well as computer software for this purpose. The validation of constructed models and introduction of reliability criteria of models are also within the scope of this research project (Lam *et al.*, 2004: 79). The model created for simulating static, dynamic and cyclic behavior of timber structures were validated against other experimental data obtained from previously conducted research, and yet the computational demands are still very high.

Lam *et al.* (2004) underlines that, in spite of these studies, "Very few numerical models capable of analyzing the seismic behavior of three-dimensional woodframe structures currently exist" and "Currently available commercial structural analysis packages are not very efficient in modeling woodframe buildings" (Lam *et al.*, 2004: 80). The key point especially tried to be reflected in the models constructed in this project is, as underlined also in experimental discussions, the hysteresis behavior of nails. This behavior cannot be reflected in the models constructed using available software. For this reason, two computer programs for the reproduction of seismic behavior of timber structures were developed by the research project, called CASHEW and SAWS, the latter being a more simplified version (Lam *et al.*, 2002: 81).

Ayoub (2007) proposed a single degree of freedom system with degrading pinched hysteretic behavior for the modeling of timber shear panels (Ayoub, 2007: 215). Choi, *et al.* (2007) developed two algorithms to assess and locate damage in timber structures (Choi, *et al.*, 2007: 1128). The study of Vintzileou *et al.* (2005), on the other hand, aimed assessing the structural characteristics of the historical construction system of the island of Lefkada. For this reason, an analytical model of a typical structure of the island was constructed where mainly shell and frame elements were used, to then verify it with the results of previous analytical works and site survey (Vintzileou *et al.*, 2005: 231).

As a continuation of the experimental work, mentioned above, Yasumura *et al.* (2006: 74) reproduced the results obtained from the pseudodynamic tests, carried out with two story frames, and concluded that, based on the results of pseudodynamic tests, the simulation work gives the response of the first story very well, while underestimates that of the second story.

In the relevant literature, the most frequently used computer software for the modeling of timber structures are the package programs like ANSYS (e.g. Chen *et al.*, 2003), Abaqus (e.g. Cointe *et al.*, 2007), Diana (e.g. Feio, 2005; Ayoub, 2007), SAP 2000 (Vintzileou *et al.*, 2005) etc. and other software developed specially for modeling of timber structures like Drain 3D, RUAUMOKO, CANNY-E, ISTAR-WD 46 (Ayoub, 2007).

The difference between the results of analytical modeling and experimental studies can be attributed to material degradation that cannot be fully reflected at the analytical model, as well as the weight of loading equipment in case the structure was experimented *in-situ* (Fujita *et al.*, 2004: 46).

According to the sensitivity analysis carried out by Cointe *et al.* (2007), the most influential variable with respect to a given critical response is the stiffness of connection. Joint clearance is another important factor that determines the overall structural response (Cointe *et al.*, 2007: 340-341).

Again for modeling studies, it may be concluded that little attention was paid to traditional/heritage structures in timber.

1.5. AIM AND CONTENT OF THE STUDY

Even though there are many studies reporting timber frame "*hımış*" structures have an inherent stability against seismic actions, it is seen that these reports are based mainly on qualitative observations and lack engineering data. In addition, there are also a smaller number of reports controversially stating bad behaviour of such structures under earthquakes. Nearly all of the experimental and modelling studies in the relevant literature are on contemporary timber frame structures and standardized modern connections.

Considering this problem, this PhD thesis was defined and the studies were carried out within the framework of TUBITAK project numbered 106M499, namely "Tarihi Geleneksel Ahşap Karkas/Hımış Konutların Sismik Performansının Değerlendirilmesi" (Evaluation of the Seismic Resistance of Traditional Historic Timber Frame *Hımış* Houses), amining to evaluate the seismic resistance of traditional Ottoman timber frame "*hımış*" structures.

Considering this aim, these studies that were included in this thesis PhD study and also presented in the TUBITAK project are related only to the timber frame section and are composed of (1) experimental studies, (2) seismic capacity evaluation based on ATC-40 procedure, (3) material tests, (4) optimization studies and (5) analytical studies.

In the experimental studies part of this thesis, 8 frames of different geometrical constructions, which were constructed in laboratory conditions as replicas of the selected frames from the existing houses in Safranbolu, were tested under reversed cyclic loading without and with infill/covering. Capacity calculations were carried out, again, for each of 8 frames without and with infill/covering. Material tests include plaster, mortar, adobe and brick compression tests as well as nail tests and nail pull-in/pull-out tests. In the optimization studies section, the stiffness and energy dissipation capacity values, obtained by means of experimental studies, were used to develop a series of empirical equations.

1.6. METHODOLOGY

The TÜBİTAK project no 106M499 entitled "SEISMIC ASSESSMENT OF HISTORIC TRADITIONAL TIMBER FRAMED / HIMIŞ HOUSES" was defined by Prof. Dr. Uğurhan Akyüz and Assoc. Prof. Dr. Neriman Şahin Güçhan as a doctorate project in 2006. The project was aiming to support two PhD candidates, who were willing to study on this topic. One of these PhD candidates was to work on experimental part, and the other was to work on the analytical part of this study.

Then, after the approval of the project by TUBITAK, the PhD candidate Sinan Akarsu was selected as the fellow to be supported by this project. In addition, Assoc. Prof. Dr. Ahmet Türer joined to the project team in 2007, especially to support the experimental studies in the laboratory. In the first year of the project, Akarsu continued to the studies related with TUBITAK project. During this time, a site survey was made by the project team, consisting of Prof. Dr. Uğurhan Akyüz, Assoc. Prof. Dr. Neriman Şahin Güçhan, Sinan Akarsu and Dr. Reşat Sümerkan from Karadeniz Technical University.

Eastern Black Sea Region was selected for the aim of site surveys. Settlements on 8 different axes were visited in the Eastern Black Sea Region (Figure 40), which are Yeşilyurt, Sevinç, Kiremitli, Dikkaya(Maçka) in the 1st Axis, Aksu (Sürmene) – Büyükdoğanlı (Sürmene) in the 2nd Axis, Fındıkoba(Of) – Ulucami (Çaykara)– Taşkıran (Çaykara)-Uzungöl in the 3rd Axis, Yağcılar (İkizdere) in the 4rt Axis, Bilenköy (Pazar), Yolkıyı, Şenyuva, Ayder (Çamlıhemşin) in the 5th Axis, Çağlayan (Fındıklı) in the 6th Axis, Konaklı (Arhavi) in the 7th Axis and Çavuşlu (Hopa) in the 8th Axis. The aim of this site survey was to define the characteristics of the construction techniques of timber frame *hımış* houses. Then, the first report of the project including a review on the construction techniques of traditional Ottoman timber frame houses was concluded by this team.

Figure 40: Eastern Black Sea Region Site Survey Axes (Şahin Güçhan, 2007b)

During this time, the selection of the timber frames from Safranbolu was also done by the project team. The reasons for selecting the frames from Safranbolu are given in Section 2.1. The frames were selected so as to cover as many geometrical configurations as possible. Among the 6 frames selected for testing purposes, 1 has no openings, 3 has two window openings, and 2 has 3 window openings. The replicas of the selected timber frames were reproduced by the building masters, brought from Safranbolu, based on the drawings made by PhD candidate Sinan Akarsu.

2 of these 6 selected frames were built by using two different timber types, yellow pine and fir, in order to reflect the effect of timber type on the results. Therefore, 8 frames with different geometrical configurations were obtained to test without and with infill. The detailed information regarding the tested frames are given in Section 2.1. The author of this thesis joined the project team at this stage in 2007 to carry out analytical modelling. Unfortunately, after the completion of the construction of the frames in laboratory conditions, Sinan Akarsu had to withdraw from the TUBITAK project due to personal reasons. The author of this thesis, therefore, became responsible both from experimental and analytical studies.

In the meantime, the author of this thesis carried out a comprehensive literature survey on the previous studies regarding traditional Ottoman timber frame houses, and qualitative studies, as well as experimental and analytical work carried out on timber frame structures. A summary of this literature survey is presented in **Chapter 1**, together with the aim, content and methodology of this study.

A single frame, forming façade of a room or a *sofa*, is the smallest ***module forming the timber frame section*** in an Ottoman house. In this study, in order to have an idea on the overall structural behaviour of a whole traditional Ottoman timber frame "*hımış"* house, it was decided to test not the whole floors but frames only, since the out-of-plane strength of a frame is assumed to be zero. Therefore, in case that a whole floor was tested, the results were assumed to be unaltered. On the other hand, in case a whole floor was tested, the connections of the frame, loaded in the out-of-plane direction, would have been forced as well. The effect of connections, therefore, might be investigated in a future study.

At this stage, prior to start to the experimental studies in the laboratory conditions, it was noticed that there were slight changes between the built frames and selected frames from Safranbolu (Appendix A). These changes can be defined as: missing or addition of some of the timber tie beams, misplacement of some of the secondary timber elements and/or differences in thicknesses of some elements. Moreover, the reproduced timber frame replicas were not in the same quality both in terms of workmanship and design with the existing houses in Safranbolu. However, due to the lack of standards in traditional timber structures, by the members of the project team, it was decided that these mistakes are in the acceptable limits considering the aim and content of this study. Besides most of the projects funds were spent on the frames' construction, the frames could not been adjusted. Detailed information regarding the differences between the frames, which were observed in-situ, and those built at the Structural Mechanics Laboratory for the aim of frame tests are given in **Section 2.1.**

Parallel to the literature survey, the first work done after the author's inclusion to the project was to design the test set-up for the built frames. The test-set was designed in such a way that the frame can easily slide inside the test-set-up in the in-plane direction under top lateral loading, while it cannot move in the out-of-plane direction. The test set-up was designed as sufficiently large for any of the 8 frames, therefore, only the height of the hydraulic piston was arranged for different frames with different heights. The hydraulic piston used to apply the lateral reverse cyclic load had a 50 cm long stroke; half of this stroke was used for pushing the frame and the other half for pulling the frame. The loading was carried out by using a load cell, whose capacity is 500 kN in compression and 250 kN in tension. In addition, a number of devices were used to measure displacements during testing. These were (1) two LVDT's of 200 mm, placed at both sides of the frame, to measure diagonal displacement, (2) two LVDT's of 50 mm, placed at both sides of the frame, to check the bottom lateral displacement, (3) an LVDT of 500 mm to measure the top lateral displacement, (4) two LVDT's of 300 mm, placed at both sides of the frame to measure the top lateral displacement. The LVDT's mentioned in the item (3) and (4) were used together to check the top lateral displacement. The LVDT of 500 mm measured the top lateral displacement in all cycles, while one of the LVDT's of 300 mm was measuring the top lateral displacement in push cycles and the other LVDT of 300 mm was measuring the top lateral displacement in pull cycles. The detailed information regarding the test set-up and instrumentation is given in **Section 2.2.**

All the frames were tested without infill/covering. After that, a group of construction masters brought from Beypazarı and repaired each frame at the failed connections, by using the same number and same type of nails. Therefore, these frames could be tested again with infill/covering, by assuming that they are all recovered after repair.

Two different types of infill and two different types of covering were used in this study. The infill materials are brick and adobe, while the covering techniques are *bağdadi* and *şamdolma*, which are both traditional lath and plaster techniques, applied on timber frames and covered with plaster. The bricks used for infilling purposes in this study were solid bricks and transported from demolished traditional timber frame houses by building masters. However, they are not as old as timber frame structures, and they are considered to be from 1960's. The bricks were 21x10x6 cm in size. The adobe blocks were prepared by the local building masters from Beypazarı by using traditional recipes and they were 9-11.5 cm x 9-11.5 cm x 20-21 cm in size. *Bağdadi* is a traditional lath and plaster technique, where approximately 2-4 centimeters wide laths are nailed onto the timber frame so as to leave about a-centimeter-wide gaps between each other (Figure 41). So that, when the surface is plastered, the plaster is hold onto the surface more easily. *Şamdolma* is another lath and plaster technique, probably specific to Beypazarı, where, on the contrary to *bağdadi*, approximately 8-10 cm wide laths are used to nail on the frame (Figure 41). Also in *şamdolma* technique, approximately one-centimeter-wide gaps are left between the laths so that plaster holds on the frame's surface more easily.

The construction masters brought both from Safranbolu and Beypazarı were contacted with the help and advises of municipalities and professionals in the local construction sector. On the other hand, it was noticed that these construction masters had not an exact command on tradition construction methods of timber frame structures. The poor quality of the built replicas against the actual frames selected from Safranbolu was apparent. In spite of these uncontrollable contingencies, the experimental part of this study was carried out as previously scheduled. The detailed information related to the tests that were carried out by using frames without and with infill/covering is presented in Sections **2.3-2.18.**

Figure 41: *Bağdadi* and *şamdolma* covering techniques, respectively

Based on the top lateral load – top lateral displacement relations obtained at the end of frame tests, the parameters that directly or indirectly related to the seismic performance were obtained for each test, such as energy dissipation capacity, energy absorption capacity and energy recovery capacity as well as overall and initial stiffness etc. to distinguish the effects of different geometrical configurations and different infill/covering techniques on the frames' performance. As mentioned also by Ceccotti (1994: 169),

> "quasi-static cyclic tests remain fundamental in order to determine some of the most important parameters influencing the final performance (initial stiffness, yield and ultimate strength, ductility, hardening and/or softening ratios, shape of the hysteresis, dissipating energy and damping…)".

The mentioned parameters, obtained for each test, are collectively given in the Appendix I-XVI at the end of the thesis.

After the completion of frame tests, each frame without and with infill/covering was weighed by means of a system composed of a load cell and a data acquisition system. The load cell was mounted to the crane and then, each frame without and with infill/covering was lifted. In some of the frames, the timber elements forming the frame were so detached from each other that they were weighed separately, and then the weights of these elements were summed up to find out the weight of a whole frame. In some other frames, on the other hand, especially in the ones with adobe or brick infill, the infill was partially torn down during the tests. In these cases, the unit weight of adobe or brick infill was determined, and the weight of the whole frame with infill was calculated by summing up the weight of the incomplete frame and the calculated value for the torn-down section. Therefore, the increase in weight after infill/covering was determined for each frame. Detailed information regarding the weights of each frame is presented in **Section 2.19.**

Next, the capacity calculations were made of each frame, based on the experimentally obtained lateral load-lateral displacement values, in order to obtain linear and non-linear period and damping values. For this aim, ATC-40 was used. Detailed information about these capacity calculations is given in **Chapter 3.**

In this study, a series of material tests were carried out in order to determine (1) the compressive strength values lime-based plaster and mortar (**Section 4.1**), (2) the compressive strength values of adobe and brick blocks (**Section 4.2**), (3) the compressive strength values of adobe and brick masonry samples (**Section 4.3**), (4) the tensile strength values of nails (**Section 4.4.1**), (5) the push-in/pull-out strength values of nails (**Section 4.4.2**), (6) the flexural strength values of timber (**Section 4.5.1**) and (7) the compressive strength values of timber (**Section 4.5.2**). It is important to point out that the push-in/pull-out strength values of nails were determined by using fir only, and not yellow pine. Investigating the change in push-in/pull-out strength values of nails by using different types of timber might be a future study.

By using the results obtained at the end of frame tests, a number of curve-fit studies were carried out. For this aim, the energy dissipation capacity and overall stiffness parameters were selected. The obtained energy dissipation capacity and overall stiffness values for each test, without and with infill/cladding, were normalized in such a way that the data points got closer to each other; therefore a curve could be fit to the whole data. The empirical formulas obtained in such a way can be seen in **Chapter 5.**

In **Chapter 6**, the obtained results were discussed in terms of the changes in load bearing capacity, weight, stiffness and drift ratio when the frames were infilled / covered. Moreover, the period values obtained by means of capacity calculations were used to calculate demand values in the linear and non-linear ranges and compared them against the experimentally obtained linear and non-linear capacity values for each frame without and with infill/covering. For this aim, the Turkish code was used, and it was decided if the frames could bear the seismic demand in linear or non-linear range. In this study, a number of macro and micro modelling was also carried out, while most of those were inconclusive. Therefore, the limitations of the commercially available software for modelling timber frame structures with nailed connections were clearly seen. The limitations regarding the modelling of timber frames were also briefly discussed in this chapter.

In **Chapter 7**, the conclusions drawn at the end of this study are presented.

CHAPTER 2

EXPERIMENTAL STUDIES

In this part of the research, a number of timber frames resembling traditional Ottoman timber frame "*hımış*" houses were reproduced and tested under reverse cyclic lateral loading. For this aim, Safranbolu, which is in the UNESCO World Heritage List since 1994, was chosen as study case, since Safranbolu is one of the most excellently preserved Ottoman towns, where all the characteristics of an Ottoman house, mentioned in the previous chapter, are affirmed (Sözen, 2001: 166-173) (Figure 42-Figure 43).

Figure 42: Traditional Safranbolu houses in 2011

Figure 43: Traditional Safranbolu houses in 1993 (Neriman Şahin Güçhan archive)

Other reasons to select Safranbolu are as follows:

1. Safranbolu is a settlement, where *hımış* tradition has successfully been used and the examples of traditional dwellings with timber frame construction have to a large extent been preserved with their authentic features,

2. This is a settlement located in a first degree seismic zone (Figure 44). Therefore, the experimental and analytical studies can be supported by means of site observations in terms of seismic performances of the structures.

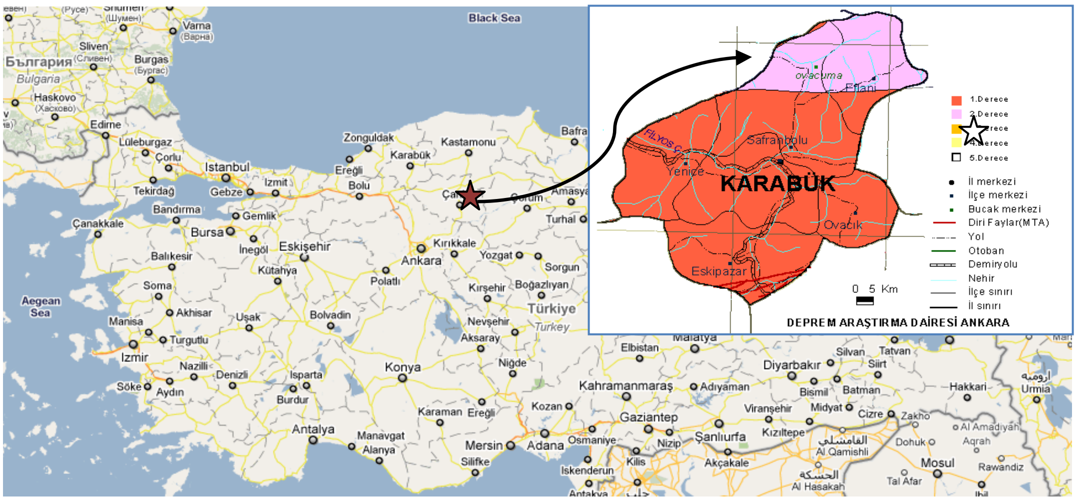

Figure 44: Turkey map (taken from Google Maps) and map of Seismicity for the city of Karabük (taken from the website of General Directorate of Disaster Affairs, http://www.deprem.gov.tr/linkhart.htm)

2.1. SELECTION OF FRAMES

The frames to then use in the experimental studies were selected

(a) So as to cover the most common types, as well as to reflect as many geometrical configurations as possible in the experimental analysis, and

(b) From the modules in the non-plastered facades that can be easily observed.

The tested frame, the façade from which the frame was selected and the actual frame are shown respectively in Figure 45-Figure 50. In order to distinguish the differences in seismic behavior of frames having different opening ratios, 1 of the 6 selected frames has no openings, while 3 of them have 2 window openings and 2 have 3 window openings.

Figure 45: Solid frame module from Akpınar St. No: 43, Karaali District, Safranbolu

Figure 46: Frame module with two window openings from Akpınar St. No: 20, Karaali District, Safranbolu

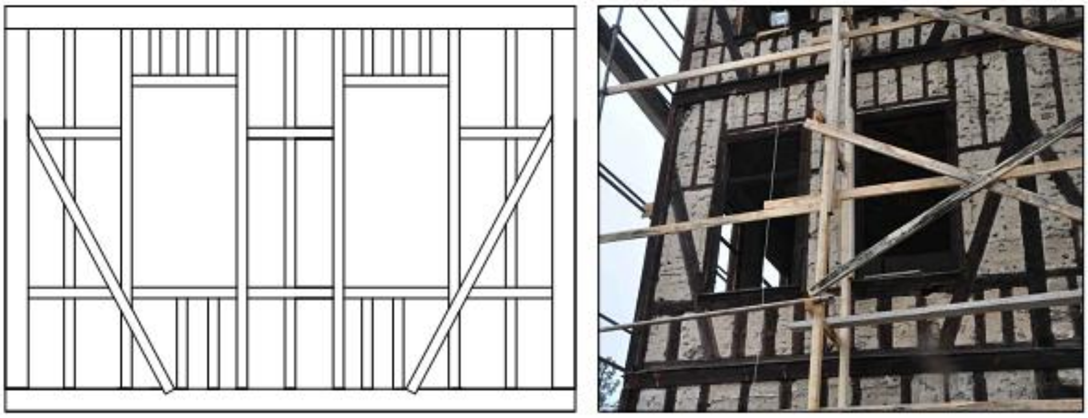

Figure 47: Frame module with two window openings from Köyiçi Square No: 4, Bağlarbağı District, Safranbolu

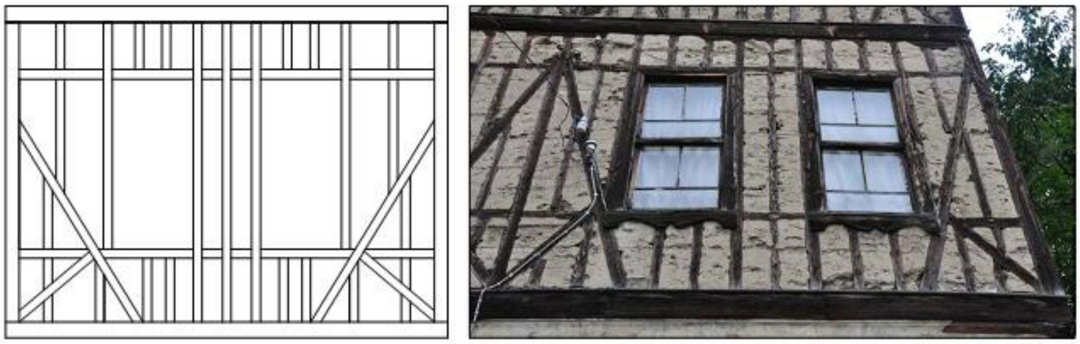

Figure 48: Frame module with two window openings from Değirmenbaşı St. No 69, Bağlarbağı District, Safranbolu

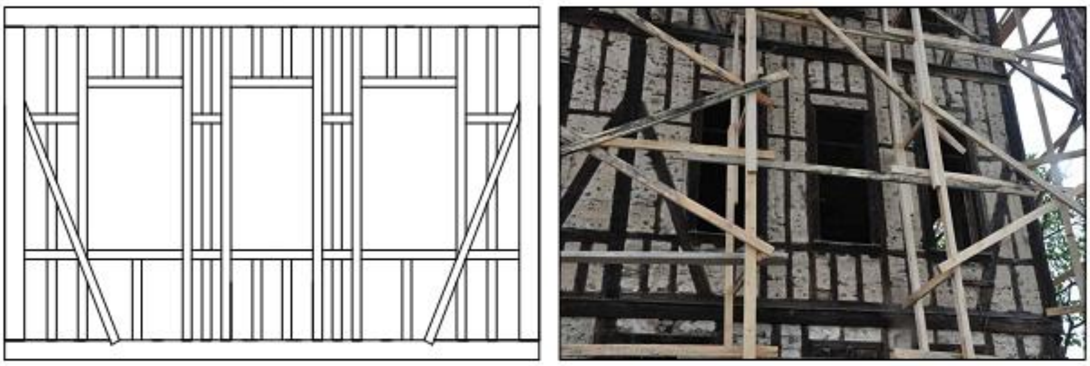

Figure 49: Frame module with three window openings from Köyiçi Square No: 4, Bağlarbağı District, Safranbolu

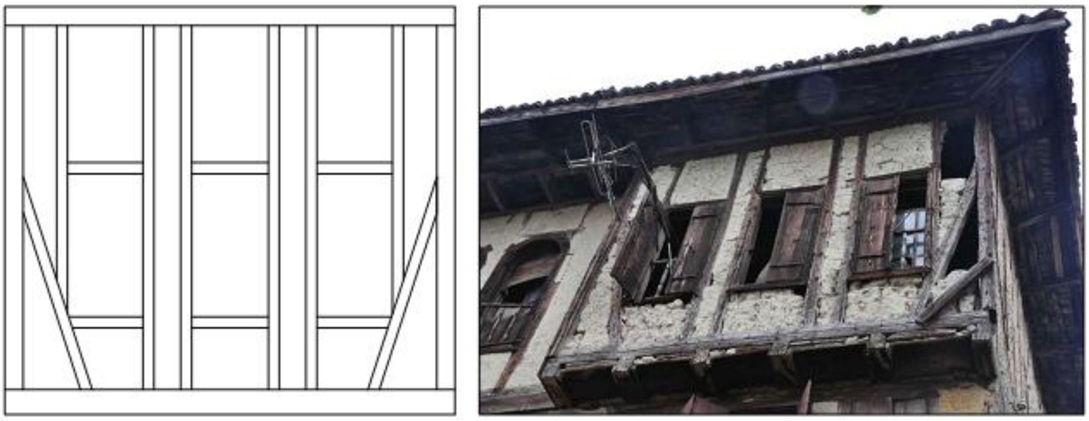

Figure 50: Frame module with three window openings from Akpınar St. No: 43, Karaali District, Safranbolu

Two of the selected 6 frames were constructed in laboratory conditions by using two different wood types, yellow pine and fir. All 8 frames having different geometrical configuration and material properties were constructed by a local building master from Beypazarı, to be able to reflect all traditional features intrinsic to traditional housing. As connection elements, solely nails were used, as the case in the houses the frames were chosen from. The frames were then tested under reverse cyclic loading at the Structural Mechanics Laboratory of the Middle East Technical University.

2.2. TEST SET-UP AND INSTRUMENTATION

The test set up designed for the purpose of frame experiments mentioned above, is basically composed of a foundation part, vertical masts and horizontal ones securing them to the wall (Figure 51).

Figure 51: An overall view of the test set-up

The frame to be tested was placed in and secured to a U profile by means of plates, placed on each side of the frame, and bolted to the frame. For small frames, three of these plates were used on each side, while for big frames the number of the plates used on each side is five (Figure 52). In addition, an eventual lateral slippage of frames was prevented by plates bolted to foundation at two ends of the frame (Figure 53).

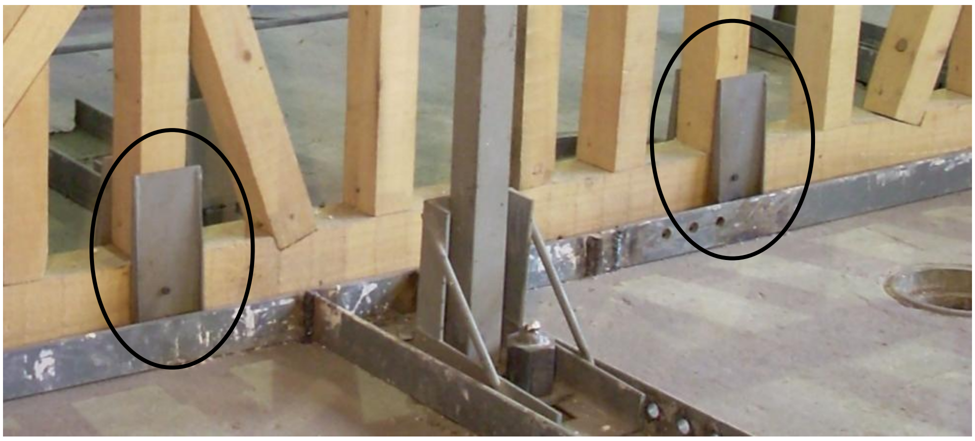

Figure 52: Plates securing the frame inside the profile

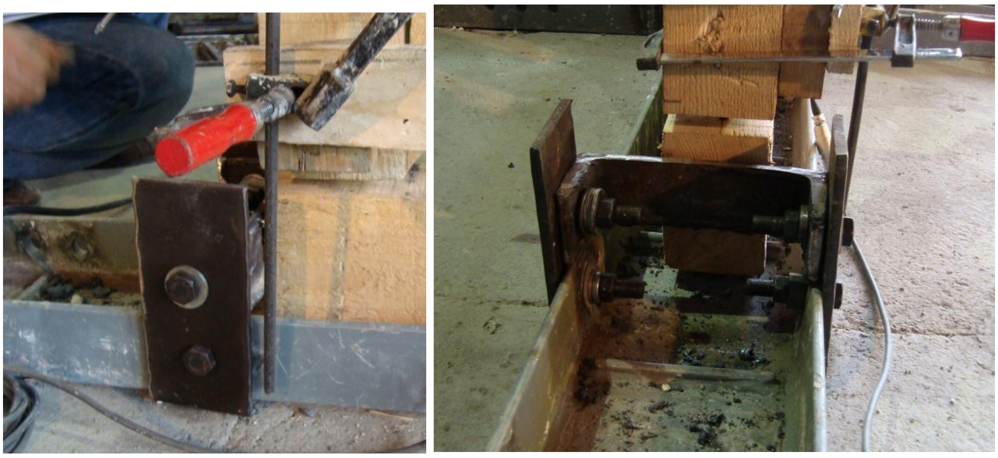

Figure 53: Plates bolted to foundation at two ends of the frame to prevent frames' eventual lateral slippage

Vertical masts were welded inside the lugs. Then horizontal elements were placed between them, to which rollers were secured. Each roller touched to the frame at one point. By means of horizontal masts, bolted to the vertical ones at one end and to the wall at the other, the out-of-the-plane movement of the frame was prevented (Figure 54).

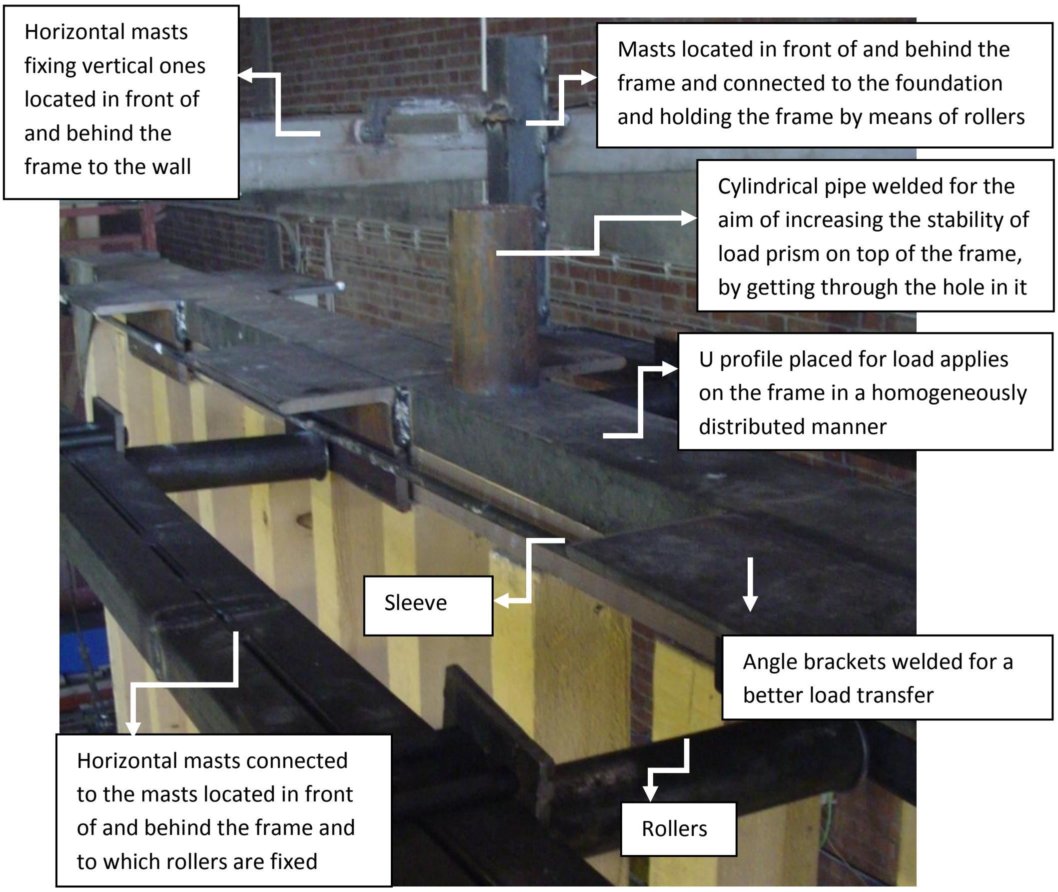

Figure 54: Top portion of the test set-up

At top of the frame, another inverted U profile is placed. Angle brackets were welded at intervals to the profile for a better load transfer. Furthermore, a cylinder pipe was also welded on top of the profile to further increase the stability of one load prism by placing the cylinder through one of the two holes the prism held (Figure 55).

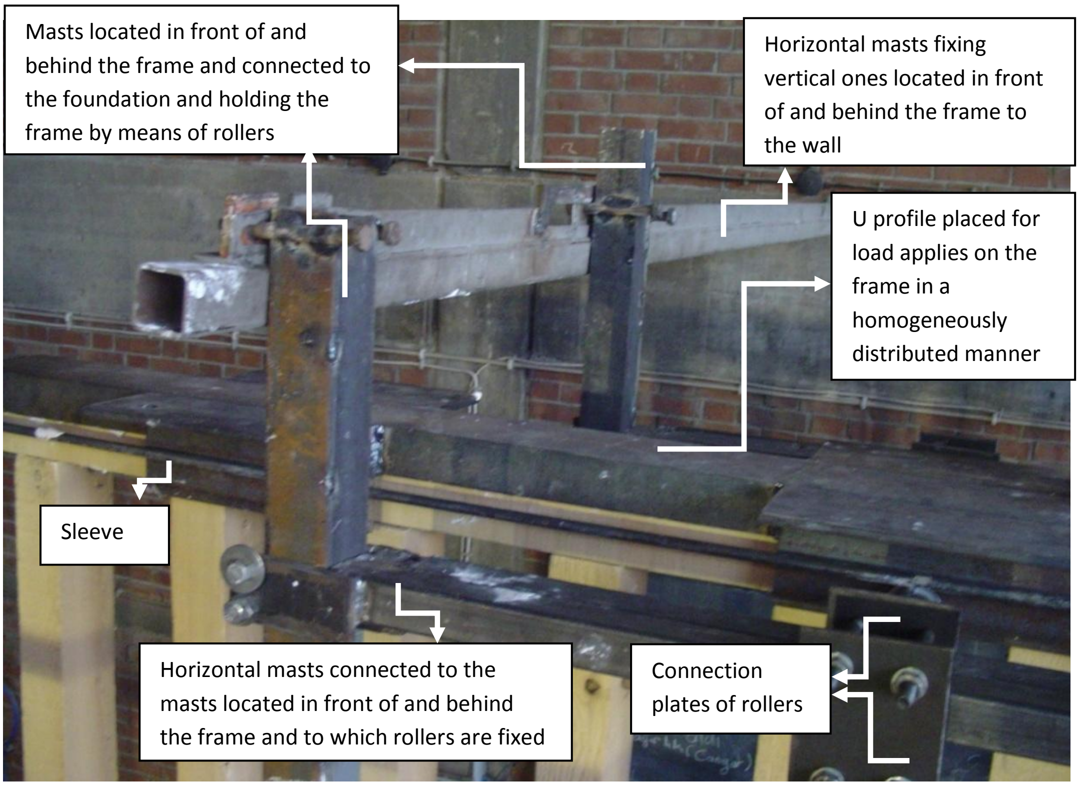

Figure 55: Top portion of the test set-up

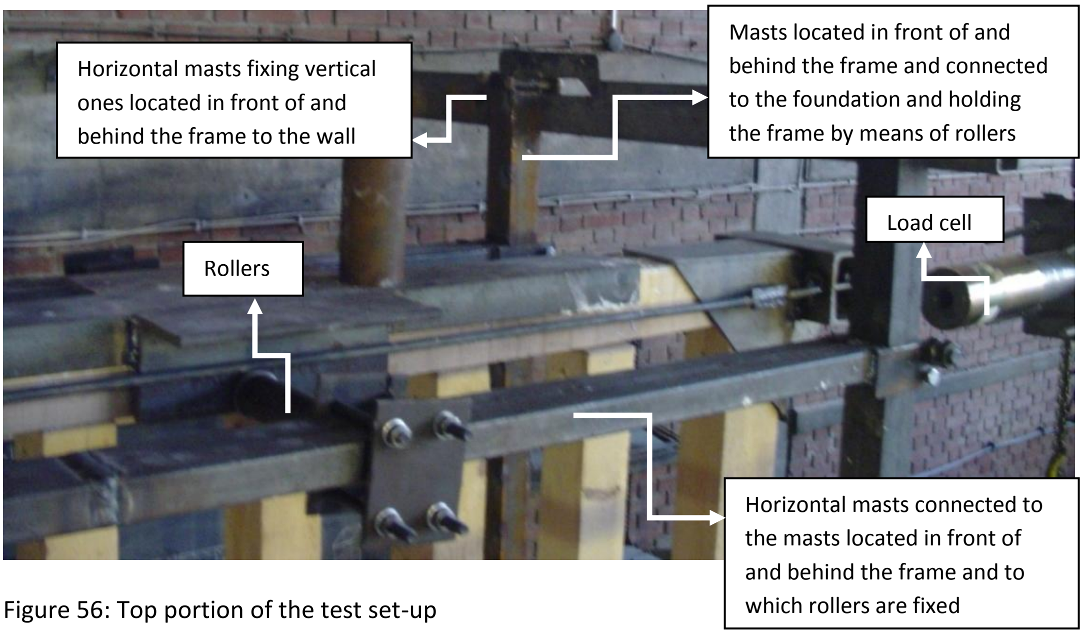

Figure 56: Top portion of the test set-up

At both top corners of the frame, angle elements were placed through which the sleeves pass. The angle element at the side of the hydraulic piston is fixed to it by means of a connector (Figure 57-Figure 58). CAD drawings of the test set-up can be seen in Figure 59.

Figure 57: Angle elements to which sleeves are connected

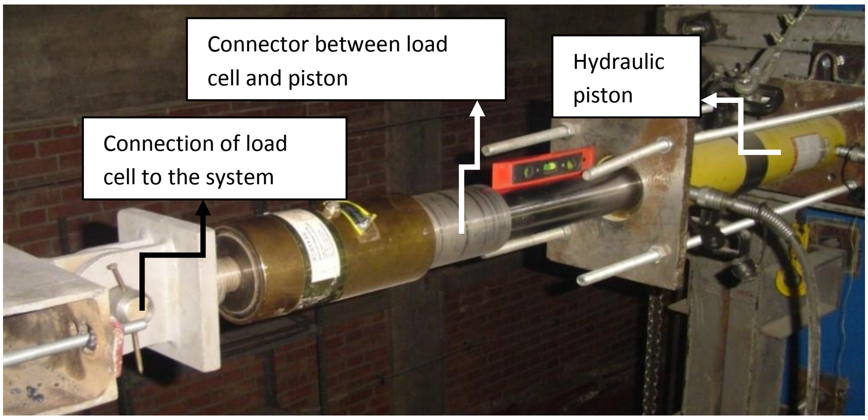

Figure 58: Piston connected to strong wall and load cell, used in the experiments

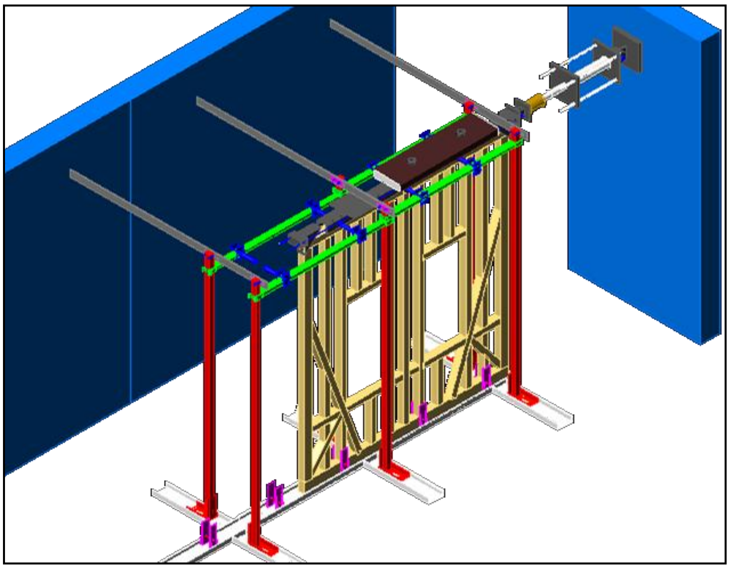

Figure 59: CAD drawing of the test set-up

The loading was carried out by using a load cell, whose capacity is 500 kN in compression and 250 kN in tension, and a piston with 50 cm stroke length. Half of the stroke length was used to push and the other half to pull the frame.

For the first five experiments (frames#1-5 without infill/covering), four Linear Variable Differential Transformers (LVDT) were used. For their locations, see Figure 60-Figure 62.

Figure 60: LVDTs of 200 mm placed at both sides of the frame to measure diagonal displacement

Figure 61: LVDT of 200 mm to measure diagonal displacement and that of 50 mm to check bottom lateral displacement

Figure 62: LVDT of 500 mm to measure the lateral top displacement and hydraulic piston

For the next experiments, on the other hand, more sensors were used with an addition of two LVDT's of 50 mm, placed on the horizontal masts securing the system to the wall. Besides, two LVDT's of 300 mm were placed on both sides of the frame to measure lateral displacements in push and pull directions separately, however the LVDT of 500 mm that had placed previously to measure lateral top displacement was not removed and kept functioning. The LVDT of 50 mm stroke length that was used to check possible lateral displacement at the bottom of the frame was used also on the other side of the frame (Figure 63-Figure 64).

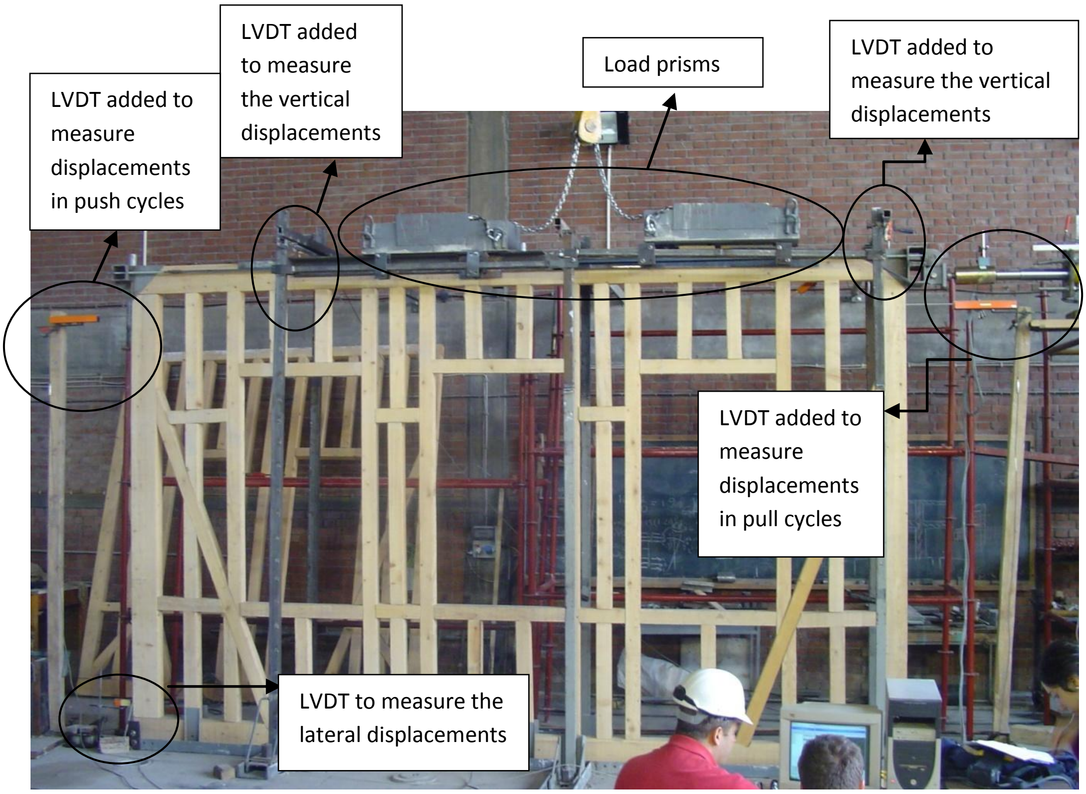

Figure 63: Additional sensors

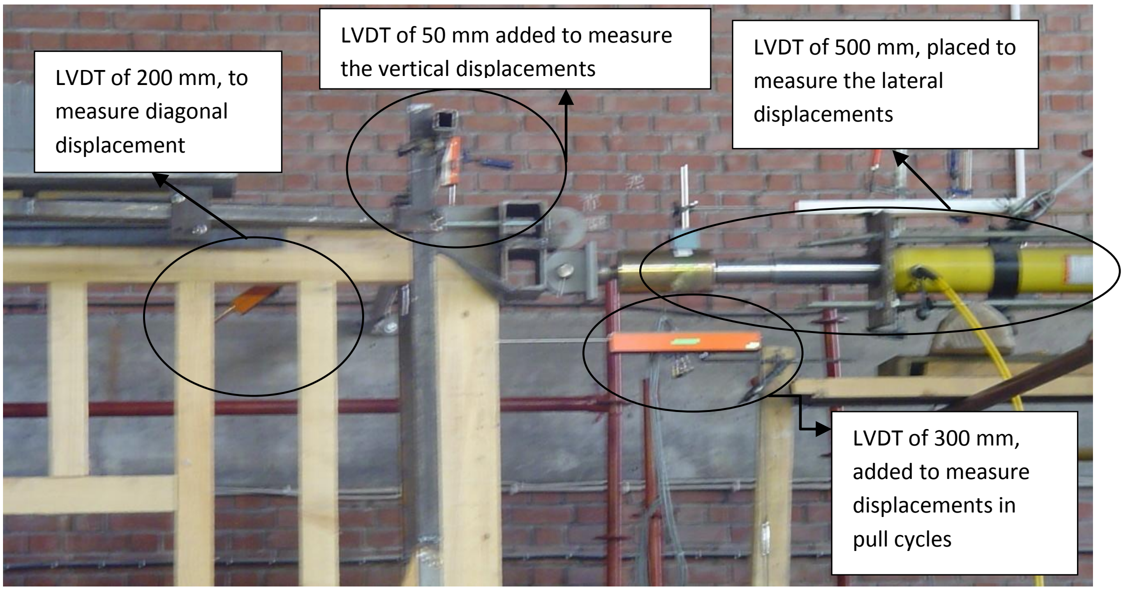

Figure 64: Additional sensors

All tests were conducted using two load prisms, each 100 cm x 40 cm x 10 cm in size and weighing approximately 320 kg, which were held by means of a crane during tests (Figure 65).

Figure 65: Load prisms held by means of crane

2.3. FRAME#1

The first experiment was carried out with a 325 cm x 310 cm (H x L) sized yellow pine frame, having two window openings of 67 cm x 135 cm (Figure 66-Figure 67).

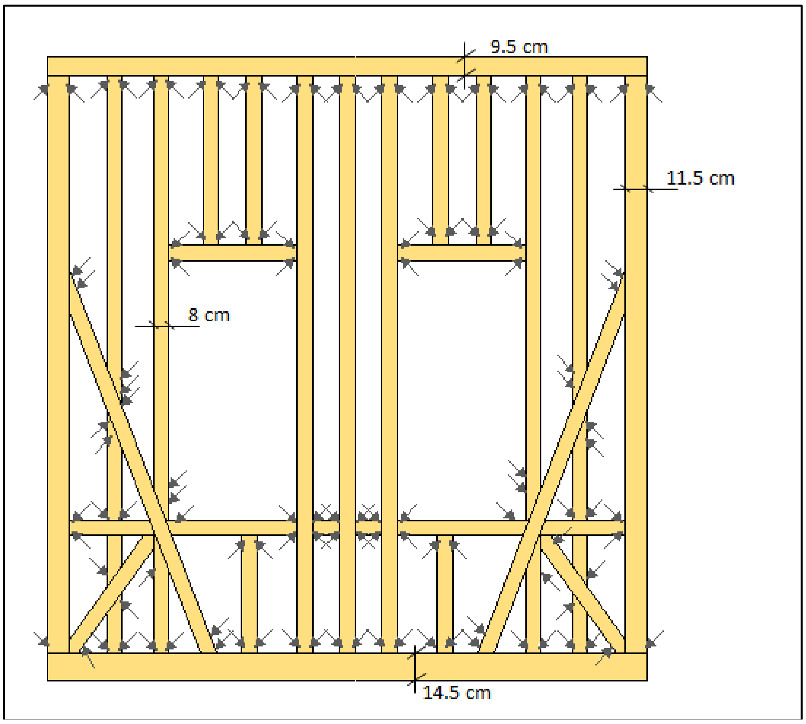

Figure 66: Drawing of Frame#1 (arrows indicate the nails at each connection)

Figure 67: Frame#1

In this experiment, loading was done in the load-controlled manner by increasing the load value 1 kN (approximately 100 kgf) at a time, for successive push and pull cycles, until 4kN (approximately 400 kgf) is reached. After this point, displacement-controlled loading was done with an increment of 10 mm at a time for each cycle (Figure 68).

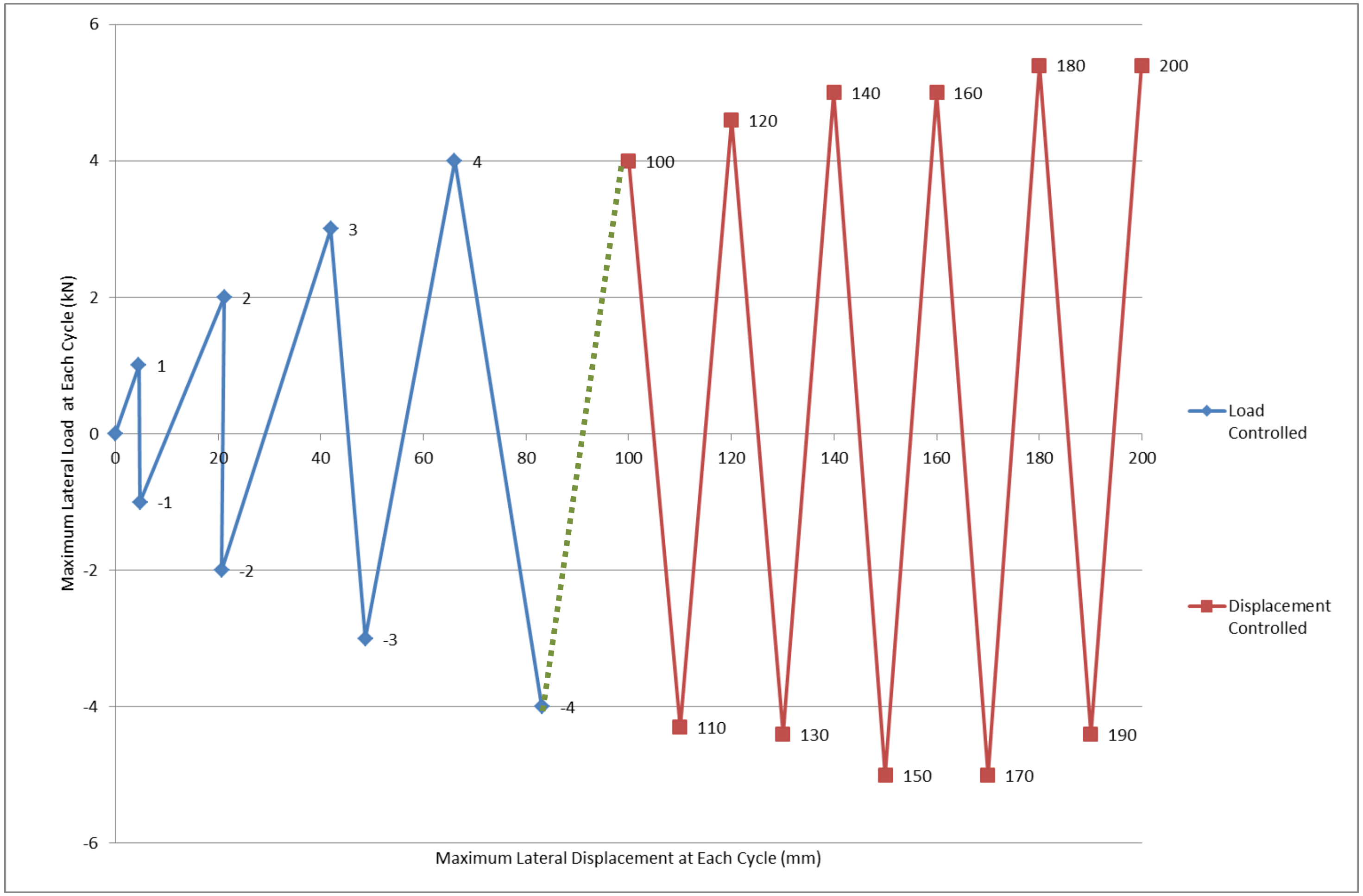

Figure 68: Load controlled and displacement controlled phases of the testing of Frame#1 (data labels shown are load and displacement values for load controlled and displacement controlled data series, respectively)

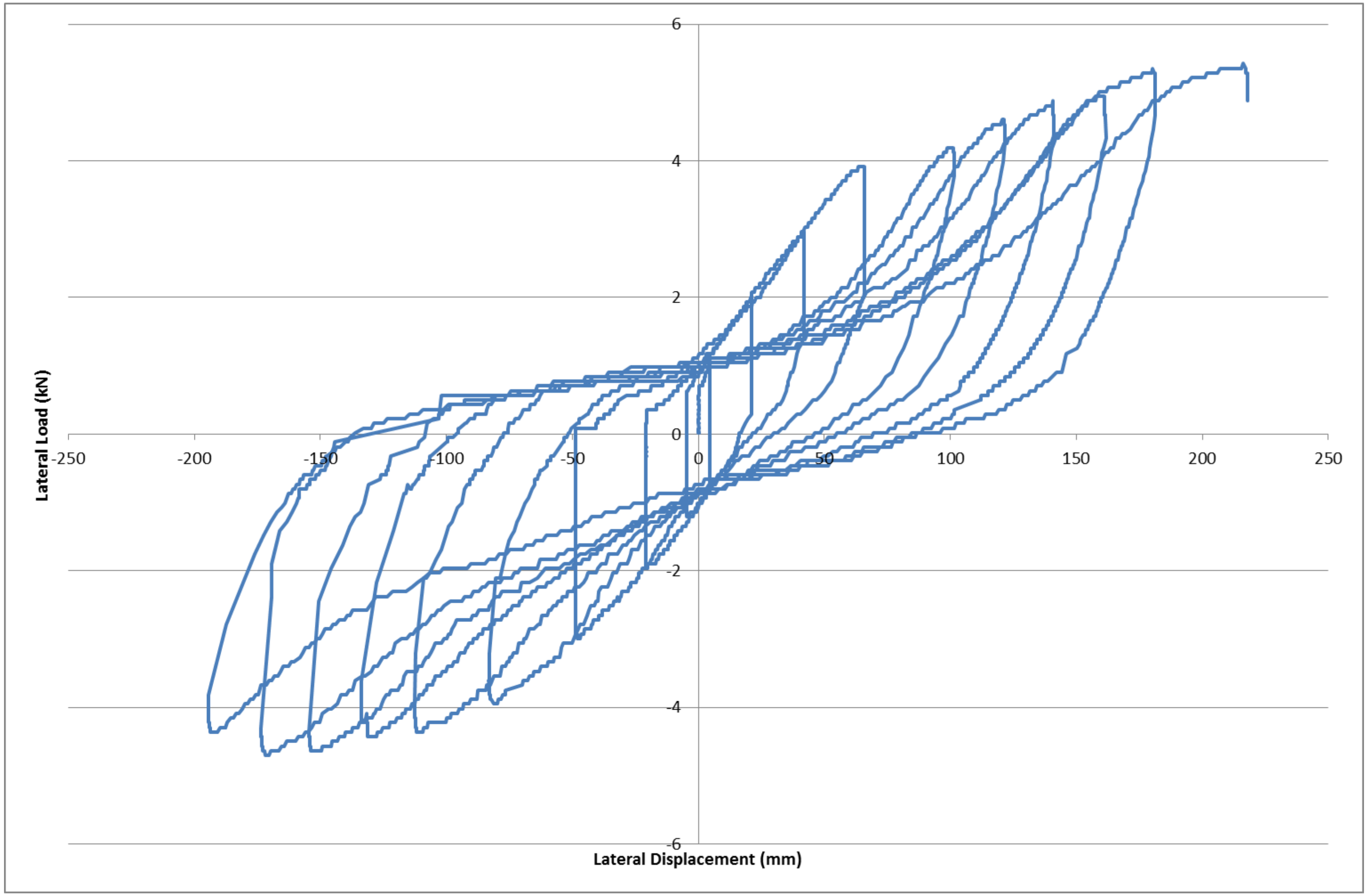

Figure 69: Lateral load – lateral displacement graph of Frame#1

In Figure 69, the load-displacement behavior obtained at the end of the experiment can be observed. The experiment was to the point where first indication of strength loss was observed. The test was terminated before the frame was totally damaged since the same frame was planned to be used with infill/covering. The maximum lateral load that was observed in the push direction is about 5.4 kN (approximately 553 kgf) and the corresponding lateral displacement is 218 mm, while in the pull direction these values are 4.7 kN (approximately 479 kgf) and 173 mm, respectively. More information related to the results obtained at the end of the testing of Frame#1 can be found in Appendix B.

The failures occurred at the nailed joints in the form of dilatation are shown in Figure 70. The inclined views of the frame at the end of the test can be seen in Figure 71.

Figure 70: Several examples to joint failure in the testing of Frame#1

Figure 71: Two figures taken during the testing of Frame#1

2.4. FRAME#1 WITH ADOBE INFILL

In this test, the first frame was tested with infill. Before testing the frame, the failed connections were repaired using the same type and number of nails. The infill was carried out by 9-11.5 cm x 9-11.5 cm x 20-21 cm adobe blocks, prepared by local construction workers (Figure 72). Mortar and plaster were prepared according to traditional methods.

Figure 72: Infilling and plastering processes

In the testing of Frame#1 with adobe infill, loading was done in the load-controlled manner by increasing the load value 1kN (approximately 100 kgf) at a time, for successive push and pull cycles, until 4kN (approximately 400 kgf) is reached. After this point, displacement-controlled loading was done with an increment of, first, 2, next 5 and finally 10 mm at a time for each cycle (Figure 73).

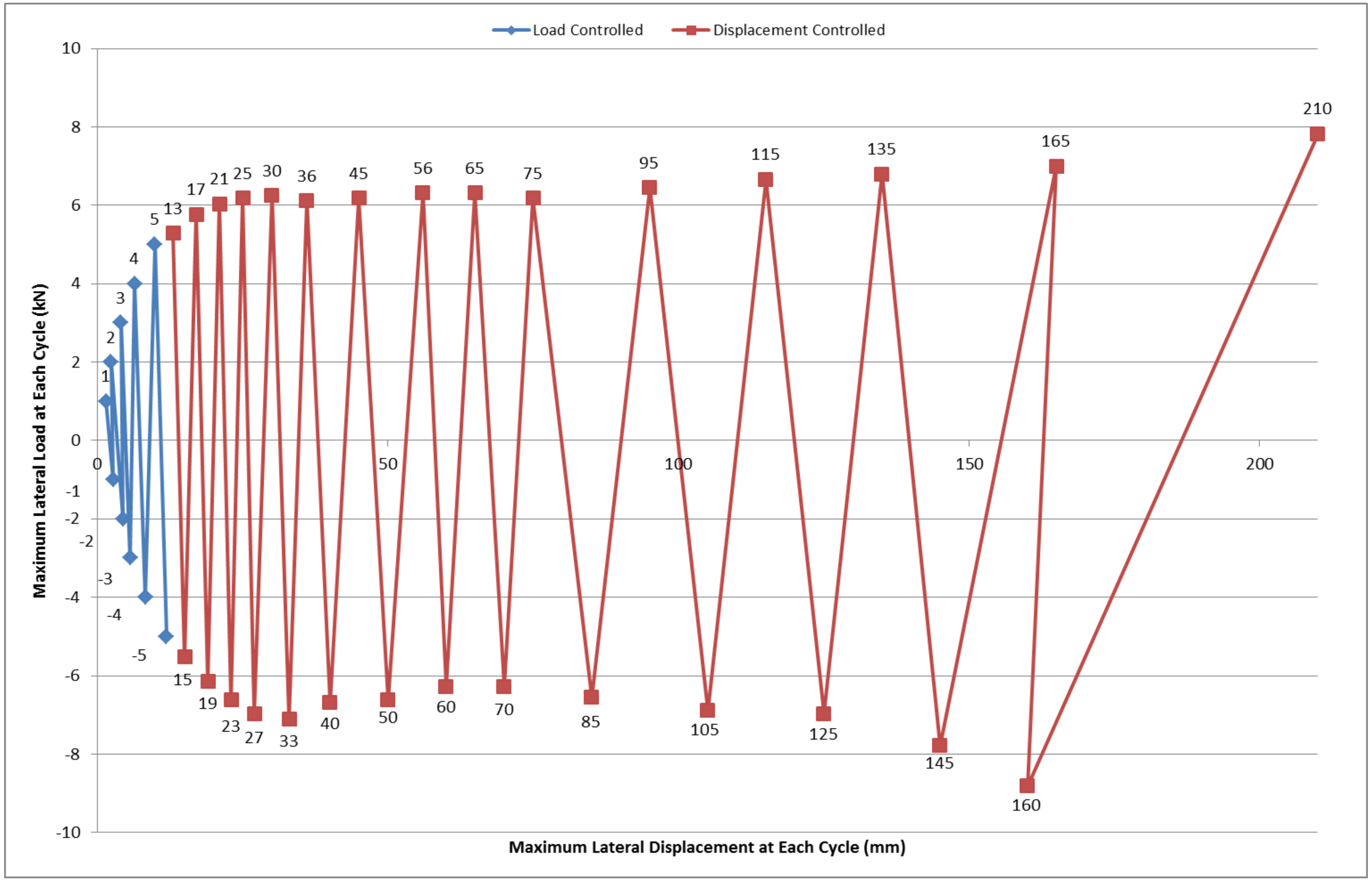

Figure 73: Load controlled and displacement controlled phases of the testing of Frame#1 with adobe infill (data labels shown are load and displacement values for load controlled and displacement controlled data series, respectively)

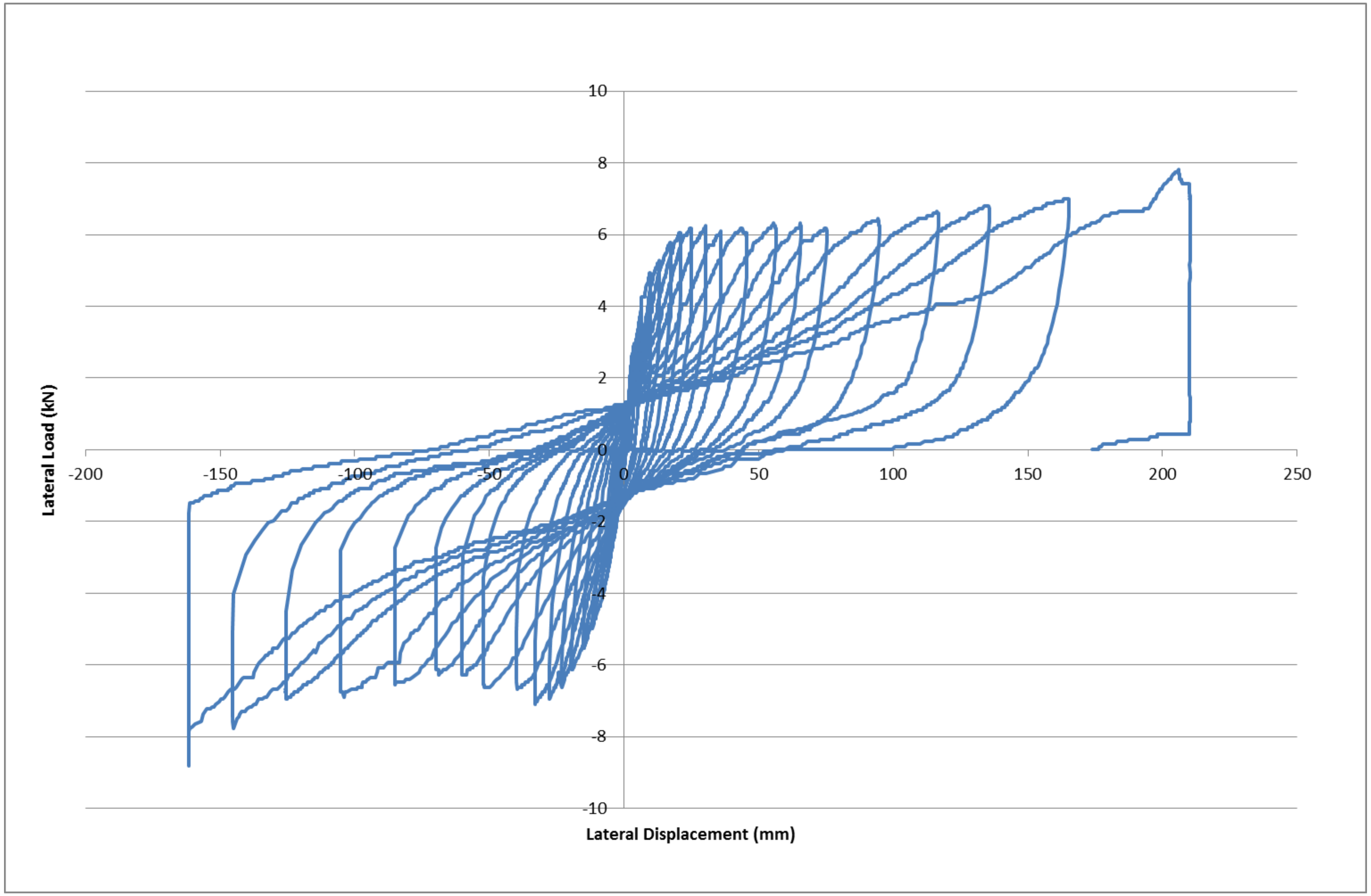

Figure 74: Lateral load – lateral displacement graph of Frame#1 with adobe infill

In Figure 74, the load-displacement behavior obtained at the end of the experiment can be observed. The experiment was to the point where first indication of strength loss was observed. The maximum lateral load that was observed in the push direction is 7.8 kN (approximately 800 kgf) and the corresponding lateral displacement is 210 mm, while in the pull direction these values are approximately 8.8 kN (approximately 900 kgf) and 160 mm, respectively. More information related to the results obtained at the end of the testing of Frame#1 with adobe infill can be found in Appendix C.
A typical failure at the nailed connections in the form of dilatation is shown in Figure 75.

Figure 75: Connection failures

2.5. FRAME#2

The second experiment was carried out with a 360 cm x 330 cm (H x L) sized yellow pine frame, having no openings (Figure 77).

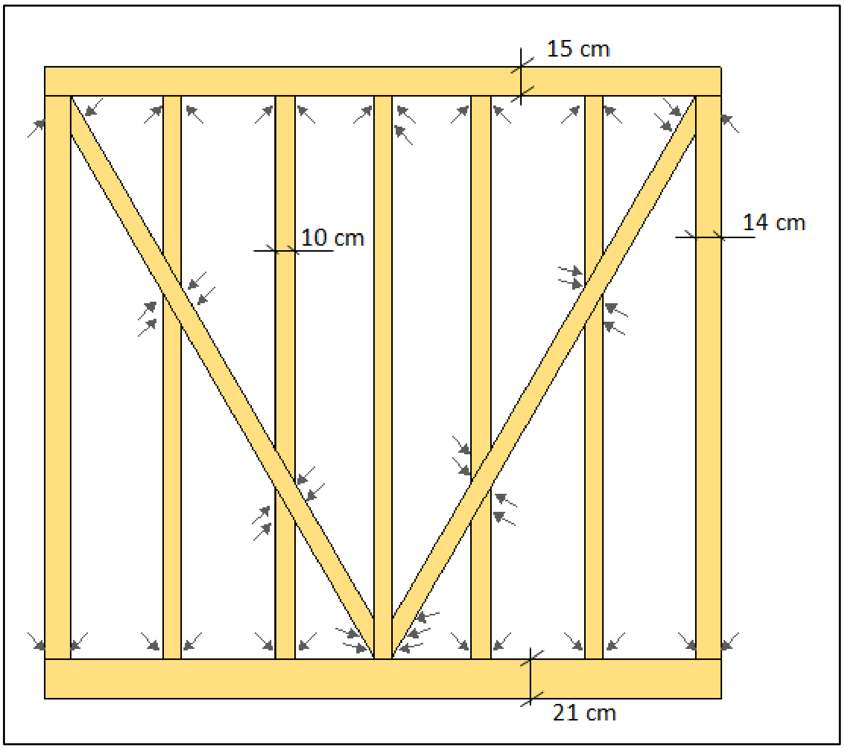

Figure 76: Drawing of Frame#2 (arrows indicate the nails at each connection)

Figure 77: Second frame to be tested

Also in this test, until 4 kN (approximately 400 kgf) is reached, loading was done in the load controlled manner by increasing the load value 1 kN (approximately 100 kgf) at a time, for successive push and pull cycles. After this point, displacement controlled loading was done with an increment first of 5 mm and then 10 mm at a time for each cycle (Figure 78).

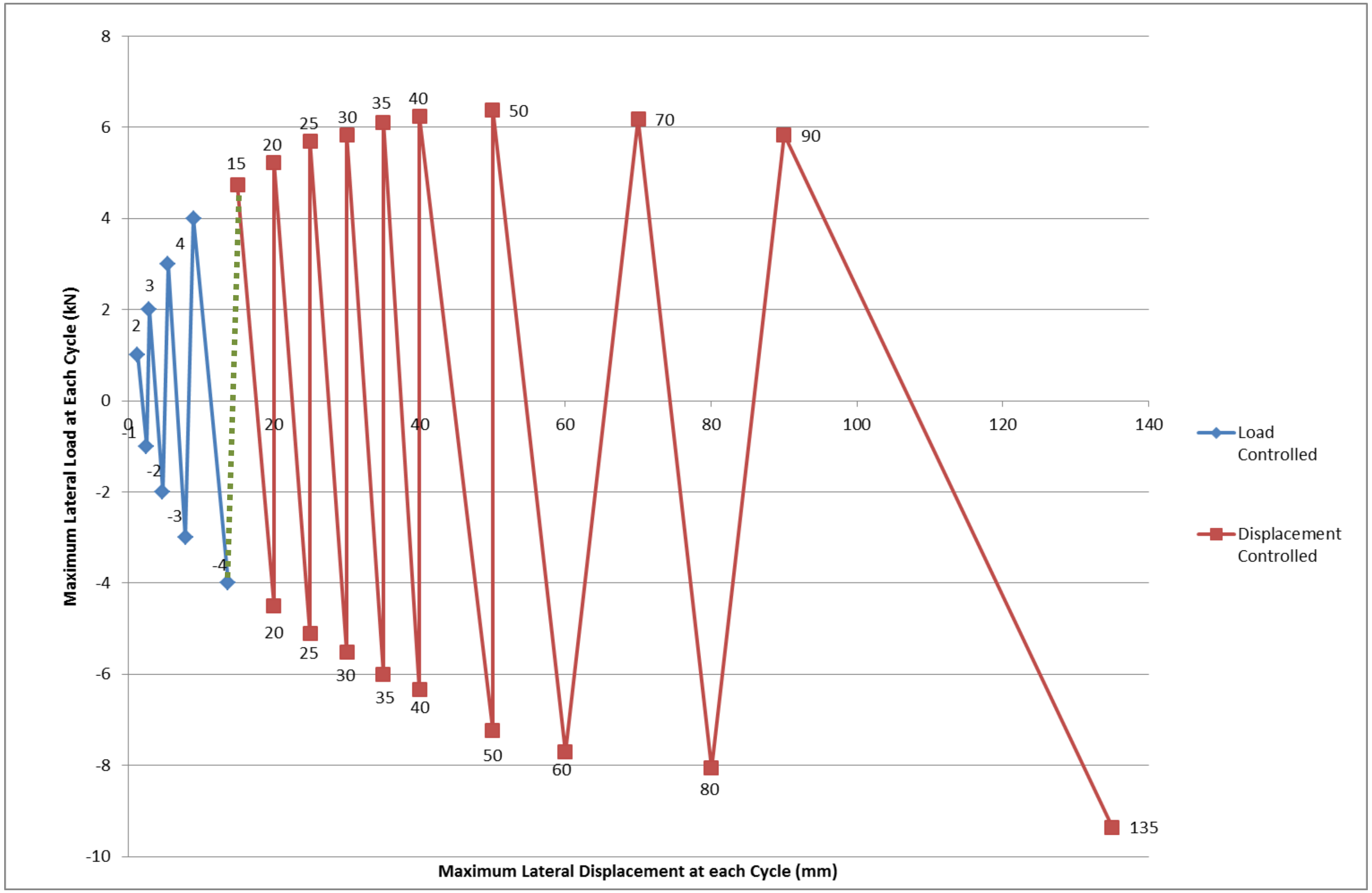

Figure 78: Load controlled and displacement controlled phases of the testing of Frame#2 (data labels shown are load and displacement values for load controlled and displacement controlled data series, respectively)

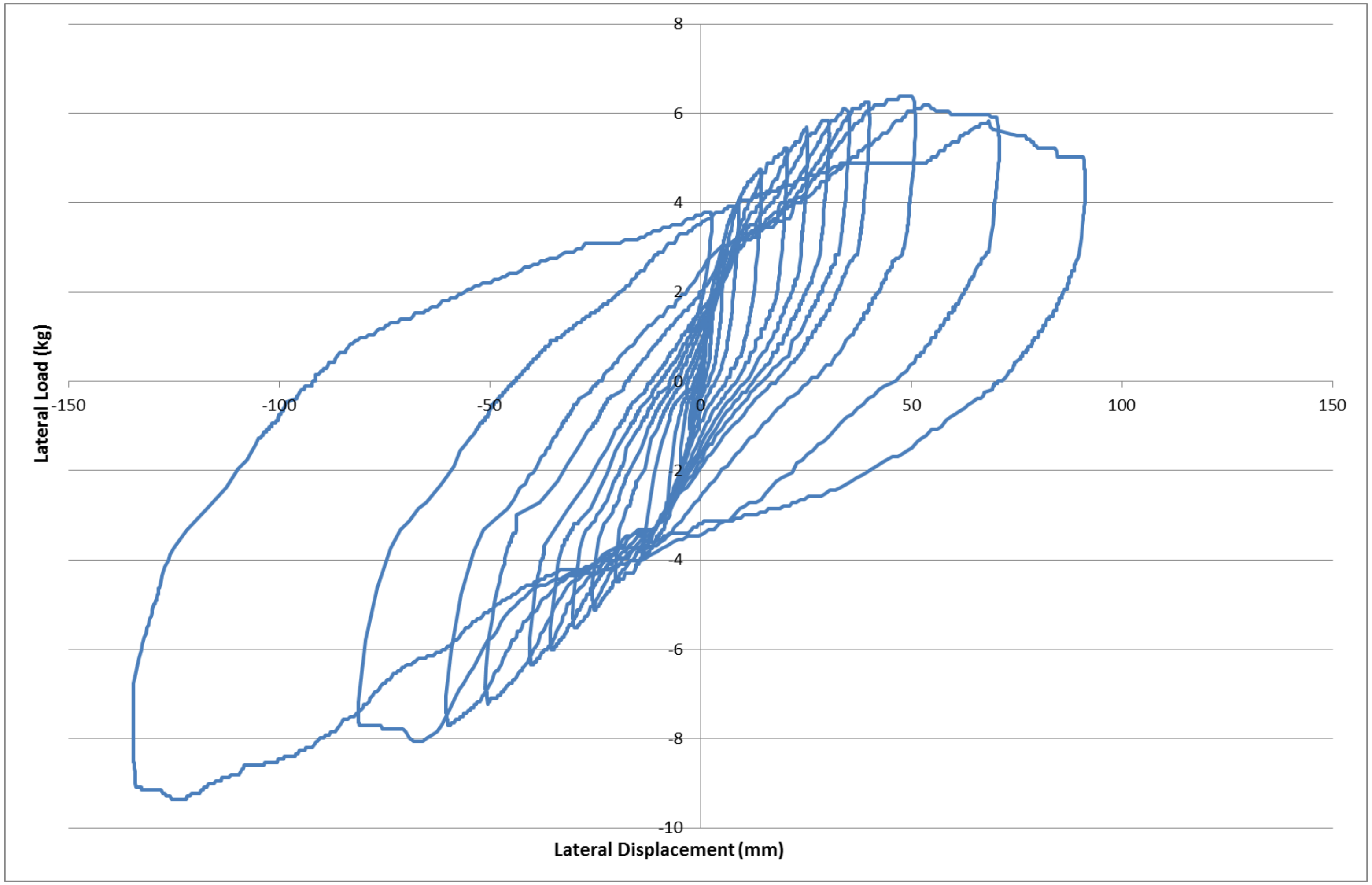

Figure 79: Lateral load – lateral displacement graph of Frame#2

In Figure 79, the load-displacement behavior obtained at the end of the experiment can be observed. The experiment was to the point where first indication of strength loss was observed. The test was terminated before the frame was totally damaged since the same frame was planned to be used with infill/covering. The maximum lateral load that was observed in the push direction is about 6.4 kN (approximately 651 kgf) and the corresponding lateral displacement is 51 mm, while in the pull direction these values are 9.3 kN (approximately 953 kgf) and 135 mm respectively. More information related to the results obtained at the end of the testing of Frame#2 can be found in Appendix D.

The failures at the nailed joints in the form of joint dilatation and nail distortion are shown in Figure 80 and Figure 81.

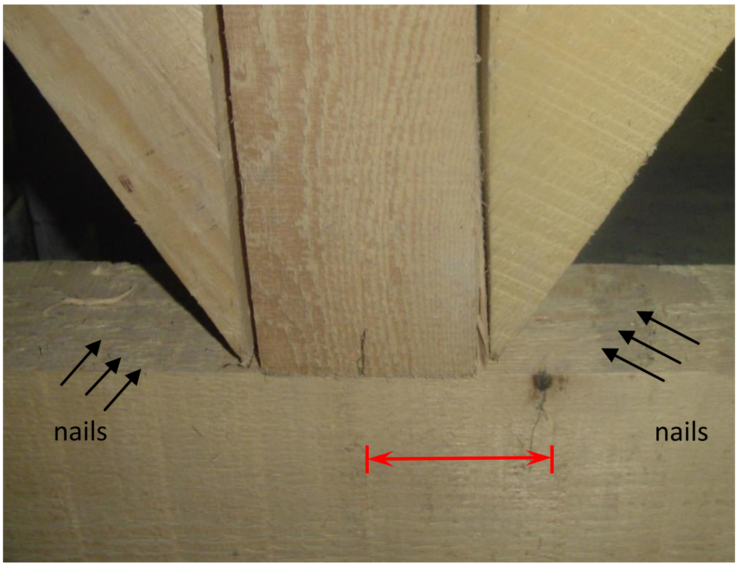

Figure 80: Displacement occurred at the middlemost upright element during the test of Frame#2

Figure 81: Trace of the slipped nail

2.6. FRAME#2 WITH ADOBE INFILL

In this test, the Frame#2 was tested with adobe infill. Before testing the frame, the failed connections were repaired using the same type and number of nails (Figure 82). The infill was carried out by 9-11.5 cm x 9-11.5 cm x 20-21 cm adobe blocks, prepared by local construction workers (Figure 72). Mortar and plaster were prepared according to traditional methods.

Figure 82: Frame#2 after repairing all connections

Figure 83: Adobe infilling

Figure 84: Addition of *hatıls* between existing timber elements

In this test, loading was done in the load-controlled manner by increasing the load value 1 kN (approximately 100 kgf) at a time, for successive push and pull cycles, until 4 kN (approximately 400 kgf) is reached. After this point, displacement-controlled loading was done with an increment of, first 5 and then 10 mm at a time for each cycle (Figure 85).

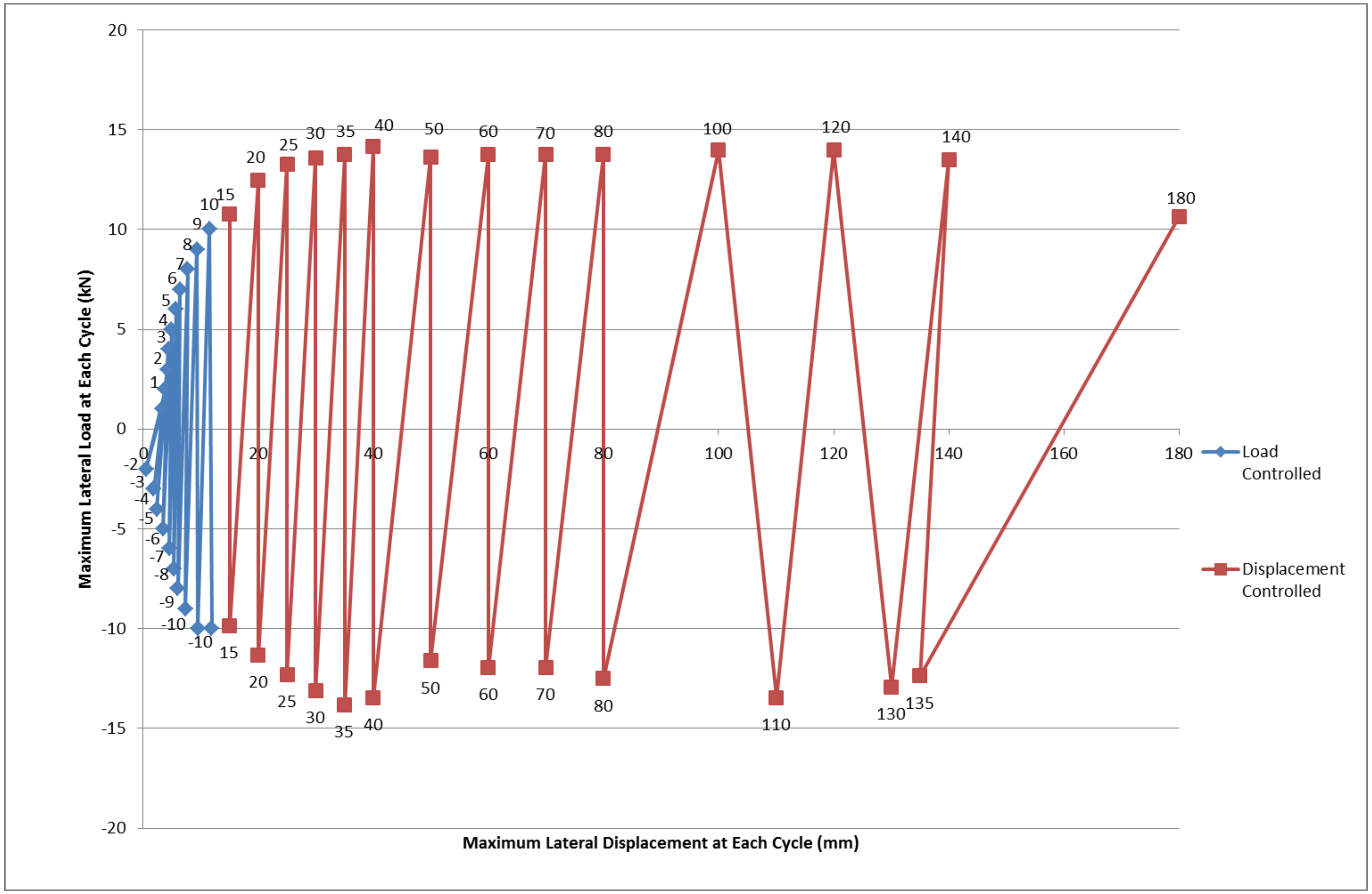

Figure 85: Load controlled and displacement controlled phases of the testing of Frame#2 with adobe infill (data labels shown are load and displacement values for load controlled and displacement controlled data series, respectively)

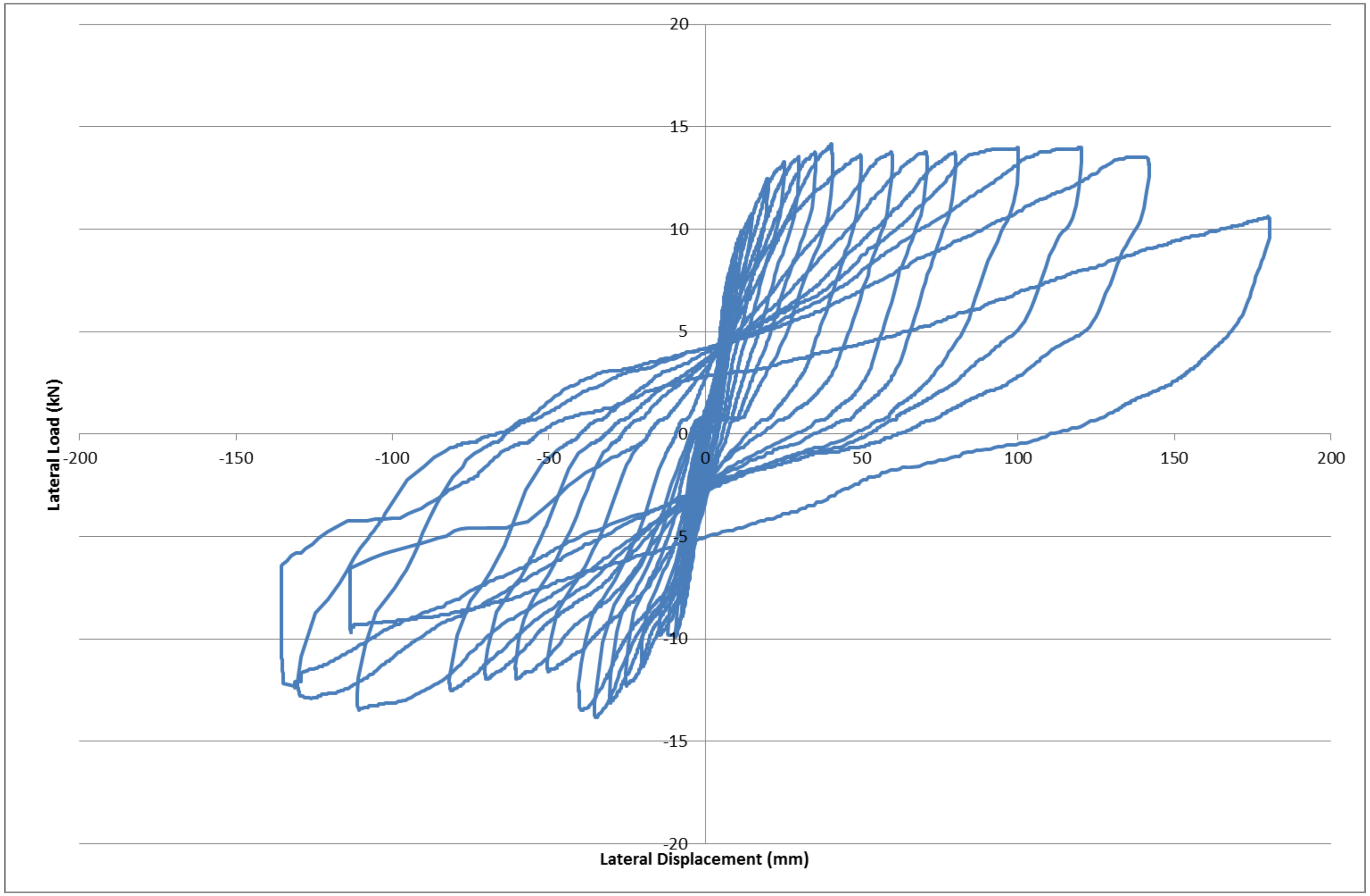

Figure 86: Lateral load – lateral displacement graph of Frame#2 with adobe infill

In Figure 86, the load-displacement behavior obtained at the end of the experiment can be observed. The experiment was to the point where first indication of strength loss was observed. The maximum lateral load that was observed in the push direction is nearly 14.2 kN (1450 kgf) and the corresponding lateral displacement is 180 mm, while in the pull direction these values are approximately 13.7 kN (1400 kgf) and 135 mm, respectively. More information related to the results obtained at the end of the testing of Frame#2 with adobe infill can be found in Appendix E.

The failures at the nailed connections in the form of dilatation are shown in Figure 87 and Figure 88.

Figure 87: Frame#2 with adobe infill after test

Figure 88: An example to connection failures

2.7. FRAME#3

The third test was carried out with a 360 cm x 330 cm (H x L) sized fir frame, having no window openings. The frame is actually the same with the frame tested in the second experiment in terms of geometrical configuration; however the wood type is different (Figure 90).

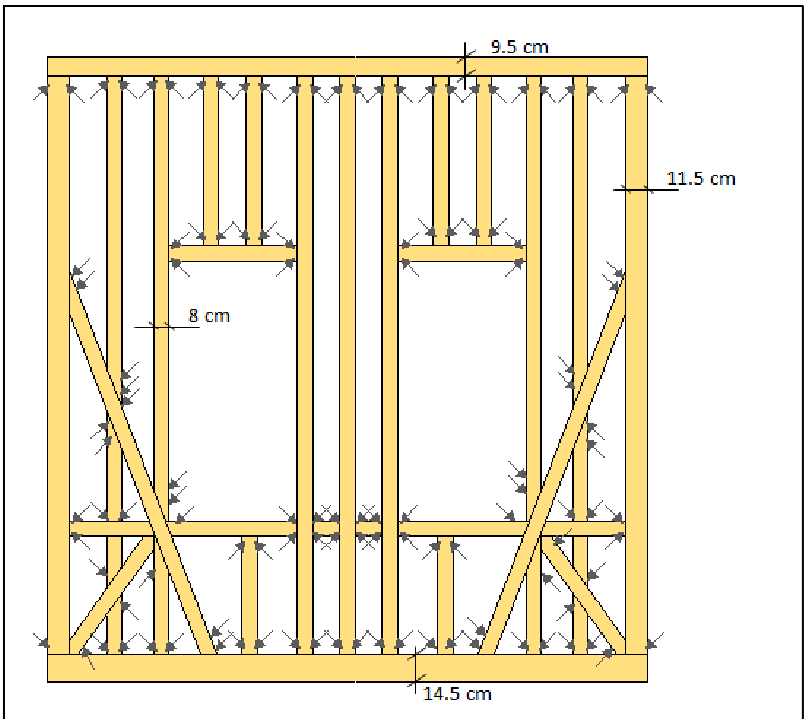

Figure 89: Drawing of Frame#3 (arrows indicate the nails at each connection)

A remarkable point is that Frame#3 had a distinguishably bad workmanship in comparison to the other frames. At certain connections, the nails were not drawn completely and timber elements' surfaces were not in the same plane. This point will be borne in mind, while considering the obtained results.

Figure 90: Third frame to be tested

Since the geometrical configuration of this frame is the same as the previous one, loading was tried to be carried out in the same manner to compare the results more easily. Therefore, just like the previous experiment, also in this one until 4 kN (approximately 400 kgf) is reached, loading was done in the load controlled manner by increasing the load value 1 kN (approximately 100 kgf) at a time, for successive push and pull cycles. After this point, displacement controlled loading was done with an increment first of 5 mm and then 10 mm at a time for each cycle (Figure 91).

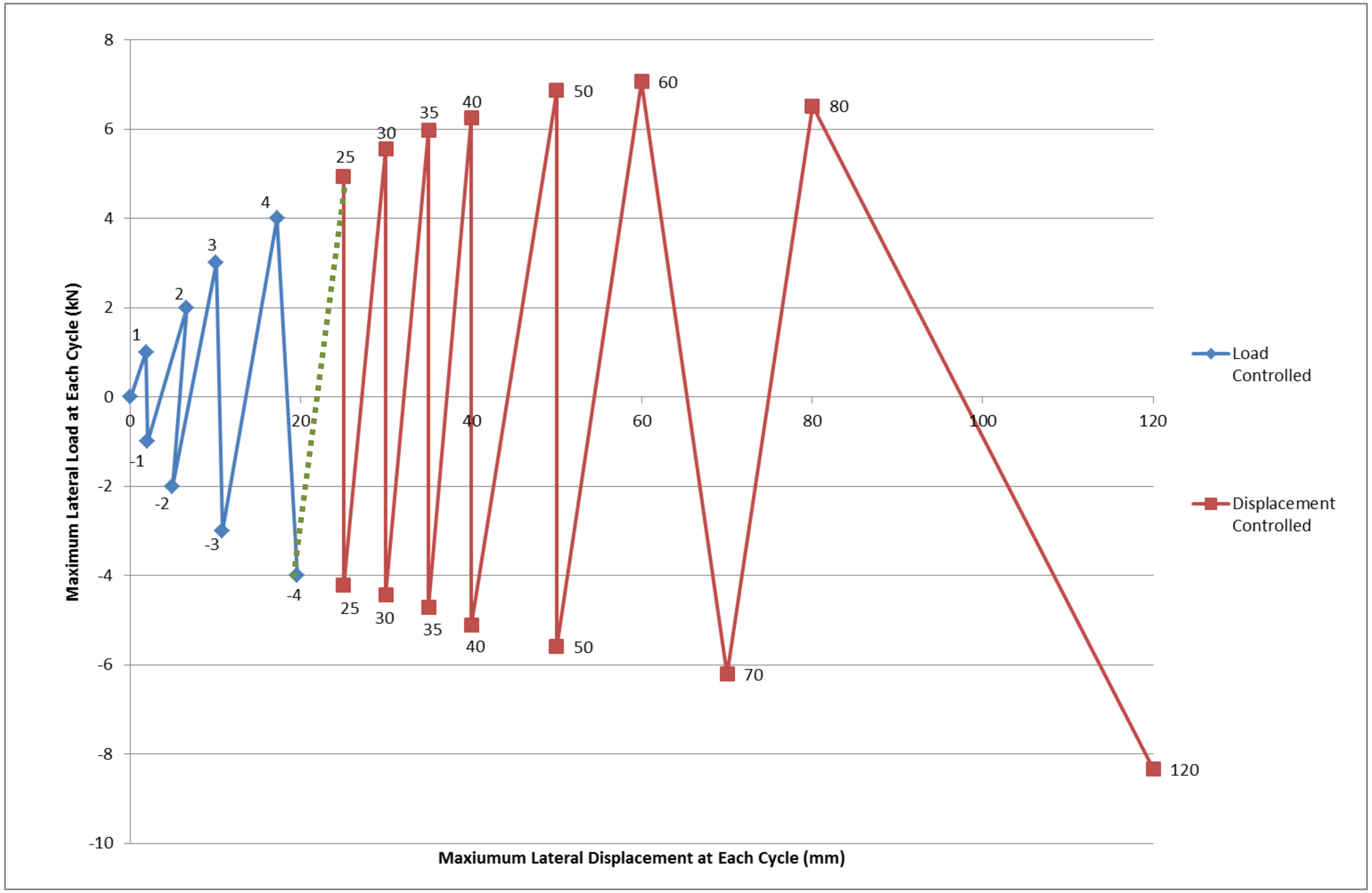

Figure 91: Load controlled and displacement controlled phases of the experiment for the testing of Frame#3 (data labels shown are load and displacement values for load controlled and displacement controlled data series, respectively)

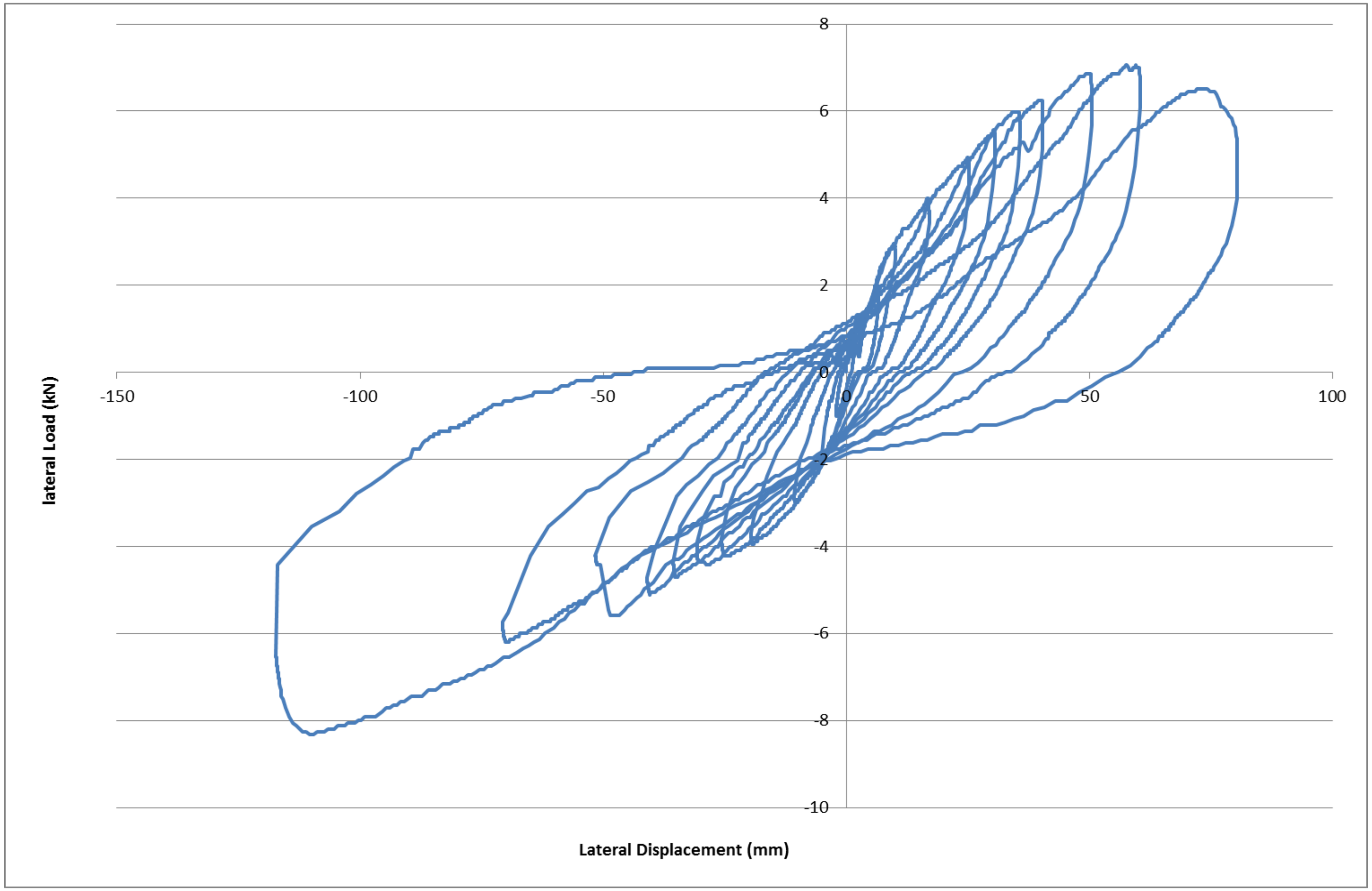

Figure 92: Lateral load – lateral displacement graph of Test#3

In Figure 92, the load-displacement behavior obtained at the end of the experiment can be observed. The experiment was to the point where the first indication of strength loss was observed. The test was terminated before the frame was totally damaged, since the same frame was planned to be used with infill/covering. The maximum lateral load that was observed in the push direction is approximately 7 kN (720 kg) and the corresponding lateral displacement is 80 mm, while in the pull direction these values are nearly 8.3 kN (850 kgf) and 117 mm respectively. More information related to the results obtained at the end of the testing of Frame#3 can be found in Appendix F.

The failures occurred at the nailed joints in the form of joint dilatation and nail distortion as well as complete detachment of the timber elements from each other (Figure 93-Figure 94).

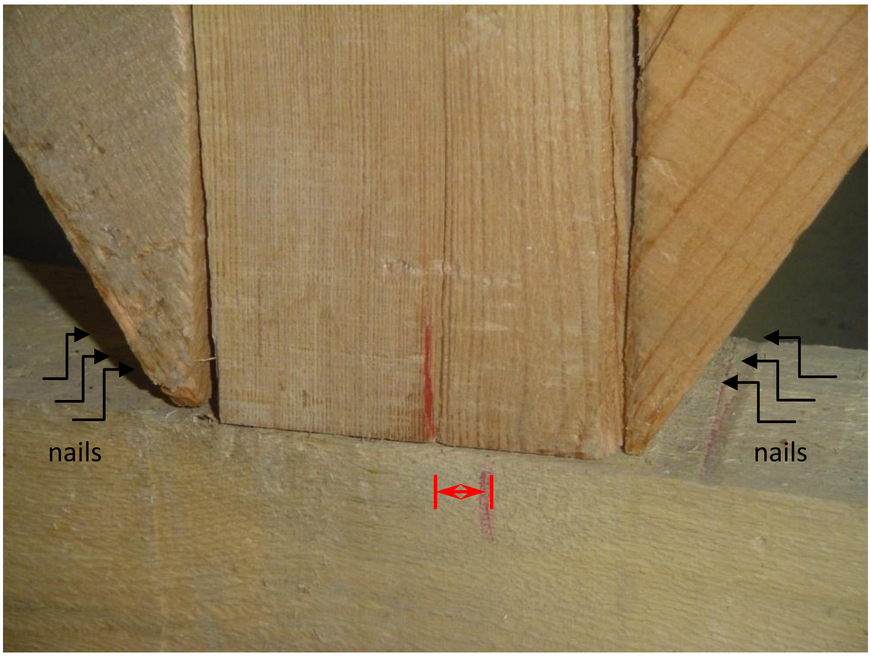

Figure 93: Displacement occurred at the middlemost upright element during Test#3

Figure 94: Elements completely detached from each other

2.8. FRAME#3 WITH ŞAMDOLMA COVERING

In this test, the Frame#3 was tested with covering. Before testing the frame, the failed connections were repaired using the same type and number of nails. Also In this case, *şamdolma* was used as covering technique. In *şamdolma* covering technique, approximately 10 cm wide laths are nailed to the frame in such a way that a gap of several centimeters is left between them, and then the surface is plastered. Plaster was prepared according to traditional methods (Figure 95-Figure 96).

Figure 95: Nailing of laths

Figure 96: Plastering and the final state of the Frame#3 with *şamdolma* covering

In this test, loading was done in the load-controlled manner by increasing the load value 1 kN (approximately 100 kgf) at a time, for successive push and pull cycles, until 8kN (approximately 800 kgf) is reached. After this point, displacement-controlled loading was done with an increment of, first 2.5 and then 5 and finally 10 mm at a time for each cycle (Figure 97).

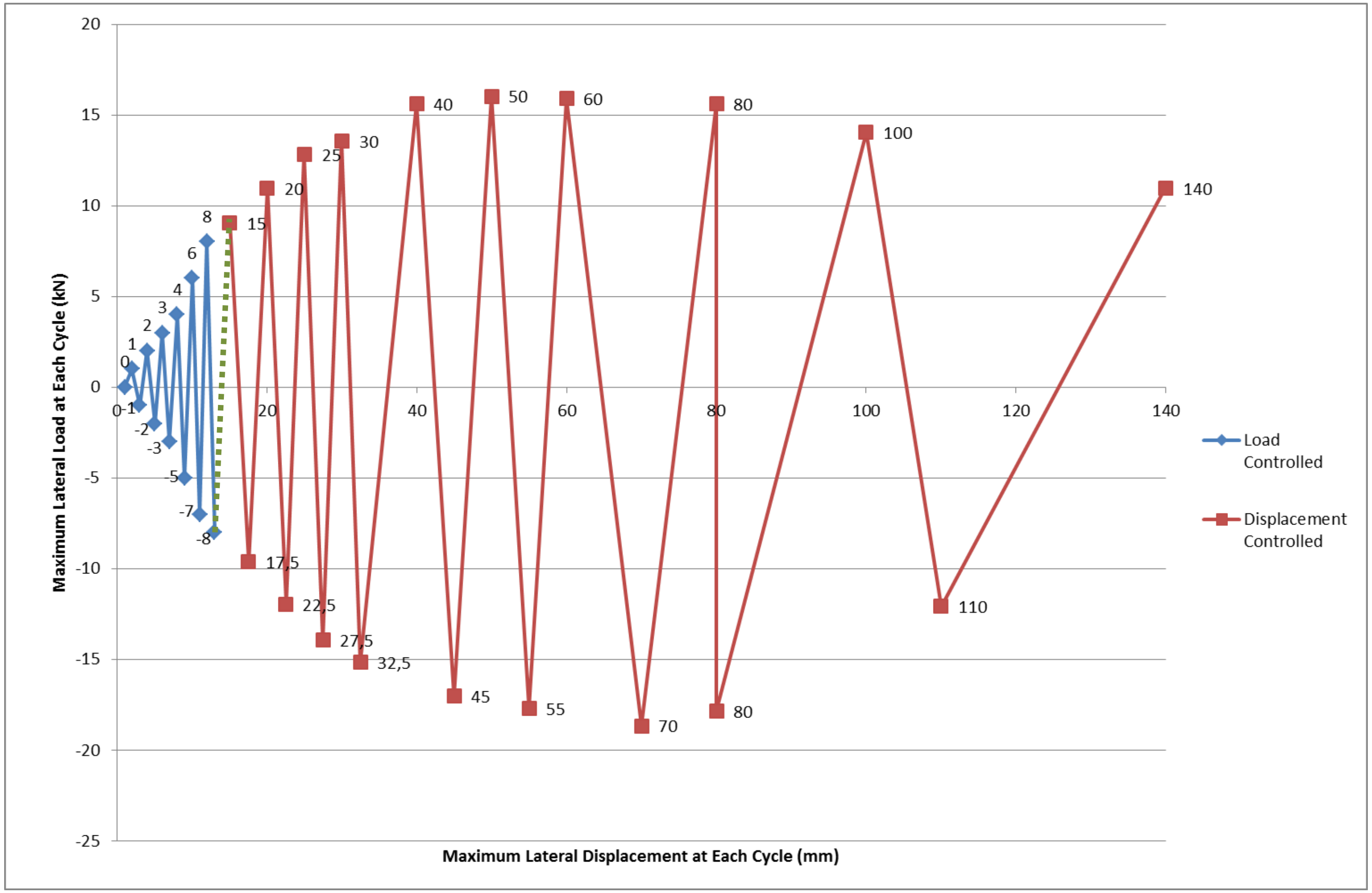

Figure 97: Load controlled and displacement controlled phases of the testing of Frame#3 with *şamdolma* covering (data labels shown are load and displacement values for load controlled and displacement controlled data series, respectively)

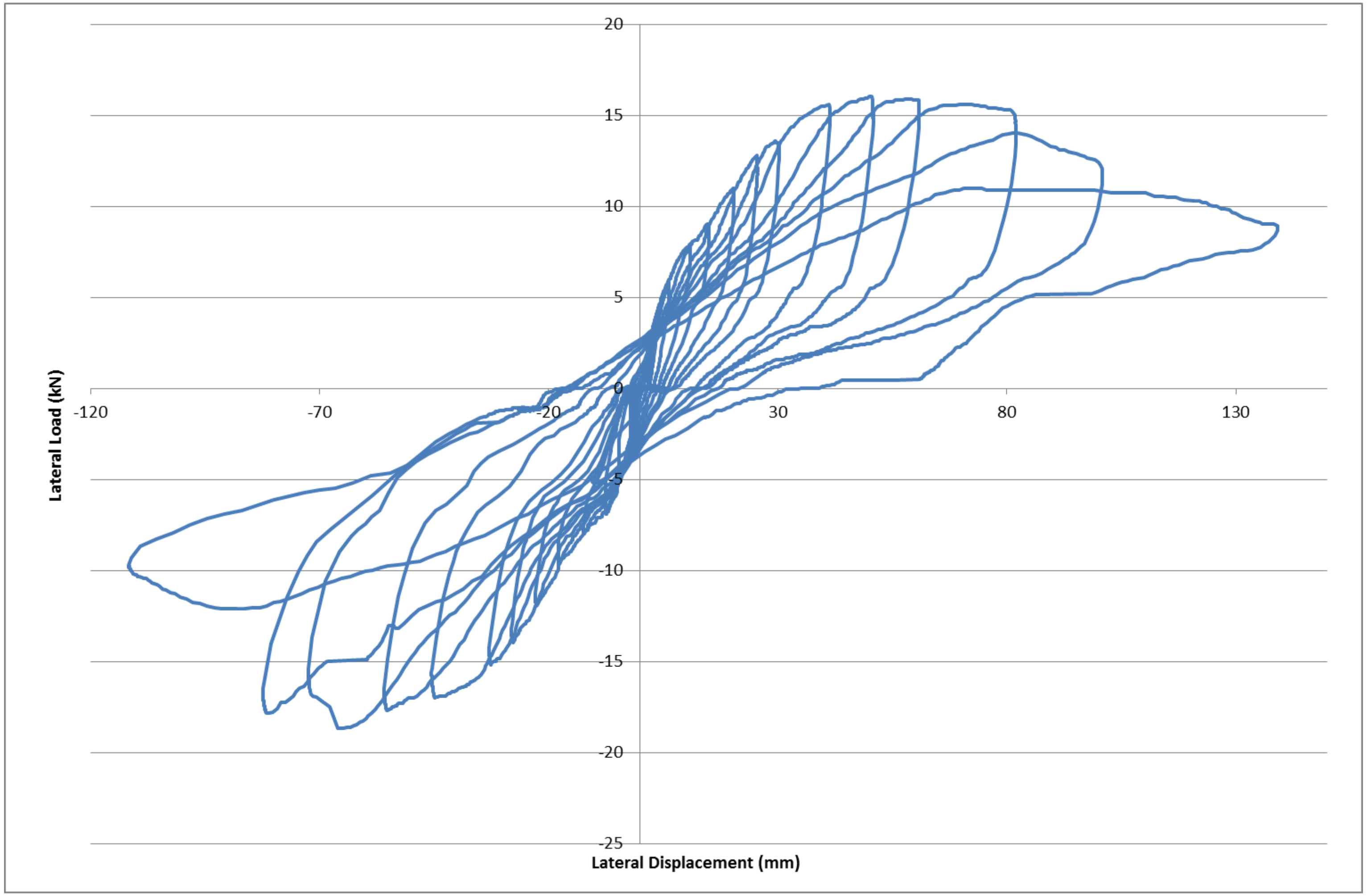

Figure 98: Lateral load – lateral displacement graph of Frame#3 with *şamdolma* covering

In Figure 98, the load-displacement behavior obtained at the end of the experiment can be observed. The experiment was to the point where first indication of strength loss was observed. The maximum lateral load that was observed in the push direction is nearly 16 kN (1634 kgf) and the corresponding lateral displacement is 139 mm, while in the pull direction these values are approximately 18.7 kN (1902 kgf) and 112 mm, respectively. Again, in the case of testing of Frame#3 with *şamdolma* covering, high dilatations in connections were observed (Figure 99). More information related to the results obtained at the end of the testing of Frame#2 with adobe infill can be found in Appendix G.

Figure 99: Dilatation at the frame bottom

2.9. FRAME#4

The testing of Frame#4 was carried out with a 325 cm x 310 cm (H x L) sized fir frame, having two window openings. The frame is actually the same with the frame tested in the first experiment in terms of geometrical configuration; however the wood type is different. The Frame#1 was made of yellow pine, while Frame#4 was made of fir (Figure 100-Figure 101).

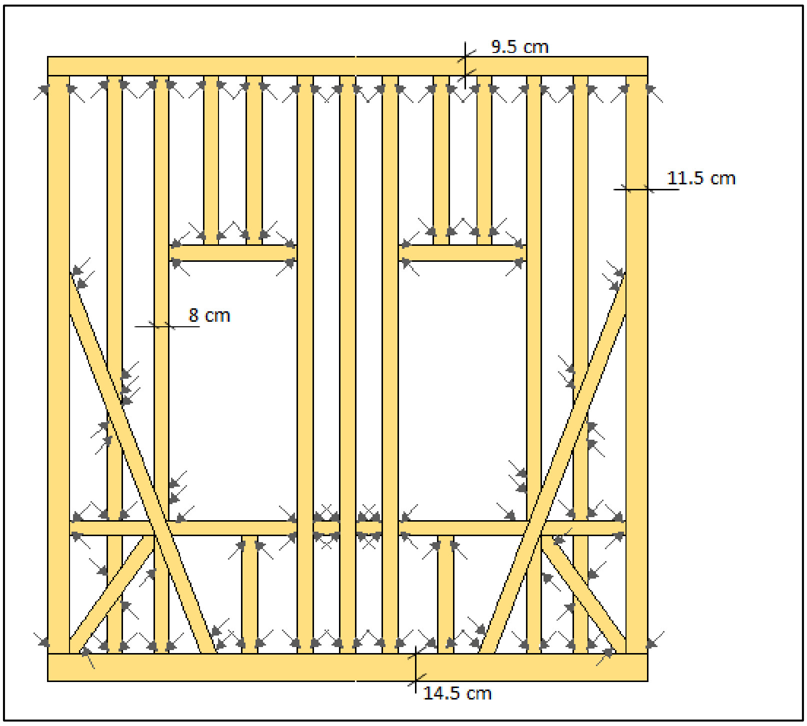

Figure 100: Drawing of Frame#4 (arrows indicate the nails at each connection)

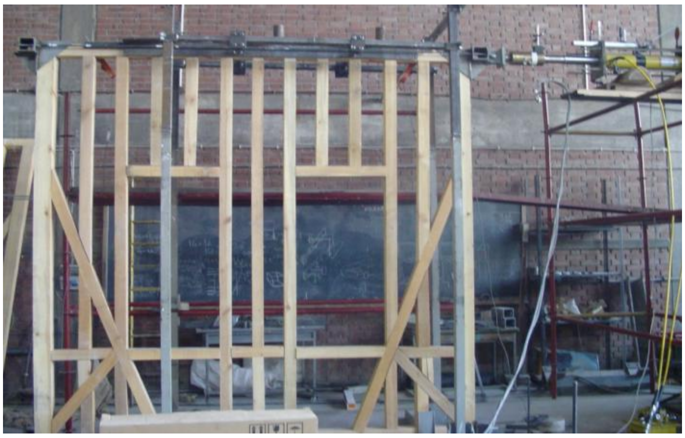

Figure 101: Forth frame to be tested

In the testing of Frame#4, loading was carried out in the same manner as testing of Frame#1, since their geometrical configuration are the same. Therefore, just like the testing of Frame#1, also in this one until 4 kN (approximately 400 kgf) is reached, loading was done in the load controlled manner by increasing the load value 1 kN (approximately 100 kgf) at a time, for successive push and pull cycles. After this point, displacement controlled loading was done with an increment of 10 mm at a time for each cycle (Figure 102).

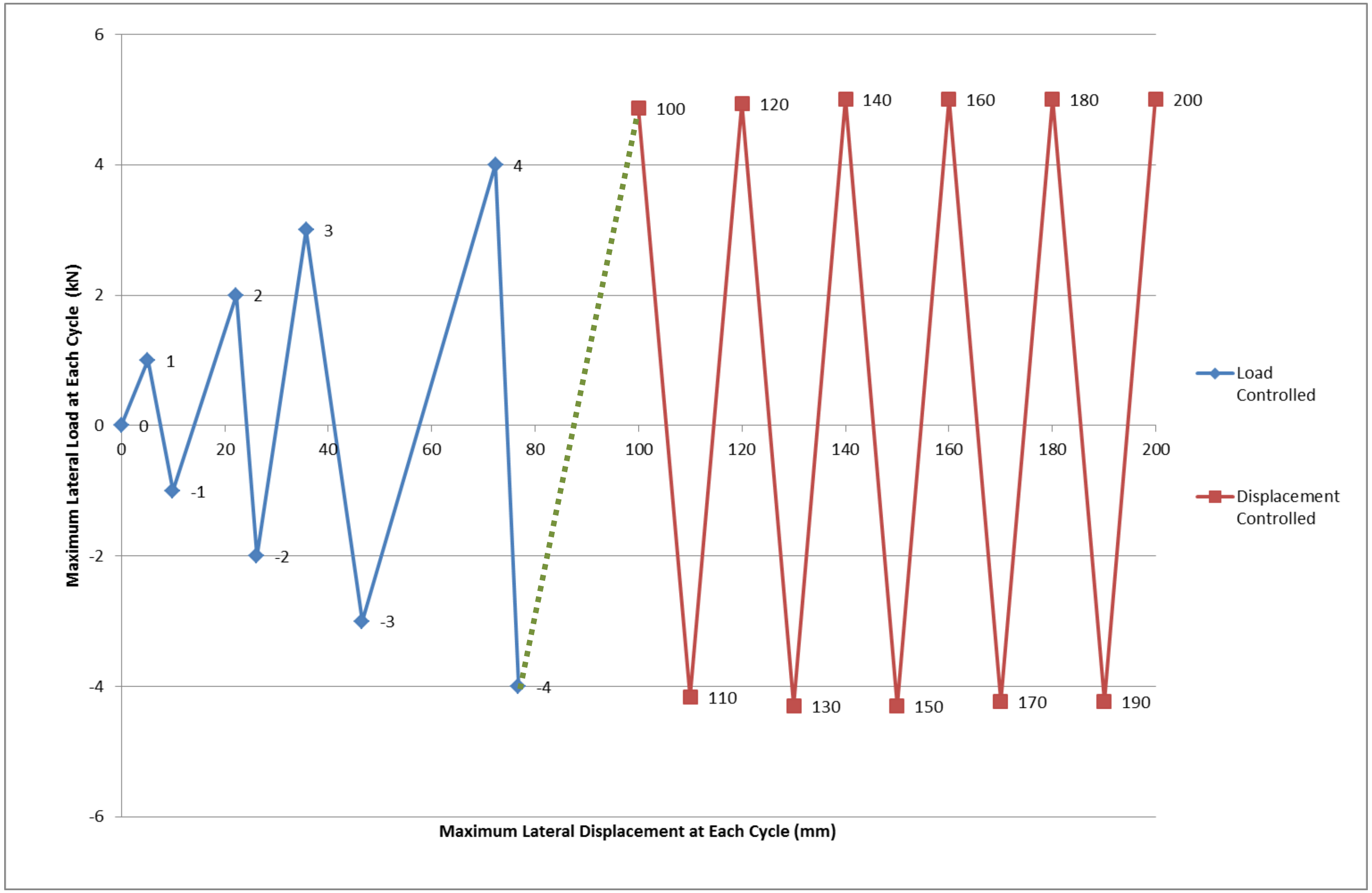

Figure 102: Load controlled and displacement controlled phases of the experiment for Test#4 (data labels shown are load and displacement values for load controlled and displacement controlled data series, respectively)

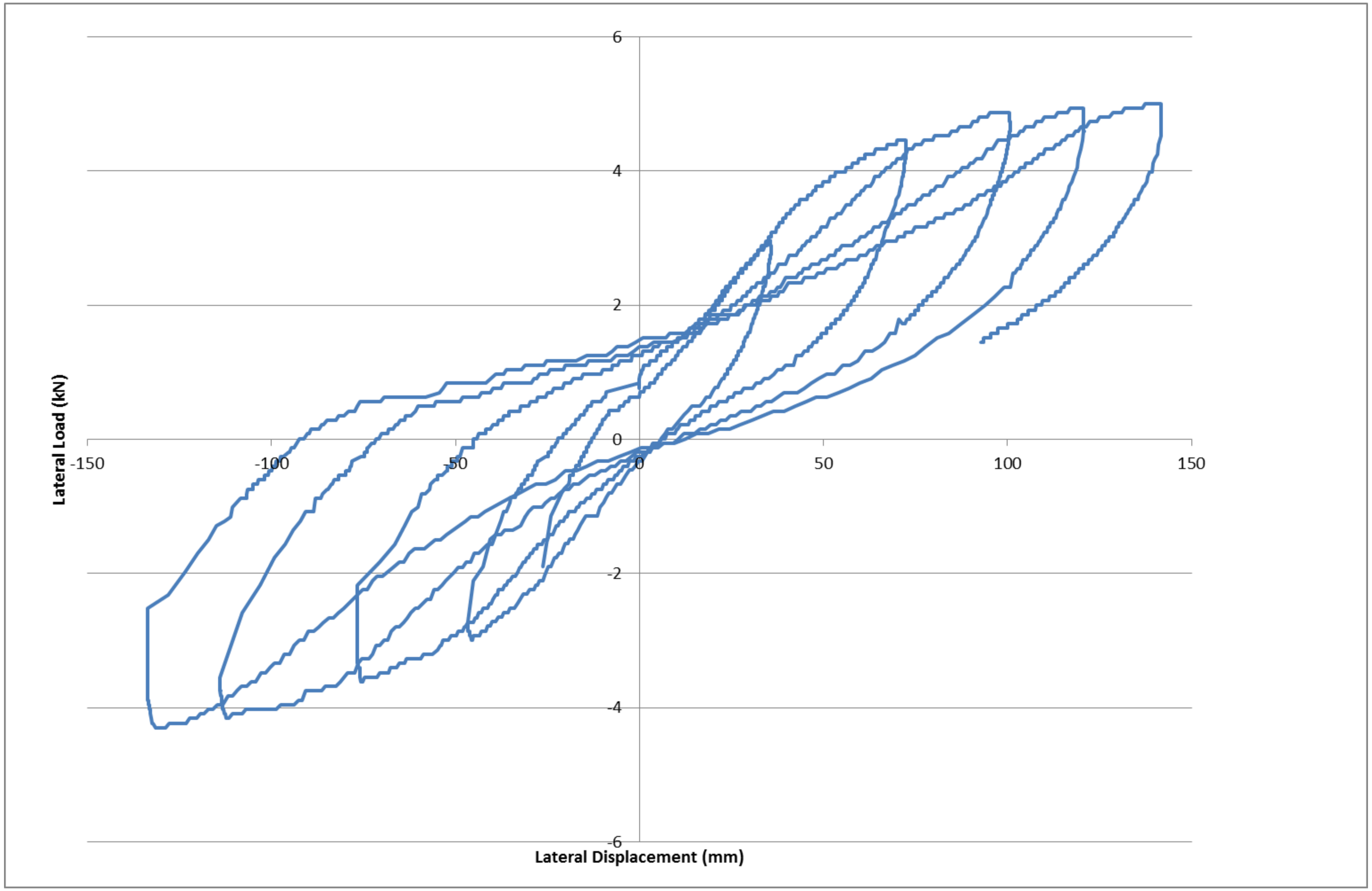

Figure 103: Lateral load – lateral displacement graph of Test#4

In Figure 103, the load-displacement behavior obtained at the end of the experiment can be observed. The experiment was to the point where first indication of strength loss was observed. The test was terminated before the frame was totally damaged since the same frame was planned to be used with infill/covering. The maximum lateral load that was observed in the push direction is about 5 kN (510 kgf) and the corresponding lateral displacement is 200 mm, while in the pull direction these values are 4.3 kN (438 kgf) and 150 mm respectively. For more information related to the results obtained at the end of the testing of Frame #4, please refer to Appendix H.

The failures occurred at the nailed joints in the form of joint dilatation and nail distortion as well as complete detachment of the timber elements from each other (Figure 104-Figure 105).

Figure 104: Permanently dislocated nails during Test#4

Figure 105: Details of dislocated connections observed during the testing of Frame#4

2.10. FRAME#4 WITH BRICK INFILL

In this test, the Frame#4 was tested with infill. Before testing the frame, the failed connections were repaired using the same type and number of nails (Figure 106-Figure 109). For infill, solid bricks, gathered from demolished historic houses, which are 21x10x6 cm in size, were used. Mortar and plaster were prepared according to traditional methods.

Figure 106: Solid bricks used for infill

Figure 107: Infilling process

Figure 108: Plastering of Frame#4 with brick infill

Figure 109: The final state of the Frame#4 with brick infill

In this test, first of all 3 kN (approximately 300 kgf) was applied in the pull direction. Then, 3 kN (approximately 300 kgf) is reached in the push direction with 1 kN (approximately 100 kgf) increment in each cycle. Next, 1 kN (approximately 100 kgf) increment was applied in both directions until 5 kN (approximately 500 kgf) is reached. In the displacement controlled phase, on the other hand, 180 mm was reached first with 10 mm, then with 20 mm increments (Figure 110).

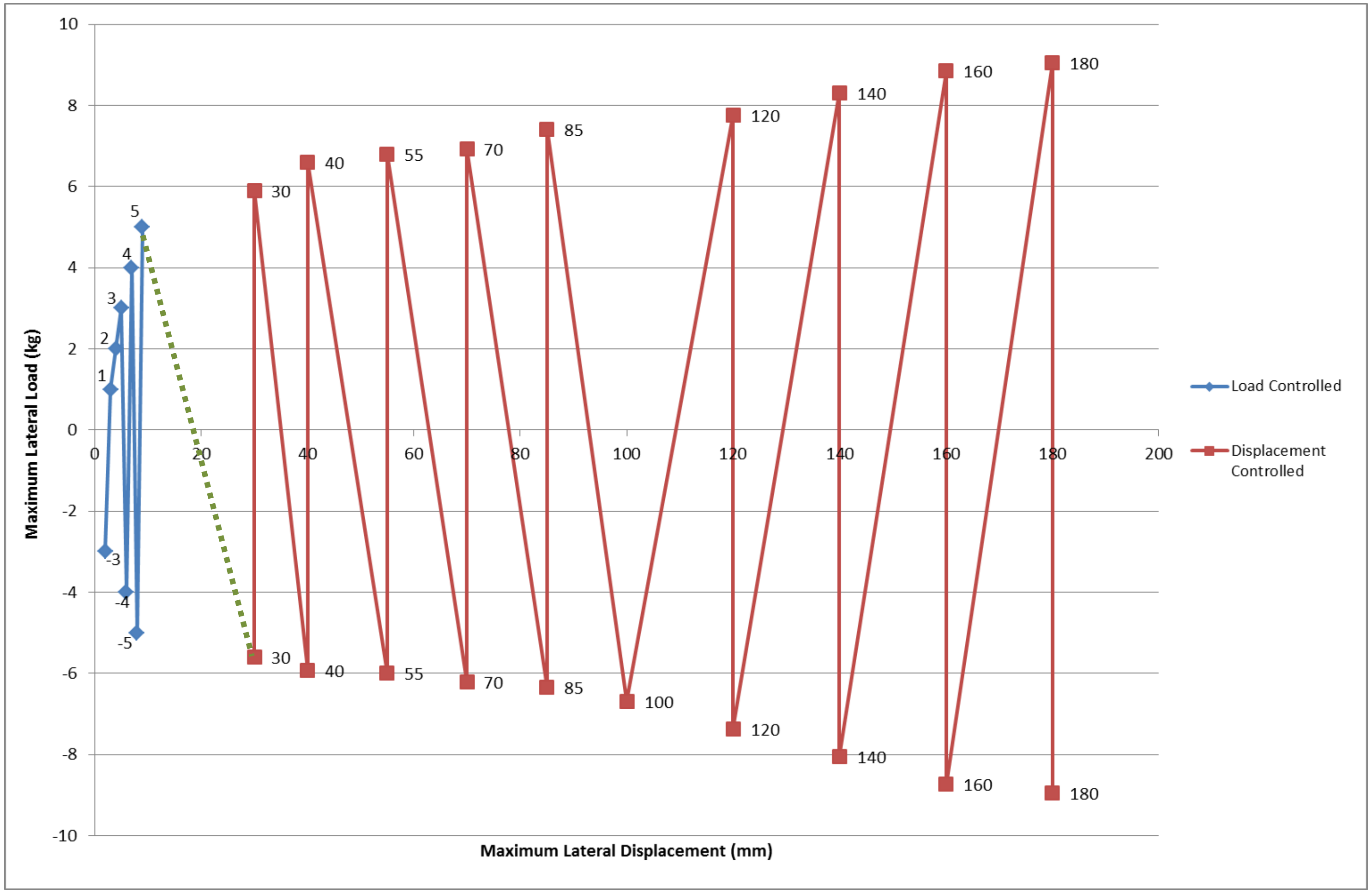

Figure 110: Load controlled and displacement controlled phases of the experiment for the testing of Frame#4 with brick infill (data labels shown are load and displacement values for load controlled and displacement controlled data series, respectively)

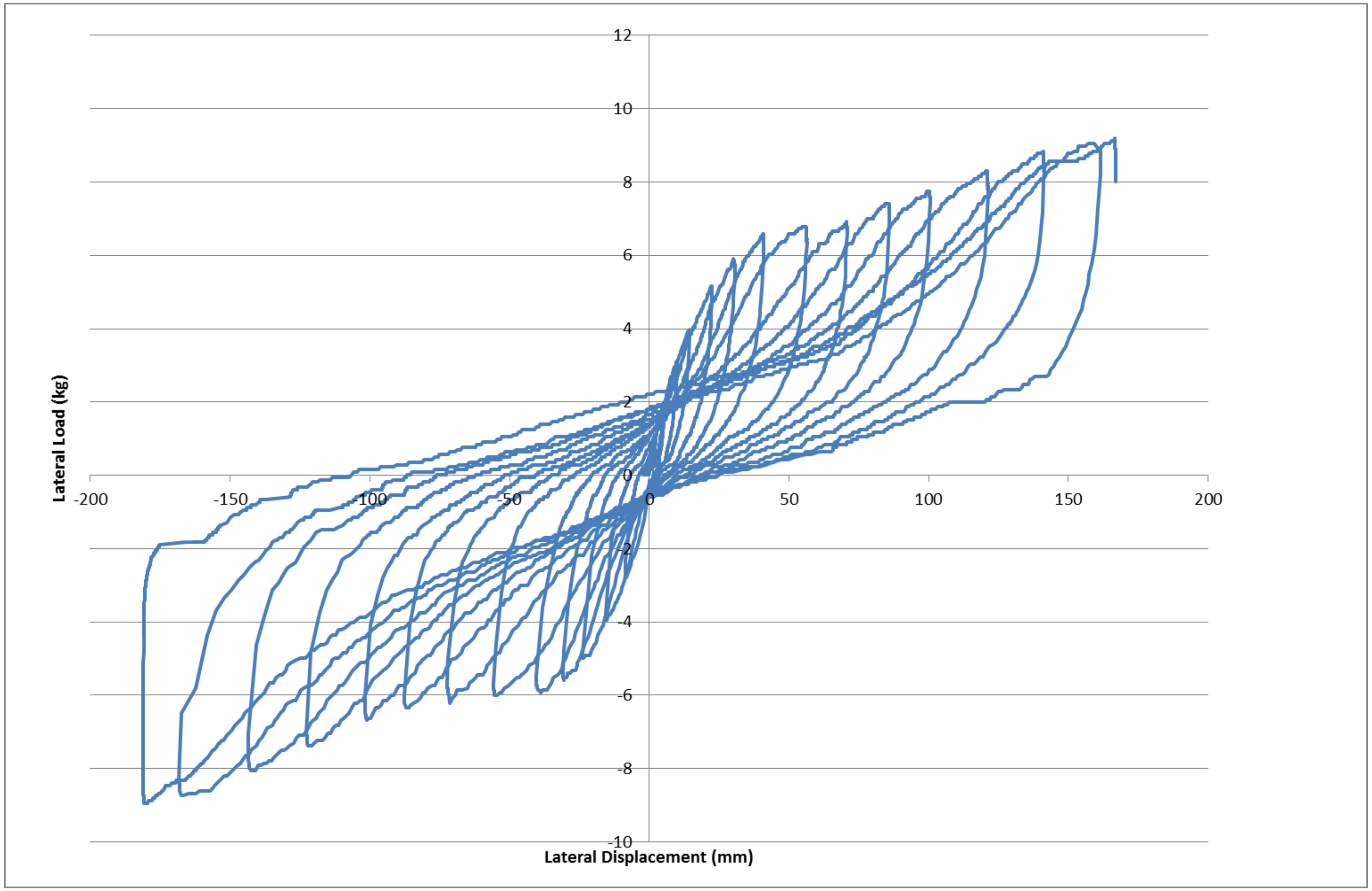

Figure 111: Lateral load – lateral displacement graph of Frame#4 with brick infill

The resulting lateral load- lateral displacement relation is shown in Figure 111. The maximum lateral load that was observed in the push direction is 9.2 kN (936 kgf) and the corresponding lateral displacement is 166 mm, while in the pull direction these values are 8.9 kN (911 kgf) and 181 respectively. For more information related to the results obtained at the end of the testing of Frame#4 with brick infill, please refer to Appendix I.

Also in the testing of Frame#4 with brick infill, connections failed in the form of permanent openings (Figure 112-Figure 113).

Figure 112: Examples to connection failure

Figure 113: Frame#4 with brick infill after the test

2.11. FRAME#5

The testing of Frame#5 was carried out with a 330 cm x 370 cm (H x L) sized yellow pine frame, having three window openings, each of which is 116 cm x 63 cm in size (Figure 114-Figure 115).

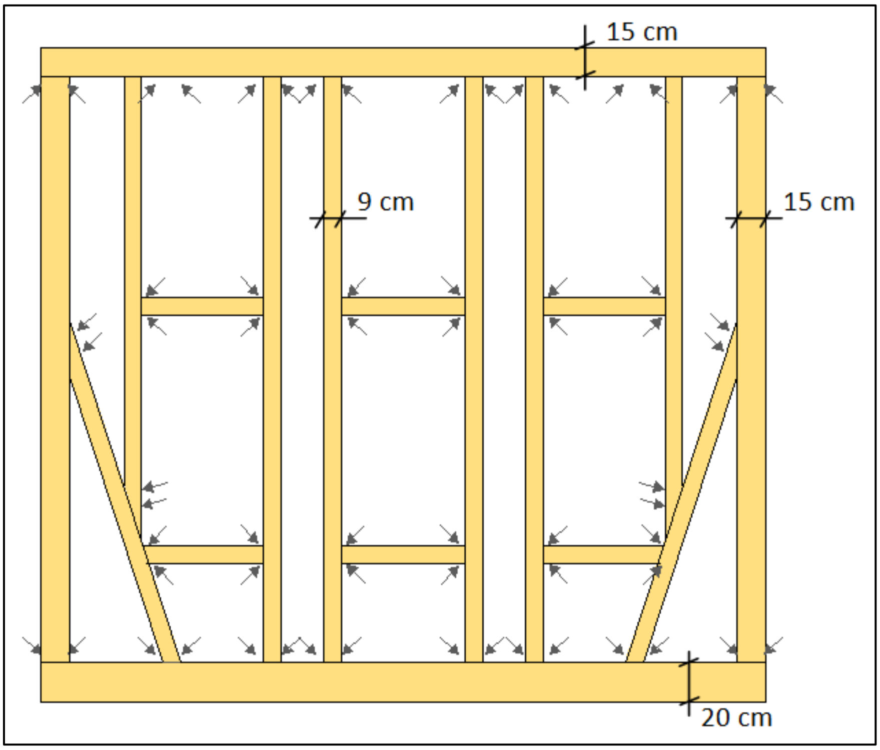

Figure 114: Drawing of Frame#5 (arrows indicate the nails at each connection)

Figure 115: Frame#5

In this test, right after 1 kN (approximately 100 kgf) is reached, loading was started to be done in the displacement controlled manner with an increment first of 10 mm at a time for each pair of cycles in the same direction and then 10 mm at a time for each cycle as can be seen in Figure 116.

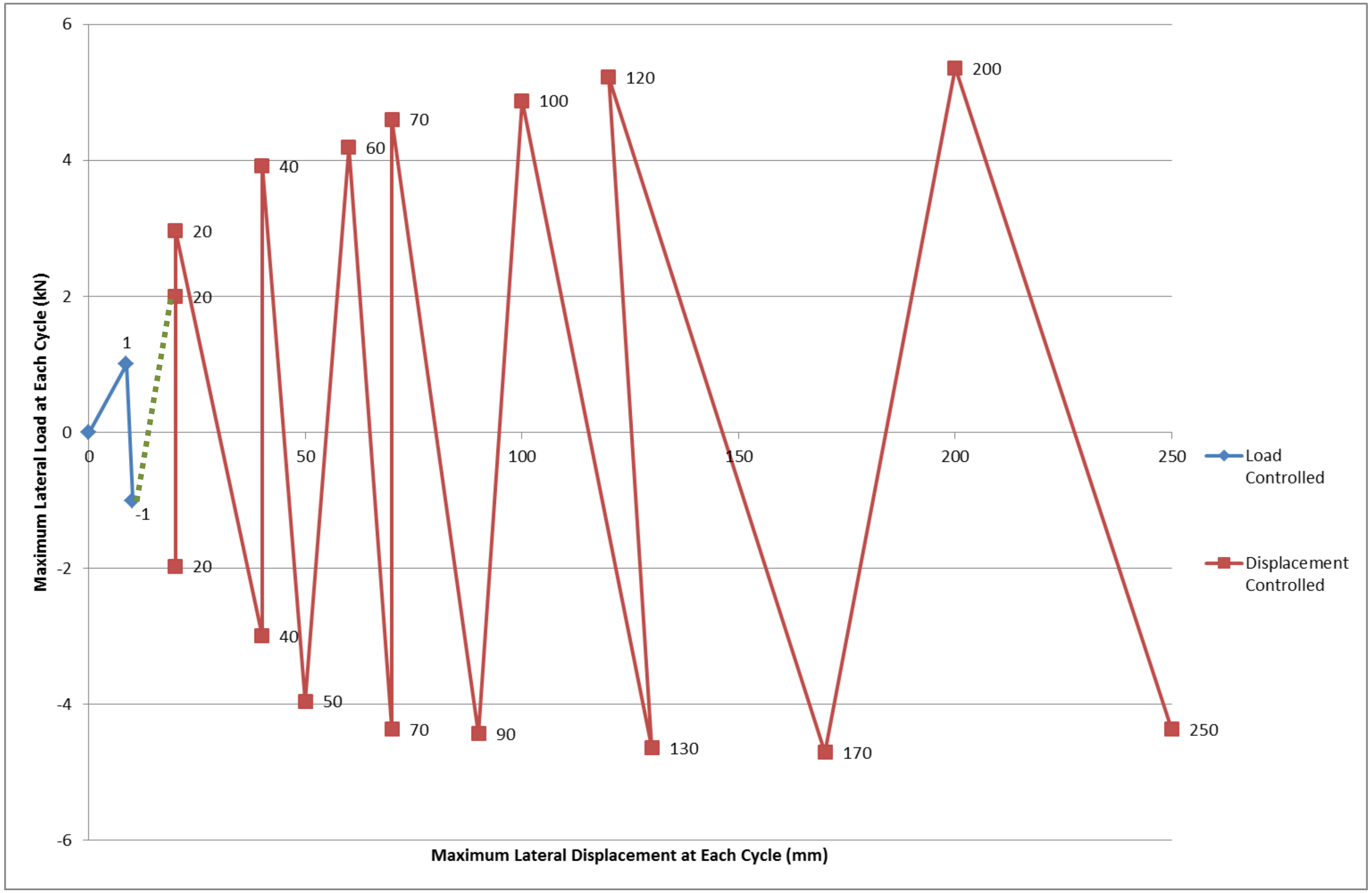

Figure 116: Load controlled and displacement controlled phases of the testing of Frame#5 (data labels shown are load and displacement values for load controlled and displacement controlled data series, respectively)

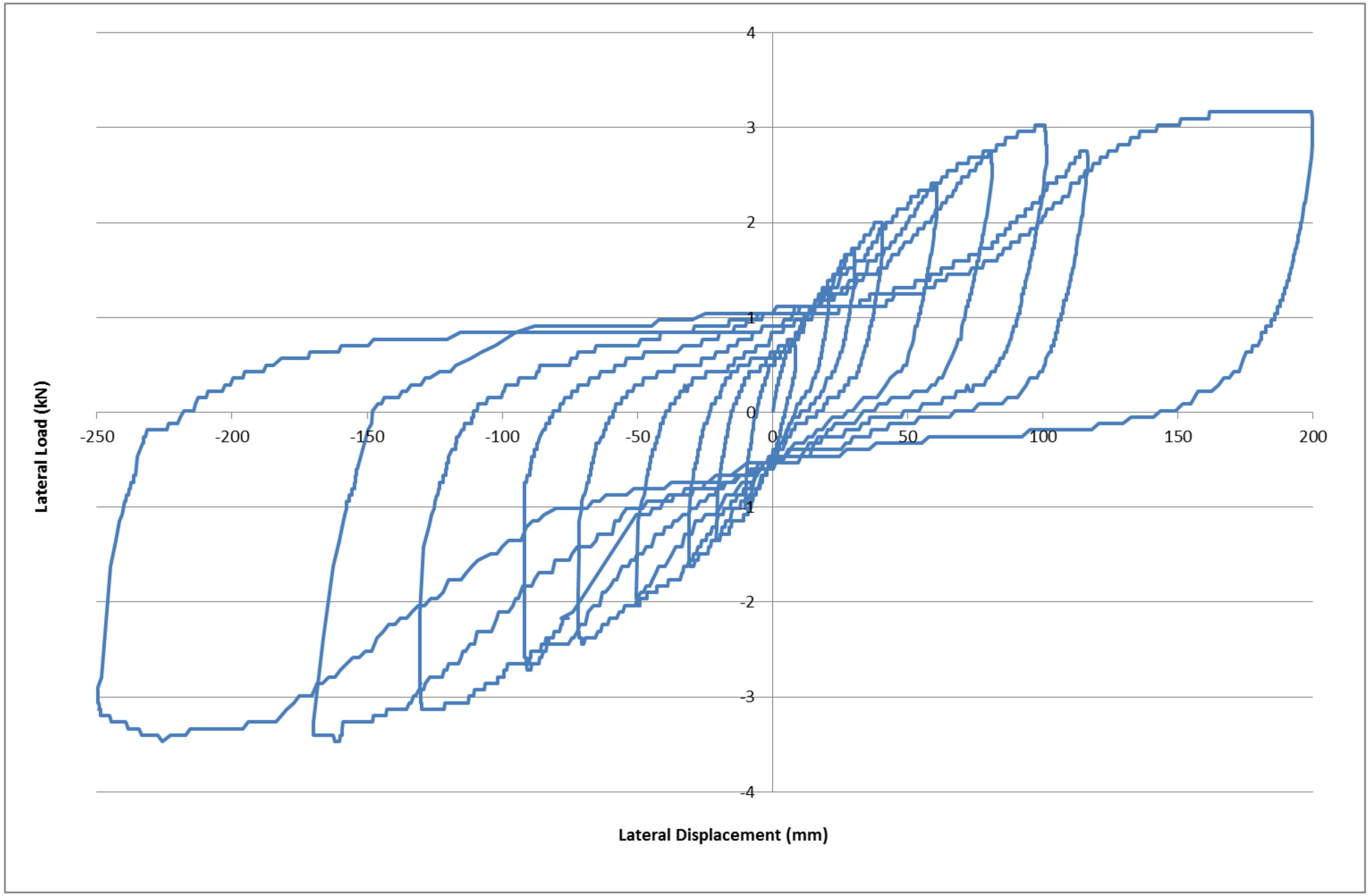

Figure 117: Lateral load – lateral displacement graph of Frame#5

The load-displacement behavior obtained at the end of the test can be seen in Figure 117. The experiment was to the point where first indication of strength loss was observed. The test was terminated before the frame was totally damaged since the same frame was planned to be used with infill/covering. The maximum lateral load that was observed in the push direction is around 5.4 kN (552 kgf) and the corresponding lateral displacement is 218 mm, while in the pull direction these values are 4.7 kN (479 kgf) and 170 mm, respectively. For more information related to the results obtained at the end of the testing of Frame#5, refer to Appendix J.

The failures occurred at the nailed joints in the form of joint dilatation and nail distortion as well as complete detachment of the timber elements from each other (Figure 118).

Figure 118: Examples to joint dilatation

2.12. FRAME#5 WITH BAĞDADİ COVERING

In this test, the Frame#5 was tested with *bağdadi* covering. Before testing the frame, the failed connections were repaired using the same type and number of nails. In *bağdadi* covering technique, 3-4 cm wide laths are nailed to the frame so as to leave a gap of several centimeters between each successive lath (Figure 119). Then, the surface is plastered. Plaster was prepared according to traditional methods.

Figure 119: *Bağdadi* covering

In this test, loading was done in the load controlled manner by increasing the load value 1 kN (approximately 100 kgf) at a time, for successive push and pull cycles, until 8 kN (approximately 800 kgf) is reached. After this point, displacement controlled loading was done with an increment of 10 mm at a time for each cycle (Figure 120).

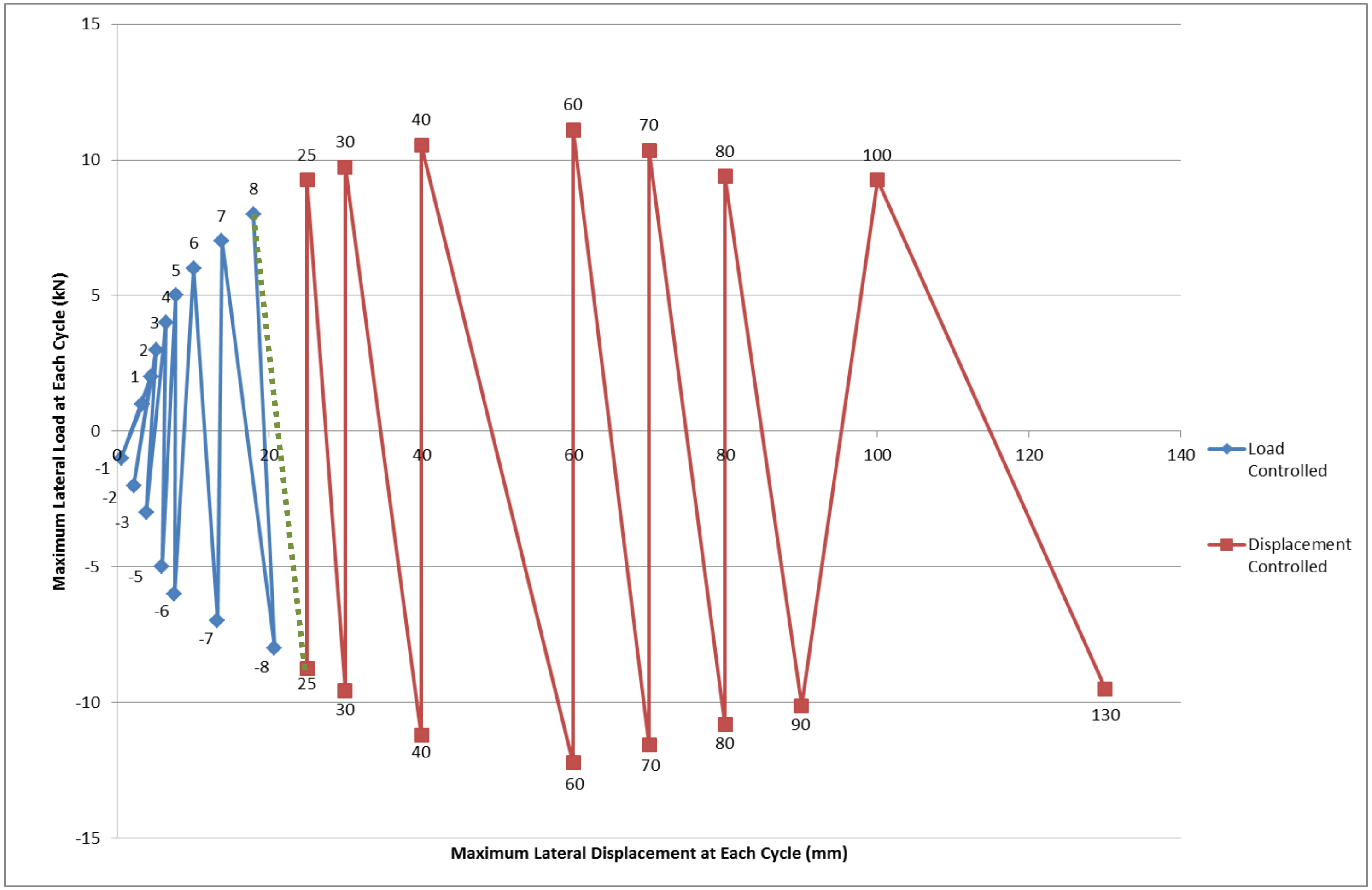

Figure 120: Load controlled and displacement controlled phases of the testing of Frame#5 with *bağdadi* covering (data labels shown are load and displacement values for load controlled and displacement controlled data series, respectively)

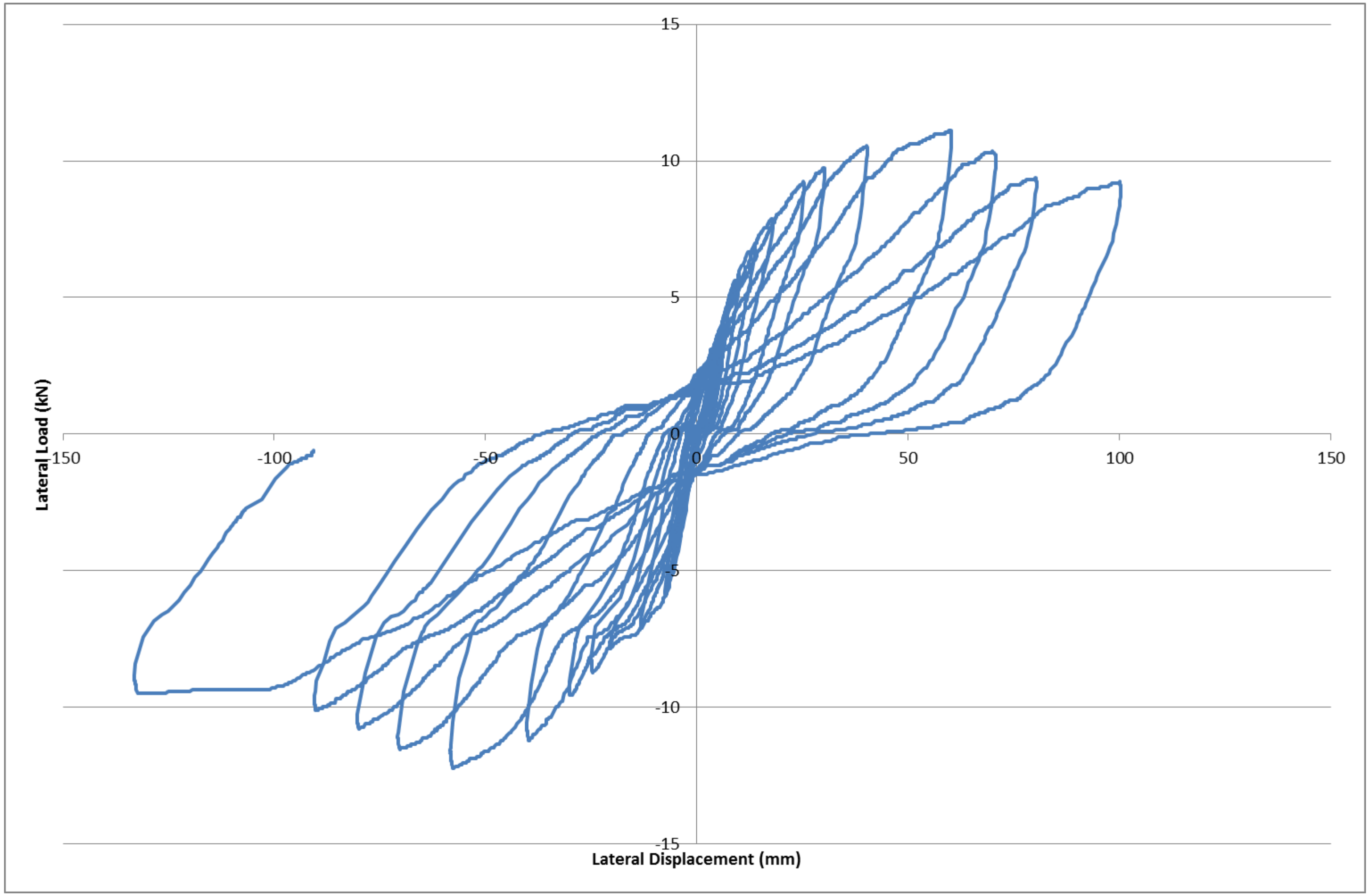

Figure 121: Lateral load – lateral displacement graph of Frame#5 with *bağdadi* covering

In Figure 121, top resulting top lateral load - displacement relation obtained at the end of the test is shown. The maximum lateral load that is observed in the push direction is 11 kN (1130 kgf) and the corresponding lateral displacement is 100 mm, while in the pull direction these values are 12.3 kN (1250 kgf) and 133 mm respectively. For more information related to the results obtained at the end of the testing of Frame #5 with *bağdadi* covering, please refer to Appendix K.

The failures occurred at the nailed joints in the form of joint dilatation and nail distortion (Figure 104).

Figure 122: An example to connection dilatations observed in the testing of Frame#5 with *bağdadi* covering

2.13. FRAME#6

The sixth experiment was carried out with a 340 cm x 520 cm (H x L) sized yellow pine frame, having three window openings, each of which 93 cm x 157 cm in size (Figure 123).

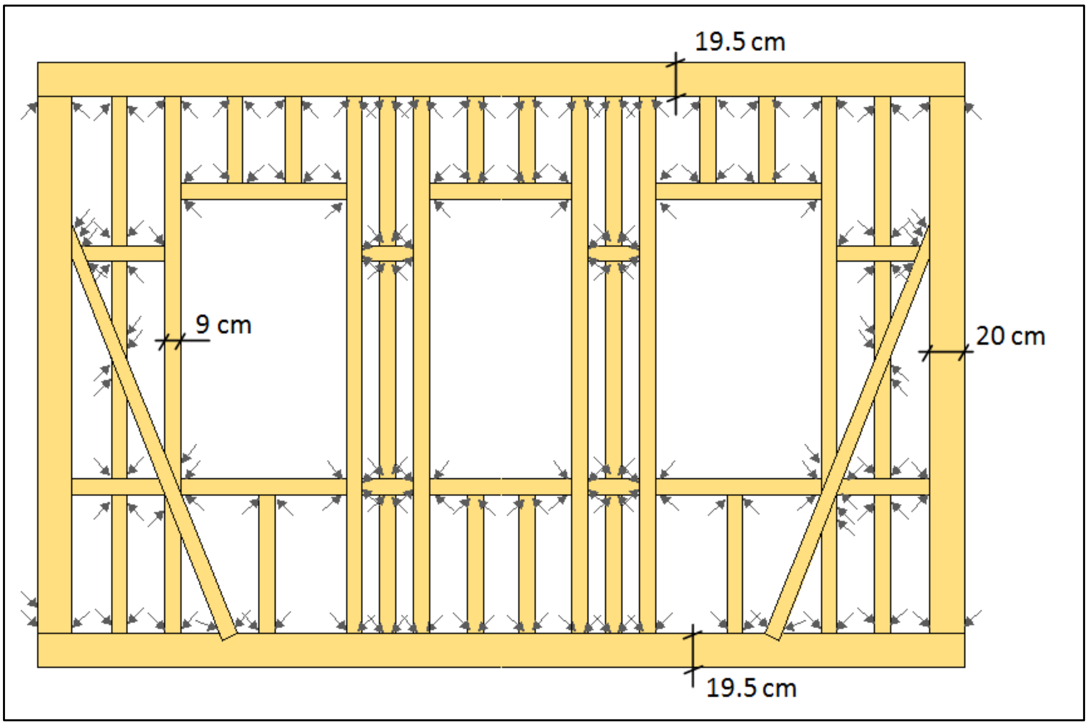

Figure 123: Drawing of Frame#6 (arrows indicate the nails at each connection)

In this test, until 4 kN (approximately 400 kg) is reached, loading was done in the load controlled manner by increasing the load value 1 kN (approximately 100 kg) at a time, for successive push and pull cycles. After this point, displacement controlled loading was done with an increment of 10 mm at a time for each cycle (Figure 124).

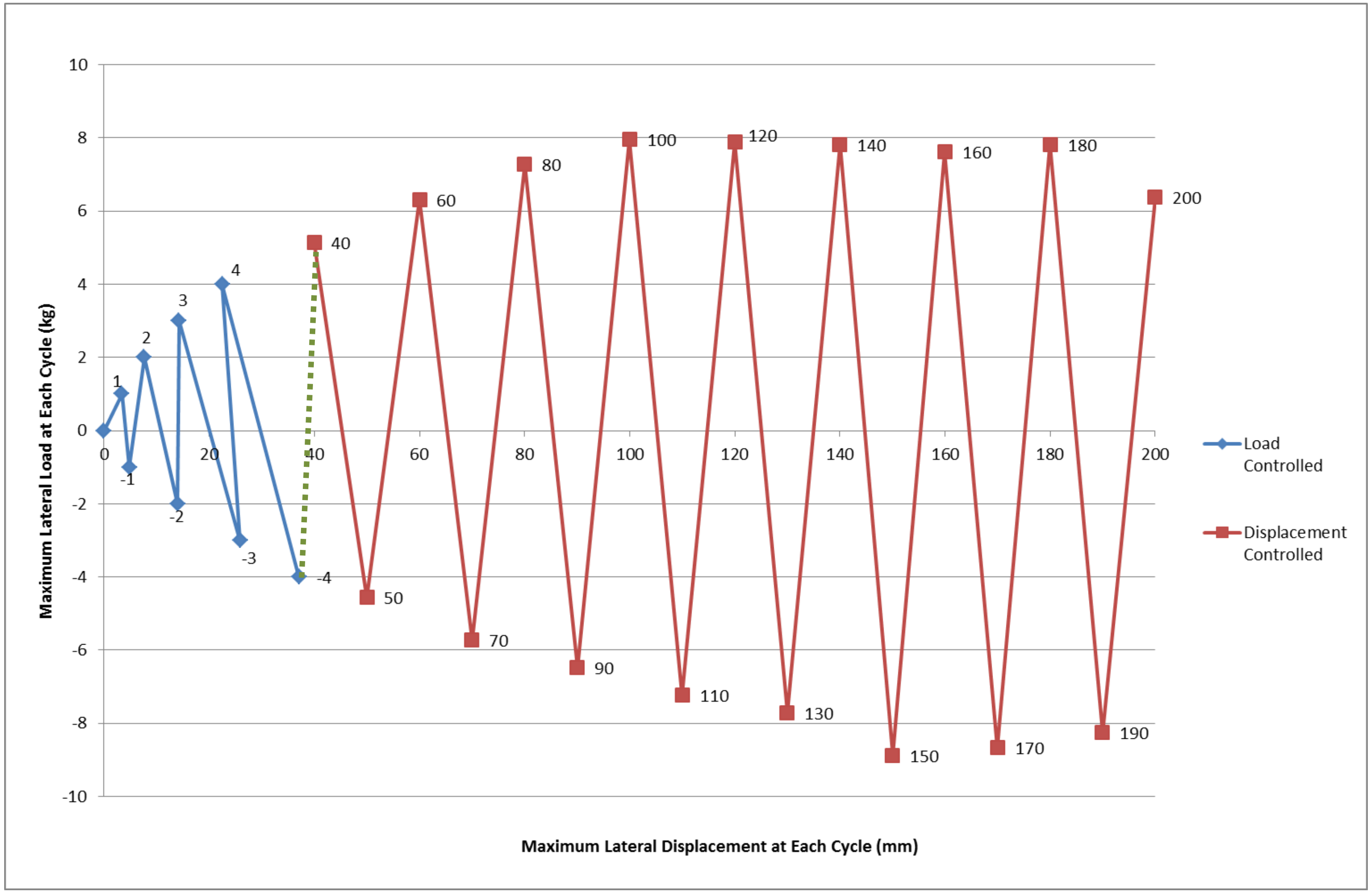

Figure 124: Load controlled and displacement controlled phases of the testing of Frame#6 (data labels shown are load and displacement values for load controlled and displacement controlled data series, respectively)

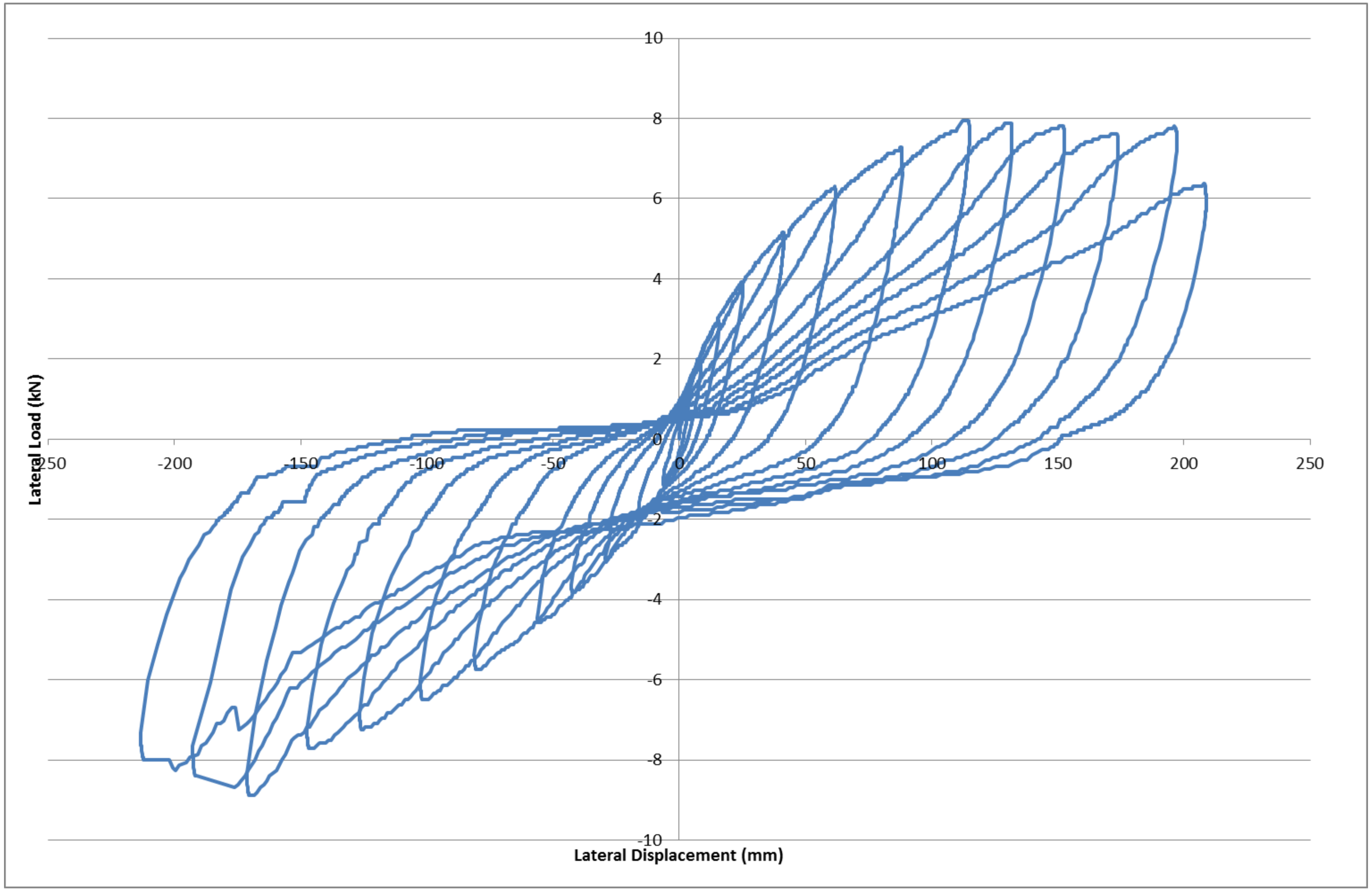

Figure 125: Lateral load – lateral displacement graph of Frame#6

The resulting top lateral load – top lateral displacement graph obtained at the end of testing of Frame#6 is seen in Figure 125. The experiment was to the point where first indication of strength loss was observed. The test was terminated before the frame was totally damaged since the same frame was planned to be used with infill/covering. The maximum lateral load that was observed in the push direction is 7.9 kN (810 kgf) and the corresponding lateral displacement is 208 mm, while in the pull direction these values are 8.9 kN (904 kgf) and 213 mm respectively. For more information related to the results obtained at the end of the testing of Frame #5 with *bağdadi* covering, please refer to Appendix L. Some examples to connection failures are shown in Figure 126.

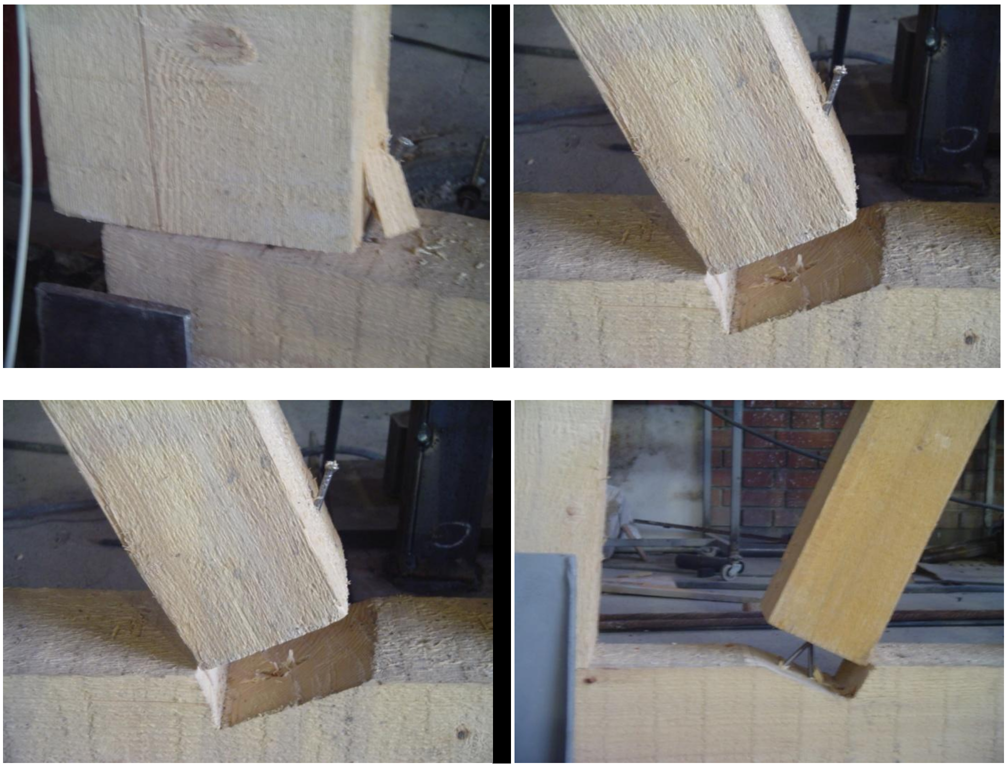

Figure 126: Examples to joint dilatation in Test#6

2.14. FRAME#6 WITH ŞAMDOLMA COVERING

In this test, Frame#6 was tested with covering. Before testing the frame, the failed connections were repaired using the same type and number of nails. In this case, *şamdolma* was used as covering technique (Figure 127-Figure 128). Plaster was prepared according to traditional methods.

Figure 127: Nailing of laths

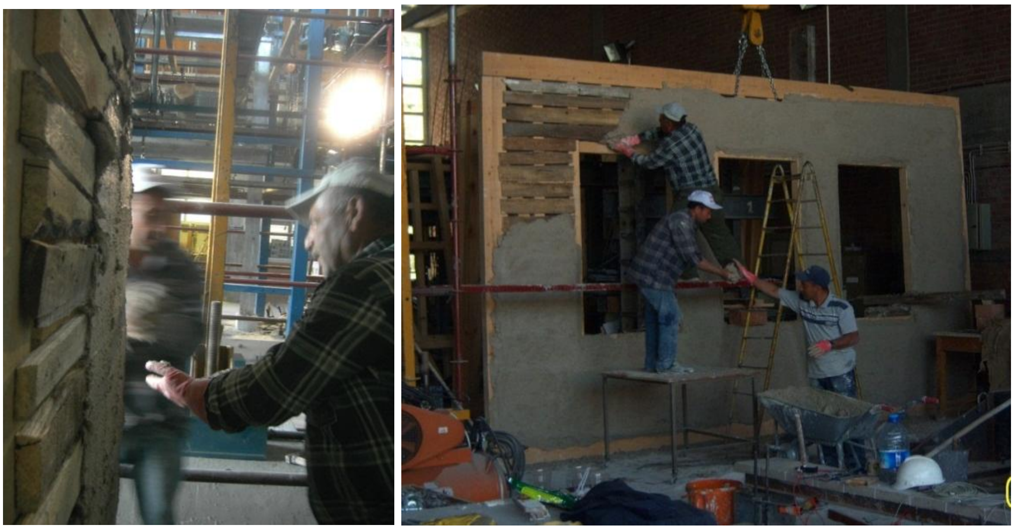

Figure 128: Plastering process

While loading this frame, in the load displacement range, 8 kN (approximately 800 kgf) was reached with 1 kN (approximately 100 kgf) of increment in each cycle. Next, the test was continued by controlling displacement, with 20 mm increment in each cycle.

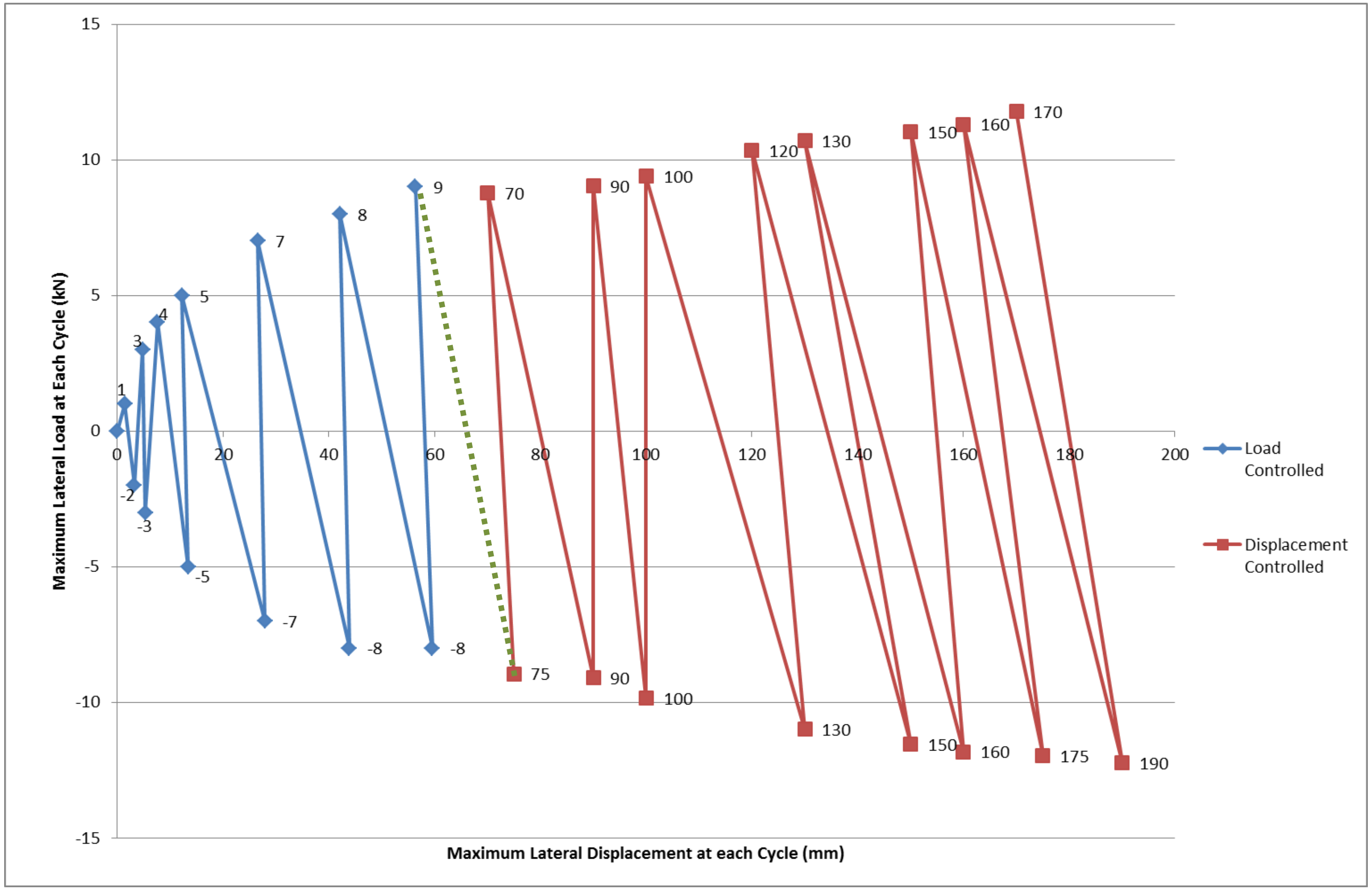

Figure 129: Load controlled and displacement controlled phases of the testing of Frame#6 with *şamdolma* covering (data labels shown are load and displacement values for load controlled and displacement controlled data series, respectively)

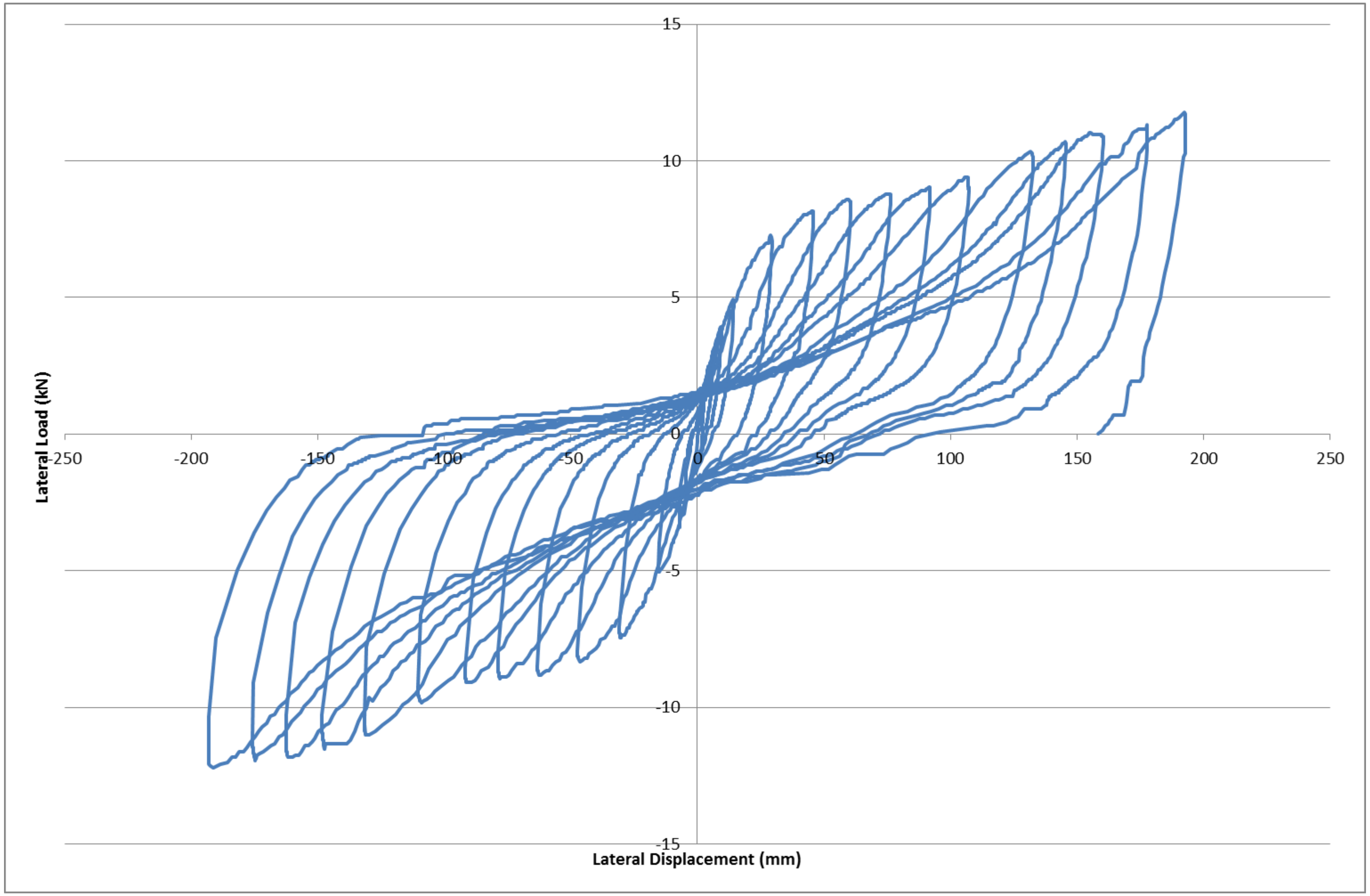

Figure 130: Lateral load – lateral displacement graph of Frame#6 with *şamdolma* covering

The resulting top lateral load - displacement relationship is shown in Figure 130. The maximum lateral load that was observed in the push direction is 11.7 kN (1200 kgf) and the corresponding lateral displacement is 192 mm, while in the pull direction these values are 12.2. kN (1246 kgf) and 193 mm respectively. For more information related to the results obtained at the end of the testing of Frame#6 with *şamdolma* covering, please refer to Appendix M.

After the test, apart from crumbled plaster, also connection failures, similar to the ones observed in the previous tests, were observed (Figure 131).

Figure 131: Frame#6 with infill after the test

2.15. FRAME#7

The seventh frame that was tested is 485 cm x 340 cm (H x L) in size, was constructed from yellow pine and has two window openings, each of which 169 cm x 89.5 cm in size (Figure 132-Figure 133).

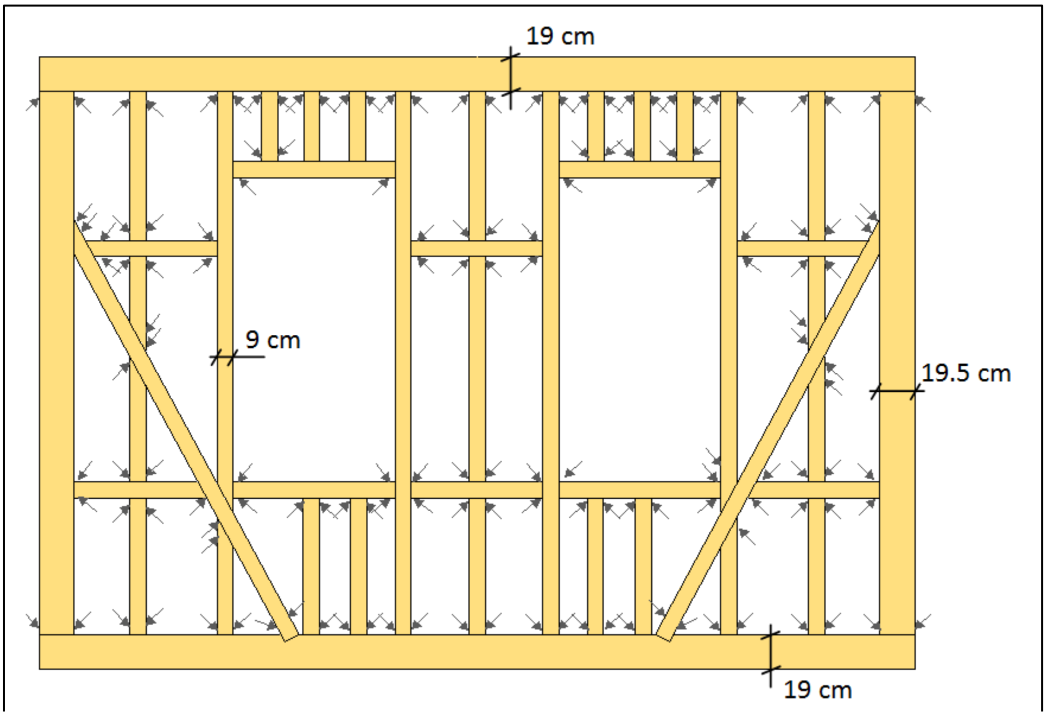

Figure 132: Drawing of Frame#7 (arrows indicate the nails at each connection)

Figure 133: Frame#7

In this test, load was increased 100 kg at each cycle until 4 kN (approximately 400 kgf) is reached. Then, test was continued in a displacement controlled way, by increasing displacement 20 mm each cycle (Figure 134).

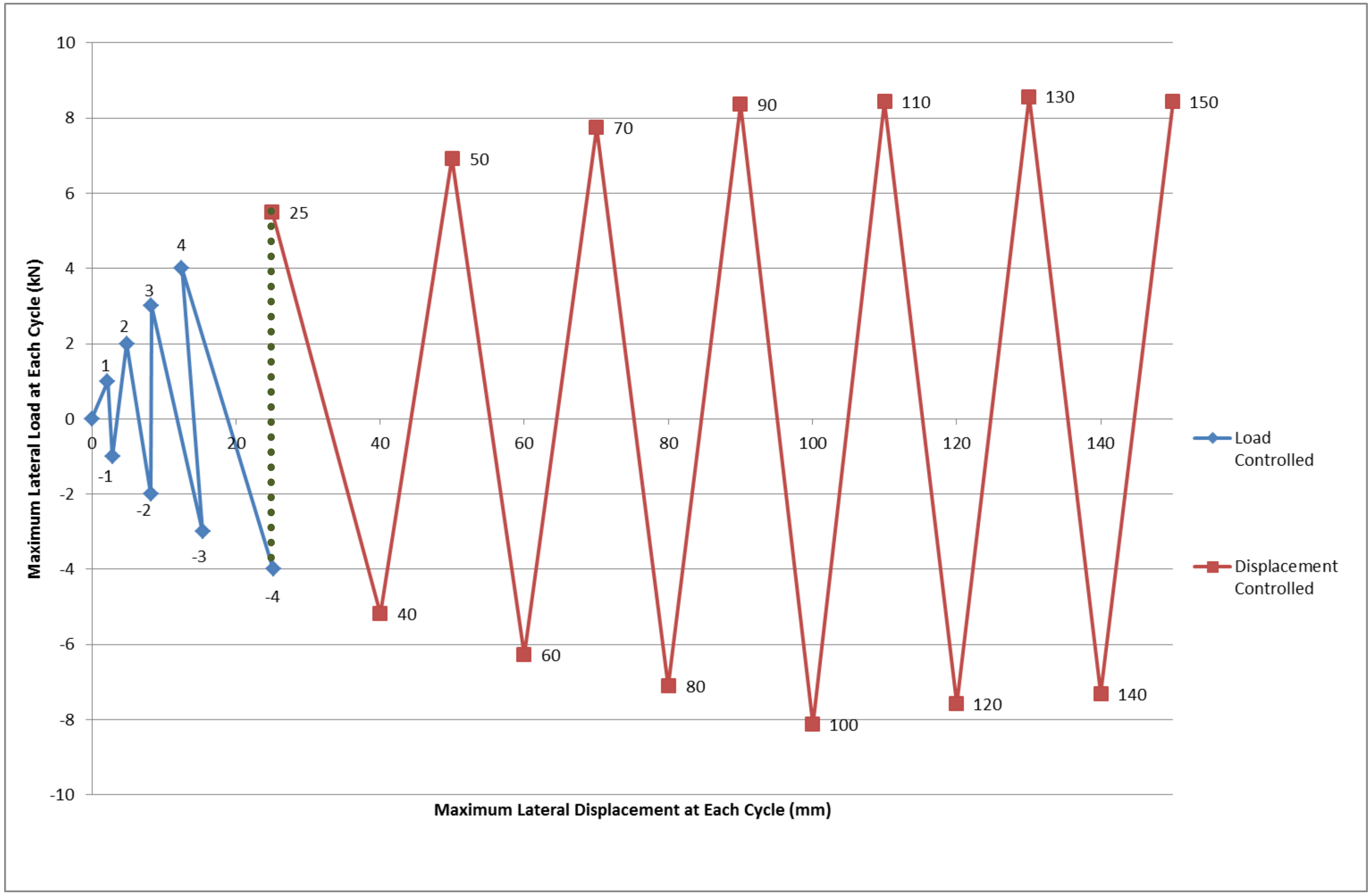

Figure 134: Load controlled and displacement controlled phases of the experiment for the testing of Frame#7 (data labels shown are load and displacement values for load controlled and displacement controlled data series, respectively)

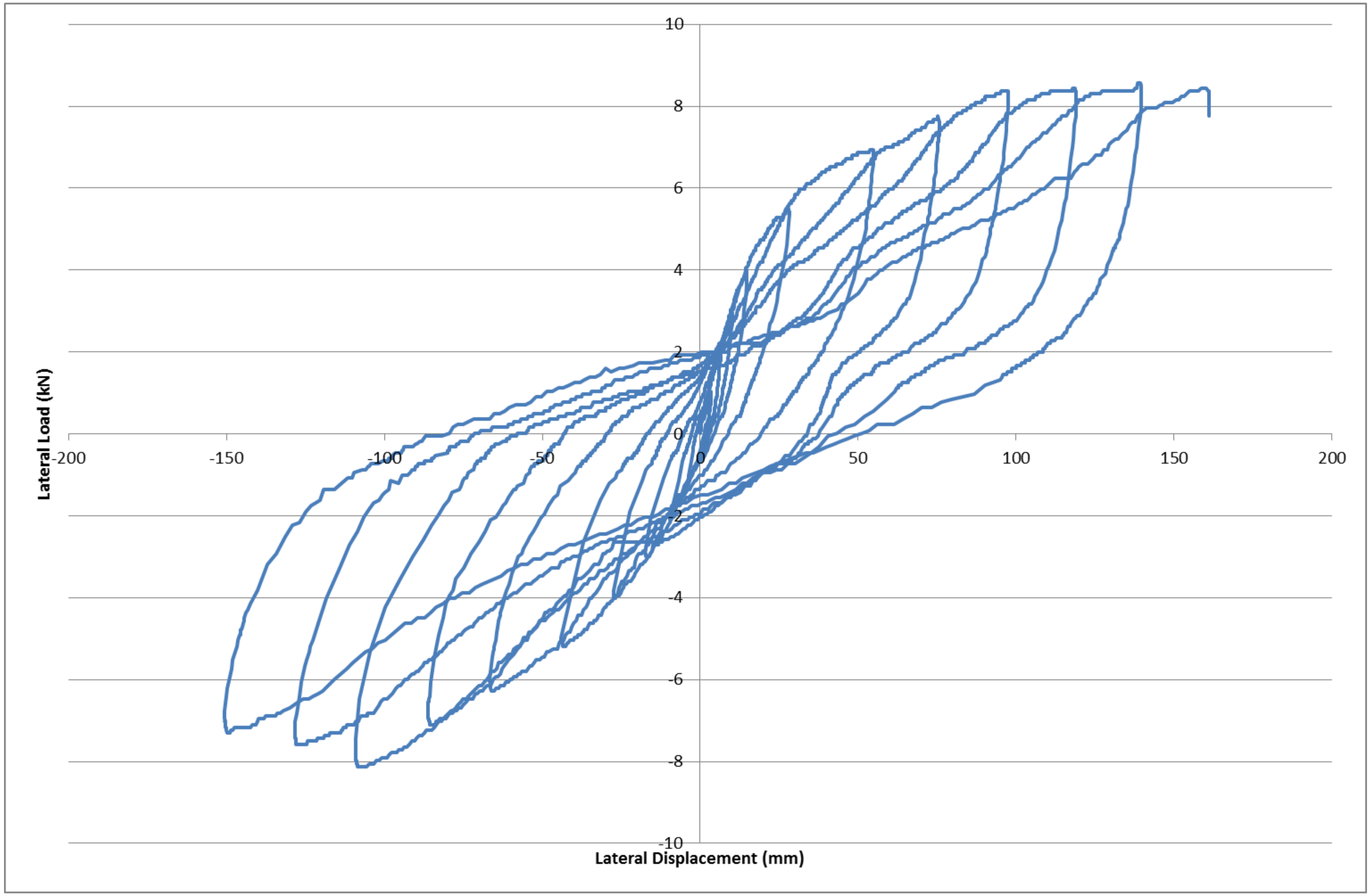

Figure 135: Lateral load – lateral displacement graph of Frame#7

The resulting top lateral load –displacement graph is seen in Figure 135. The experiment was to the point where first indication of strength loss was observed. The test was terminated before the frame was totally damaged since the same frame was planned to be used with infill/covering. The maximum lateral load that is observed in the push direction is 8.6 kN (873 kgf) and the corresponding lateral displacement is 160 mm, while in the pull direction these values are 8.1 kN (830 kgf) and 150 mm respectively. For more information related to the results obtained at the end of the testing of Frame#7, please refer to Appendix N.

Again, in this test, permanent openings were formed at the connections, and nails were buckled (Figure 136).

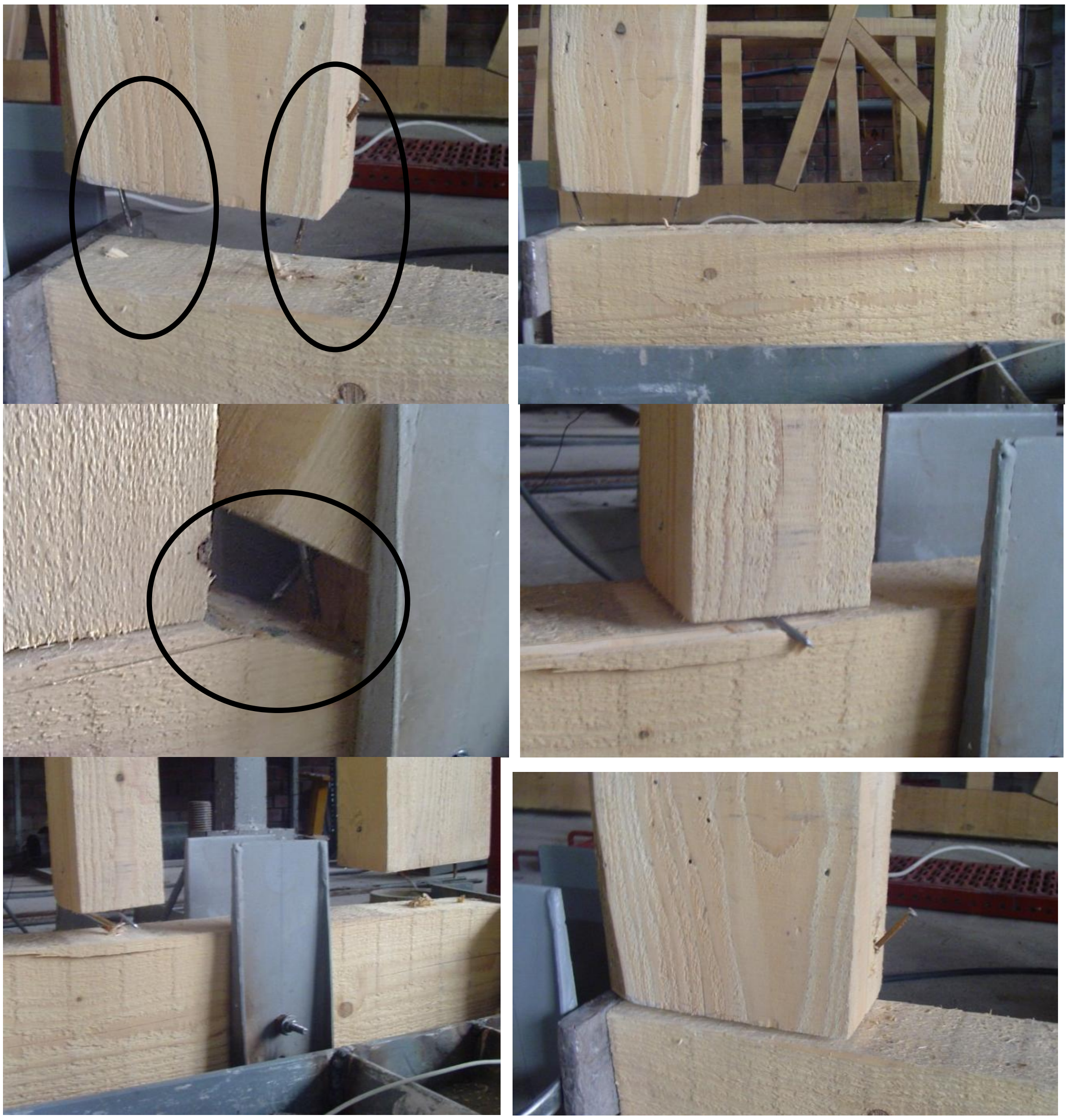

Figure 136: Examples to connection failures observed during Test#7

2.16. FRAME#7 WITH BRICK INFILL

In this test, Frame#7 was tested with infill. Before testing the frame, the failed connections were repaired using the same type and number of nails. For infill, solid bricks gathered from demolished historic houses were used. Mortar and plaster were prepared according to traditional methods (Figure 137-Figure 139).

Figure 137: Preparation of mortar for the infill

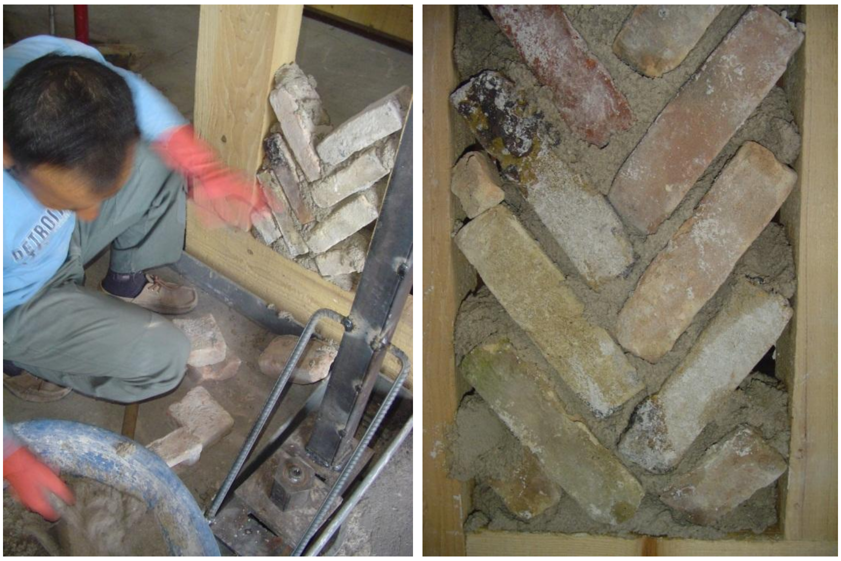

Figure 138: The infill was laid in the herring bond style

Figure 139: During infilling

Figure 140: Plastering and the final state of the Frame#7 with infill

The test was started in load controlled manner, with 1 kN (approximately 100 kgf) increment until 6 kN (approximately 600 kgf) is reached, and then with 2 kN (approximately 200 kgf) increment until 10 kN (approximately 1000 kgf) is reached. After this point, the test was continued in displacement controlled way, first with 1, and then 2 and finally 10 mm increment (Figure 141).

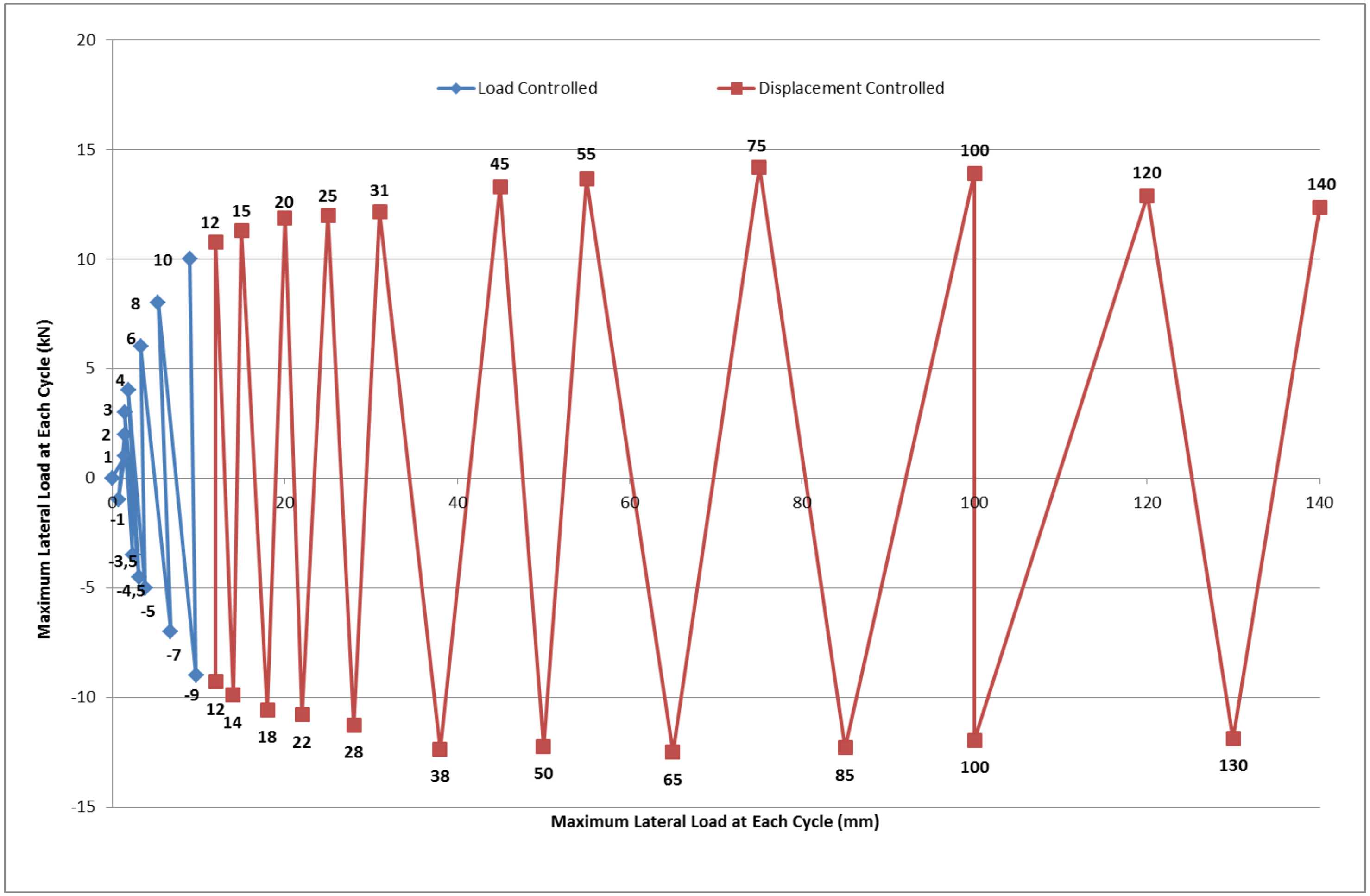

Figure 141: Load controlled and displacement controlled phases of the experiment for the testing of Frame#7 with brick infill (data labels shown are load and displacement values for load controlled and displacement controlled data series, respectively)

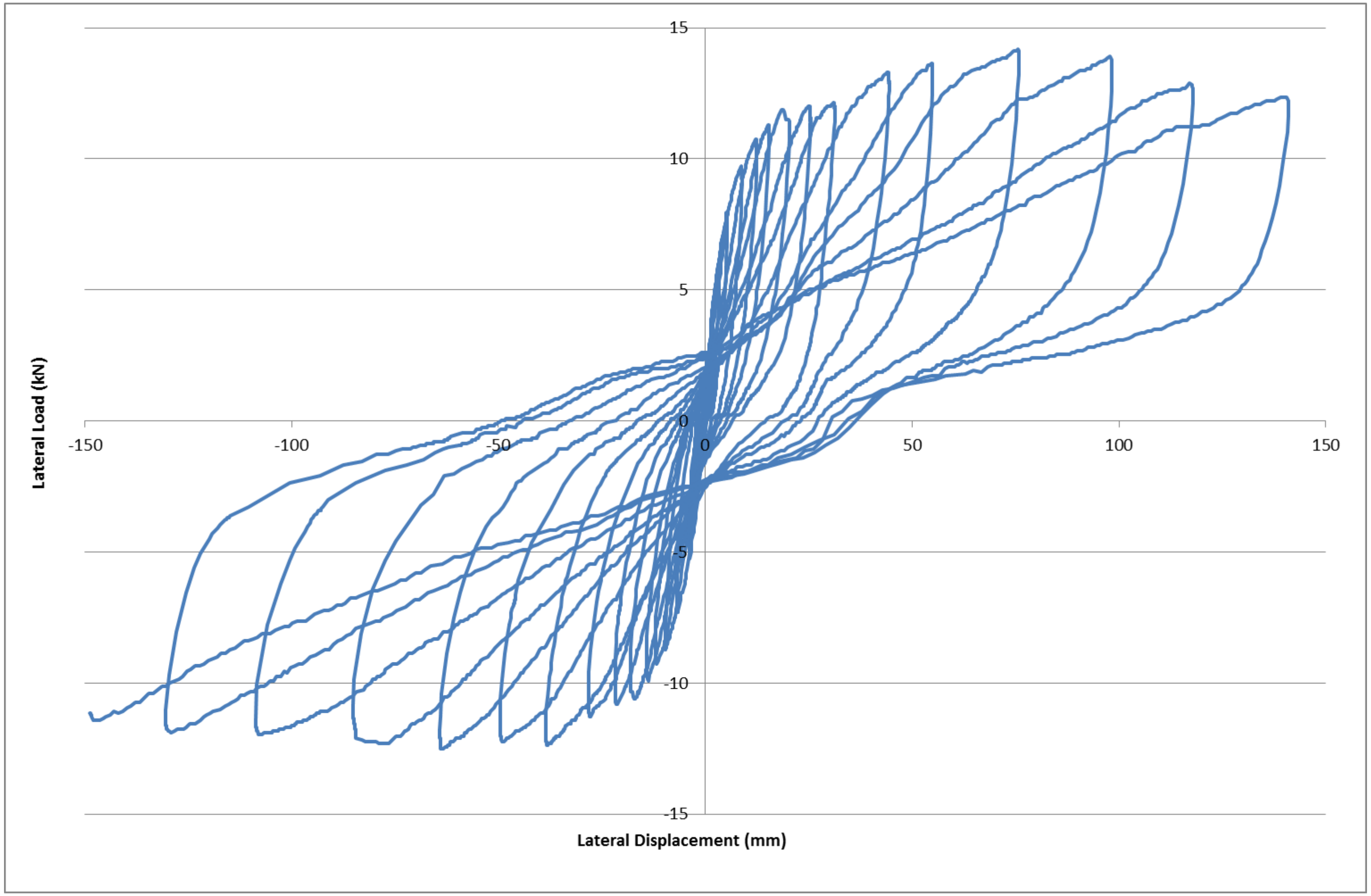

Figure 142: Lateral load – lateral displacement graph of Frame#7 with brick infill

The resulting lateral load-lateral displacement graphs are given in Figure 142. The maximum lateral load that is observed in the push direction is 14.2 kN (1445 kgf) and the corresponding lateral displacement is 141 mm, while in the pull direction these values are 12.5 kN (1275 kgf) and 148 mm respectively. For more information related to the results obtained at the end of the testing of Frame#7 with brick infill, please refer to Appendix O. Also in this case, connections failed in the form of permanent openings and buckling in nails (Figure 143-Figure 144).

Figure 143: Frame#7 with infill after the test

Figure 144: Examples to buckled nails

2.17. FRAME#8

The seventh frame that was tested is 304 cm x 409 cm (H x L) in size, was constructed from yellow pine and has two window openings, each of which is 156 cm x 75 cm in size (Figure 144-Figure 146).

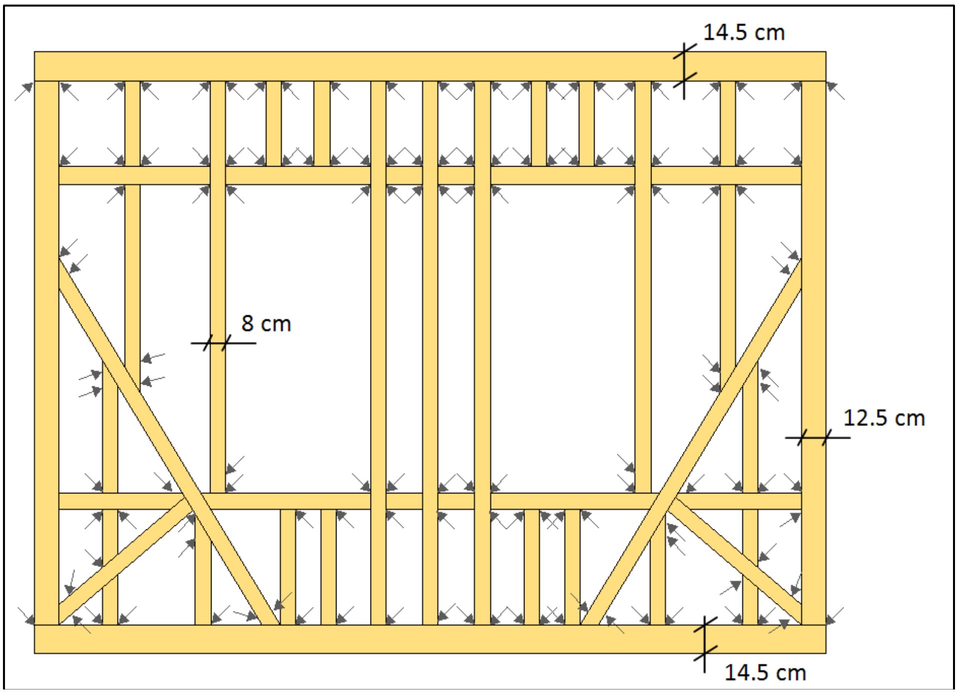

Figure 145: Drawing of Frame#8 (arrows indicate the nails at each connection)

Figure 146: Eight frame during the test

In this test, load was increased 1 kN (approximately 100 kgf) at each cycle until 5 kN (approximately 500 kgf) is reached. Then, test was continued in a displacement controlled way, by increasing displacement first 20, and then 25 mm each 2 cycles (Figure 147).

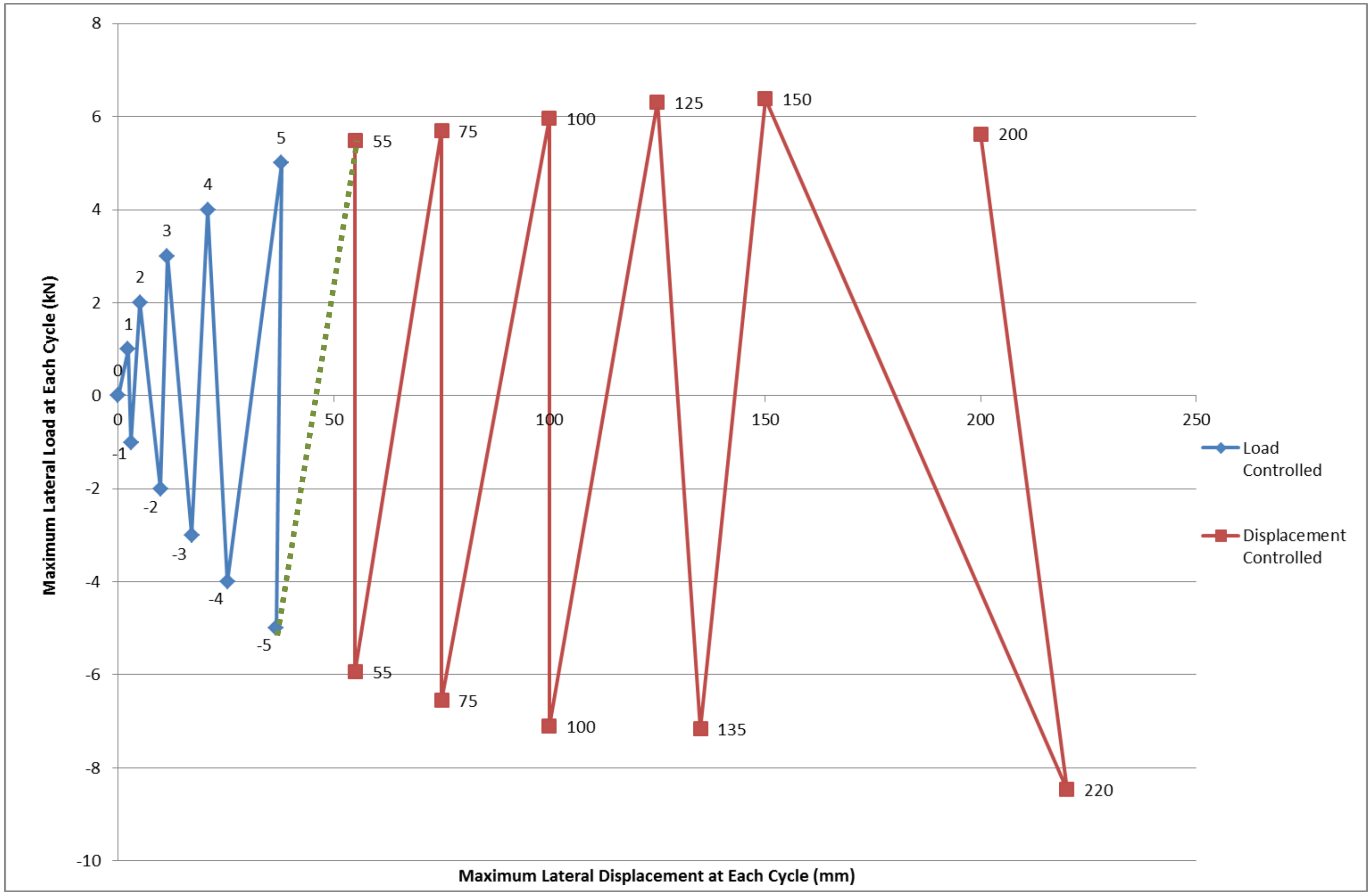

Figure 147: Load controlled and displacement controlled phases of the experiment for the testing of Frame#8 (data labels shown are load and displacement values for load controlled and displacement controlled data series, respectively)

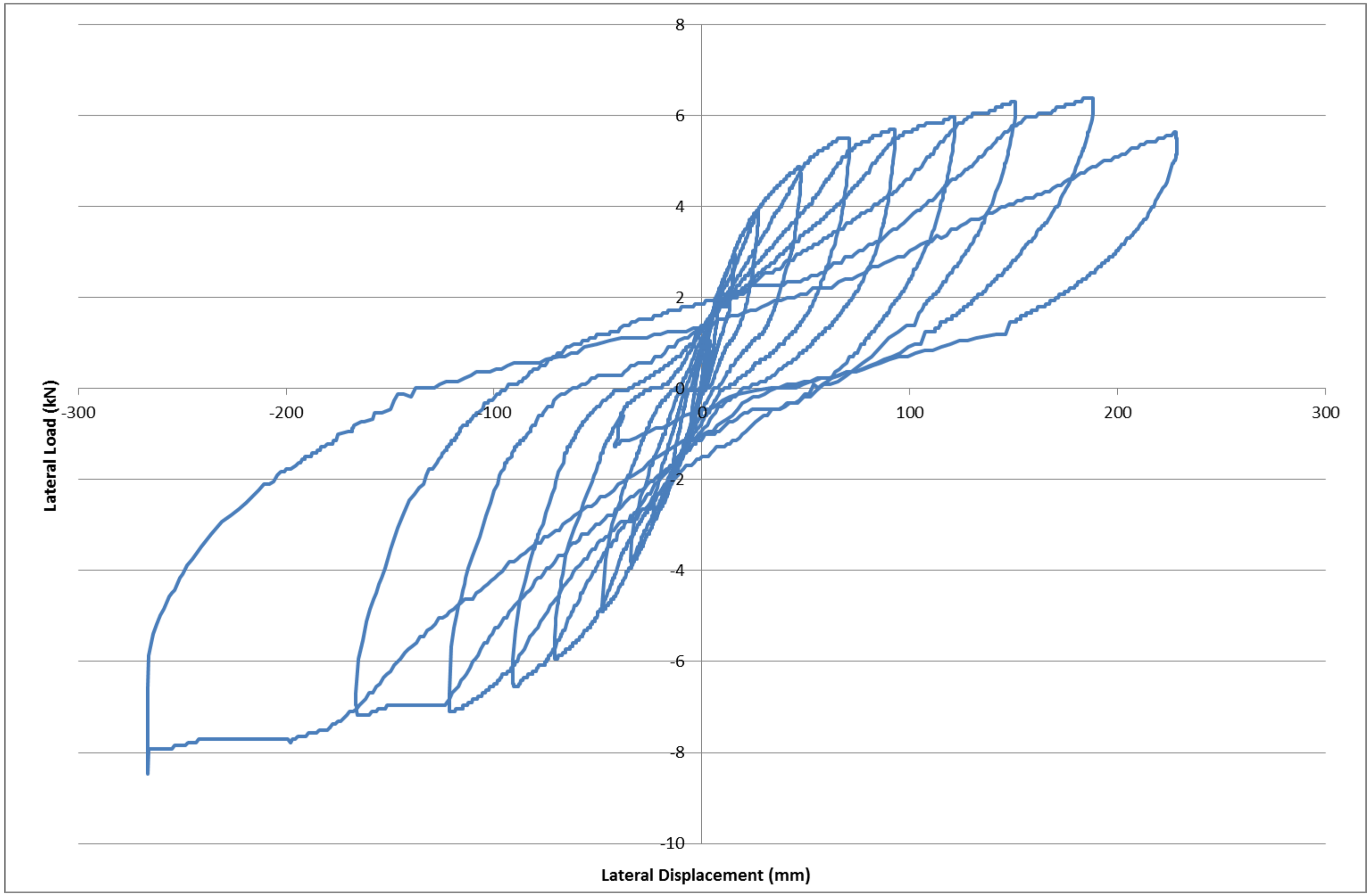

Figure 148: Lateral load – lateral displacement graph of Frame#8

The resulting lateral load-lateral displacement relation is given in Figure 148. The experiment was to the point where first indication of strength loss was observed. The test was terminated before the frame was totally damaged since the same frame was planned to be used with infill/covering. The maximum lateral load that was observed in the push direction is 6.4 kN (650 kgf) and the corresponding lateral displacement is 228 mm, while in the pull direction these values are 8.5 kN (863 kgf) and 266 mm respectively. For more information related to the results obtained at the end of the testing of Frame#8, please refer to Appendix P.

Also in the testing of Frame#8, connections failed in the form of permanent openings and buckling in nails (Figure 143-Figure 144).

Figure 149: Permanent connection failures of the Frame#8 after the test

Figure 150: Examples to out-of-plane displacements occurred at the connections after the testing of Frame#8

Figure 151: Examples to connection dilatations observed during the testing of Frame#8

Figure 152: Overall permanent out-of-plane displacement after the testing of Frame#8

2.18. FRAME#8 WITH BAĞDADİ INFILL

In this test, the Frame#8 was tested with *bağdadi* covering. Before testing the frame, the failed connections were repaired using the same type and number of nails.

Figure 153: *Bağdadi* covering and plastering

The testing of Frame#8 with *bağdadi* covering started in a load controlled manner with 1 kN (approximately 100 kgf) increment each cycle until 8 kN (approximately 800 kgf) is reached. After this point, the test was continued in displacement controlled way, first with 2, and then 4 and finally 5 mm increment (Figure 154).

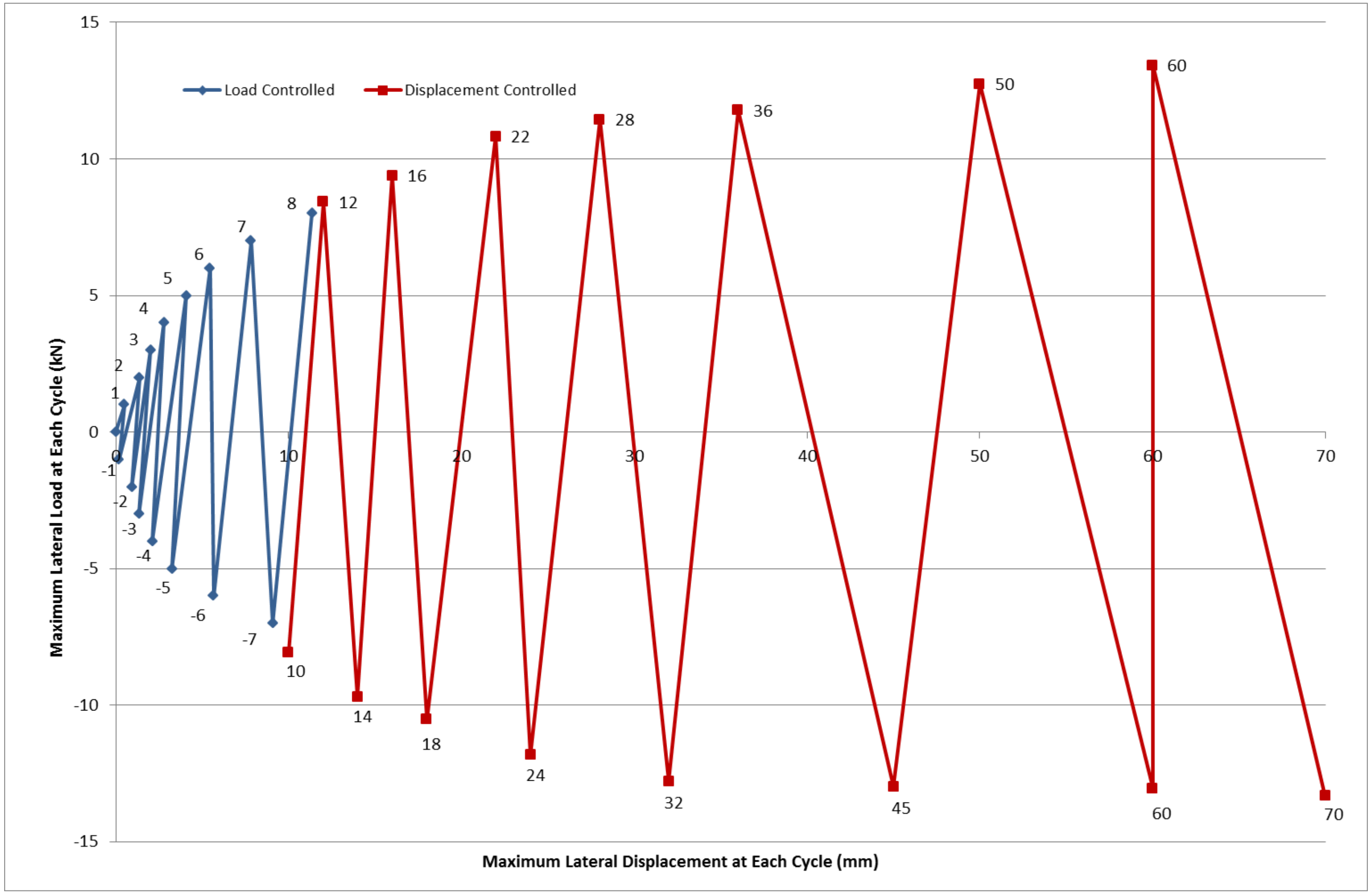

Figure 154: Load controlled and displacement controlled phases of the experiment for the testing of Frame#8 with *bağdadi* covering (data labels shown are load and displacement values for load controlled and displacement controlled data series, respectively)

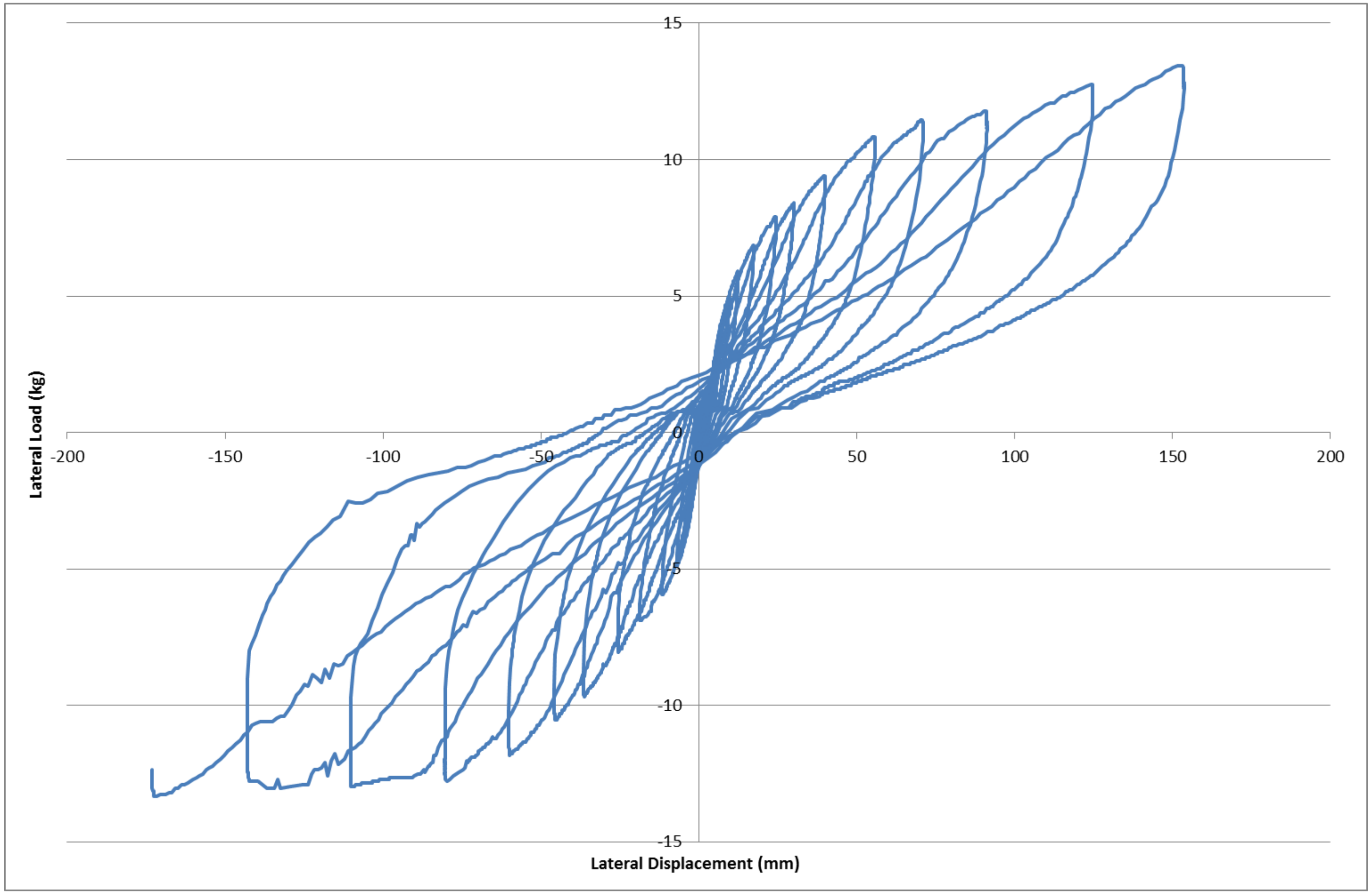

Figure 155: Lateral load – lateral displacement graph of Frame#8 with *bağdadi* covering

The resulting lateral load-lateral displacement relationship is shown in Figure 155. The maximum lateral load that is observed in the push direction is 13.4 kN (1370 kgf) and the corresponding lateral displacement is 153 mm, while in the pull direction these values are 13.3 kN (1360 kgf) and 173 mm respectively. For more information related to the results obtained at the end of the testing of Frame#8 with *bağdadi* covering, please refer to Appendix R.

After the test, connection failures which are similar to the ones observed in previous tests were observed (Figure 156).

Figure 156: Examples to connection failures observed during the testing of Frame#8 with *bağdadi* covering

2.19. FRAME WEIGHING

For the aim of determining the weights of the frames without and with infill/covering, most of the frames were lifted by means of a crane, the tip of which was equipped by a load cell. A metal cylinder of known weight was lifted first for control purposes (Figure 157). The weights of the other frames without or with infill/covering, on the other hand, were calculated by using the unit weight of each infill/covering type.

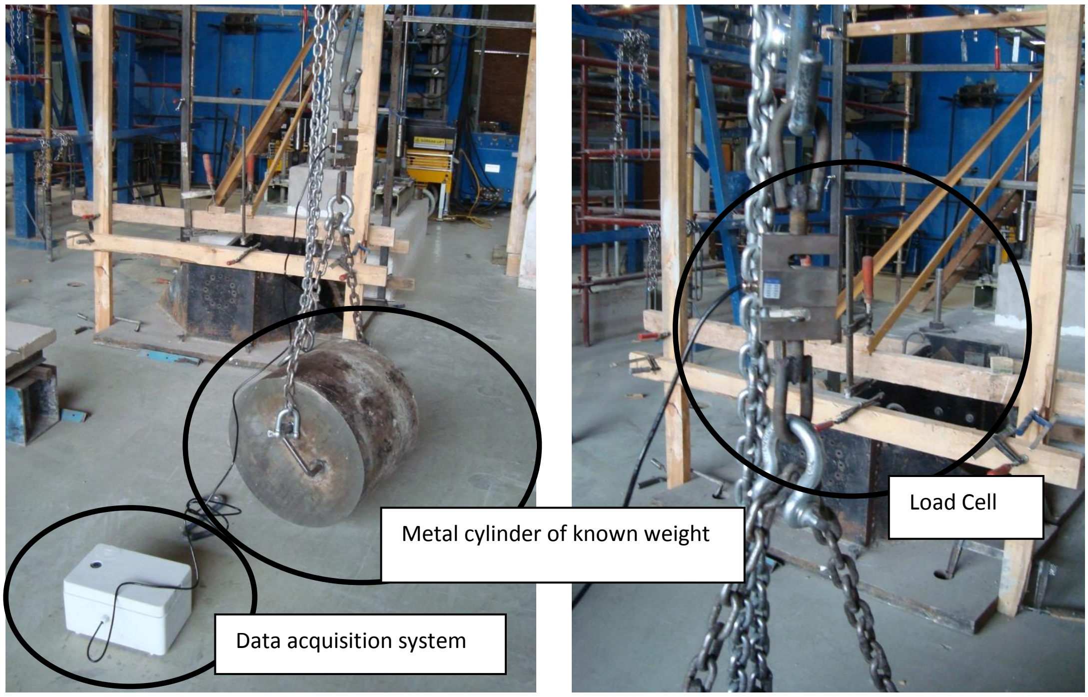

Figure 157: Metal cylinder of known weight and load cell used for determining the weights of the frames

A typical data obtained at the end of this process is as follows:

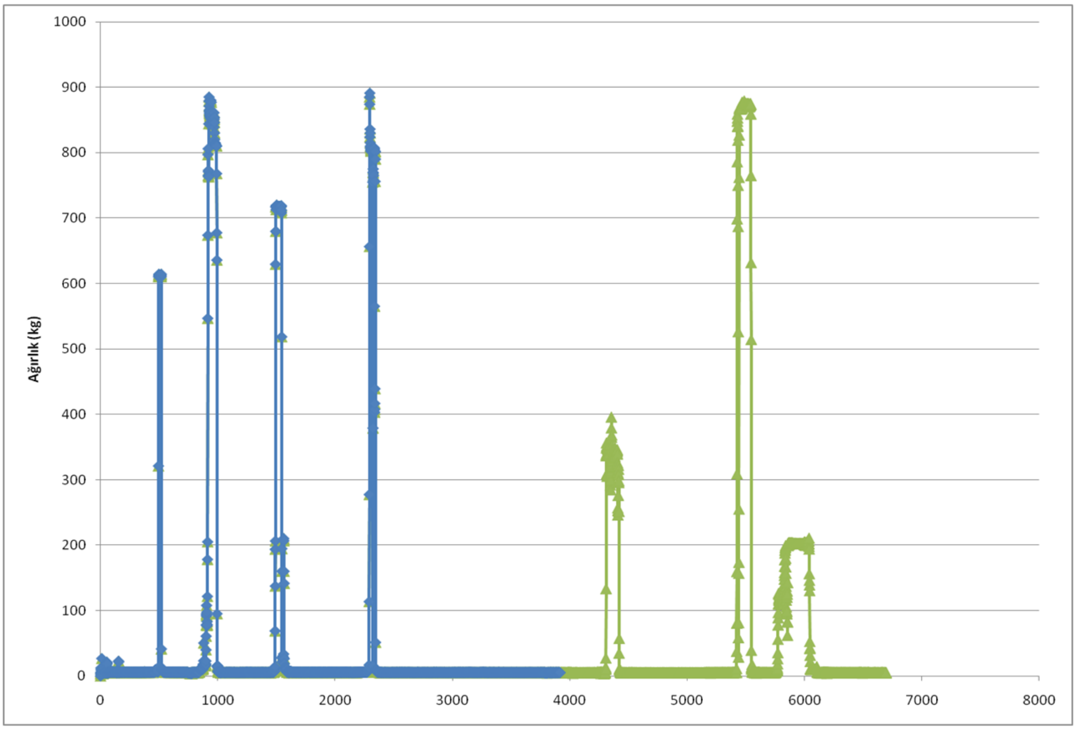

Figure 158: Graph showing typical data obtained at the end of weighing the frames

The results are shown in Table 2.

Table 2: Weights of the frames tested without and with infill/covering

Frame No	Without Infill	With Infill		Increase in Weight after Infilling
	Weight (kN)	Infill/Covering Type	Weight (kN)	
1	1.83	Adobe	7.75	4.23
2	1.55	Adobe	10.53**	6.79
3	1.80	*Şamdolma*	7.55**	4.18
4	1.83	Brick	8.39*	4.57
5	2.25*	*Bağdadi*	6.51	2.90
6	3.72	*Şamdolma*	12.27	3.29
7	2.69	Brick	13.36*	4.97
8	2.05	*Bağdadi*	6.33**	3.09

* Calculated

** Weighed incomplete and rest calculated

CHAPTER 3

SEISMIC CAPACITY EVALUATION OF TIMBER FRAMES WITH AND WITHOUT INFILL BY MEANS OF CAPACITY CALCULATIONS

In this chapter, the seismic capacities of timber frames, which were investigated experimentally (and whose results were reported in previous chapters) were evaluated by using the procedure C among the three procedures offered the nonlinear static analysis procedures described in ATC-40 (1996: 8-1). According to this, first of all, the top lateral displacement-top lateral load curves were transformed into ADRS format (acceleration-displacement response spectrum format) capacity curves, i.e. Sa versus Sd representation, by the following equations:

$$Sa = \frac{V/_W}{\alpha_1} \tag{1}$$

$$Sd = \frac{\Delta_{roof}}{PF_1 \emptyset_{roof,1}} \tag{2}$$

where,

S_a: spectral acceleration

S_d: spectral displacement

$W_i/_g$: mass assigned to level i (in our case, total number of levels is 1)

$\emptyset_i 1$: amplitude of mode 1 at level i

N: level N, the level which is the uppermost in the main portion of the structure

V: base shear.

W: building dead weight plus likely live loads (in our case, half of the frame weight plus the weight of load prisms)

Δ_{roof}: roof displacement

PF_1 = modal participation factor for the first natural mode (taken as 1.4 – see Figure 159)

$$PF_1 = \left[\frac{\sum_{i=1}^{N} {(w_i \vartheta_{i1})}/{g}}{\sum_{i=1}^{N} {(w_i \vartheta^2{}_{i1})}/{g}} \right] \tag{3}$$

α_1: modal mass coefficient for the first natural mode (taken as 0.8 – see Figure 159).

$$\propto_1 = \frac{\left[\sum_{i=1}^{N} {(w_i \vartheta_{i1})}/{g} \right]^2}{\left[\sum_{i=1}^{N} {w_i}/{g} \right] \left[\sum_{i=1}^{N} {(w_i \vartheta_{i1}{}^2)}/{g} \right]} \tag{4}$$

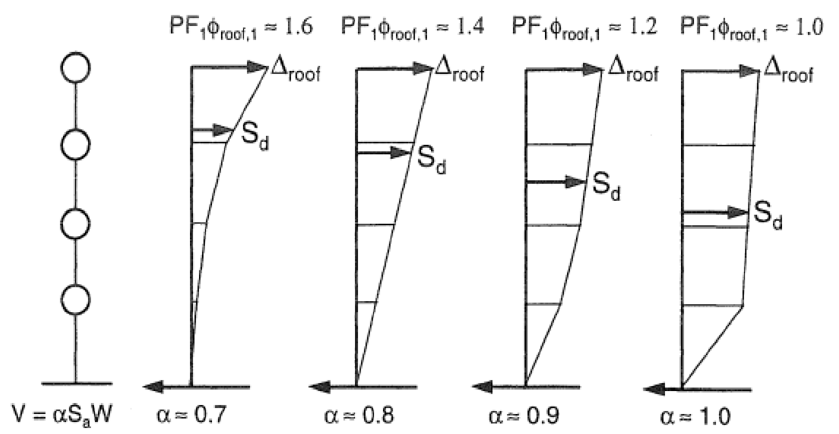

Figure 159: Example modal participation factors and modal mass coefficients (taken from ATC-40)

Once the ADRS format capacity curve is obtained, the period, T, value at any point can be calculated by the following equation:

$$T = 2\pi \sqrt{\frac{S_d}{S_a}} \tag{5}$$

After the formation of capacity curve, a bilinear representation of it is needed. According to this, the capacity curve should be represented by two lines, where the sum of the areas between these lines and the actual capacity curve must be equal to each other below and under the capacity curve (Figure 160). In Figure 160, A_1 must be equal to A_2. Please note that K_i is the initial stiffness.

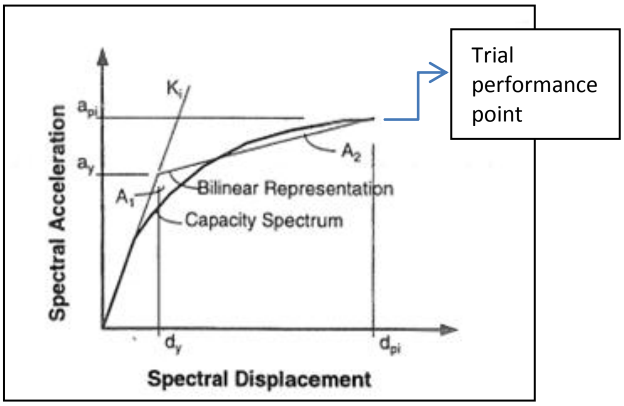

Figure 160: Formation of bilinear representation (taken from ATC-40)

For the aim of bilinear representation, a trial performance point is selected as seen in Figure 160. Whenever a bilinear representation by using the trial performance and a point on K_i line is successful, the damping ratio value is obtained for the obtained configuration by using the following equations:

$$\beta_{eq} = \beta_0 + 0.05 \tag{6}$$

where,

0.05: 5% viscous damping inherent in the structure (assumed to be constant)

β_0: hysteretic damping represented as equivalent viscous damping

$$\beta_0 = \frac{1}{4\pi}\frac{E_D}{E_{So}} \tag{7}$$

where,

E_D: energy dissipated by damping (see Figure 161-Figure 162)

$$E_D = 4(a_y d_{pi} - d_y a_{pi}) \tag{8}$$

$\mathrm{E_{So}}$: maximum strain energy (see Figure 161-Figure 162)

$$E_{So} = a_{pi} d_{pi}/2 \tag{9}$$

Therefore, the equations become:

$$\beta_0 = \frac{63.7(a_y d_{pi} - d_y a_{pi})}{a_{pi} d_{pi}} \tag{10}$$

$$\beta_{eq} = \beta_0 + 5 = \frac{63.7(a_y d_{pi} - d_y a_{pi})}{a_{pi} d_{pi}} + 5 \tag{11}$$

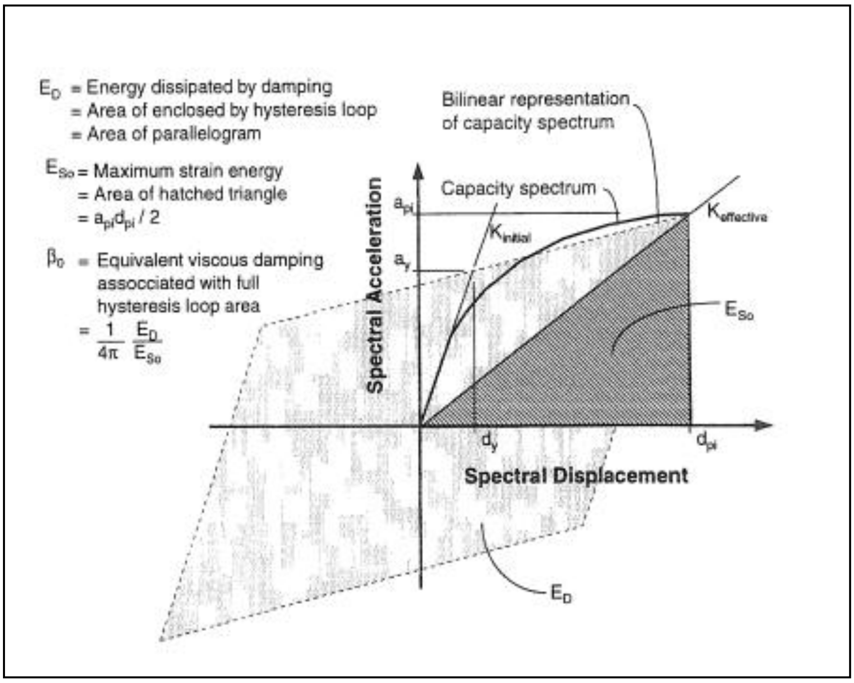

Figure 161: Derivation of damping for spectral reduction (taken from ATC-40)

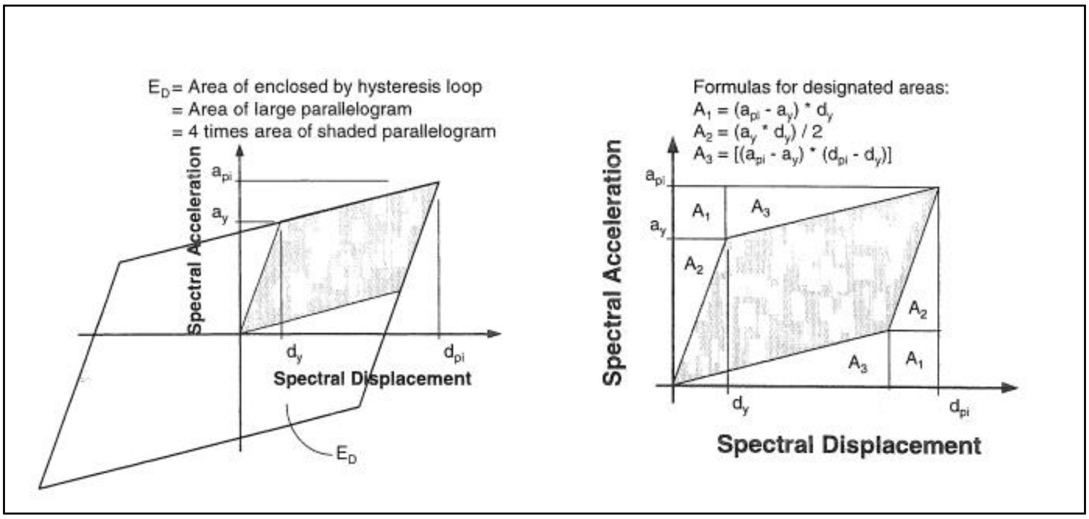

Figure 162: Derivation of energy dissipated by damping E_D (taken from ATC-40)

The elastic response spectrum of 5% is used to draw a reduced response spectrum with a different damping value based on the site seismic coefficients C_A and C_B (ATC-40: 4-14) (Figure 163).

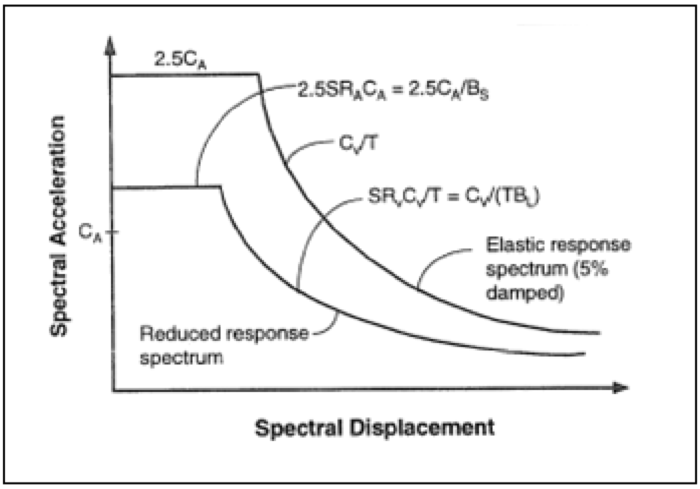

Figure 163: Reduced response spectrum (taken from ATC-40)

$$SR_A \cong \frac{3.21-0.68ln\left[\frac{63.7\kappa\left(a_y d_{pi}-d_y a_{pi}\right)}{a_{pi}d_{pi}}+5\right]}{2.12} \geq \text{value given in Table 3} \quad (12)$$

Table 3: Minimum allowable SR_A and SR_V values given in ATC-40

Structural Behavior Type	SR_A	SR_V
Type A	0.33	0.50
Type B	0.44	0.56
Type C	0.56	0.67

$$SR_V \cong \frac{2.31-0.41ln\left[\frac{63.7\kappa\left(a_y d_{pi}-d_y a_{pi}\right)}{a_{pi}d_{pi}}+5\right]}{1.65} \geq \text{value given in Table 3} \quad (13)$$

where, the κ factor "is a measure of extent to which the actual building hysteresis is well represented by the parallelogram " shown in Figure 161.

The structural behaviors are defined in Table 4.

Table 4: Structural behavior types given in ATC-40

Shaking Duration	Essentially new building	Average existing building	Poor existing building
Short	Type A	Type B	Type C
Long	Type B	Type C	Type C

In our study, the structural behavior type was selected as Type C, which complies both with average and poor existing buildings, and short and long shaking durations. κ factor is defined as shown in Table 5, therefore is taken as 0.33, and SR_A and SR_V values were calculated accordingly.

Table 5: Values for damping modification factor, κ, given in ATC-40

Structural behavior type	β_0 (percent)	κ
Type A	≤16.25	1.0
	>16.25	$1.13 - \frac{0.51(a_y d_{pi} - d_y a_{pi})}{a_{pi} d_{pi}}$
Type B	≤25	0.67
	>25	$0.847 - \frac{0.446(a_y d_{pi} - d_y a_{pi})}{a_{pi} d_{pi}}$
Type C	Any value	0.33

In case that the trial performance point is on the the calculated damping curve, then the trial performance point can be accepted as the performance point, if not the next iteration step is checked. Please note that the threshold interval for performance point is $0.95d_{pi} \leq d_i \leq 1.05d_p$ for a given damping value (Figure 164).

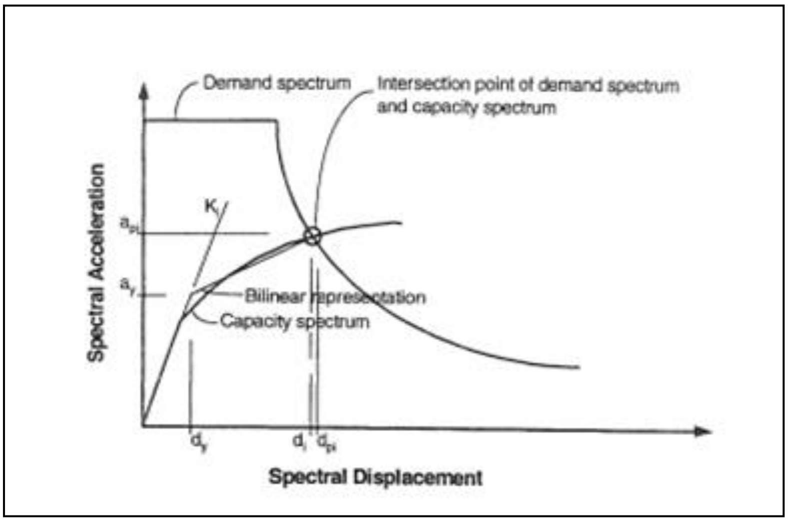

Figure 164: Intersection point of demand and capacity spectrum within acceptable tolerance (taken from ATC-40)

Based on the explained method, the capacity calculations of each frame without and with infill/covering were made. The results are shown in Table 6, and Figure 165-Figure 172.

Table 6: Results of the capacity calculations for each frame without and with infill/covering

Frame no	Frame Drawing	Direction	Empty State	Spectral Acceleration Graph for Empty State	Infill/ Covering Type	Direction	With Infill/Covering	Spectral Acceleration Graph for With-Infill/Covering State	General Information	Notes
1	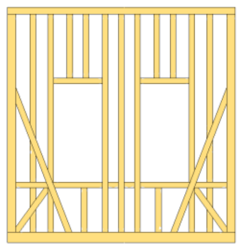	push	Ti=0.27 s	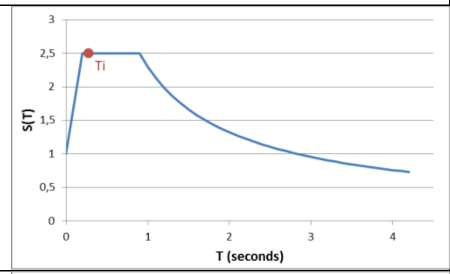	Adobe	push	Ti=0.18 s Ta= 0.78 s Sd= 135 mm ξ= 8.8%	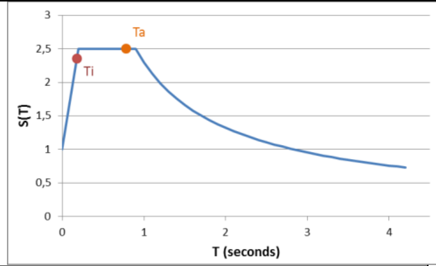	(H x L): 325 cm x 310 cm Yellow Pine 2 windows of 135 cm x 67 cm each Window Openings per Total Surface of the Frame: 0.180	Figure 165 No performance point was obtained in empty state
		pull	Ti=0.26 s	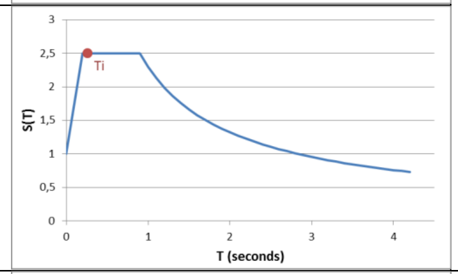		pull	Ti=0.22 s Ta= 0.71 s Sd= 113 mm ξ= 9.2%	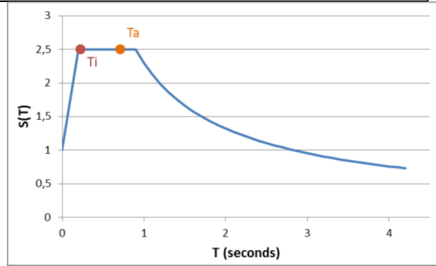		
2	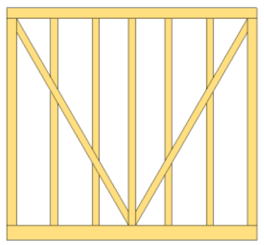	push	Ti=0.17 s Ta=0.26 s Sd= 17 mm ξ= 7.2%	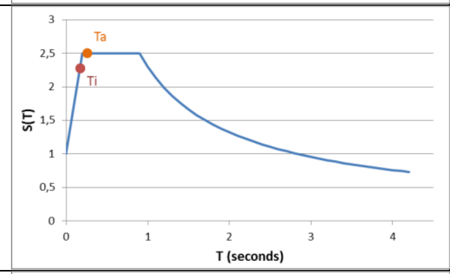	Adobe	push	Ti=0.12 s Ta= 0.17 s Sd= 7.5 mm ξ= 7.1%	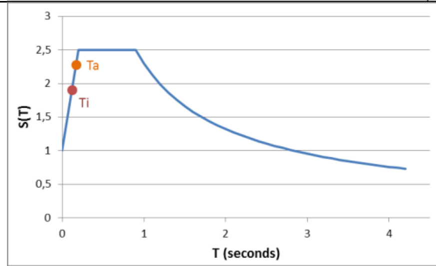	(H x L): 360 cm x 330 cm Yellow Pine No Windows	Figure 166
		pull	Ti=0.21 s Ta=0.31 s Sd= 24 mm ξ= 6.7%	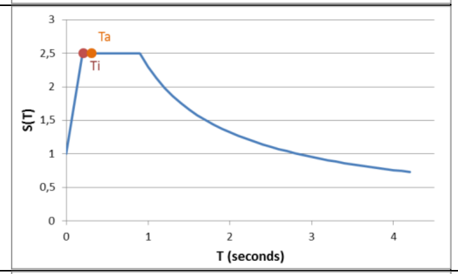		pull	Ti=0.14 s Ta=0.16 s Sd= 6.5 mm ξ= 6.3%	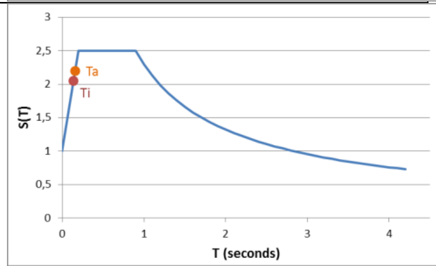		
3	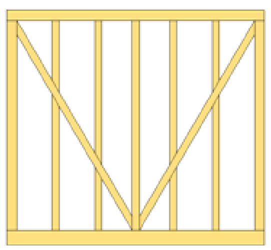	push	Ti=0.18 s Ta=0.31 s Sd= 25.5 mm ξ= 6.4%	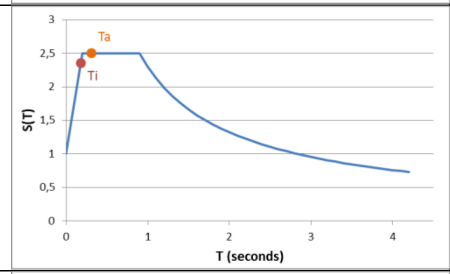	*Şamdolma*	push	Ti=0.10 s Ta=0.13 s Sd= 4 mm ξ= 7.3%	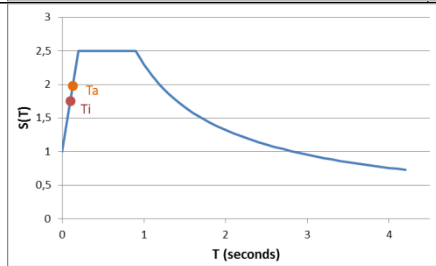	(H x L): 360 cm x 330 cm Fir No Windows	Figure 167
		pull	Ti=0.20 s Ta=0.39 s Sd= 36.9 mm ξ= 7.1%	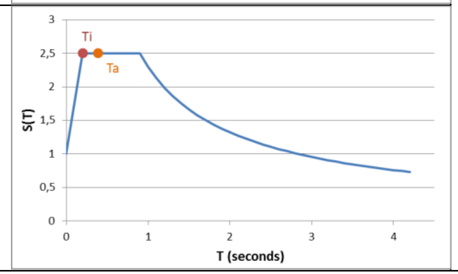		pull	Ti=0.11 s Ta=0.16 s Sd= 6.6 mm ξ= 8%	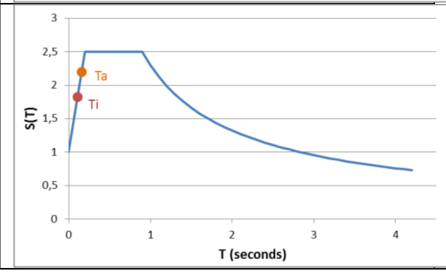		

“Table 6 (continued)”

4	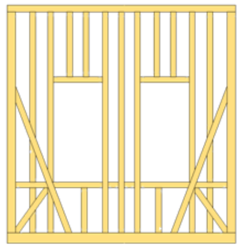	push	Ti=0.29 s	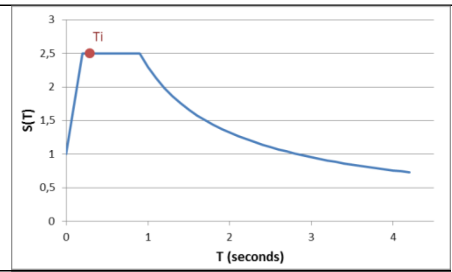	Brick	push	Ti=0.17 s Ta=0.53 s Sd= 65 mm ξ= 8%	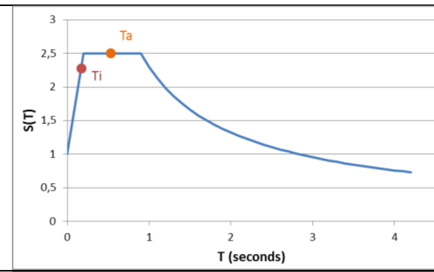	(H x L): 325 cm x 310 cm Fir 2 windows of 135 cm x 67 cm each Window Openings per Total Surface of the Frame: 0.180	Figure 168 No performance point was obtained in empty state
		pull	Ti=0.40 s	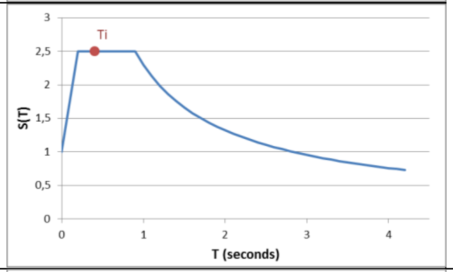		pull	Ti=0.22 s Ta=0.62 s Sd= 93.2 mm ξ= 7.6%	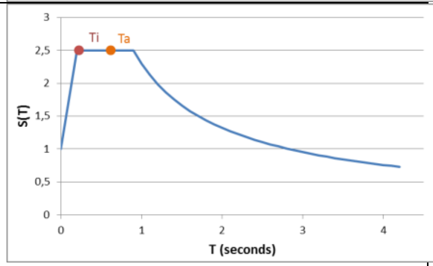		
5	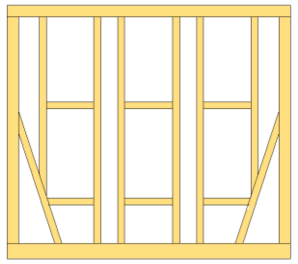	push	Ti=0.42 s	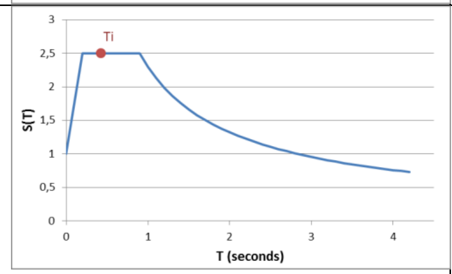	*Bağdadi*	push	Ti=0.16 s Ta=0.23 s Sd= 13.5 mm ξ= 6.9%	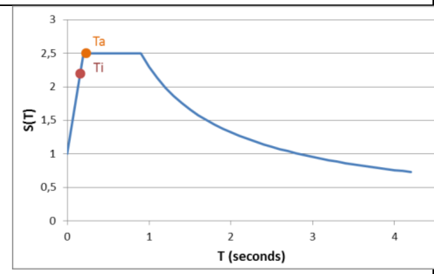	(H x L): 330 cm x 370 cm Yellow Pine 3 windows of 116 cm x 62 cm each Window Openings per Total Surface of the Frame: 0.177	Figure 169 No performance point was obtained in empty state
		pull	Ti=0.43 s	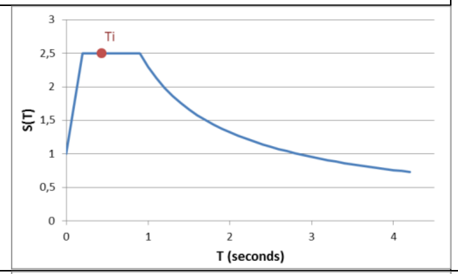		pull	Ti=0.16 s Ta=0.23 s Sd= 12.9 mm ξ= 7.3%	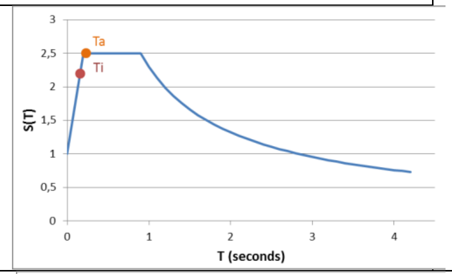		
6	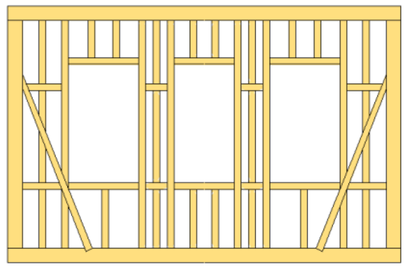	push	Ti=0.33 s	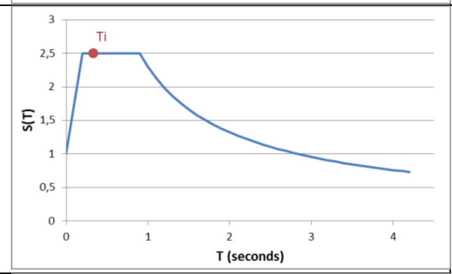	*Şamdolma*	push	Ti=0.21 s Ta=0.56 s Sd= 72.5 mm ξ= 8.2%	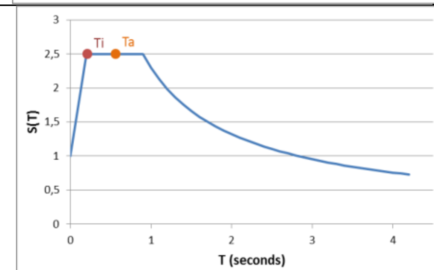	(H x L): 340 cm x 520 cm Yellow Pine 3 windows of 157 cm x 93 cm each Window Openings per Total Surface of the Frame: 0.248	Figure 170 No performance point was obtained in empty state
		pull	Ti=0.18 s	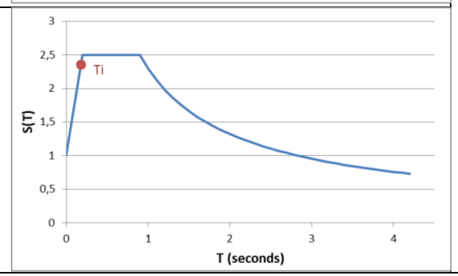		pull	Ti=0.21 s Ta=0.54 s Sd= 68 mm ξ= 8.1%	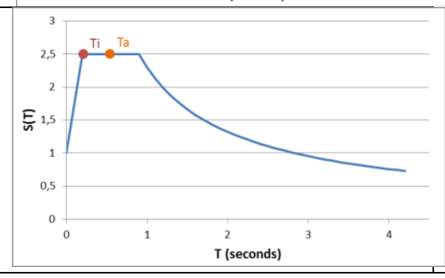		

"Table 6 (continued)"

<table>
<tr><td rowspan="2">7</td><td rowspan="2">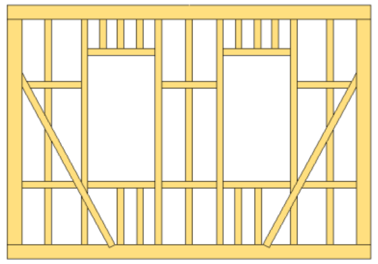</td><td>push</td><td>push:
Ti=0.22 s Ta=0.32 s
Sd= 26 mm ξ= 7.0%</td><td>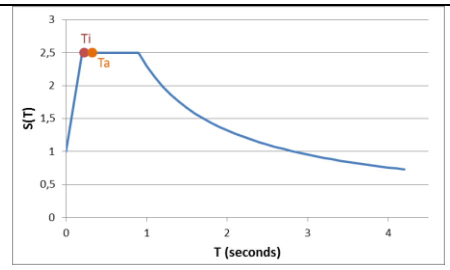</td><td rowspan="2">Brick</td><td>push</td><td>Ti=0.08 s Ta=0.16 s
Sd= 5.6 mm ξ= 7.4%</td><td>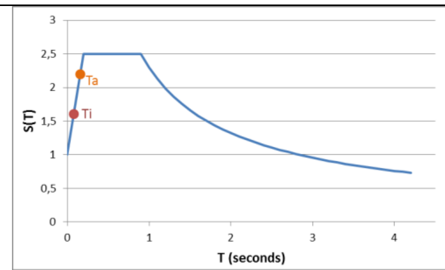</td><td rowspan="2">(H x L): 340 cm x 485 cm

Yellow Pine

2 windows of 169 cm x 89.5 cm each

Window Openings per Total Surface of the Frame: 0.184</td><td rowspan="2">Figure 171</td></tr>
<tr><td>pull</td><td>pull:
Ti=0.26 s Ta=0.42 s
Sd= 46 mm ξ= 6.6%</td><td>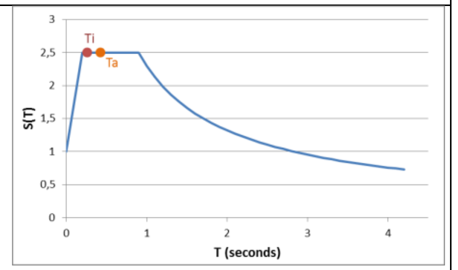</td><td>pull</td><td>Ti=0.11 s Ta=0.19 s
Sd= 8.9 mm ξ= 7.5%</td><td>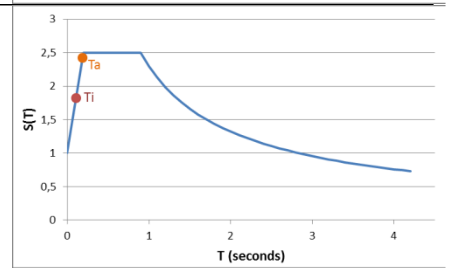</td></tr>
<tr><td rowspan="2">8</td><td rowspan="2">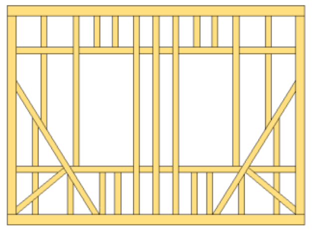</td><td>push</td><td>push:
Ti=0.20 s Ta=0.45 s
Sd= 49 mm ξ= 7.7%</td><td>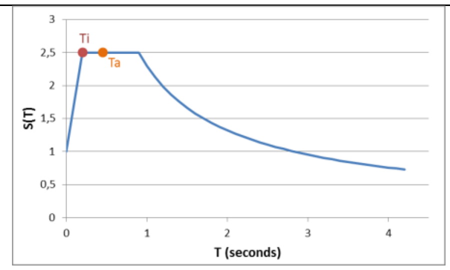</td><td rowspan="2">Bağdadi</td><td>push</td><td>Ti=0.11 s Ta=0.18 s
Sd= 6.3 mm ξ= 6.8%</td><td>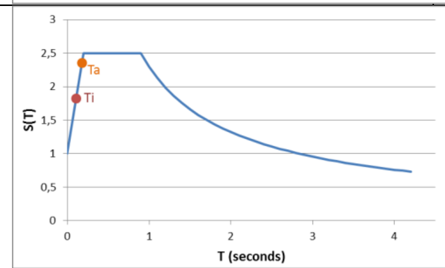</td><td rowspan="2">(H x L): 300 cm x 400 cm

Yellow Pine

2 windows of 156 cm x 75 cm each

Window Openings per Total Surface of the Frame: 0.195</td><td rowspan="2">Figure 172</td></tr>
<tr><td>pull</td><td>pull:
Ti=0.25 s Ta=0.40 s
Sd= 41 mm ξ= 6.6%</td><td>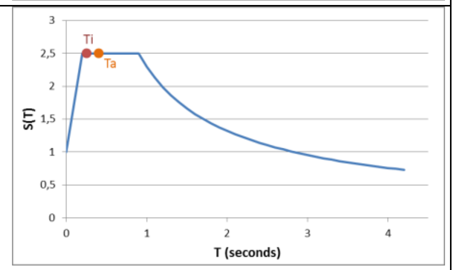</td><td>pull</td><td>Ti=0.09 s Ta=0.16 s
Sd= 6.5 mm ξ= 7.3%</td><td>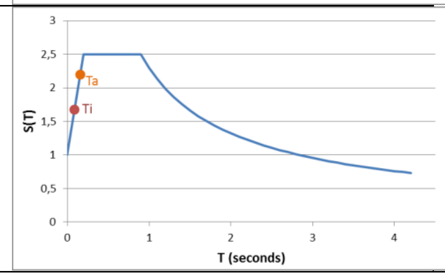</td></tr>
</table>

Notes:

- The frame drawings are proportional to each other.
- The design acceleration spectrum was drawn according to Turkish Earthquake code and the local site class was taken as Z4, to be on the safe side.
- Ti is the initial period, while Ta is the period gained after inelastic displacement, Sd.
- The case Ta value could not been reached, as in Frame#1, 4, 5 and 6 without infill/covering, means that the frame does not have a capacity under seismic loading.

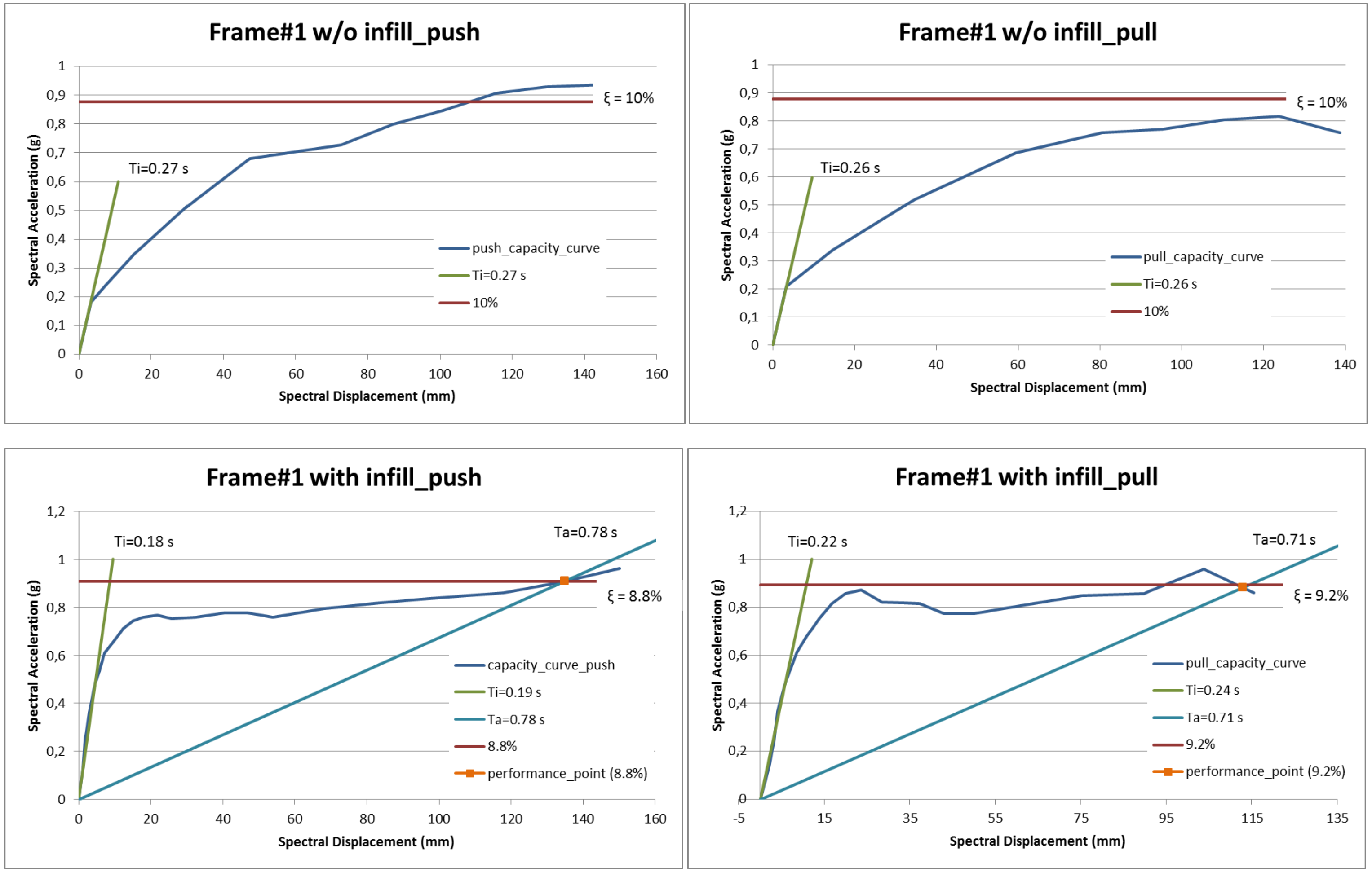

Figure 165: Sd-Sa graphs of Frame#1 without and with infill, and for push and pull directions, respectively (10% damping line was indicated as a reference for tests where performance point was not obtained)

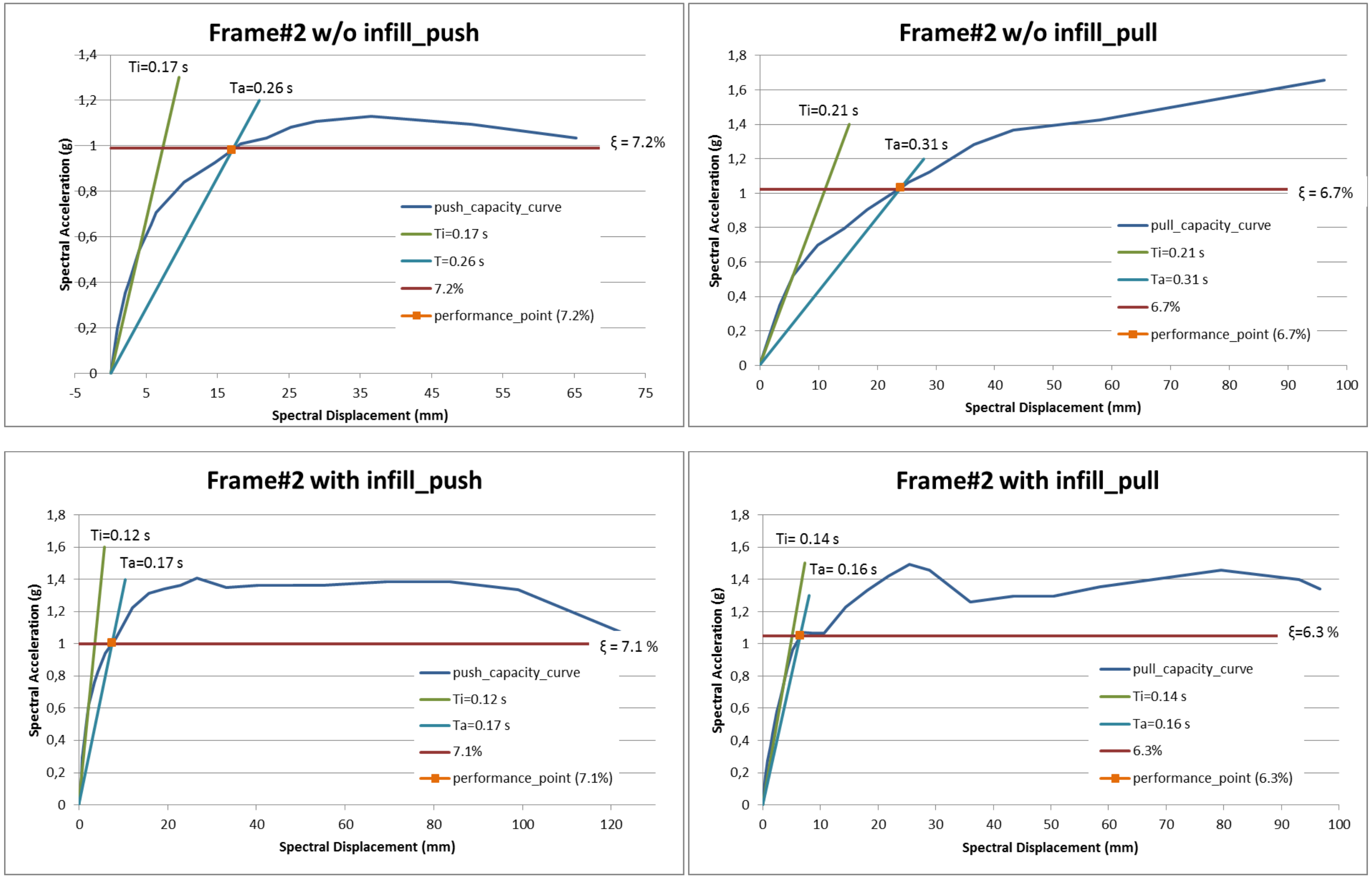

Figure 166: Sd-Sa graphs of Frame#2 without and with infill, and for push and pull directions, respectively

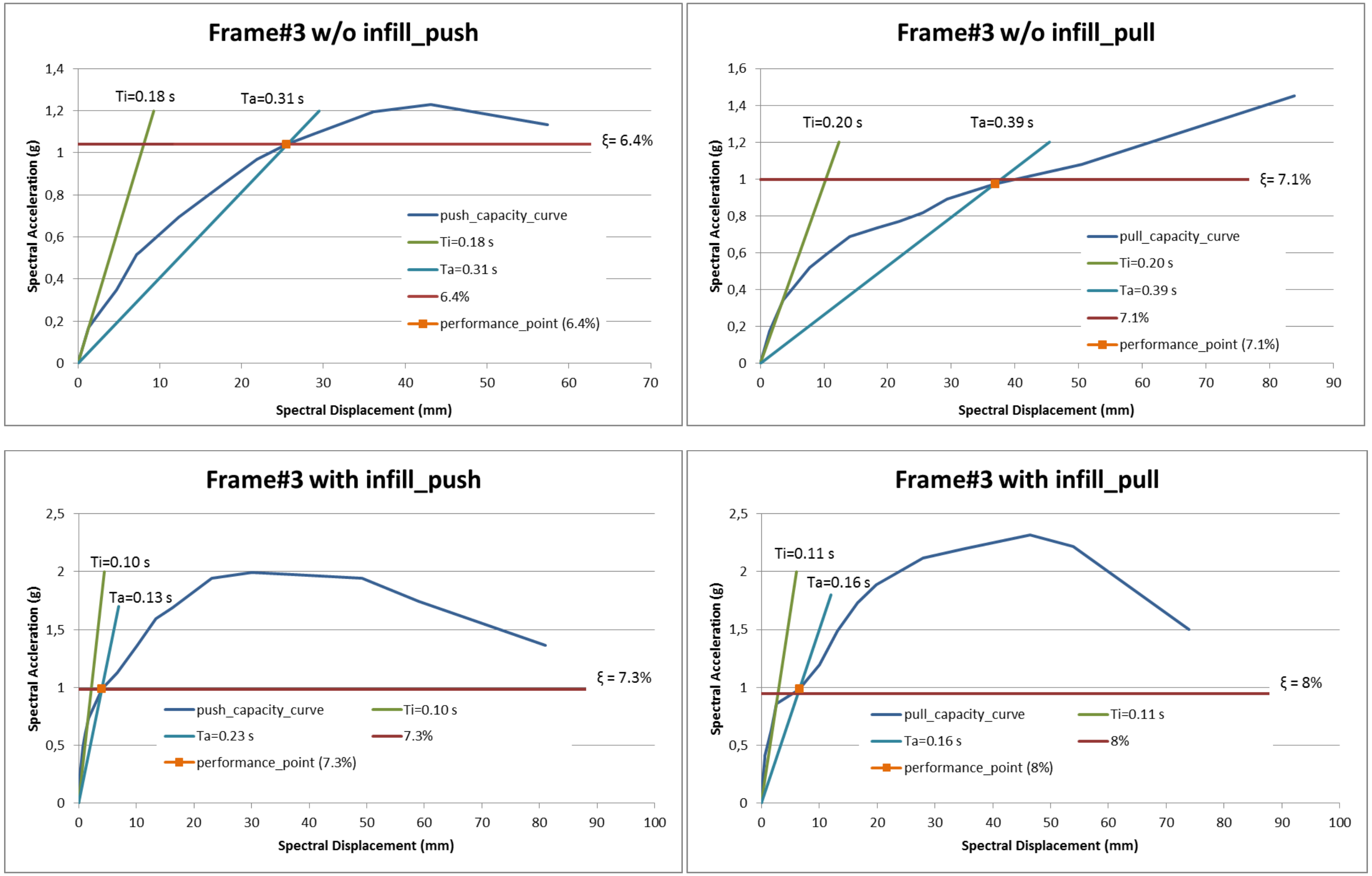

Figure 167: Sd-Sa graphs of Frame#3 without and with infill, and for push and pull directions, respectively

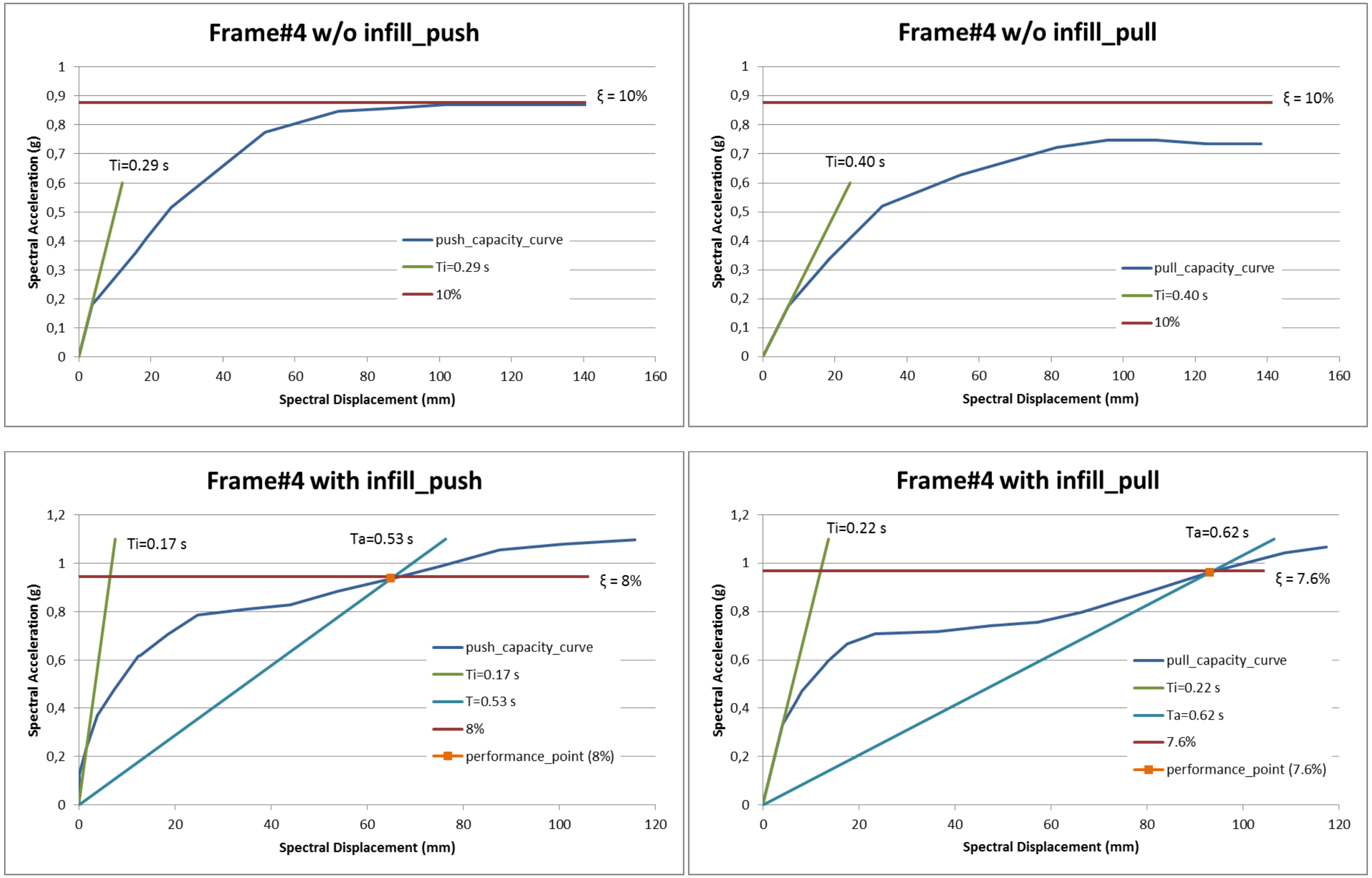

Figure 168: Sd-Sa graphs of Frame#4 without and with infill, and for push and pull directions, respectively (10% damping line was indicated as a reference for tests where performance point was not obtained)

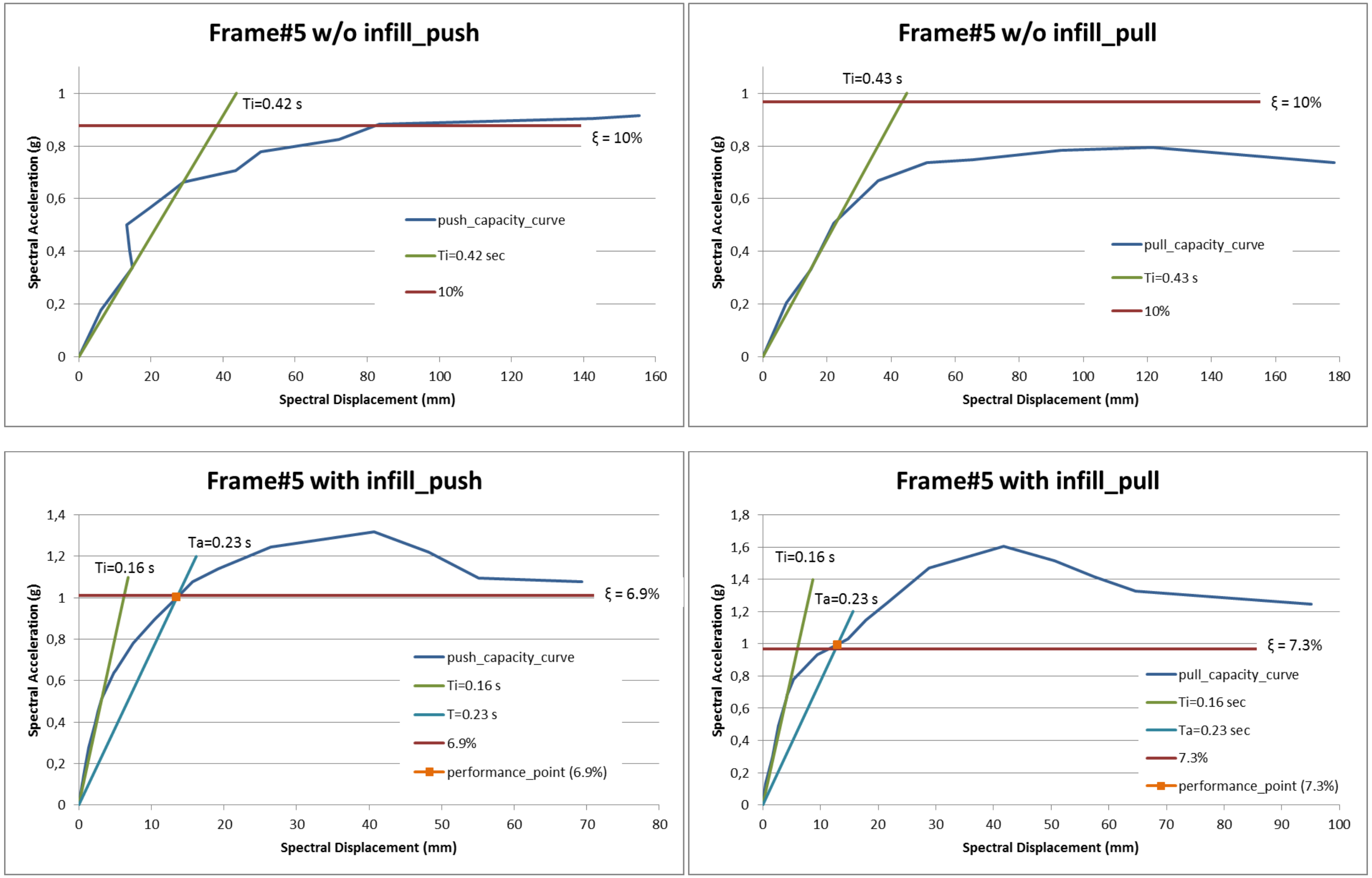

Figure 169: Sd-Sa graphs of Frame#5 without and with infill, and for push and pull directions, respectively (10% damping line was indicated as a reference for tests where performance point was not obtained)

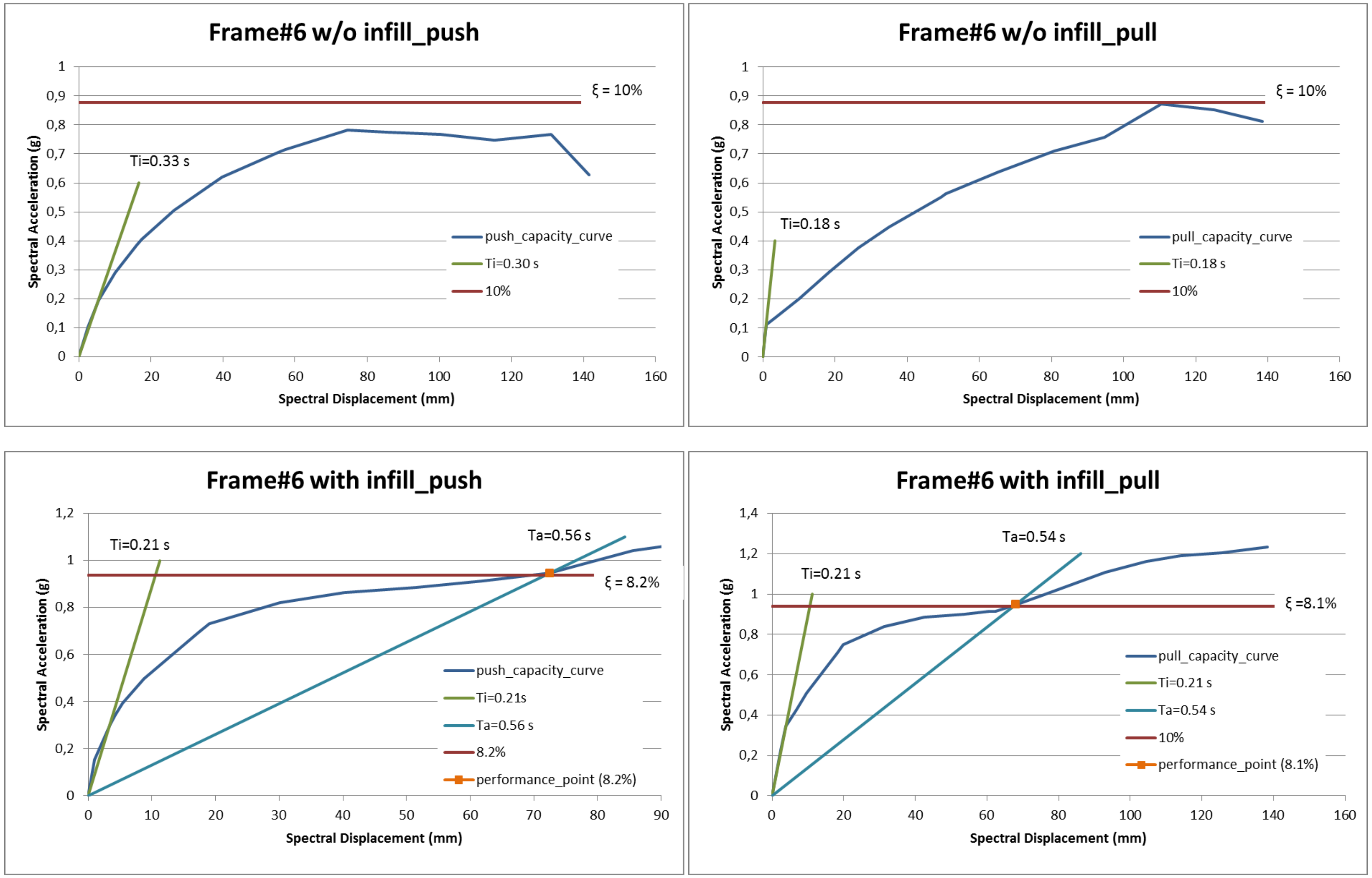

Figure 170: Sd-Sa graphs of Frame#6 without and with infill, and for push and pull directions, respectively (10% damping line was indicated as a reference for tests where performance point was not obtained)

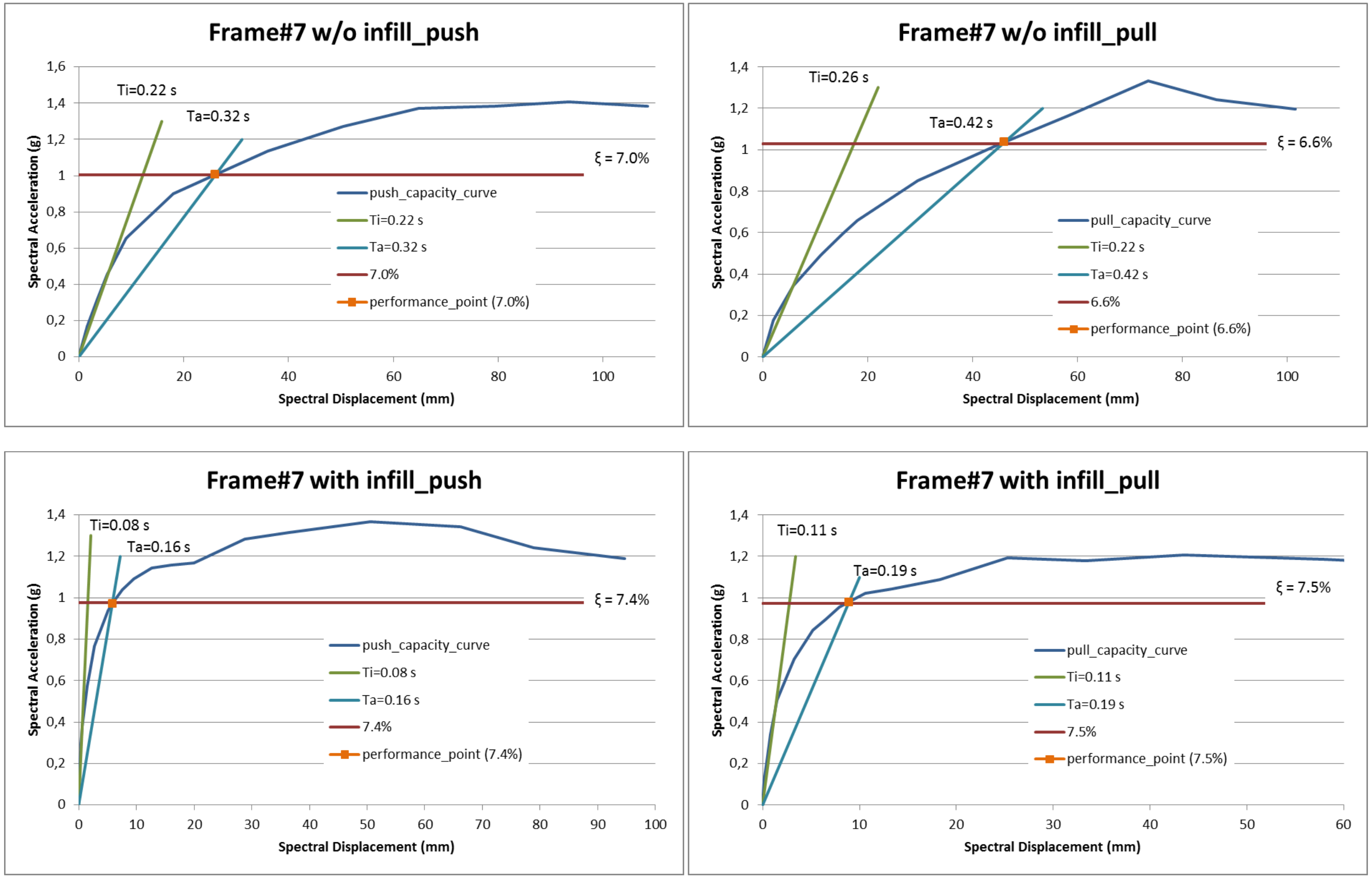

Figure 171: Sd-Sa graphs of Frame#7 without and with infill, and for push and pull directions, respectively

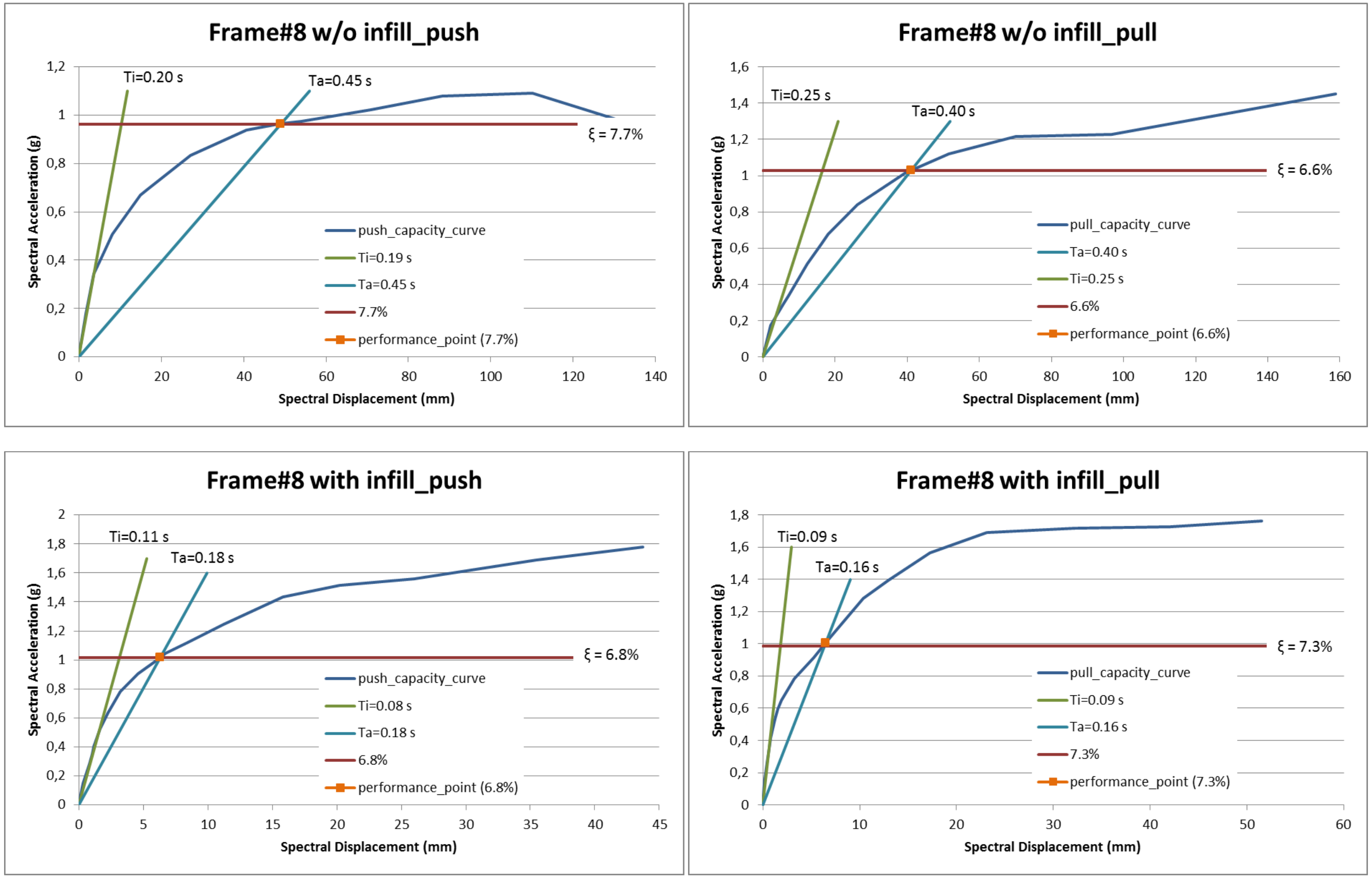

Figure 172: Sd-Sa graphs of Frame#8 without and with infill, and for push and pull directions, respectively

In addition to these, a two story structure composed of 2 Frame#8's with *bağdadi* covering on top of each other was also solved by means of the ATC-40 procedure. For this aim, an envelope curve for such a structure was manually formed and capacity calculations were carried out for 1st and 2nd story top movement, and these curves were subjected to the above-explained procedure. The results are shown in Figure 173-Figure 174 and Table 7.

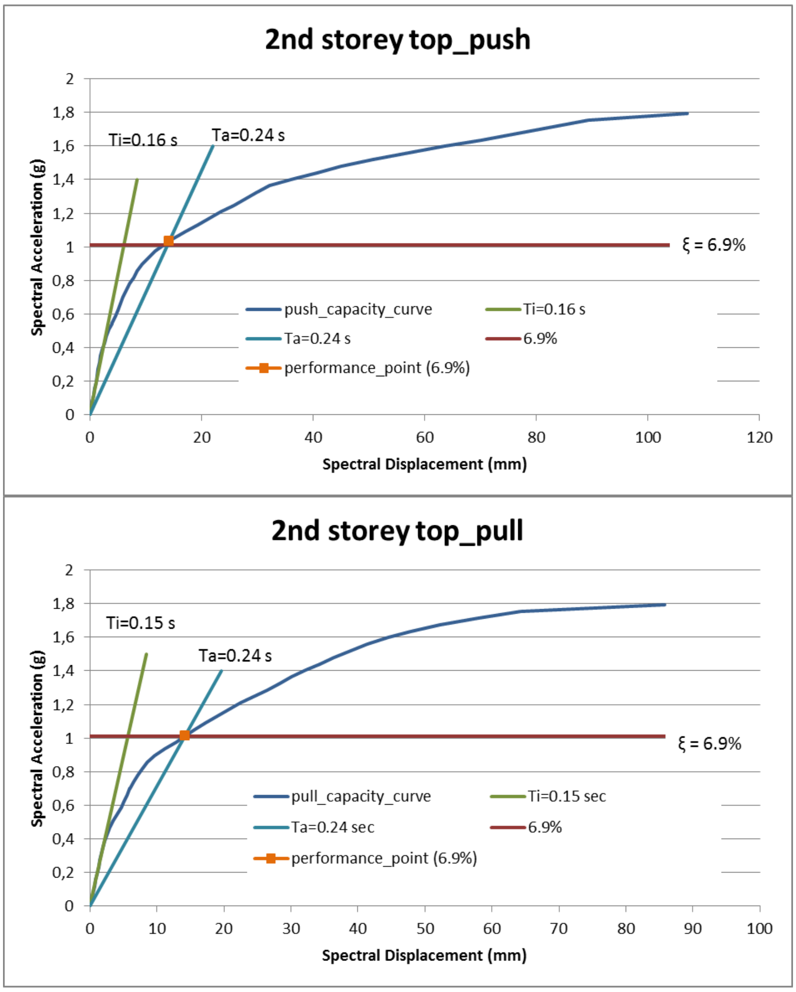

Figure 173: Sd-Sa graphs of the second story of a two story structure composed of 2 Frame#8 with *bağdadi* covering, and for push and pull directions, respectively

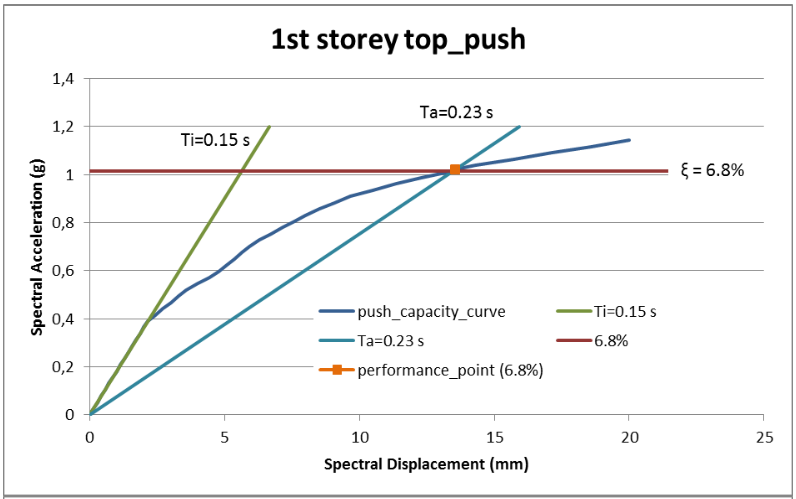

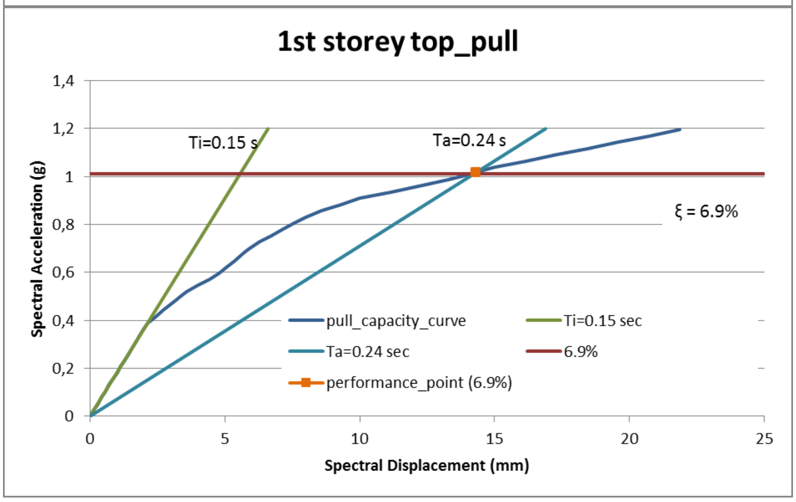

Figure 174: Sd-Sa graphs of the first story of a two story structure composed of 2 Frame#8 with *bağdadi* covering, and for push and pull directions, respectively

Table 7: Results of the capacity calculations for each frame without and with infill/covering

			Spectral Acceleration Graph			Spectral Acceleration Graph
2nd story	push	Ti=0.16 s Ta= 0.24 s Sd= 14.2 mm ξ= 6.9%	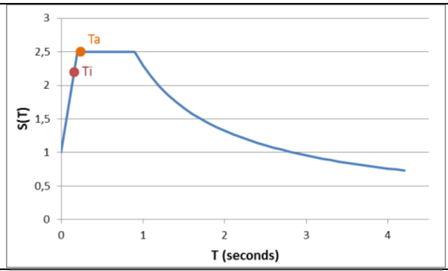	pull	Ti=0.15 s Ta= 0.24 s Sd= 14.1 mm ξ= 6.9%	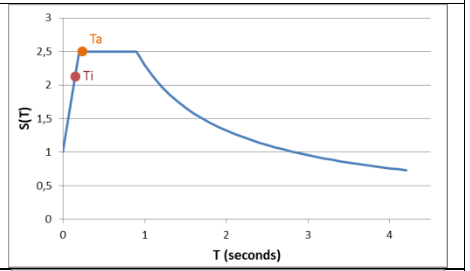
1st story	push	Ti=0.15 s Ta= 0.23 s Sd= 13.6 mm ξ= 6.8%	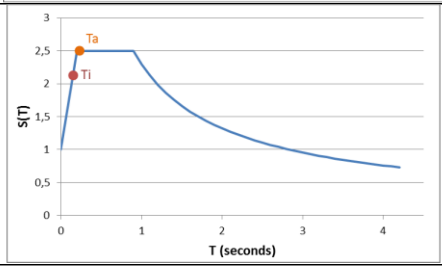	pull	Ti=0.15 s Ta= 0.23 s Sd= 14.3 mm ξ= 6.8%	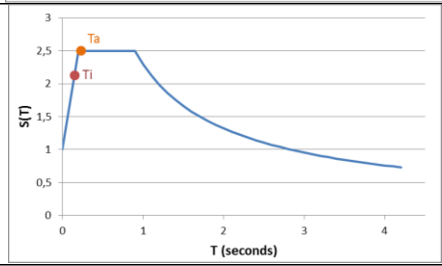

CHAPTER 4

MATERIAL TESTS

In this study, a number of material tests were carried out in order to determine the certain material properties of lime-based plaster and mortar, adobe and brick blocks and adobe and brick masonry samples, as well as nails, used in the tested frames. Adobe and brick blocks and adobe and brick masonry samples as well as samples taken from plaster and mortar by means of standard cylinders were tested under compressive loading. Nails, on the other hand, were subjected to tensile loading. A series of pull-in/pull-out test were also carried out to determine the load-displacement behavior of a nailed connection. In addition, yellow pine and fir timber samples were tested under bending and compression in parallel-to-grains and perpendicular-to-grains directions.

4.1. COMPRESSION TESTS ON PLASTER AND MORTAR SAMPLES

In this section, the results of compression tests carried out on lime-based plaster and mortar samples are given. In the frame tests, mortar and plaster were prepared according to traditional recipes by local construction workers from Beypazarı, a district of Ankara, known for its historical tissue composed of Ottoman timber frame houses. The preparation techniques for mortar and plaster are as follows:

PLASTER: 1 unit of soil is mixed with 1 unit of lime called *tekke kireci*[10], and then, again, some water, whose amount is determined according to the consistency of the final compost, is added.

MORTAR: Mortar preparation differs from each other based on where to be used. In the brick masonry infill walls, mortar is prepared by mixing 2 units of soil, 1 unit of lime and water. Water is added slowly and its amount is adjusted according to the consistency of the final compost. When mortar is to be used in adobe infill walls, on the other hand, soil, water and straw is mixed, in undefined proportions, until the compost has the desired consistency.

---

[10] The raw material of *tekke kireci* (*Tekke* lime) is obtained from the stone quarries around Beypazarı and then processed in Tekke village of Beypazarı. The plaster obtained using *Tekke kireci* is called *Tatlı Sıva* (*Tatlı* plaster) (Urak and Çelebi; 2005: 401- 403).

All plaster and mortar samples were taken by means of 15 cm long standard sampling cylinders, with a diamater of 7.5 cm (Figure 175). The soil-based mortar samples crumbled as soon as they were taken out of the sampler, therefore could not been tested. The compressive strength values obtained for the lime-based plaster and mortar samples as given in Table 8 and Table 9.

Figure 175: Plaster and mortar samples taken by standard sampling cylinders

Table 8: Compressive strength values of lime-based plaster samples

SAMPLE NO	DIAMETER (CM)	HEIGHT (CM)	FAILURE LOAD (KG)	STRENGTH (MPa)
1	7*	13.5*	500	0.318526
2	7*	13.5*	510	0.324896
3	7*	13.5*	480	0.305785
			average	0.316402

*The plaster samples shrank in both dimensions.

Table 9: Compressive strength values of lime-based mortar samples

SAMPLE NO	DIAMETER (CM)	HEIGHT (CM)	FAILURE LOAD (KG)	STRENGTH (MPa)
1	7.5	15	1109	0.615432
2	7.5	15	1320	0.732525
3	7.5	15	1110	0.615987
			average	0.654648

4.2. COMPRESSION TESTS ON ADOBE AND BRICK BLOCKS

The adobe and brick blocks were also tested under compression. Before, the testing, the edges of the blocks were adjusted (Figure 176), and the samples were capped in order to apply the compressive loading in a homogeneous manner. The capping was done by usign a cement-based compost (Figure 177), since the conventional sulphur-based compost did not adhere to the samples. As seen in Figure 178, the capping was first done at one face of the blocks, and when the cemen-based compost is dried, it was applied to the other face.

Figure 176: Before capping the adobe and brick samples, their edges were adjusted by cutting

Figure 177: Cement based mortar was prepared for capping

Figure 178: Capping

The adobe blocks, used as an infill material in the tested frames, were prepared by the local construction masters from Beypazarı. The preparation technique of adobe blocks is given below:

ADOBE BLOCKS: 3 units of soil are mixed with 1 unit of straw. Please note that soil is taken from the vicinity of a river bed. Then, water is added to the mixture. The workers cannot define the amount of water. Water is added slowly and its amount is adjusted according to the consistency of the final compost. The mixture is kept for one day, and the next day, it is mixed once more and poured into molds.

The adobe blocks were 9-11.5 cm x 9-11.5 cm x 20-21 cm, while the brick blocks were 21x10x6 cm in size. The compressive strength values obtained for adobe and brick blocks are given in Table 10 and Table 11.

Table 10: Compressive strength values of adobe samples

SAMPLE NO	BOTTOM SURFACE (CM)	UPPER SURFACE (CM)	FAILURE LOAD (KG)	STRENGTH (MPa)
1	21 x 9.5	20 x 10	3700	1.211506
2	20 x 10	21.5 x 9	2950	0.974882
3	20.5 x 10.5	20.5 x 10	5050	1.558571
4	21.5 x 11.5	20 x 11.5	3000	0.812145
			average	1.137296

Table 11: Compressive strength values of brick samples

SAMPLE NO	BOTTOM AND UPPER SURFACE (CM)	INTERNAL GAP (CM) (ON ONE SIDE)	FAILURE LOAD (KG)	STRENGTH (MPa)
1	21 x 10	14.5 x 4.5	18930	10.46596
2	21 x 10	14.5 x 4.5	27740	15.3368
3	21 x 10	14.5 x 4.5	15870	8.774153
4	21 x 10	14.5 x 4.5	11140	6.159046
			average	10.18399

4.3. COMPRESSION TESTS ON ADOBE AND BRICK MASONRY SAMPLES

In addition to these tests on adobe and brick blocks, a number of masonry samples were also tested (Figure 179). For this aim, 4 brick and 4 adobe masonry samples were prepared. 3 of these samples were 1.5 masonry blocks long, while the 4th one was 2 masonry blocks long. Before testing them under compression, capping was carried out, again by using cement-based compost (Figure 180-Figure 181).

Figure 179: Adobe and brick masonry samples

Figure 180: Capping procedure

Figure 181: Adobe and brick masonry samples after capping

The tests were carried out using the instrument shown in Figure 182.

Figure 182: The equipment where compression tests were achieved

Two examples to samples failures are shown in Figure 183.

Figure 183: Two examples to the failures of adobe and brick masonry samples under compression

The compressive strength values obtained at the end of the tests carried out on adobe and brick masonry samples are shown in Table 12.

Table 12: Compressive strength values of masonry samples

SAMPLE	SURFACE AREA (CM)	FAILURE LOAD (KG)	STRENGTH (MPa)
Adobe	33 x 9.5	1500	0.469
Adobe	33 x 10	1200	0.357
Adobe	36 x 9	1580	0.478
Adobe	44 x 12	2240	0.416
		average	0.430
Brick 1	30 x 8.5	4750	1.827
Brick 2	29.5 x 8.5	3600	1.408
Brick 3	30 x 8.5	4000	1.538
Brick 4	39 x 9	5250	1.467
		average	1.560

4.4. NAIL TESTS

Nails can be of a variety of shape, length, quality and treatments, and connections may fail due to insufficient friction between the fastener and timber, as well as low strength (ASCE; 1996: 29, 43). In this study, all nails that were used at the connections of the tested frames were 12 cm long and 4.5 mm thick. The nails were first tested under tensile loading. Next, a series of push-in/pull-out were carried out.

4.4.1. TENSION TESTS

For the purpose of determining the tensile strength of the material, which the nail was manufactured from, tension test was carried out. For this aim, first of all, the head of the nail was cut so that the testing instrument can hold it. The resulting failure modes are shown in Figure 184. As seen, both ductile and brittle failure observed at the nails.

Figure 184: Nails after tension test

The nail failed at 1300 kg, therefore the tensile strength of the material is 82 kgf/mm^2 (~820 MPa).

4.4.2. PUSH-IN/PULL-OUT TESTS

A series of tests were carried out to determine the pull-out strength of a nail. For this aim, the head of the nails was cut so that the testing instrument can hold it (Figure 185). Next, the nail was pulled from the timber in order to determine the load value at which the nail comes completely out of the timber block (Figure 186). The pull-out test was repeated for all four faces of a timber block in order to understand the effect of the grains on the results. The pull-out load values obtained for four sides of a fir timber blocks are seen in Figure 187.

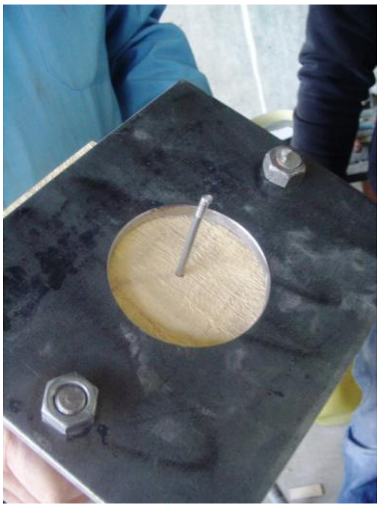

Figure 185: The nail inside the instrument

Figure 186: Pull-out test

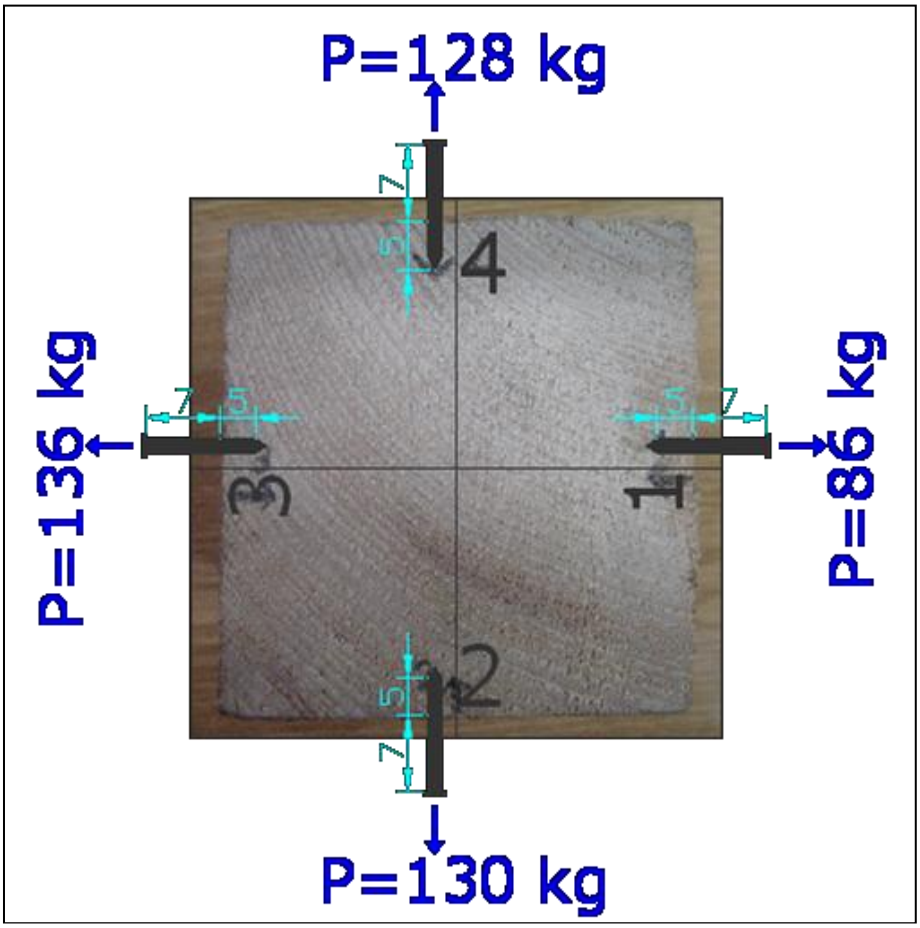

Figure 187: Pull-out load values obtained for all of the four faces of a timber block

In addition to this test, also a number of tests were carried out by using a different test set-up in order not only to determine pull-out load but also pull-in load in a cyclic manner. For this aim, a test set-up composed of an LVDT of 100 mm and a load cell of 5 tons was formed. A timber block, on which a nail is driven, was connected to a base, which can be elevated and lowered with the help of a motor. The head of nail was cut, and welded to the screw at the tip of load cell (Figure 188).

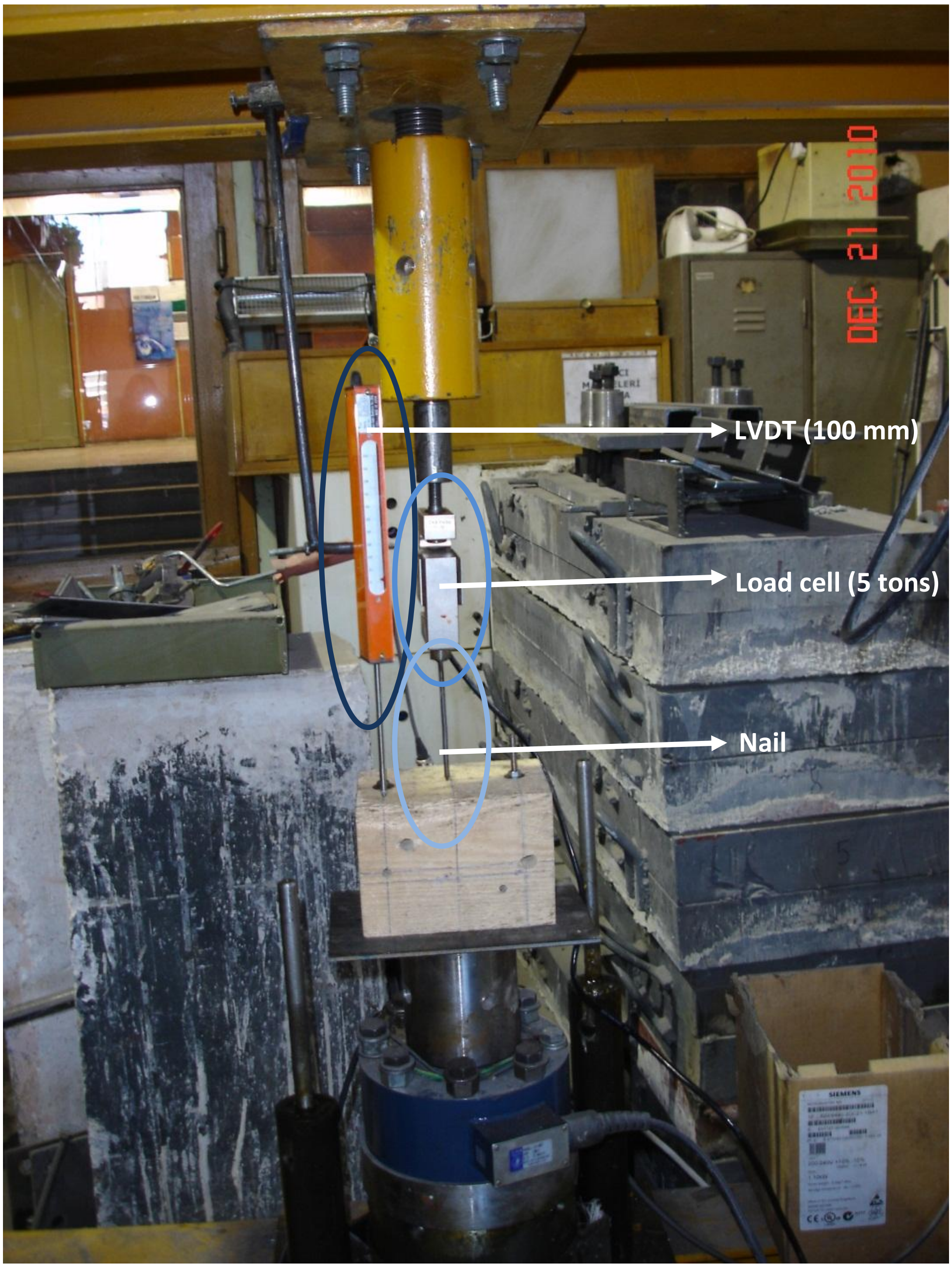

Figure 188: Test set-up used for pull-in/out tests

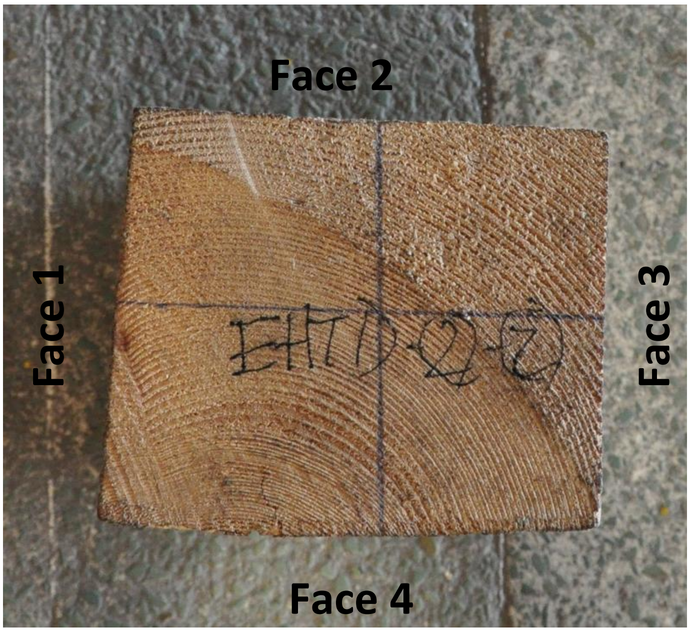

Figure 189: Numbering of pull-out faces

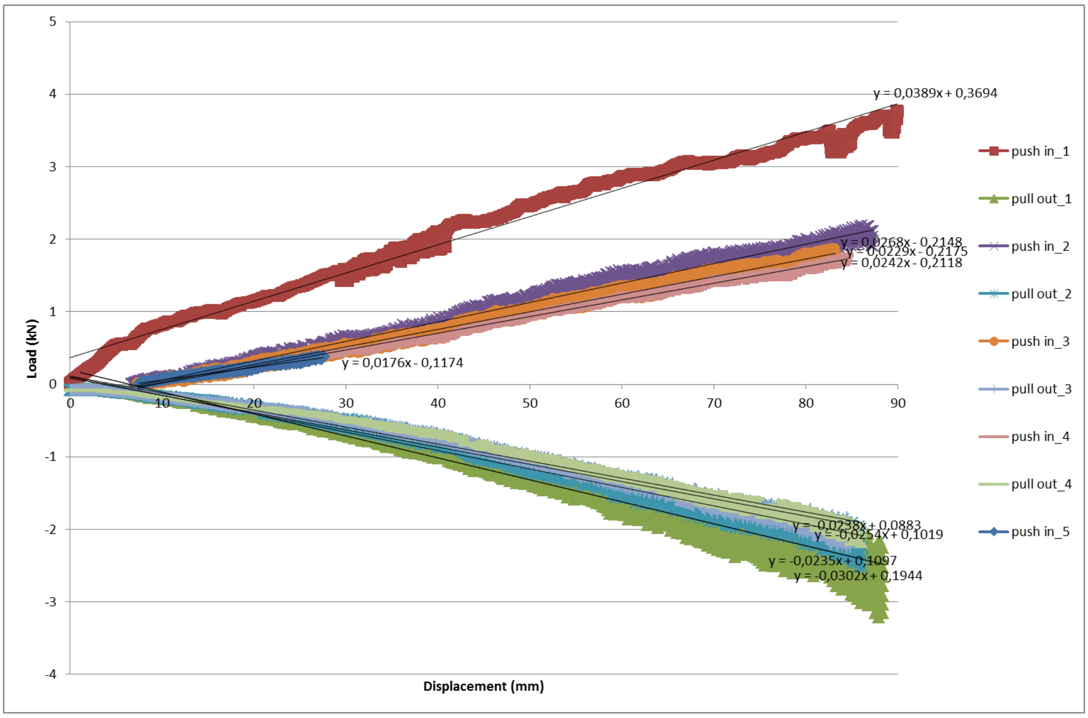

Figure 190: Decrease in stiffness shown in load-displacement graph (Face 1)

As seen in Figure 190, the stiffness of the first push-in cycle (shown in red) is higher than the others, since this is the first cycle where the nail is driven in the timber block. The stiffness values decrease each time it comes out and is driven again back to the timber block. The amount of decrease, on the other hand, is smaller each time; therefore, the decrease in stiffness seems to converge to zero.

The same procedure was repeated for the other three faces of the timber block. The results are shown in Figure 191-Figure 193.

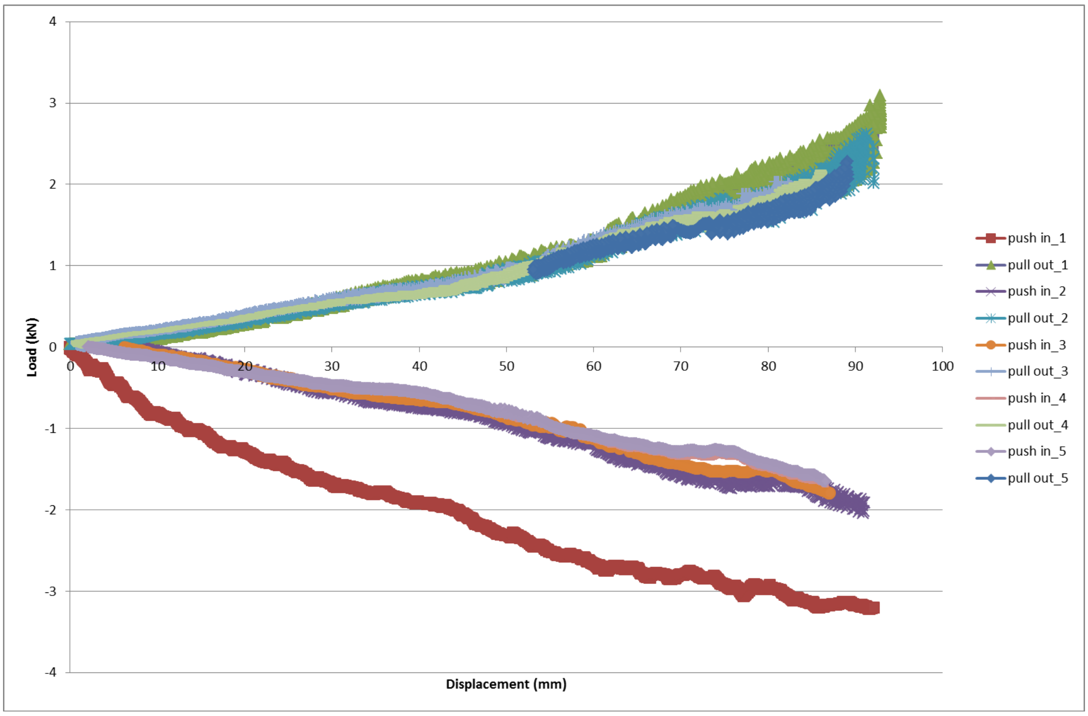

Figure 191: Decrease in stiffness shown in load-displacement graph (Face 2)

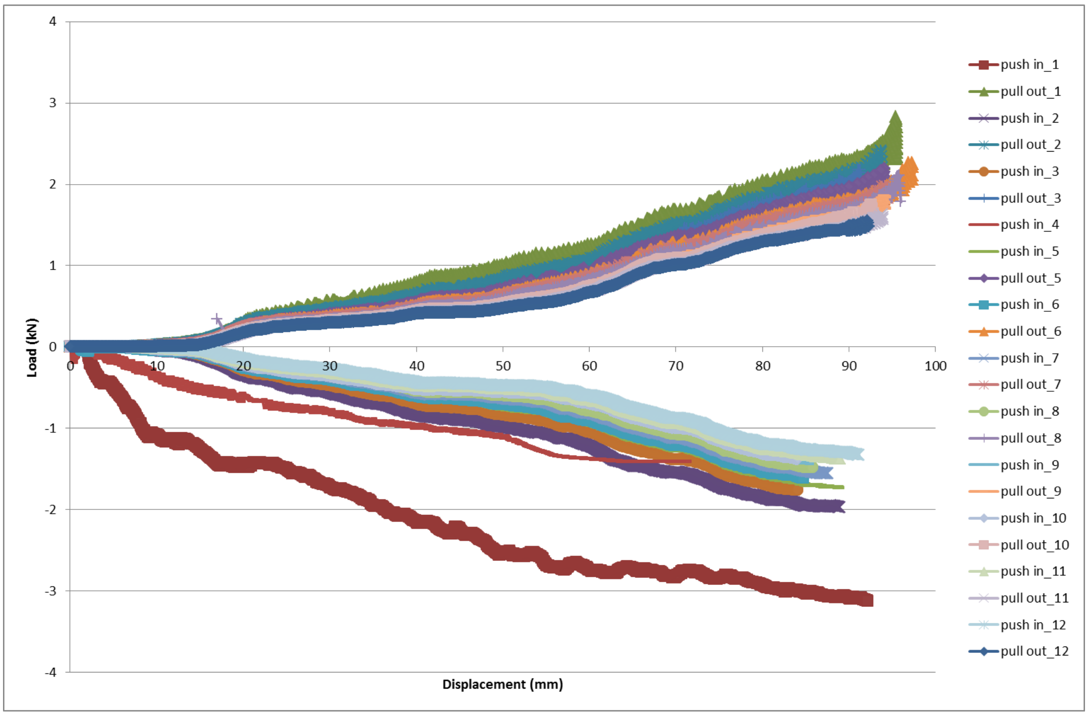

Figure 192: Decrease in stiffness shown in load-displacement graph (Face 3)

Figure 193: Decrease in stiffness shown in load-displacement graph (Face 4)

As seen from Figure 187, and Figure 190-Figure 193, the results obtained from two different pull-out tests are consistent.

4.5. TIMBER TESTS

In addition to the material tests, mentioned in the previous sections, timber specimens were also tested under bending and compression. The tests were carried out in accordance with the procedures given in ASTM D143-09.

4.5.1. BENDING TESTS

For the aim of bending tests, 50 x 50 x 760 mm yellow pine and fir specimens were prepared and centrally loaded with a span length of 710 mm according to ASTM D143-09 procedure. The recommended loading rate of 2.5 mm/min was respected (Figure 194-Figure 198).

Figure 194: Overall view of the instrument, where bending tests were carried out

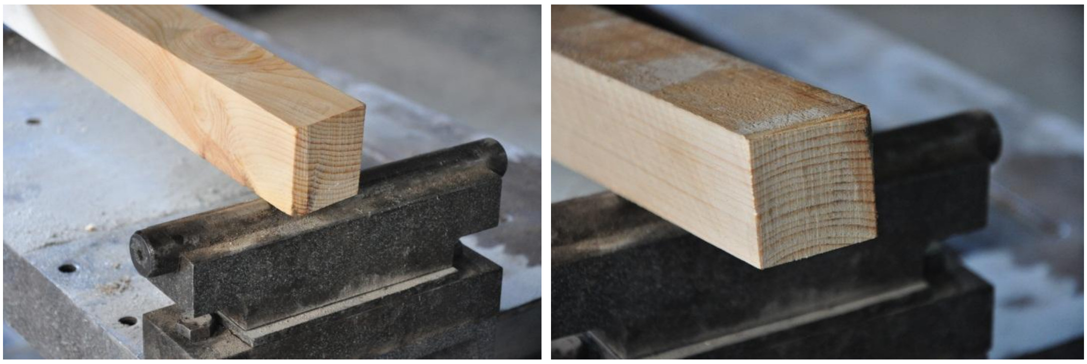

Figure 195: Placement of specimens

Figure 196: Adjusting the specimen for a central loading

Figure 197: Testing of the specimens

Figure 198: Specimens after testing

According to ASTM D143-09, the failure mode of Y.P.#1 is brash tension, that of F.#1 is horizontal shear and finally that of F.#2 is cross-grain tension (Figure 198). The obtained flexural strength values from bending tests as well as calculated flexural stress values are given in Table 13 and Figure 199. The flexural stress values were calculated by using the following formula:

$$\sigma = \frac{M * c}{I} \tag{15}$$

where

σ: bending stress (MPa)

M: moment (kN.mm)

c: distance to the neutral surface (mm)

I: moment of inertia (mm^4)

$$I = \frac{b * h^3}{12} \tag{16}$$

where

b: section width (mm)

h: section height (mm)

In our case, $c = {50}/{2} = 25\ mm$, $b = h = 50\ mm$, $M = P * \frac{710}{2} = 355P\ kN.mm$ and $I = \frac{50*50^3}{12} = 26.04x10^6\ mm^4$.

Table 13: Results of bending tests, carried out on yellow pine and fir specimens

Yellow pine	Ultimate flexural strength (P) (kN)	Moment (M) (kN.mm)	Flexural stress (σ)(MPa)	Fir	Ultimate flexural strength (P) (kN)	Moment (M) (kN.mm)	Flexural stress (σ)(MPa)
#1	5.5	1952.5	1.88	#1	8.8	3124.0	3.00
#2	4.9	1739.5	1.67	#2	7.4	2627.0	2.52
#3	7.9	2804.5	2.69	#3	8.3	2946.5	2.83
#4	8.8	3124.0	3.00	#4	8.3	2946.5	2.83
average	6.8	2414.0	2.32	average	8.2	2911.0	2.80

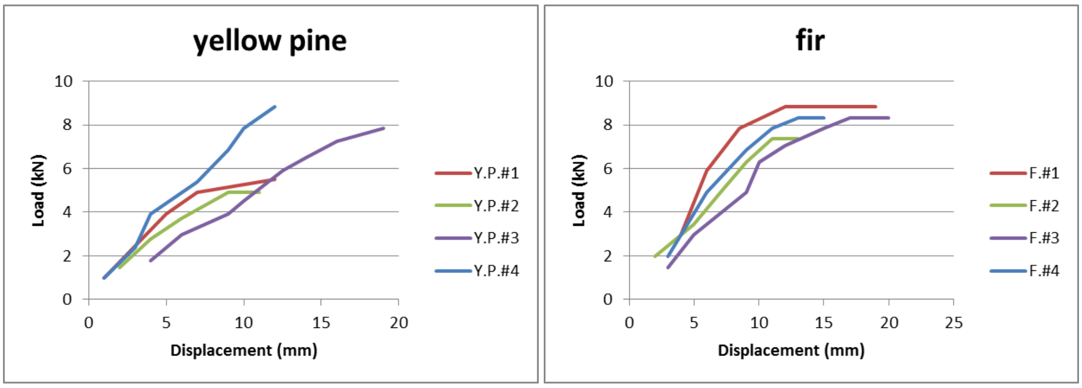

Figure 199: Results of bending tests, carried out on yellow pine and fir specimens

4.5.2. COMPRESSION TESTS

The timber specimens were also tested under compression perpendicular and parallel to grains. Also in this case, ASTM D-143-09 was taken as reference. The instrument used for the aim of compression tests is shown in Figure 200.

Figure 200: Views of the instrument, where compression tests were carried out

(a) Compression tests parallel to grains: According to ASTM D143-09, in order to test the compressive strength in the weaker direction of yellow pine and fir, 50 x 50 x 200 mm specimens are needed. However, in these tests 50 x 50 x 150 mm specimens could be prepared. The recommended loading rate of 0.305 mm/min could not been applied due to the settings of the instrument used, therefore the tests were carried out by using the lowest possible rate, which was 90 kg/sec.

Figure 201: Measurement of the specimen lengths

The lengths of the specimens were measured before and after the test by means of an electronic caliper (Figure 201). The obtained results are given in Table 14.

In addition the compressive stress values were calculated by using the following formula:

$$\sigma = \frac{P}{A} \tag{17}$$

where,

P: Compressive strength (kN)

A: Surface area (mm2)

σ: Compressive stress (MPa)

In this case, $A = 50 * 50 = 2500\ mm^2$.

Table 14: Results of compression tests parallel to grains, carried out on yellow pine and fir specimens, 50 x 50 x 150 mm in size (note that Y.P. stands for yellow pine ad F. stands for fir)

Specimen	Compressive Stress (P) (kN)	Ultimate compressive strength (σ)(MPa)	Initial Length (mm)	Last length (mm)	Decrease in Length (%)
Y.P.#1	93.8	0.038	*	*	*
Y.P.#2	83.0	0.033	148	146.5	1.01
Y.P.#3	108.7	0.043	144.5	142.5	1.38
Y.P.average	85.2	0.038	146.3	144.5	1.20
F.#1	126.5	0.051	147.6	146	1.08
F.#2	98.9	0.040	147.2	146.2	0.68
F.#3	111.7	0.045	152	150.8	0.79
F.#4	115.8	0.046	151.7	149.7	1.32
F.average	113.2	0.045	149.6	148.2	0.97

* The first specimen was loaded beyond its ultimate limit to see the deformed shape more clearly (Figure 202).

Figure 202: A distorted specimen (yellow pine #1) after compression test parallel to grains

(b) Compression tests perpendicular to grains: According to ASTM D143-09, compression tests perpendicular to grains should be carried out on specimens, 50 x 50 x 150 mm in size. However, within the framework of this thesis, the specimens to be tested under compression were taken from the frames previously tested under in-plane reverse cyclic lateral loading, and it was seen that 50 x 50 x 150 mm timber specimens are not available for compression test parallel to grain. For this reason, 50 x 50 x 50 mm and 50 x 59 x 95 mm specimens were prepared, and they were tested not only under compression parallel to grains but also perpendicular to grains to see how the ultimate strength values change according to specimen size. The recommended loading rate of 0.305 mm/min could not be applied due to the settings of the instrument used, therefore the tests were carried out by using the lowest possible rate, which was 90 kg/sec.

Figure 203: Compression test perpendicular to grains

Table 15: Results of compression tests perpendicular to grains, carried out on yellow pine and fir specimens, 50 x 50 x 50 mm in size (Y.P. stands for yellow pine ad F. stands for fir)

Specimen	Compressive Stress (P) (kN)	Ultimate compressive strength (σ)(MPa)
Y.P.#1	14.8	0.006
Y.P.#2	11.5	0.005
Y.P.#3	16.3	0.007
Y.P.#4	16.4	0.007
Y.P.average	14.7	0.006
F.#1	9.9	0.003
F.#2	11.8	0.005
F.#3	7.5	0.003
F.#4	8.4	0.003
F.average	9.4	0.004

Table 16: Results of compression tests perpendicular to grains, carried out on yellow pine and fir specimens, 50 x 50 x 95 mm in size (Y.P. stands for yellow pine ad F. stands for fir)

Specimen	Compressive Stress (P) (kN)	Ultimate compressive strength (σ)(MPa)
Y.P.#1	13.7	0.006
Y.P.#2	13.2	0.005
Y.P.#3	14.2	0.006
Y.P.#4	15.3	0.006
Y.P.average	13.7	0.006
F.#1	8.8	0.035
F.#2	8.8	0.035
F.#3	10.0	0.004
F.#4	9.6	0.004
F.average	9.3	0.004

After compression test perpendicular to grains, the specimens are distorted and sometimes cracked as shown in Figure 204 and Figure 205.

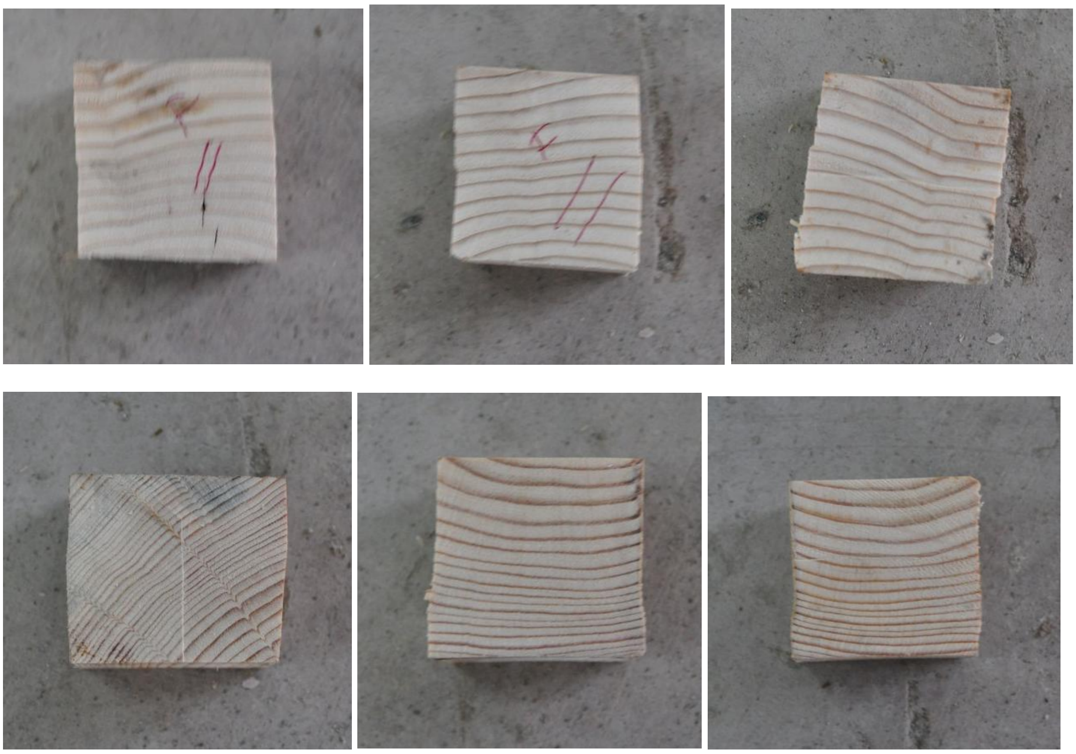

Figure 204: Distorted specimens after compression test parallel to grains

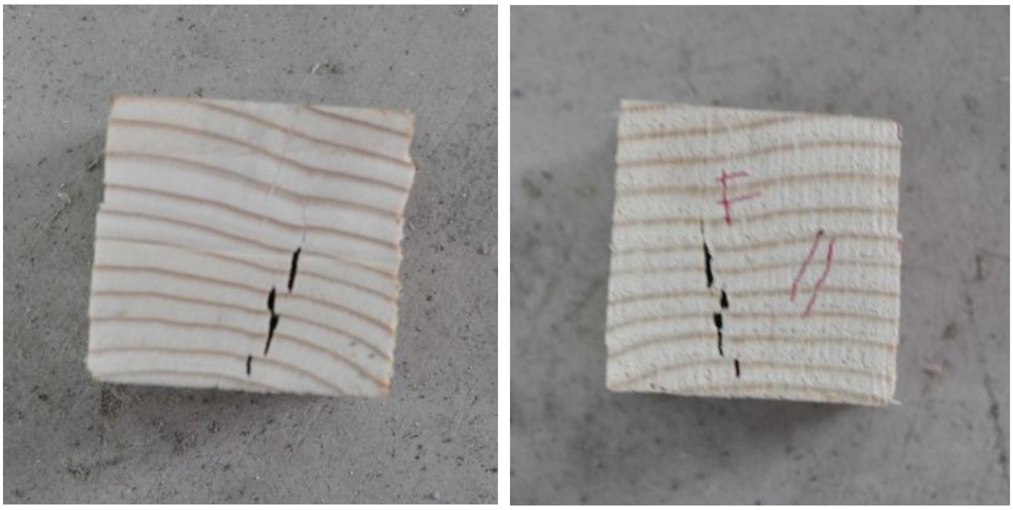

Figure 205: A distorted and cracked specimen after compression test parallel to grains

Figure 206: Distorted shapes of two 50x50x95 specimens, loaded beyond their ultimate strengths

The compression parallel to grains tests were repeated by using two specimens, 50 x 50 x 50 mm in size. The obtained results are given in Table 17. Specimens are mostly cracked as can be seen in Figure 207.

Table 17: Results of compression tests parallel to grains, carried out on yellow pine and fir specimens, 50 x 50 x 50 mm in size (Y.P. stands for yellow pine ad F. stands for fir)

Yellow pine	Compressive Stress (P) (kN)	Ultimate compressive strength (σ)(MPa)
Y.P.#1	14.8	0.0059
Y.P.#2	11.5	0.0046
Y.P.#3	16.3	0.0065
Y.P.#4	14.2	0.0057
Y.P.average	14.2	0.0057
F.#1	9.9	0.0040
F.#2	11.7	0.0047
F.#3	7.5	0.0030
F.#4	8.4	0.0034
F.average	9.4	0.0038

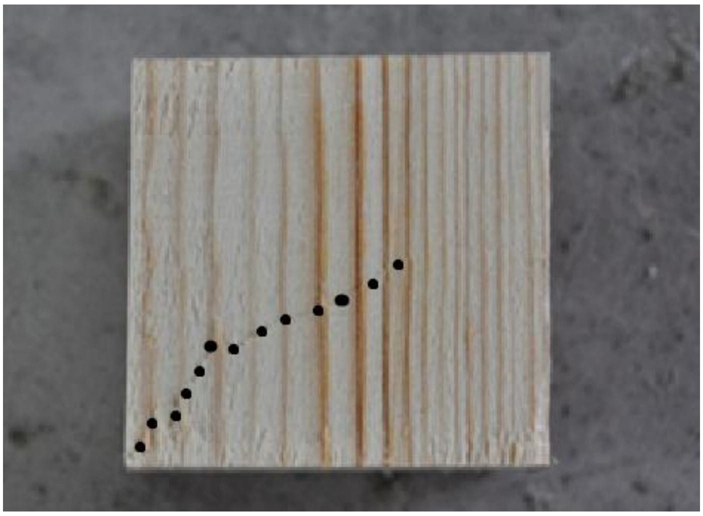

Figure 207: A cracked specimen after compression test parallel to grains

CHAPTER 5

CURVE-FIT STUDIES

In this study, a number of curve-fit studies were carried out in order to develop a series of empirical formulas for energy dissipation capacity and stiffness. For this aim, the cumulative energy dissipation and overall stiffness values' set, obtained for each frame without and with infill/covering, was tried to be normalized in such a way that the values set for each test gets closer to each other (Figure 208-Figure 209, and Figure 210-Figure 211 for energy dissipation capacity and overall stiffness, respectively).

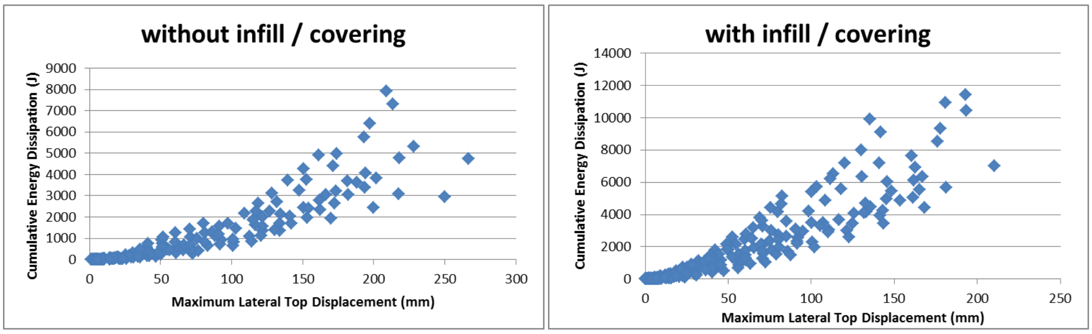

Figure 208: Maximum lateral top displacement versus cumulative energy dissipation relationship before normalization

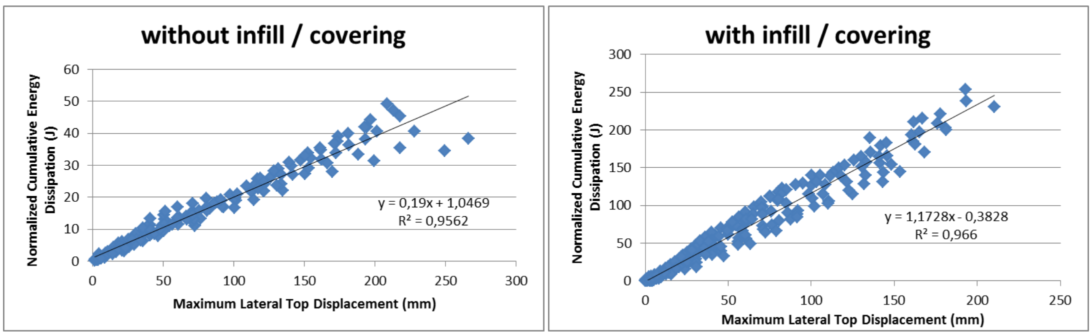

Figure 209: Maximum lateral top displacement versus normalized cumulative energy dissipation relationship

Next, a curve was tried to be fit to obtained point set. According to this, the obtained equations are as follows:

$$E_{diss} = \left(W_{eff} + 0.0638A_{eff}\right) * (0.19D_{max} + 1.0469)^2 \qquad \text{without infill case} \qquad (18)$$

$$E_{diss} = \left(0.873W_{eff} + 0.055A_{eff}\right) * (1.1865D_{max} + 0.5697)^{3/2} \qquad \text{with infill case} \qquad (19)$$

E_{diss}: Energy dissipation (J)

W_{eff}: Effective width = Frame width – total width of openings (m)

A_{eff}: Effective area = Frame area – total area of openings (m^2)

D_{max}: Maximum lateral top displacement (mm)

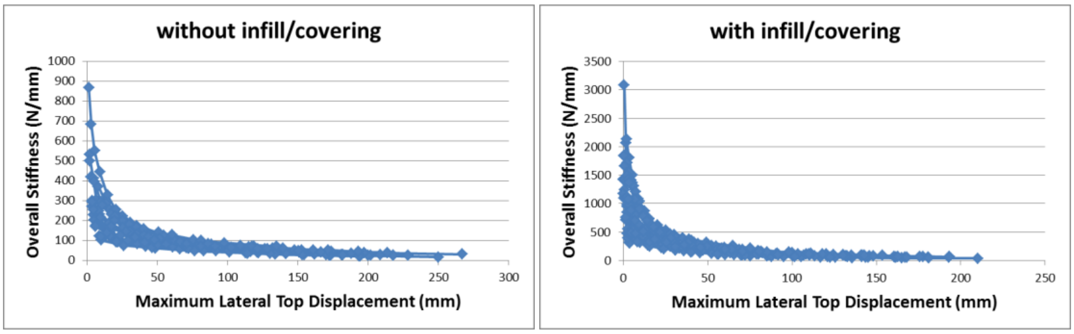

Figure 210: Maximum lateral top displacement versus overall stiffness relationship before normalization

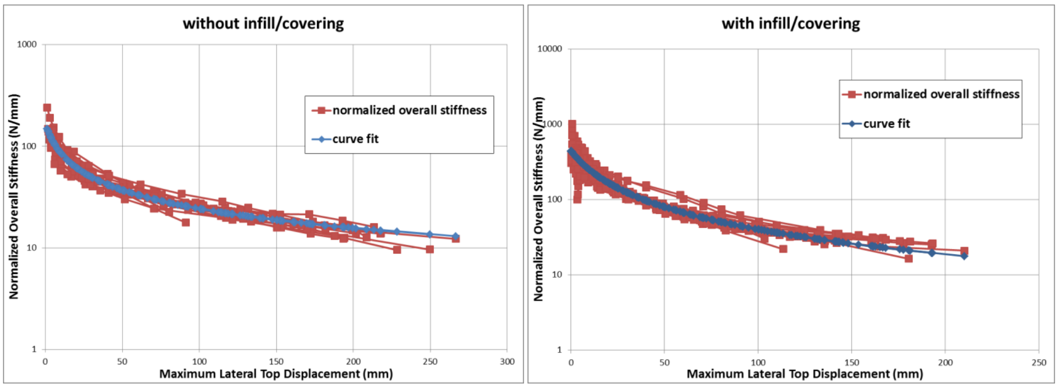

Figure 211: Maximum lateral top displacement versus normalized overall stiffness relationship

$k_{overall} = W_{eff} * (104.187/[0.2 * (D_{max} + 5.39)^{0.66}]$ without infill case (20)

$k_{overall} = W_{eff} * (337/[0.025 * (D_{max} + 16.19)^{1.22}]$ with infill case (21)

$k_{overall}$: Overall stiffness (N/mm)

W_{eff}: Effective width = Frame width – total width of openings (m)

D_{max}: Maximum lateral top displacement (mm)

Effective width and effective area values for the frame set, tested within the framework of this thesis work, is as shown in Table 18.

Table 18: Effective width and effective area values of the frames

Frame	Effective width (m)	Effective area (m^2)
1	1.78	8.2998
2	3.6	11.88
3	3.6	11.88
4	1.78	8.2998
5	1.81	10.0176
6	2.42	13.3337
7	3.06	13.4649
8	2.59	10.0936

CHAPTER 6

RESULTS AND DISCUSSIONS

Turkey is a seismically active country and prone to earthquake induced damages. Taking into consideration that a major part of the registered built heritage in Turkey is composed of traditional Ottoman timber frame "*hımış*" houses, the need for an evaluation of these structures from an engineering point of view is apparent. For this reason, in this study, seismic resistance of traditional Ottoman *hımış* houses with timber frame construction was aimed to be investigated, by means of experimental and analytical studies, for the aim of support their proper conservation. The results obtained at the end of this study can be listed as follows:

- Total of 16 cyclic reversed loading tests were conducted on 8 different *hımış* frames for without and with infill/covering conditions. The test results showed that failures are always governed by the failures at the connections. Under in-plane lateral loading, especially the bottom connections on the far right and left, as well as those at the both ends of diagonal braces are the first ones to loosen, dilate and eventually fail. At each loading cycle, nails at the opposite side of loading direction, were pulled out partially, and at the next cycle they are driven back to their original places, until a point where the nail gets buckled and the connection is completely lost.

- The pull-out and push-in tests carried out on nails showed that the resistance of the nail slightly reduced under repetitive pull-out and push in cycles and converges to a constant. The calculated average stiffness of a 12 long nail with Ø4.5mm diameter is measured 26 N/mm on an average. The average energy dissipated by a nail, on the other hand, is 82J.

- In the frame tests, two different types of wood were used: yellow pine, and fir. However, wood type seems not to be very important since failures always occur at the connections and wood is not stressed to its strength limits.

- Within the timber frames that were tested under reverse cyclic lateral loading, within the framework of this study, there were certain randomnasses that affect the behavior. First of all, the connections were made of the sole use of nails, in line with the traditional construction methods of traditional Ottoman timber frames, and the number and driving angle of nails at each connection was not standard. The number of nails at each connection changed between 1 and 5, based on the construction worker's appreciation. Therefore, the stiffness of connections was uneven throughout a frame. Another point is workmanship. Among the frame set, the workmanship was not standard, even though all frames were constructed, and repaired and infilled/cladded by the same two groups of construction masters. The timber elements forming the frame were occasionally not connected well. Slightly out-of-plane connections were in some cases observed. The laths used for *bağdadi* and *şamdolma* covering were not necessarily nailed to each timber element of the frame, they covered. These workmanship irregularities were not fixed before frame testing, since they are thought to be an intrinsic characteristic of the construction of traditional timber frame "*hımış*" houses.

- The timber frame set, tested within the framework of this thesis work, appeared to have high energy dissipation capacity, which is one the most important factor defining a structures seismic performance (Figure 212-Figure 213).

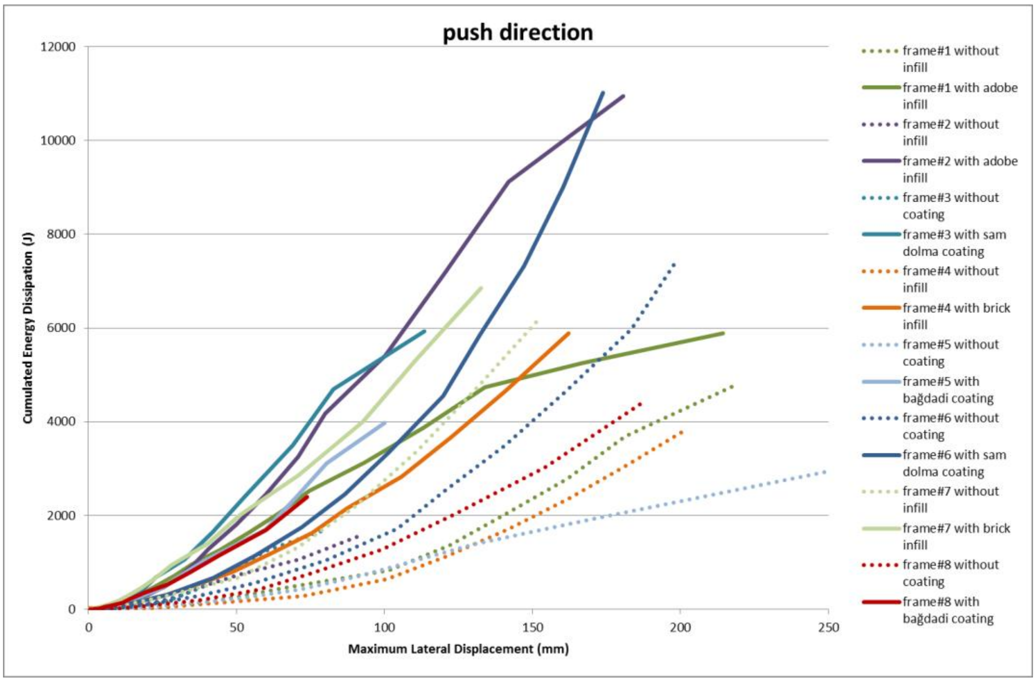

Figure 212: Maximum lateral displacement – Cumulative energy dissipation change in push direction

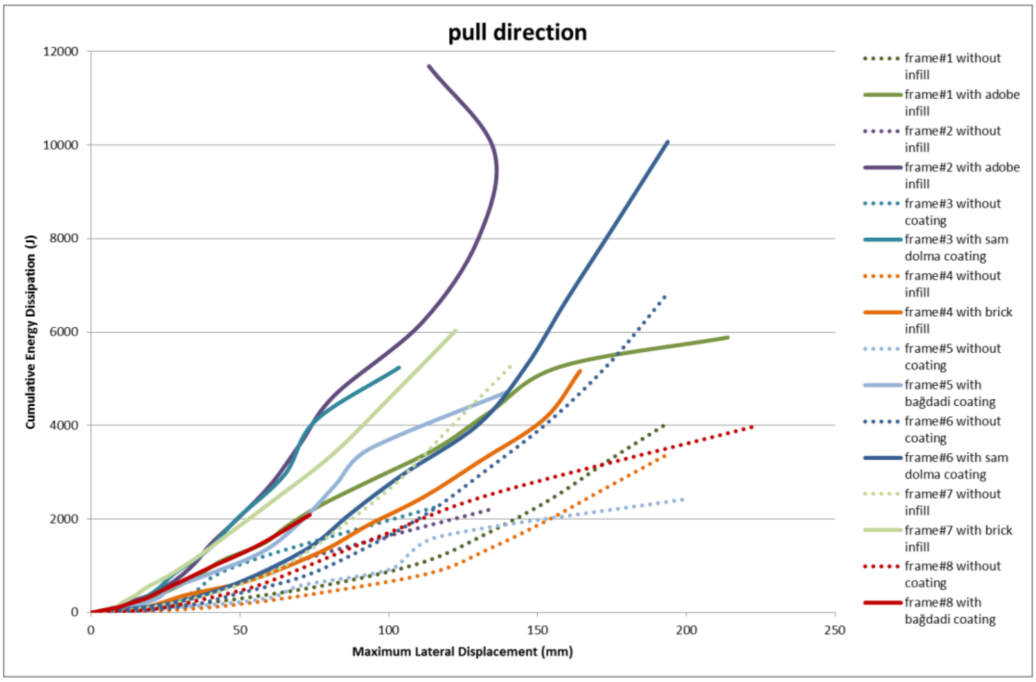

Figure 213: Maximum lateral displacement – Cumulative energy dissipation change in pull direction

- The load bearing capacity of a timber frame increases with infill/covering (Table 19). In with-infill/covering state, the overall stiffness values also increase (Figure 214-Figure 216 and Table 20).

Table 19: Load bearing capacity values without and with infill/covering (infill and covering techniques are shown in blue and pink, respectively)

Frame	Load bearing capacity without infill/covering (kN)	Infill/covering type	Load bearing capacity with infill/covering (kN)
1	>5.06	Adobe	>8.31
2	>7.87	Adobe	14.00
3	>7.70	*Şamdolma*	17.35
4	>4.65	Brick	>9.07
5	>3.32	*Bağdadi*	11.67
6	8.42	*Şamdolma*	>12.00
7	>8.35	Brick	13.34
8	>7.42	*Bağdadi*	>13.38

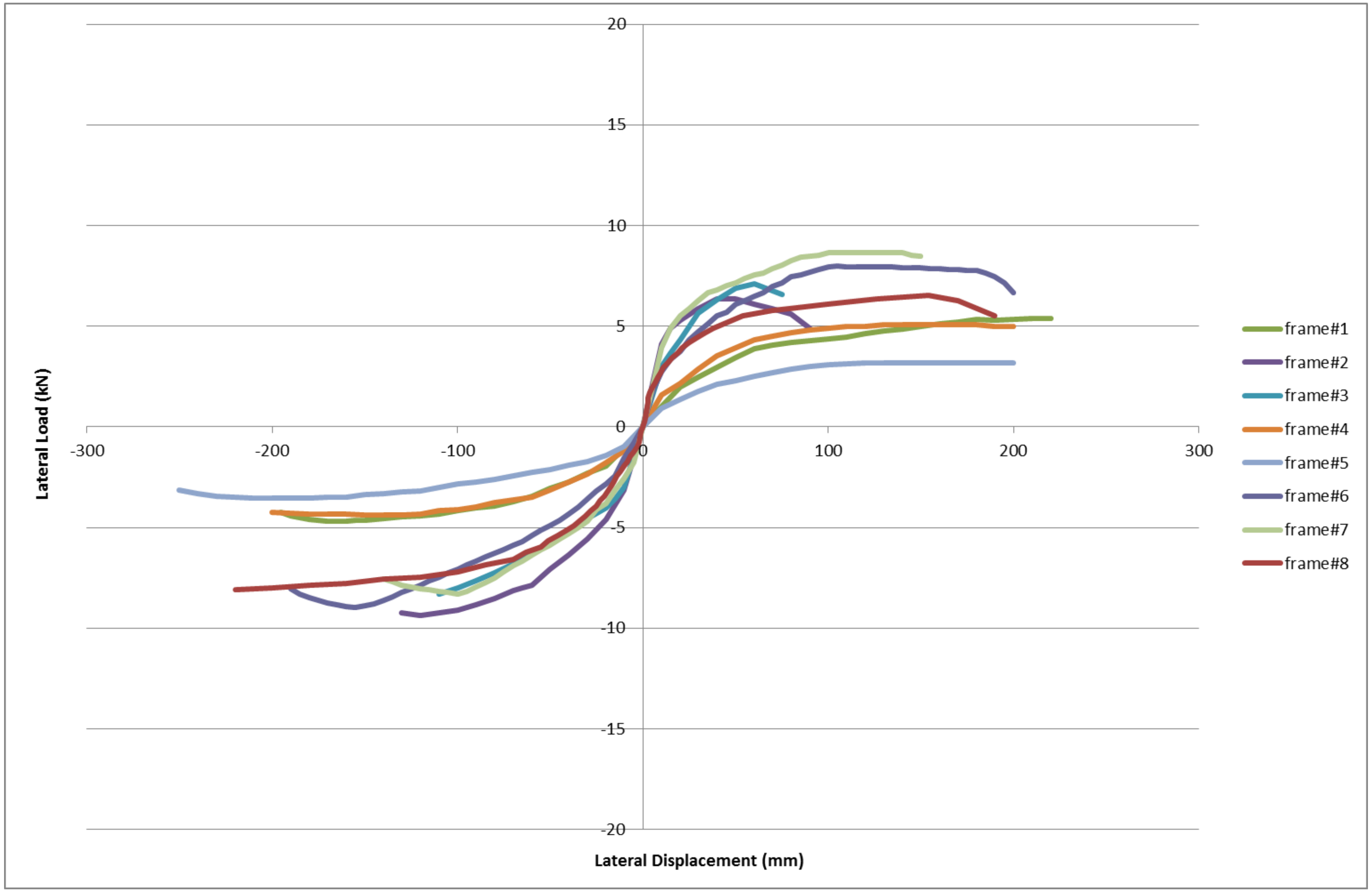

Figure 214: Envelope curves of frames without infill

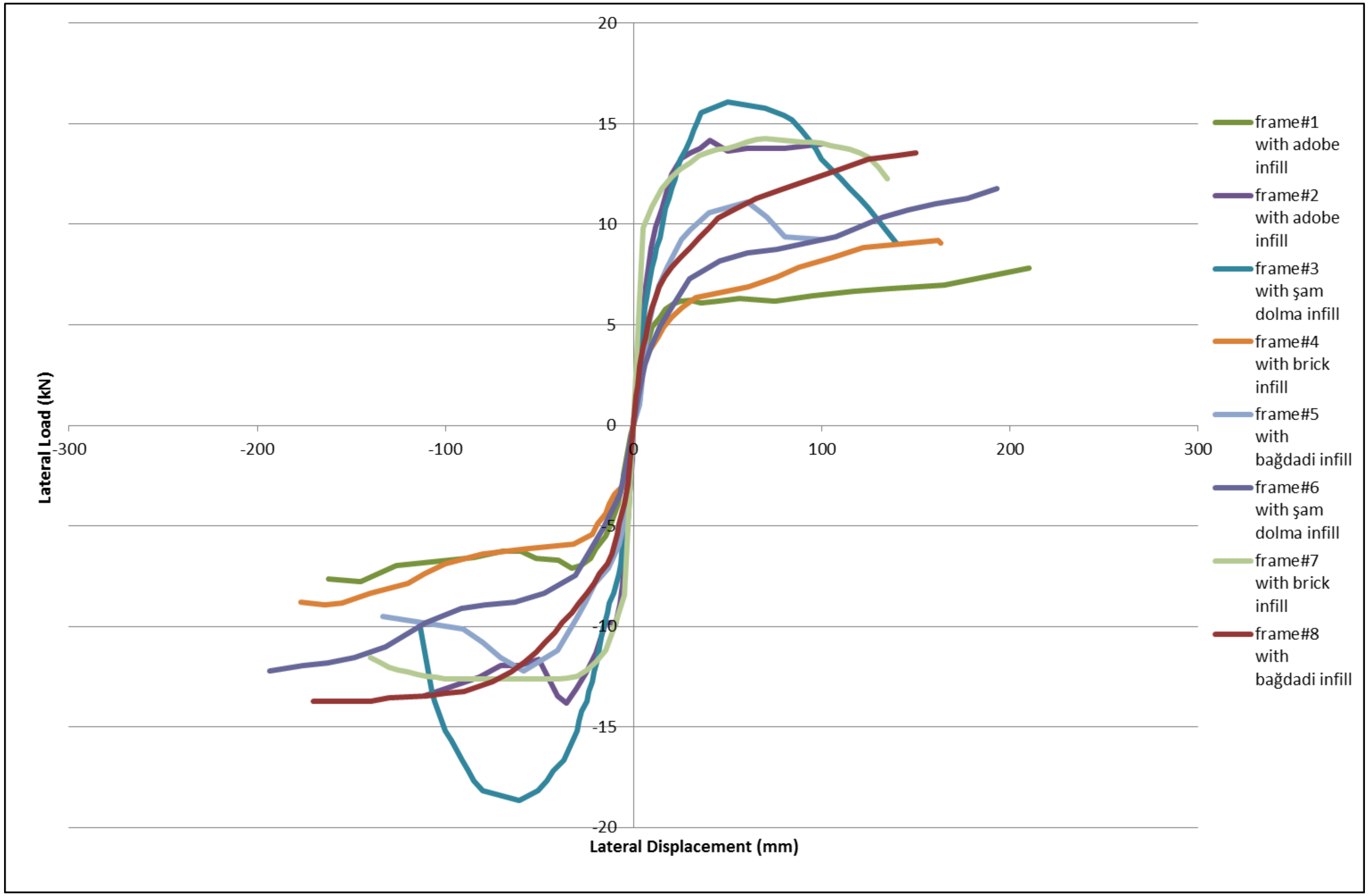

Figure 215: Envelope curves of frames with infill

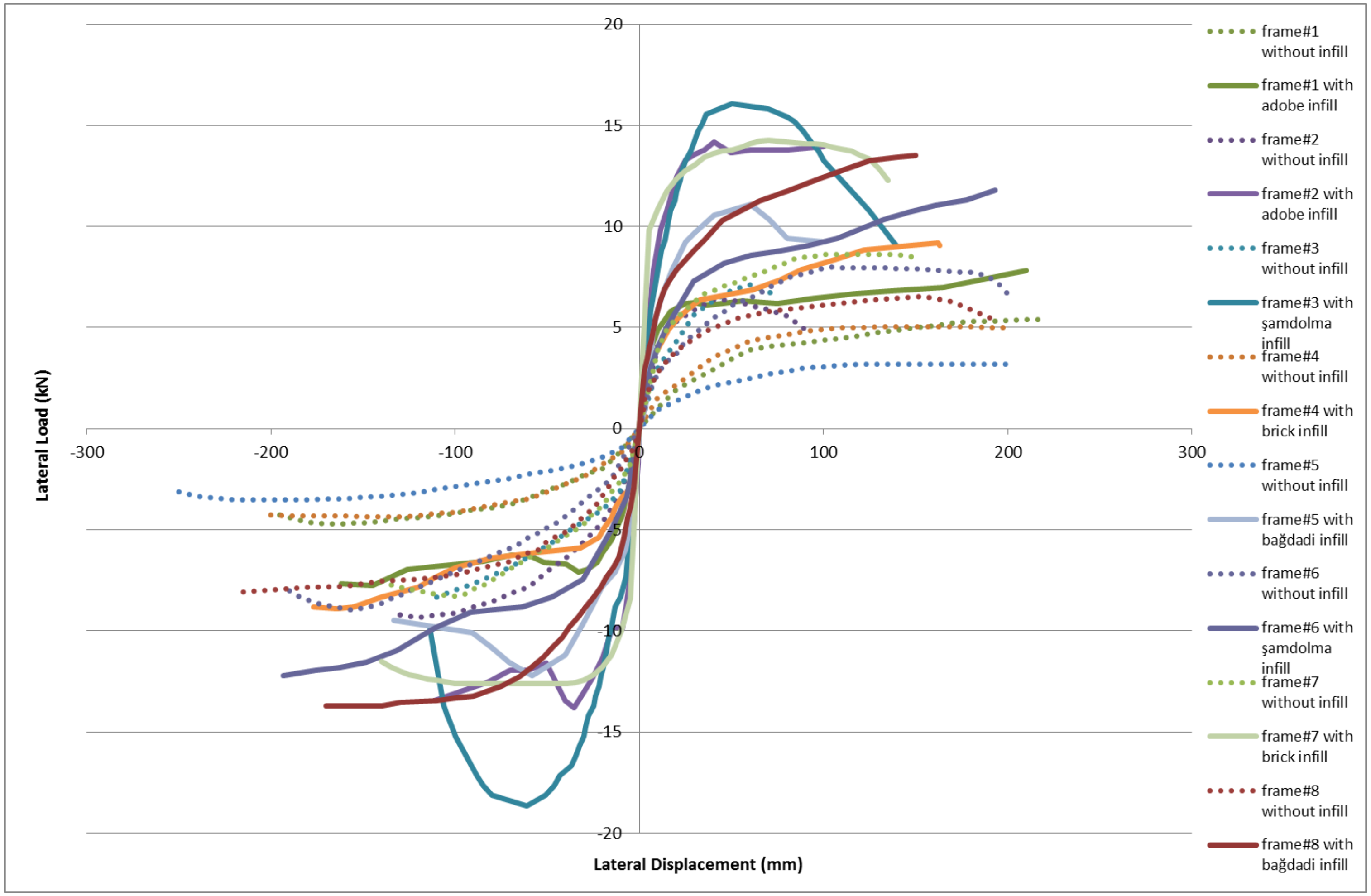

Figure 216: Envelope curves of the frames without and with infill

- On the other hand, infill/covering results also in weight increase and changes the period of the structure. As can be seen from Table 20, increase in weight is always higher than increase in load bearing capacity, except for Frame#5 with *bağdadi* covering. On the contrary, increase in stiffness is always higher than 1.

Table 20: Table showing average increases in load bearing capacity, stiffness and in weight in with-infill/cover state in comparison to without-infill/cover states (rows shown in blue indicates frames made of yellow pine, while those in green indicates frame made of fir)

Infill		Frame		Average Increase in Load Bearing Capacity	Average Increase in Overall Stiffness*	Average Increase in Initial Stiffness**	Increase in Weight	Increase in Load / Increase in Weight
Masonry Infill	Brick Masonry	4	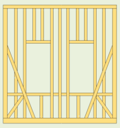	>1.95	>2.22	3.70	4.57	>0.43
		7	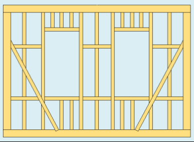	<1.60	<1.72	4.57	4.97	<0.32
	Adobe Masonry	1	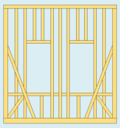	>1.64	>3.73	4.26	4.23	>0.39
		2	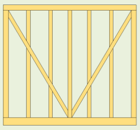	<1.78	<1.30	**7.93**	6.79	<0.26
Covering	*Şamdolma*	6	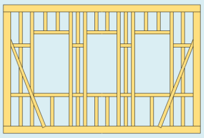	>1.43	>1.56	2.85	3.29	>0.44
		3	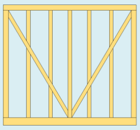	<2.25	<1.78	**10.14**	4.18	<0.54
	Bağdadi	5	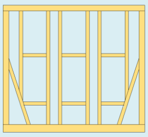	**>3.52**	**>6.87**	5.69	**2.90**	**>1.21**
		8	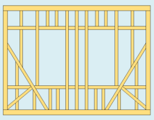	>1.80	**>5.61**	3.09	3.09	>0.58

* Overall stiffness values were calculated by using the maximum load value that the frame borne and the corresponding displacement value.

** Initial stiffness values were calculated using 1.5 kN load value and the corresponding displacement value.

- Frames#1, 4, 5 and 6 do not have a capacity against seismic loading, according to the calculations made for seismic capacity evaluation on the basis of ATC-40 procedure, i.e. a period value after a certain amount of inelastic displacement cannot be calculated. In addition, it is seen that the frames behave linearly for higher spectral displacement (Sd) values, when they are empty, in comparison to frame with infill/covering. Another important point is that the difference between Sd values, obtained for performance points, which is especially remarkable for frames with infill. For instance, Frame#1 with adobe infill reaches performance point after 135 mm of spectral displacement, while this value is 4 mm for Frame#3 with *şamdolma* infill, both in push direction. The frames with infill/covering having Sd values larger than 40 mm, which is the average value of the Sd values of all frame with infill/covering are Frame#1, #4, #6, #7 and #8. The infill/covering types of these frames are adobe, brick, *şamdolma*, brick and *bağdadi*, respectively. Since infill types do not indicate a certain infill or covering type, the reason may be sought in geometrical configuration of these frames. The window opening ratios of these frames are 0.180, 0.180, 0.248, 0.184 and 0.195, respectively. Frames#1 and #4 have the same geometrical configuration and in terms of this discussion, both give consistent results. Similarly, Frame#2 and #3 have the same geometrical configuration and have the same consistency. Therefore, it might be concluded that frames without openings behave worse under seismic loading in comparison to those with openings. On the other hand, Frame#5 has opening ratio equal to 0.177, and has high spectral acceleration values.

Table 21: Results of the capacity calculations for each frame without and with infill/covering (frames that do not have a capacity are shown in grey)

Frame		Direction	Empty State	Infill/ Covering	With Infill/Covering	General Information
1	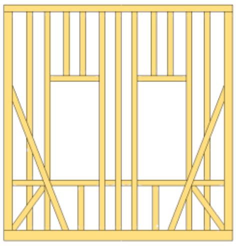	push	Ti=0.27 s	Adobe	Ti=0.18 s Ta= 0.78 s Sd= **135 mm** ξ= 8.8%	(H x L): 325 cm x 310 cm Yellow Pine 2 windows of 135 cm x 67 cm each Window openings per total surface of the frame: 0.180
		pull	Ti=0.26 s		Ti=0.22 s Ta= 0.71 s Sd= **113 mm** ξ= 9.2%	
2	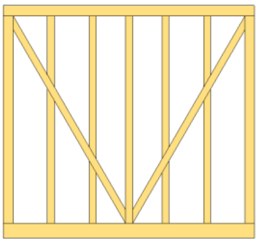	push	Ti=0.17 s Ta=0.26 s Sd= **17 mm** ξ= 7.2%	Adobe	Ti=0.12 s Ta= 0.17 s Sd= **7.5 mm** ξ= 7.1%	(H x L): 360 cm x 330 cm Yellow Pine No Windows
		pull	Ti=0.21 s Ta=0.31 s Sd= **24 mm** ξ= 6.7%		Ti=0.14 s Ta=0.16 s Sd= **6.5 mm** ξ= 6.3%	
3	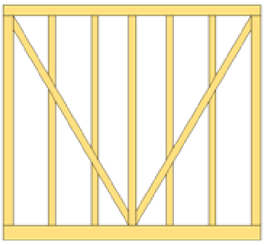	push	Ti=0.18 s Ta=0.31 s Sd= **25.5 mm** ξ= 6.4%	*Şamdolma*	Ti=0.10 s Ta=0.13 s Sd= **4 mm** ξ= 7.3%	(H x L): 360 cm x 330 cm Fir No Windows
		pull	Ti=0.20 s Ta=0.39 s Sd= **36.9 mm** ξ= 7.1%		Ti=0.11 s Ta=0.16 s Sd= **6.6 mm** ξ= 8%	
4	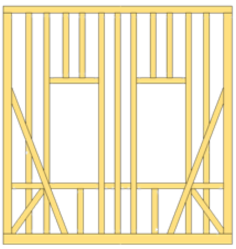	push	Ti=0.29 s	Brick	Ti=0.17 s Ta=0.53 s Sd= **65 mm** ξ= 8%	(H x L): 325 cm x 310 cm Fir 2 windows of 135 cm x 67 cm each Window openings per total surface of the frame: 0.180
		pull	Ti=0.40 s		Ti=0.22 s Ta=0.62 s Sd= **93.2 mm** ξ= 7.6%	

"Table 21 (continued)"

5	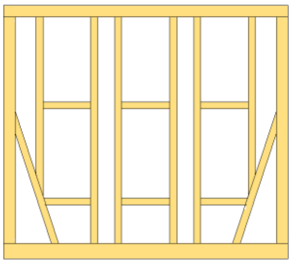	push	Ti=0.42 s	*Bağdadi*	Ti=0.16 s Ta=0.23 s Sd= **13.5 mm** ξ= 6.9%	(H x L): 330 cm x 370 cm Yellow Pine 3 windows of 116 cm x 62 cm each Window openings per total surface of the frame: 0.177
		pull	Ti=0.43 s		Ti=0.16 s Ta=0.23 s Sd= **12.9 mm** ξ= 7.3%	
6	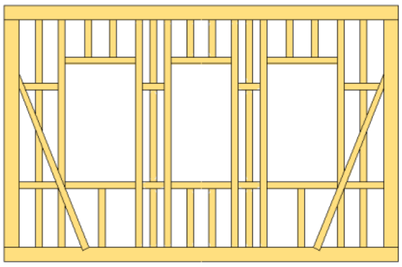	push	Ti=0.33 s	*Şamdolma*	Ti=0.21 s Ta=0.56 s Sd= **72.5 mm** ξ= 8.2%	(H x L): 340 cm x 520 cm Yellow Pine 3 windows of 157 cm x 93 cm each Window openings per total surface of the frame: 0.248
		pull	Ti=0.18 s		Ti=0.21 s Ta=0.54 s Sd= **68 mm** ξ= 8.1%	
7	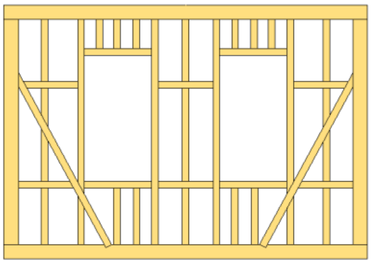	push	Ti=0.22 s Ta=0.32 s Sd= **26 mm** ξ= 7.0%	Brick	Ti=0.08 s Ta=0.16 s Sd= **5.6 mm** ξ= 7.4%	(H x L): 340 cm x 485 cm Yellow Pine 2 windows of 169 cm x 89.5 cm each Window openings per total surface of the frame: 0.184
		pull	Ti=0.26 s Ta=0.42 s Sd= **46 mm** ξ= 6.6%		Ti=0.11 s Ta=0.19 s Sd= **8.9 mm** ξ= 7.5%	
8	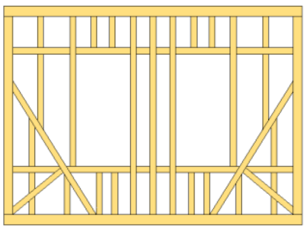	push	Ti=0.20 s Ta=0.45 s Sd= **49 mm** ξ= 7.7%	*Bağdadi*	Ti=0.11 s Ta=0.18 s Sd= **6.3 mm** ξ= 6.8%	(H x L): 300 cm x 400 cm Yellow Pine 2 windows of 156 cm x 75 cm each Window openings per total surface of the frame: 0.195
		pull	Ti=0.25 s Ta=0.40 s Sd= **41 mm** ξ= 6.6%		Ti=0.09 s Ta=0.16 s Sd= **6.5 mm** ξ= 7.3%	

- To decide whether the without-infill/covering state or with-infill/covering state is more advantageous, the capacities and demands of a frame should be compared on the basis of capacity calculations. According to Turkish Earthquake Code (2007), the demand on a structure under earthquake loading is

$$D = \frac{W * A(T)}{R_a(T)} \tag{22}$$

where,

W: weight

A(T): spectrum acceleration coefficient

$R_a(T)$: seismic load reduction factor.

$$A(T) = A_0 * I * S(T) \tag{23}$$

where,

A_0: Effective Ground Acceleration Coefficient

I: Building importance factor

$S(T)$: Spectrum Coefficient

$$R_a(T) = 1.5 + (R - 1.5) * T/T_A \quad (0 \leq T \leq T_A) \tag{24}$$

$$R_a(T) = R \quad (T > T_A) \tag{25}$$

where,

T_A: Spectrum characteristic period (s)

R: Structural behavior factor

In Eurocode 8 (2002: 160), the structural behavior factors are defined as given in Table 22. Therefore, the structural behavior factor, R, is taken as 3.

Table 22: Design Concept, structural types and behavior factors for the three ductility classes (taken from EU8)

Design concept and ductility class	q*	Examples of structures
Low capacity to dissipate energy - DCL	1.5	Cantilevers; Beams; Arches with two or three pinned joints; Trusses joined with connectors.
Medium capacity to dissipate energy - DCM	2	Glued wall panels with glued diaphragms, connected with nails and bolts; Trusses with doweled and bolted joints; Mixed structures consisting of timber framing (resisting the horizontal forces) and non-load bearing infill.
	2.5	Hyperstatic portal frames with doweled and bolted joints
High capacity to dissipate energy - DCH	3	Nailed wall panels with glued diaphragms, connected with nails and bolts; Trusses with nailed joints.
	4	Hyperstatic portal frames with doweled and bolted joints
	5	Nailed wall panels with nailed diaphragms, connected with nails and bolts.

* R in Turkish Earthquake Code R

Therefore, the equation becomes

$$D = \frac{W * A_0 * I * S(T)}{R_a(T)} \quad (26)$$

In this study, A_0 is taken as 0.4 to consider the worst case, the 1st degree seismic zone. Regarding the importance factor, the Turkish Earthquake Code makes a classification as (1) buildings to be utilized after the earthquake and buildings containing hazardous materials, (2) intensively and long-term occupied buildings, (3) schools, other educational buildings and facilities, dormitories, and (4) other buildings. Since there is no any class specified for heritage structures, in this work, they are accepted as other buildings, and I is taken as 1.0. S_T, on the other hand, is calculated as follows:

$$S(T) = 1 + 1.5 * T/T_A \ \ (0 \leq T \leq T_A) \quad (27)$$

$$S(T) = 2.5 \ \ (T_A \leq T \leq T_B) \quad (28)$$

$$S(T) = 2.5 * (T_B/T)^{0.8} \ \ (T > T_B) \quad (29)$$

where,

T_A and T_B: Spectrum characteristic periods (s)

T: Building natural vibration period (s)

T_A and T_B are defined according to the local site class, which, in this study, is taken as Z1, which is the worst case. According to Turkish Earthquake Code, T_A and T_B are 0.20 and 0.90, respectively.

The linear range load was used to compare with the linear range demand, calculated by using Ti value, while the largest load value was used to compare the non-linear range demand, calculated by using Ta value (Table 23).

Table 23: Demand and capacity values for each frame without and with infill/covering

Frame		Window openings per total surface of the frame (from smallest to largest)	direction	Without Infill/Covering: Load Bearing Capacity (kN) Linear	Without Infill/Covering: Load Bearing Capacity (kN) Non-linear	T (s)	S(T)	$R_a(T)$	$A_0 * I$	Weight (kN)	Demand (kN)	With Infill/Covering: Infill/ Covering	Load Bearing Capacity (kN) Linear	Load Bearing Capacity (kN) Non-linear	T (s)	S(T)	$R_a(T)$	$A_0 * I$	Weight (kN)	Demand (kN)	Average Increase in Demand	Capacity / Demand: Without Infill/Covering Linear	Without Infill/Covering Non-linear	With Infill/Covering Linear	With Infill/Covering Non-linear
2	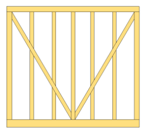	0	Push	3.029	6.382	Ti=0.17	2.275		0.4	1.55	1.41	Adobe	6.929	14.182	Ti=0.12	1.9		0.4	10.53	7.99	467%	2.15	12.27	**0.87**	4.11
						Ta=0.26	2.5	3			0.52				Ta= 0.17	2.275	2.775			3.45	564%				
			Pull	2.924	>9.356	Ti=0.21	2.5				1.56		7.235	13.804	Ti=0.14	2.05				9.82	530%	1.87	>15.09	**0.74**	4.02
						Ta=0.31	2.5	3			0.62				Ta=0.16	2.2	2.7			3.43	453%				
3		0	Push	0.976	7.066	Ti=0.18	1.35			1.80	0.98	Şamdolma	5.903	16.030	Ti=0.10	1.75			7.55	5.29	440%	**1.00**	11.78	1.12	4.70
						Ta=0.31	2.5	3			0.60				Ta=0.13	1.975	2.475			3.41	468%				
			Pull	1.966	>8.330	Ti=0.20	2.5				1.80		6.893	18.663	Ti=0.11	1.825				7.84	356%	1.09	>13.88	**0.88**	7.59
						Ta=0.39	2.5	3			0.60				Ta=0.16	2.2	2.7			2.46	310%				
5	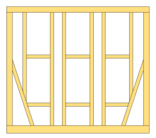	0.177	Push	2.003	3.166	Ti=0.42	2.5			2.25	2.25	Bağdadi	4.945	11.103	Ti=0.16	2.2			6.51	5.72	154%	**0.89**		**0.87**	5.12
															Ta=0.23	2.5	3			2.17					
			Pull	1.966	>3.472	Ti=0.43	2.5				2.25		5.182	12.230	Ti=0.16	2.2				5.72	154%	**0.87**		**0.91**	5.64
															Ta=0.23	2.5	3			2.17					
1	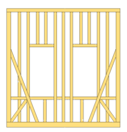	0.180	Push	1.045	>5.424	Ti=0.27	2.5			1.83	1.83	Adobe	3.919	>7.819	Ti=0.18	2.35			7.75	7.30	299%	**0.57**		**0.54**	>3.03
															Ta= 0.78	2.5	3			2.58					
			Pull	1.213	4.703	Ti=0.26	2.5				1.83		3.950	>8.809	Ti=0.22	2.5				7.74	323%	**0.66**		**0.51**	>3.41
															Ta= 0.71	2.5	3			2.58					
4			Push	1.045	>5.007	Ti=0.29	2.5			1.83	1.83	Brick	2.003	>9.188	Ti=0.17	2.275			8.39	7.63	317%	**0.57**		**0.26**	>3.28
															Ta=0.53	2.5	3			2.80					
			Pull	1.008	>4.299	Ti=0.40	2.5				1.83		2.788	>8.946	Ti=0.22	2.5				8.40	359%	**0.55**		**0.33**	>3.20
															Ta=0.62	2.5	3			2.80					
7	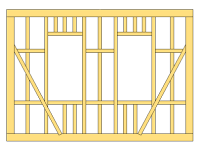	0.184	Push	2.961	8.572	Ti=0.22	2.5			2.69	2.70	Brick	3.919	14.183	Ti=0.08	1.6			13.36	8.55	217%	1.10	9.52	**0.46**	3.26
						Ta=0.32	2.5	3			0.90				Ta=0.16	2.2	2.7			4.35	383%				
			Pull	2.103	8.125	Ti=0.26	2.5				2.70		4.430	12.504	Ti=0.11	1.825				9.77	262%	**0.78**	9.03	**0.45**	2.83
						Ta=0.42	2.5	3			0.90				Ta=0.19	2.425	2.925			4.43	392%				
8	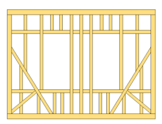	0.195	Push	2.003	6.382	Ti=0.20	2.5			2.05	2.04	Bağdadi	3.987	>13.430	Ti=0.11	1.825			6.33	4.63	127%	**0.98**	9.39	**0.86**	>6.43
						Ta=0.45	2.5	3			0.68				Ta=0.18	2.35	2.85			2.09	207%				
			Pull	1.008	>8.467	Ti=0.25	2.5				2.04		3.129	>13.325	Ti=0.09	1.675				4.24	108%	**0.49**	12.45	**0.74**	>6.47
						Ta=0.40	2.5	3			0.68				Ta=0.16	2.2	2.7			2.06	203%				
6	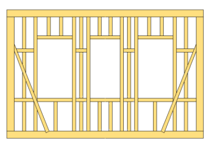	0.248	Push	2.003	7.956	Ti=0.33	2.5			3.72	3.72	Şamdolma	3.030	11.788	Ti=0.21	2.5			12.27	12.27	230%	**0.53**		**0.25**	2.88
															Ta=0.56	2.5	3			4.09					
			Pull	1.145	8.877	Ti=0.18	1.35				2.02		3.403	12.230	Ti=0.21	2.5				12.27	507%	**0.56**		**0.28**	2.99
															Ta=0.54	2.5	3			4.09					

As can be seen from Table 23, the linear capacity to demand ratio is almost always lower than 1 for the frames without and with infill/covering, which means none of the frames can bear seismic demand in linear range. Only exception to this is Frame#2 and 3 without infill/covering. On the other hand, the nonlinear capacity to demand ratio is always higher than 1. Therefore, nearly all frames are incapable of bearing seismic demand in linear range and they pass to nonlinear state after a certain amount of damage.

In Table 23, the frames were lined up from the one having smallest to the largest ratio of openings' area to the total surface area. It is seen that no significant changes occur in the capacity values based on openings.

- The same procedure for demand calculation was carried out also for the 2 story structure composed of 2 Frame#8 with *bağdadi* covering that was discussed in previous sections. The obtained results are shown in Table 24.

Table 24: Demand and capacity values for a two story structure composed of 2 Frame#8's with *bağdadi* covering

	direction	Load Bearing Capacity (kN)		T (s)	S(T)	$R_a(T)$	$A_0 * I$	Weight (kN)	Demand (kN)	Capacity / Demand	
		Linear	Non-linear							Linear	Non-linear
2nd story	Push	3.24	>13.54	Ti=0.16	2.2		0.4	6.33	5.56	0.58	>6.42
				Ta=0.24	2.5	3			2.11		
	pull	2.94	>13.54	Ti=0.15	2.125				5.38	0.55	>6.42
				Ta=0.24	2.5	3			2.11		
1st story	Push	2.94	>9.03	Ti=0.15	2.125				5.38	0.55	>4.28
				Ta=0.23	2.5	3			2.11		
	pull	2.94	>9.03	Ti=0.15	2.125				5.38	0.55	>4.28
				Ta=0.23	2.5	3			2.11		

- In Table 25, the changes in period values obtained for each frame for linear and nonlinear range and, with and without infill/covering states. Normally, the period values tend to decrease with infilling. However, in Frame#6 the period value in the pull direction increases by 17%.

Table 25: Change in period values for push and pull directions of each frame without and with infill/covering

Frame		direction	Empty State	Infill/ Covering	With Infill/ Covering	Change in Period
1	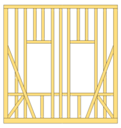	Push	push: T=0.27 s	Adobe	push: Ti=0.18 s Ta= 0.78 s	Ti: -33%
		Pull	pull: T=0.26 s		pull: Ti=0.22 s Ta= 0.71 s	Ti: -15%
2	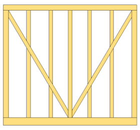	Push	push: Ti=0.17 s Ta=0.26 s	Adobe	push: Ti=0.12 s Ta= 0.17 s	Ti: -29% Ta: -34%
		Pull	pull: Ti=0.21 s Ta=0.31 s		pull: Ti=0.14 s Ta=0.16 s	Ti: -33% Ta: -48%
3	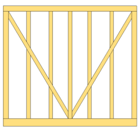	Push	push: Ti=0.18 s Ta=0.31 s	*Şamdolma*	push: Ti=0.10 s Ta=0.13 s	Ti: -44% Ta: -58%
		Pull	pull: Ti=0.20 s Ta=0.39 s		pull: Ti=0.11 s Ta=0.16 s	Ti: -45% Ta: -59%
4	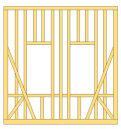	Push	push: T=0.29 s	Brick	push: Ti=0.17 s Ta=0.53 s	Ti: -41%
		pull	pull: T=0.40 s		pull: Ti=0.22 s Ta=0.62 s	Ti: -45%
5	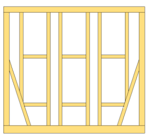	Push	push: T=0.42 s	*Bağdadi*	push: Ti=0.16 s Ta=0.23 s	Ti: -62%
		Pull	pull: T=0.43 s		pull: Ti=0.16 s Ta=0.23 s	Ti: -63%
6	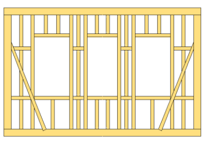	Push	push: T=0.33 s	*Şamdolma*	push: Ti=0.21 s Ta=0.56 s	Ti: -36%
		Pull	pull: T=0.18 s		pull: Ti=0.21 s Ta=0.54 s	Ti: +17%

"Table 25 (continued)"

7	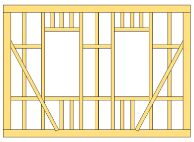	Push	push: Ti=0.22 s Ta=0.32 s	Brick	push: Ti=0.08 s Ta=0.16 s	Ti: -63% Ta: -50%
		Pull	pull: Ti=0.26 s Ta=0.42 s		pull: Ti=0.11 s Ta=0.19 s	Ti: -58% Ta: -55%
8	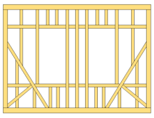	Push	push: Ti=0.20 s Ta=0.45 s	*Bağdadi*	push: Ti=0.11 s Ta=0.18 s	Ti: -45% Ta: -60%
		Pull	pull: Ti=0.25 s Ta=0.40 s		pull: Ti=0.09 s Ta=0.16 s	Ti: -64% Ta: -60%

- A series of optimization studies were carried out. According to this, a series of empirical formulas were generated for energy dissipation capacity and overall stiffness values. These formulas are as follows:

$E_{diss} = \left(W_{eff} + 0.0638A_{eff}\right) * (0.19D_{max} + 1.0469)^2$ without infill case

$E_{diss} = \left(0.873W_{eff} + 0.055A_{eff}\right) * (1.1865D_{max} + 0.5697)^{3/2}$ with infill case

where,

E_{diss}: Energy dissipation (J)

W_{eff}: Effective width = Frame width – total width of openings (m)

A_{eff}: Effective area = Frame area – total area of openings (m^2)

D_{max}: Maximum lateral top displacement (mm)

$k_{overall} = W_{eff} * (104.187/[0.2 * (D_{max} + 5.39)^{0.66}]$ without infill case

$k_{overall} = W_{eff} * (337/[0.025 * (D_{max} + 16.19)^{1.22}]$ with infill case

where,

$k_{overall}$: Overall stiffness (N/mm)

W_{eff}: Effective width = Frame width – total width of openings (m)

D_{max}: Maximum lateral top displacement (mm)

As can be seen from the derived formulas, the energy dissipation capacity changes according to $y = a * (X + b)^c$ relation, while overall stiffness changes according to $y = a * (^{b}/_{[c\, *\, (X + d)^e]})$.

- The timber frame structures are highly ductile thanks to the energy dissipative plastic behavior of connections. As can be seen from Table 26, drift ratios nearly up to 9% were observed. In addition, it was observed that covering seems to decrease drift ratio more. According to the obtained results, summarized in Table 26, for empty frames, the average drift ratio is 6%, and for frames with infill/covering, the average drift ratios are 5.5 and 4.9%, respectively. Moreover, based on the values, adobe and brick infill seem to **increase** drift ratio by around 3%, while *bağdadi* and *şamdolma* covering seem to **decrease** drift ratio by around 18% on the average.

Table 26: Drift ratios obtained for each test without and with infill/covering (infill and covering techniques are shown in blue and pink, respectively)

Frame	Frame height (cm)	Infill/ covering type	Maximum Lateral Displacement (mm)		Drift ratios (%)		Change in drift ratio with infill/ covering
			Without infill/ covering	With infill/ covering	Without infill/ covering	With infill/ covering	
1	324	Adobe	>217.948	>210.260	>6.72	>6.49	~-3%
2	330	Adobe	>134.615	180.586	>4.08	5.47	<34%
3	330	*Şamdolma*	>117.399	139.194	>3.56	4.22	<19%
4	324	Brick	>201.831	>181.135	>6.23	>5.59	~-10%
5	330	*Bağdadi*	>249.816	133.15	>7.57	4.03	<-47%
6	340	*Şamdolma*	213.553	>193.223	6.28	>5.68	>-10%
7	340	Brick	161.172	148.718	4.74	4.37	-8%
8	304	*Bağdadi*	>266.670	>173.077	>8.77	>5.69	~-35%
				average	5.99	5.19	7.54

- A number of analytical models were constructed within the framework of this study. The aim of the analytical works was to replicate the measured response of the tested frames analytically and then use the analytical models to simulate the frames' nonlinear earthquake response by time history analysis. Detailed information regarding these studies is as follows:

    - Model#1: An initial model was constructed by using commercially available SAP 2000 software, where the whole Frame#1 was modeled as an idealized single frame with lumped mass at the upper end. At the bottom of the frame, a nonlinear rotational link was assigned, where the moment-curvature relationship, based on the experimentally obtained load-displacement relationship was defined (Figure 217). Therefore, the load-displacement behavior of a certain frame could be successfully reproduced. As a second stage, a time history analysis was tried to be carried out to see whether at a certain cycle, the displacement of the frame would ever go outside of the experimentally defined range, i.e. the capacity of the frame (Figure 218). Although, SAP 2000 could generate response similar to the experimentally obtained envelope curve for static loads, it could not carry out the analysis for nonlinear time history analysis. Therefore, this modeling and simulation trial was inconclusive.

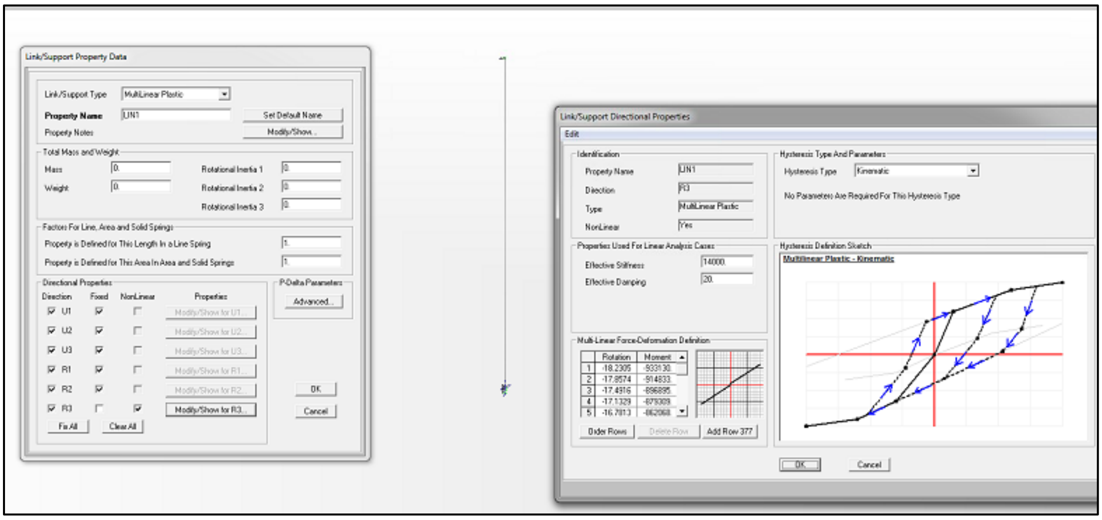

Figure 217: Model#1

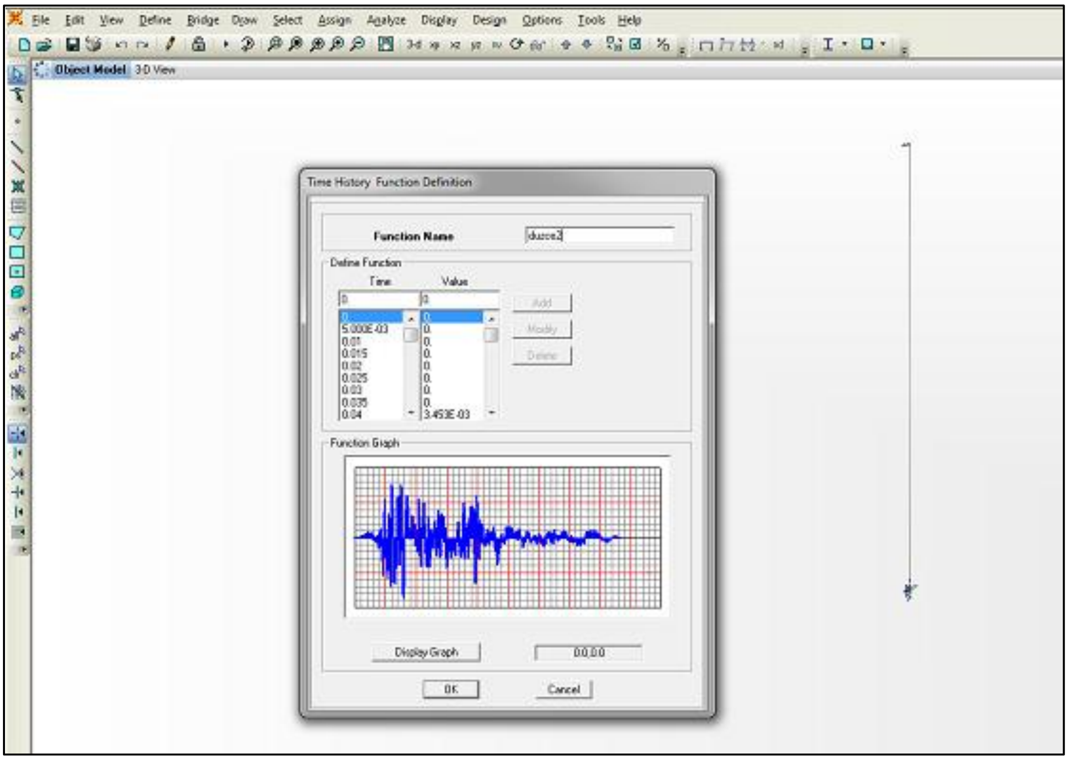

Figure 218: Time-history function assignment to Model#1

- Model#2: Another 2D model was constructed in SAP 2000, where all the timber elements in Frame#1 were modeled as they are using linear frame elements. In this case, moment releases were also assigned at the ends of the timber elements with nailed connection (Figure 219). Although nonlinear links at the nailed connections worked under static loading, the model could not be analyzed for nonlinear dynamic loading (i.e., time history analysis). Therefore, this trial was also inconclusive.

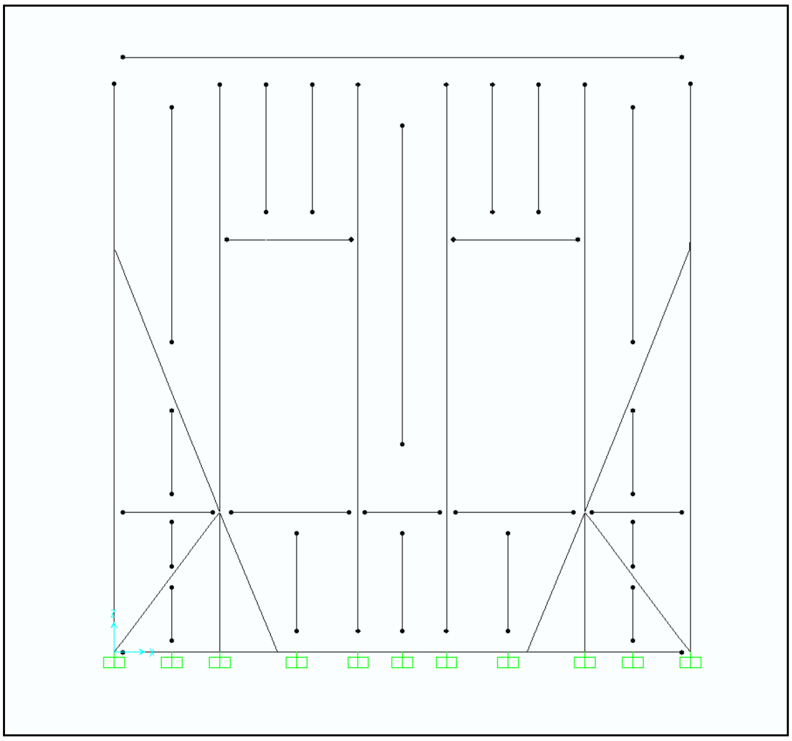

Figure 219: Model#2

- Model#3: Additional analytical modeling and analysis was conducted to understand the ultimate capacity of Frame#1 if the connections did not fail and were not the governing failure mechanism. The two dimensional frame model where each member was modeled using line elements was altered by cancelling all moment releases and nonlinear links, assuming that all connections were rigid (Figure 220). In this case, the tensile and compressive strength values (parallel to grains) of wood were taken as 2.9 MPa and 40 MPa, respectively. The results showed that if the connections did not govern the failures, the frame would have failed at 2 cm and 24 cm lateral displacements due to excessive tensile and compressive stresses, respectively. Therefore, the tensile strength would govern the failure at 2cm lateral displacement (Figure 221). The top lateral load values corresponding to these displacement values are 9.91 kN and 226.83 kN, respectively. Therefore, the failure would occur at 2 cm drift with 9.9 kN capacity, which is 80% more than the current capacity with nails. It was concluded that strong connections between members do not provide extensively large capacities for the frame system and nails would provide additional ductility and energy dissipating capability to the wooden frame system. If the connections were rigidly connected and have high capacity, the failure mode of the frame would be expected to be relatively less ductile.

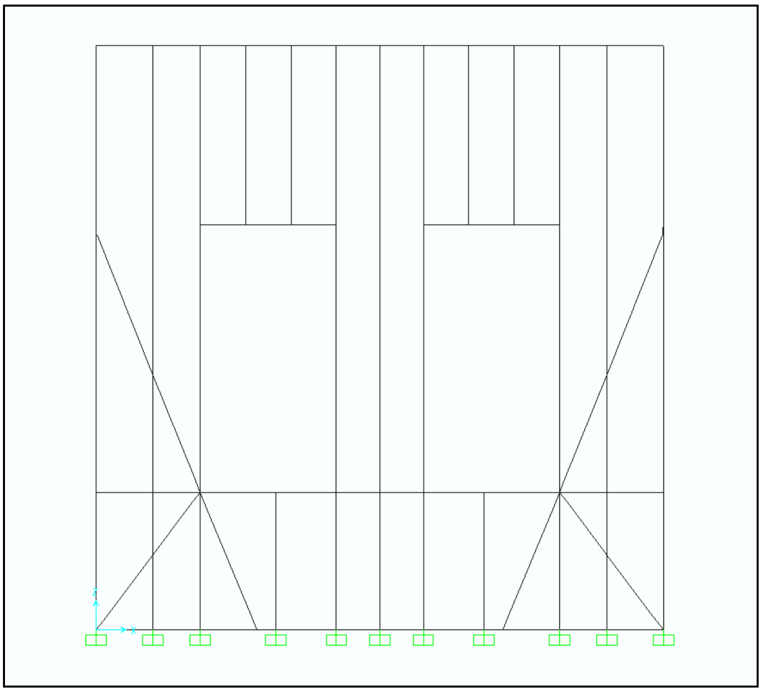

Figure 220: Model #3

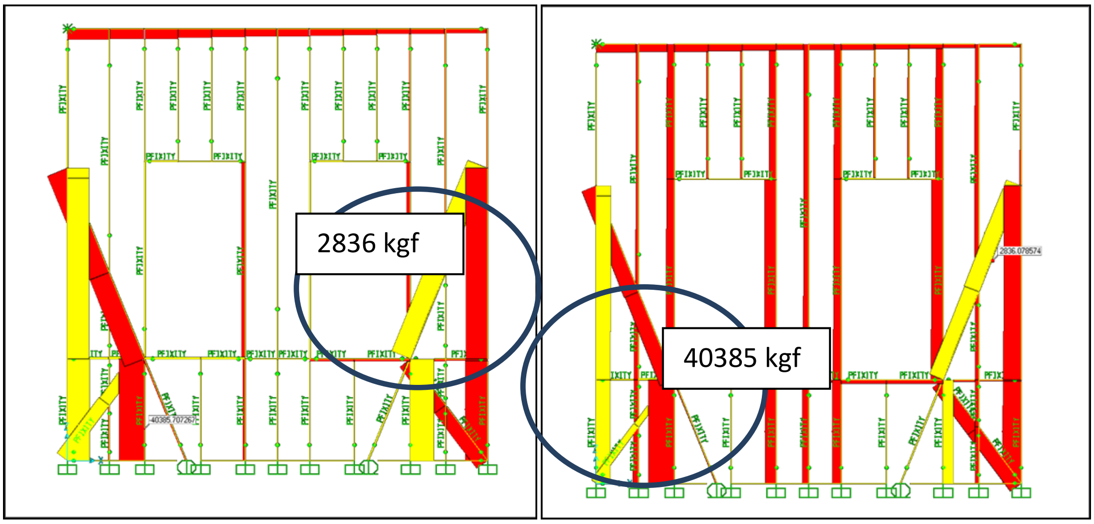

Figure 221: The axial stress diagram showing the tensile and compressive forces

CHAPTER 8

CONCLUSIONS

The conclusions drawn at the end of this study can be summarized as follows:

- The infill and covering increases the load bearing capacity of a timber frame, in an order of 1.74 and 2.25, respectively. Therefore, covering increases the load bearing capacity more.

- However, the increase in load bearing capacity by infill and covering is counterweighed by the increase in frame mass. Therefore, the frames became weaker against earthquakes as lateral seismic forces are proportional with the mass of the structure. The increase in weight is larger than the increase in load bearing capacity. The increase in weight is in the order of 5.3 for frames with infill, and 3.4 for the frames with covering. Therefore, covering results in a lower increase in weight, which is less disadvantageous than masonry infill.

- The ratio of increase in load bearing capacity to increase in weight for frames without and with infill/covering is always less than 1, except for one frame with *bağdadi* covering.

- By using the procedure given in Turkish Earthquake Code (1997), the seismic demand on each frame without and with infill was calculated based on the period values, obtained capacity calculations by ATC-40. It was seen that demand values increase in the order of 4.3 with infill/covering. However, the load bearing capacity values in with-infill/covering state is, on an average, 2 times of the load bearing capacity values in without-infill/covering state. Therefore, even though the infill/covering increases the capacity of a frame, worsens its behavior under earthquake loading.

- Considering the above mentioned results, in case another infill material is needed, it is recommended that the frames are infilled with a lighter material, such as autoclaved aerated concrete, whose density is around 400-800 kg/m^3, or gypsum boards.

- Infill and covering also increases stiffness, in the order of 2.2 and 4.0, for the frames with infill and covering, respectively. Stiffer frames have relatively smaller period of natural vibration while frames with higher mass have longer periods. Increase in stiffness and mass are in a way balance each other, while mass increase is larger than stiffness increase and therefore, periods are expected to be larger for frames with infill. Period increase of structures with already large periods, and period decrease of structures with already small periods would reduce seismic forces. Tested timber frames have initial periods of 0.18 to 0.4 seconds; therefore, earthquake forces might slightly decrease.

- Since timber frames fail always at the connections, it may be concluded that the behavior of timber frames is governed by the connections. Therefore, wood type does not govern the failure criteria and seems to be not very important. Nailed connections result in ductility in frame structures. Use of more rigid connections would result in a stiffer behavior, and timber would fail due to excessive tensile stresses at low lateral displacements.

- When brick and adobe masonry and *bağdadi* and *şamdolma* covering are investigated separately, it is seen that the increase in seismic demand in the former case is in the order of 5.16, while the increase in capacity is in the order of 1.74. For the latter case, on the other hand, these values are 3.42 and 2.25, respectively. Therefore, covering may be preferred rather than infilling with brick or adobe, as the response is less bad compared to the frames with infill.

- The aim of this study was to assess the seismic resistance of traditional Ottoman timber frame "*hımış*" structures, and it was clearly indicated that the tested timber frames are capable of resisting seismic demand, defined by the recent Turkish Earthquake Code (2007). On the other hand, to prevent unwanted increase in weight, and therefore in seismic demand, it is proposed a light technique to infill/covering purposes, such as *bağdadi.* One should bear in mind that the results are intended to be used not only in the conservation of existing traditional Ottoman timber frame "*hımış*" houses, but also for modern seismically resistant timber constructions.

REFERENCES

Acar, E. (1996). Anadolu'dan Tarihöncesi Çağlardan Tunç Çağı Sonuna Kadar Konut ve Yerleşme / Housing and Settlement in Anatolia: From Prehistoric Ages to the End of the Bronze age. In Y. Sey (ed.), *Tarihten Günümüze Anadolu'da Konut ve Yerleşme / Housing and Settlement in Anatolia: A Historical Perspective v.1* (pp. 380-394). Istanbul: Türkiye Ekonomik ve Toplumsal Tarih Vakfı.

Adam, J. P. (2006). *L'Arte di Costruire Presso i Romani - Materiali e Tecniche.* Milano: Longanesi.

Aedo, W. C., & Olmos, A. R. (2002). *Bahareque - Guía de Construccion Parasismica.* Villefontaine Cede: Ediciones CRATerre.

Akın, N. (1996). Osmanlı Döneminde Anadolu Konutuyla Balkan Konutu Arasındaki Ortaklıklar / The Common Characteristics of Anatolian and Balkan Houses During the Ottoman Period. In Y. Sey (ed.), *Tarihten Günümüze Anadolu'da Konut ve Yerleşme / Housing and Settlement in Anatolia: A Historical Perspective v.1* (pp. 269-277). Istanbul: Türkiye Ekonomik ve Toplumsal Tarih Vakfı Yayınları.

Aksoy, D., & Ahunbay, Z. (2005). Geleneksel Ahşap İskeletli Türk Konutu'nun Deprem Davranışları. *İtü Dergisi/a Mimarlık, Planlama, Tasarım* , 47-58.

Ambraseys, N. N., & Finkel, C. F. (1995). *The Seismicity of Turkey and Adjacent Areas: A Hıstorical Review, 1500-1800.* Istanbul: Eren Yayıncılık ve Kitapçılık Ltd. Şti.

Applied.Technology.Council. (1996). *Seismic Evaluation and Retrofit of Concrete Buildings ATC-40.* California: Report no SSC-96-01.

Arel, A. (1982). *Osmanlı Konut Geleneğinde Tarihsel Sorunlar.* İzmir: Ticaret Matbaacılık.

Asatekin, G. N. (1994). Anadolu'daki Geleneksel Konut Mimarisinin Biçimlenmesinde Aile Konut Karşılıklı İlişkilerinin Rolü. In İ. Tekeli, *Kent, Planlama, Politika, Sanat: Tarık Okyay Anısına Yazılar* (pp. 65-87). Ankara: Orta Doğu Teknik Üniversitesi Mimarlık Fakültesi.

ASCE. (1996). *Mechanical Connections of Wood Structures: ASCE Manuals and Reports on Engineering Practice No. 84.* New York: American Society of Engineers.

ASTM. (2009). *ASTM D143-09 Standard Test Methods for Small Clear Specimens of Timber.* West Conshohocken, USA: ASTM International.

Ayoub, A. (2007). Seismic Analysis of Wood Building Structures. *Engineering Structures 29* , 213-223.

Bammer, A. (1996). Çadır ile Anadolu Evi İlişkileri / The Relationship Between the Tent and the Anatolian House. In Y. Sey (ed.), *Tarihten Günümüze Anadolu'da Konut ve Yerleşme / Housing and Settlement in Anatolia: A Historical Perspective v.1* (pp. 234-247). Istanbul: Türkiye Ekonomik ve Toplumsal Tarih Vakfı Yayınları.

Bayındırlık.ve.İskan.Bakanlığı. (2007). *Deprem Bölgelerinde Yapılacak Binalar Hakkında Yönetmelik - Turkish Earthquake Code.* Bayındırlık ve İskan Bakanlığı.

Bayülke, N. (2001). Ahşap Yapılar. *Türkiye Mühendislik Haberleri 414/4* , 14-20.

Bommer, J., Benito, B. C.-R., Lemoine, A., López-Menjívar, M., Madariaga, R., Mankelow, et al. (2002). The El Salvador Earthquakes of January and February 2001: Context, Characteristics and Implications for Seismic Risk. *Soil Dynamics and Earthquake Engineering 22* , 389-418.

Ceccotti, A. (1994). Structural Seismic 'Action Reduction Factor'. In H. J. Blass, A. Ceccotti, C. Dyrbye, M. Gnuschke, K. F. Hansen, J. Nielsen, et al., *Behavior of Timber Structures Under Seismic Actions* (pp. 168-169). Ed. J.D. Dolan. Materials and Structures 27, 157-184: RILEM TECHNICAL COMMITTEES.

Cerasi, M. (1998). The Formation of Ottoman House Types: A Comparative Study in Interaction with Neighboring Cultures. *Muqarnas 15* , 116-156.

Chen, C., Lee, T., & Jeng, D. (2003). Finite Element Modeling for the Mechanical Behavior of Dowel-Type Timber Joints. *Computers and Structures 81* , 2731-2738.

Choi, F. C., Li, J., Samali, B., & Crews, K. (2008). Application of the Modified Damage Index Method to Timber Beams. *Engineering Structures 30* , 1124-1145.

Coeck van Aelst, P. (1873). *The Turks in MDXXXIII: A Series of Drawings Made in That Year at Constantinople.* Trans. by Sir William S. M. Bart, London & Edinburg: Privately Printed.

Cointe, A., Castéra, P., Morlier, P., & Galimard, P. (2007). Diagnosis and Monitoring of Timber Buildings of Cultural Heritage. *Structural Safety 29* , 337-348.

Cuadra, C., & Chariarse, V. (1992). Recent Research Work at CISMID on Low Cost Housing Structures. *Simposio Internacional sobre Prevención de Desastres Sísmicos*, (pp. 83-88). Mexico.

Demirtaş, R., Iravul, Y., Erkmen, C., Baran, B., Yaman, M., Baykal, M., et al. (2000). ÇankırıDepremi - 06 Haziran 2000 Orta (Çankırı) Depremi. *Jeoloji Mühendisleri Odası Haber Bülteni* , 6-15.

Diri, F. (2010). *Construction Techniques of Traditional Birgi Houses.* Ankara, Turkey: Unpublished Graduate Thesis in Middle East Technical University, Department of Architecture - Restoration.

Doğangün, A., Tuluk, Ö., Livaoğlu, R., & Acar, R. (2006). Traditional Wooden Building and Their Damages During Earthquakes in Turkey. *Engineering Failure Analysis 13* , 981-996.

Eldem, S. H. (1984). *Türk evi : Osmanlı dönemi / Turkish houses : Ottoman period.* İstanbul: Türkiye Anıt, Çevre, Turizm Değerlerini Koruma Vakfı.

Eldem, S. H. (1968). *Türk Evi Plan Tipleri.* İstanbul: İstanbul Teknik Üniversitesi Mimarlık Fakültesi Baskı Atölyesi.

Erdik, M., Sesetyan, K., Demircioglu, M. B., Celep, U., Biro, Y., & Uckan, E. (2002b). *Special Earthquake Report from the May 2002 Newsletter: Preliminary Observations on the Sultandağı, Turkey, Earthquake of February 3, 2002.* Retrieved January 14, 2011, from Earthquake Engineering Research Institute, Learning From Earthquakes - Turkey: http://www.eeri.org/lfe/pdf/Turkey_Sultandagi_Insert_May02.pdf

Erdik, M., Sesetyan, K., Demircioglu, M. B., Celep, U., Biro, Y., & Uckan, E. (2002a). *Sultandağı Earthquake, Turkey.* Retrieved November 9, 2010, from Earthquake Engineering Research Institute, Learning From Earthquakes - Turkey: http://eeri.org/lfe/pdf/turkey_sultandagi_report_erdik.pdf

Eurocode8. (2002). *Design of Structures for Earthquake Resistance Part 1: General Rules, Seismic Actions and Rules for Buildings.* Brussels: CEN: European Committee for Standardization.

Evren, M. (1959). *Türk Evinde Çıkma.* Istanbul: Fakülteler Matbaası.

Eyice, S. (1996). Türkiye'de Bizans Dönemi Yerleşimi Hakkında Notlar / Observations on Byzantine Dwellings in Turkey. In Y. Sey (ed.), *Tarihten Günümüze Anadolu'da Konut ve Yerleşme / Housing and Settlement in Anatolia: A Historical Perspective v.1* (pp. 206-220). Istanbul: Türkiye Ekonomik ve Toplumsal Tarih Vakfı.

Fang, C. P., Isawaki, S., Yu, M. H., Shen, Q. P., Miyamoto, Y., & Hikosaka, H. (2001). Ancient Chinese Timber Architecture I: Experimental Study. *Journal of Structural Engineering* , 1348-1357.

Faroqhi, S. (1998). *Osmanlı Kültürü ve Gündelik Yaşam: Ortaçağdan Yirminci Yüzyıla.* İstanbul: Tarih Vakfı Yurt Yayınları.

Feio, A. J. (2005). *Inspection and Diagnosis of Historical Timber Structures: NDT Correlation and Structural Behavior.* Guimaraes: Unpublished Thesis Work in University do Minho.

Fellows, C. (1840). *An Account of Discoveries in Lydia, Being A Journal Kept During A Second Excursion in Asia Minor.* London: John Murray.

Fujita, K. K., Koshihara, M., Iwata, S., Nakazono, M., & Sakamoto, I. (2004). On-Site Lateral loading Test of a Traditional Timber House in Japan. *Journal of Asian Architecture and Building Engineering 46* , 41-46.

Genç, M., & Mazak, M. (2001). *İstanbul Depremleri: Fotoğraf ve Belgelerde 1894 Depremi.* İstanbul: IGDAS Kültürel Yayınları.

Gilfillan, J. R., & Gilbert, S. G. (2001). Development of a Technique to Measure the Residual Strength of Woodworm Infested Timber. *Construction and Building Materials 15* , 381-388.

Grabert, H. (1971). 28 Mart 1970 Tarihinde Batı Anadolu'da Meydana Gelen Depremin Nedenini Teşkil Eden İki Önemli Arıza Elemanının Kesişmesi. *Maden Tetkik ve Arama Dergisi 77* , 22-30.

Guiliani, C. F. (1990). *L'Edilizia nell'Antichita'.* Roma: La Nuova Italia Scientifica.

Gülhan, D., & Özyörük Güney, İ. (2000). The Behaviour of Traditional Building Systems Against Earthquake and Its Comparison to Reinforced Concrete Frame Systems: Experiences of Marmara Earthquake Damage Assessment Studies in Kocaeli and Sakarya. *Earthquake-Safe:Lessons to be Learned from Traditional Buildings.* Istanbul: ICOMOS.

Günay, R. (1998). *Tradition of the Turkish Houses and Safranbolu Houses.* Istanbul: YEM.

Gürpınar, A., Erdik, M., & Ergünay, O. (May 24-28, 1981). Sitting and Structural Aspects of Adobe Buildings in Seismic Areas. *International Workshop on Earthen Buildings in Seismic Areas*, (pp. 139-158). Albuquerque, New Mexico.

Hamlin, A. D. (1904). *History of Architecture.* London and Bombay: Longmans, Green, and Co.

Heiduschke, A., Kasal, B., & Haller, P. (2009). Shake Table Tests of Small - and Full-Scale Laminated Timber Frames with Moment Connections. *Bulletin of Earthquake Engineering 7* , 323-339.

Işık, F., & İşkan Yılmaz, H. (1996). Likya'da Konut ve Gömüt Arasındaki Yapısal İlişkiler / Structural Links Between the House and the Tomb in Lycia. In Y. Sey (ed.), *Tarihten Günümüze Anadolu'da Konut ve Yerleşme / Housing and Settlement in Anatolia: A Historical Perspective v.1* (pp. 171-181). Istanbul: Türkiye Ekonomik ve Toplumsal Tarih Vakfı.

Kafesçioğlu, R. (1955). *Kuzey-Batı Anadolu'da Ahşap Ev Yapıları.* İstanbul: İstanbul Teknik Üniversitesi - Mimarlık Fakültesi Pulhan Matbaası.

Kafesçioğlu, R. (1949). *Orta Anadolu'da Köy Evlerinin Yapısı.* Istanbul: İstanbul Matbaacılık.

Kalafatçıoğlu, A. (1968). 1967 Yılı Sakarya Depremine Ait Kısa Not. *Maden Tetkik ve Arama Dergisi 70* , 129-137.

Kandemir Yücel, A., Tavukçuoğlu, A., & Caner Saltık, E. (2007). In Situ Assessment of Structural Timber Elements of a Historic Building by Infrared Thermography and Ultrasonic Velocity. *Infrared Physics & Technology 49* , 243-248.

Kasal, B., & Anthony, R. W. (2004). Advances in In-Situ Evaluation of Timber Structures. *Progress in Structural Engineering and Materials 6* , 94-103.

Kazmaoğlu, M., & Tanyeli, U. (1979). Anadolu Konut Mimarisinde Bölgesel Farklılıkla. *Yapı 33* , 29-41.

Koçyiğit, A., Bozkurt, E., Kaymakcı, N., & Şaroğlu, F. (2002, February 18). *3 Şubat 2002 Çay (Afyon) Depreminin Kaynağı ve Ağır Hasarın Nedenleri: Akşehir Fay Zonu (Jeolojik Ön Rapor).* Retrieved April 8, 2011, from http://www.metu.edu.tr/~akoc/Afyon.pdf

Kömürcüoğlu, E. (1950). *Ankara Evleri.* Istanbul: İstanbul Matbaacılık.

Kuban, D. (1996). Ev Üzerine Felsefe Kırıntıları / Scraps of Philosophy for Human Dwellings. In Y. Sey (ed.), *Tarihten Günümüze Anadolu'da Konut ve Yerleşme / Housing and Settlement in Anatolia: A Historical Perspective v.1* (pp. 1-5). Istanbul: Türkiye Ekonomik ve Toplumsal Tarih Vakfı.

Kuban, D. (1995). *The Turkish Hayat House.* Istanbul: T.C. Ziraat Bankası Kültür Yayınları.

Lam, F., Filiatrault, A., Kawai, N., Nakajima, S., & Yamaguchi, N. (2004). Performance of Timber Buildings under Seismic Load. Part 2: Modelling. *Progress in Structural Engineering and Materials 6* , 79-83.

Lam, F., Filiatrault, A., Kawai, N., Nakajima, S., & Yamaguchi, N. (2002). Performance of Timber Buildings under Seismic Load. Part I: Experimental Studies. *Progress in Structural Engineering and Materials 4* , 276-285.

Leijten, A. J. (2009). Withdrawal Capacity of Wahers in Bolted Timber Connections. *Wood Material Science and Engineering 3-4* , 131-139.

Lloyd, S., & Müller, H. W. (1998). *Architettura: Origini.* Milano: Elemond Editori Associati.

Lopes, M. (2010). Construção Pombalina: Património Histórico e Estrutura Sismo-Resistente. *Congresso Nacional de Sismologia e Engenharia Sismica*, (pp. 1-15). Aveiro.

López, M., Bommer, J. J., & Pinho, R. (2004). Seismic Hazard Assessments, Seismic Design Codes, and Earthquake Engineering in El Salvador. In W. I. Rose, J. J. Bommer, D. L. López, M. J. Carr, & J. J. Major, *Natural Disasters in El Salvador* (pp. 301-320). U.S.A.: The Geological Society of America.

López, M., Bommer, J., & Méndez, P. (2004). The Seismic Performance of Bahareque Dwellings in El Salvador. *13th World Conference on Earthquake Engineering*, (p. Paper no 2646). Vancouver, Canada.

Lugli, G. (1957). *La Tecnica Edilizia Romana con Particolare Riguardo a Roma e Lazio.* Roma: Giovanni Bardi.

Mellink, M. J. (1975). Archaeology in Asia Minor. *Americal Journal of Archaeology 79:3* , 201-222.

Minke, G. (2001). *Construction Manual for Earthquake-Resistant Houses Built of Earth.* Eschborn: GATE - BASIN.

Neve, P. (1996). Hitit Krallığı'nın Başkenti Hattuşa'da Konut / Housing in Hattuşa, the Capital of the Hittite Kingdom. In Y. Sey (ed.), *Tarihten Günümüze Anadolu'da Konut ve Yerleşme / Housing and Settlement in Anatolia: A Historical Perspective v.1* (pp. 99-115). Istanbul: Türkiye Ekonomik ve Toplumsal Tarih Vakfı.

Ousterhout, R. (1999). *Master Builders of Byzantium.* Philadelphia: Princeton University Press.

Özdoğan, M. (1996). Kulübeden Konuta: Mimarlıkta İlkeler / From Huts to Houses: "Firsts" in Architecture. In Y. Sey (ed.), *Tarihten Günümüze Anadolu'da Konut ve Yerleşme / Housing and Settlement in Anatolia: A Historical Perspective v.1* (pp. 19-30). Istanbul: Türkiye Ekonomik ve Toplumsal Tarih Vakfı.

Parisi, M., & Piazza, M. (2002). Seismic Behavior and Retrofitting of Joints in Traditional Timber Roof Structures. *Soil Dynamics and Earthquake Engineering 22* , 1183-1191.

Perrot, G., & Chipiez, C. (1892). *Art in Phyrigia, Lydia, Caria and Lycia.* London: Chapman and Hall Limited.

Popovski, M., Prion, H. G., & Karacabeyli, E. (2002). Seismic Performance of Connections in Heavy Timber Construction. *Canadian Journal of Civil Engineering 29* , 389-399.

Popovski, M., Prion, H. G., & Karacabeyli, E. (2003). Shake Table Tests on Single-Storey Braced Timber Frames. *Canadian Journal of Civil Engineering 30* , 1089-1100.

Rai, D. C., & Murty, C. V. (2005). *Preliminary Report on the 2005 North Karshmir Earthquake of October 8, 2005. Kanpur.* India: National Information Centre of Earthquake Engineering.

Rainer, J., & Karacabeyli, E. (2000). Wood-Frame Construction in Past Earthquakes. *Proceedings of the 6th World Conference on Timber Engineering.* Whistler Resort, British Columbia, Canada.

Rheidt, K. (1996). Kent mi, Köy mü? Orta ve Geç Bizans Anadolu'sunda Konut ve Yerleşme / City or Village? Housing and Settlement in Middle and Late Byzantine Anatolia. In Y. Sey (ed.), *Tarihten Günümüze Anadolu'da Konut ve Yerleşme / Housing and Settlement in Anatolia: A Historical Perspective v.1* (pp. 221-233). Istanbul: Türkiye Ekonomik ve Toplumsal Tarih Vakfi.

Sawaka, K., Sasaki, T., Doi, S., & Iijima, Y. (2008). Effect of Decay on Shear Performance of Dowel-Type Timber Joints. *Journal of Wood Science 54* , 356-361.

Shaji, T., Somayaji, S., & Mathews, M. S. (2000). Ultrasonic Pulse Velocity Technique for Inspection and Evaluation of Timber. *Journal of Materials in Civil Engineering* , 180-185.

Soygeniş, M. (2008). *Yapı 3-4-5.* İstanbul: Birsen Yayınevi.

Sözen, M. (2001). *Türklerde Ev Kültürü.* Istanbul: Doğan Kitapcilik A.S.

Şahin Güçhan, N. (2001). Ahşap Karkas Yapılar ve Bunların Restorasyonunda İnşaat Mühendislerinin Rolü. *Türkiye Mühendislik Haberleri 414/4* , 21-26.

Şahin Güçhan, N. (2007a). Observations on Earthquake Resistance of Traditional Timber Framed Houses in Turkey. *Building and Environment 42* , 840-851.

Şahin Güçhan, N. (2007b). *Tarihi Geleneksel Ahşap Karkas/Hımış Konutların Sismik Performansının Değerlendirilmesi.* Ankara: Project No: 106M499, unpublished TUBITAK report no 1.

Şahin, N. (1995). *A Study on Conservation and Rehabilitation Problems of Historic Timber Houses in Ankara.* Ankara: Unpublished Doctorate Dissertation in Middle East Technical University, Department of Architecture - Restoration.

Tanyeli, U. (1996). Anadolu'da Bizans, Osmanlı Öncesi ve Osmanlı Dönemlerinde Yerleşme ve Barınma Düzeni / Houseing and Settlement Patterns in the Byzantine, Pre-Ottoman and Ottoman Periods in Anatolia. In Y. Sey (ed.), *Tarihten Günümüze Anadolu'da Konut ve Yerleşme / Housing and Settlement in Anatolia: A Historical Perspective v.1* (pp. 405-471). Istanbul: Türkiye Ekonomik ve Toplumsal Tarih Vakfı.

Tobriner, S. (1997). La Casa Baraccata: Un Sistema antisismico nella Calabria del XVIII Secolo. *Costruire in Laterizio* , 110-115.

Tobriner, S. (1998). *Response of Traditional Japanese Construction to the Kobe (Hyogoken-Nanbu) Earthquake.* Retrieved March 12, 2010 , from Earthquake Engineering Research Center of the University of California, Berkeley, Library of the National Information Service for Earthquake Engineering: http://nisee.berkeley.edu/kobe/tobriner.html

Tobriner, S. (1999). Safety and Reconstruction of Noto after the Sicilian Earthquake of 1963 - The Eighteeneth Century Context. In A. Johns, *Dreadful Visitations: Confronting Natural Catastrophe in the Age of Enlightenment* (pp. 49-73). New York: Routledge.

Tobriner, S. (2000). Wooden Architecture and Earthquakes in Turkey: A Renaissance Report and Commentary on the Performance of Wooden Structures in the Turkish Earthquakes of 17 August and 12 November 1999. *Earthquake-Safe:Lessons to be Learned from Traditional Buildings.* Istanbul: ICOMOS.

Uchida, A., Kawai, N., & Maekawa, H. (2000). Diagnosis Method for Seismic Performance of Japanese Traditional Timber Buildings. *Proceedings of the 6th World Conference on Timber Engineering.* Whistler Resort, British Columbia, Canada.

Ulrich, R. B. (2007). *Roman Woodworking.* Yale: Yale University Press.

Urak, G., & Çelebi, G. (2005). Beypazarı Geleneksel Evlerinde Uygulanan "Tatlı Sıva" Üzerine Bir İnceleme. *Gazi Üniversitesi Mühendislik Mimarlık Fakültesi Dergisi 20-3* , 401-409.

Ünlü, A. (1996). Origins of Anatolian Sofa Houses. *IAPS 12 International Conference on Socio-Environmental Metamorphoses*, (pp. 248-255). Chalkidiki, Greece.

Van de Kuilen, J. W. (2007). Service Life Modelling of Timber Structures. *Materials and Structures 40* , 151-161.

Vintzileou, E., Zagkotsis, A., Repapis, C., & Zeris, C. (2007). Seismic Behaviour of the Historical System of the Island of Lefkada, Greece. *Construction and Building Materials 21* , 225-236.

Vitruvius. (1914 Translation by Morris Hicky Morgan). *The Ten Books of Architecture.* Cambridge: Harvard University Press.

Wright, G. (2000). *Ancient Building Technology I-II-III.* Leiden, Boston: Köln: Brill.

Yasamaki, A., Sasaki, Y., & Iijima, Y. (2010). Determining Young's Modulus of Timber on the Basis of a Strength Database and Stress Wave Propogation Velocity II: Effect of the Reference Distribution Database on the Determination. *Journal of Wood Science 56* , 380-386.

Yasumura, M., & Yasui, S. (2006). Pseudodynamic Tests and Earthquake Response Analysis of Timber Structures I: Plywood-Sheathed Conventional Wooden Walls With Openings. *Journal of Wood Science 52* , 63-68.

Yasumura, M., Kamada, T., Imura, Y., Uesugi, M., & Daudeville, L. (2006). Pseudodynamic Tests and Earthquake Response Analysis of Timber Structures II: Two Level Conventional Wooden Structures With Plywood Sheathed Shear Walls. *Journal of Wood Science 52* , 69-74.

Yoshimura, K., & Kuroki, M. (2001). Damage to Masonry Structures Caused by the El Salvador Earthquake of January 13, 2001. *Journal of Natural Disaster Science 23* , 53-63.

APPENDIX A

A. DIFFERENCES BETWEEN FRAMES SELECTED FROM SAFRANBOLU AND BUILT REPLICAS IN LABORATORY

The detailed drawings of the differences between the frames selected from Safranbolu and built replicas in the laboratory environment are given in Figure 222-Figure 227.

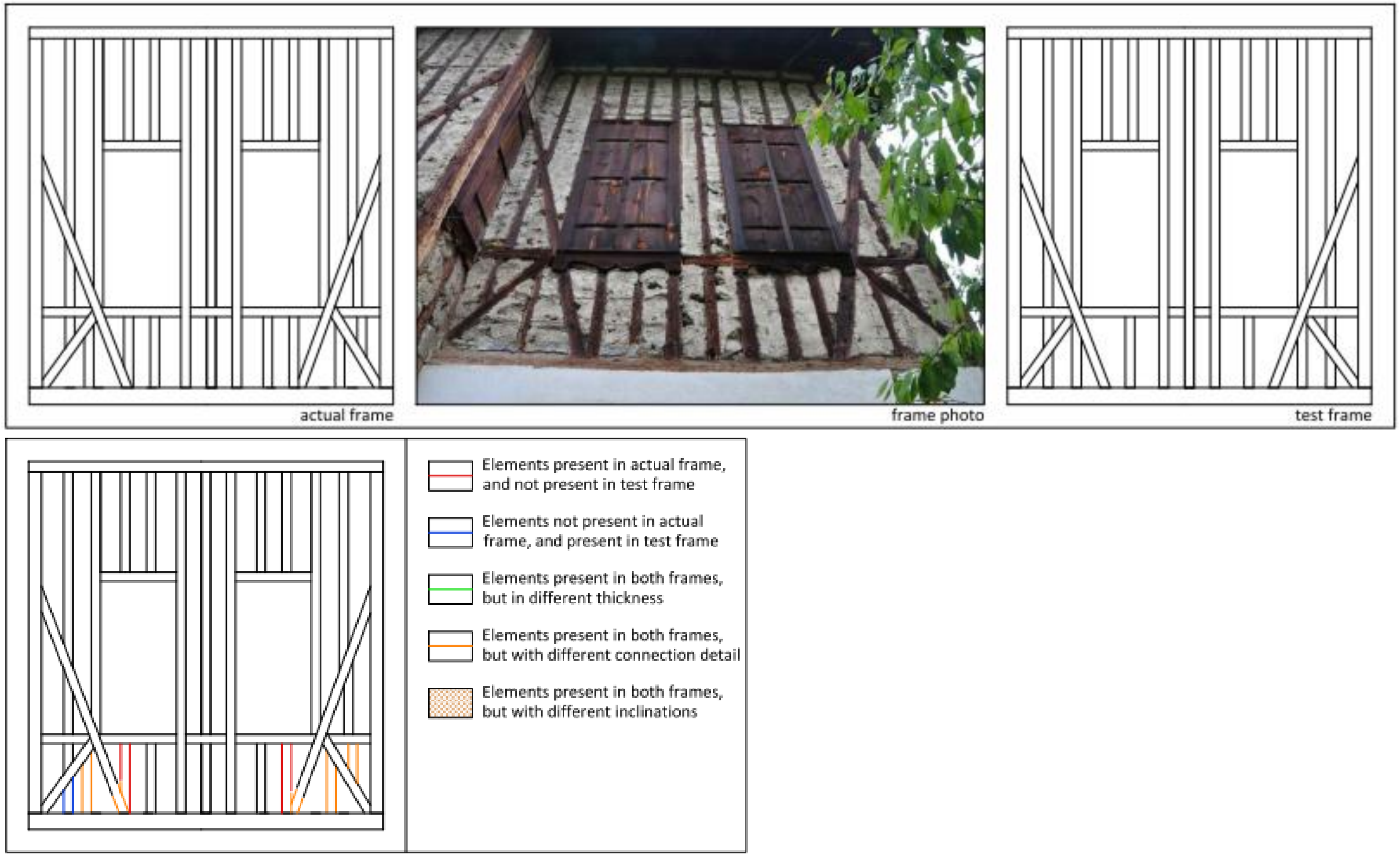

Figure 222: Drawings of actual frame and test frames#1 and #4, showing the differences between them

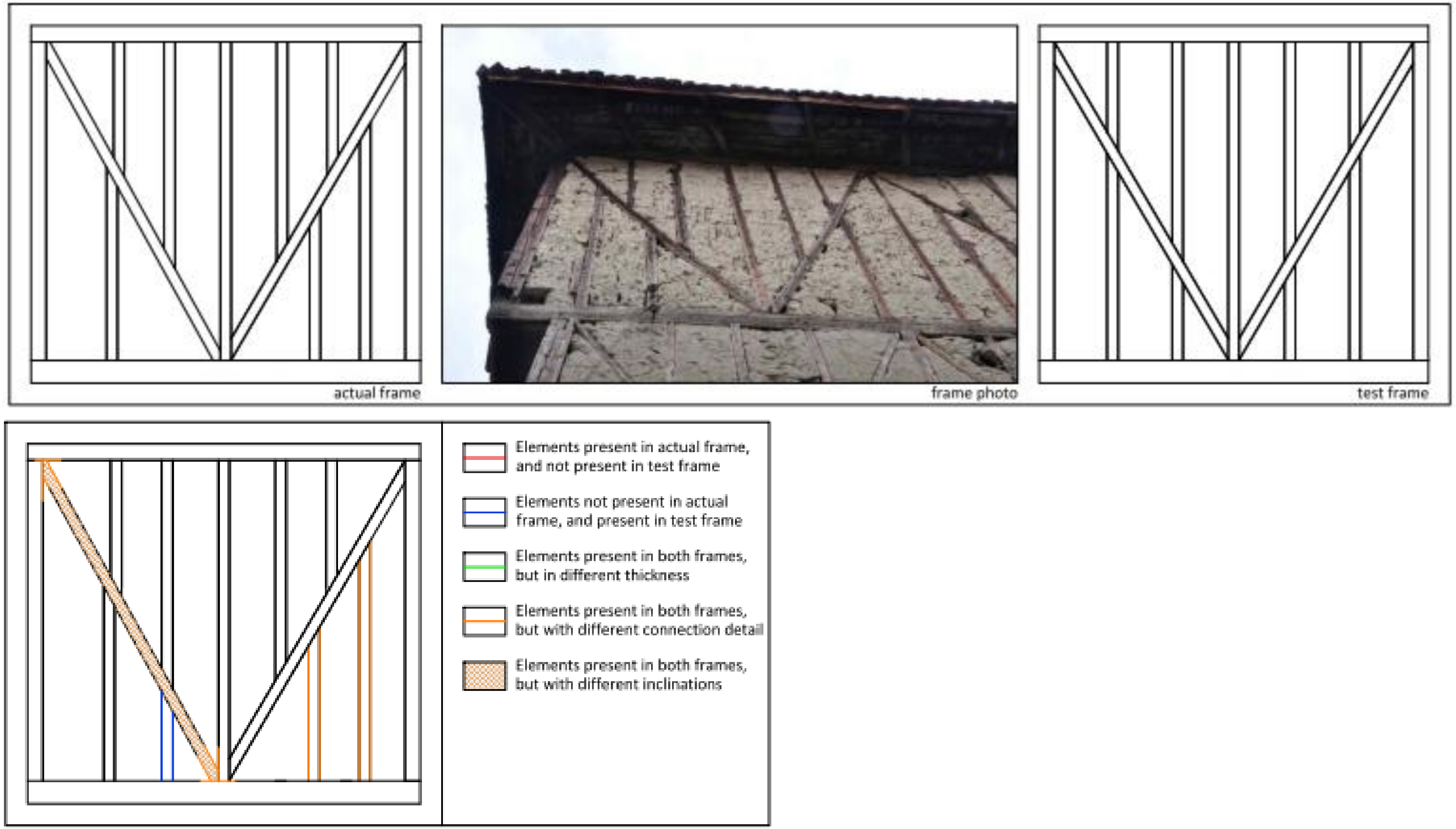

Figure 223: Drawings of actual frame and test Frames#2 and #3, showing the differences between them

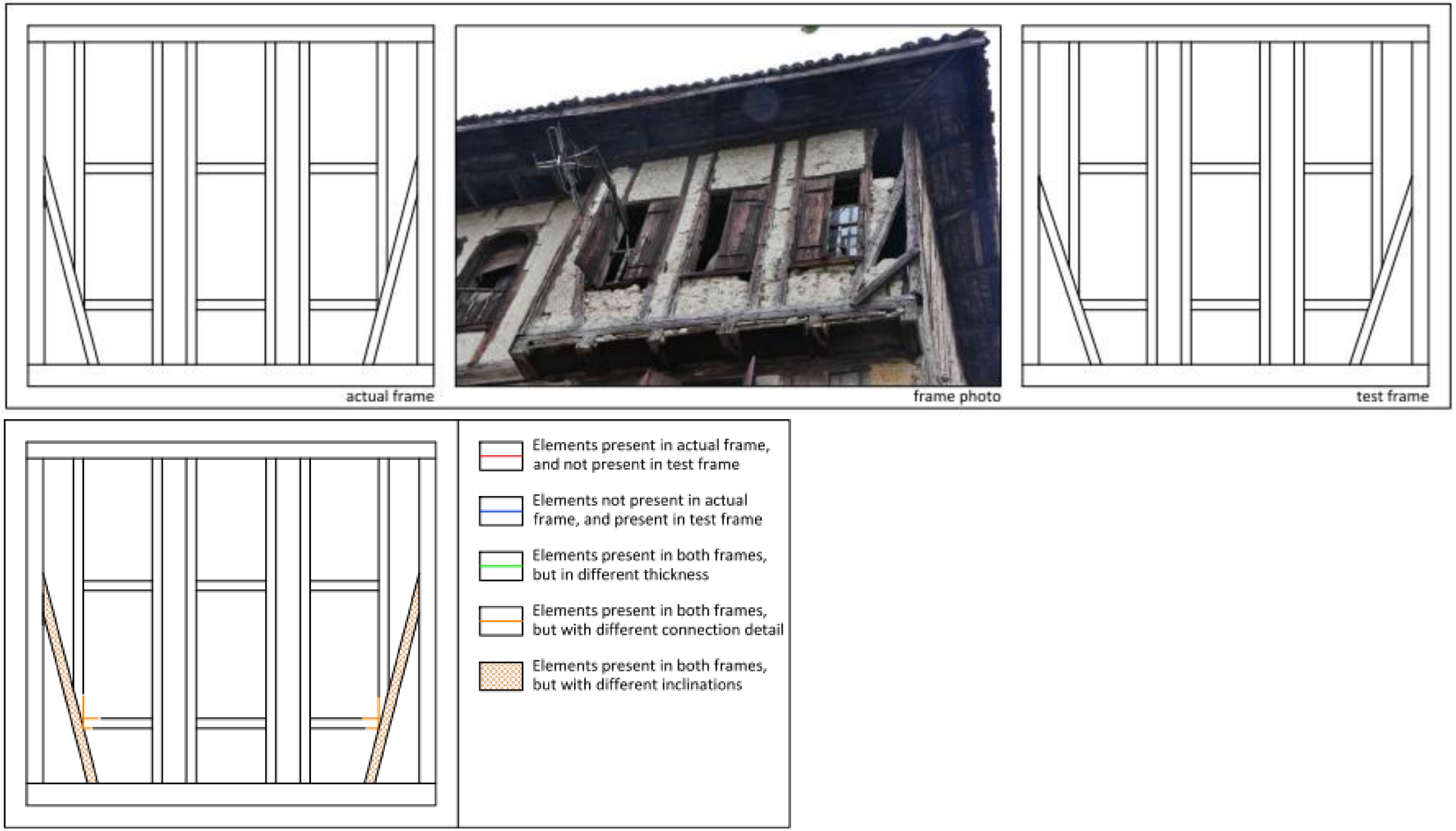

Figure 224: Drawings of actual frame and test Frame#5, showing the differences between them

Figure 225: Drawings of actual frame and test Frame#6, showing the differences between them

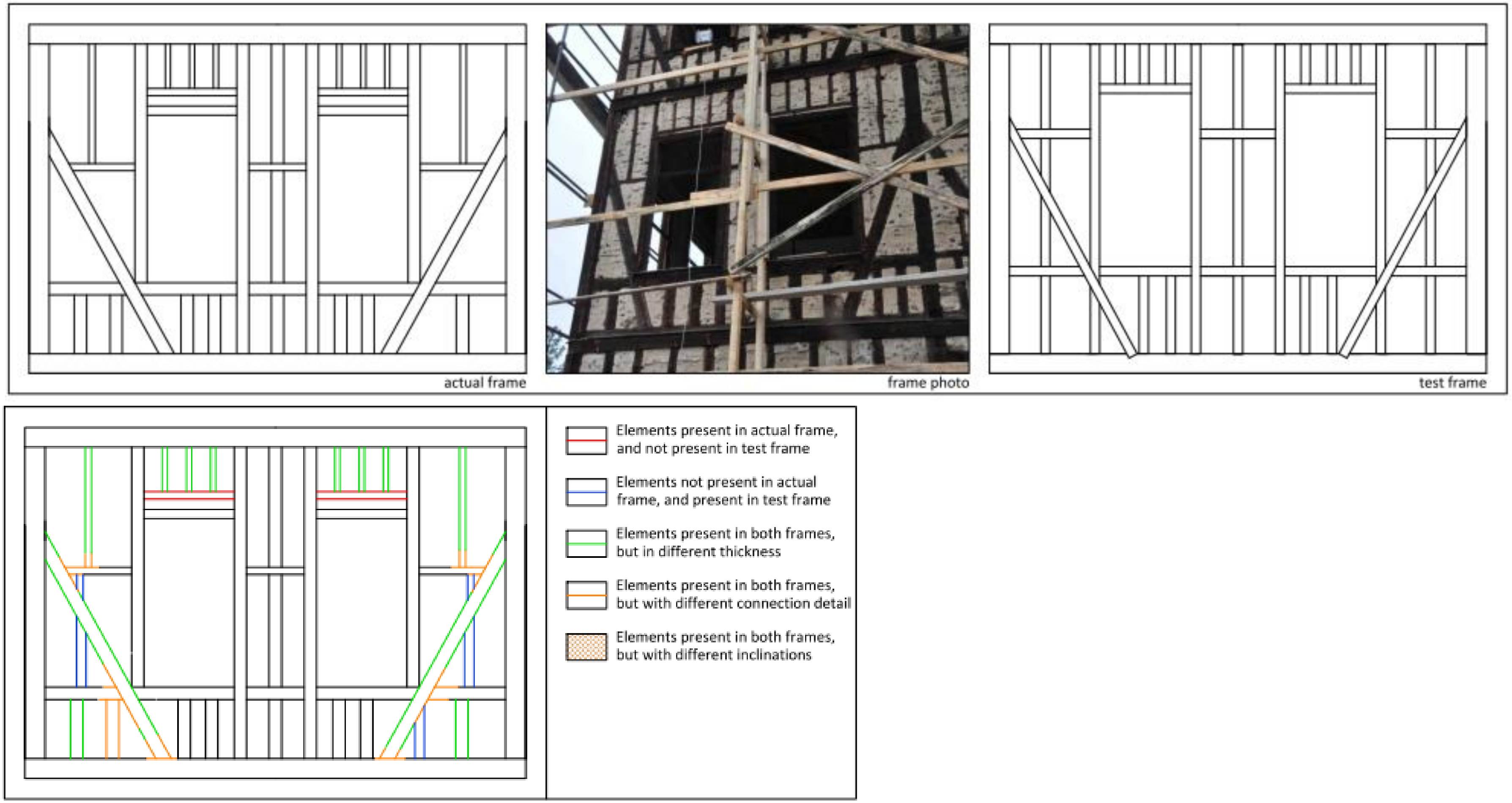

Figure 226: Drawings of actual frame and test Frame#7, showing the differences between them

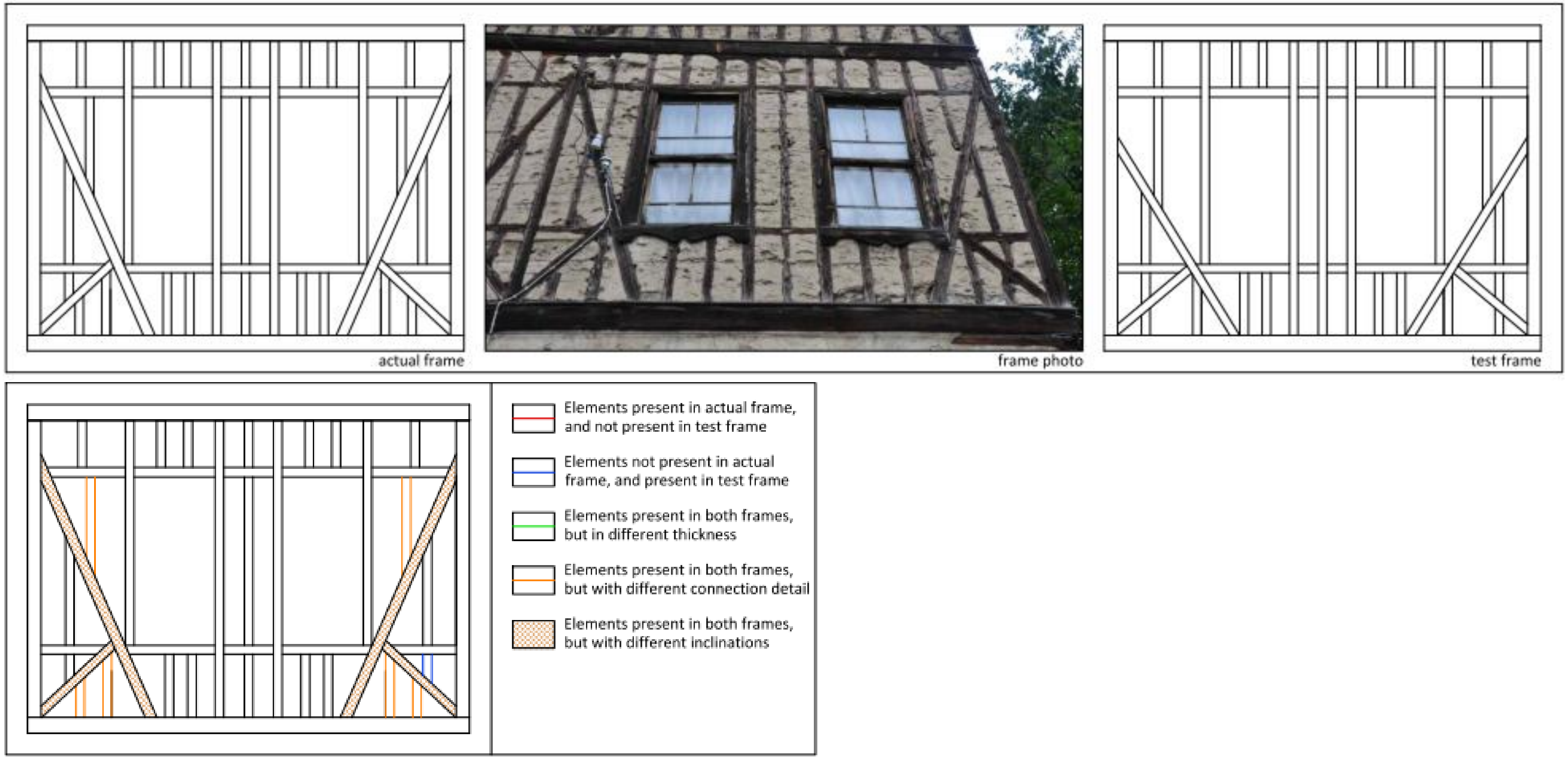

Figure 227: Drawings of actual frame and test Frame#8, showing the differences between them

APPENDIX B

B. RESULTS OBTAINED AT THE END OF TESTING OF FRAME#1

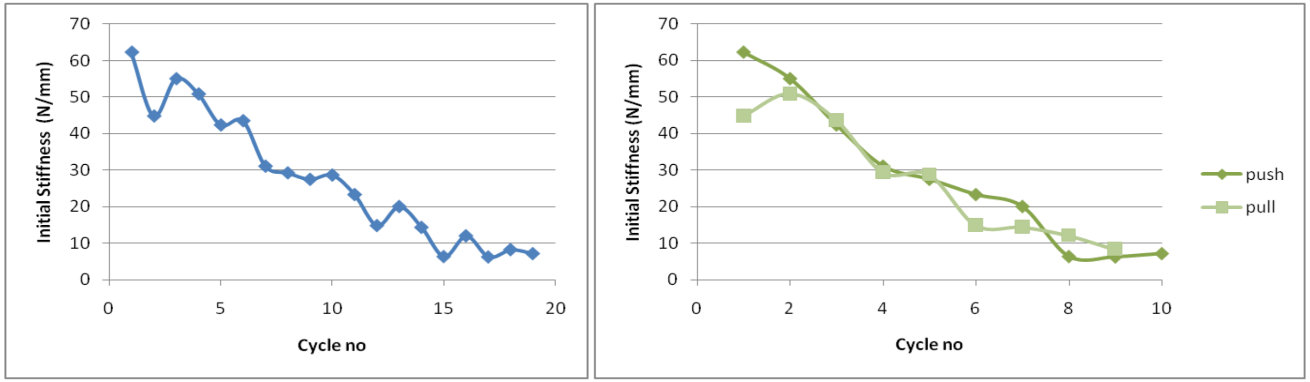

Figure 228: Change in initial stiffness of Frame#1 for all cycles and for push and pull cycles separately, respectively

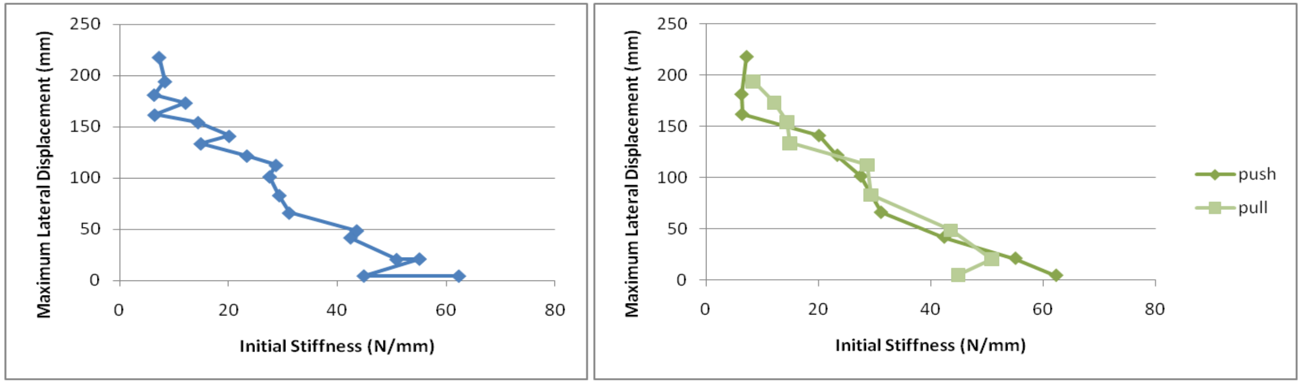

Figure 229: Change in initial stiffness – maximum lateral displacement relation of Frame#1 for all cycles and for push and pull cycles separately, respectively

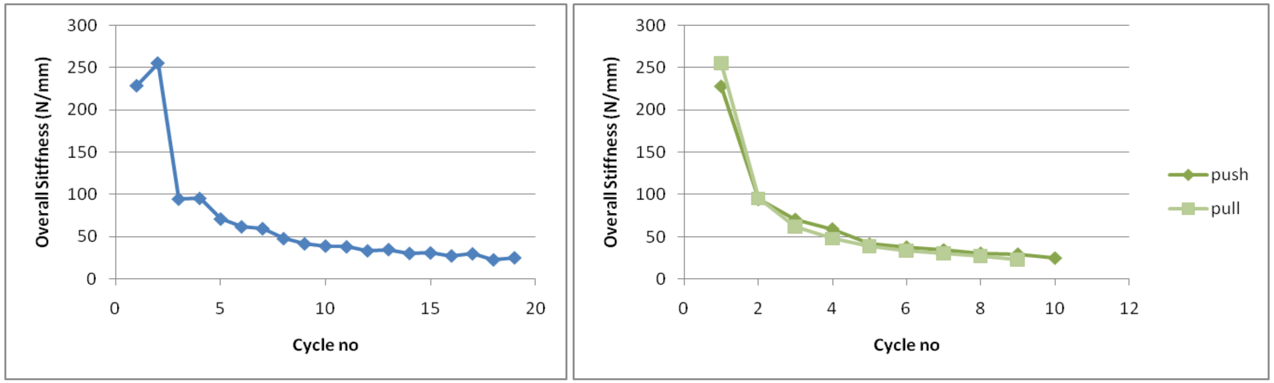

Figure 230: Change in overall stiffness of Frame#1 for all cycles and for push and pull cycles separately, respectively

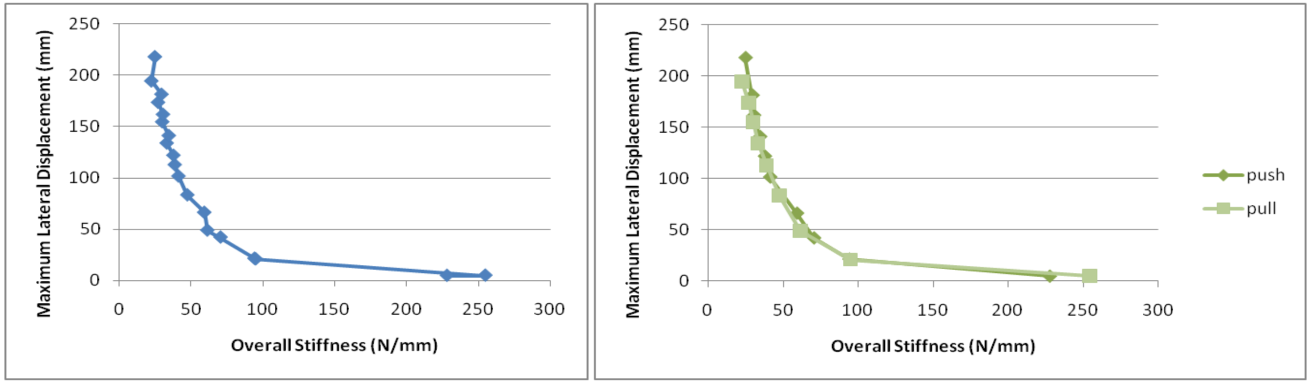

Figure 231: Change in overall stiffness – maximum lateral displacement relation of Frame#1 for all cycles and for push and pull cycles separately, respectively

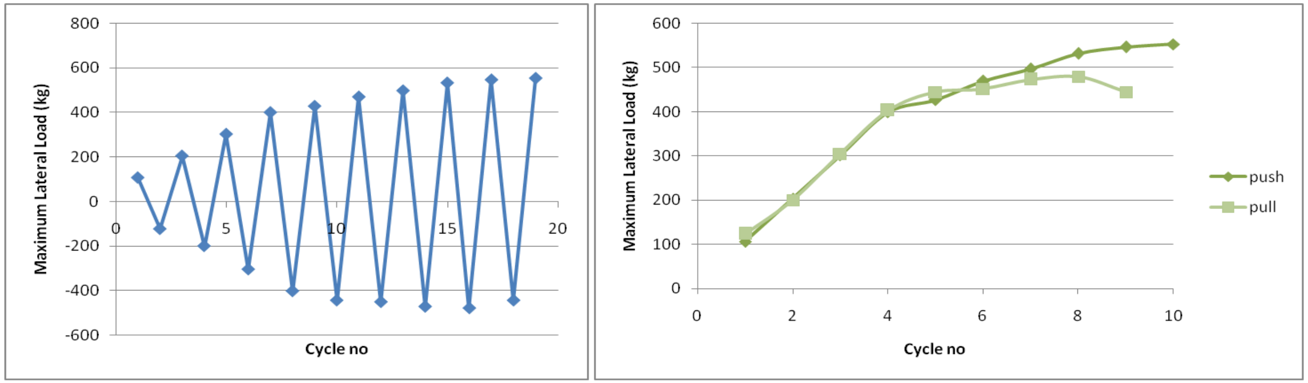

Figure 232: Change in maximum lateral load of Frame#1 for all cycles and for push and pull cycles separately, respectively

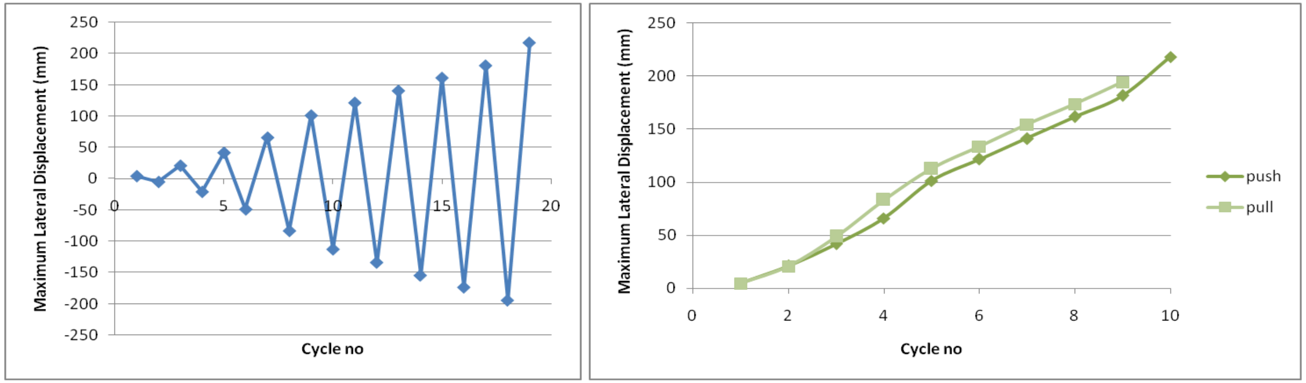

Figure 233: Change in maximum lateral displacement of Frame#1 for all cycles and for push and pull cycles separately, respectively

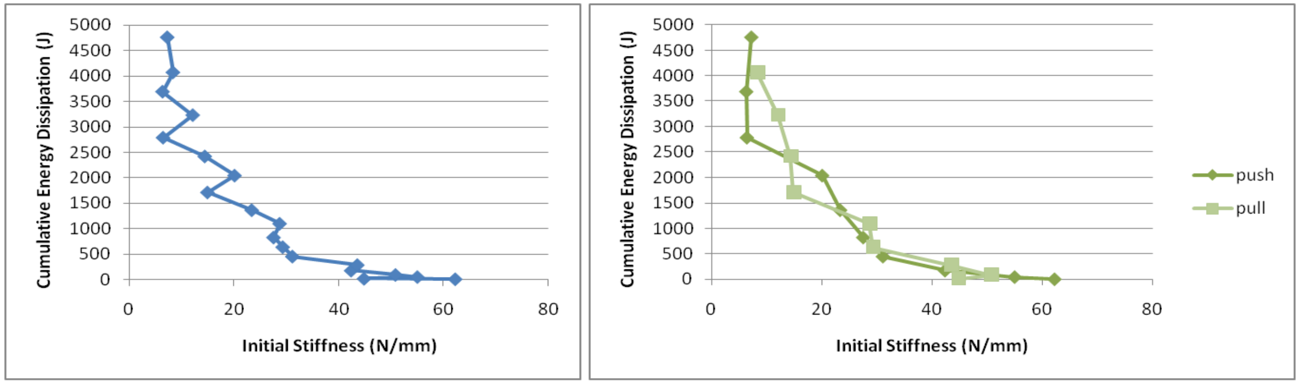

Figure 234: Change in cumulative dissipated energy – initial stiffness relation of Frame#1 for all cycles (positive push / negative pull, and absolute values, respectively) and for push and pull cycles separately

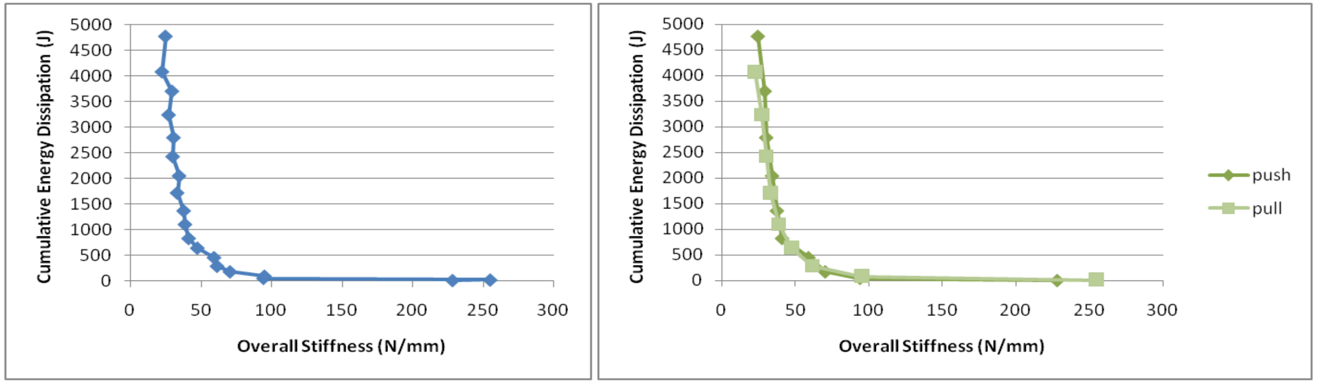

Figure 235: Change in cumulative dissipated energy – overall stiffness relation of Frame#1 for all cycles (positive push / negative pull, and absolute values, respectively) and for push and pull cycles separately

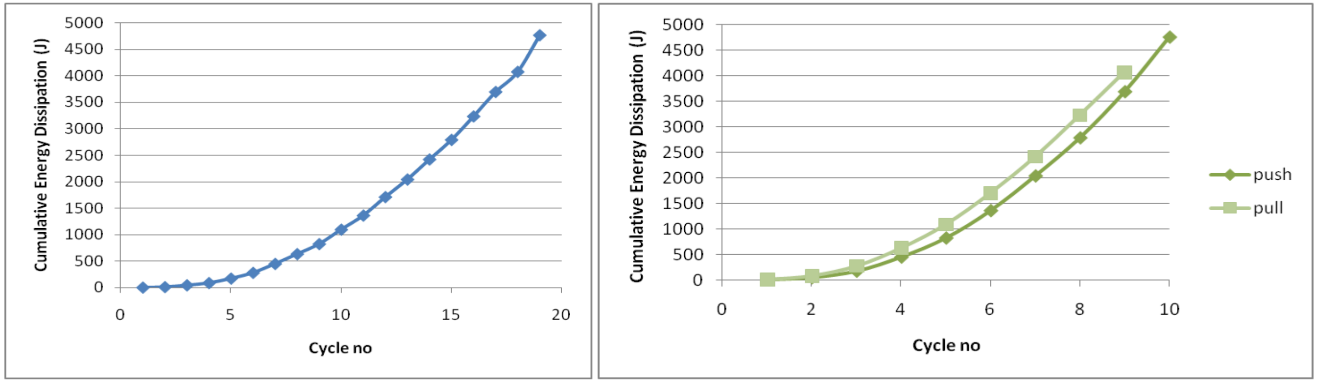

Figure 236: Change in cumulative dissipated energy of Frame#1 for all cycles and for push and pull cycles separately, respectively

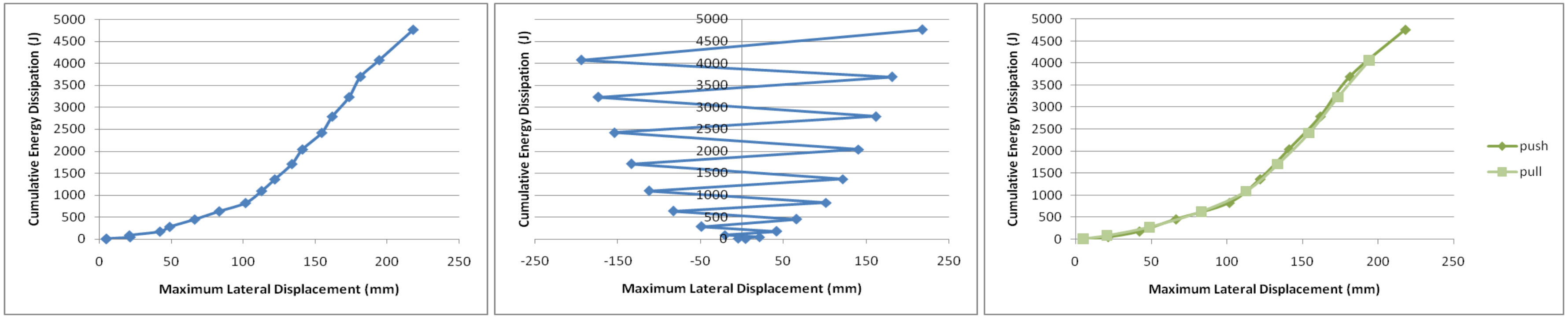

Figure 237: Change in cumulative dissipated energy – maximum lateral displacement relation of Frame#1 for all cycles (positive push / negative pull, and absolute values, respectively) and for push and pull cycles separately

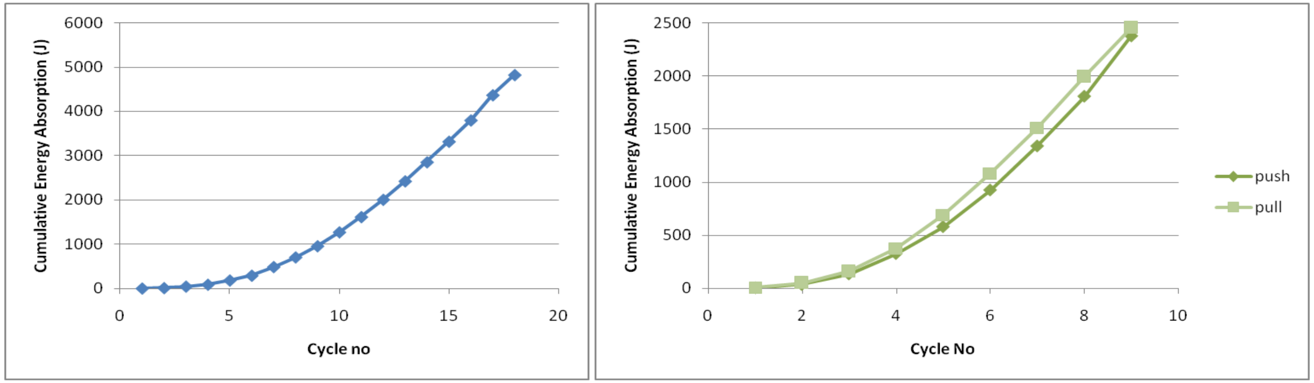

Figure 238: Change in cumulative absorbed energy of Frame#1 for all cycles and for push and pull cycles separately, respectively

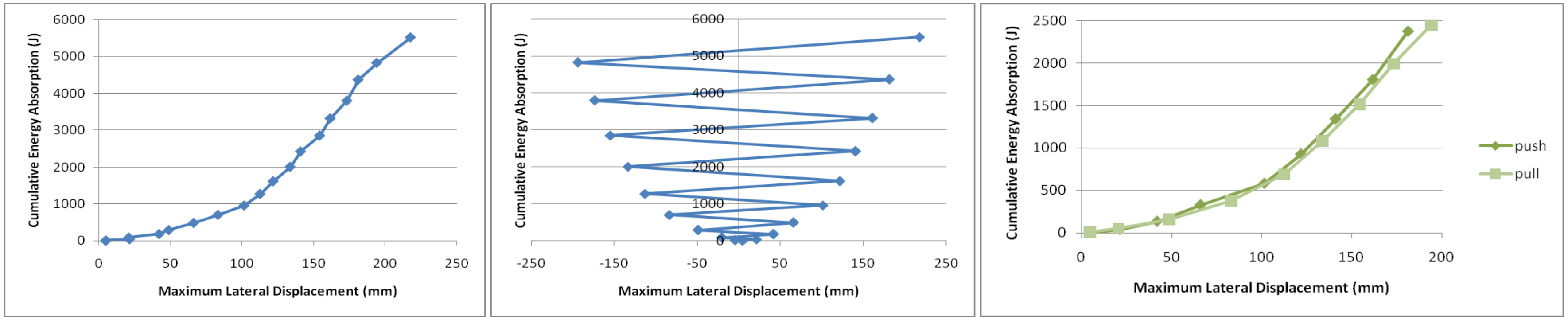

Figure 239: Change in cumulative absorbed energy – maximum lateral displacement relation of Frame#1 for all cycles (positive push / negative pull, and absolute values, respectively) and for push and pull cycles separately

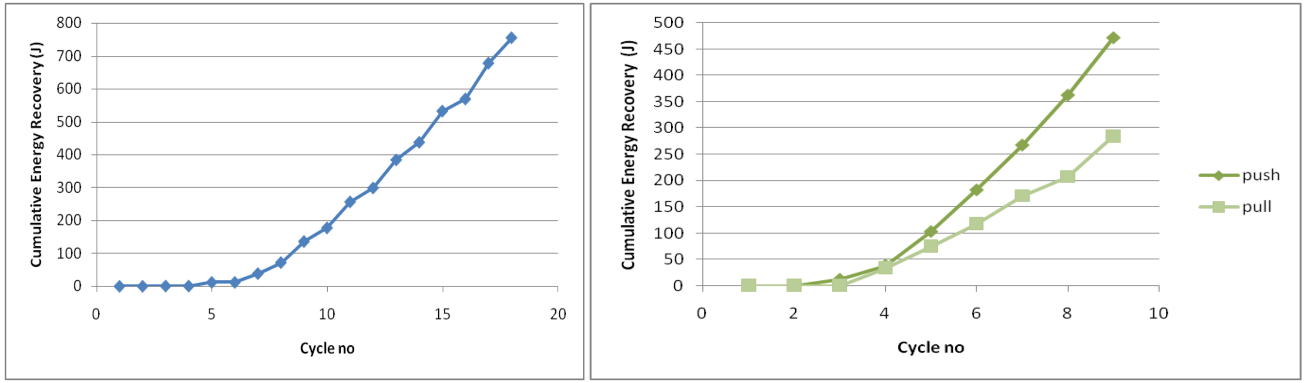

Figure 240: Change in cumulative recovered energy of Frame#1 for all cycles and for push and pull cycles separately, respectively

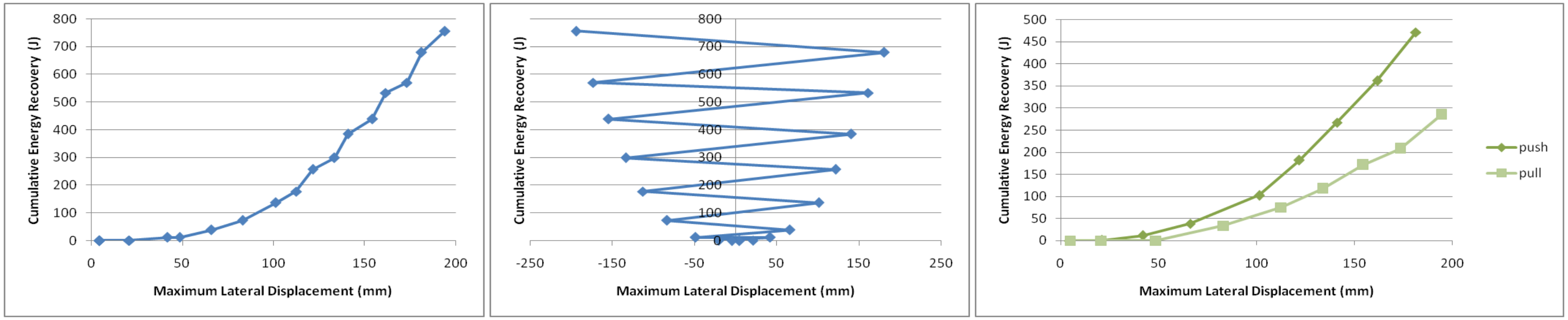

Figure 241: Change in cumulative recovered energy – maximum lateral displacement relation of Frame#1 for all cycles (positive push / negative pull, and absolute values, respectively) and for push and pull cycles separately

APPENDIX C

C. RESULTS OBTAINED AT THE END OF TESTING OF FRAME#1 WITH ADOBE INFILL

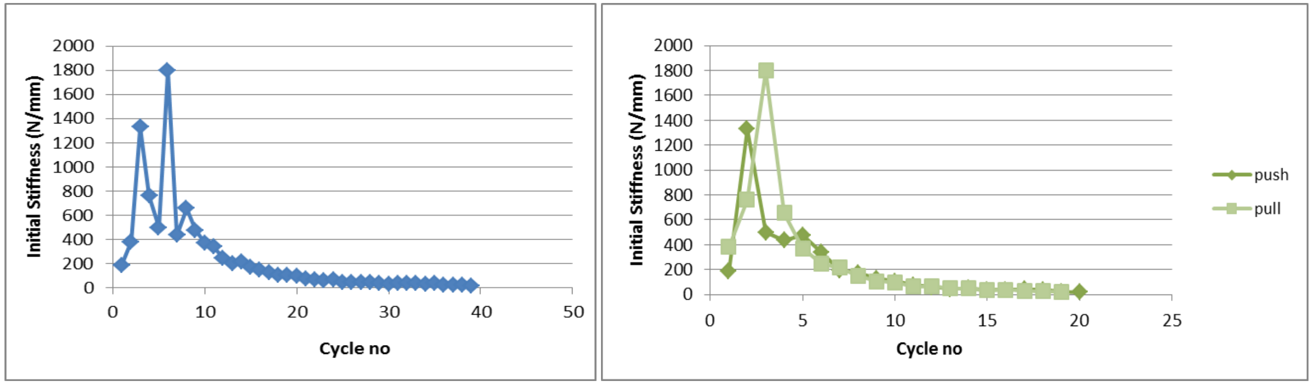

Figure 242: Change in initial stiffness of Frame#1 with infill for all cycles and for push and pull cycles separately, respectively

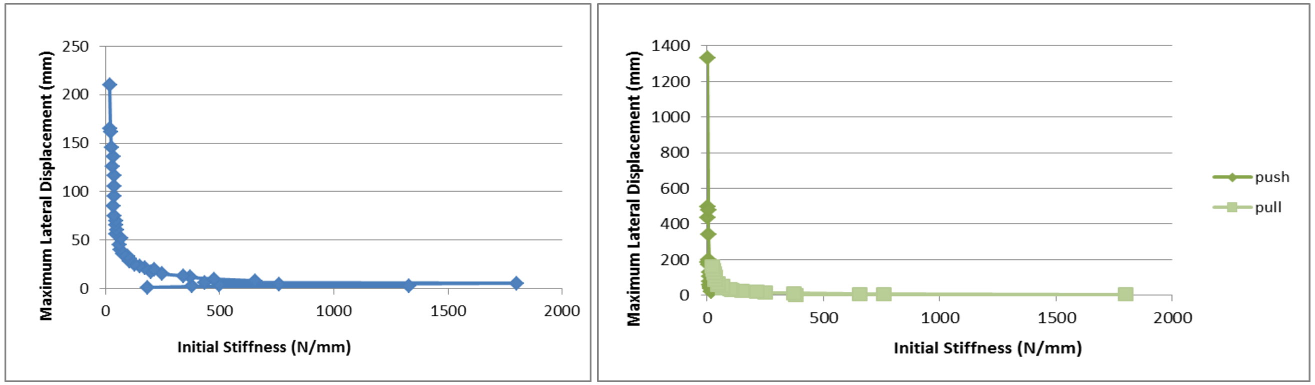

Figure 243: Change in initial stiffness – maximum lateral displacement relation of Frame#1 with infill for all cycles and for push and pull cycles separately, respectively

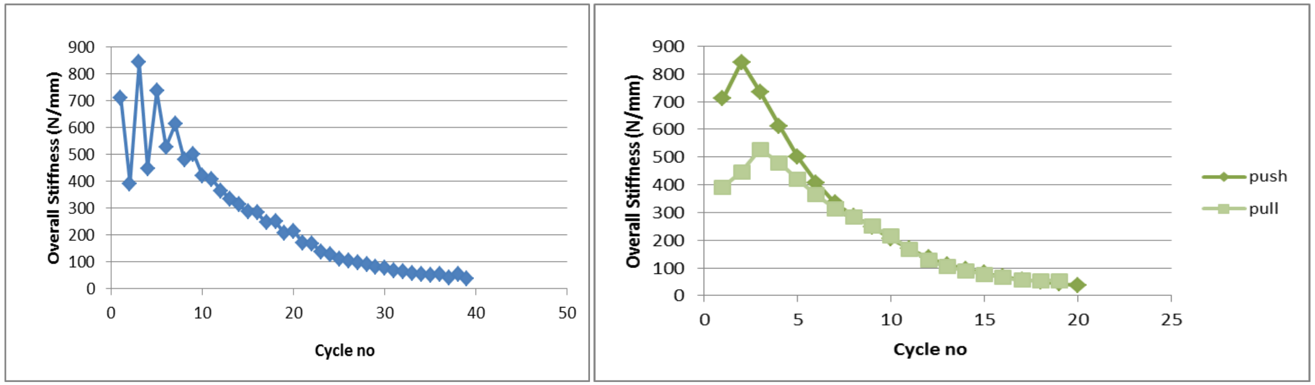

Figure 244: Change in overall stiffness of Frame#1 with infill for all cycles and for push and pull cycles separately, respectively

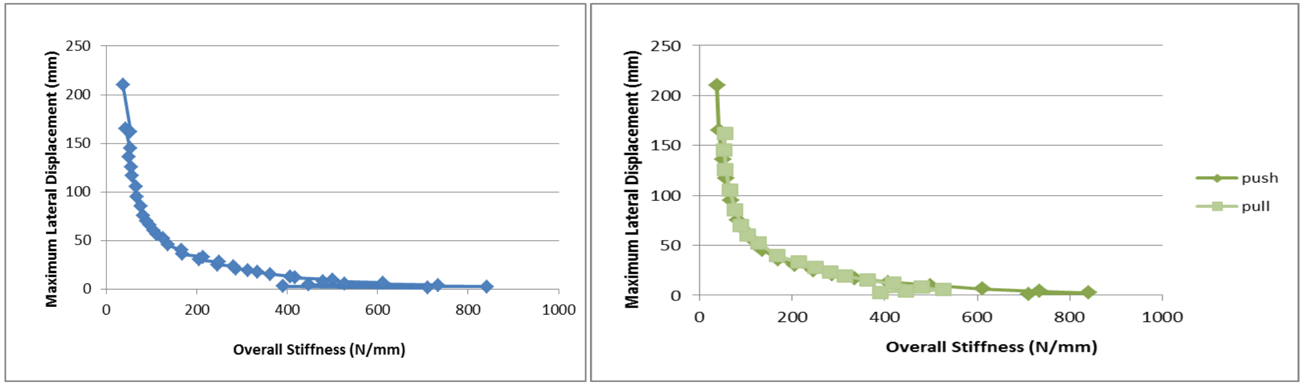

Figure 245: Change in overall stiffness – maximum lateral displacement relation of Frame#1 with infill for all cycles and for push and pull cycles separately, respectively

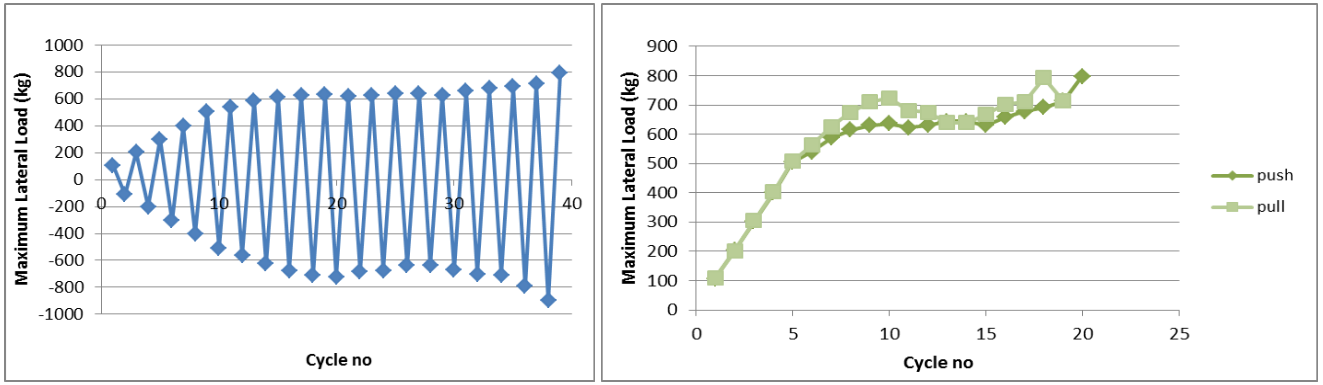

Figure 246: Change in maximum lateral load of Frame#1 with infill for all cycles and for push and pull cycles separately, respectively

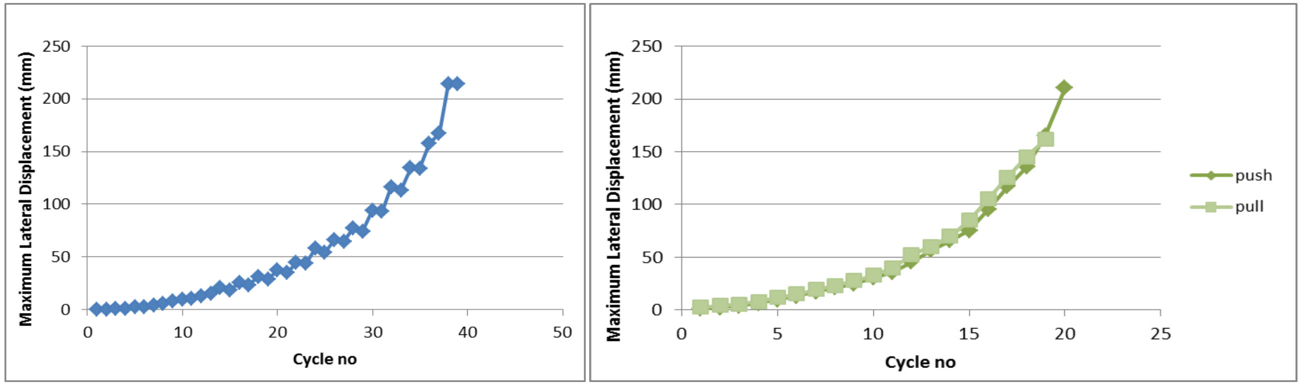

Figure 247: Change in maximum lateral displacement of Frame#1 with infill for all cycles and for push and pull cycles separately, respectively

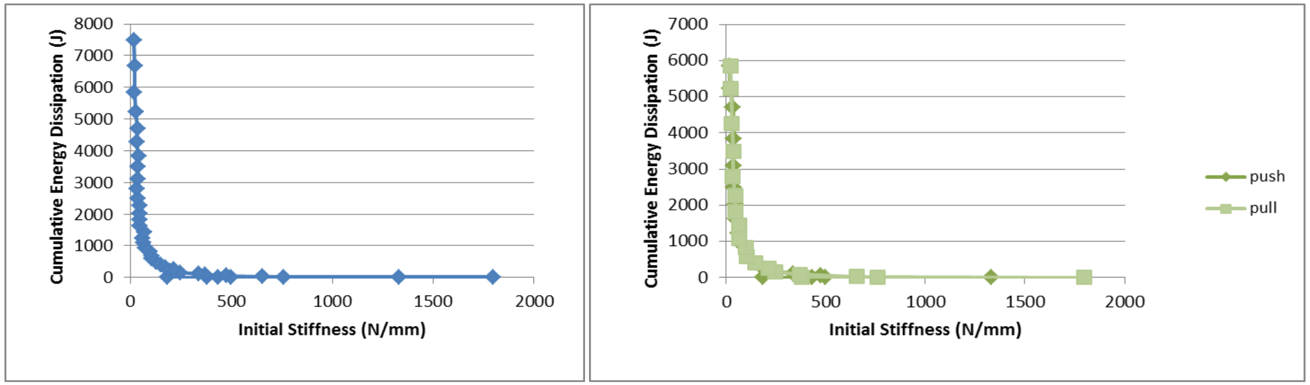

Figure 248: Change in cumulative dissipated energy – initial stiffness relation of Frame#1 with infill for all cycles (positive push / negative pull, and absolute values, respectively) and for push and pull cycles separately

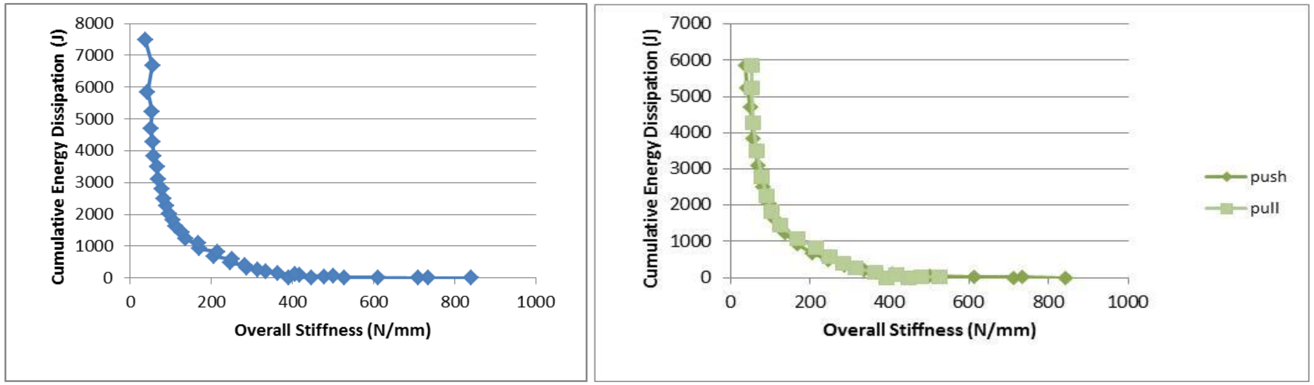

Figure 249: Change in cumulative dissipated energy – overall stiffness relation of Frame#1 with infill for all cycles (positive push / negative pull, and absolute values, respectively) and for push and pull cycles separately

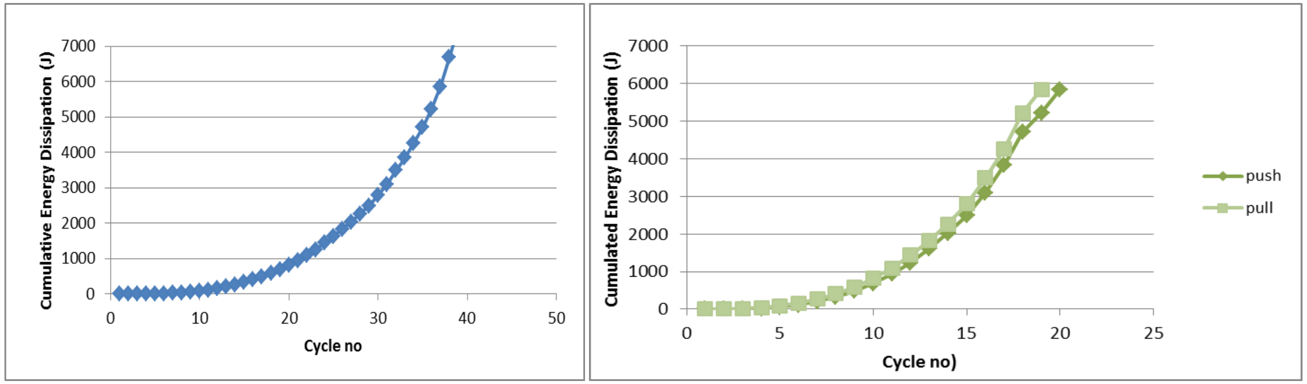

Figure 250: Change in cumulative dissipated energy of Frame#1 with infill for all cycles and for push and pull cycles separately, respectively

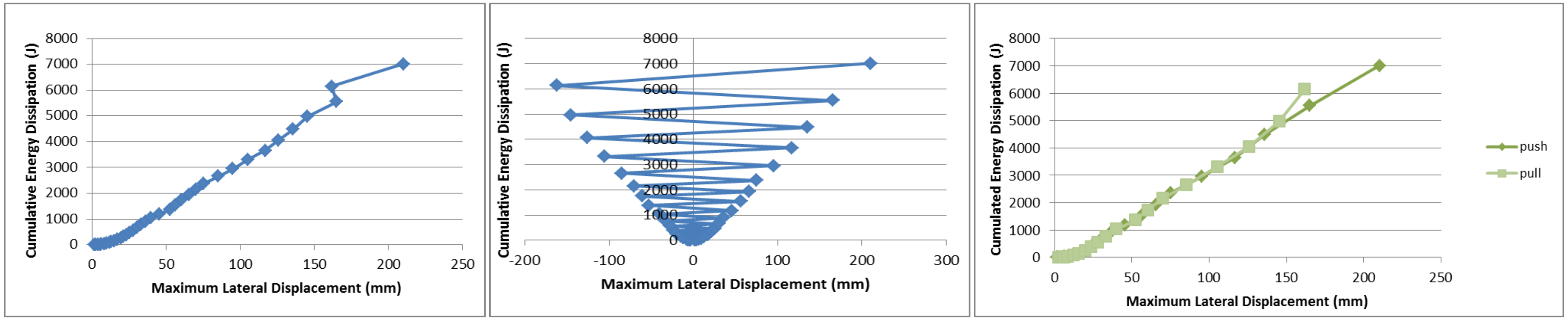

Figure 251: Change in cumulative dissipated energy – maximum lateral displacement relation of Frame#1 with infill for all cycles (positive push / negative pull, and absolute values, respectively) and for push and pull cycles separately

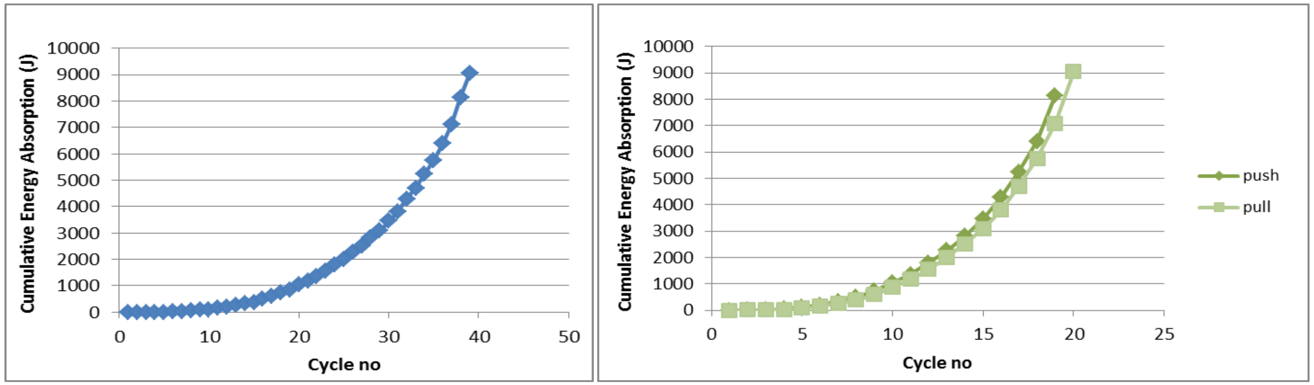

Figure 252: Change in cumulative absorbed energy of Frame#1 with infill for all cycles and for push and pull cycles separately, respectively

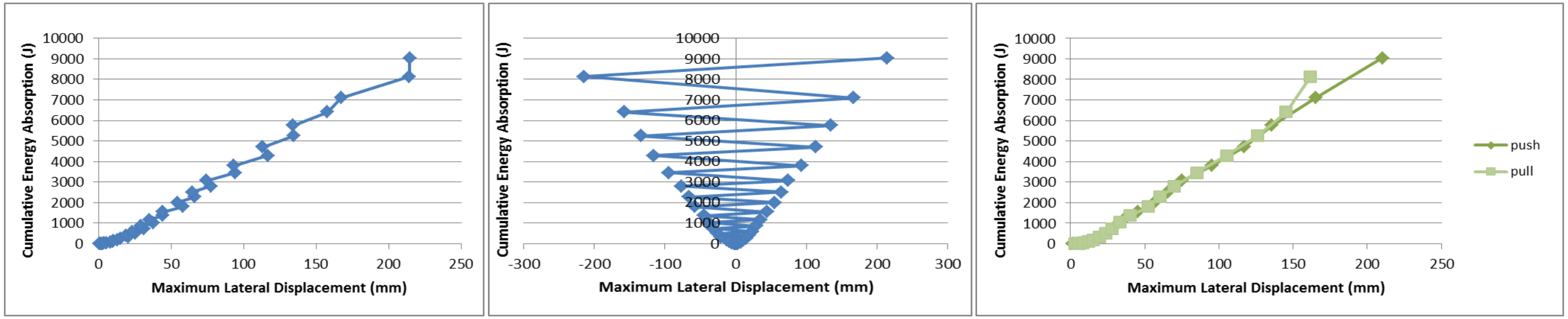

Figure 253: Change in cumulative absorbed energy – maximum lateral displacement relation of Frame#1 with infill for all cycles (positive push / negative pull, and absolute values, respectively) and for push and pull cycles separately

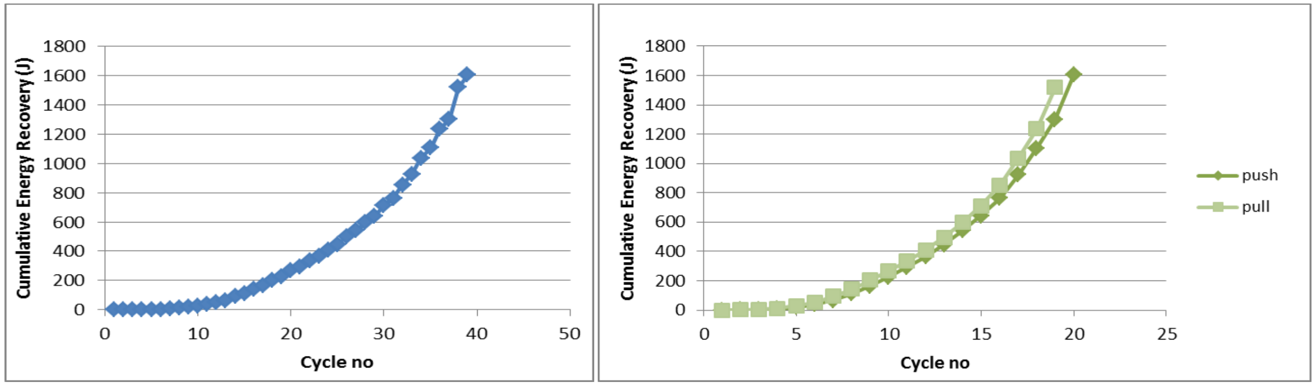

Figure 254: Change in cumulative recovered energy of Frame#1 with infill for all cycles and for push and pull cycles separately, respectively

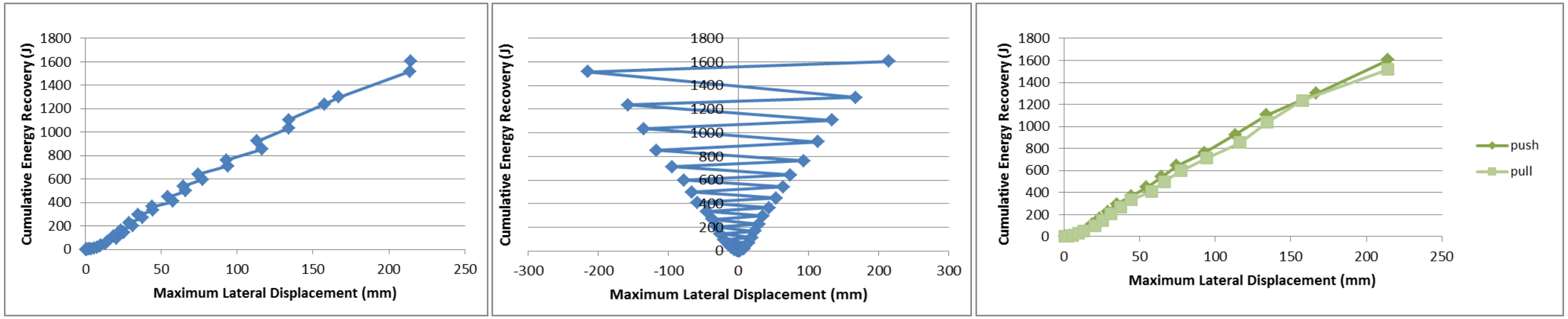

Figure 255: Change in cumulative recovered energy – maximum lateral displacement relation of Frame#1 with infill for all cycles (positive push / negative pull, and absolute values, respectively) and for push and pull cycles separately

APPENDIX D

D. RESULTS OBTAINED AT THE END OF TESTING OF FRAME#2

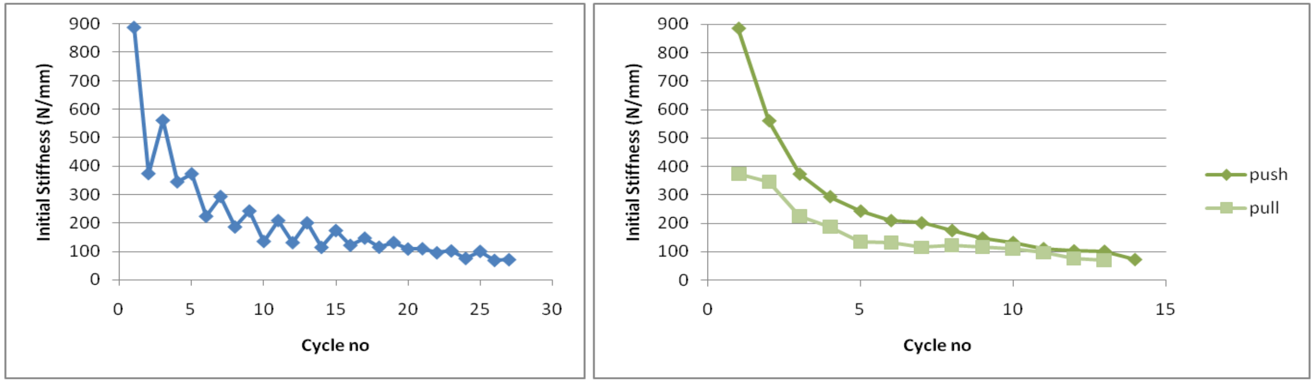

Figure 256: Change in initial stiffness of Frame#2 for all cycles and for push and pull cycles separately, respectively

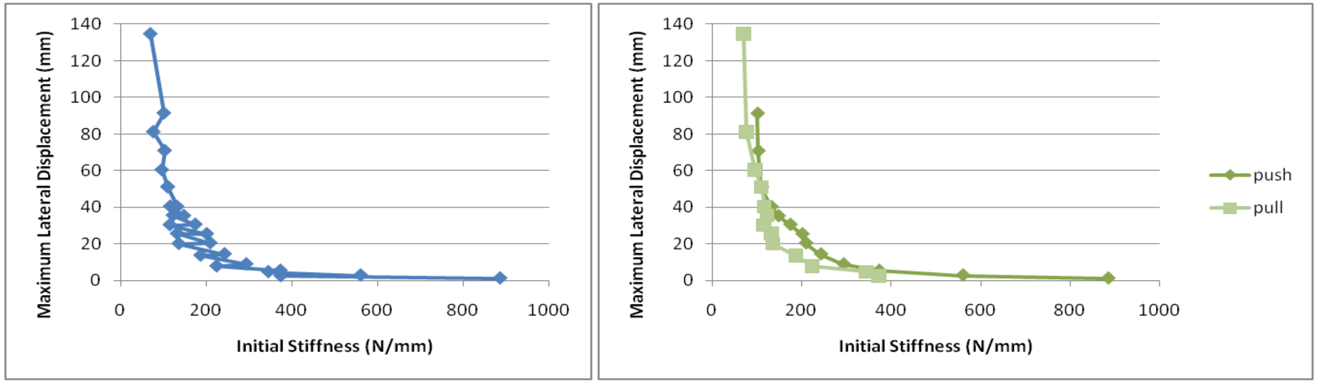

Figure 257: Change in initial stiffness – maximum lateral displacement relation of Frame#2 for all cycles and for push and pull cycles separately, respectively

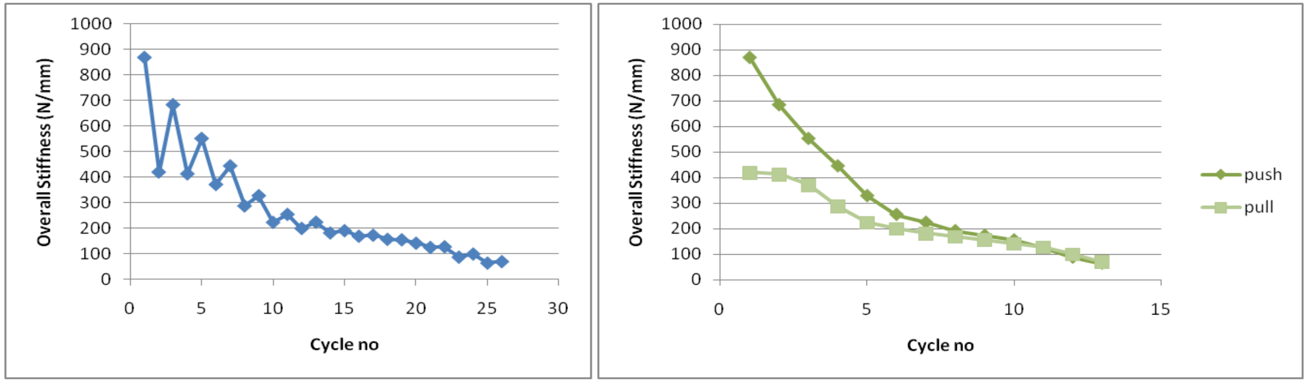

Figure 258: Change in overall stiffness of Frame#2 for all cycles and for push and pull cycles separately, respectively

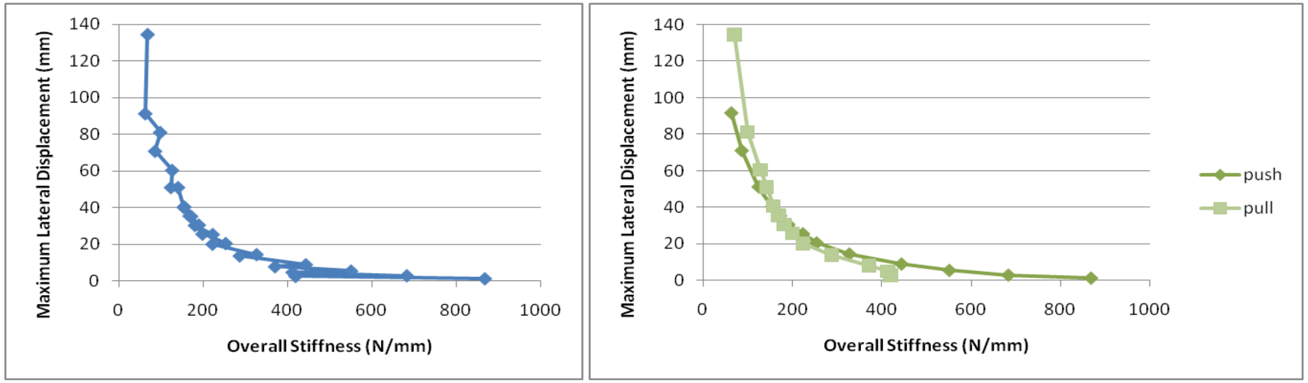

Figure 259: Change in overall stiffness – maximum lateral displacement relation of Frame#2 for all cycles and for push and pull cycles separately, respectively

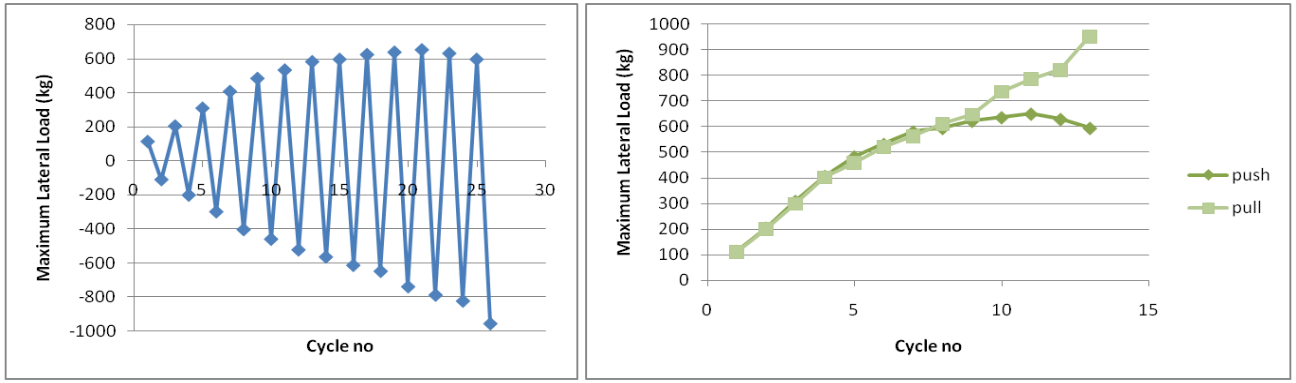

Figure 260: Change in maximum lateral load of Frame#2 for all cycles and for push and pull cycles separately, respectively

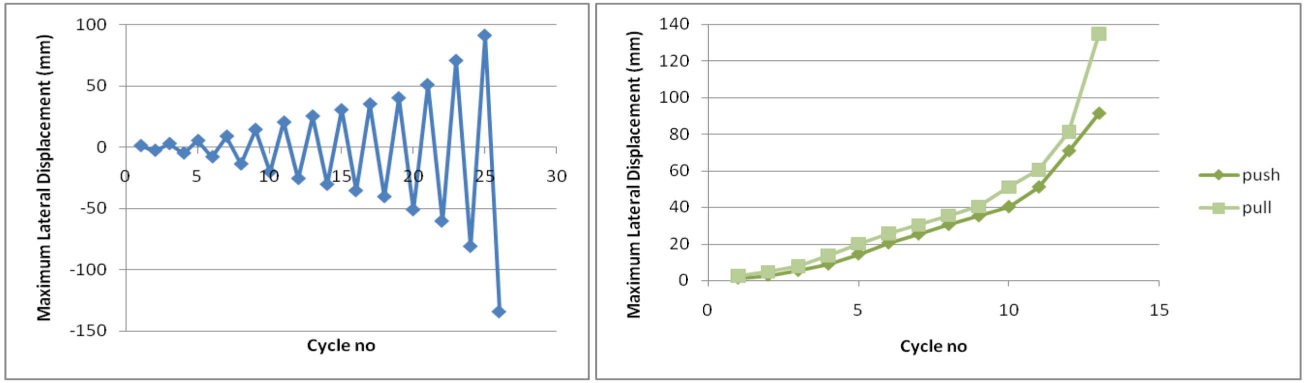

Figure 261: Change in maximum lateral displacement of Frame#2 for all cycles and for push and pull cycles separately, respectively

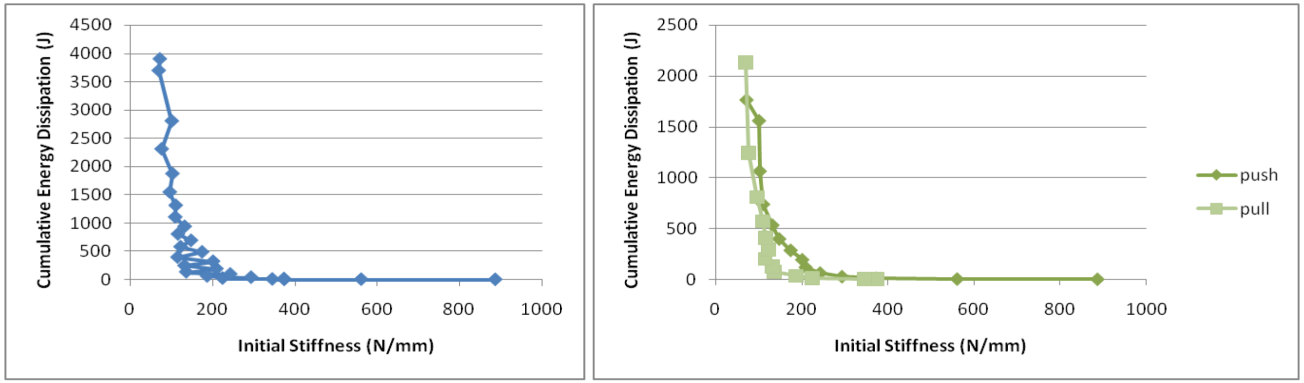

Figure 262: Change in cumulative dissipated energy – initial stiffness relation of Frame#2 for all cycles (positive push / negative pull, and absolute values, respectively) and for push and pull cycles separately

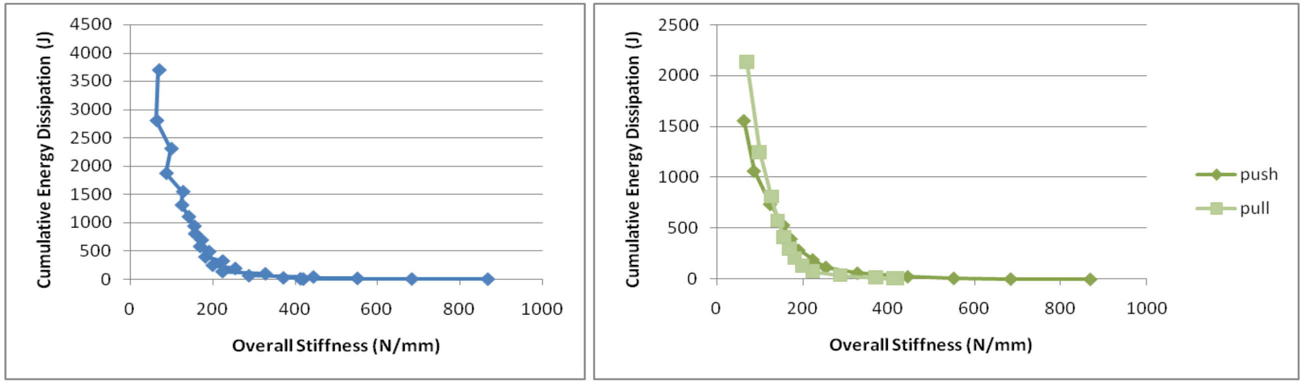

Figure 263: Change in cumulative dissipated energy – overall stiffness relation of Frame#2 for all cycles (positive push / negative pull, and absolute values, respectively) and for push and pull cycles separately

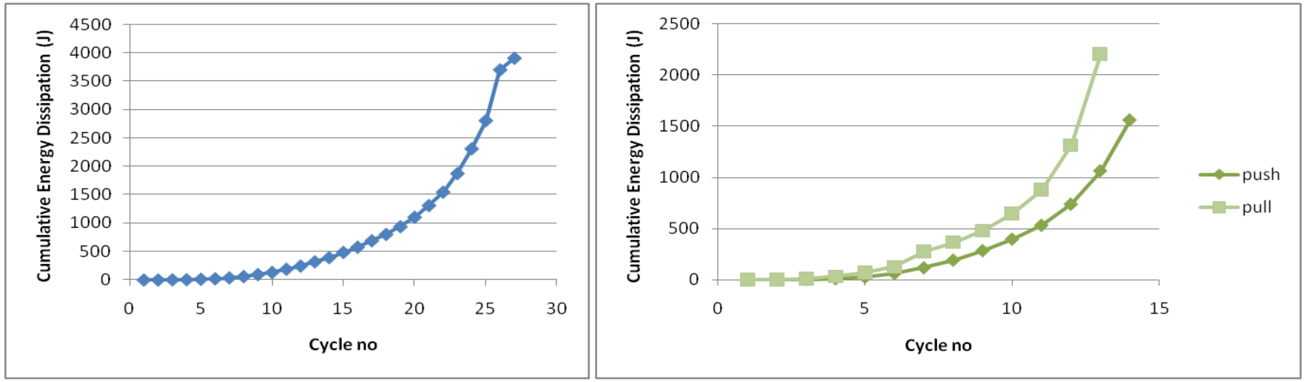

Figure 264: Change in cumulative dissipated energy of Frame#2 for all cycles and for push and pull cycles separately, respectively

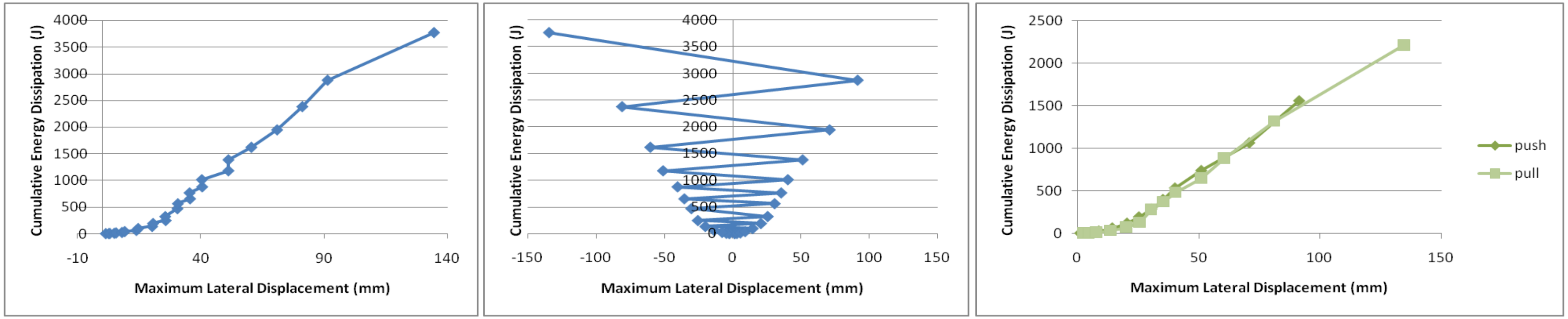

Figure 265: Change in cumulative dissipated energy – maximum lateral displacement relation of Frame#2 for all cycles (positive push / negative pull, and absolute values, respectively) and for push and pull cycles separately

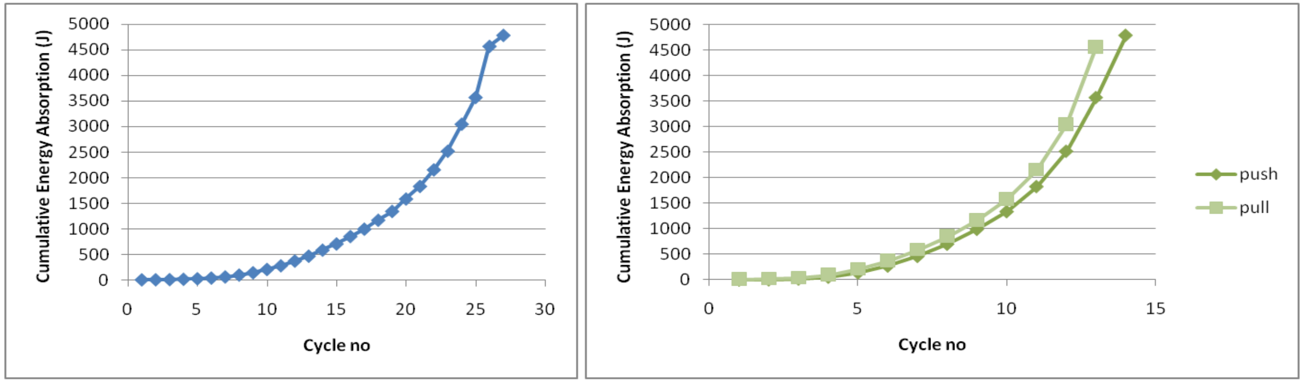

Figure 266: Change in cumulative absorbed energy of Frame#2 for all cycles and for push and pull cycles separately, respectively

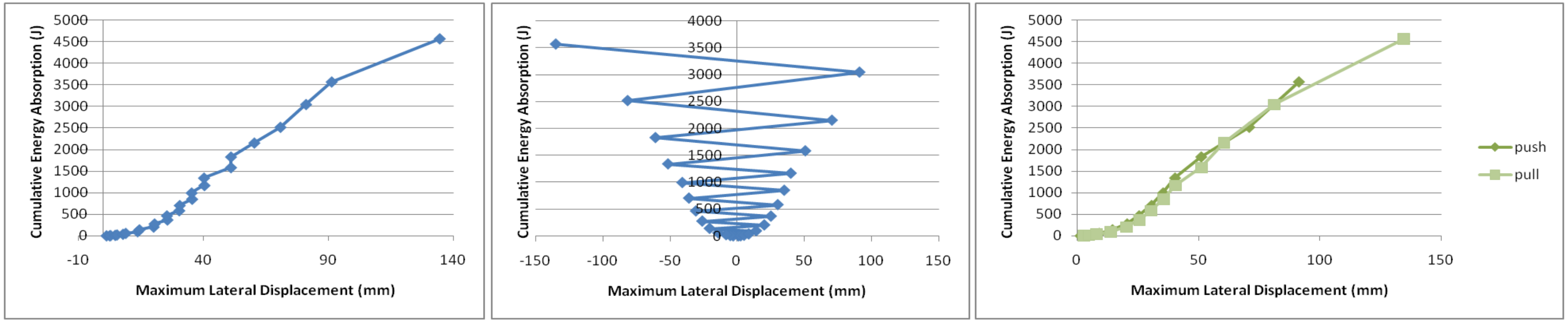

Figure 267: Change in cumulative absorbed energy – maximum lateral displacement relation of Frame#2 for all cycles (positive push / negative pull, and absolute values, respectively) and for push and pull cycles separately

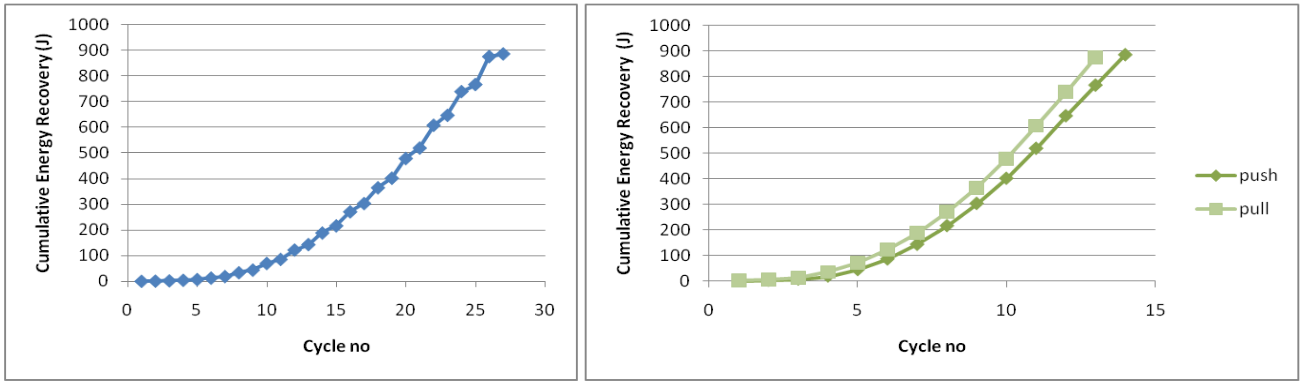

Figure 268: Change in cumulative recovered energy of Frame#2 for all cycles and for push and pull cycles separately, respectively

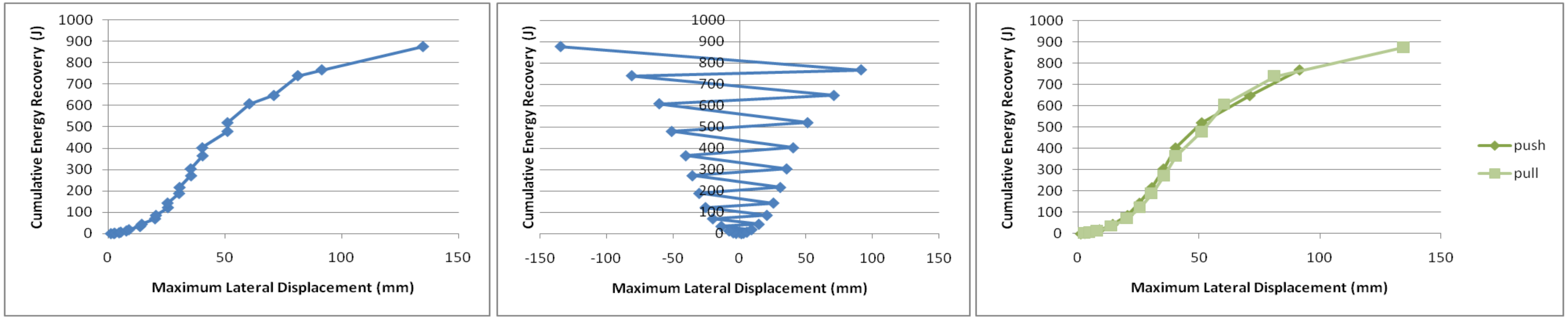

Figure 269: Change in cumulative recovered energy – maximum lateral displacement relation of Frame#2 for all cycles (positive push / negative pull, and absolute values, respectively) and for push and pull cycles separately

APPENDIX E

E. RESULTS OBTAINED AT THE END OF TESTING OF FRAME#2 WITH ADOBE INFILL

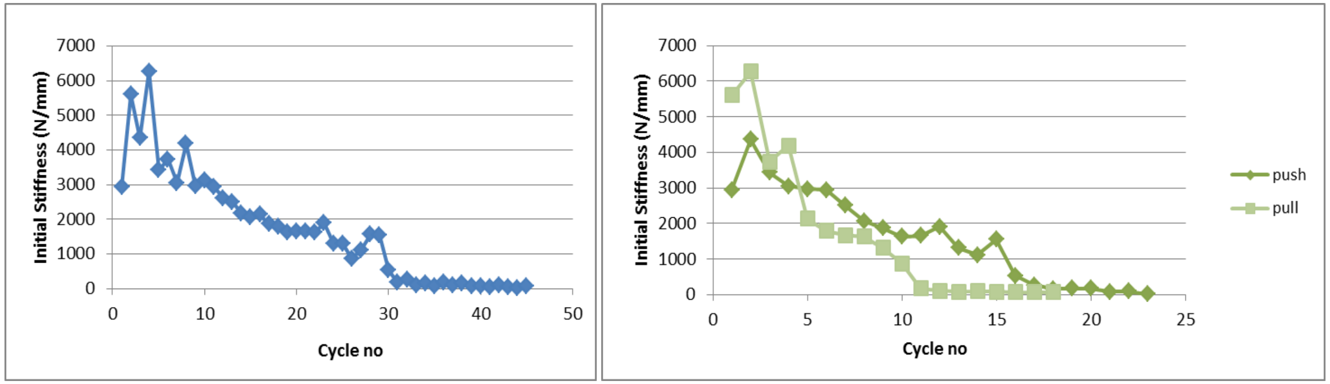

Figure 270: Change in initial stiffness of Frame#2 with infill for all cycles and for push and pull cycles separately, respectively

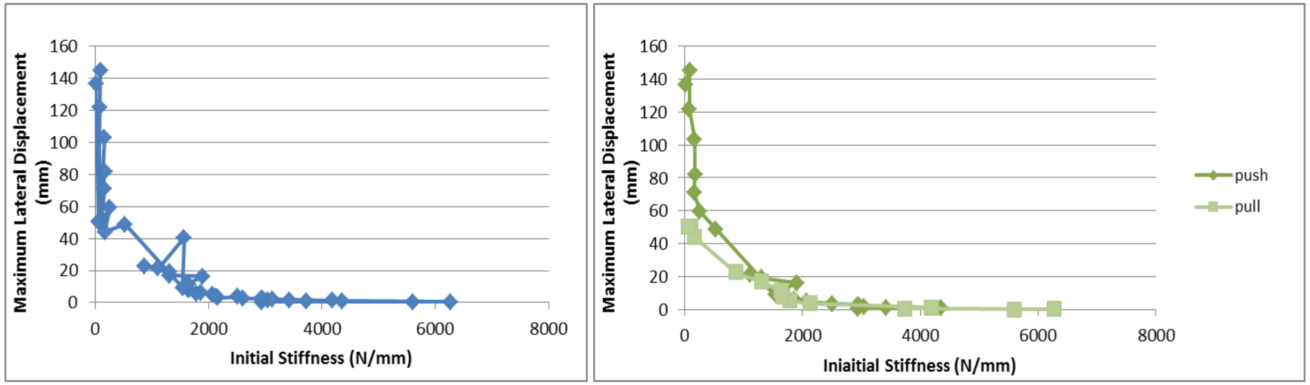

Figure 271: Change in initial stiffness – maximum lateral displacement relation of Frame#2 with infill for all cycles and for push and pull cycles separately, respectively

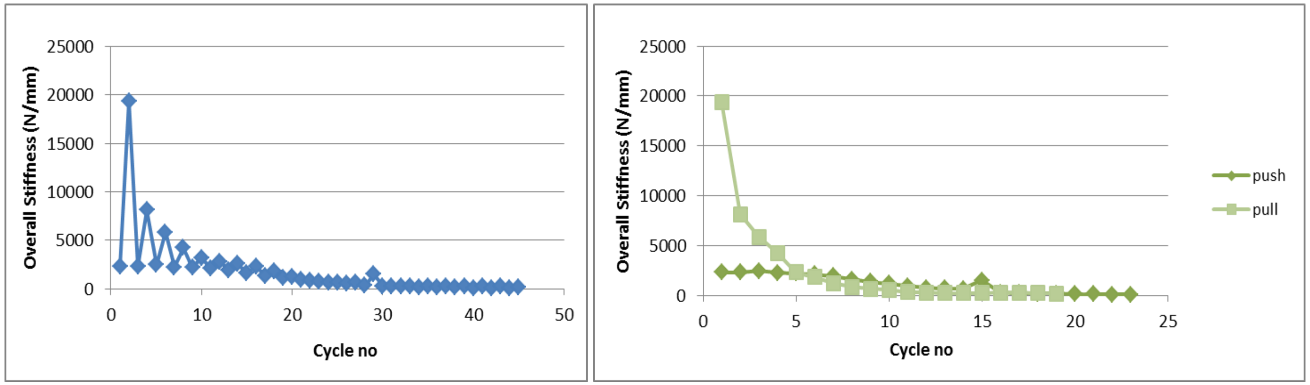

Figure 272: Change in overall stiffness of Frame#2 with infill for all cycles and for push and pull cycles separately, respectively

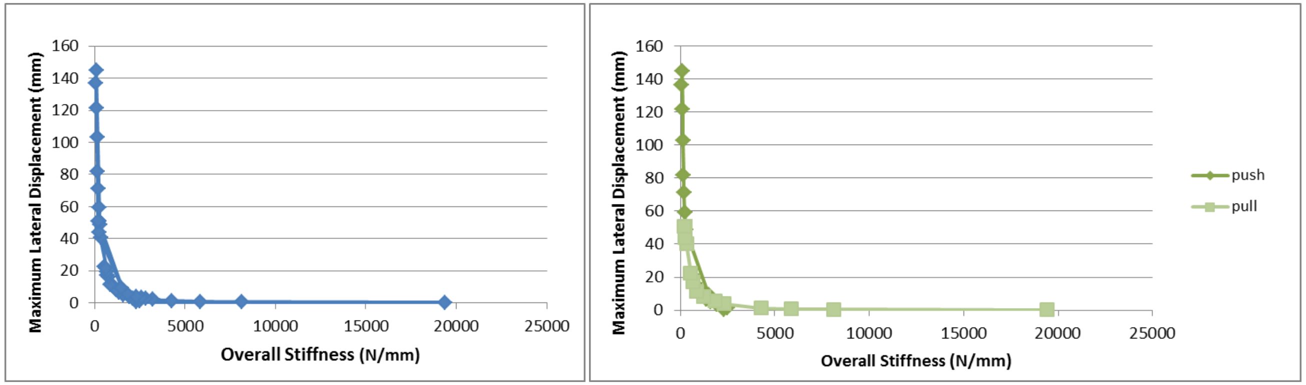

Figure 273: Change in overall stiffness – maximum lateral displacement relation of Frame#2 with infill for all cycles and for push and pull cycles separately, respectively

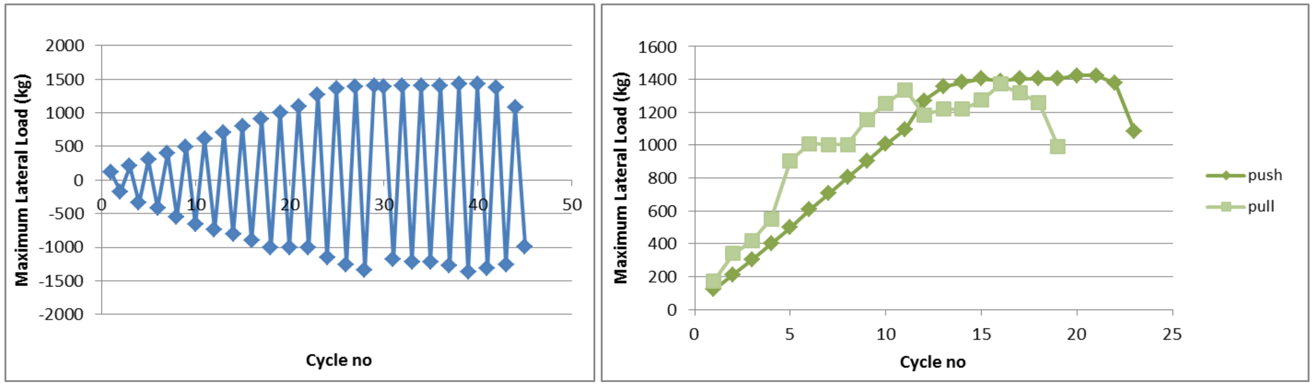

Figure 274: Change in maximum lateral load of Frame#2 with infill for all cycles and for push and pull cycles separately, respectively

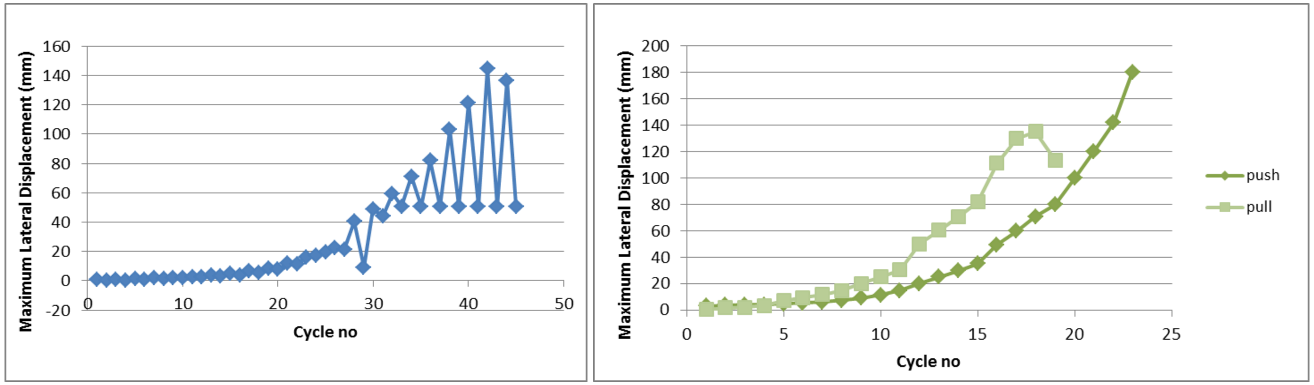

Figure 275: Change in maximum lateral displacement of Frame#2 with infill for all cycles and for push and pull cycles separately, respectively

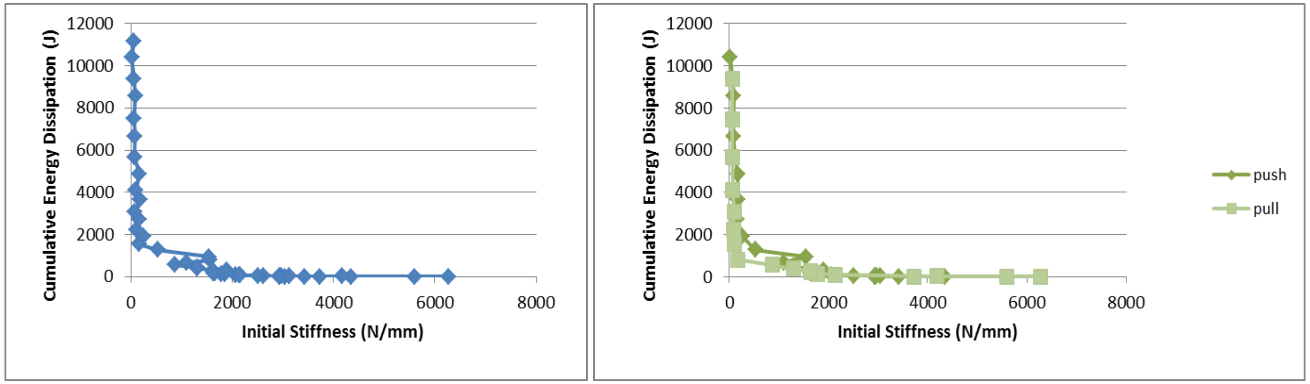

Figure 276: Change in cumulative dissipated energy – initial stiffness relation of Frame#2 with infill for all cycles (positive push / negative pull, and absolute values, respectively) and for push and pull cycles separately

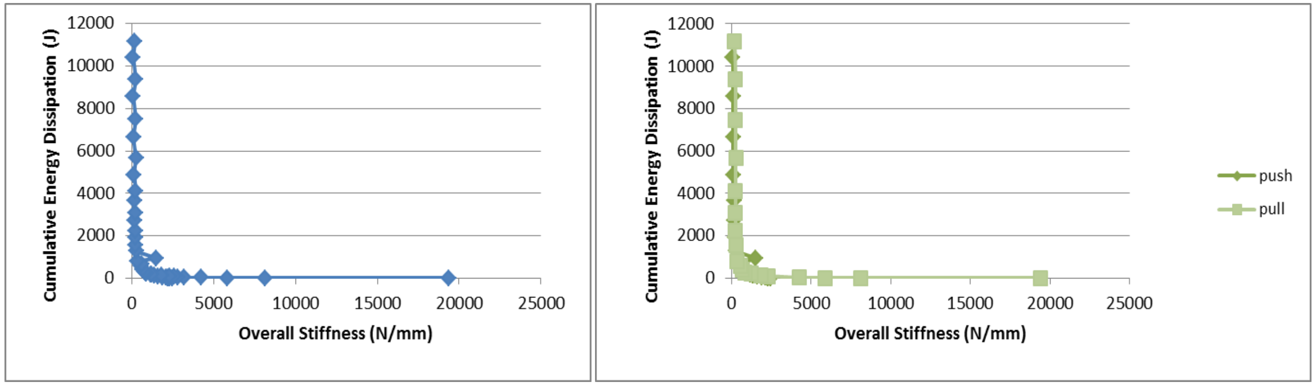

Figure 277: Change in cumulative dissipated energy – overall stiffness relation of Frame#2 with infill for all cycles (positive push / negative pull, and absolute values, respectively) and for push and pull cycles separately

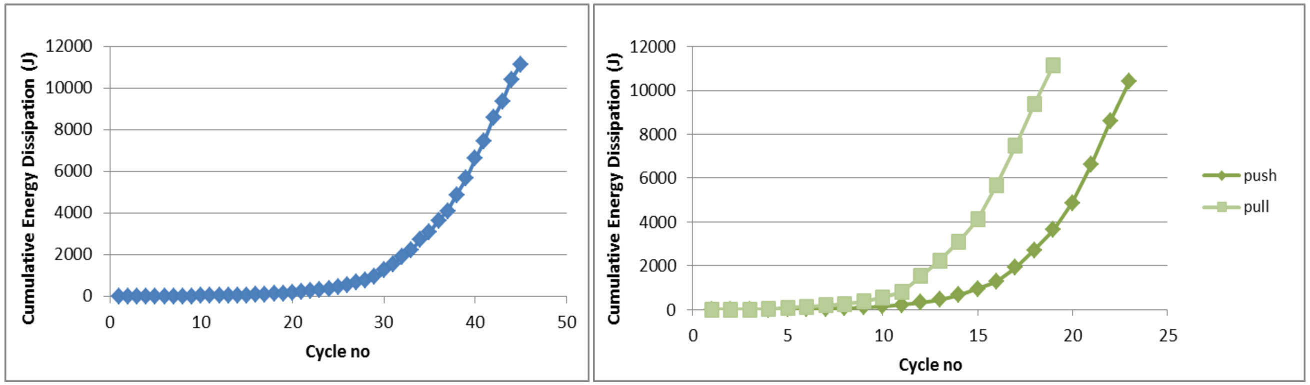

Figure 278: Change in cumulative dissipated energy of Frame#2 with infill for all cycles and for push and pull cycles separately, respectively

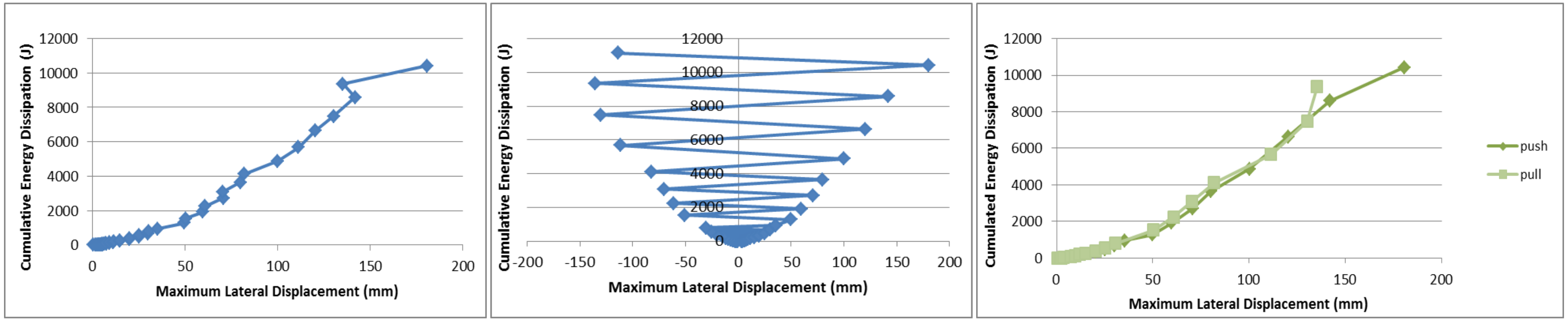

Figure 279: Change in cumulative dissipated energy – maximum lateral displacement relation of Frame#2 with infill for all cycles (positive push / negative pull, and absolute values, respectively) and for push and pull cycles separately

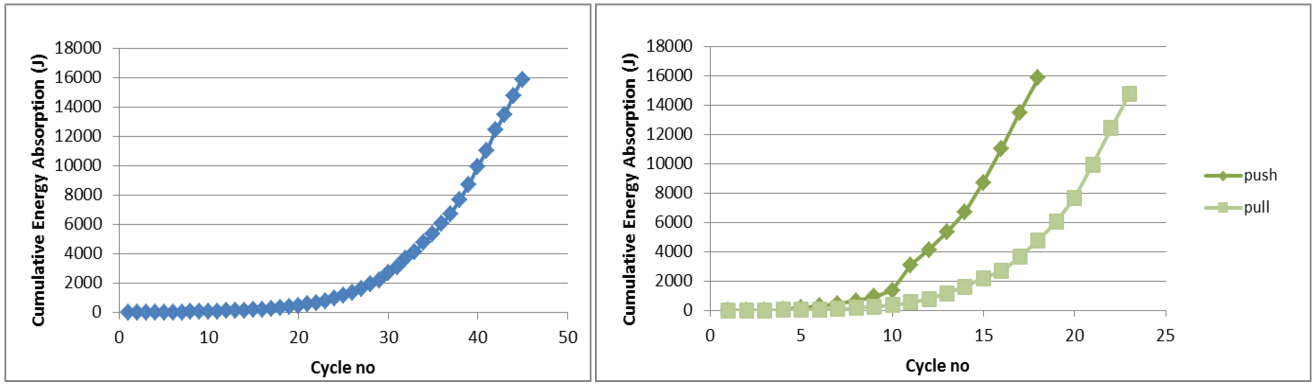

Figure 280: Change in cumulative absorbed energy of Frame#2 with infill for all cycles and for push and pull cycles separately, respectively

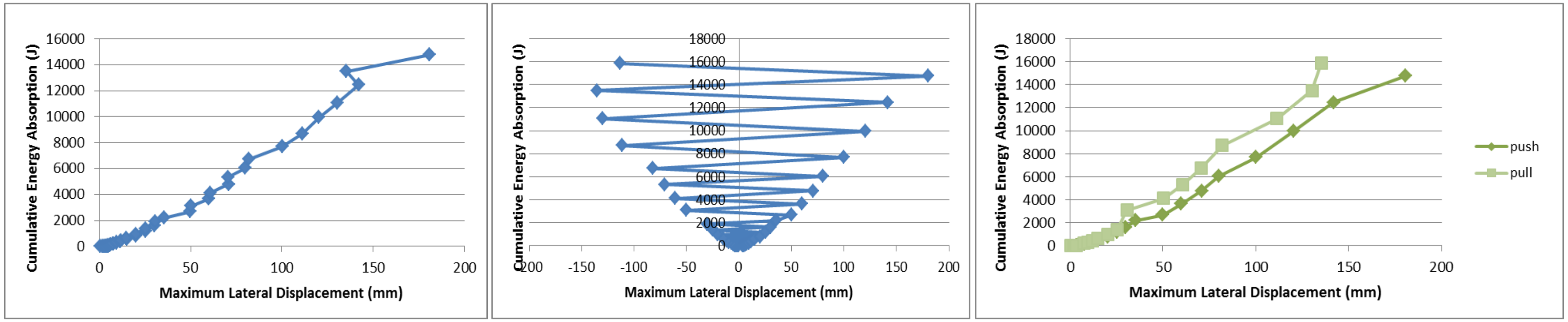

Figure 281: Change in cumulative absorbed energy – maximum lateral displacement relation of Frame#2 with infill for all cycles (positive push / negative pull, and absolute values, respectively) and for push and pull cycles separately

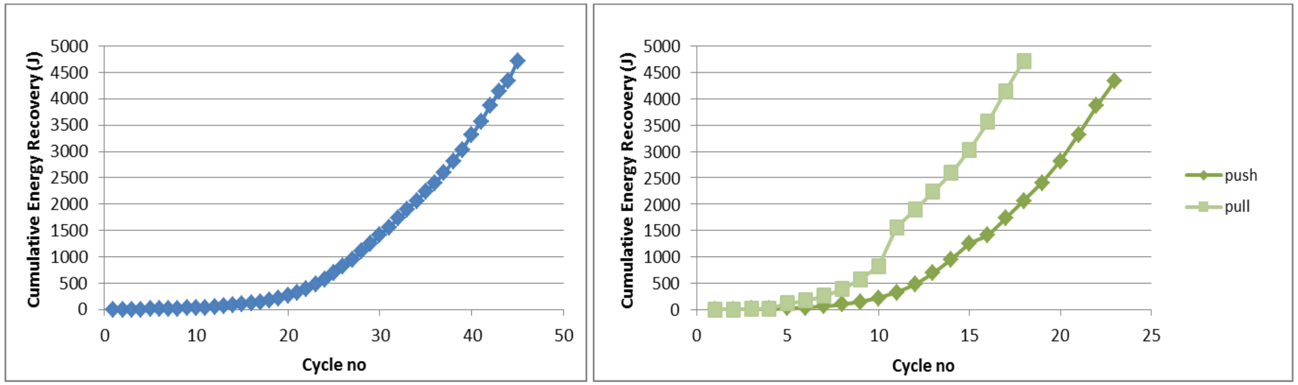

Figure 282: Change in cumulative recovered energy of Frame#2 with infill for all cycles and for push and pull cycles separately, respectively

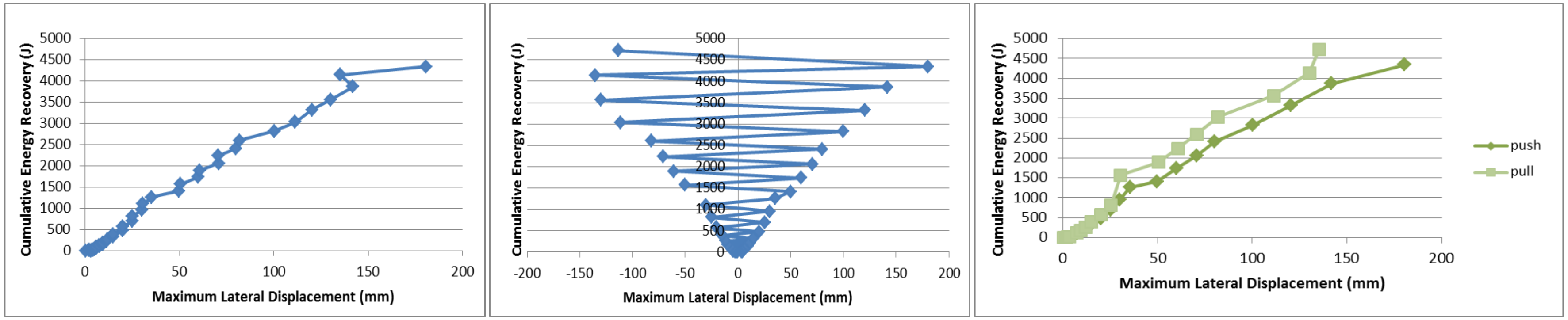

Figure 283: Change in cumulative recovered energy – maximum lateral displacement relation of Frame#2 with infill for all cycles (positive push / negative pull, and absolute values, respectively) and for push and pull cycles separately

APPENDIX F

F. RESULTS OBTAINED AT THE END OF TESTING OF FRAME#3

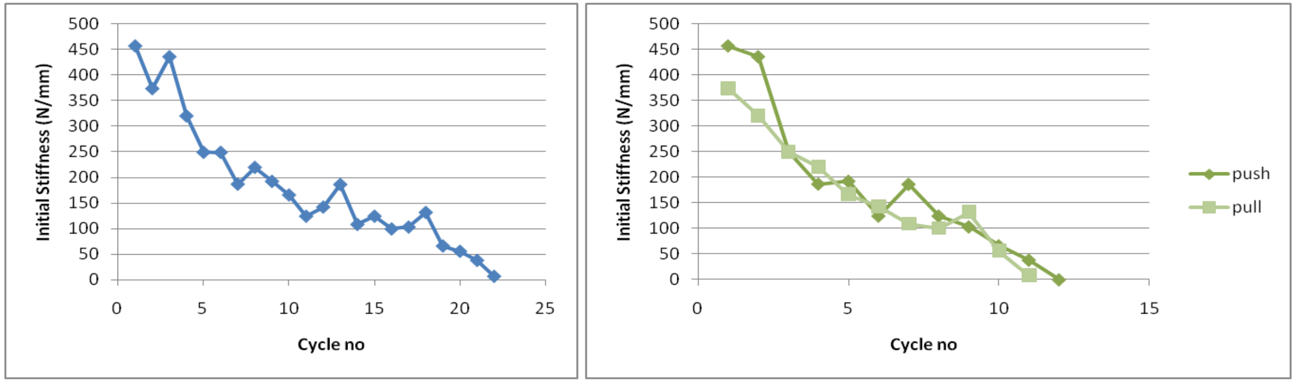

Figure 284: Change in initial stiffness of Frame#3 for all cycles and for push and pull cycles separately, respectively

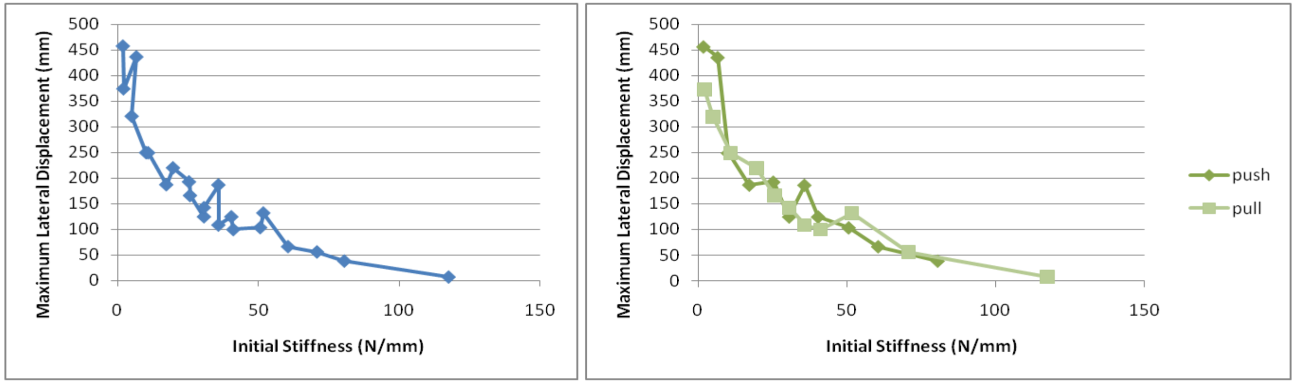

Figure 285: Change in initial stiffness – maximum lateral displacement relation of Frame#3 for all cycles and for push and pull cycles separately, respectively

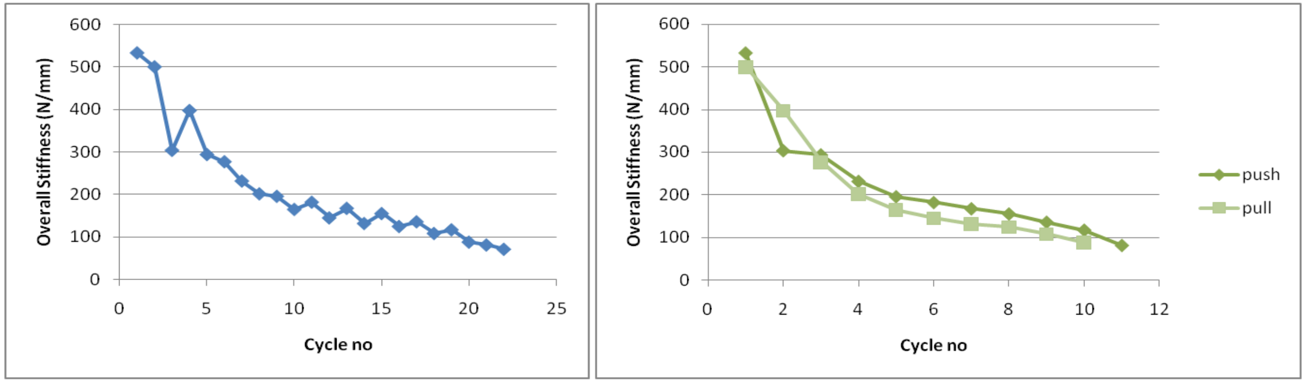

Figure 286: Change in overall stiffness of Frame#3 for all cycles and for push and pull cycles separately, respectively

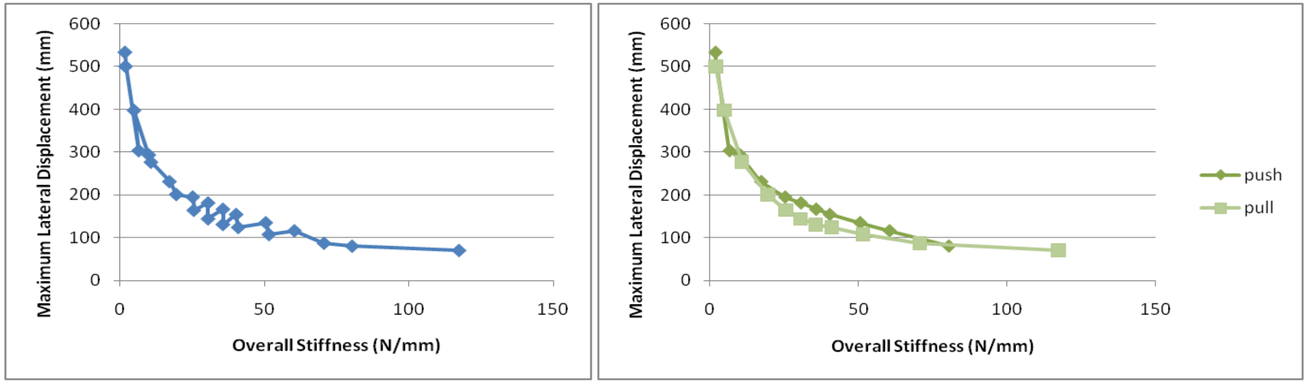

Figure 287: Change in overall stiffness – maximum lateral displacement relation of Frame#3 for all cycles and for push and pull cycles separately, respectively

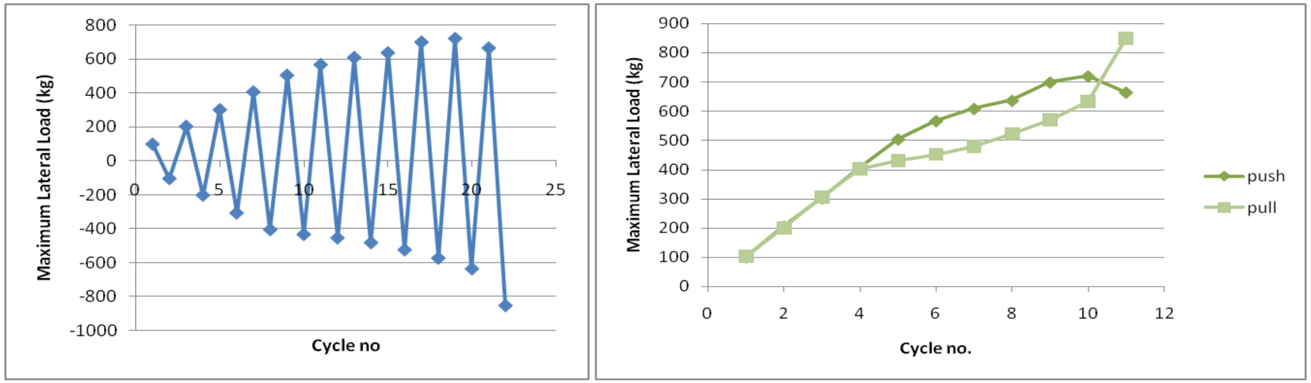

Figure 288: Change in maximum lateral load of Frame#3 for all cycles and for push and pull cycles separately, respectively

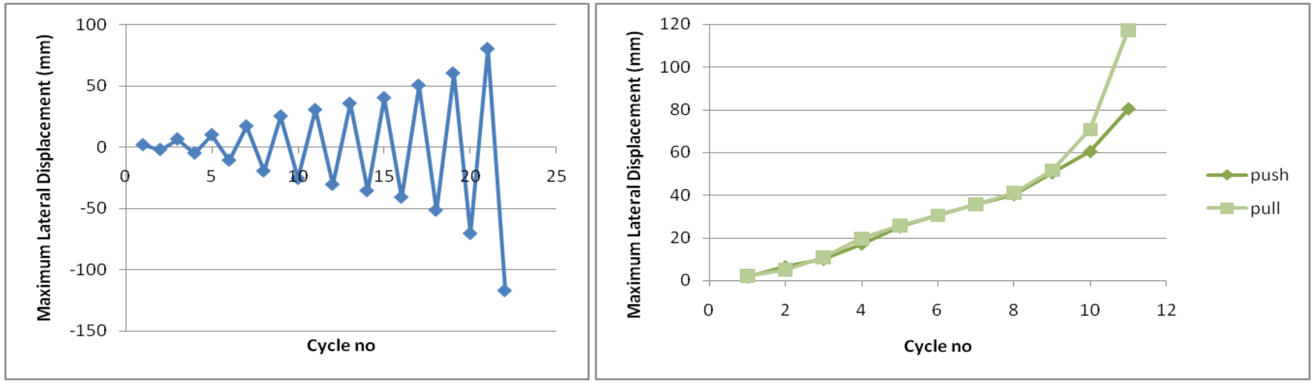

Figure 289: Change in maximum lateral displacement of Frame#3 for all cycles and for push and pull cycles separately, respectively

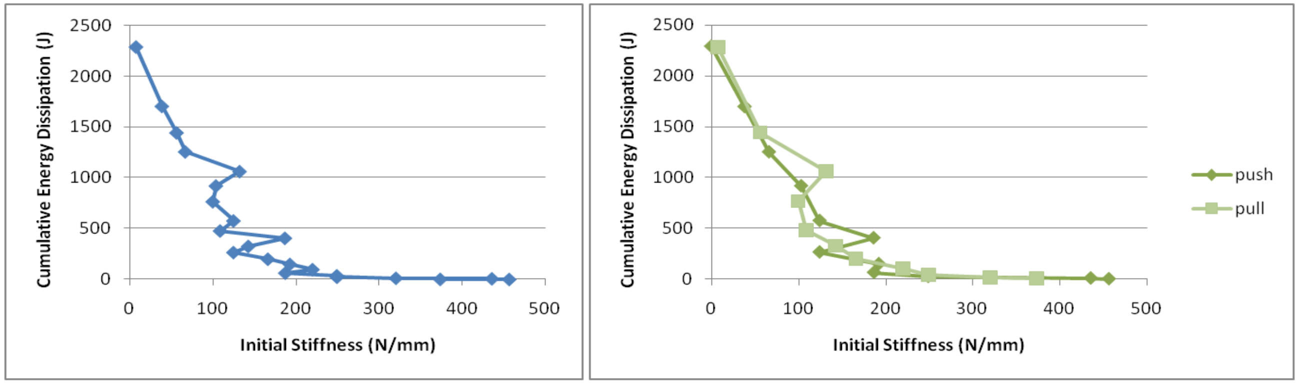

Figure 290: Change in cumulative dissipated energy – initial stiffness relation of Frame#3 for all cycles (positive push / negative pull, and absolute values, respectively) and for push and pull cycles separately

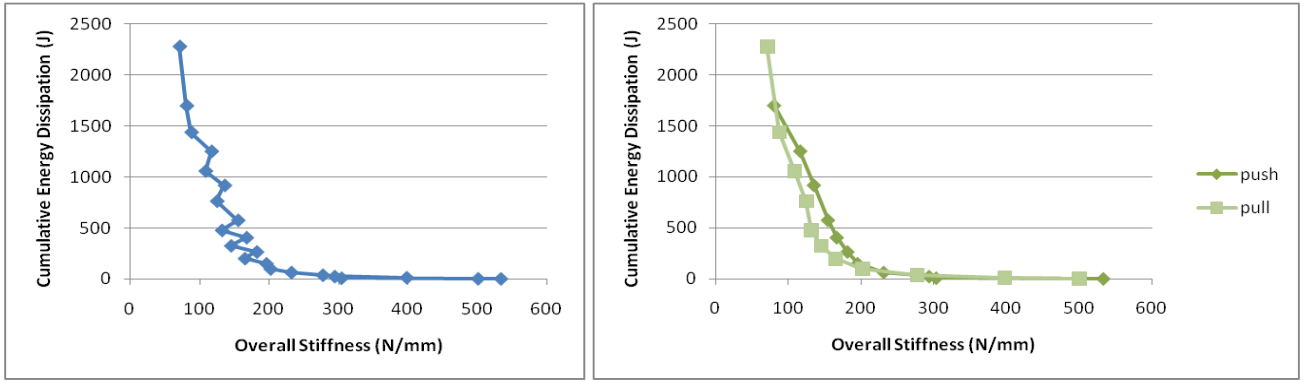

Figure 291: Change in cumulative dissipated energy – overall stiffness relation of Frame#3 for all cycles (positive push / negative pull, and absolute values, respectively) and for push and pull cycles separately

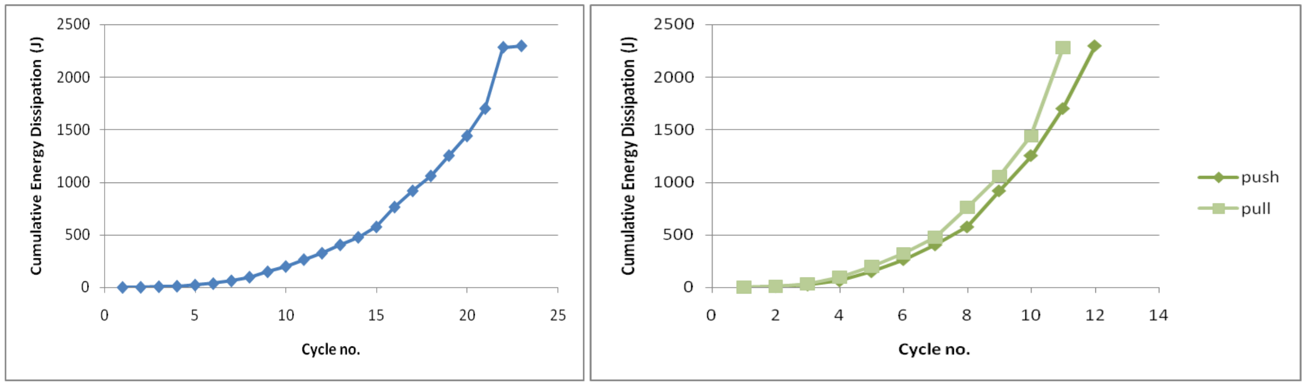

Figure 292: Change in cumulative dissipated energy of Frame#3 for all cycles and for push and pull cycles separately, respectively

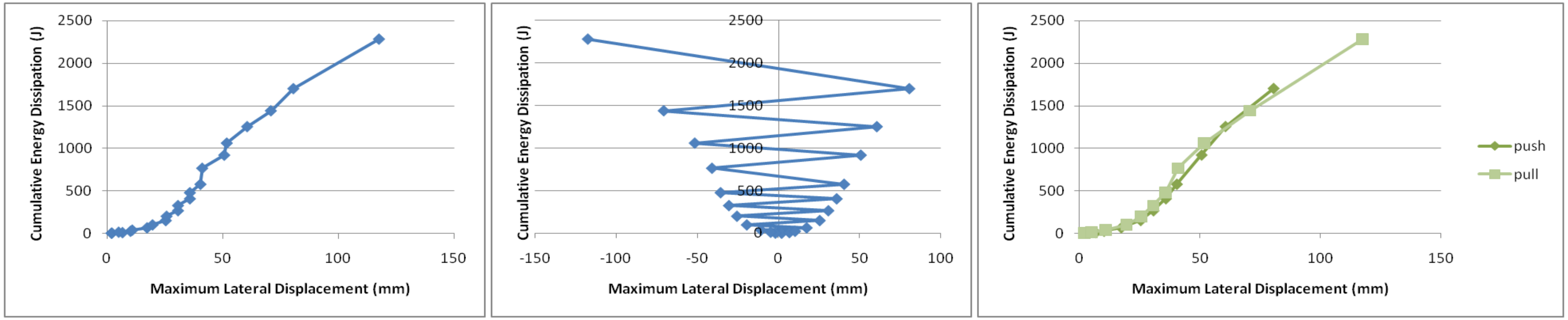

Figure 293: Change in cumulative dissipated energy – maximum lateral displacement relation of Frame#3 for all cycles (positive push / negative pull, and absolute values, respectively) and for push and pull cycles separately

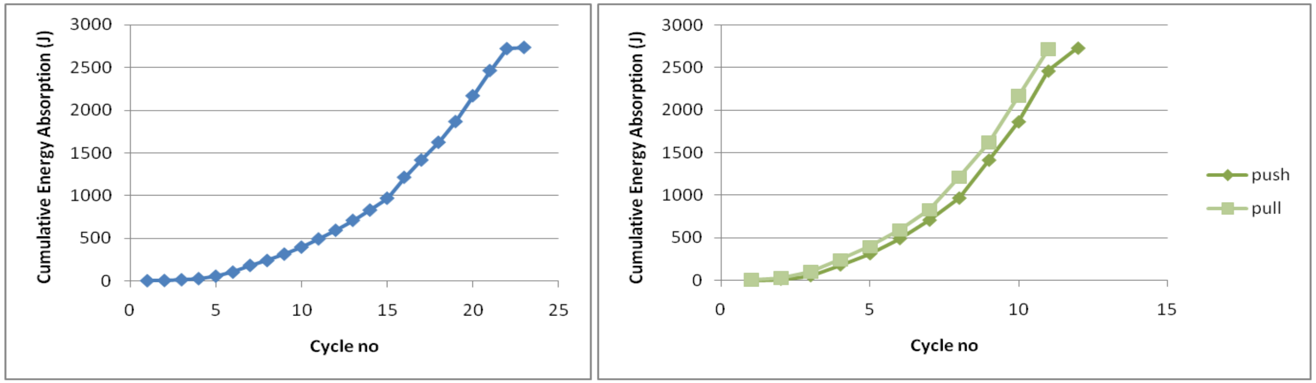

Figure 294: Change in cumulative absorbed energy of Frame#3 for all cycles and for push and pull cycles separately, respectively

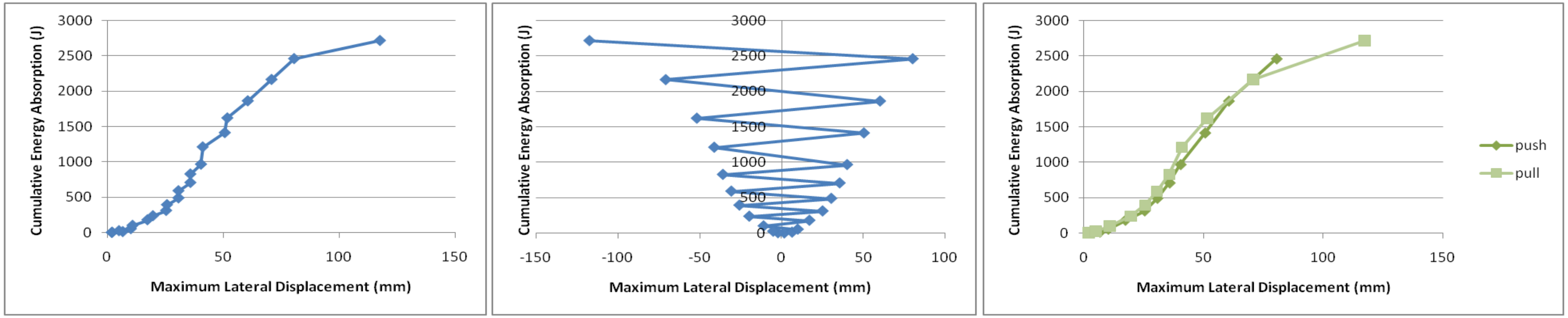

Figure 295: Change in cumulative absorbed energy – maximum lateral displacement relation of Frame#3 for all cycles (positive push / negative pull, and absolute values, respectively) and for push and pull cycles separately

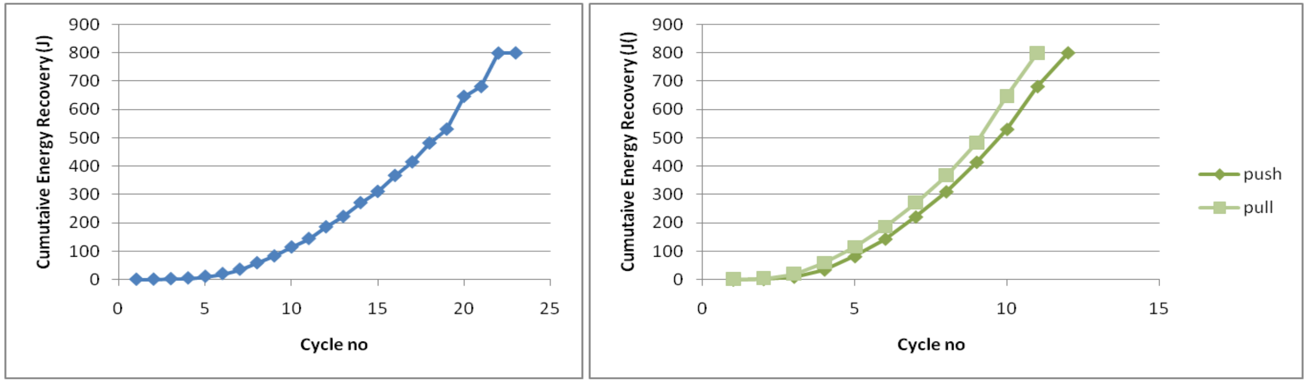

Figure 296: Change in cumulative recovered energy of Frame#3 for all cycles and for push and pull cycles separately, respectively

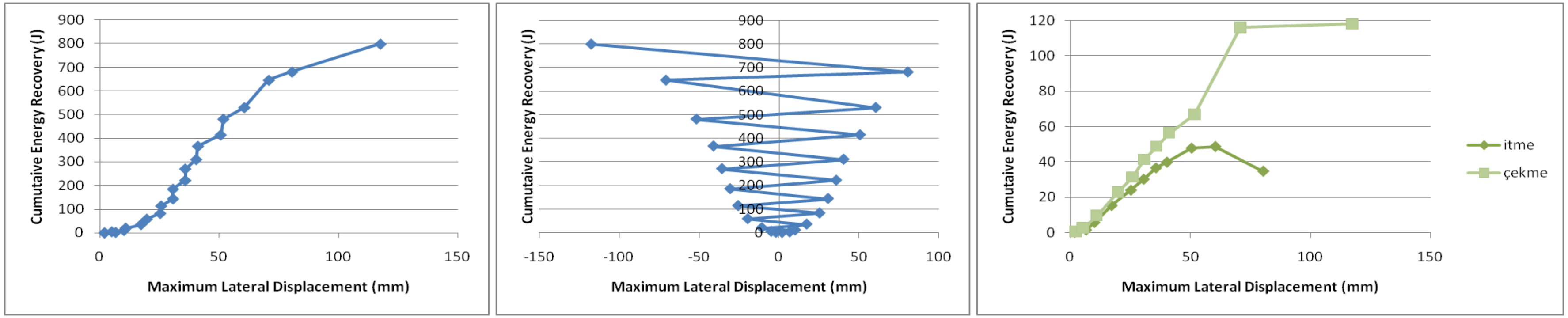

Figure 297: Change in cumulative recovered energy – maximum lateral displacement relation of Frame#3 for all cycles (positive push / negative pull, and absolute values, respectively) and for push and pull cycles separately

APPENDIX G

G. RESULTS OBTAINED AT THE END OF TESTING OF FRAME#3 WITH ŞAMDOLMA COVERING

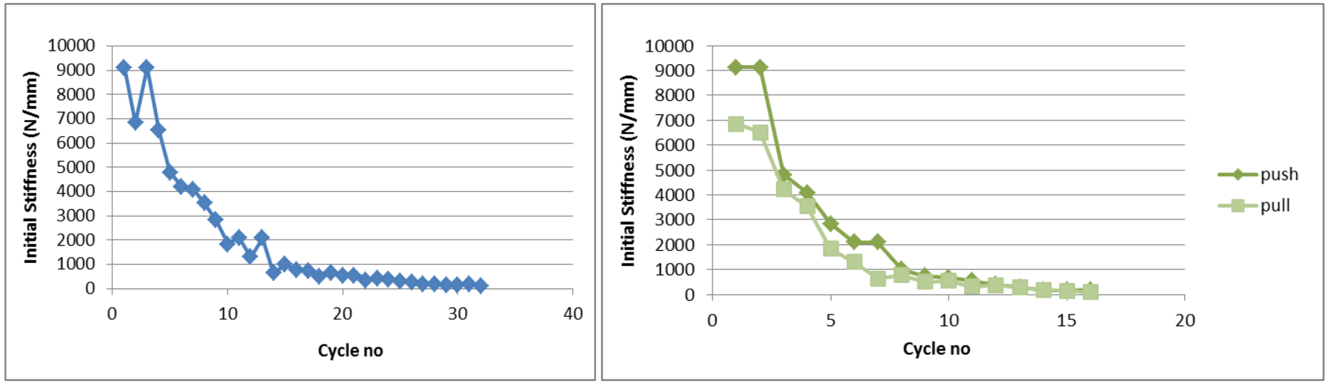

Figure 298: Change in initial stiffness of Frame#3 with infill for all cycles and for push and pull cycles separately, respectively

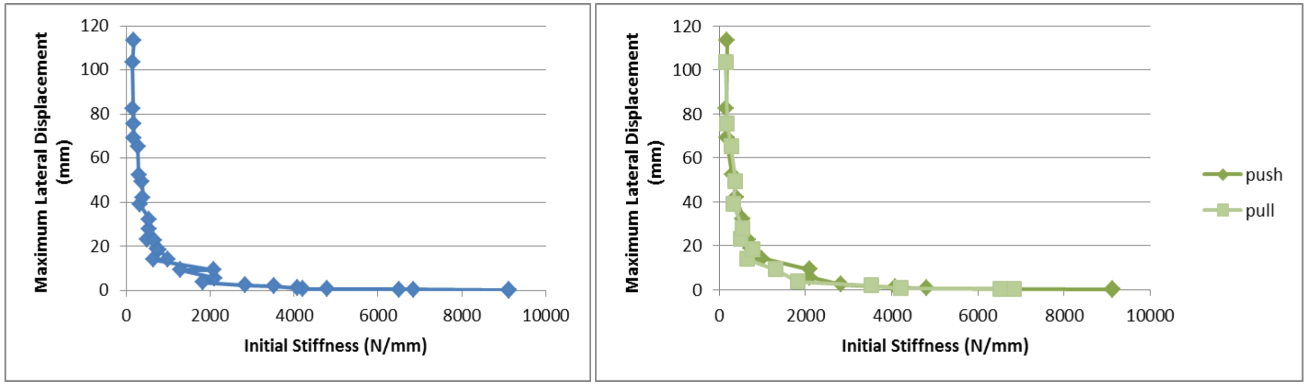

Figure 299: Change in initial stiffness – maximum lateral displacement relation of Frame#3 with infill for all cycles and for push and pull cycles separately, respectively

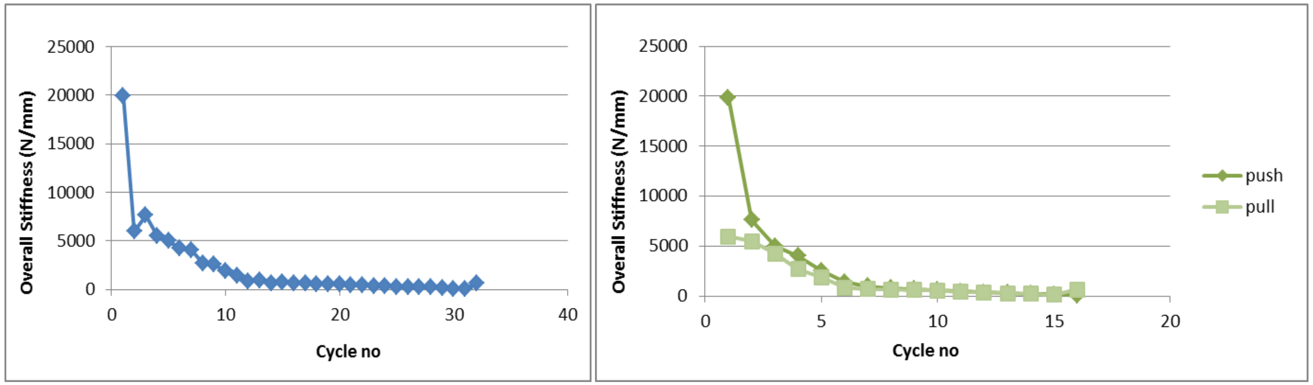

Figure 300: Change in overall stiffness of Frame#3 with infill for all cycles and for push and pull cycles separately, respectively

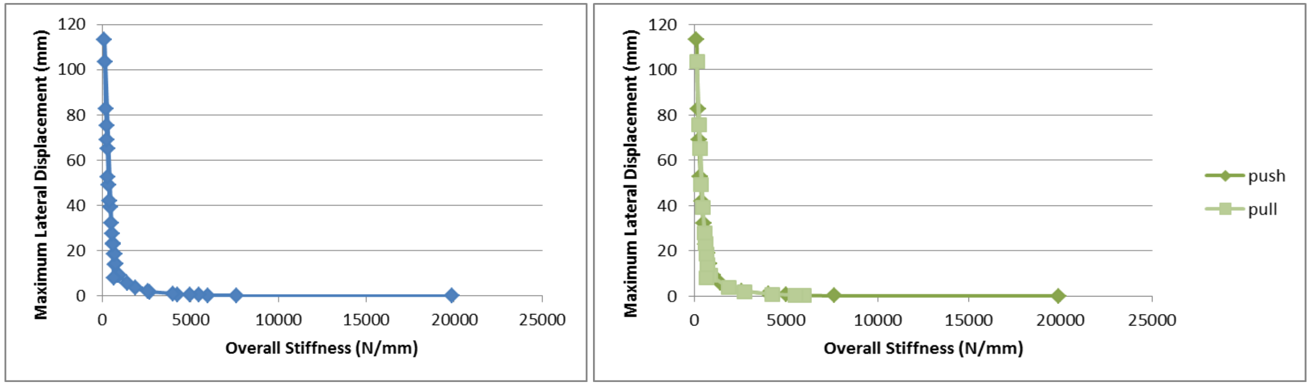

Figure 301: Change in overall stiffness – maximum lateral displacement relation of Frame#3 with infill for all cycles and for push and pull cycles separately, respectively

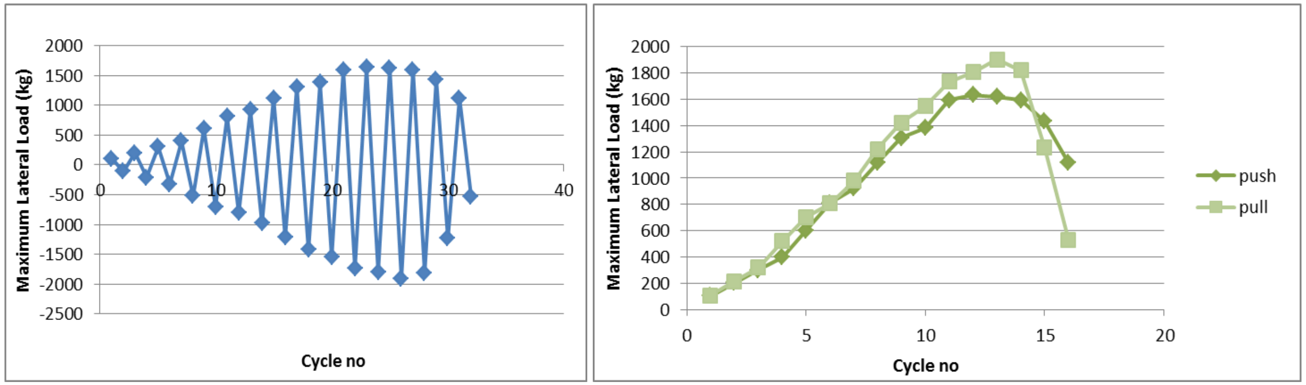

Figure 302: Change in maximum lateral load of Frame#3 with infill for all cycles and for push and pull cycles separately, respectively

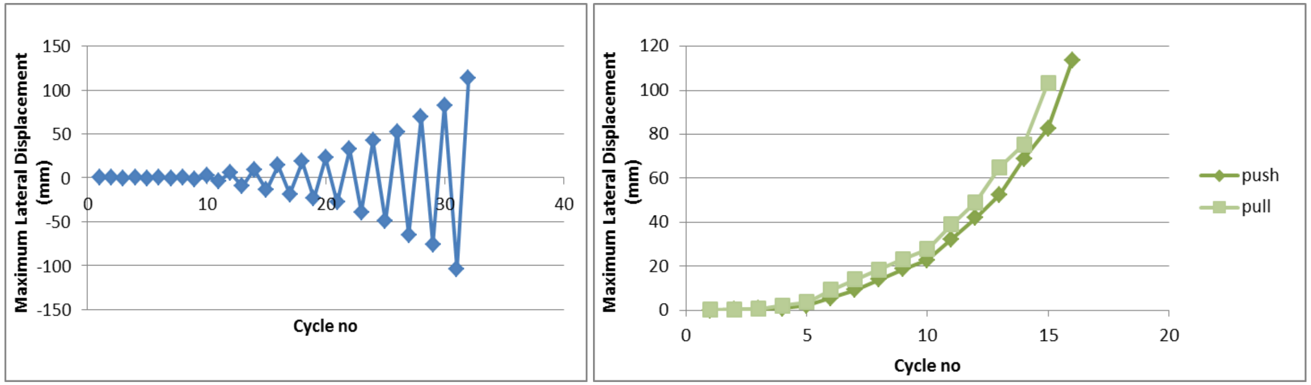

Figure 303: Change in maximum lateral displacement of Frame#3 with infill for all cycles and for push and pull cycles separately, respectively

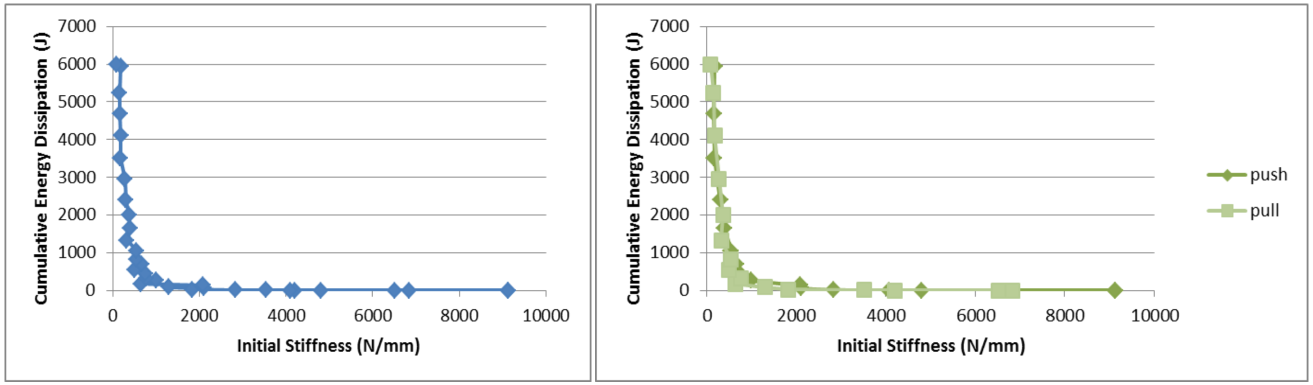

Figure 304: Change in cumulative dissipated energy – initial stiffness relation of Frame#3 with infill for all cycles (positive push / negative pull, and absolute values, respectively) and for push and pull cycles separately

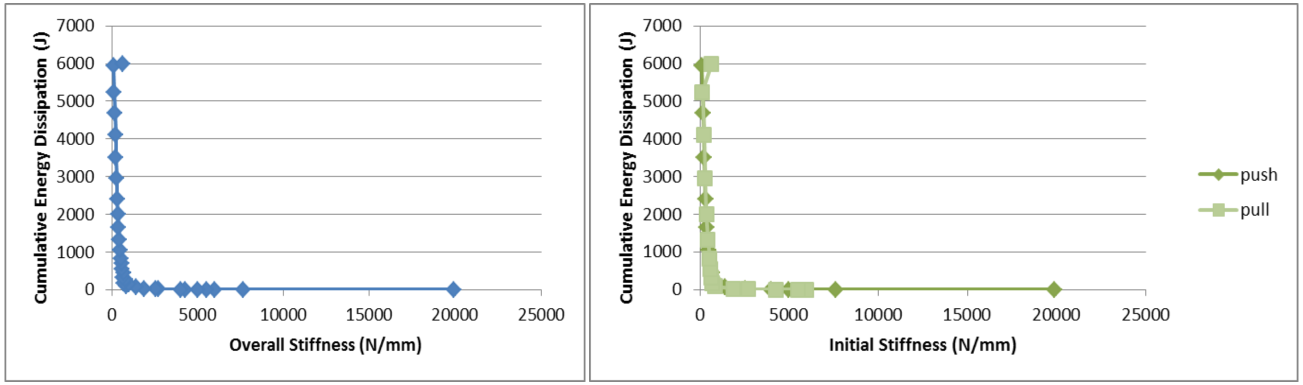

Figure 305: Change in cumulative dissipated energy – overall stiffness relation of Frame#3 with infill for all cycles (positive push / negative pull, and absolute values, respectively) and for push and pull cycles separately

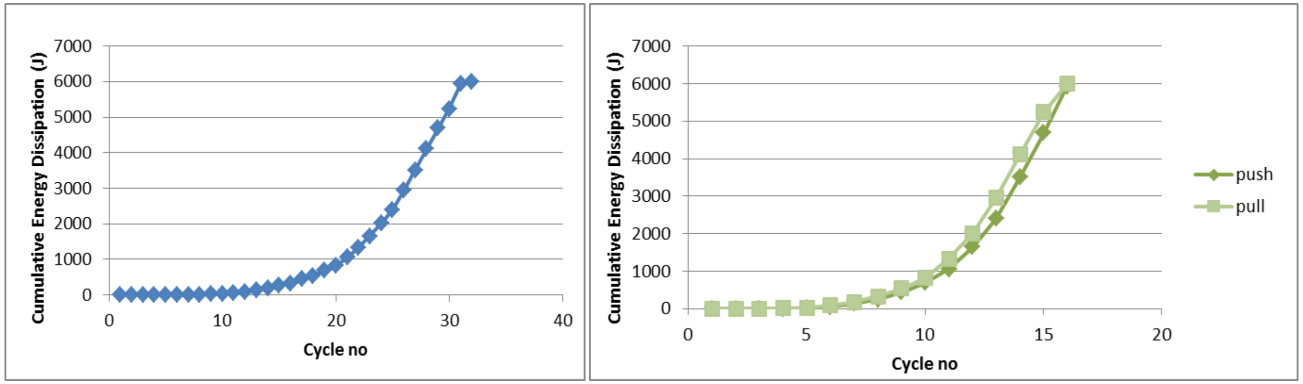

Figure 306: Change in cumulative dissipated energy of Frame#3 with infill for all cycles and for push and pull cycles separately, respectively

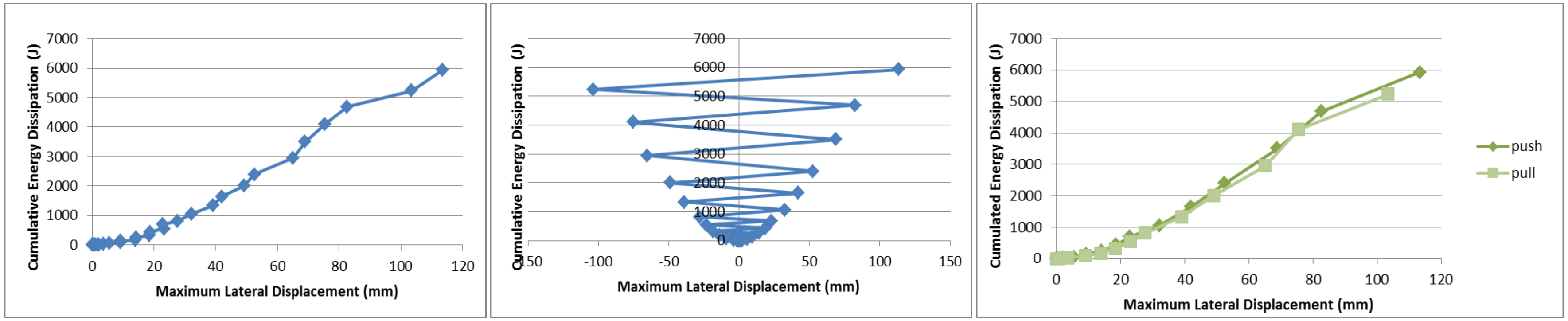

Figure 307: Change in cumulative dissipated energy – maximum lateral displacement relation of Frame#3 with infill for all cycles (positive push / negative pull, and absolute values, respectively) and for push and pull cycles separately

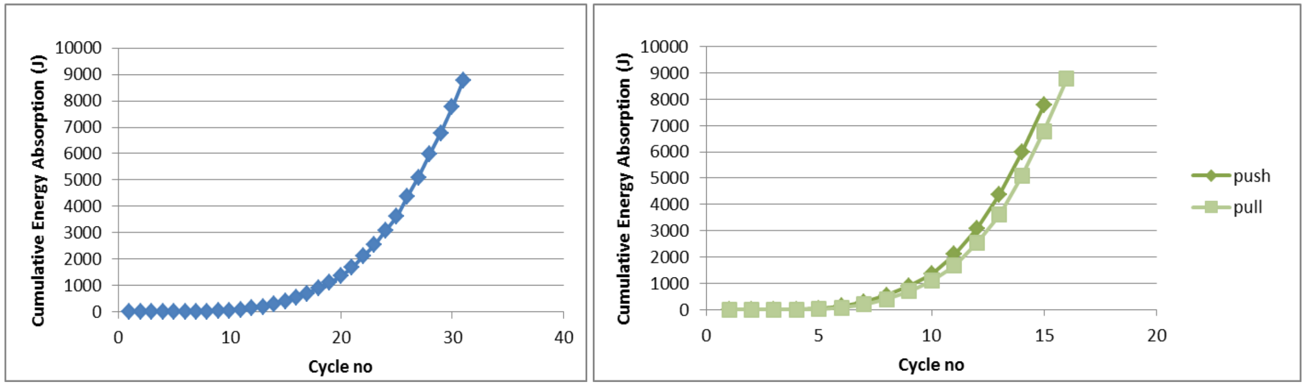

Figure 308: Change in cumulative absorbed energy of Frame#3 with infill for all cycles and for push and pull cycles separately, respectively

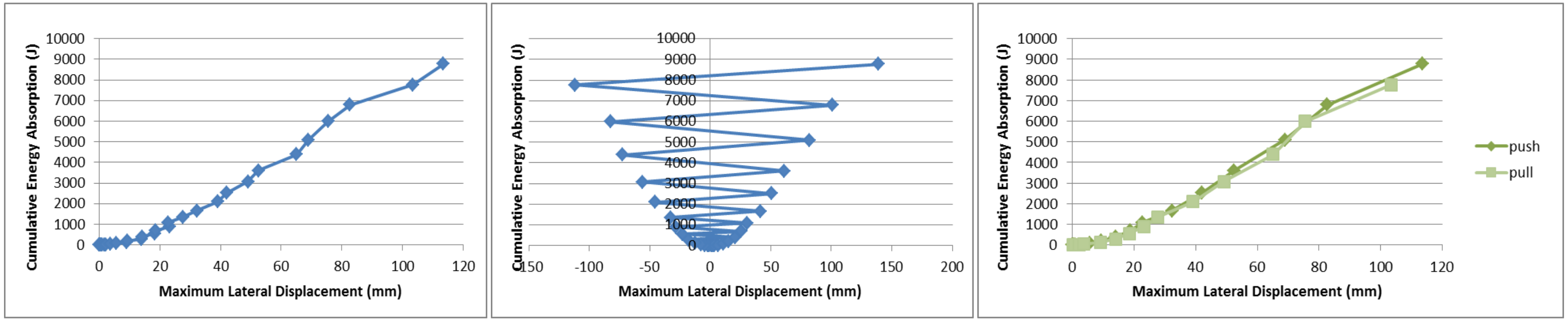

Figure 309: Change in cumulative absorbed energy – maximum lateral displacement relation of Frame#3 with infill for all cycles (positive push / negative pull, and absolute values, respectively) and for push and pull cycles separately

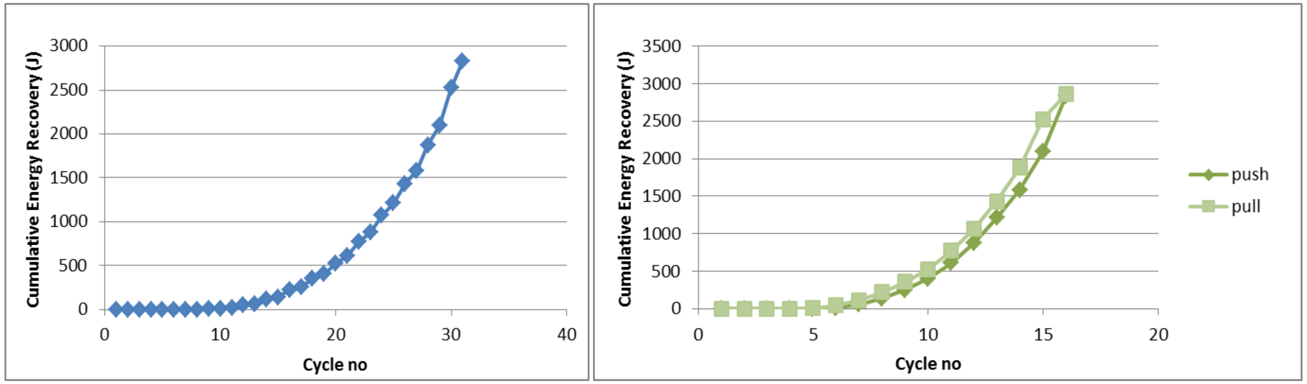

Figure 310: Change in cumulative recovered energy of Frame#3 with infill for all cycles and for push and pull cycles separately, respectively

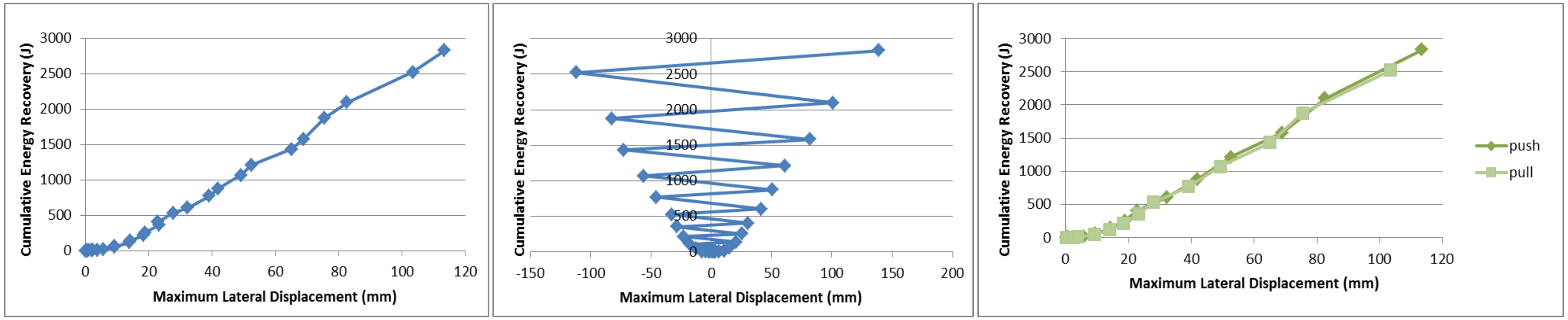

Figure 311: Change in cumulative recovered energy – maximum lateral displacement relation of Frame#3 with infill for all cycles (positive push / negative pull, and absolute values, respectively) and for push and pull cycles separately

APPENDIX H

H. RESULTS OBTAINED AT THE END OF TESTING OF FRAME#4

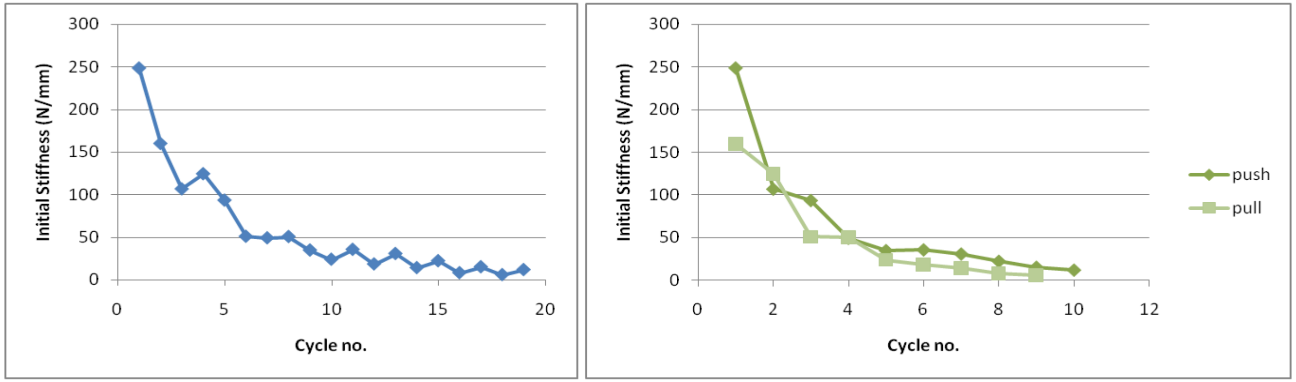

Figure 312: Change in initial stiffness of Frame#4 for all cycles and for push and pull cycles separately, respectively

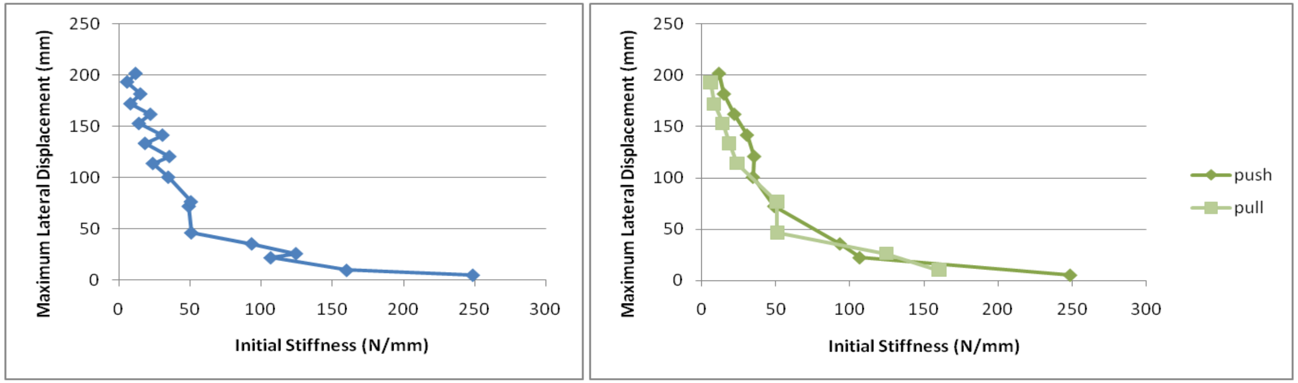

Figure 313: Change in initial stiffness – maximum lateral displacement relation of Frame#4 for all cycles and for push and pull cycles separately, respectively

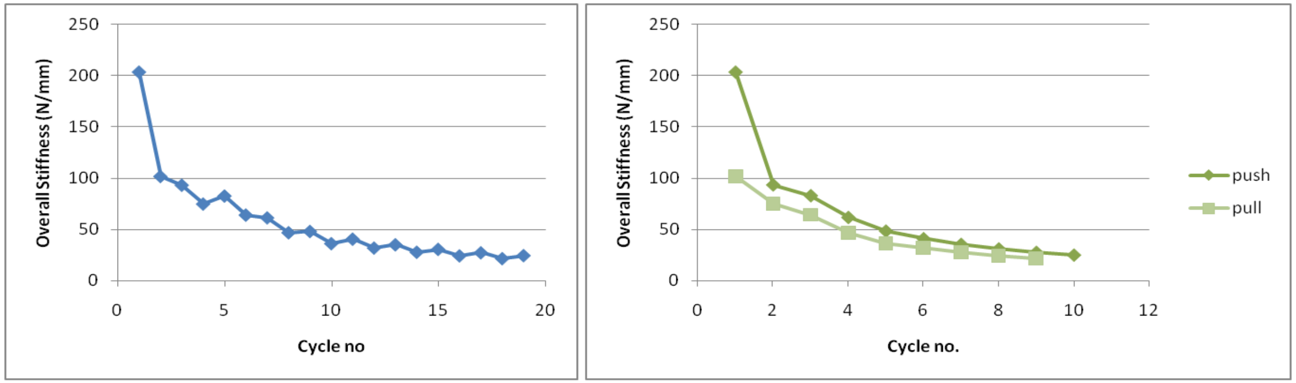

Figure 314: Change in overall stiffness of Frame#4 for all cycles and for push and pull cycles separately, respectively

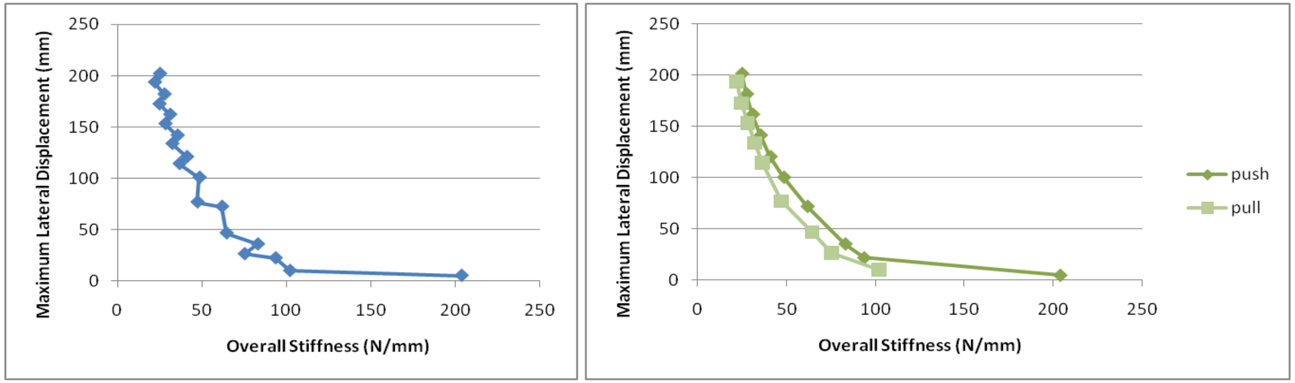

Figure 315: Change in overall stiffness – maximum lateral displacement relation of Frame#4 for all cycles and for push and pull cycles separately, respectively

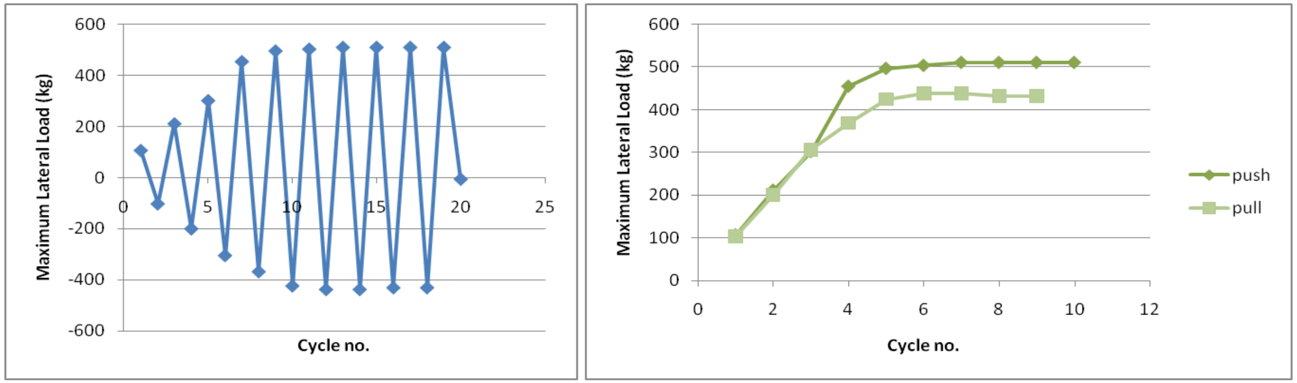

Figure 316: Change in maximum lateral load of Frame#4 for all cycles and for push and pull cycles separately, respectively

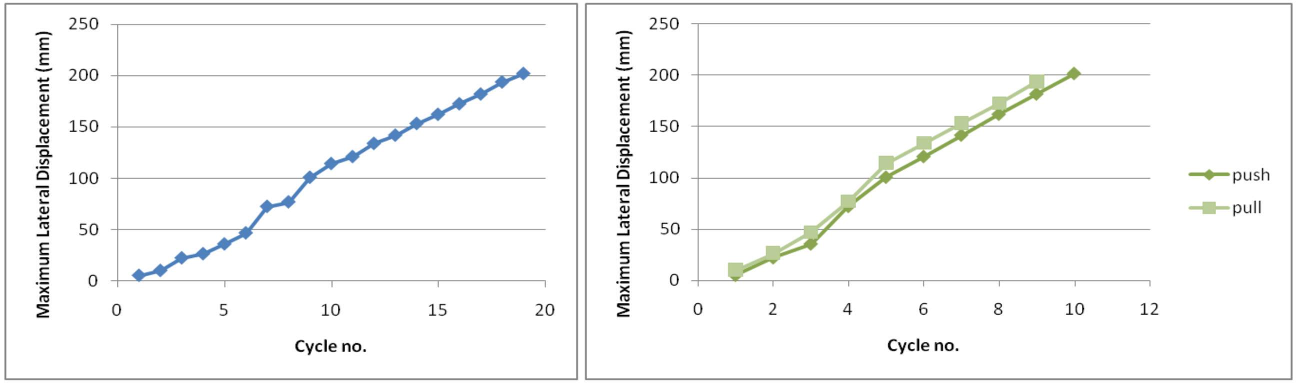

Figure 317: Change in maximum lateral displacement of Frame#4 for all cycles and for push and pull cycles separately, respectively

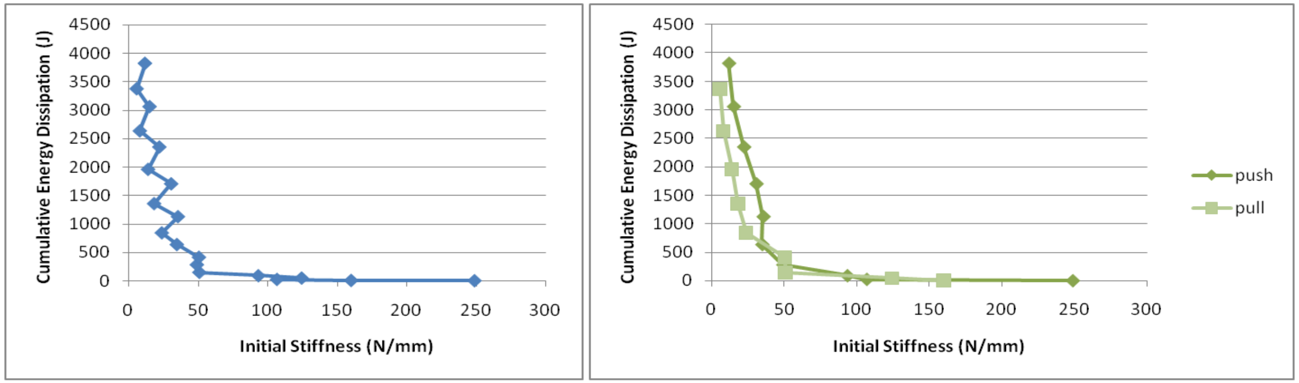

Figure 318: Change in cumulative dissipated energy – initial stiffness relation of Frame#4 for all cycles (positive push / negative pull, and absolute values, respectively) and for push and pull cycles separately

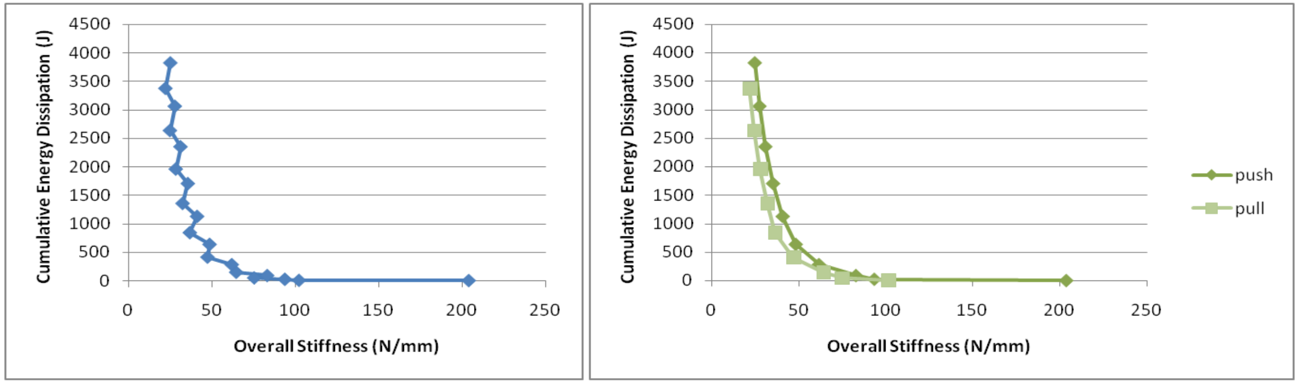

Figure 319: Change in cumulative dissipated energy – overall stiffness relation of Frame#4 for all cycles (positive push / negative pull, and absolute values, respectively) and for push and pull cycles separately

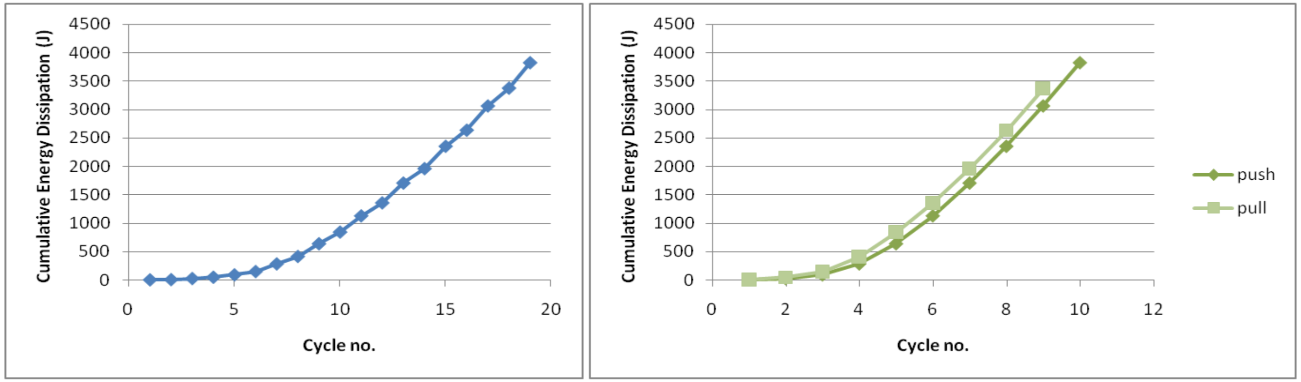

Figure 320: Change in cumulative dissipated energy of Frame#4 for all cycles and for push and pull cycles separately, respectively

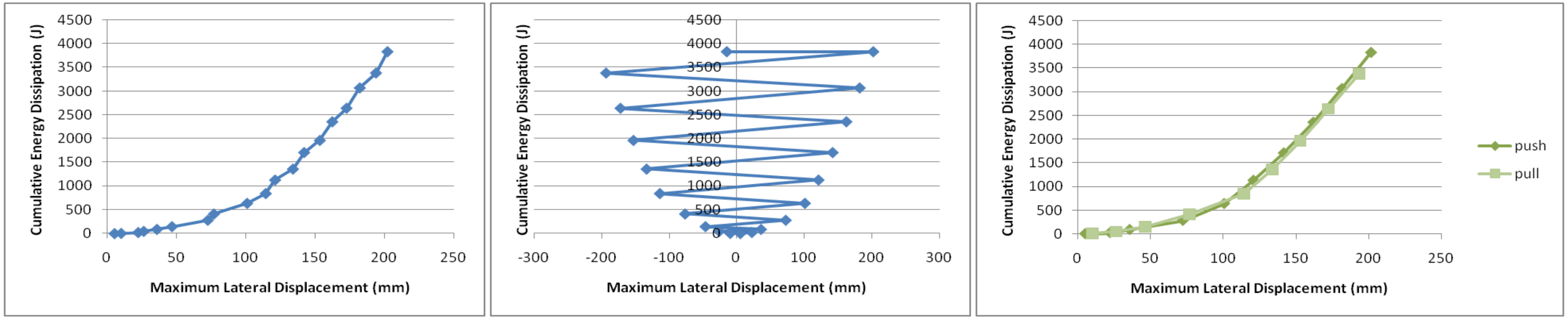

Figure 321: Change in cumulative dissipated energy – maximum lateral displacement relation of Frame#4 for all cycles (positive push / negative pull, and absolute values, respectively) and for push and pull cycles separately

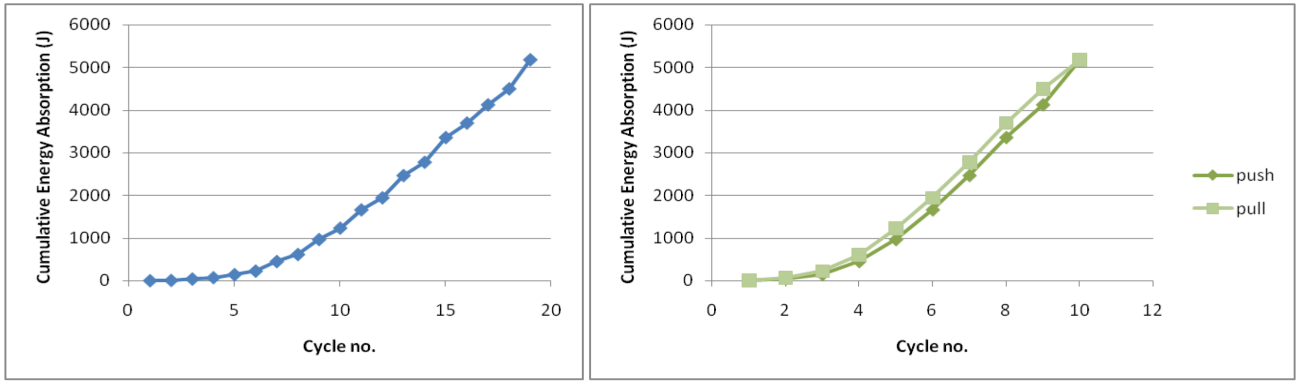

Figure 322: Change in cumulative absorbed energy of Frame#4 for all cycles and for push and pull cycles separately, respectively

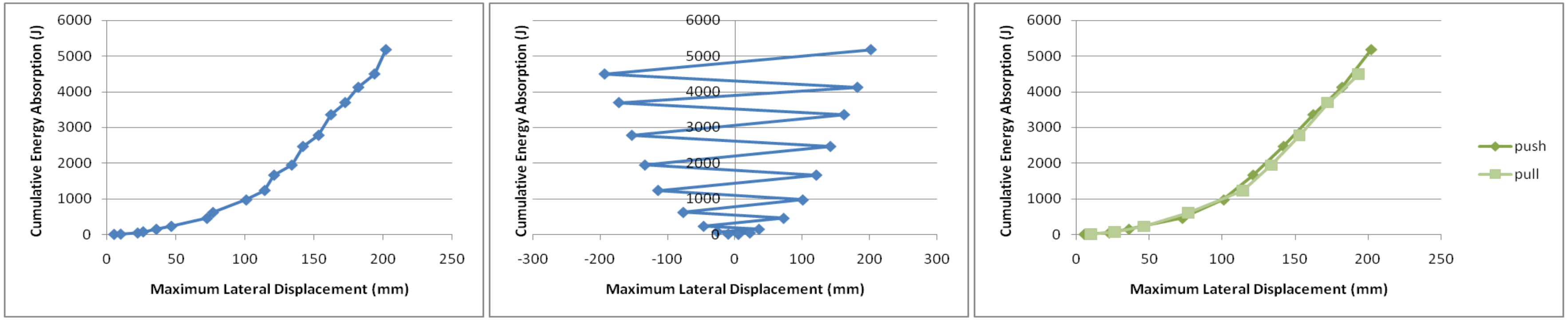

Figure 323: Change in cumulative absorbed energy – maximum lateral displacement relation of Frame#4 for all cycles (positive push / negative pull, and absolute values, respectively) and for push and pull cycles separately

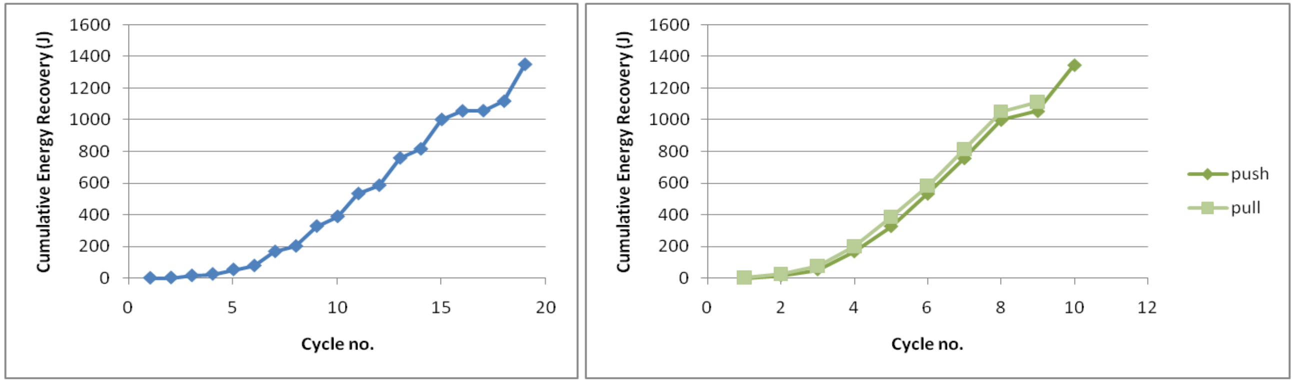

Figure 324: Change in cumulative recovered energy of Frame#4 for all cycles and for push and pull cycles separately, respectively

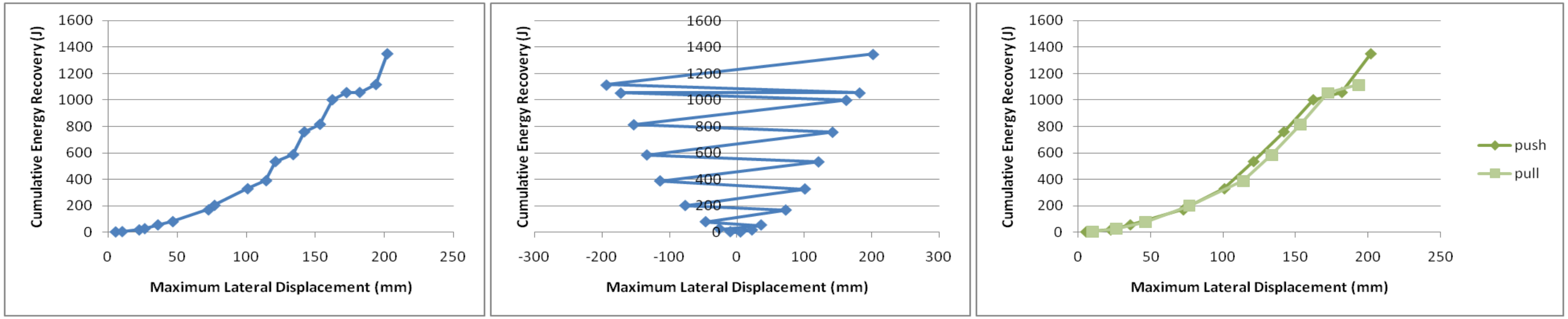

Figure 325: Change in cumulative recovered energy – maximum lateral displacement relation of Frame#4 for all cycles (positive push / negative pull, and absolute values, respectively) and for push and pull cycles separately

APPENDIX I

I. RESULTS OBTAINED AT THE END OF TESTING OF FRAME#4 WITH BRICK INFILL

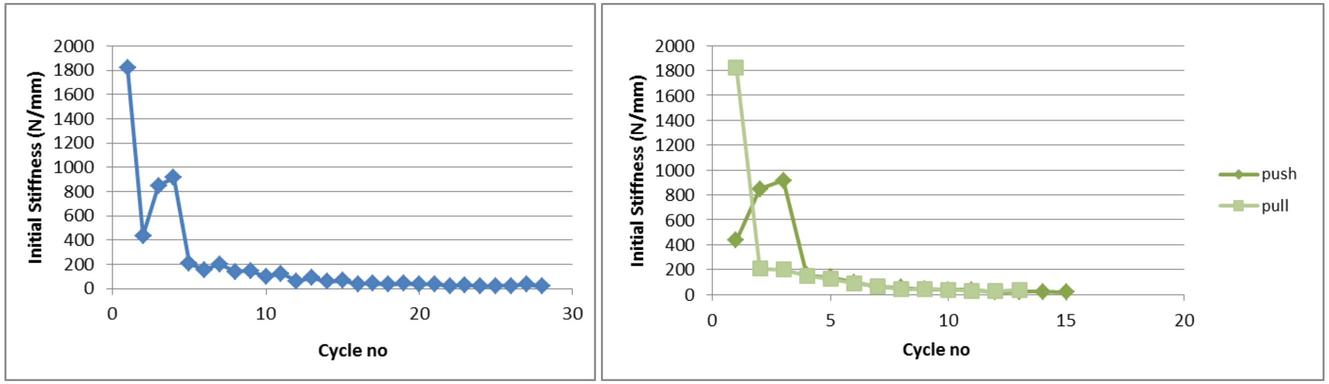

Figure 326: Change in initial stiffness of Frame#4 with infill for all cycles and for push and pull cycles separately, respectively

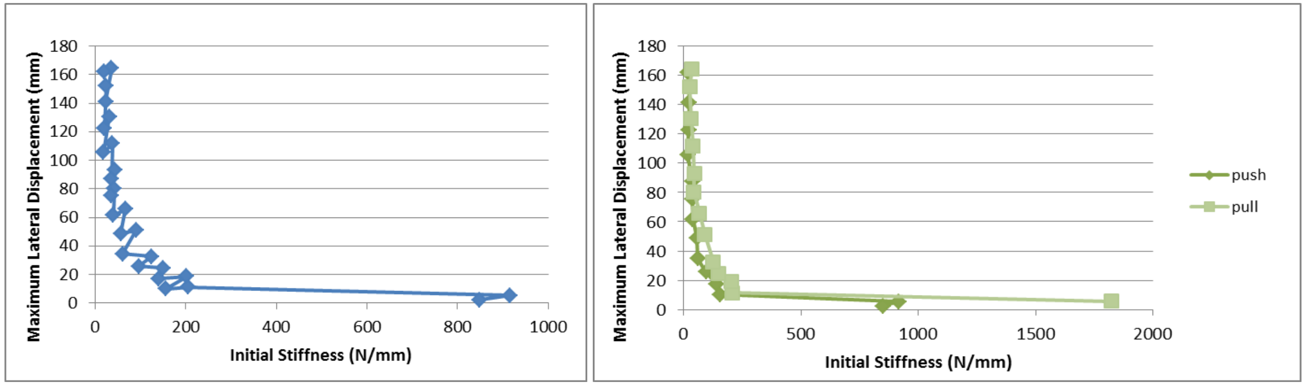

Figure 327: Change in initial stiffness – maximum lateral displacement relation of Frame#4 with infill for all cycles and for push and pull cycles separately, respectively

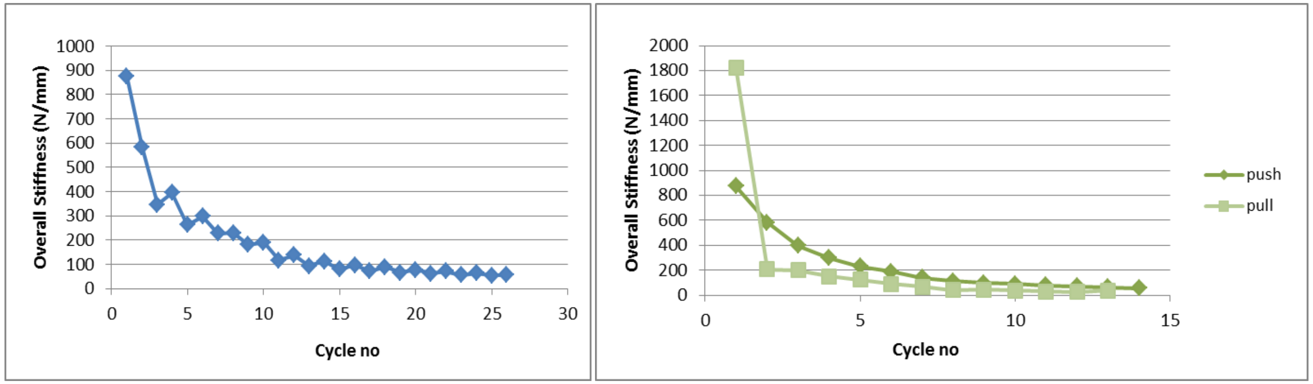

Figure 328: Change in overall stiffness of Frame#4 with infill for all cycles and for push and pull cycles separately, respectively

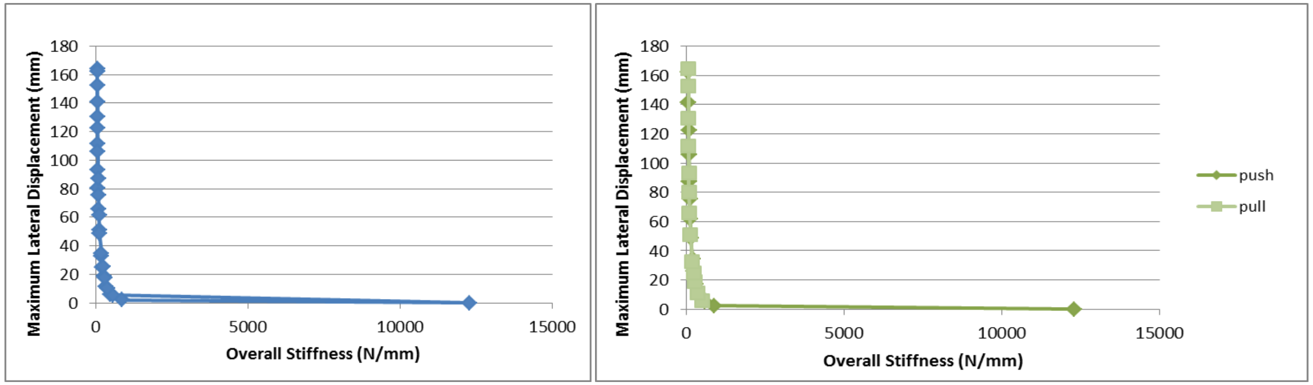

Figure 329: Change in overall stiffness – maximum lateral displacement relation of Frame#4 with infill for all cycles and for push and pull cycles separately, respectively

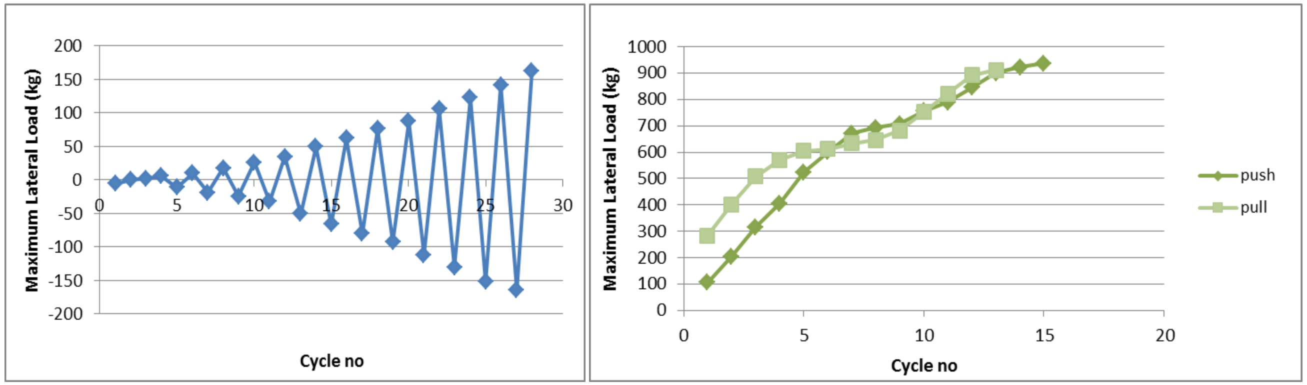

Figure 330: Change in maximum lateral load of Frame#4 with infill for all cycles and for push and pull cycles separately, respectively

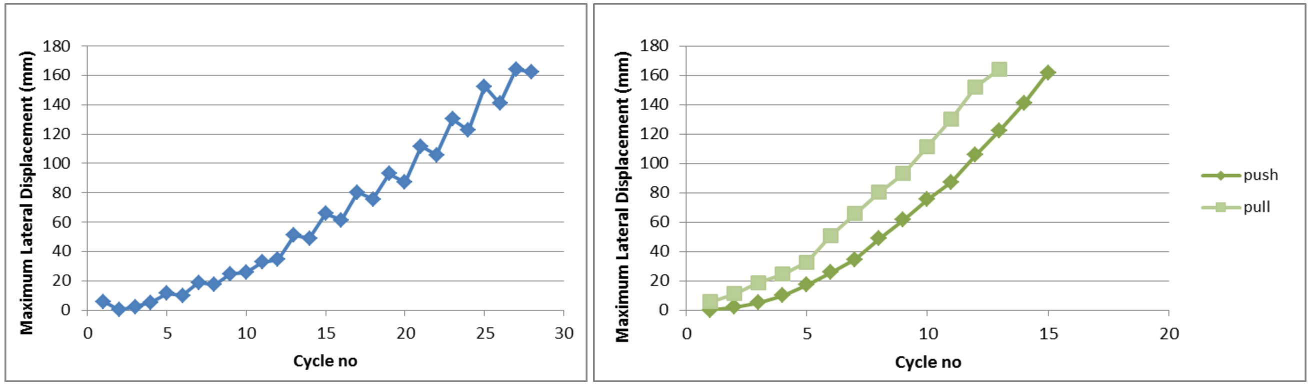

Figure 331: Change in maximum lateral displacement of Frame#4 with infill for all cycles and for push and pull cycles separately, respectively

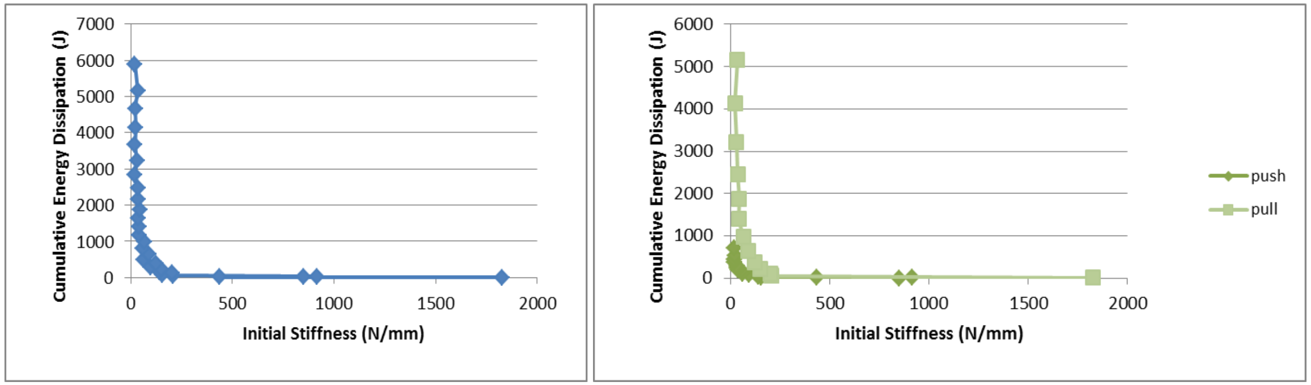

Figure 332: Change in cumulative dissipated energy – initial stiffness relation of Frame#4 with infill for all cycles (positive push / negative pull, and absolute values, respectively) and for push and pull cycles separately

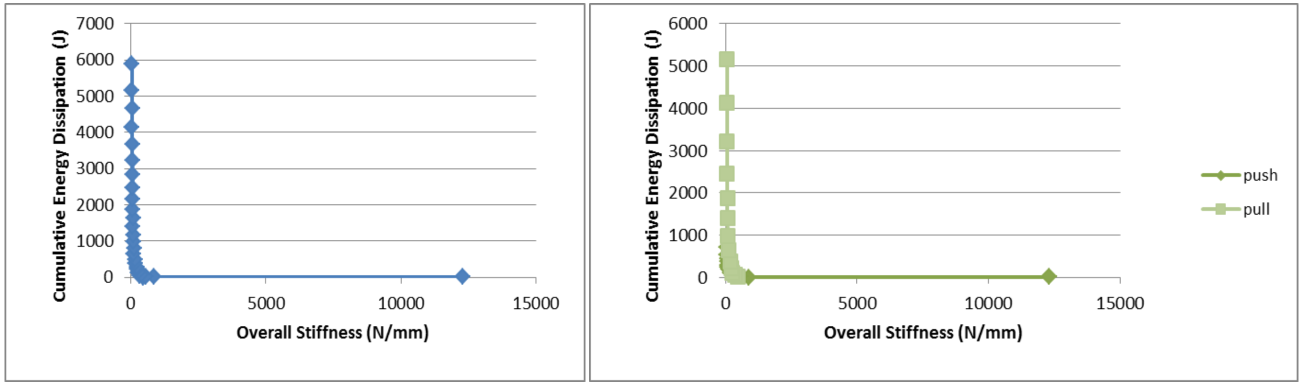

Figure 333: Change in cumulative dissipated energy – overall stiffness relation of Frame#4 with infill for all cycles (positive push / negative pull, and absolute values, respectively) and for push and pull cycles separately

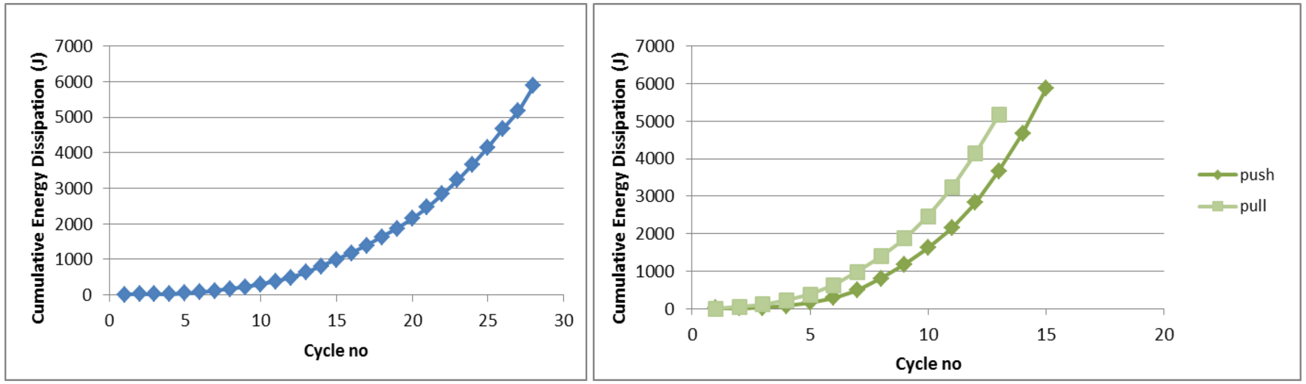

Figure 334: Change in cumulative dissipated energy of Frame#4 with infill for all cycles and for push and pull cycles separately, respectively

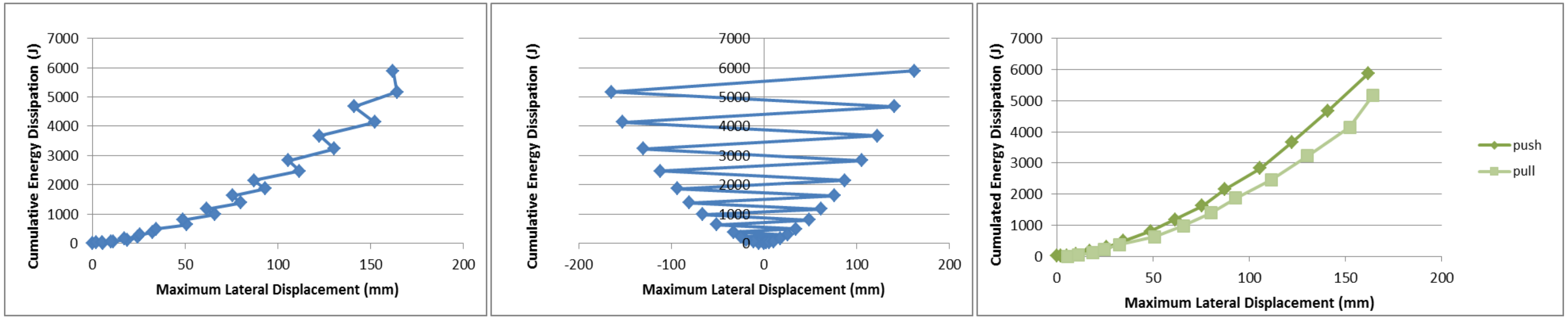

Figure 335: Change in cumulative dissipated energy – maximum lateral displacement relation of Frame#4 with infill for all cycles (positive push / negative pull, and absolute values, respectively) and for push and pull cycles separately

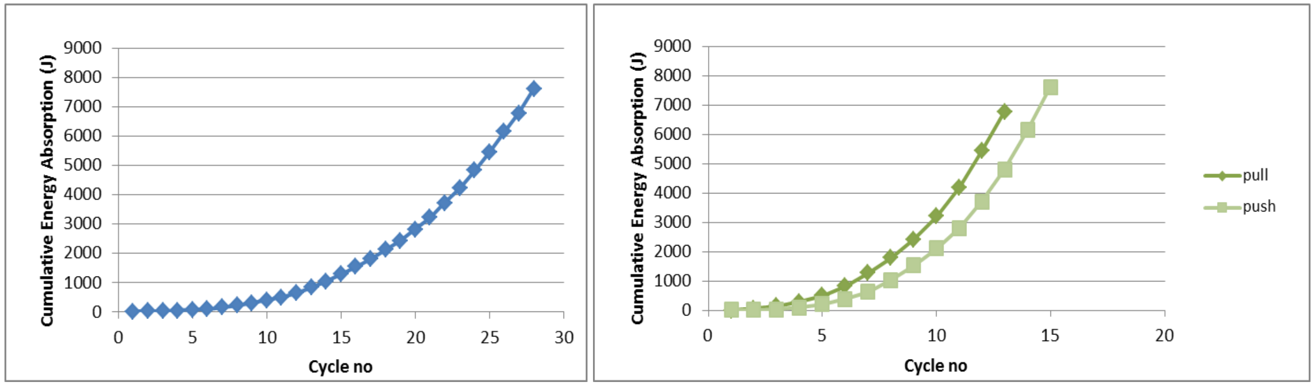

Figure 336: Change in cumulative absorbed energy of Frame#4 with infill for all cycles and for push and pull cycles separately, respectively

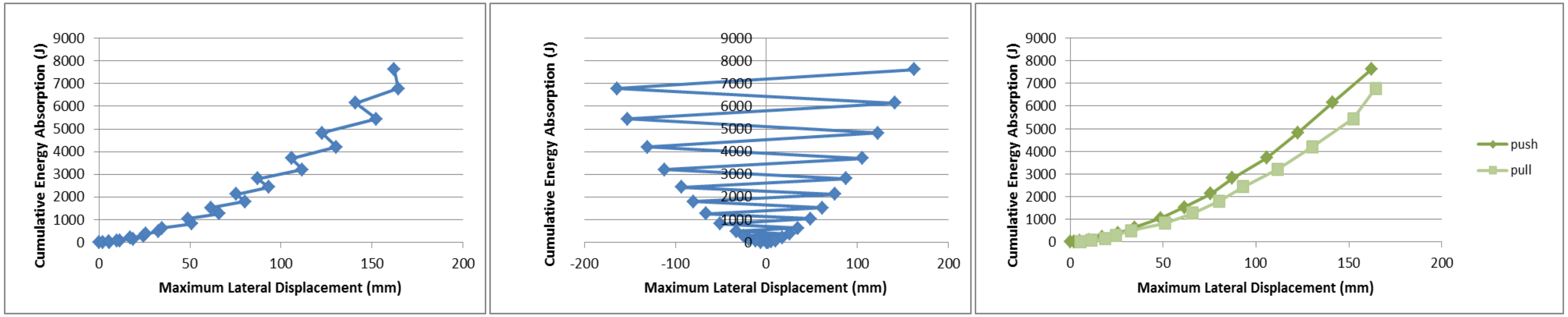

Figure 337: Change in cumulative absorbed energy – maximum lateral displacement relation of Frame#4 with infill for all cycles (positive push / negative pull, and absolute values, respectively) and for push and pull cycles separately

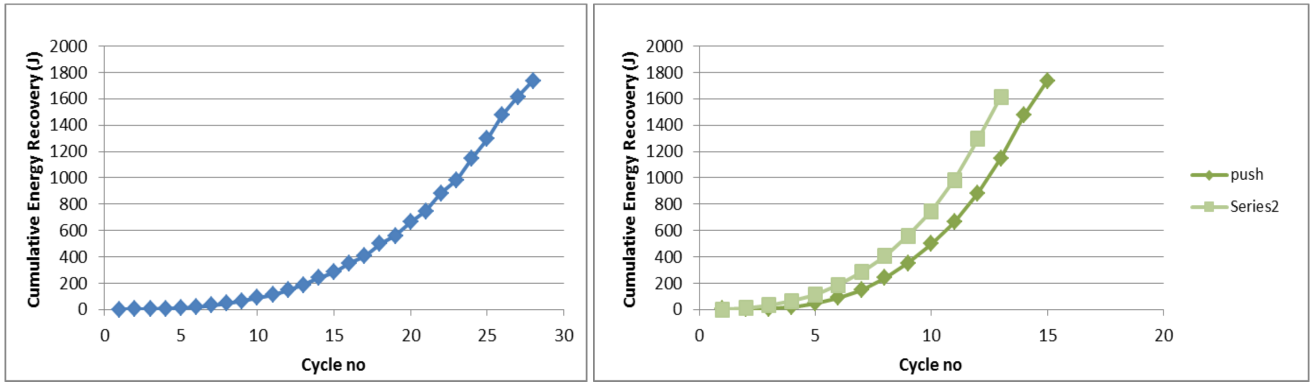

Figure 338: Change in cumulative recovered energy of Frame#4 with infill for all cycles and for push and pull cycles separately, respectively

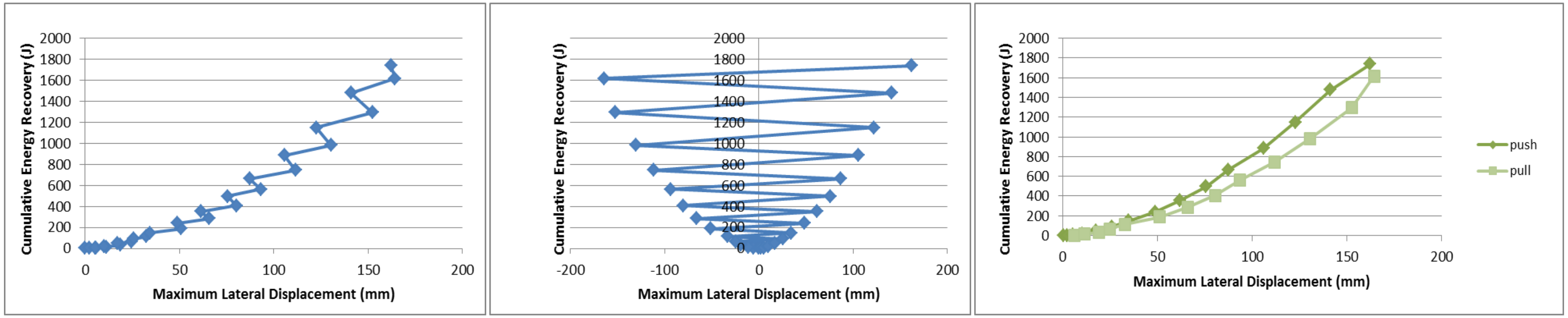

Figure 339: Change in cumulative recovered energy – maximum lateral displacement relation of Frame#4 with infill for all cycles (positive push / negative pull, and absolute values, respectively) and for push and pull cycles separately

APPENDIX J

J. RESULTS OBTAINED AT THE END OF TESTING OF FRAME#5

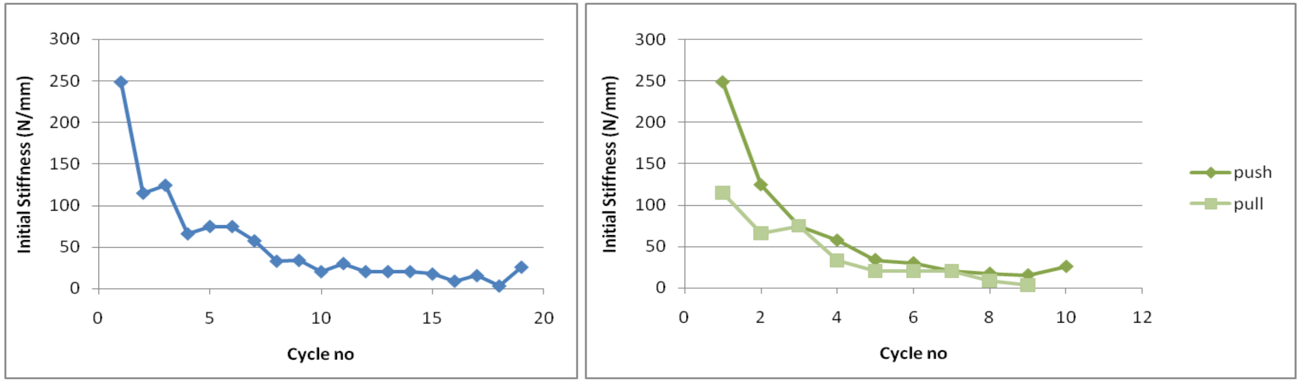

Figure 340: Change in initial stiffness of Frame#5 for all cycles and for push and pull cycles separately, respectively

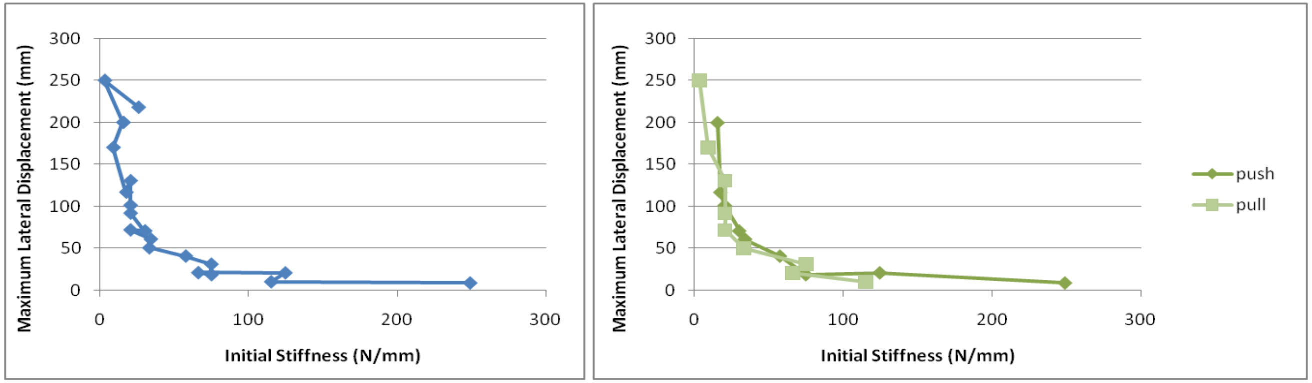

Figure 341: Change in initial stiffness – maximum lateral displacement relation of Frame#5 for all cycles and for push and pull cycles separately, respectively

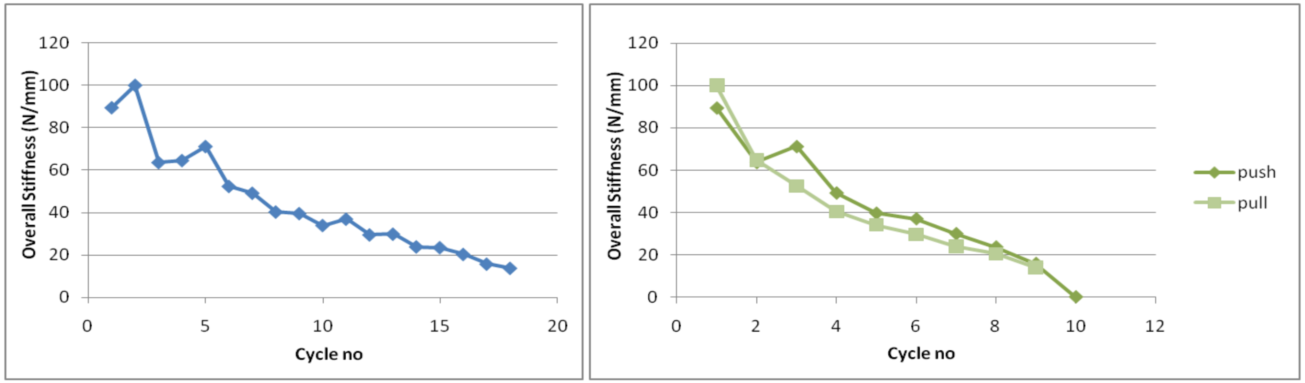

Figure 342: Change in overall stiffness of Frame#5 for all cycles and for push and pull cycles separately, respectively

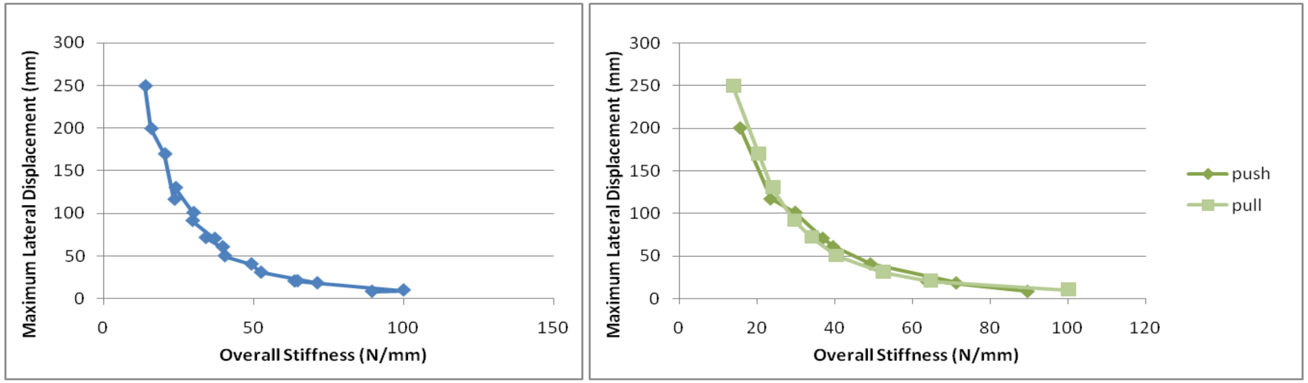

Figure 343: Change in overall stiffness – maximum lateral displacement relation of Frame#5 for all cycles and for push and pull cycles separately, respectively

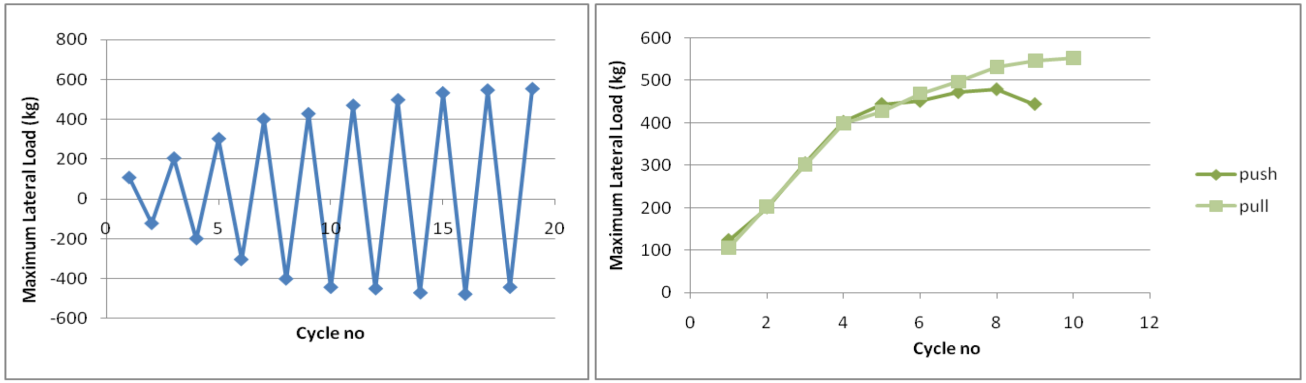

Figure 344: Change in maximum lateral load of Frame#5 for all cycles and for push and pull cycles separately, respectively

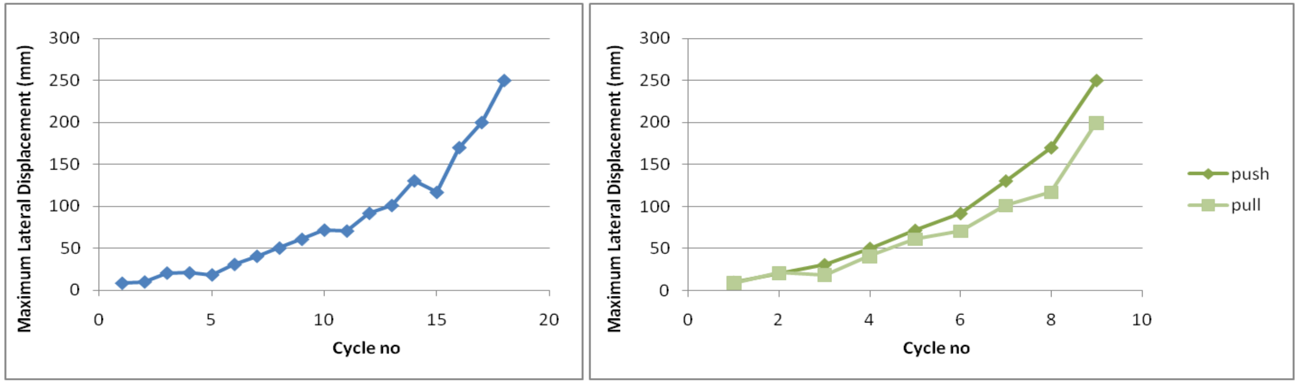

Figure 345: Change in maximum lateral displacement of Frame#5 for all cycles and for push and pull cycles separately, respectively

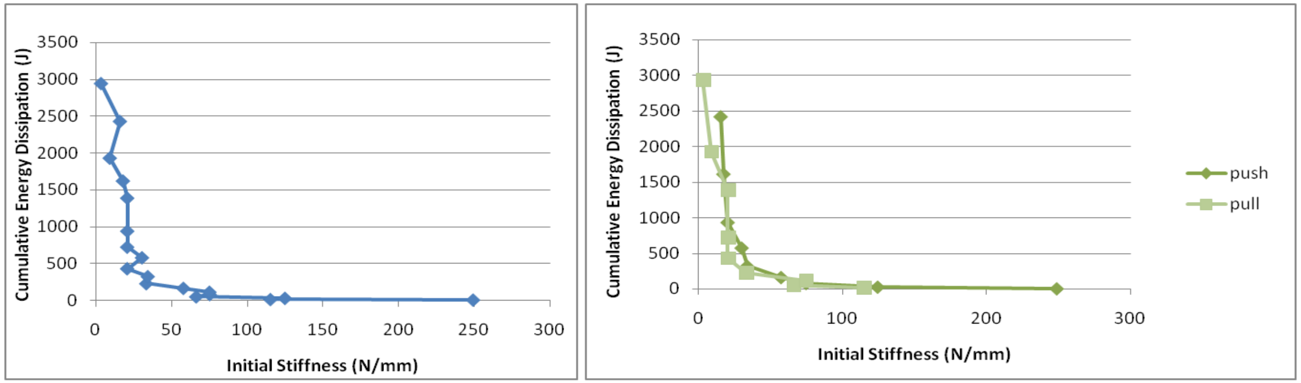

Figure 346: Change in cumulative dissipated energy – initial stiffness relation of Frame#5 for all cycles (positive push / negative pull, and absolute values, respectively) and for push and pull cycles separately

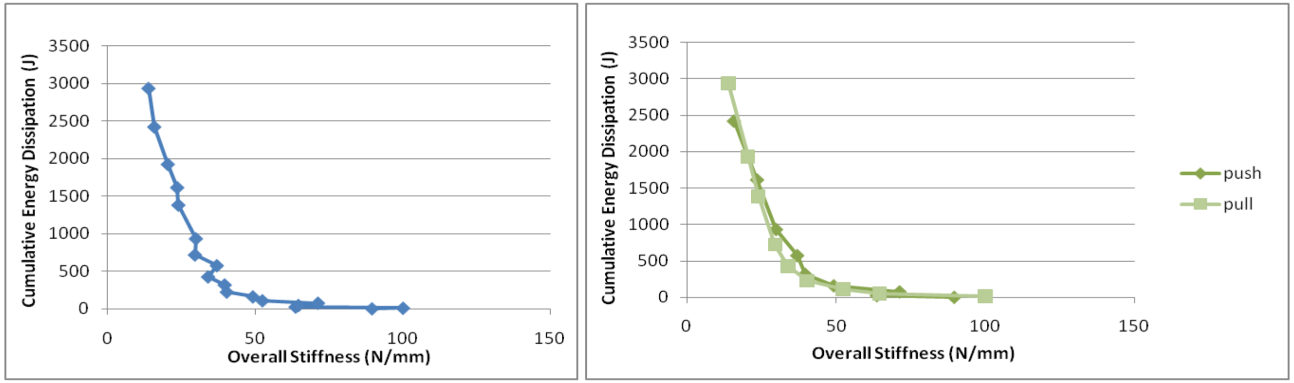

Figure 347: Change in cumulative dissipated energy – overall stiffness relation of Frame#5 for all cycles (positive push / negative pull, and absolute values, respectively) and for push and pull cycles separately

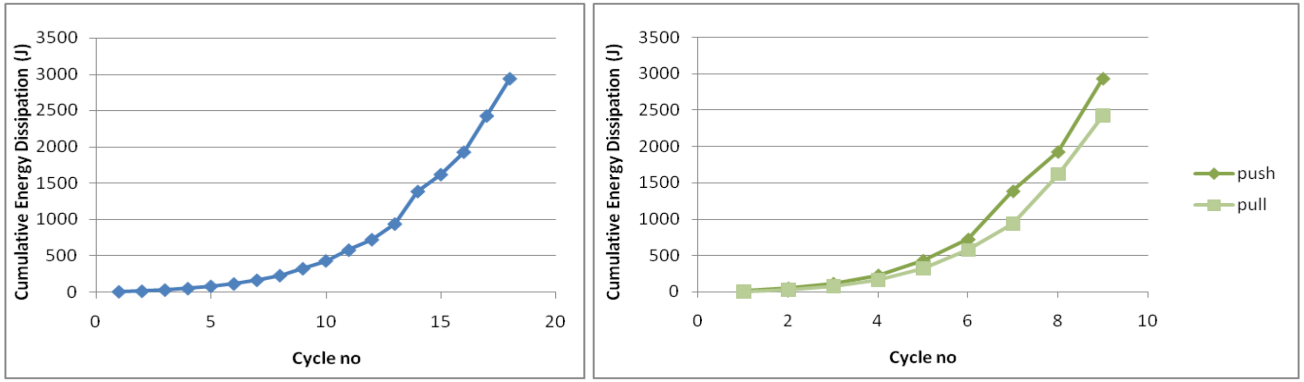

Figure 348: Change in cumulative dissipated energy of Frame#5 for all cycles and for push and pull cycles separately, respectively

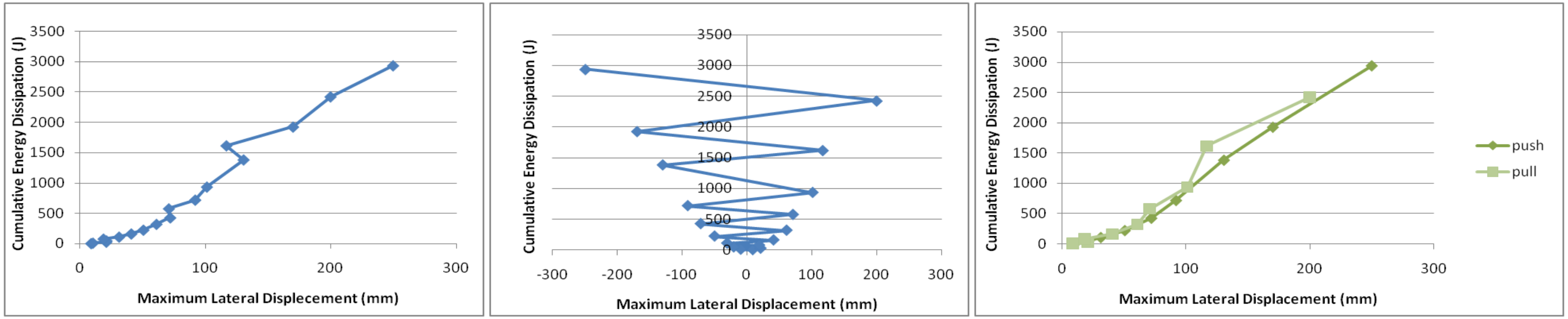

Figure 349: Change in cumulative dissipated energy – maximum lateral displacement relation of Frame#5 for all cycles (positive push / negative pull, and absolute values, respectively) and for push and pull cycles separately

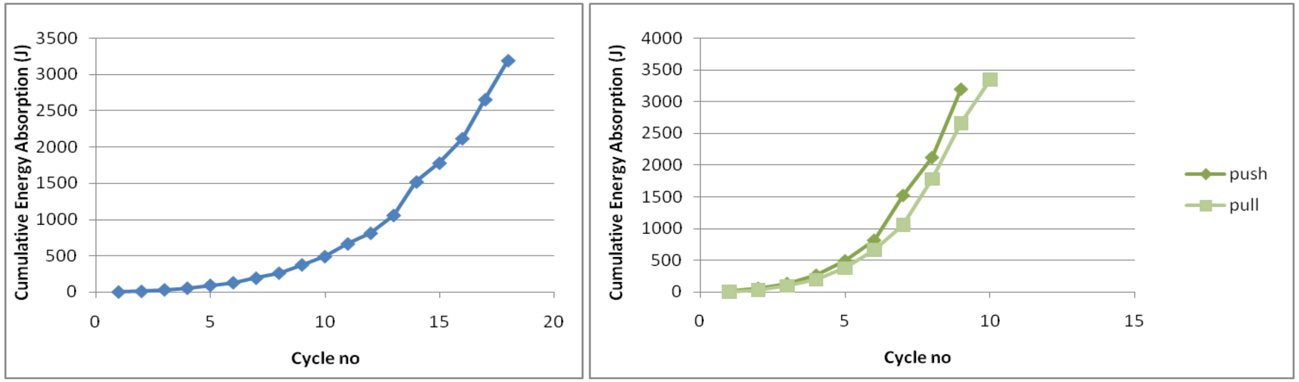

Figure 350: Change in cumulative absorbed energy of Frame#5 for all cycles and for push and pull cycles separately, respectively

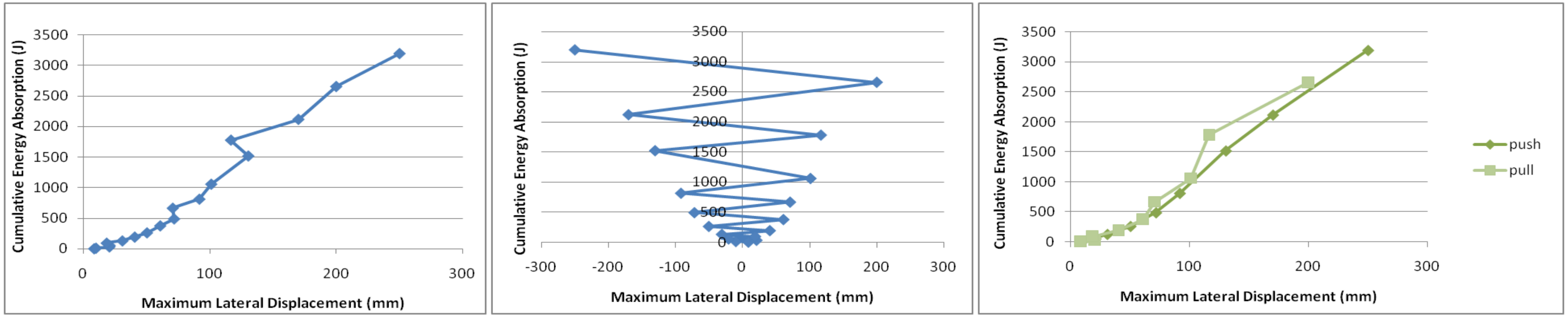

Figure 351: Change in cumulative absorbed energy – maximum lateral displacement relation of Frame#5 for all cycles (positive push / negative pull, and absolute values, respectively) and for push and pull cycles separately

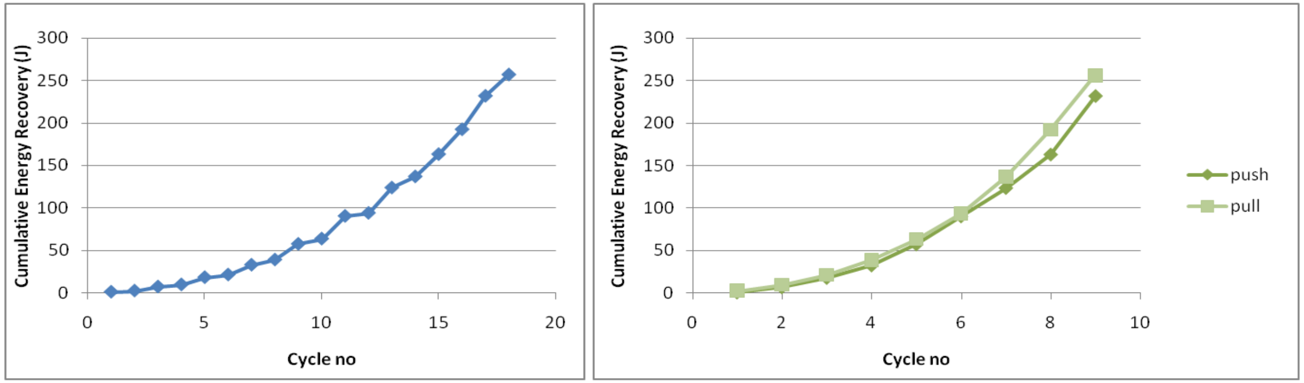

Figure 352: Change in cumulative recovered energy of Frame#5 for all cycles and for push and pull cycles separately, respectively

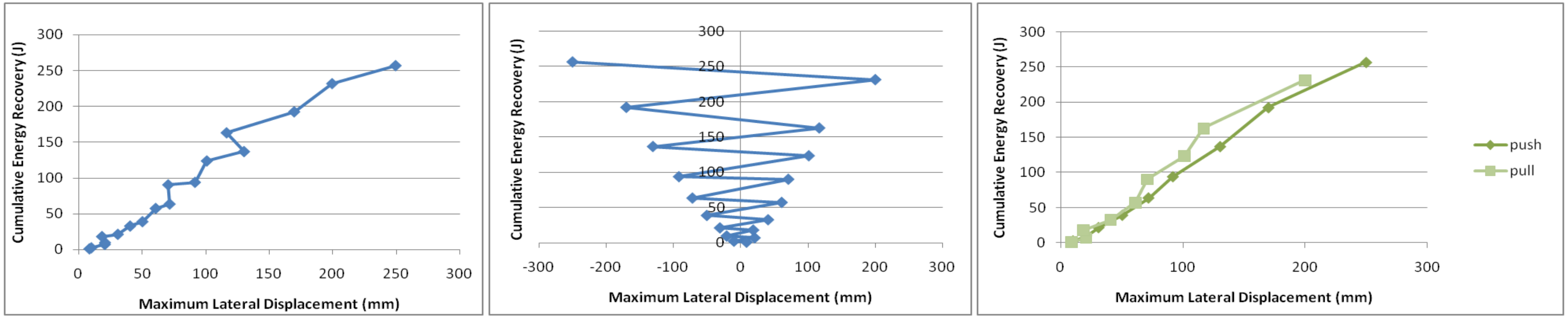

Figure 353: Change in cumulative recovered energy – maximum lateral displacement relation of Frame#5 for all cycles (positive push / negative pull, and absolute values, respectively) and for push and pull cycles separately

APPENDIX K

K. RESULTS OBTAINED AT THE END OF TESTING OF FRAME#5 WITH BAĞDADİ COVERING

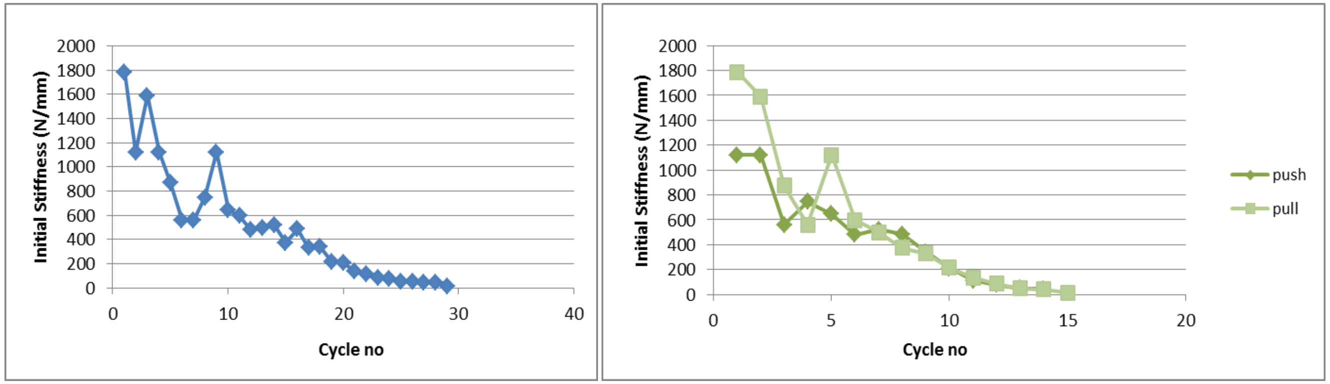

Figure 354: Change in initial stiffness of Frame#5 with infill for all cycles and for push and pull cycles separately, respectively

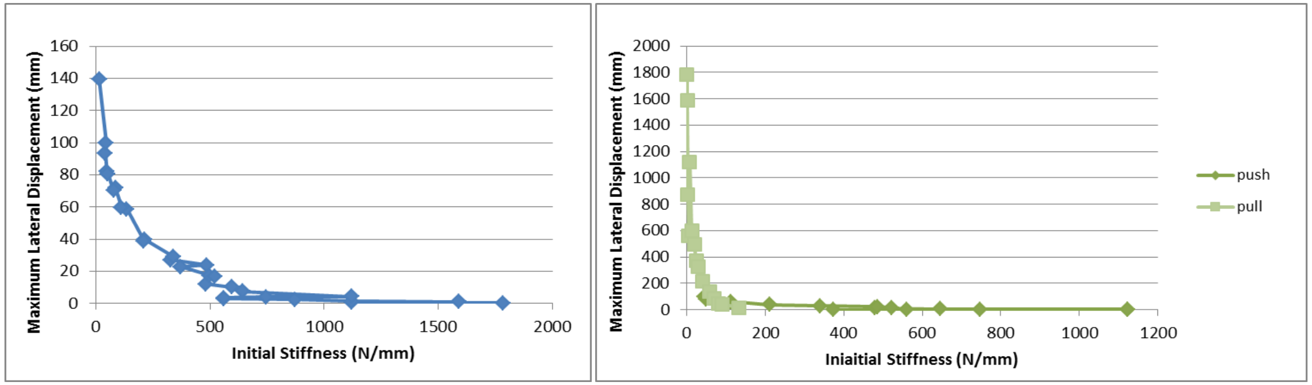

Figure 355: Change in initial stiffness – maximum lateral displacement relation of Frame#5 with infill for all cycles and for push and pull cycles separately, respectively

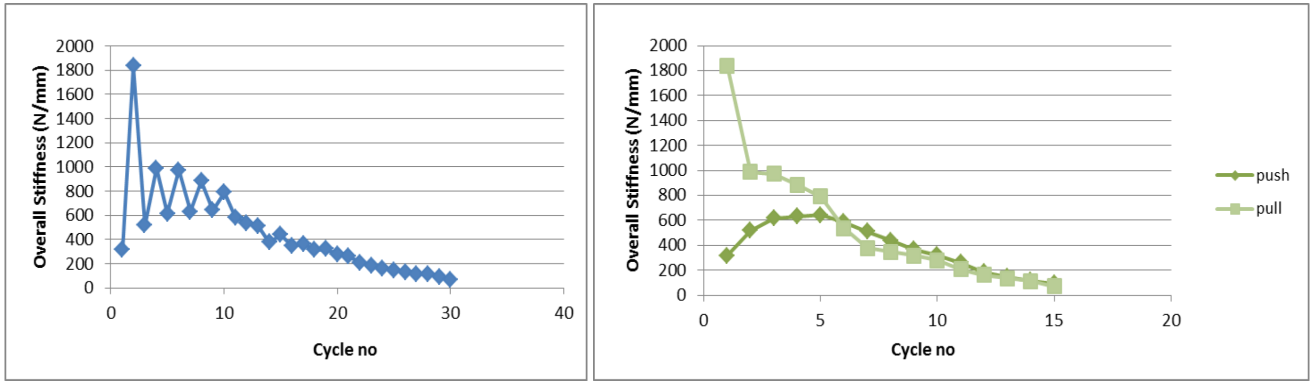

Figure 356: Change in overall stiffness of Frame#5 with infill for all cycles and for push and pull cycles separately, respectively

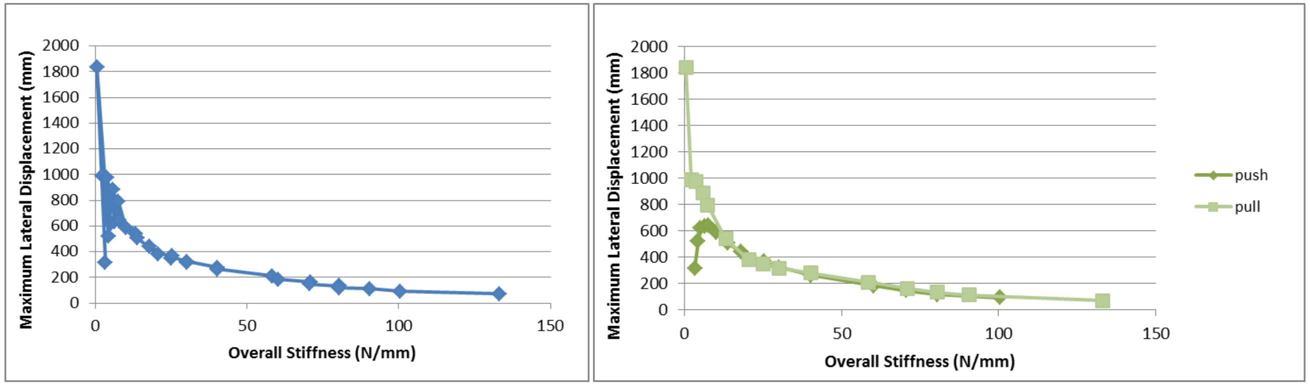

Figure 357: Change in overall stiffness – maximum lateral displacement relation of Frame#5 with infill for all cycles and for push and pull cycles separately, respectively

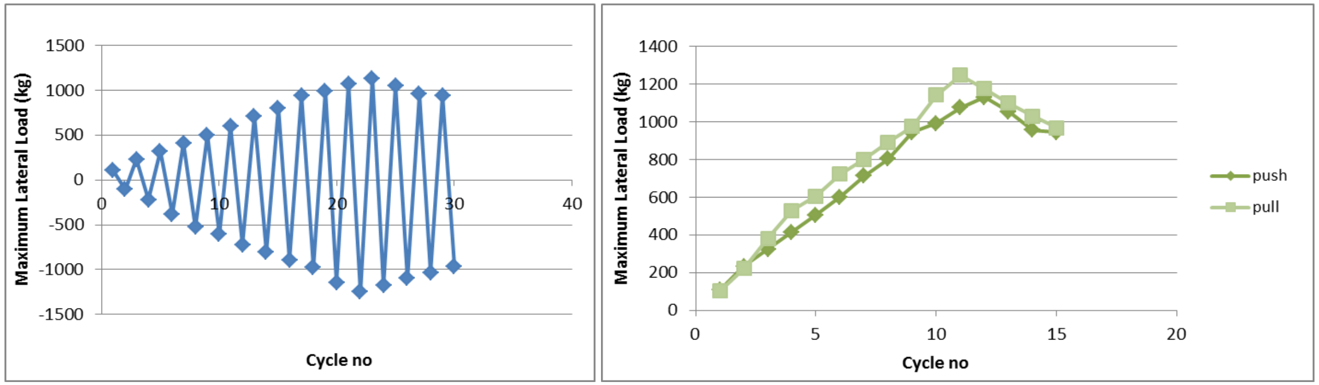

Figure 358: Change in maximum lateral load of Frame#5 with infill for all cycles and for push and pull cycles separately, respectively

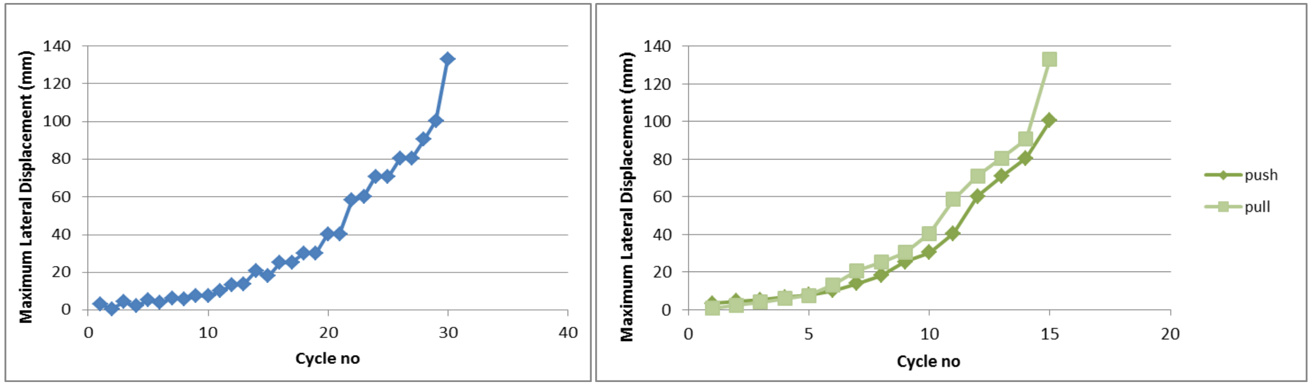

Figure 359: Change in maximum lateral displacement of Frame#5 with infill for all cycles and for push and pull cycles separately, respectively

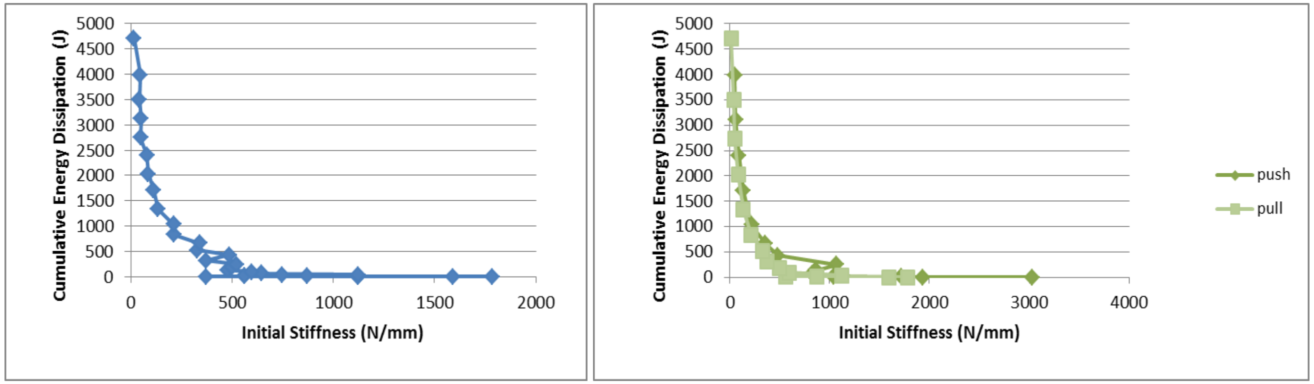

Figure 360: Change in cumulative dissipated energy – initial stiffness relation of Frame#5 with infill for all cycles (positive push / negative pull, and absolute values, respectively) and for push and pull cycles separately

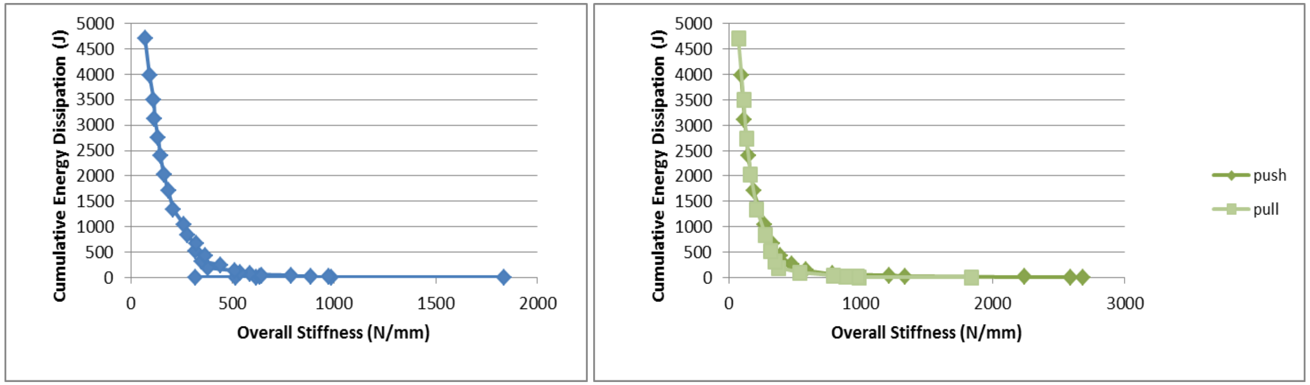

Figure 361: Change in cumulative dissipated energy – overall stiffness relation of Frame#5 with infill for all cycles (positive push / negative pull, and absolute values, respectively) and for push and pull cycles separately

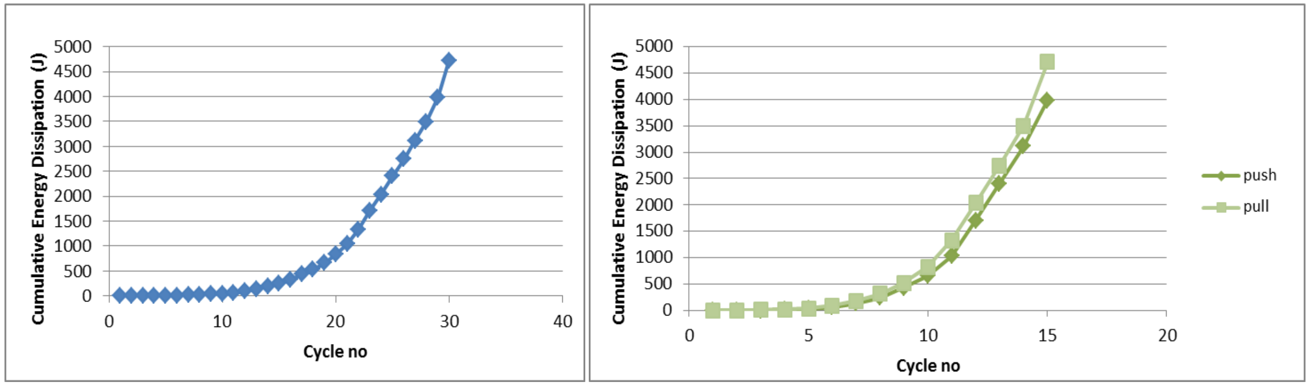

Figure 362: Change in cumulative dissipated energy of Frame#5 with infill for all cycles and for push and pull cycles separately, respectively

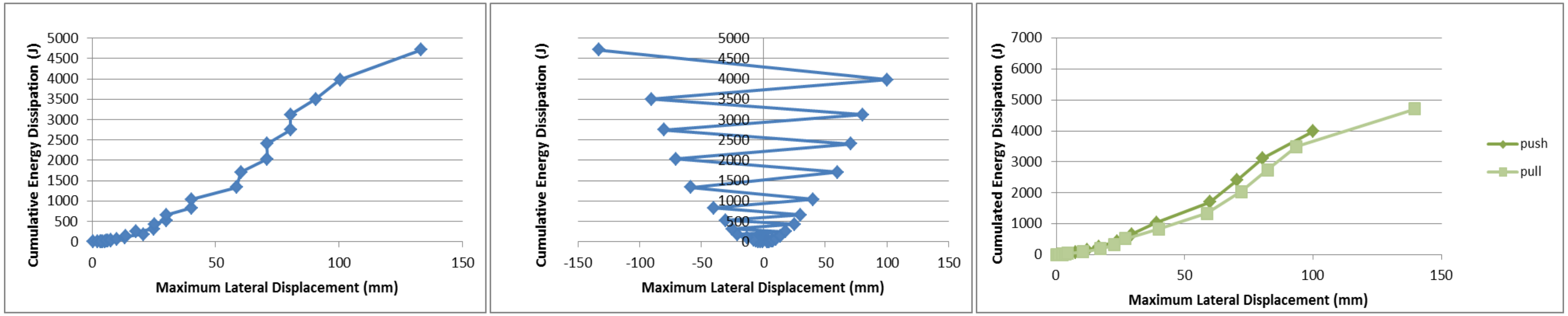

Figure 363: Change in cumulative dissipated energy – maximum lateral displacement relation of Frame#5 with infill for all cycles (positive push / negative pull, and absolute values, respectively) and for push and pull cycles separately

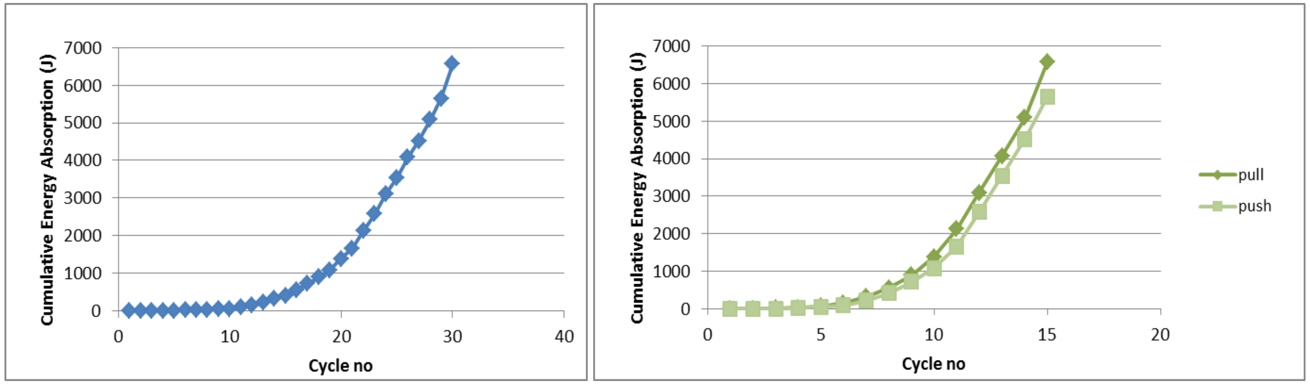

Figure 364: Change in cumulative absorbed energy of Frame#5 with infill for all cycles and for push and pull cycles separately, respectively

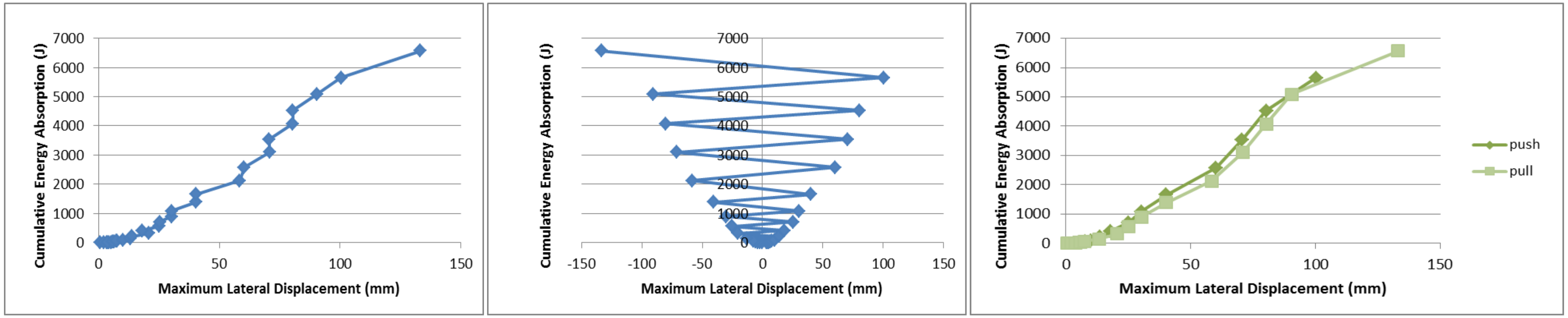

Figure 365: Change in cumulative absorbed energy – maximum lateral displacement relation of Frame#5 with infill for all cycles (positive push / negative pull, and absolute values, respectively) and for push and pull cycles separately

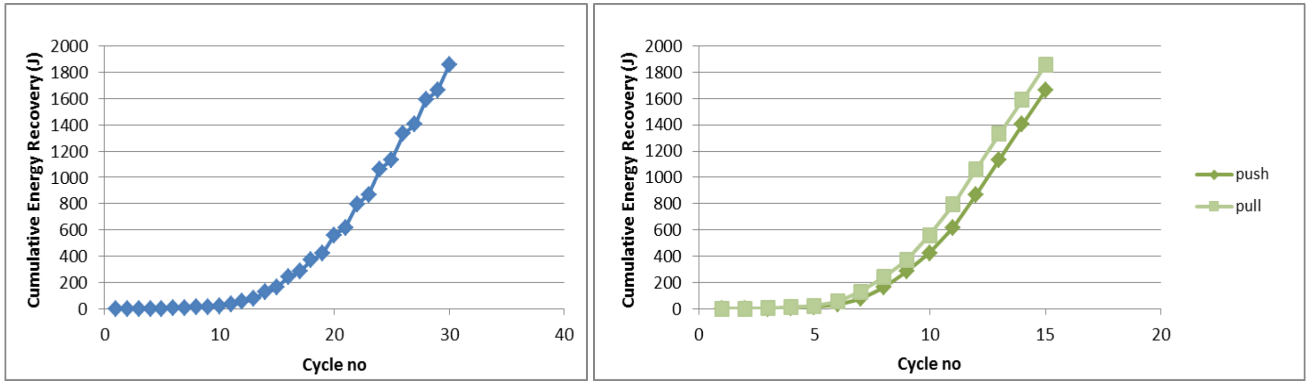

Figure 366: Change in cumulative recovered energy of Frame#5 with infill for all cycles and for push and pull cycles separately, respectively

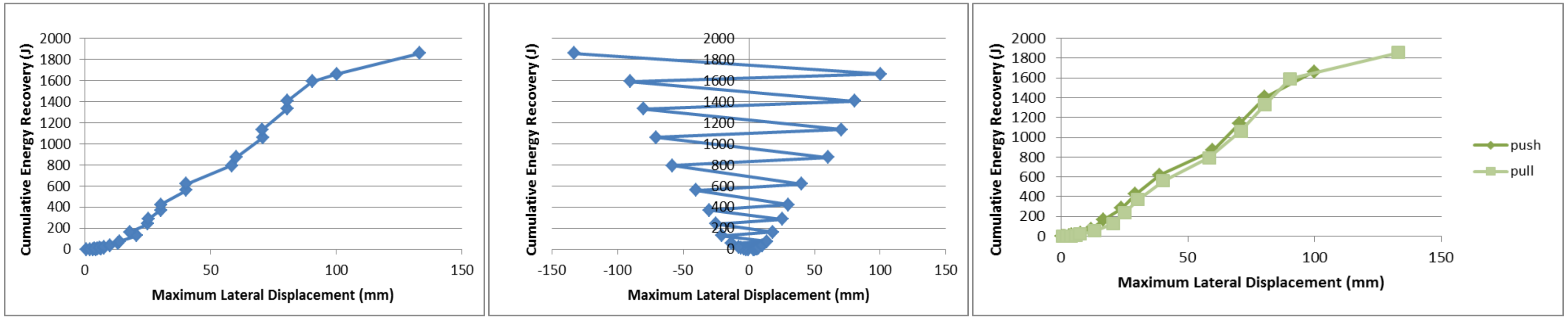

Figure 367: Change in cumulative recovered energy – maximum lateral displacement relation of Frame#5 with infill for all cycles (positive push / negative pull, and absolute values, respectively) and for push and pull cycles separately

APPENDIX L

L. RESULTS OBTAINED AT THE END OF TESTING OF FRAME#6

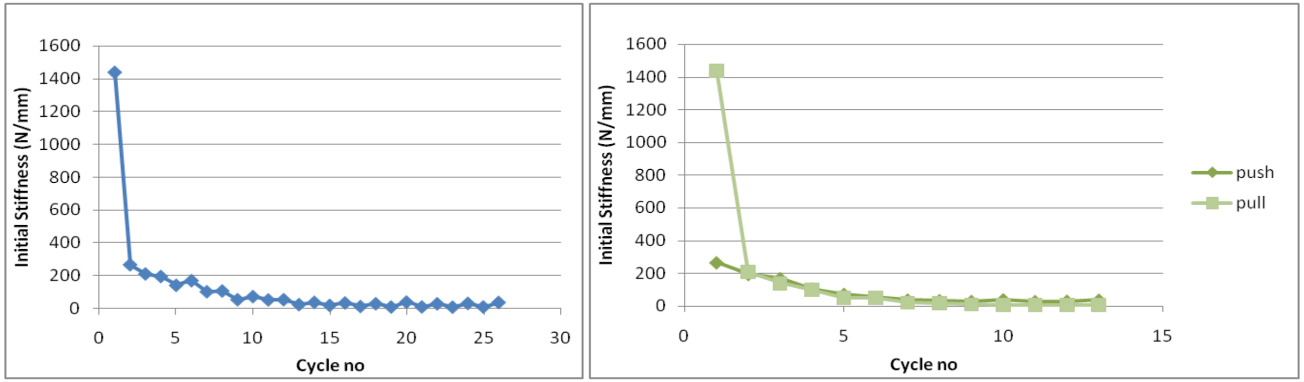

Figure 368: Change in initial stiffness of Frame#6 for all cycles and for push and pull cycles separately, respectively

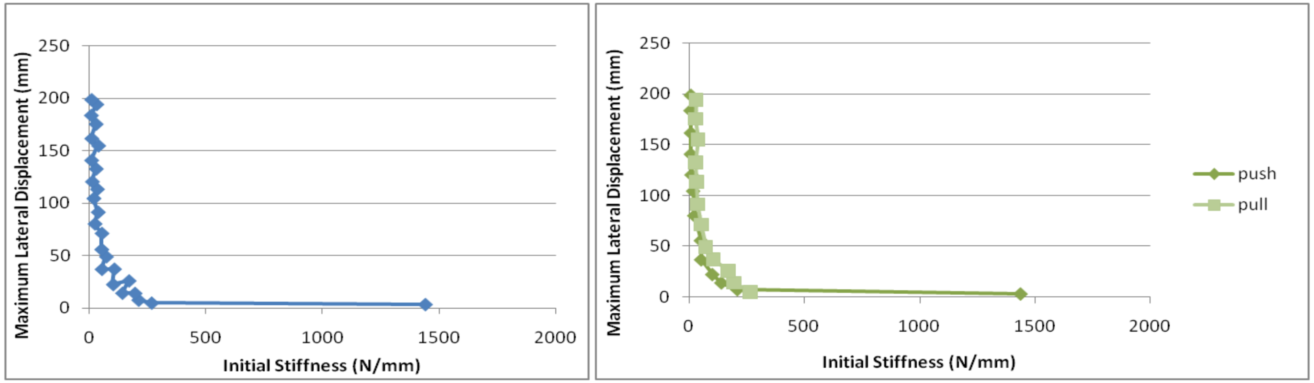

Figure 369: Change in initial stiffness – maximum lateral displacement relation of Frame#6 for all cycles and for push and pull cycles separately, respectively

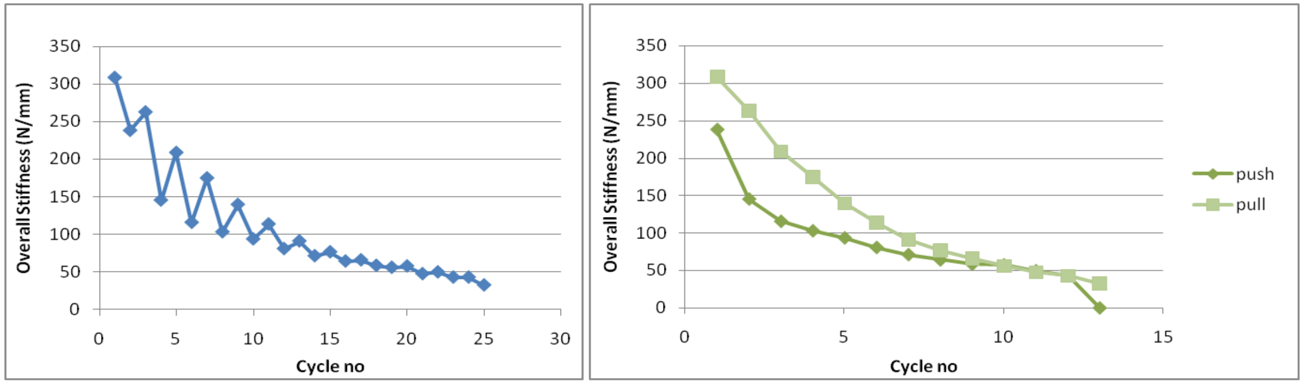

Figure 370: Change in overall stiffness of Frame#6 for all cycles and for push and pull cycles separately, respectively

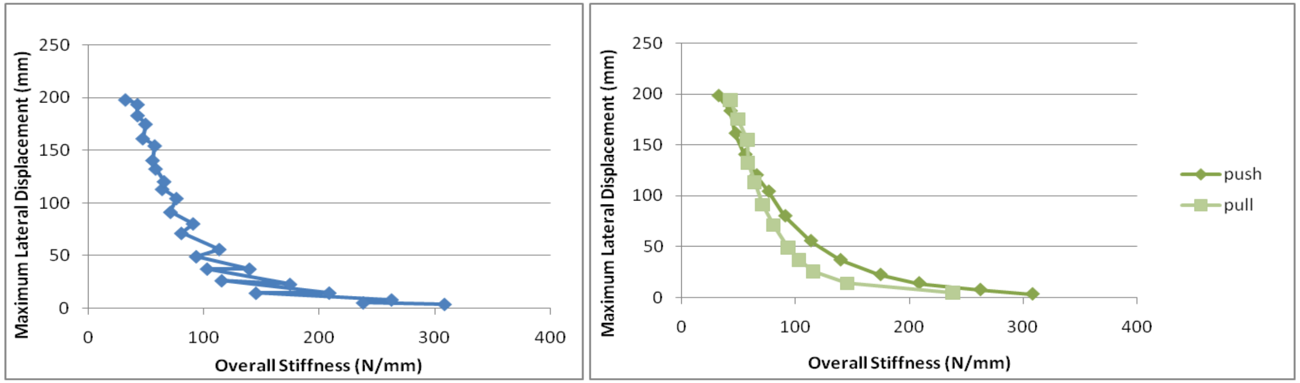

Figure 371: Change in overall stiffness – maximum lateral displacement relation of Frame#6 for all cycles and for push and pull cycles separately, respectively

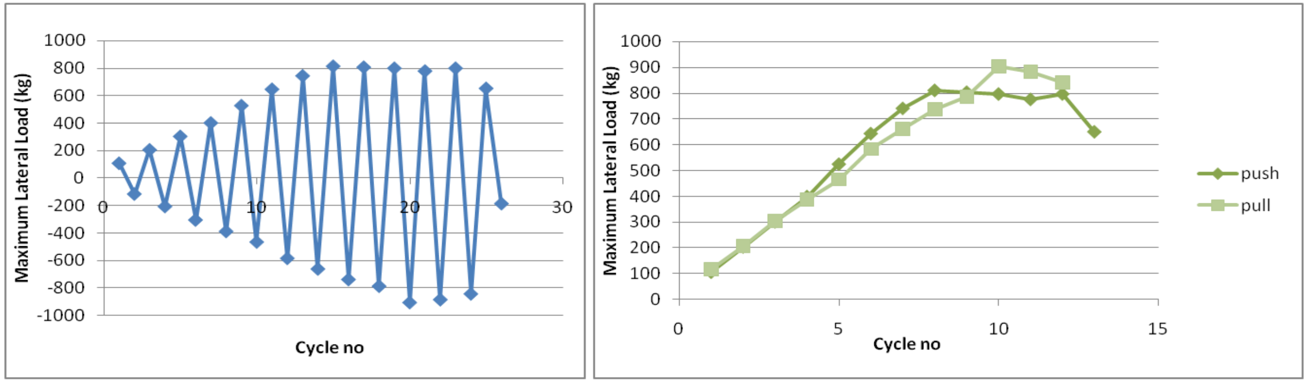

Figure 372: Change in maximum lateral load of Frame#6 for all cycles and for push and pull cycles separately, respectively

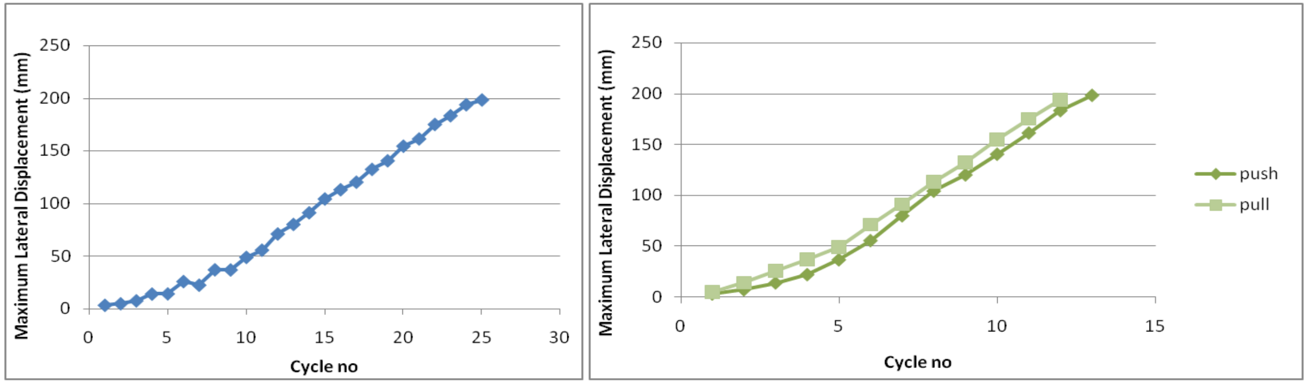

Figure 373: Change in maximum lateral displacement of Frame#6 for all cycles and for push and pull cycles separately, respectively

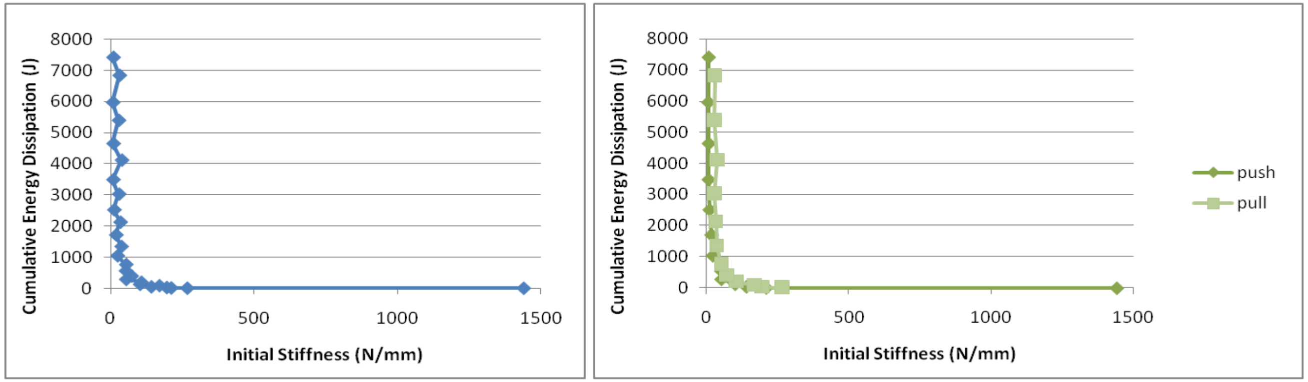

Figure 374: Change in cumulative dissipated energy – initial stiffness relation of Frame#6 for all cycles (positive push / negative pull, and absolute values, respectively) and for push and pull cycles separately

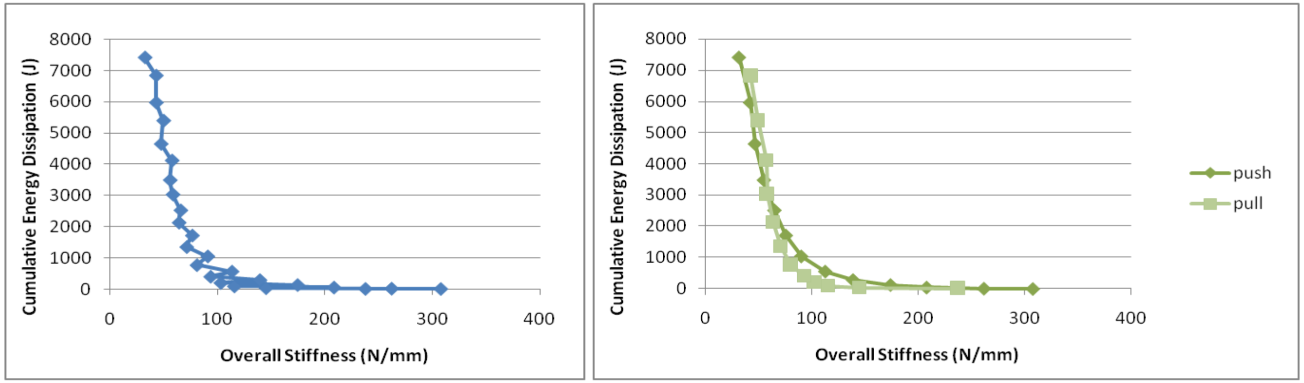

Figure 375: Change in cumulative dissipated energy – overall stiffness relation of Frame#6 for all cycles (positive push / negative pull, and absolute values, respectively) and for push and pull cycles separately

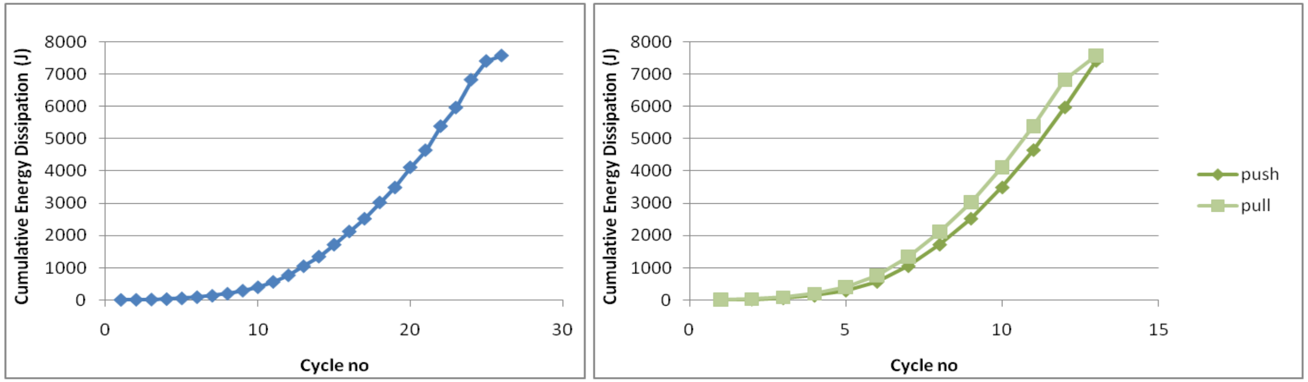

Figure 376: Change in cumulative dissipated energy of Frame#6 for all cycles and for push and pull cycles separately, respectively

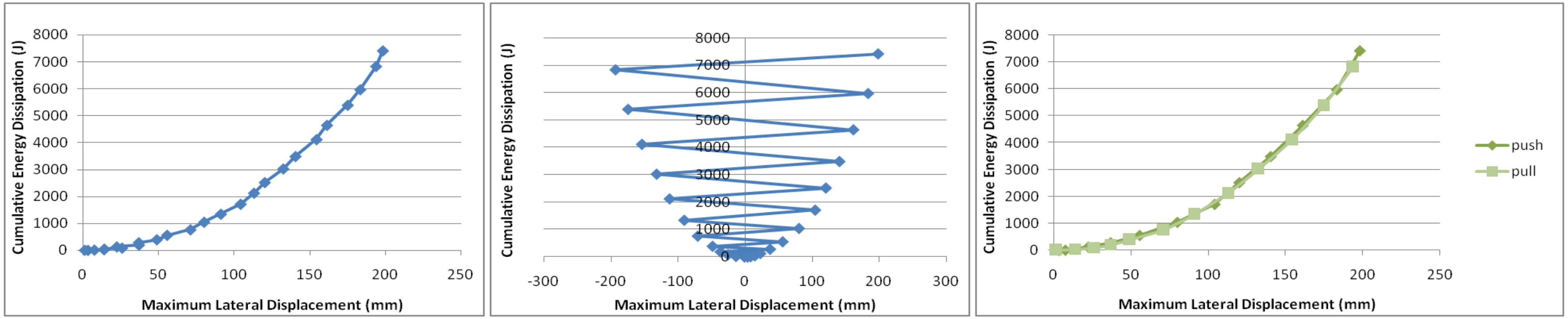

Figure 377: Change in cumulative dissipated energy – maximum lateral displacement relation of Frame#6 for all cycles (positive push / negative pull, and absolute values, respectively) and for push and pull cycles separately

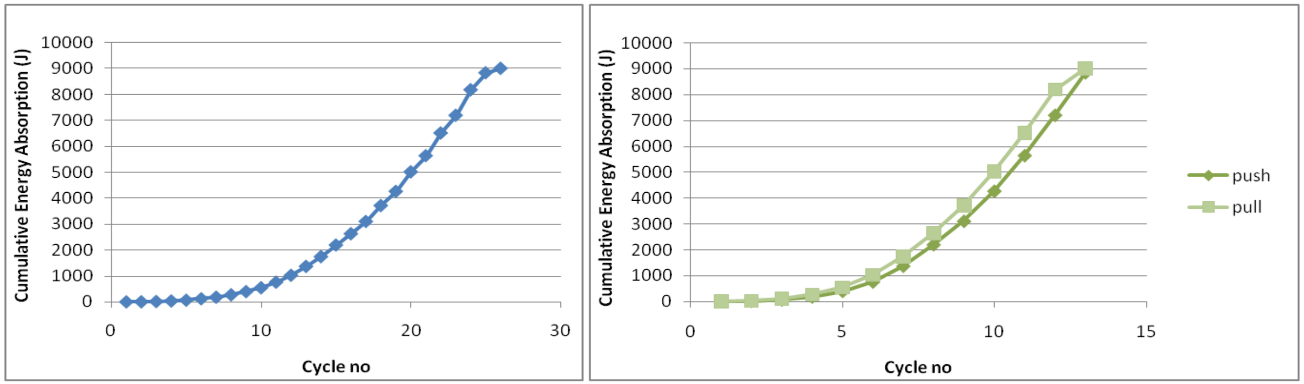

Figure 378: Change in cumulative absorbed energy of Frame#6 for all cycles and for push and pull cycles separately, respectively

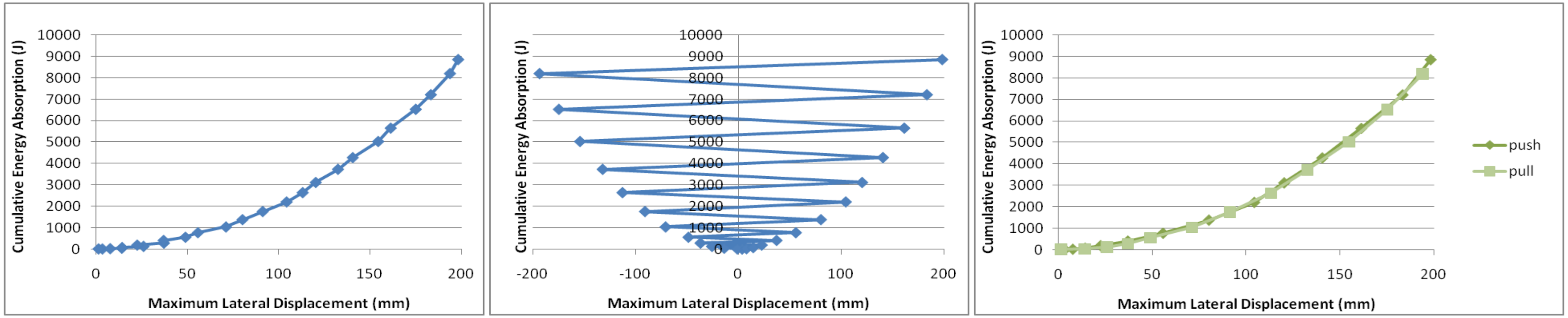

Figure 379: Change in cumulative absorbed energy – maximum lateral displacement relation of Frame#6 for all cycles (positive push / negative pull, and absolute values, respectively) and for push and pull cycles separately

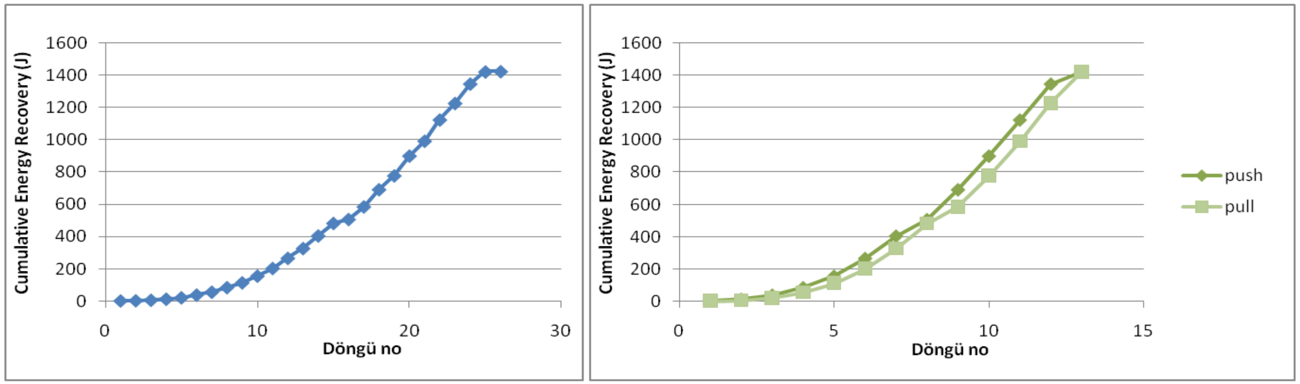

Figure 380: Change in cumulative recovered energy of Frame#6 for all cycles and for push and pull cycles separately, respectively

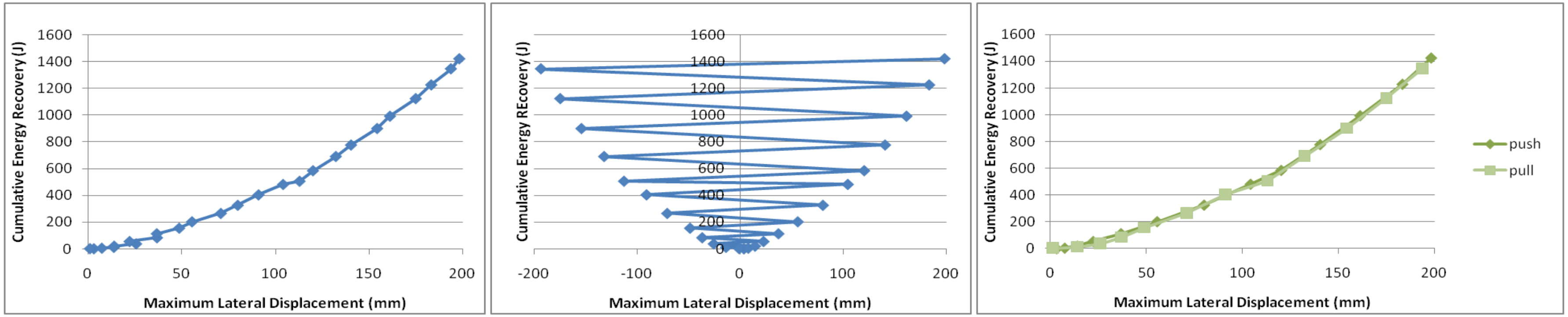

Figure 381: Change in cumulative recovered energy – maximum lateral displacement relation of Frame#6 for all cycles (positive push / negative pull, and absolute values, respectively) and for push and pull cycles separately

APPENDIX M

M. RESULTS OBTAINED AT THE END OF TESTING OF FRAME#6 WITH ŞAMDOLMA COVERING

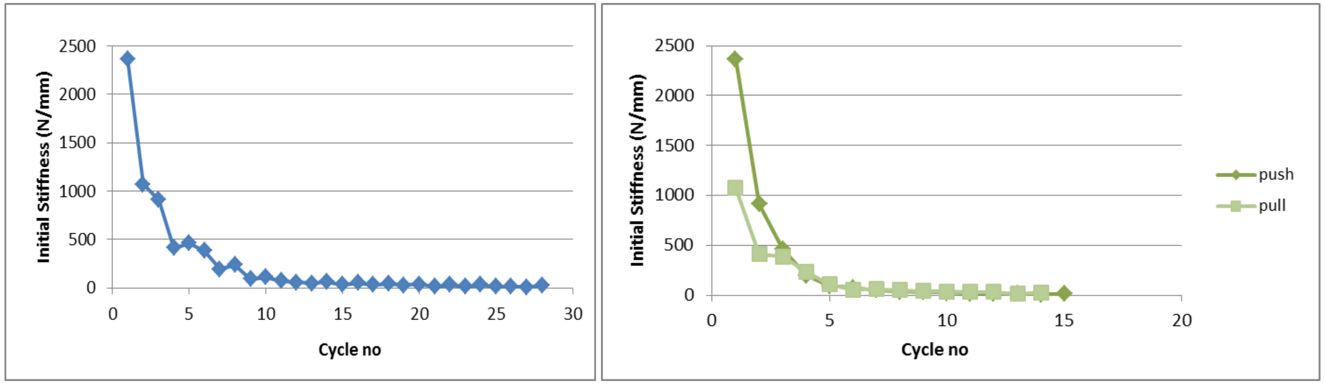

Figure 382: Change in initial stiffness for all cycles and for of Frame#6 with infill push and pull cycles separately, respectively

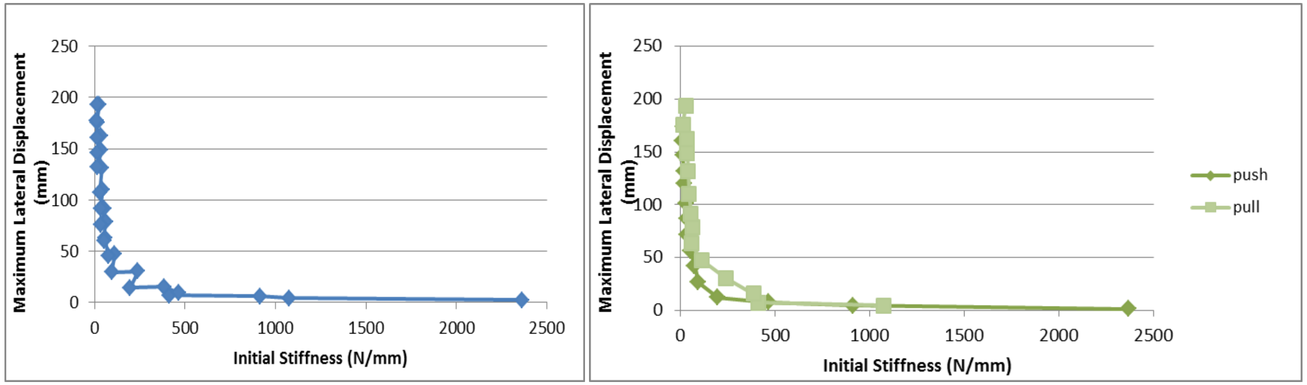

Figure 383: Change in initial stiffness – maximum lateral displacement relation of Frame#6 with infill for all cycles and for push and pull cycles separately, respectively

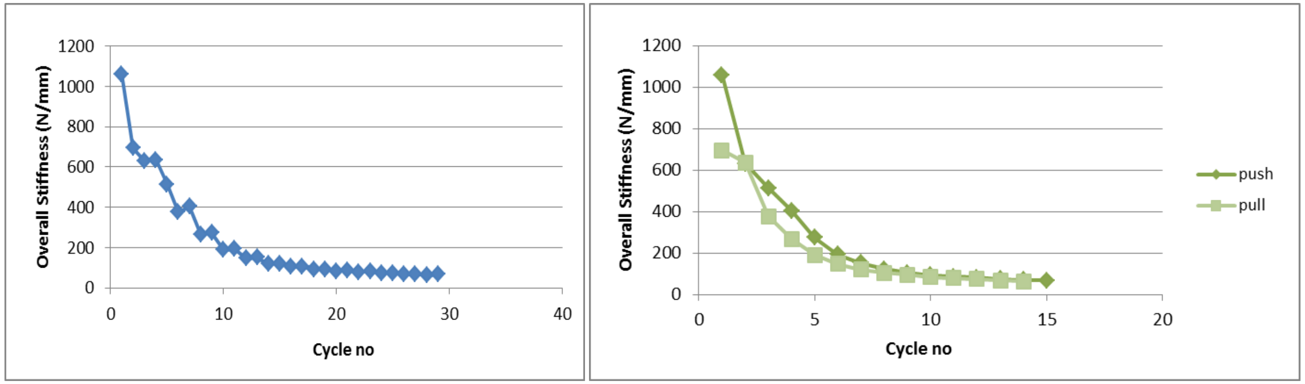

Figure 384: Change in overall stiffness for all cycles and for of Frame#6 with infill push and pull cycles separately, respectively

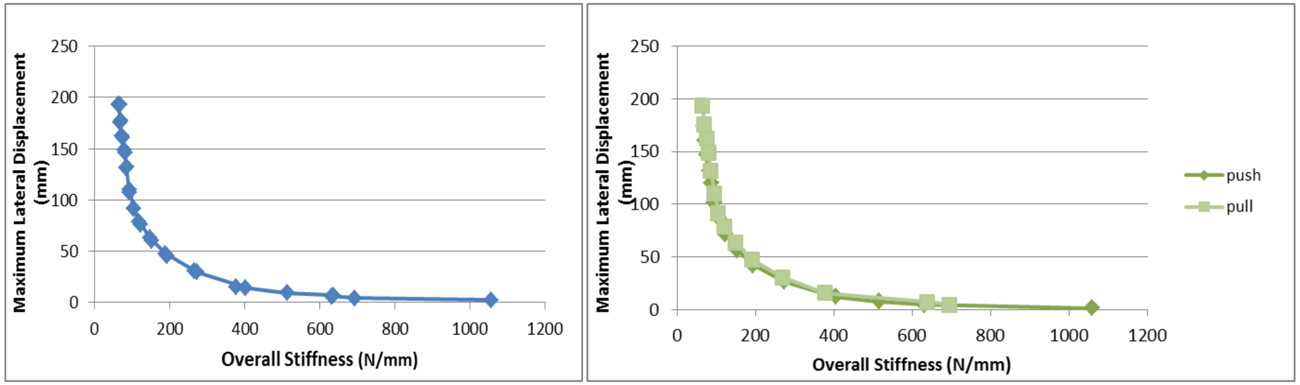

Figure 385: Change in overall stiffness – maximum lateral displacement relation of Frame#6 with infill for all cycles and for push and pull cycles separately, respectively

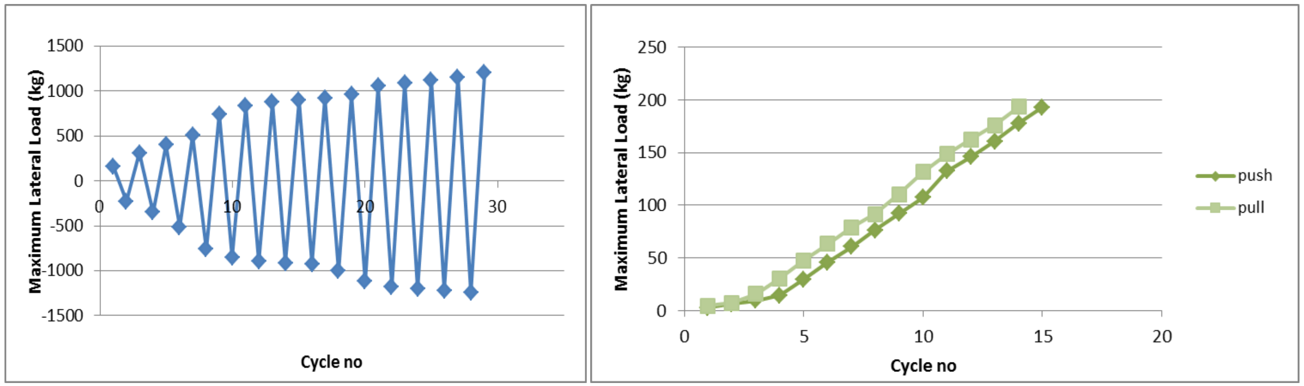

Figure 386: Change in maximum lateral displacement of Frame#6 with infill for all cycles and for push and pull cycles separately, respectively

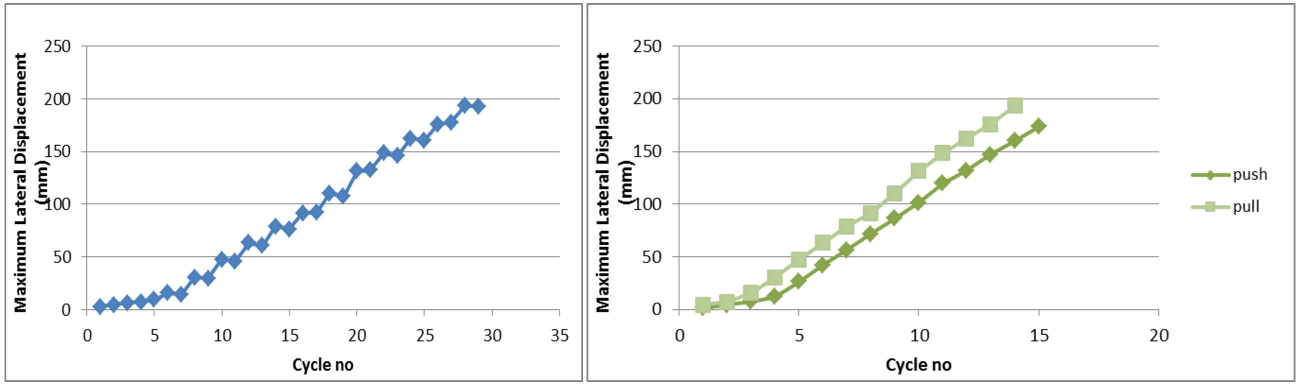

Figure 387: Change in maximum lateral displacement of Frame#6 with infill for all cycles and for push and pull cycles separately, respectively

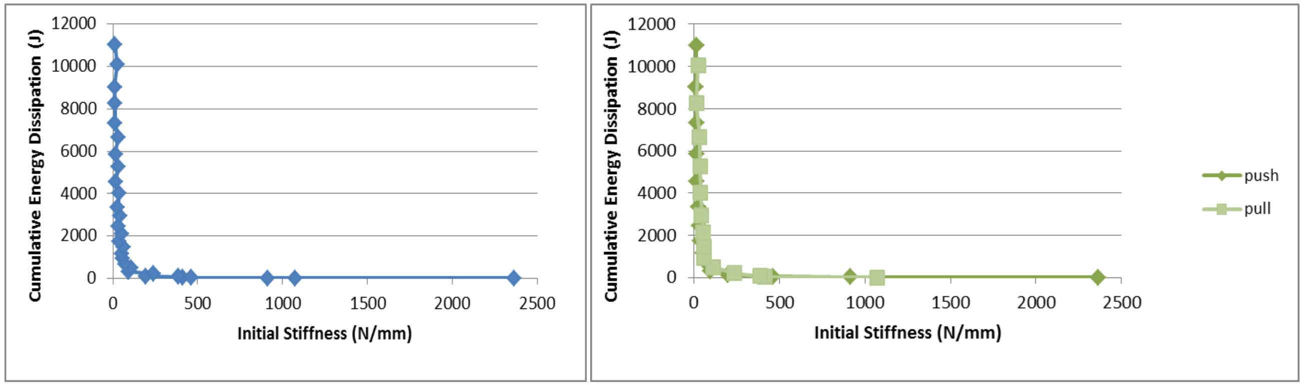

Figure 388: Change in cumulative dissipated energy – initial stiffness relation of Frame#6 with infill for all cycles (positive push / negative pull, and absolute values, respectively) and for push and pull cycles separately

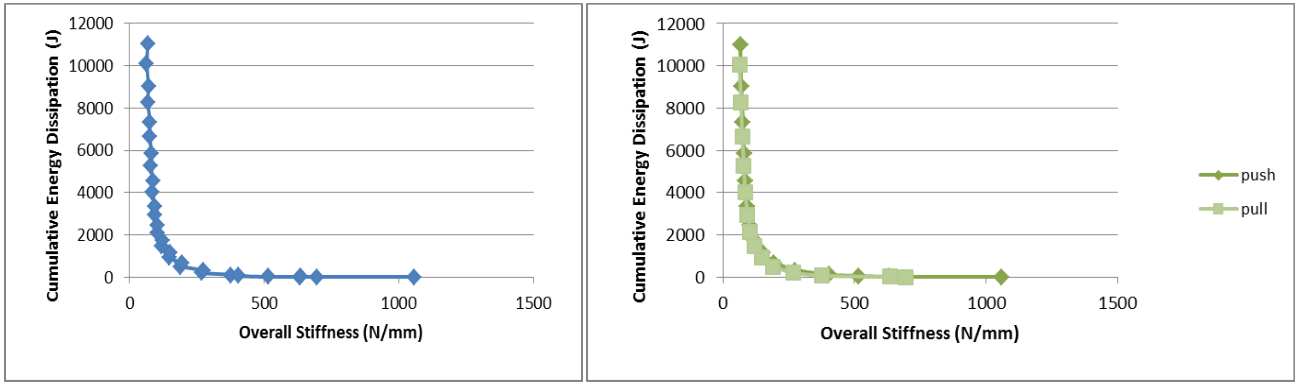

Figure 389: Change in cumulative dissipated energy – overall stiffness relation of Frame#6 with infill for all cycles (positive push / negative pull, and absolute values, respectively) and for push and pull cycles separately

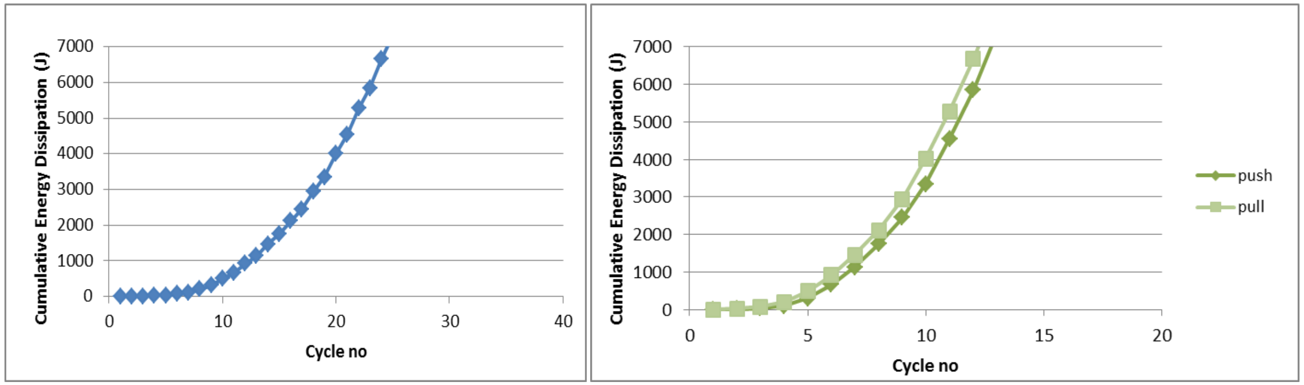

Figure 390: Change in cumulative dissipated energy of Frame#6 with infill for all cycles and for push and pull cycles separately, respectively

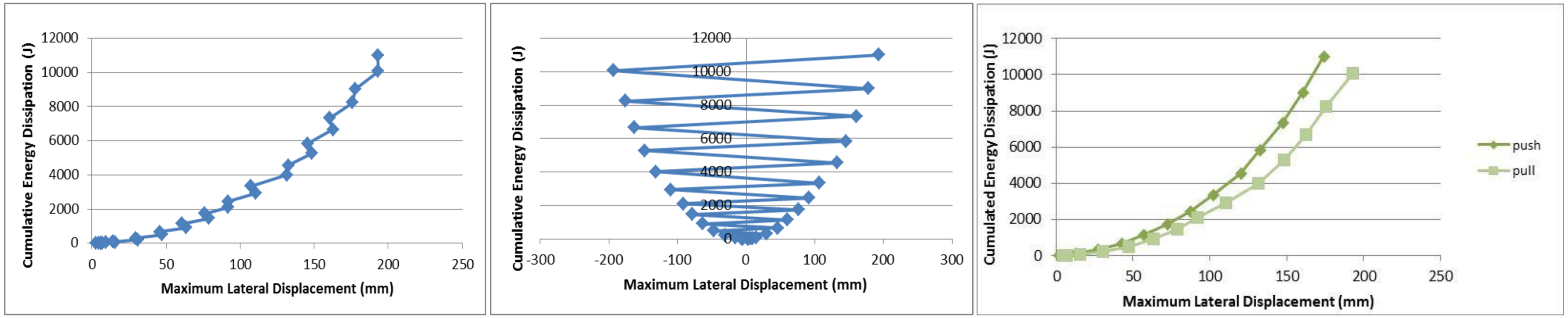

Figure 391: Change in cumulative dissipated energy – maximum lateral displacement relation of Frame#6 with infill for all cycles (positive push / negative pull, and absolute values, respectively) and for push and pull cycles separately

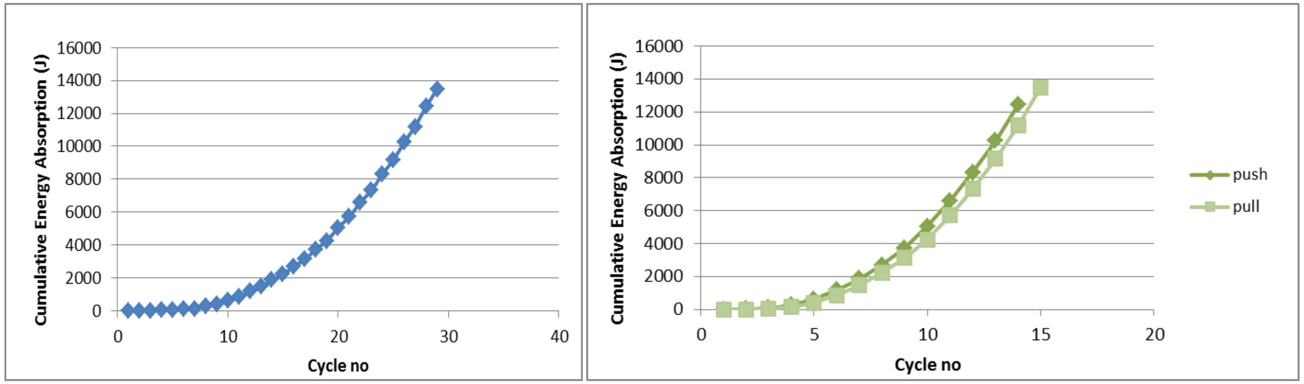

Figure 392: Change in cumulative absorbed energy of Frame#6 with infill for all cycles and for push and pull cycles separately, respectively

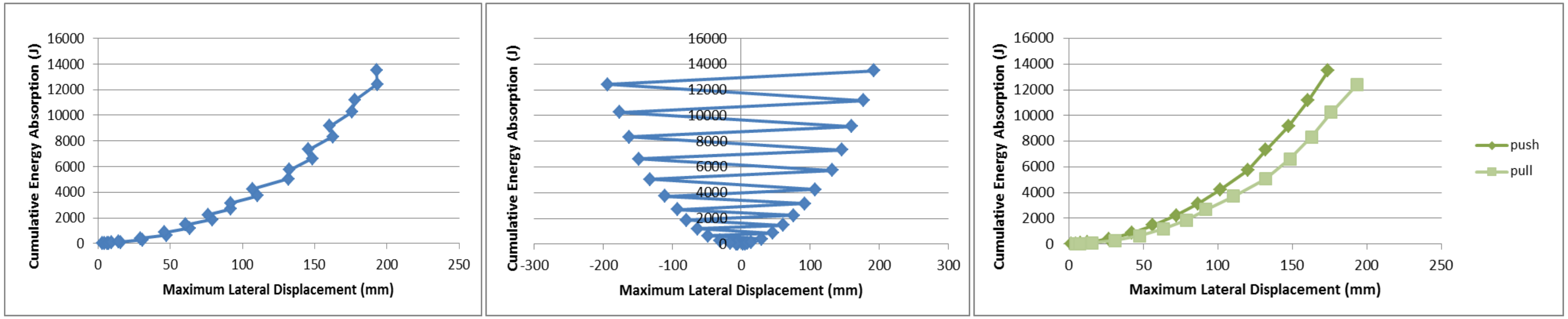

Figure 393: Change in cumulative absorbed energy – maximum lateral displacement relation of Frame#6 with infill for all cycles (positive push / negative pull, and absolute values, respectively) and for push and pull cycles separately

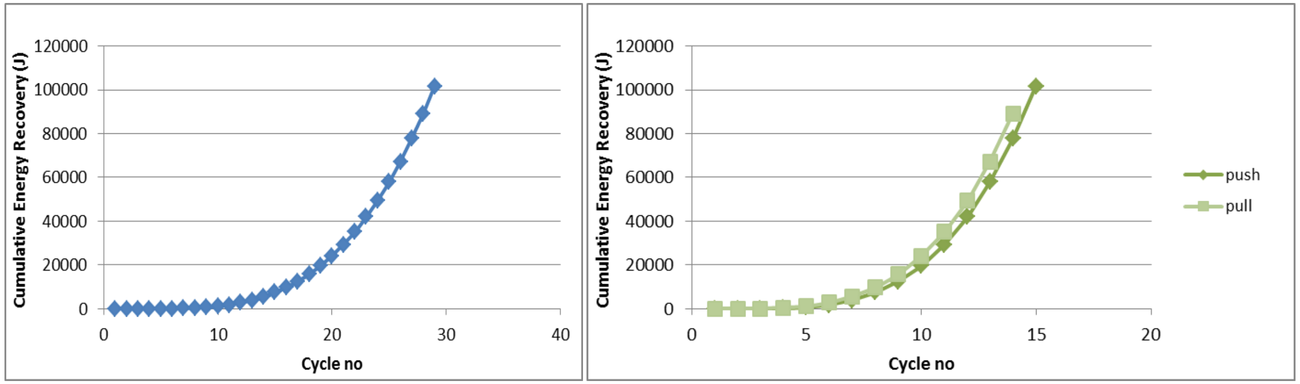

Figure 394: Change in cumulative recovered energy of Frame#6 with infill for all cycles and for push and pull cycles separately, respectively

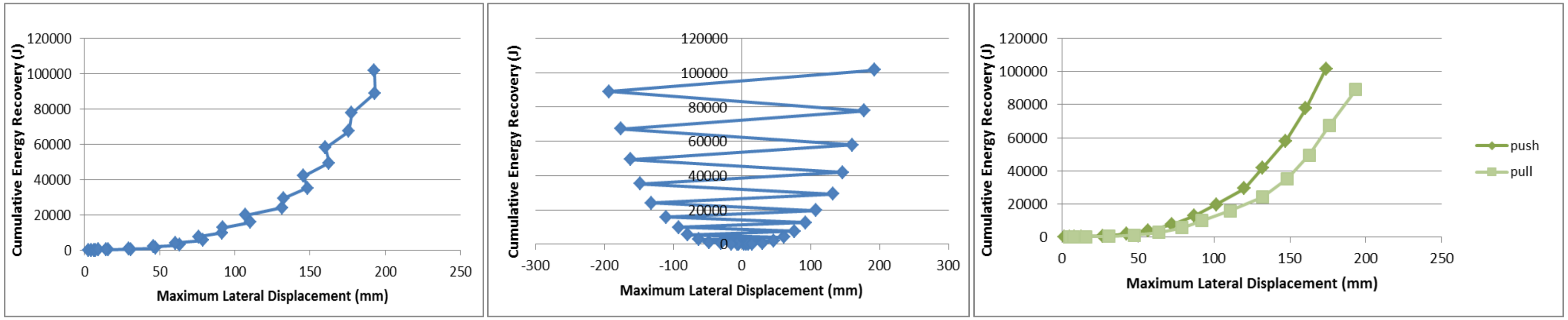

Figure 395: Change in cumulative recovered energy – maximum lateral displacement relation of Frame#6 with infill for all cycles (positive push / negative pull, and absolute values, respectively) and for push and pull cycles separately

APPENDIX N

N. RESULTS OBTAINED AT THE END OF TESTING OF FRAME#7

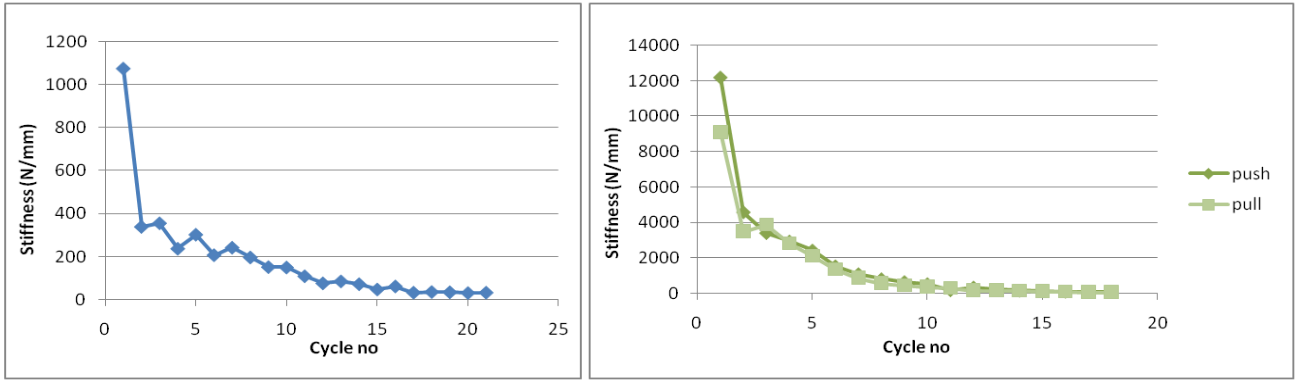

Figure 396: Change in initial stiffness for all cycles and for of Frame#7 push and pull cycles separately, respectively

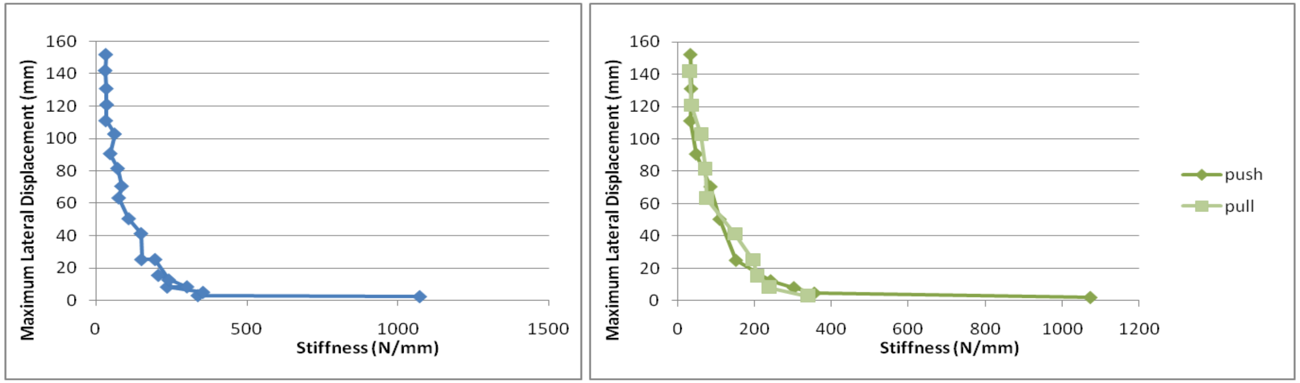

Figure 397: Change in initial stiffness – maximum lateral displacement relation of Frame#7 for all cycles and for push and pull cycles separately, respectively

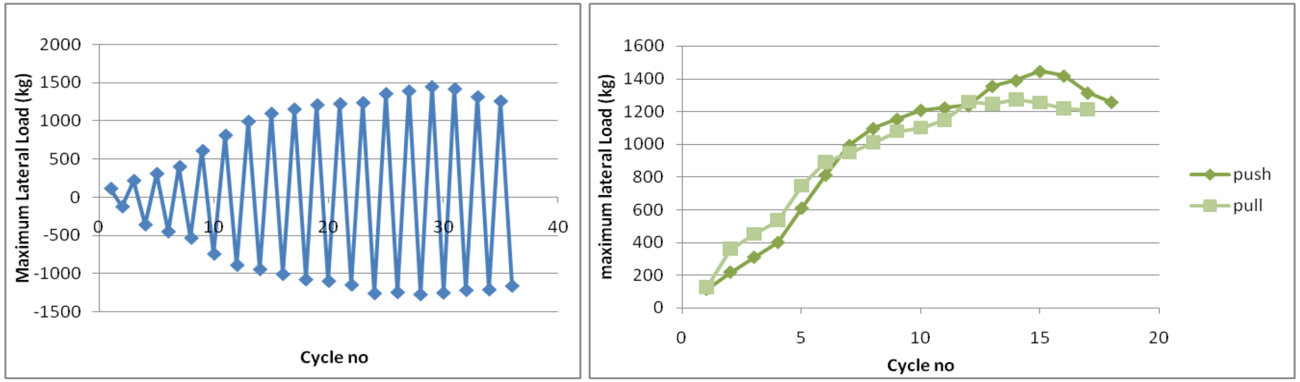

Figure 398: Change in maximum lateral displacement of Frame#7 for all cycles and for push and pull cycles separately, respectively

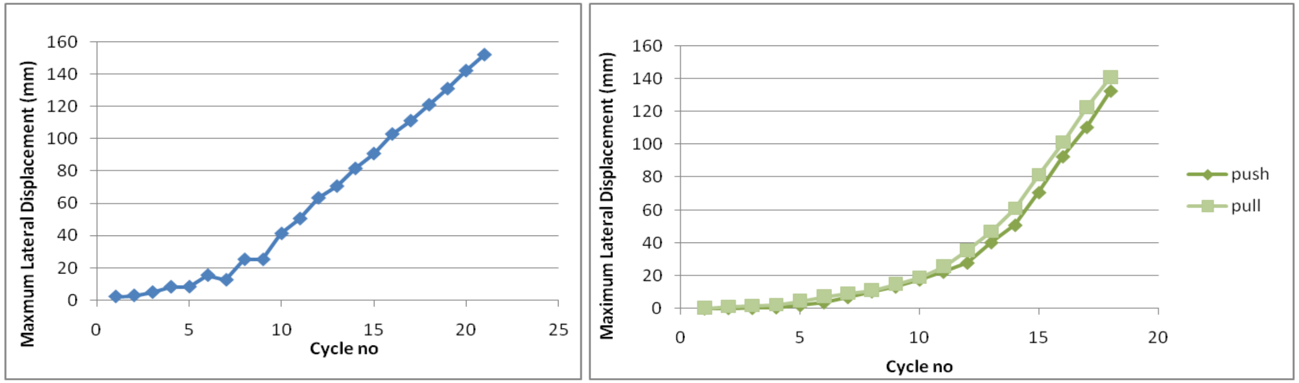

Figure 399: Change in maximum lateral displacement of Frame#7 for all cycles and for push and pull cycles separately, respectively

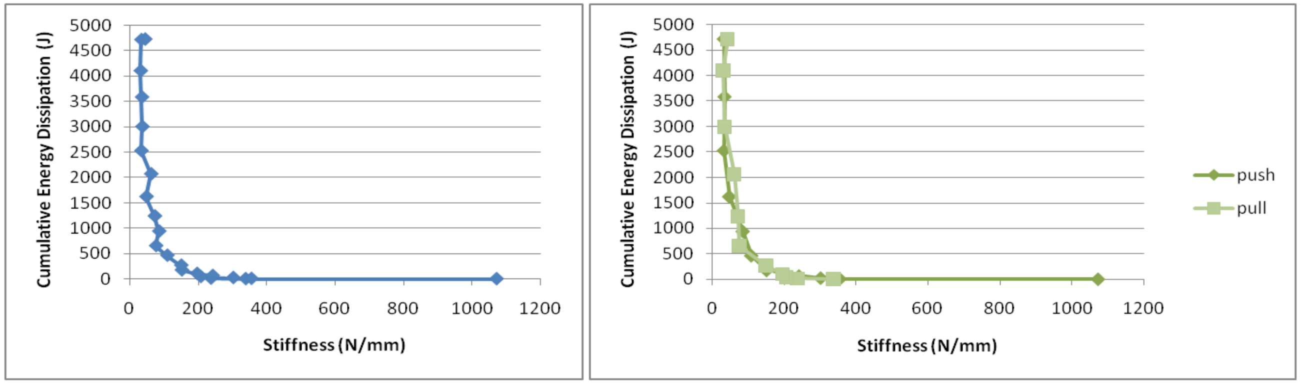

Figure 400: Change in cumulative dissipated energy – initial stiffness relation of Frame#7 for all cycles (positive push / negative pull, and absolute values, respectively) and for push and pull cycles separately

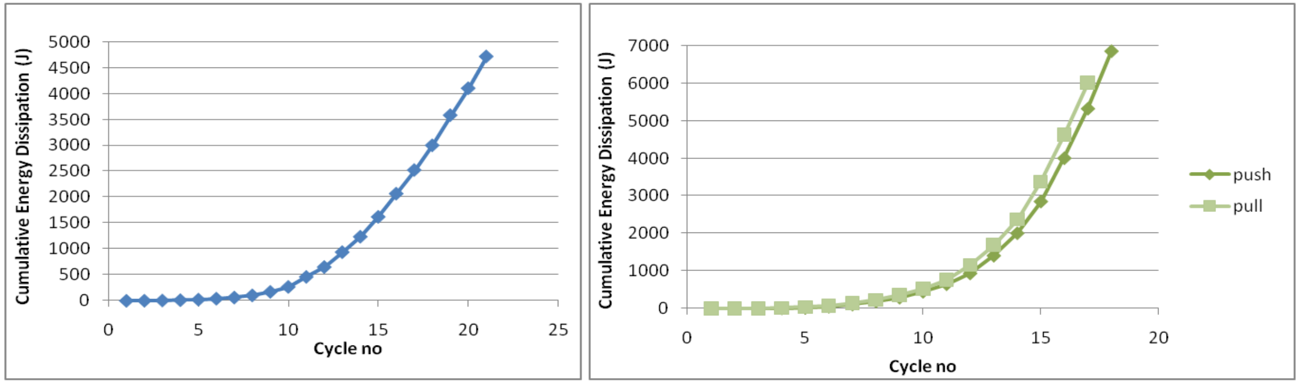

Figure 401: Change in cumulative dissipated energy of Frame#7 for all cycles and for push and pull cycles separately, respectively

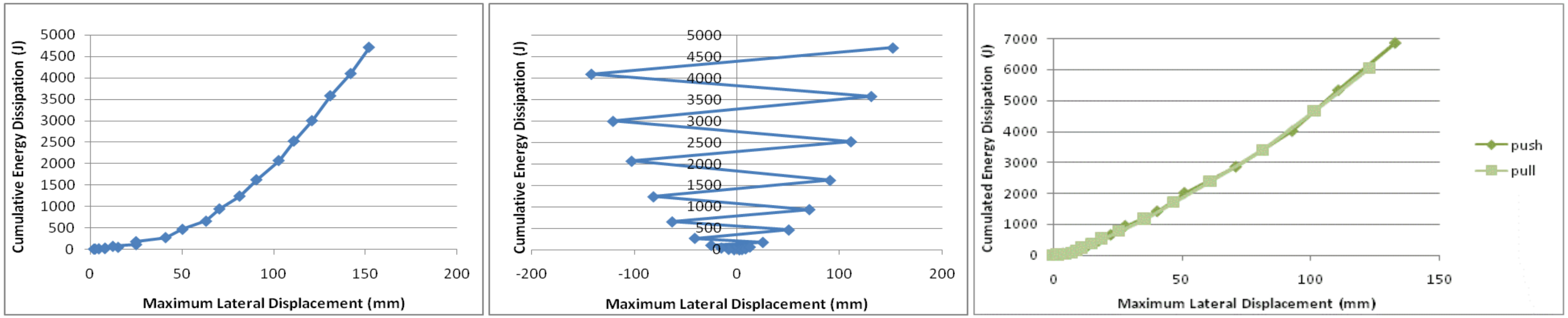

Figure 402: Change in cumulative dissipated energy – maximum lateral displacement relation of Frame#7 for all cycles (positive push / negative pull, and absolute values, respectively) and for push and pull cycles separately

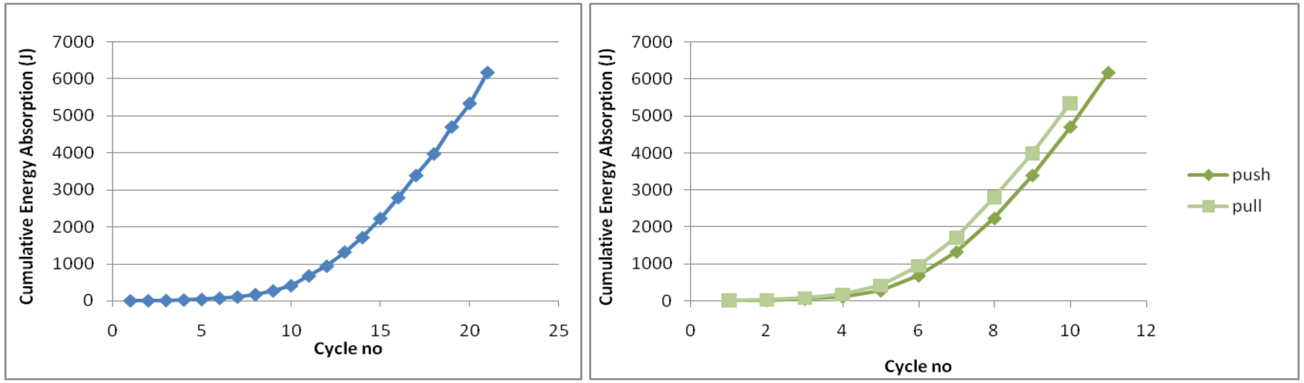

Figure 403: Change in cumulative absorbed energy of Frame#7 for all cycles and for push and pull cycles separately, respectively

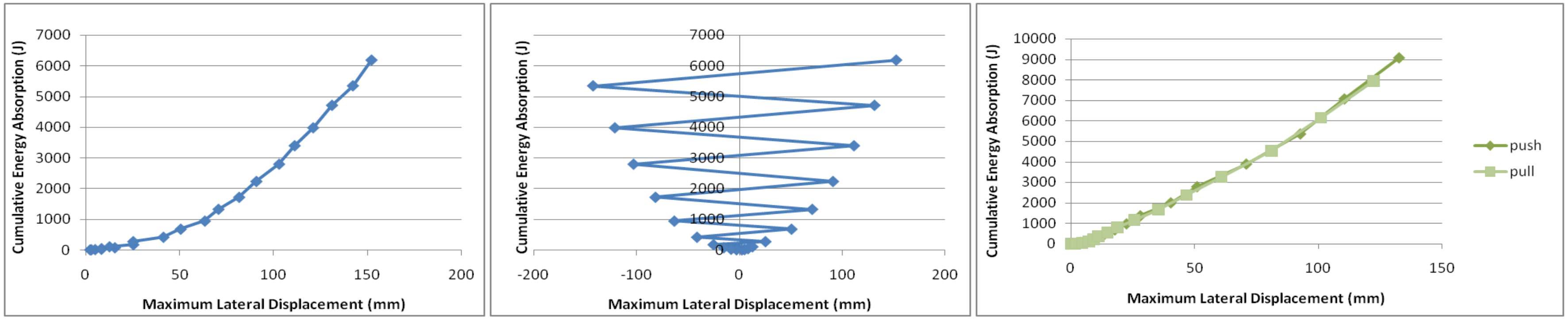

Figure 404: Change in cumulative absorbed energy – maximum lateral displacement relation of Frame#7 for all cycles (positive push / negative pull, and absolute values, respectively) and for push and pull cycles separately

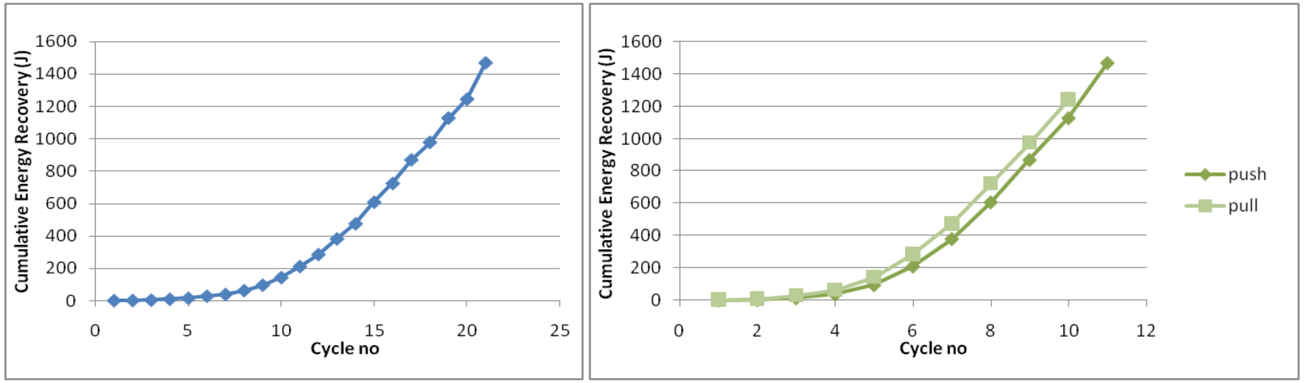

Figure 405: Change in cumulative recovered energy of Frame#7 for all cycles and for push and pull cycles separately, respectively

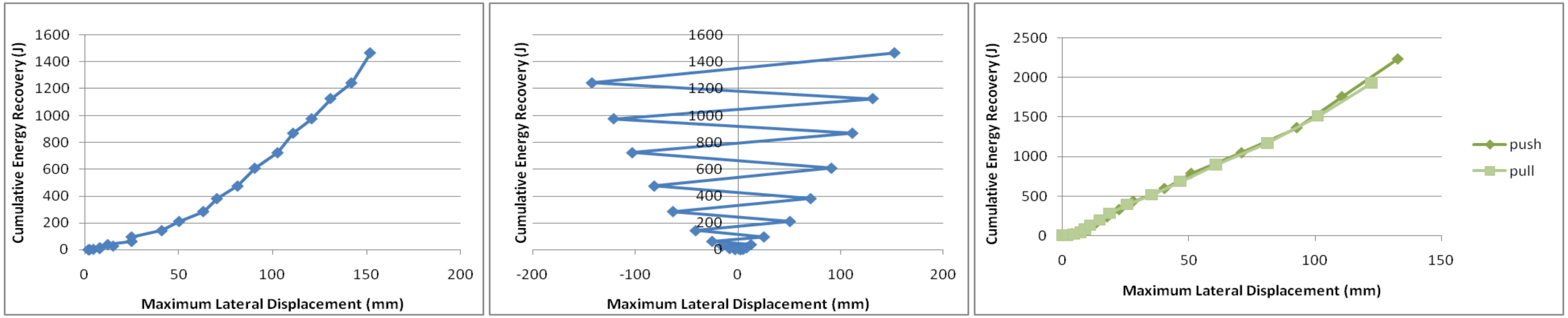

Figure 406: Change in cumulative recovered energy – maximum lateral displacement relation of Frame#7 for all cycles (positive push / negative pull, and absolute values, respectively) and for push and pull cycles separately

APPENDIX O

O. RESULTS OBTAINED AT THE END OF TESTING OF FRAME#7 WITH BRICK INFILL

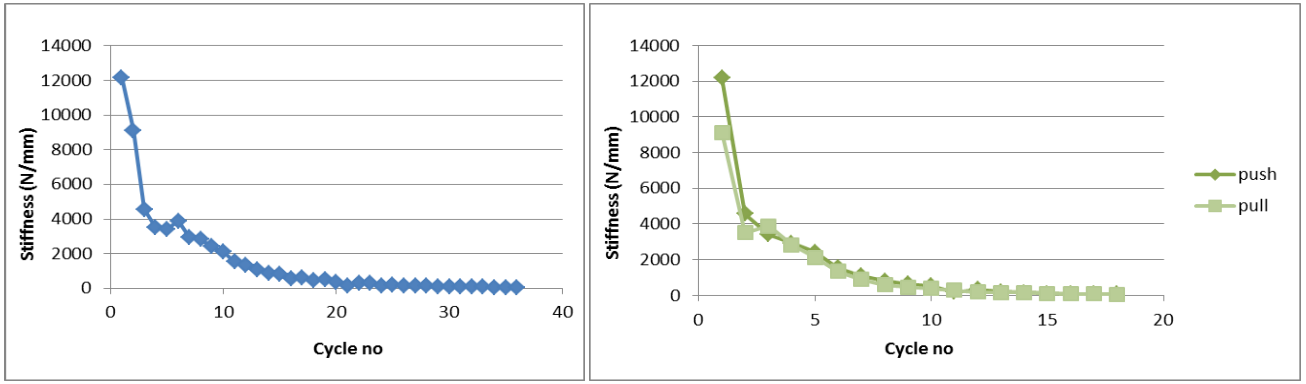

Figure 407: Change in stiffness for all cycles and for of Frame#7 with infill push and pull cycles separately, respectively

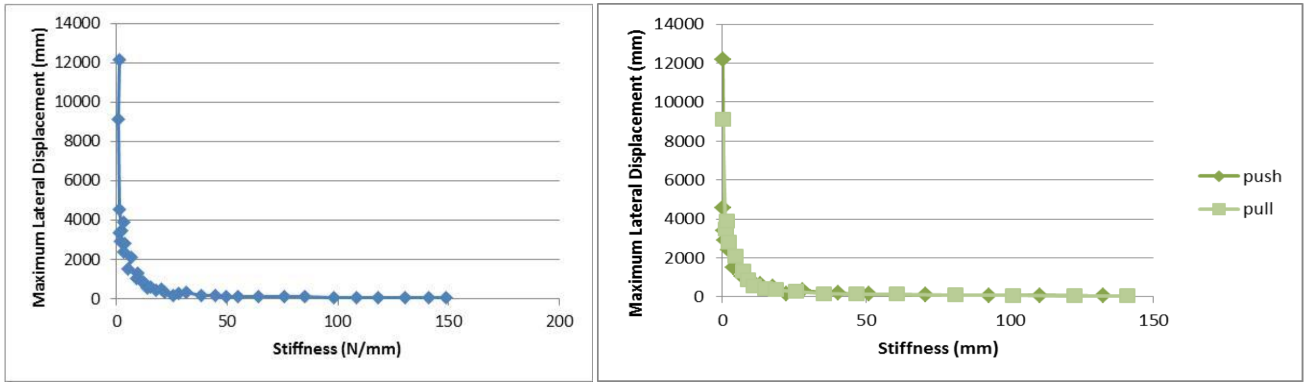

Figure 408: Change in stiffness – maximum lateral displacement relation of Frame#7 with infill for all cycles and for push and pull cycles separately, respectively

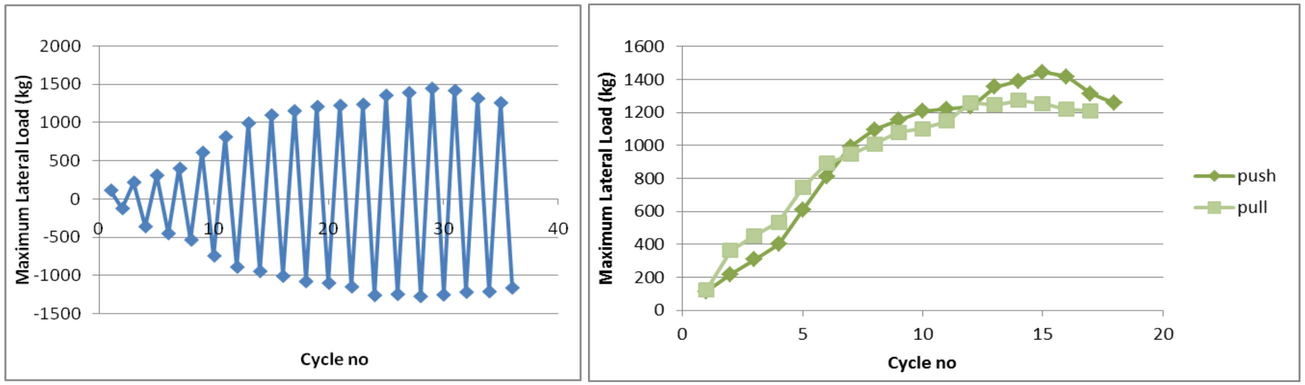

Figure 409: Change in maximum lateral displacement of Frame#7 with infill for all cycles and for push and pull cycles separately, respectively

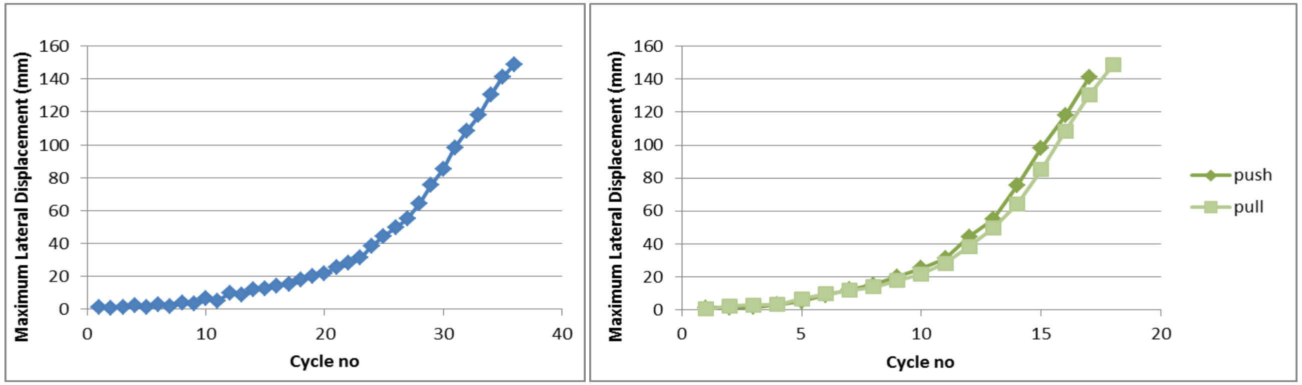

Figure 410: Change in maximum lateral displacement of Frame#7 with infill for all cycles and for push and pull cycles separately, respectively

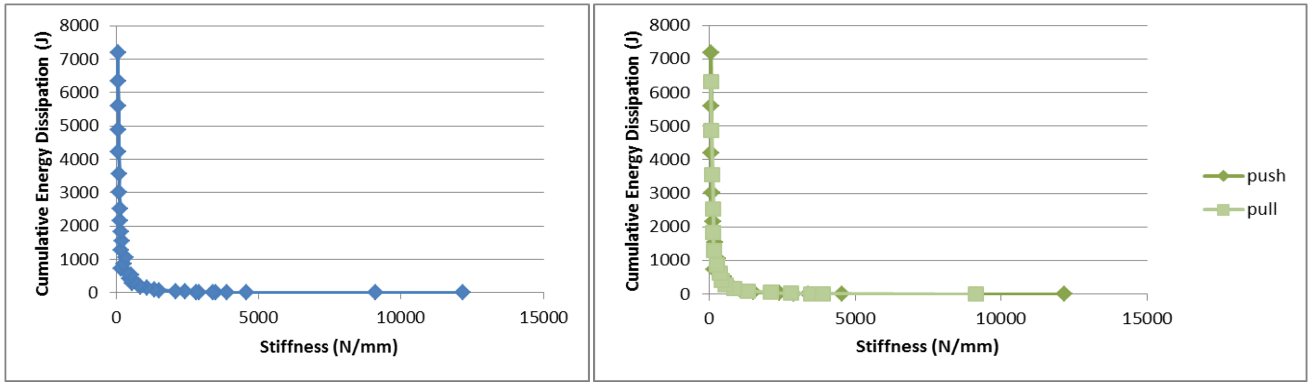

Figure 411: Change in cumulative dissipated energy –stiffness relation of Frame#7 with infill for all cycles (positive push / negative pull, and absolute values, respectively) and for push and pull cycles separately

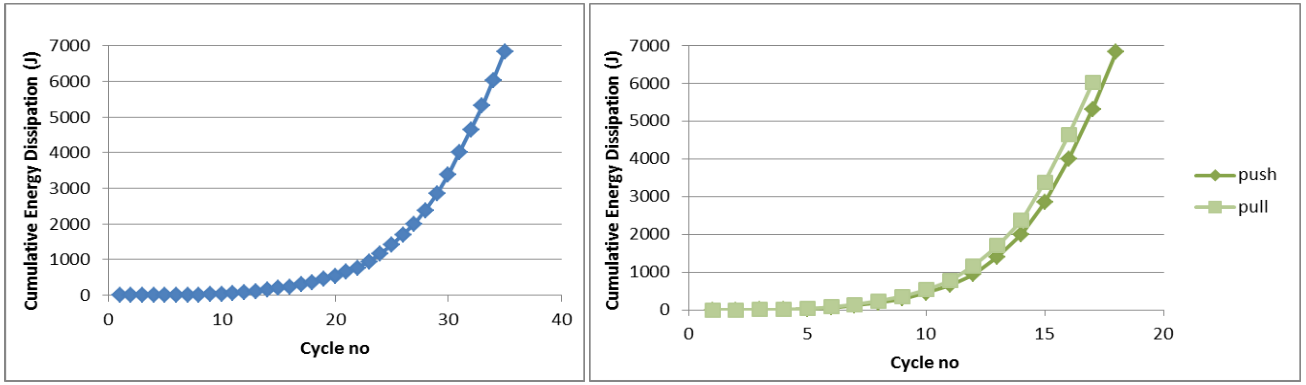

Figure 412: Change in cumulative dissipated energy of Frame#7 with infill for all cycles and for push and pull cycles separately, respectively

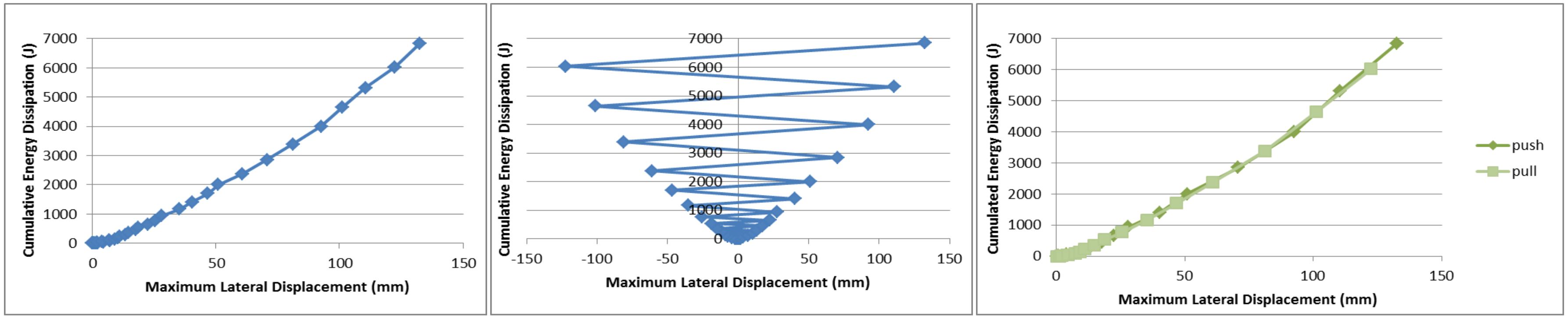

Figure 413: Change in cumulative dissipated energy – maximum lateral displacement relation of Frame#7 with infill for all cycles (positive push / negative pull, and absolute values, respectively) and for push and pull cycles separately

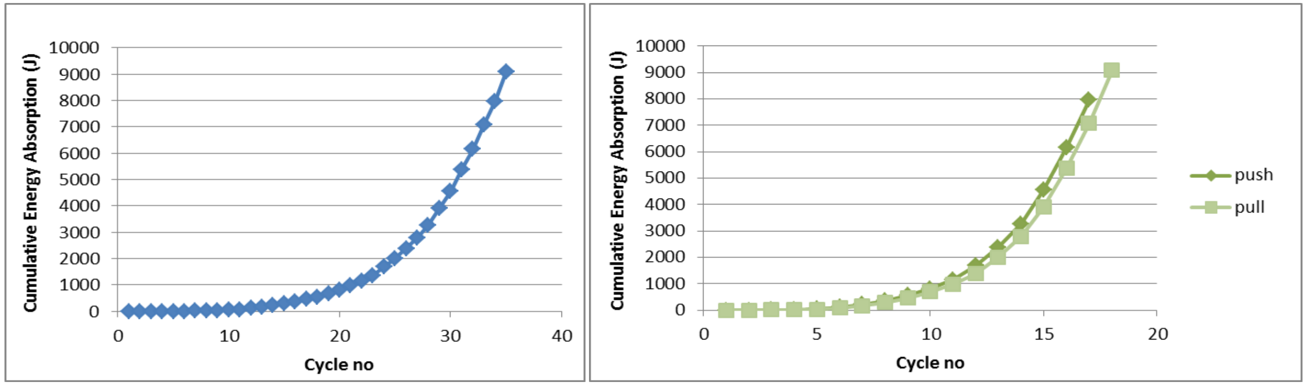

Figure 414: Change in cumulative absorbed energy of Frame#7 with infill for all cycles and for push and pull cycles separately, respectively

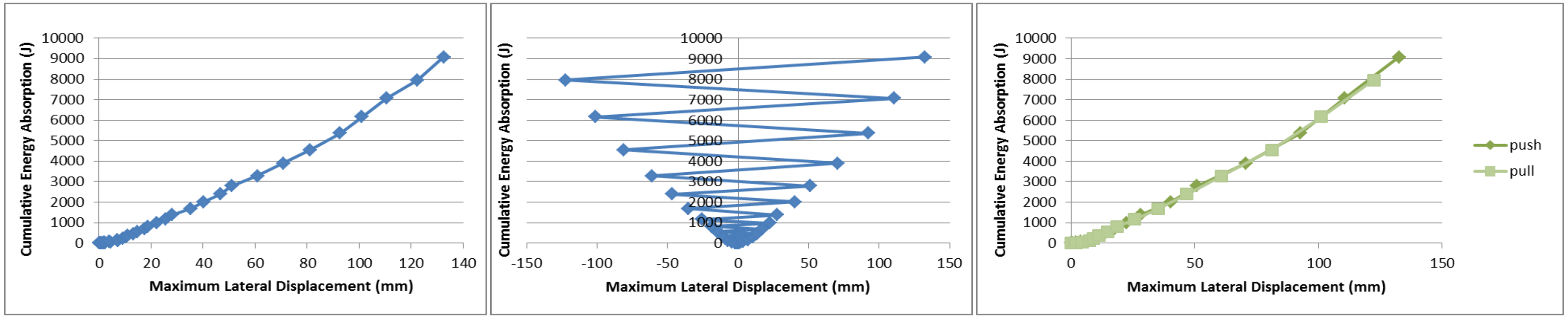

Figure 415: Change in cumulative absorbed energy – maximum lateral displacement relation of Frame#7 with infill for all cycles (positive push / negative pull, and absolute values, respectively) and for push and pull cycles separately

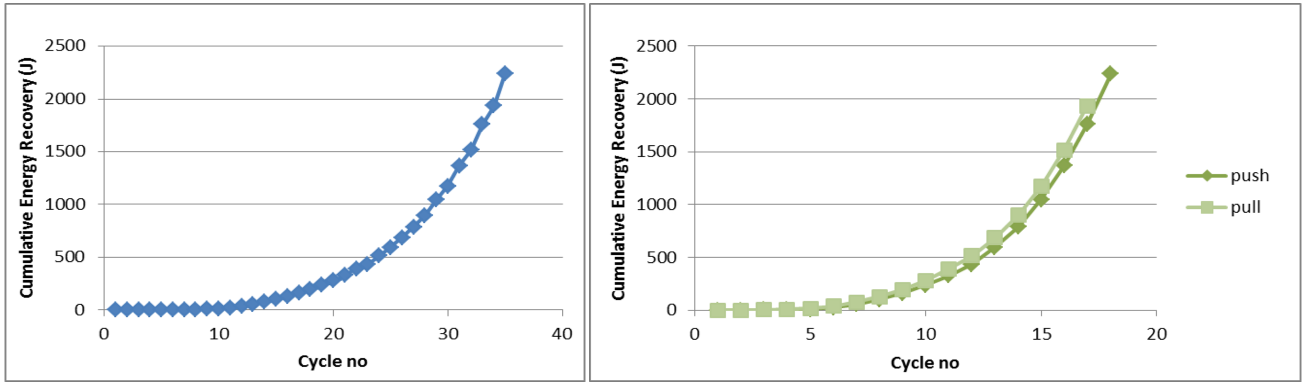

Figure 416: Change in cumulative recovered energy of Frame#7 with infill for all cycles and for push and pull cycles separately, respectively

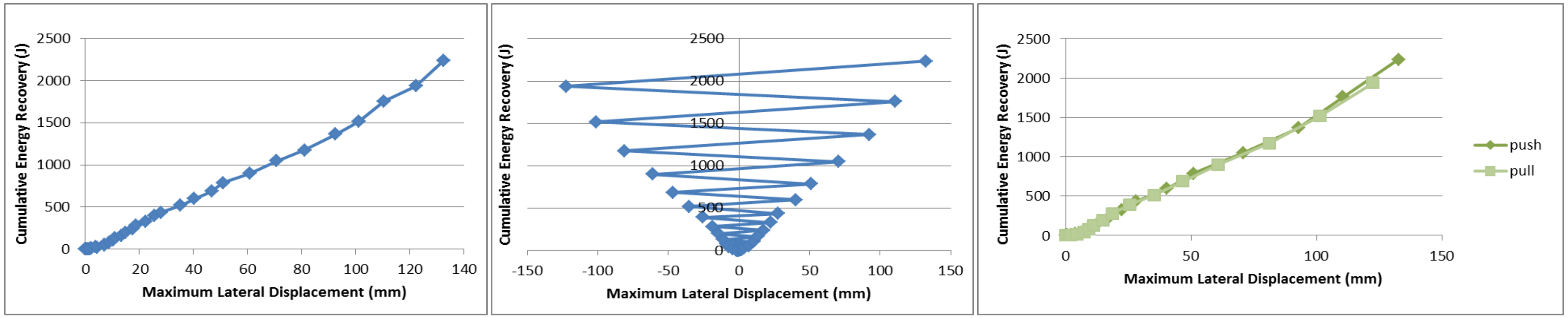

Figure 417: Change in cumulative recovered energy – maximum lateral displacement relation of Frame#7 with infill for all cycles (positive push / negative pull, and absolute values, respectively) and for push and pull cycles separately

APPENDIX P

P. RESULTS OBTAINED AT THE END OF TESTING OF FRAME#8

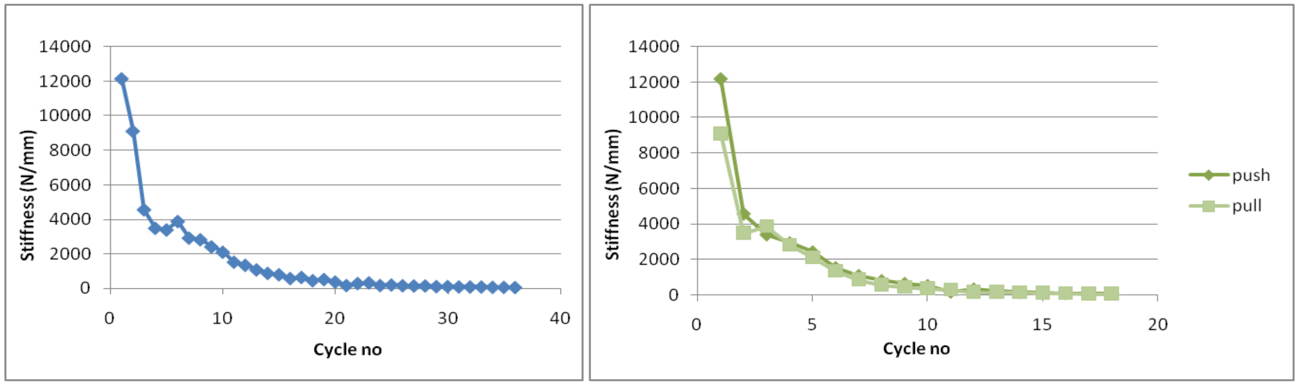

Figure 418: Change in initial stiffness of Frame#8 for all cycles and for push and pull cycles separately, respectively

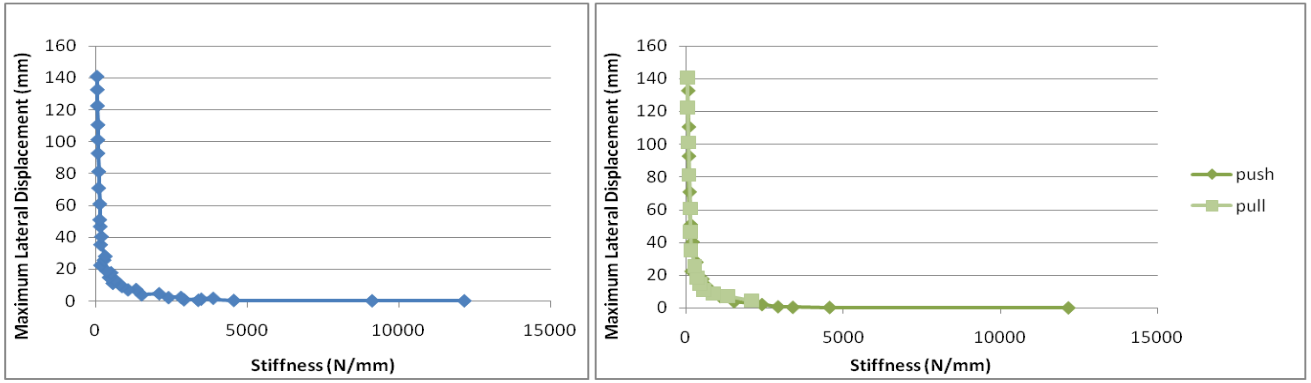

Figure 419: Change in initial stiffness – maximum lateral displacement relation of Frame#8 for all cycles and for push and pull cycles separately, respectively

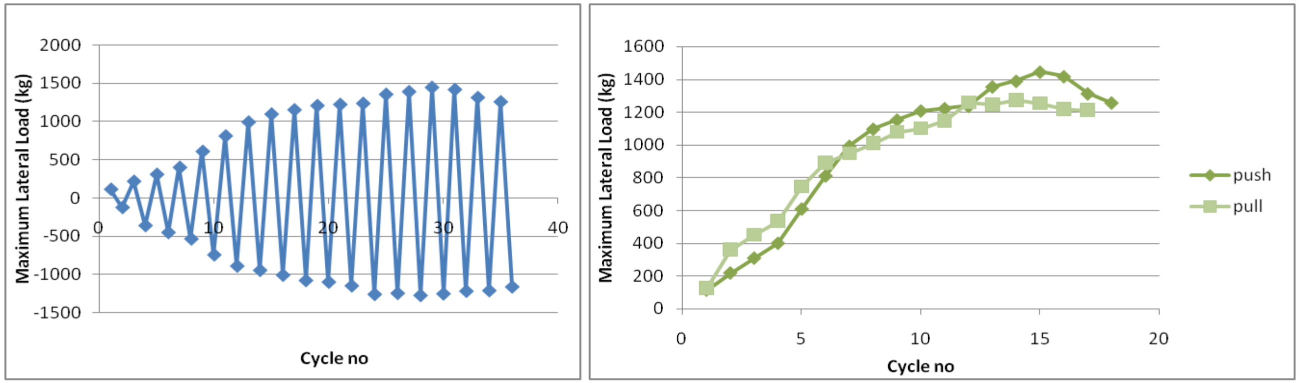

Figure 420: Change in maximum lateral load of Frame#8 for all cycles and for push and pull cycles separately, respectively

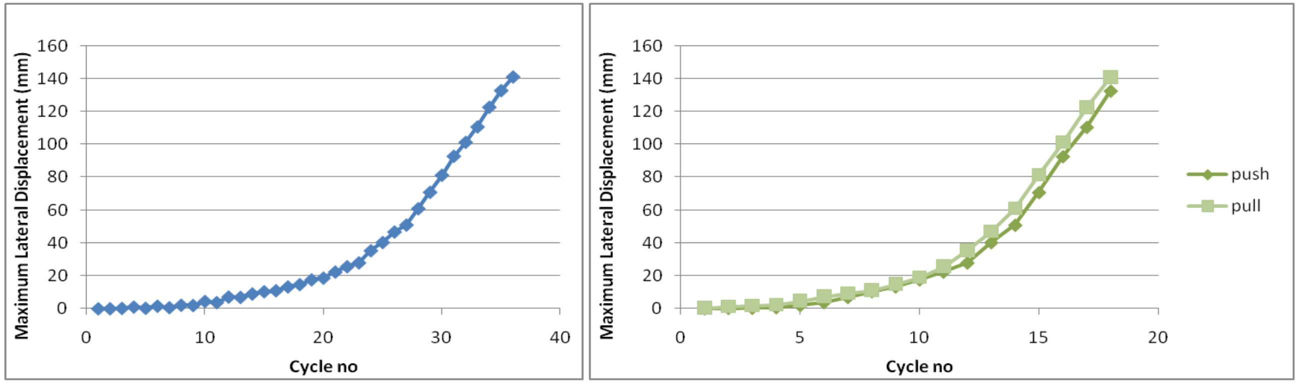

Figure 421: Change in maximum lateral displacement for all cycles and for push and pull cycles separately, respectively

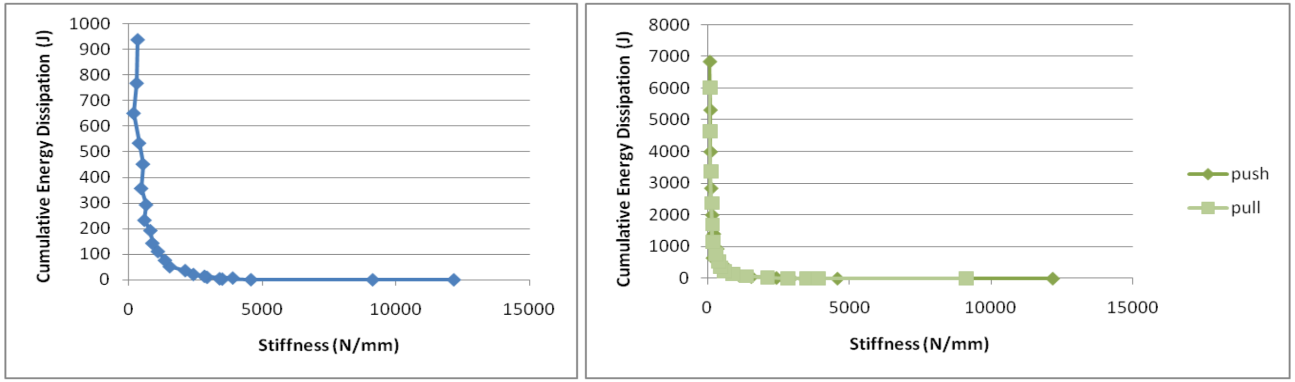

Figure 422: Change in cumulative dissipated energy – initial stiffness relation of Frame#8 for all cycles (positive push / negative pull, and absolute values, respectively) and for push and pull cycles separately

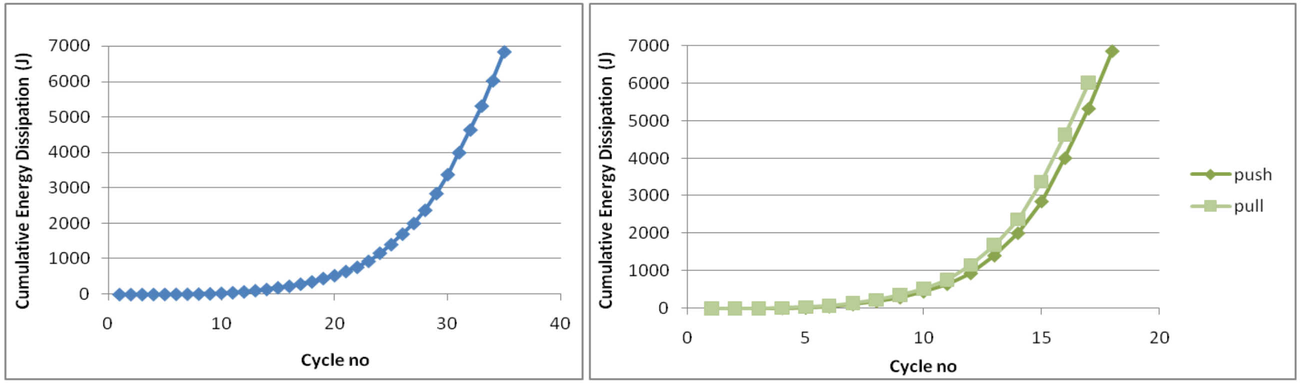

Figure 423: Change in cumulative dissipated energy of Frame#8 for all cycles and for push and pull cycles separately, respectively

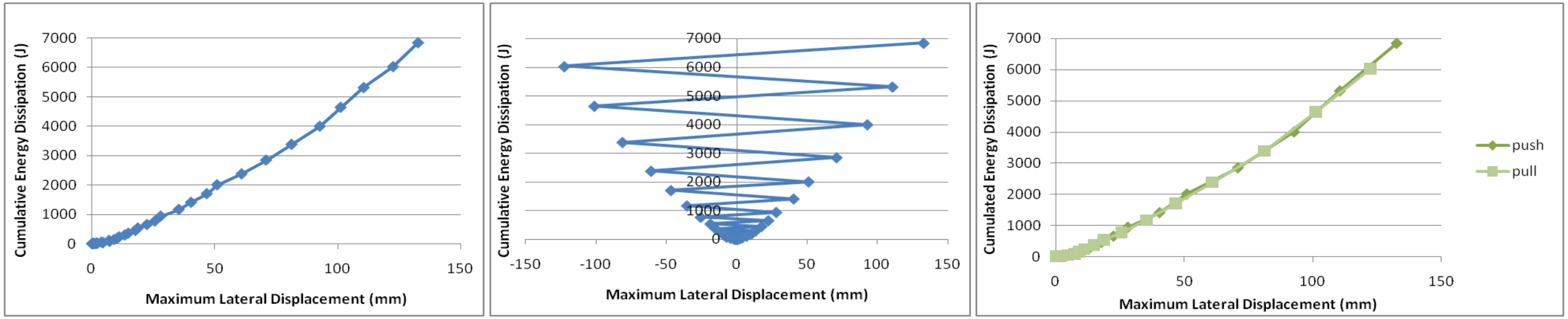

Figure 424: Change in cumulative dissipated energy – maximum lateral displacement relation of Frame#8 for all cycles (positive push / negative pull, and absolute values, respectively) and for push and pull cycles separately

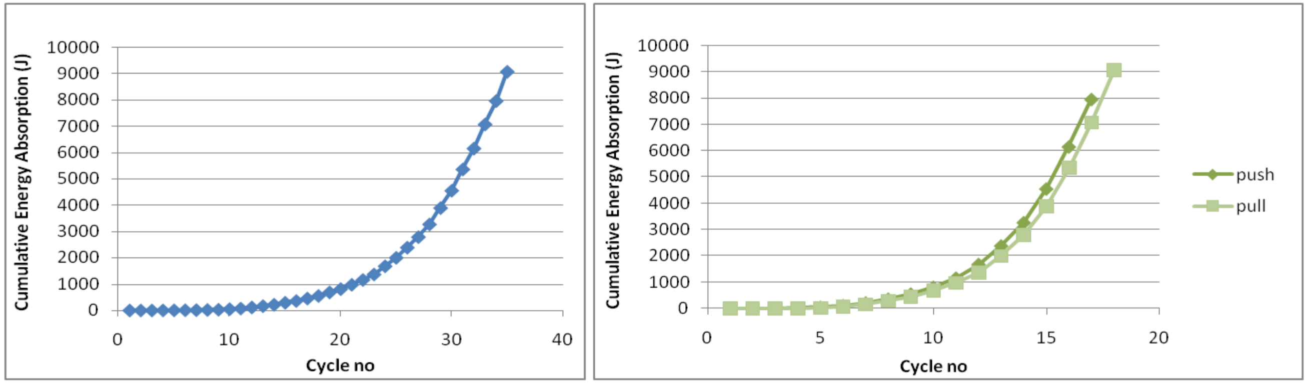

Figure 425: Change in cumulative absorbed energy of Frame#8 for all cycles and for push and pull cycles separately, respectively

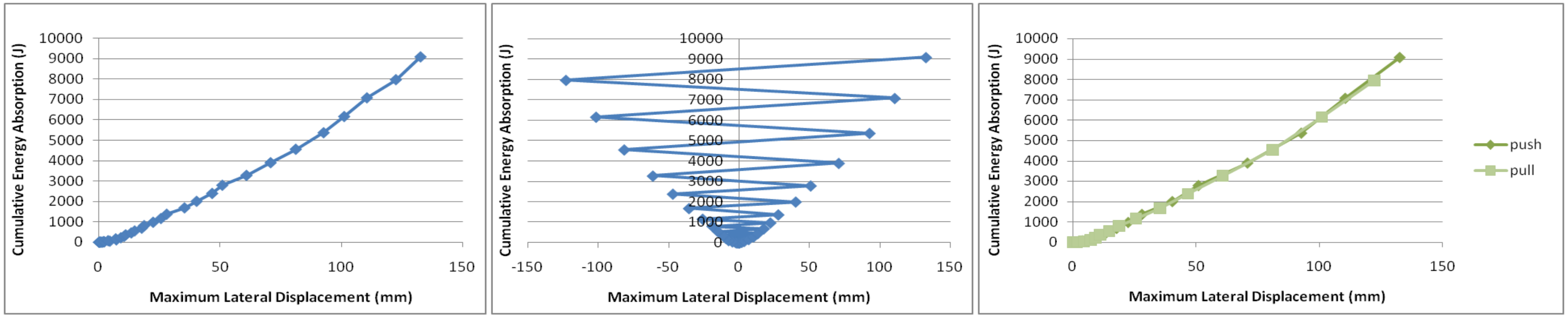

Figure 426: Change in cumulative absorbed energy – maximum lateral displacement relation of Frame#8 for all cycles (positive push / negative pull, and absolute values, respectively) and for push and pull cycles separately

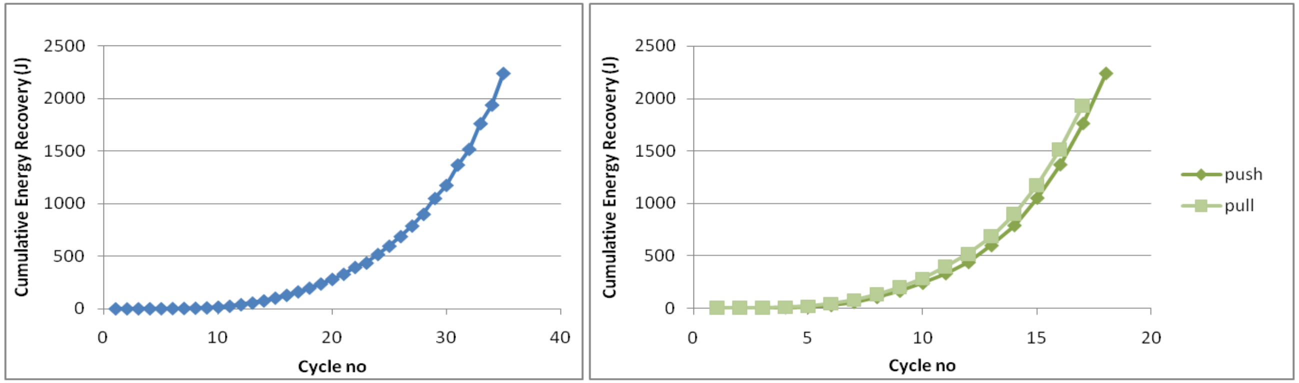

Figure 427: Change in cumulative recovered energy of Frame#8 for all cycles and for push and pull cycles separately, respectively

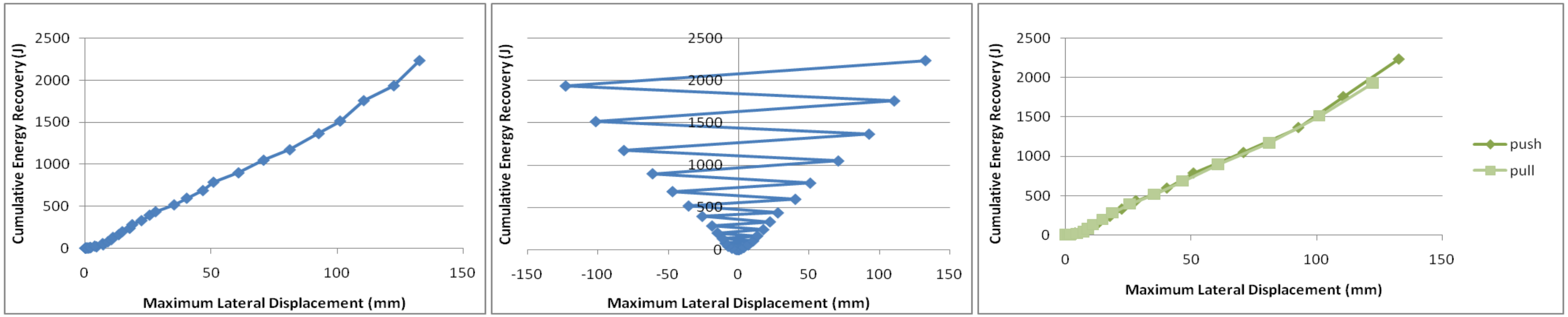

Figure 428: Change in cumulative recovered energy – maximum lateral displacement relation of Frame#8 for all cycles (positive push / negative pull, and absolute values, respectively) and for push and pull cycles separately

APPENDIX R

R. RESULTS OBTAINED AT THE END OF TESTING OF FRAME#8 WITH BAĞDADİ COVERING

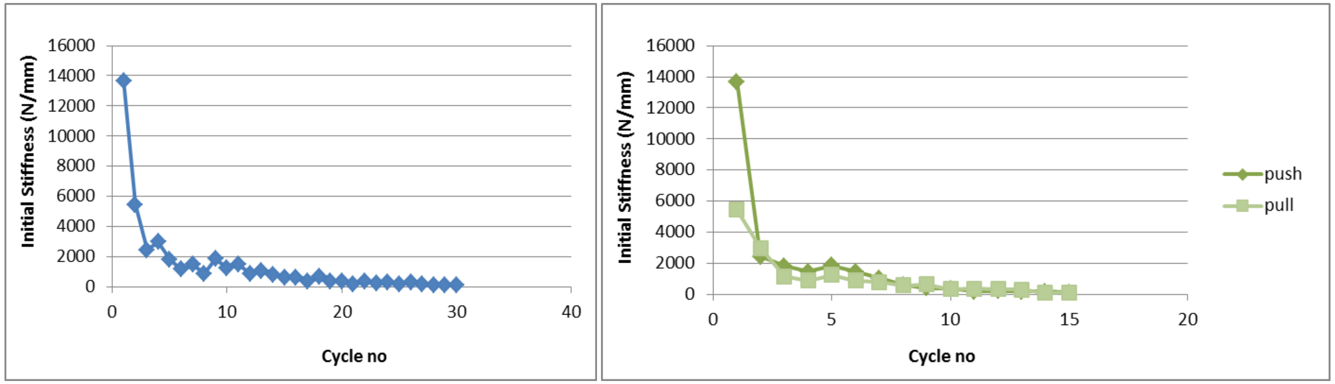

Figure 429: Change in initial stiffness of Frame#8 with infill for all cycles and for push and pull cycles separately, respectively

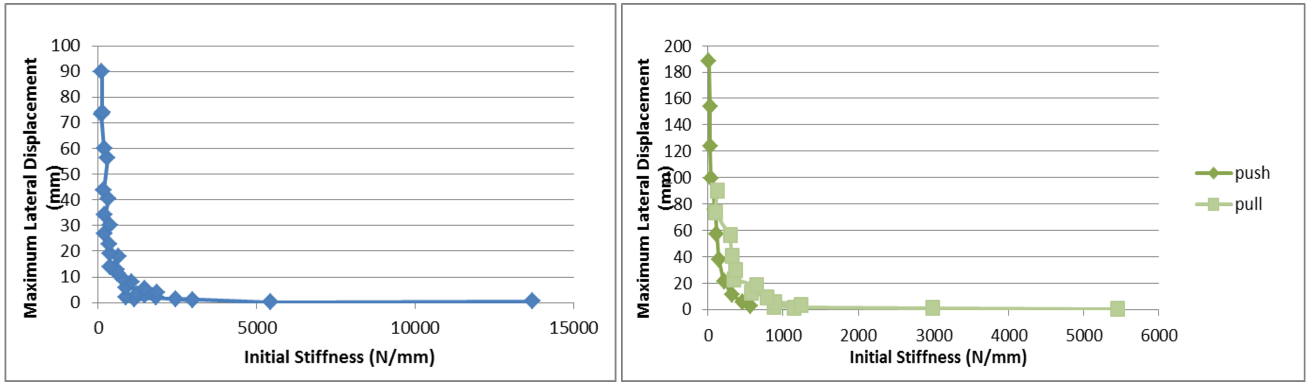

Figure 430: Change in initial stiffness – maximum lateral displacement relation of Frame#8 with infill for all cycles and for push and pull cycles separately, respectively

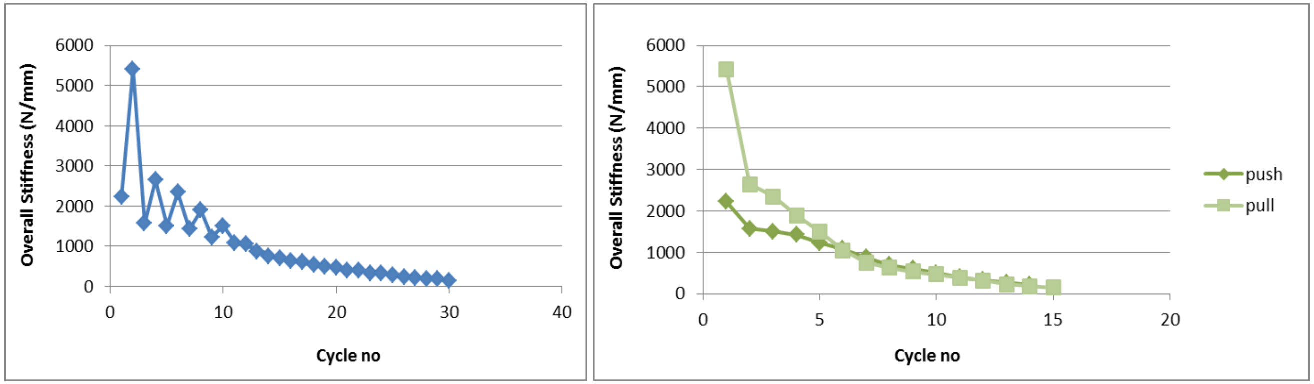

Figure 431: Change in overall stiffness of Frame#8 with infill for all cycles and for push and pull cycles separately, respectively

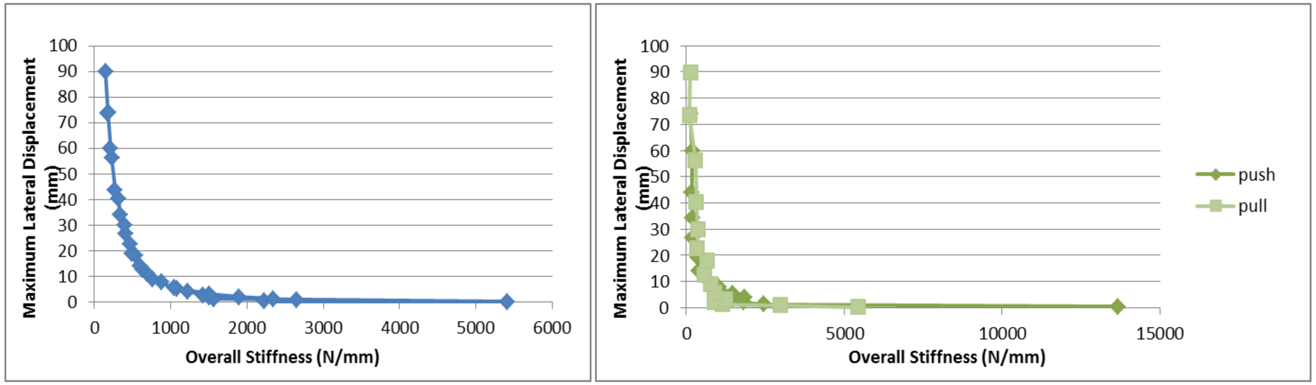

Figure 432: Change in overall stiffness – maximum lateral displacement relation of Frame#8 with infill for all cycles and for push and pull cycles separately, respectively

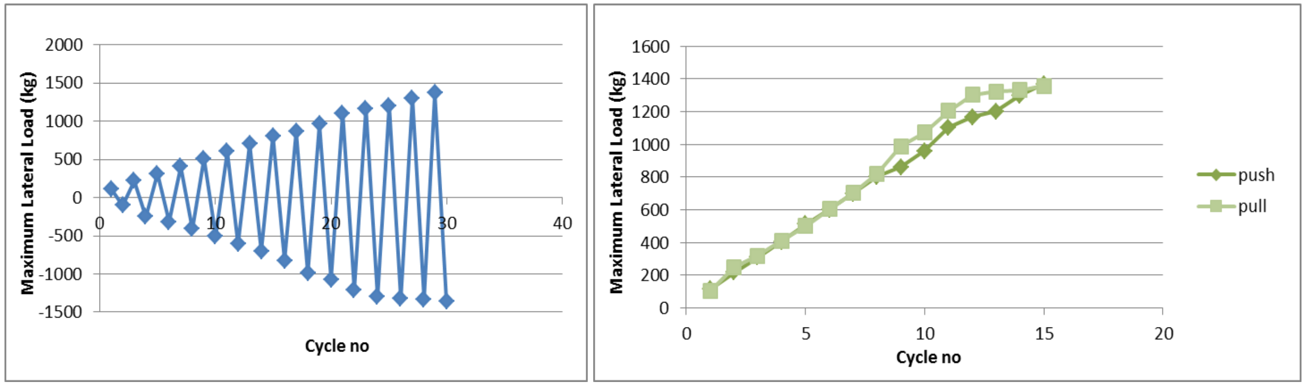

Figure 433: Change in maximum lateral load of Frame#8 with infill for all cycles and for push and pull cycles separately, respectively

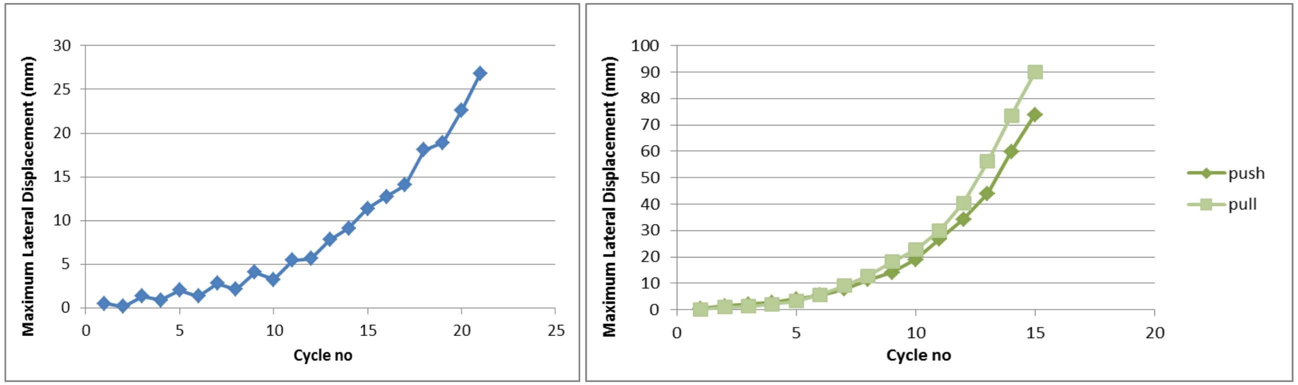

Figure 434: Change in maximum lateral displacement of Frame#8 with infill for all cycles and for push and pull cycles separately, respectively

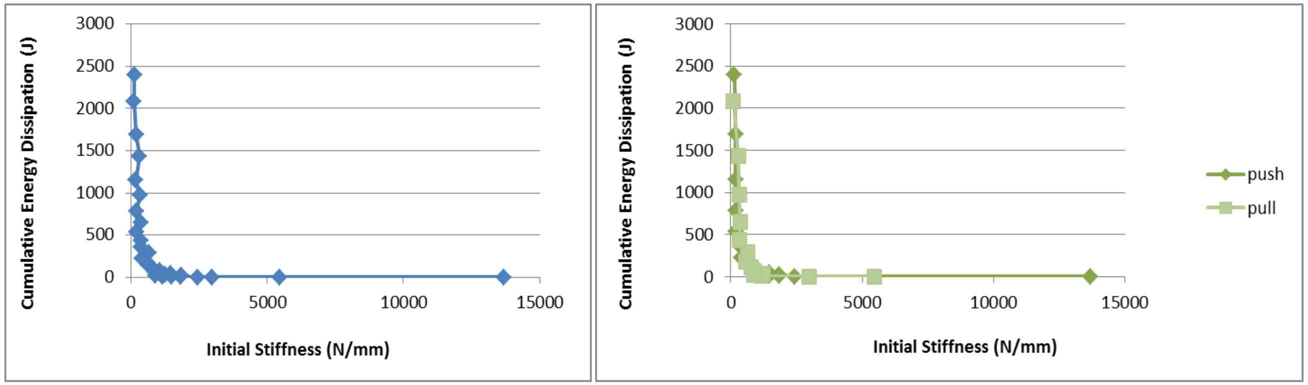

Figure 435: Change in cumulative dissipated energy – initial stiffness relation of Frame#8 with infill for all cycles (positive push / negative pull, and absolute values, respectively) and for push and pull cycles separately

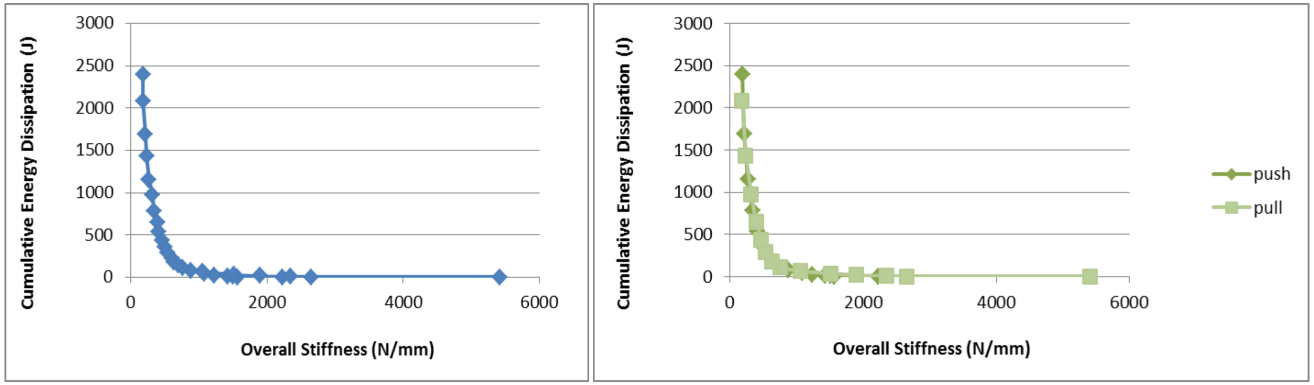

Figure 436: Change in cumulative dissipated energy – overall stiffness relation of Frame#8 with infill for all cycles (positive push / negative pull, and absolute values, respectively) and for push and pull cycles separately

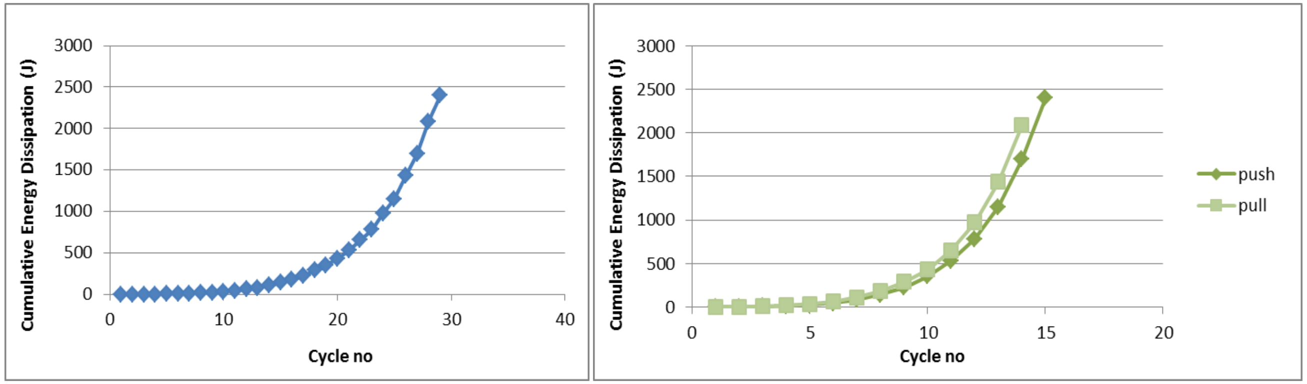

Figure 437: Change in cumulative dissipated energy of Frame#8 with infill for all cycles and for push and pull cycles separately, respectively

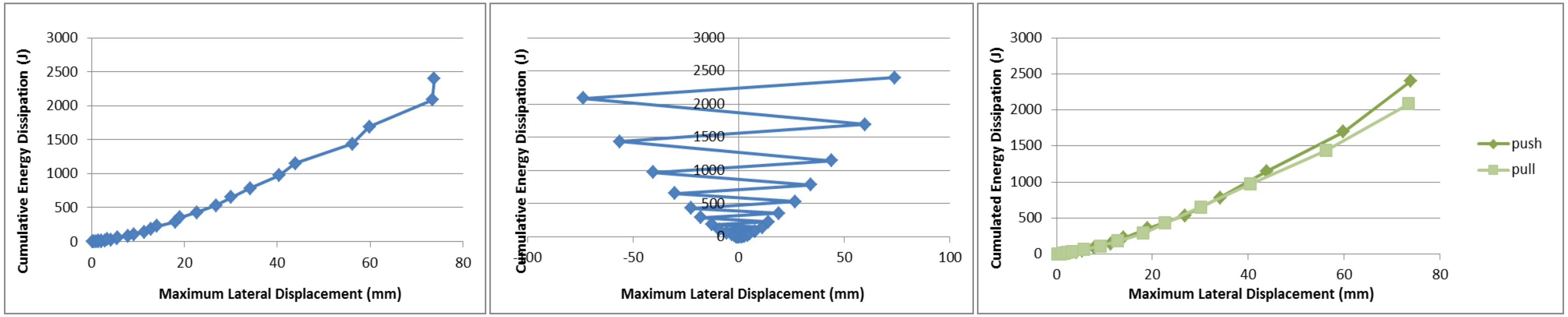

Figure 438: Change in cumulative dissipated energy – maximum lateral displacement relation of Frame#8 with infill for all cycles (positive push / negative pull, and absolute values, respectively) and for push and pull cycles separately

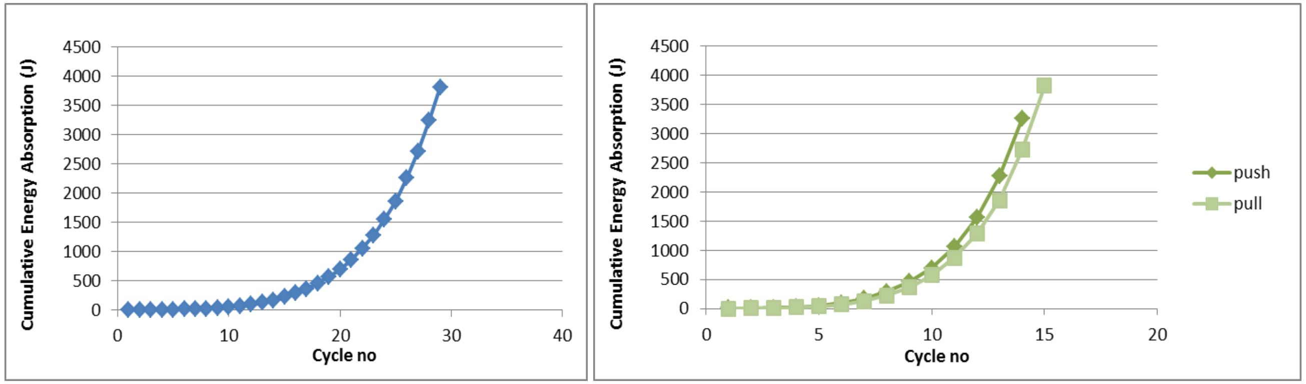

Figure 439: Change in cumulative absorbed energy of Frame#8 with infill for all cycles and for push and pull cycles separately, respectively

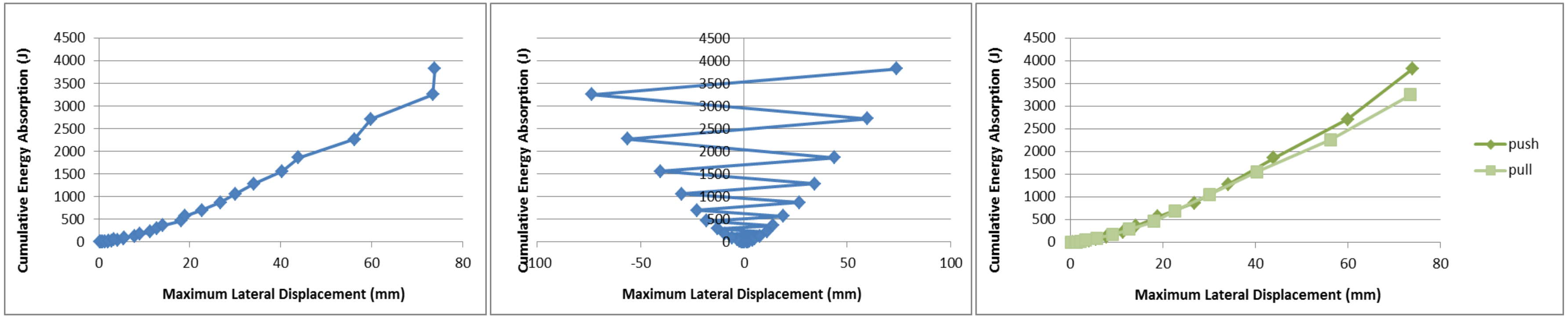

Figure 440: Change in cumulative absorbed energy – maximum lateral displacement relation of Frame#8 with infill for all cycles (positive push / negative pull, and absolute values, respectively) and for push and pull cycles separately

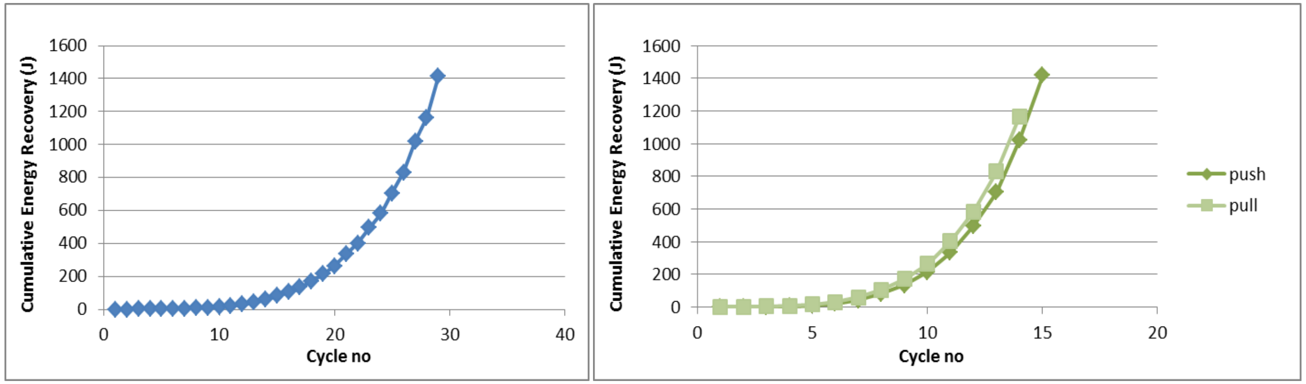

Figure 441: Change in cumulative recovered energy of Frame#8 with infill for all cycles and for push and pull cycles separately, respectively

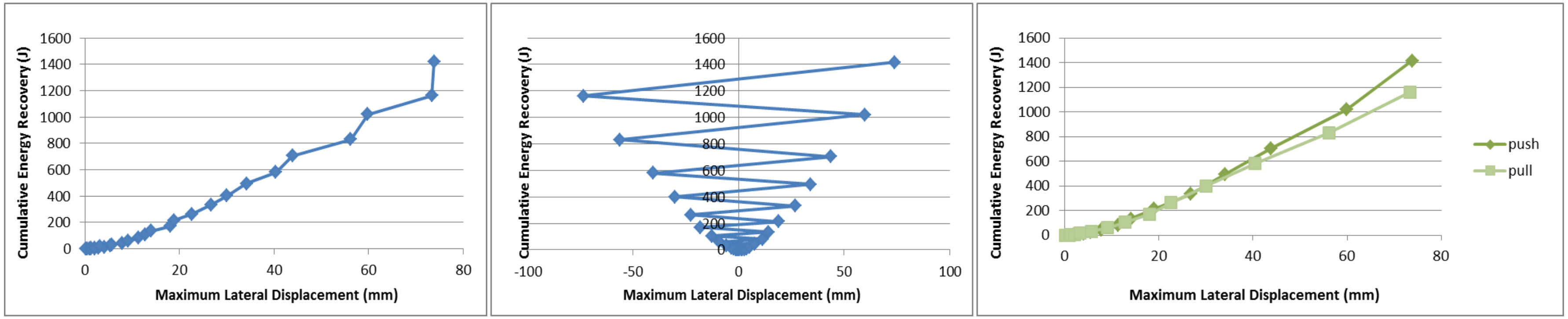

Figure 442: Change in cumulative recovered energy – maximum lateral displacement relation of Frame#8 with infill for all cycles (positive push / negative pull, and absolute values, respectively) and for push and pull cycles separately

CURRICULUM VITAE

PERSONAL INFORMATION

Surname, Name: Aktaş Erdem, Yasemin Didem

Nationality: Turkish (TC)

Date and Place of Birth: 20 December 1980, Ankara

E-mail: yasemindidem@yahoo.com

EDUCATION

2007-2011	Middle East Technical University METU, PhD, Program of Restoration
2003-2006	Middle East Technical University METU, M.S., Program of Archaeometry
M.s. Thesis	Technological Characteristics of Historical Brick Masonry Structures and Their Relationship with the Structural Behavior (Supervised by Assoc. Prof. Dr. Ahmet Türer and Prof. Dr. Emine Caner Saltık)
1997-2003	Middle East Technical University METU, Bachelor's Degree, Department of Civil Engineering (Structural Engineering Division)

WORK EXPERIENCE

2006-2008	Structural Analysis Team Membership in Commagene Nemrut Conservation Development Program, supported by Ministry of Culture.
	Analytical modeling of the monuments, Finite element analyses carried out using synthetic and recorded earthquake data and blast loading simulations, in Ls-Dyna. Dynamic tests and environmental monitoring. Investigation of possible reasons for collapse.
2008-2010	Assistantship of project no 106M499 supported by TUBITAK (The Scientific and Technological Research Council of Turkey) Seismic Assessment of Traditional Ottoman Timber Frame Houses (*Hımış*).
2010	Perge Hellenistic Period Defense Towers
	Finite element modeling and analyses carried out using synthetic and recorded earthquake data in Ls-Dyna.
2010-2011	Divriği Great Mosque
	Finite element modeling and analyses carried out using synthetic and recorded earthquake data

PUBLICATIONS

INTRNATIONAL CONFERENCE PAPERS

1. **Aktaş, Y.D.**, Türer, A., Caner-Saltık, E.N.; FE modeling and material characterization of Tahir ile Zühre Mescidi, Konya, Turkey; Structural Analysis of Historical Constructions SAHC 2006 Proceedings; Ed. Lourenco, P.B., Roca, P., Modena, C., Agrawal, S.; New Delhi; pp. 2013-2022.
2. **Aktaş, Y.D.**, Türer, A.; Preliminary Structural Monitoring and 3D Modeling of Nemrut Monuments, Turkey; Proceedings of International Symposium on Studies on Historical Heritage SHH 2007; Antalya; pp. 441-448.
3. **Aktaş, Y.D.**, Türer, A.; Issues in the Identification and Monitoring of Historical Structures – Monuments; Proceedings of 11th International Conference on Durability of Building Materials and Components DBMC, May 11-14 2008; Istanbul; pp. 1259-1266.
4. **Aktaş, Y.D.**, Türer, A.; A General Procedure for the Structural Condition Assessment of Historical Earthen Masonry Structures through Structural Identification and Monitoring; Proceedings of 10th International Conference on Study and Conservation of Earthen Architectural Heritage, January 1-5 2008; Bamako, Mali, pp. 352-357.
5. Türer, A., **Aktaş, Y.D.**, Şahin-Güçhan, N.; Structural Stability valuation of Nemrud Monuments; International Symposium on Historical Earthquakes and Conservation of Monuments and Sites in the Eastern Mediterranean Region for the 500th Anniversary Year of the 1509 September 10, Marmara Earthquake, September 10-12 2009; Istanbul, Turkey; pp. 224-226.
6. **Aktaş, Y.D.**, Erdil B., Akyüz, U., Şahin-Güçhan, N., Türer, A.; Structural Behavior of Timber Frame Ottoman Traditional "*Hımış*" Houses – Frame Loading Experiments; International Symposium on Historical Earthquakes and Conservation of Monuments and Sites in the Eastern Mediterranean Region for the 500th Anniversary Year of the 1509 September 10, Marmara Earthquake, September 10-12 2009; Istanbul, Turkey; pp. 364-366.
7. **Aktaş Erdem Y.D.**, Türer A.; Condition assessment of historic masonry structures by NDE and monitoring; Proceedings of Structures and Architecture; July, 21-23, Guimaraes, Portugal; ed. Cruz P.; Taylor and Francis Group, pp. 1785-1792.
8. **Aktaş Erdem Y.D.**, Akyüz U., Erdil B., Türer A., Şahin Güçhan N.; Assessment of seismic behavior of traditional timber frame Ottoman Houses: Frame tests; Proceedings of Structures and Architecture; July, 21-23, Guimaraes, Portugal; ed. Cruz P.; Taylor and Francis Group, pp. 1130-1137.
9. **Aktaş Erdem Y. D.**, Türer A., Erdil B., Akyüz, U., Şahin Güçhan N.; Testing and Seismic Capacity Evaluation of a Typical Traditional Ottoman Timber Frame; Proceedings of the 7th International Conference on Structural Analysis of Historical Constructions (SAHC) – Strengthening and Retrofitting; Trans Tech Publications Ltd., Switzerland; Advanced

Material Research Vols. 133-134, ed. Xianglin Gu and Xiaobin Song; October 6-8, 2010, Shanghai, People's Republic of China, pp. 629-634 (published in Advanced Materials Research, Volumes 133 – 134).

10. **Aktaş Erdem Y.D.**, Yaman C., Kandemir A., Cengiz S., Açan S., Türer A.; Analytical Modeling of Sivas Divrigi Great Mosque and Hospital; WCCE-ECCE-TCCE Joint Conference 2 on Seismic Protection of Cultural Heritage; October 31 – November 1, 2011, Antalya, Turkey, *forthcoming article*
11. **Aktaş Erdem Y. D.,** Türer A., Akyüz, U., Erdil, B., Şahin Güçhan N.; Behavior of Timber Frames with Adobe Infill Under Reverse Cyclic Loading; XIth International Conference on the Study and Conservation of Earthen Architectural Heritage, Terra 2012; April 22-27, 2012, Lima, Peru, *forthcoming article*

INTERNATIONAL JOURNAL PAPERS

1. Türer, A., **Aktaş Erdem, Y. D.**, Şahin Güçhan, N.; Reverse Engineering Evaluation and Monitoring of Nemrut Monuments, International Journal of Architectural Heritage 2, 2012 *forthcoming article*
2. **Aktaş Erdem, Y.D.**, Türer, A., Caner Saltık, E.; Adverse Structural Effects of Concrete Repairs on an Original Brick Masonry Dome Structure Under Temperature Loading (submitted to Construction and Building Materials)
3. **Aktaş Erdem, Y.D.**, Türer, A.; Akyüz, U.; Erdil, B., Şahin Güçhan, N.; Seismic Resistance Evaluation of Traditional Ottoman Timber-Frame *Hımış* Houses: Frame Loading and Material Tests (submitted to Engineering Structures)

GRANTS

2005	Suna-İnan Kıraç Research Institute of Mediterranean Civilizations
2005 - 2006	Research Grant by Italian Government
2008 - 2010	PhD Grant by TUBITAK

FOREIGN LANGUAGES

	Understanding	Speaking	Writing
English	Advanced	Advanced	Advanced
Italian	Advanced	Advanced	Advanced
Spanish	Intermediate	Intermediate	Intermediate